



**EMIL OTT**

**1902-1963**

Dr. Emil Ott, Research Professor at Stevens Institute of Technology, Trustee Plastics Institute of America and Consultant, died on September 29, 1963, in his home at Princeton. He was born in 1902 in Zurich, Switzerland, and received his Ph.D. from the Swiss Institute of Technology in 1928. A year earlier he came to the USA and worked as a chemist for Stauffer Chemical in San Francisco; then he studied at Johns Hopkins under an American Petroleum Institute Fellowship and there soon became assistant professor of chemistry.

In 1933 he joined the Hercules Powder staff as a research chemist and rose to director of research in 1939. He edited the book *Cellulose and Cellulose Derivatives* (Interscience, 1943) which is a standard reference both in this country and abroad, and published many papers in the entire field of cellulose chemistry. In 1955 he joined Food Machinery and Chemical Corporation (now FMC) as vice president in charge of research and development of the Chemical Divisions of the company.

Since 1929 he was a member of the ACS and developed great activity in the Wilmington Section; he also was a member of the ACS Board of Directors, 1948-51, together with many other responsible posts in the Society.

Dr. Ott was elected president of the American Institute of Chemists for the 1959 term, and devoted much time to the International Union of Pure

and Applied Chemistry, the Society of Chemical Industry, and the Société de Chimie Industrielle, which he represented at various international meetings abroad.

In 1933 Dr. Ott married Dorothy Aiken Wright. Their children are John Wright, Joan Nancy (Mrs. John Guyton), Dorothy Ann (Mrs. George Darmstatter), and David Emil.

Please look at the photograph and you will vividly remember Emil as we all loved to see him for so many years and as he will always remain in our memory.

Dr. Ott came up with polymers and polymer science from the early beginnings and was one of the last representatives of cellulose chemistry and technology in its transition from a chapter on sugar chemistry to its present dominating position in the science of macromolecules. The well-known book on *Cellulose and Cellulose Derivatives* which first appeared in 1943 under his editorship represents a very interesting and successful amalgamation of the older European tradition—Haworth, Staudinger, Meyer, Duclaux—with the more recent American contributions—Carothers, Kraemer, Flory, Spurlin—and can truly be called a classic in its field. A second edition, published together with his life long friend and distinguished co-worker, Harold Spurlin, has put the final touches on this merger, added the results of Russian and Japanese efforts, and has given cellulose its proper place in the wider fields of Polymer Science.

The Hercules Powder Company, which in the thirties already had a distinguished record in the field of explosives, Naval Stores, and cellulose, succeeded, during the twenty years of Dr. Ott's activities on its staff, to assemble a scientific and technical group of worldwide reputation and prestige. It is probably correct to surmise that the company's enlightened management contributed as much to Dr. Ott's growing stature as he did to the ultimate success of the research and development activities of Hercules Powder.

However, Emil was not only interested in science and engineering, but even more so in scientists and engineers and, as his position became more and more elevated, he developed from the things to the people, from the doing of scientific research to its organization and its correlation with the aims of our Society. It must have been very difficult for him to move from specialization to integration without being considered an amateur both by the professional scientists with whom he started and by the professional administrators amongst whom he spent most of his advanced career. Two qualities are above all necessary to span the gap and to maintain an influential position amongst specialists even if one cannot any longer be in contact with all pertinent details of the daily progress, and they are instinct and personality.

Emil possessed both qualities to an unusual degree and used them with great skill, diplomacy, and persuasion. How often have we all admired him when he entered the discussion of a Gordon Conference, an IUPAC Symposium or any other high level Scientific Meeting with a minimum of factual information on the topic and yet, all of a sudden, enlivened the atmosphere by a stimulating and progressive contribution. How often

has he impressed all of us in Commissions, Committees, Board Meetings, and Trustee Conferences with his thoughtful and pointed remarks: constructive for the organizations involved, full of sound advice for his colleagues, and of paternal benevolence for the younger generation.

We all are going to miss him terribly whenever we meet now that he will not be with us any longer and that we can no longer enjoy the sparks of his matchless sense of humor and the warm atmosphere of his good natured self.

Our sympathy goes to Dorothy and to all members of the Ott family together with the assurances that we all shall keep a fond and lasting memory of our dear friend and of the inimitable way in which he blended strong and profound effort with soft human spirit and with the image of a perfect gentleman.

*H. Mark*

## Stereoregular Polymerization of Vinyl Alkyl Ethers with Metal Sulfate-Sulfuric Acid Complex Catalysts

JOGINDER LAL and JAMES E. McGRATH, *Research Laboratories,  
The Goodyear Tire and Rubber Company, Akron, Ohio*

### Synopsis

The polymerization of vinyl alkyl ethers at room temperature or above, to give crystallizable polymers is of considerable interest for both theoretical and practical considerations. The polymerization of these monomers has been studied with metal sulfate-sulfuric acid complex catalysts at 0°C. or above to give high molecular weight, isotactic polymers. Ferric hydrosulfate hydrate and aluminum hexahydrosulfate heptahydrate (AHS) were used as catalysts. The nature of the solvent employed during polymerization with these heterogeneous catalysts was found to be quite important from the point of view of polymerization rate and stereoregularity of the polymer. A vinyl ether having a linear alkyl group polymerizes considerably faster than a monomer having a branched alkyl group. The apparent first-order rate constant values for the AHS-catalyzed polymerization of vinyl alkyl ethers having *n*-alkyl groups indicate the following sequence: ethyl > *n*-butyl > *n*-hexyl = *n*-octyl. In the temperature range of 30–58°C. the overall activation energy for the polymerization of vinyl *n*-butyl ether in heptane with AHS catalyst was found to be 9.7 kcal./mole. Vinyl *n*-butyl ether was copolymerized with  $\beta$ -vinyloxyethyl methacrylate ( $M_2$ ) using AHS catalyst. The average values of  $r_1 = 0.82$  and  $r_2 = 0.004$  were obtained.

### INTRODUCTION

The slow polymerization of vinyl alkyl ethers with boron trifluoride-diethyl ether catalyst at  $-78^\circ\text{C}$ . to give stereoregular, crystallizable polymers was reported by Schildknecht and co-workers.<sup>1</sup> Natta et al.<sup>2</sup> showed that poly(vinyl isobutyl ether) prepared in this fashion has an isotactic structure. A number of other catalyst systems capable of giving crystalline poly(vinyl alkyl ethers) have since been reported.<sup>3-7</sup> During our work on the cationic polymerization of vinyl isobutyl ether with triisobutylaluminum-titanium tetrachloride system, we observed that if the temperature of polymerization was allowed to exceed about  $-20^\circ\text{C}$ . the polymer produced was amorphous. Natta et al.<sup>4</sup> also reported that when the polymerization of vinyl isobutyl ether with triamylaluminum-biscyclopentadienyltitanium dichloride was carried out at  $-30^\circ\text{C}$ . or higher, amorphous polymers were obtained. Okamura et al.<sup>8</sup> found that during the polymerization of vinyl isobutyl ether with  $\text{BF}_3$ -ether in a "homogeneous" cationic system, the polymer obtained at  $-20^\circ\text{C}$ . was very tacky and had a very low precipitation temperature of  $-46^\circ\text{C}$ . in

methyl ethyl ketone solution. This value is presumably due to the irregular structure of the polymer. All these observations on the influence of temperature on the stereoregular polymerization of vinyl isobutyl ether are in marked contrast to the well-known formation of stereoregular polymers at relatively elevated temperatures in the anionic coordinated polymerization catalyzed by Ziegler- and Natta-type heterogeneous catalysts.

Polymerization of vinyl alkyl ethers at about room temperature or above to give crystallizable polymers is of considerable interest for both theoretical and practical considerations. The polymerization of vinyl alkyl ethers with aluminum hexahydrosulfate heptahydrate catalyst (AHS) at 0°C. or above to give high molecular weight polymers was reported by Mosley.<sup>9</sup> This catalyst has been found useful in synthesizing copolymers of vinyl alkyl ether with vinyl allyl ether<sup>10</sup> or with 1-methoxy-1,3-butadiene.<sup>11</sup> We had previously reported<sup>12</sup> our discovery that the reaction product of ferric sulfate with sulfuric acid (FHS) not only polymerizes vinyl alkyl ethers at about room temperature to high molecular weight materials, but that these materials also crystallize on stretching and give fiber diagrams on x-ray diffraction. At about that time we also discovered that Mosley's catalyst similarly gave crystallizable polymers from vinyl alkyl ethers. Furthermore, these polymers were more crystalline if polymerization was carried out in carbon disulfide instead of pentane.<sup>13</sup> A recent publication indicates that Okamura et al.<sup>14</sup> have also been interested in the polymerization of vinyl isobutyl ether with metal sulfate-sulfuric acid complex catalysts.

It has also been reported that crystalline polymers are produced if vinyl ethers are polymerized with the reaction product of aluminum selenate with aluminum isopropoxide,<sup>15</sup> aluminum alkoxide or aluminum alkyl with sulfuric acid,<sup>16, 17</sup> and a metal sulfate with a metal alkyl or a metal alkoxide.<sup>18</sup> The polymerization of vinyl isobutyl ether with *n*-butylmagnesium bromide at 80°C. to give a crystalline polymer has been reported by Kray.<sup>19</sup> We wish to report here some additional work in connection with the polymerization of vinyl alkyl ethers with the metal sulfate-sulfuric acid complex salts.

## EXPERIMENTAL

### Reaction of Ferric Sulfate with Sulfuric Acid

A 20-g. portion of powdered ferric sulfate hexahydrate and 100 ml. of concentrated sulfuric acid were placed in a 250-ml. flask fitted with a drying tube containing Drierite. The mixture was stirred with a glass-coated magnetic stirrer and maintained at 80°C. for about 4½ hr. After cooling, it was carefully added to 500 ml. of anhydrous diethyl ether. This treatment precipitated a white material from the reaction mixture. The white material obtained was filtered under a blanket of nitrogen, washed with additional ether three times and dried for 64 hr. at 35°C. and 2 Torr. A yield of 14 g. of white powder containing 19.85% iron and 22.7% sulfur

was obtained. These analytical data correspond to an overall composition of  $\text{Fe}_2(\text{SO}_4)_3 \cdot \text{H}_2\text{SO}_4 \cdot x\text{H}_2\text{O}$  where  $x$  is about 3 or 4.

Aluminum hexahydrosulfate heptahydrate was prepared by heating aluminum sulfate octadecahydrate with concentrated sulfuric acid according to the procedure described by Mosley.<sup>9</sup>

Catalyst suspensions were made in dry decalin or heavy mineral oil by rolling the mixture in a bottle in the presence of dried porcelain spheres.

### Monomers

Vinyl ethyl, *n*-butyl, and isobutyl ethers were obtained from Union Carbide Chemicals Company. Vinyl isopropyl ether, vinyl *n*-hexyl ether, and vinyl *n*-octyl ether were synthesized according to the method of Watanabe and Conlon<sup>20</sup> by the transesterification of analytical grade isopropyl alcohol, *n*-hexyl alcohol, and *n*-octyl alcohol with vinyl *n*-butyl ether with the use of mercuric acetate catalyst. They were fractionally distilled through a 1-m. column containing protruded metal packing, 0.16 in.  $\times$  0.16 in. and fitted with a constant temperature distillation head. All these monomers were then washed thoroughly with water, dried over potassium hydroxide pellets and distilled twice over sodium wire. For a study on their rates of polymerization, they were distilled over calcium hydride and the middle cuts were used for polymerization.  $\beta$ -Vinyloxyethylmethacrylate (VEM) was obtained from Rohm and Haas Company. It was distilled under vacuum to free it from hydroquinone stabilizer. The middle cut was used for copolymerization studies.

The refractive indices of the monomers are given in Table I.

TABLE I  
Refractive Indices of Vinyl Ethers

Monomer	$n_D^{30}$
Vinyl ethyl ether	1.3718
Vinyl isopropyl ether	1.3792
Vinyl <i>n</i> -butyl ether	1.3968
Vinyl isobutyl ether	1.3912
Vinyl <i>n</i> -hexyl ether	1.4125
Vinyl <i>n</i> -octyl ether	1.4224
$\beta$ -Vinyloxyethyl methacrylate	1.4436

### Solvents

*n*-Heptane (Phillips pure grade) and hexane (Phillips commercial grade) were treated with concentrated sulfuric acid, washed thoroughly with water, and dried over silica gel. Thereafter, they were distilled over phosphorus pentoxide under nitrogen. *n*-Pentane (Phillips pure grade) was used directly without any treatment. Thiophene-free benzene (Baker and Adamson, ACS reagent grade) and carbon disulfide (J. T. Baker, technical grade) were also distilled over phosphorus pentoxide under nitrogen.

### Polymerization

Polymerization was carried out by mixing monomer and solvent in the required ratio in a bottle and subsequently purging with dry nitrogen. The bottle was then fitted with a screw cap and a self-sealing rubber gasket. The bottle was chilled to about  $-20^{\circ}\text{C}.$ , the required amount of catalyst suspension was injected through the sealing gasket, and the bottle was tumbled in a  $5^{\circ}\text{C}.$  water bath. The polymerization was generally allowed to proceed to a high conversion. In the case of poly(vinyl ethyl ether), the polymerization was terminated with methanol containing phenyl  $\beta$ -naphthylamine stabilizer. The polymer was then precipitated in water. For the other poly(vinyl alkyl ethers), the precipitating medium was methanol. The polymers were dried for 64 hr. at  $40^{\circ}\text{C}.$  and 2 Torr.

Study of the rate of polymerization was carried out in a four-necked 1-liter flask fitted with a stirrer, a thermometer, a condenser with a drying tube on its top, and a serum cap. The flask was suspended in a constant temperature bath. After the mixture of 50 ml. of vinyl *n*-butyl ether (0.39 mole) and 500 ml. of heptane in the flask had attained the temperature of the bath, 0.5 ml. of 2.05% suspension of aluminum hexahydrosulfate heptahydrate (AHS) in dried mineral oil was injected through the gasket. Samples of the reaction mixture were withdrawn at regular intervals and injected into weighed bottles through their self-sealing gaskets. A known amount of phenyl  $\beta$ -naphthylamine in methanol was present in these bottles. The polymers were dried first under aspirator vacuum and finally at  $40^{\circ}\text{C}.$  and 2 Torr. to constant weight.

In an analogous manner, the rates of polymerization of other vinyl alkyl ethers were determined by diluting 0.39 mole of the monomer with heptane to a volume of 550 ml. and polymerizing with 0.5 ml. of 2.05% suspension of AHS.

To characterize more fully the molecular weight dependence on conversion a larger-scale polymerization was carried out in a small internally stirred reactor. The polymerization was carried out at  $50^{\circ}\text{C}.$  in hexane under 10 psig pressure of nitrogen. The volume ratio of the solvent to the monomer (vinyl *n*-butyl ether) was 5:1. The weight ratio of the monomer to the AHS catalyst was  $2.33 \times 10^4$ :1. The catalyst was introduced into the reactor as a 4% suspension in dry mineral oil. The reaction mixture was stirred continuously.

The inherent viscosity of the polymer was determined at  $30^{\circ}\text{C}.$  on a 0.1% solution of the polymer in benzene.

### Copolymerization

A 20-ml. portion of vinyl *n*-butyl ether and VEM mixture of known composition and 100 ml. of pentane were placed in cleaned 4-oz. bottles and screw-capped. The bottles were suspended in a water bath at  $26^{\circ}\text{C}.$  and after 1 hr. 20 mg. of powdered AHS catalyst was added to each of the bottles. The bottles were shaken frequently during the copolymerization

interval (13–41 min.). The copolymers were precipitated with a mixture of 80% methanol and 20% water containing 0.5% phenyl  $\beta$ -naphthylamine. The precipitated copolymers were suspended in the fresh precipitant overnight and were dried to constant weight at 40°C. and 2 Torr. Polymerizations were carried out in duplicate to 5% or lower conversions. The copolymer composition was determined by measuring the absorption due to the carbonyl group at 1725  $\text{cm}^{-1}$  and estimating the VEM content from a calibration curve obtained from a physical mixture of poly(vinyl *n*-butyl ether) and poly (VEM) in carbon tetrachloride.

## RESULTS AND DISCUSSION

Data typical of those obtained from polymerizations done in the internally stirred reactor are presented in Figures 1 and 2. The polymerization rate decreased and became very slow above 80% conversion (Fig. 1).

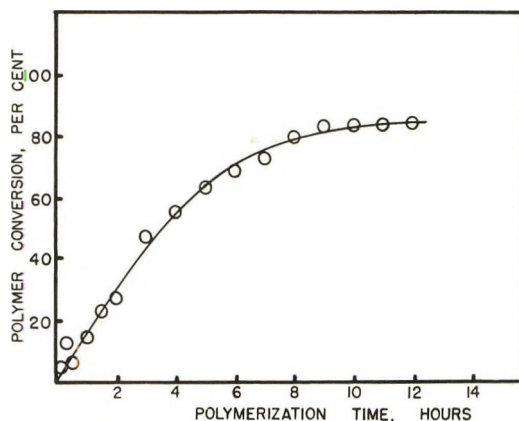


Fig. 1. Polymerization of vinyl *n*-butyl ether with AHS catalyst (suspension No. 1) at 50°C. in hexane. Dependence of polymer conversion on polymerization time.

The inherent viscosity increased rapidly as the polymerization progressed and leveled off at about 40% conversion (Fig. 2).

The conditions for bottle polymerization of several vinyl alkyl ethers are shown in Table II. The various polymers, without fractionation, gave crystalline x-ray diffraction patterns, some of which are shown in Figure 3. The identity periods of four poly(vinyl alkyl ethers) and their solubility behavior in various organic solvents are given in Table III. The identity period of 6.7 Å. for our poly(vinyl isobutyl ether) and poly(vinyl *n*-butyl ether) is in reasonable agreement with the identity period of 6.5 Å. reported by Natta et al.<sup>2</sup> for the  $\text{BF}_3$ -catalyzed poly(vinyl isobutyl ether) and by Dall'Asta and Bassi<sup>21</sup> for ethylaluminum dichloride- or ethylaluminum difluoride-catalyzed poly(vinyl *n*-butyl ether). These investigators have assigned isotactic, ternary helical structure to these two polymers. The similarity in identity period suggests that poly(vinyl

TABLE II  
 Polymerization of Vinyl Alkyl Ethers at 5°C.

Alkyl group in polymer	Solvent	Vol. ratio solvent/ monomer	Catalyst <sup>a</sup>	Molar ratio monomer/ catalyst $\times 10^3$	Polymeri- zation time, hr.	Conver- sion, %	Inherent viscosity, dl./g.
Ethyl	Pentane	6	AHS	3	2	100	4.7
Ethyl	Carbon disulfide	6	AHS	3	2	100	4.7
Ethyl	Pentane	6	FHS	1.9	18	95	3.5
Ethyl	Pentane	6	Ferric Sulfate hydrate	3.2	18	16	Liquid
Isopropyl	Pentane	5	AHS	3.3	64	64	<sup>b</sup>
Isopropyl	Pentane	5	FHS	4.8	70	14	1.7
<i>n</i> -Butyl	Pentane	6	AHS	2.5	16	80	9.0
<i>n</i> -Butyl	Carbon disulfide	6	AHS	2.5	16	84	6.2
Isobutyl	Pentane	5	AHS	15	—	47	2.4

<sup>a</sup> AHS is aluminum hexahydrosulfate (suspension preparation No. 2 in decalin); FHS is ferric hydrosulfate.

<sup>b</sup> Acetone-soluble fraction (46%), inherent viscosity 2.3 dl./g.; acetone-insoluble fraction (54%), inherent viscosity 5.7 dl./g.

TABLE III  
Identity Period and Solubility Data on Poly (vinyl Alkyl Ethers)

Polymer	Preparation of polymer	Identity period, A.		Remarks on the solubility of the polymer (25°C.)
		Our data	Literature	
Poly(vinyl ethyl ether)	AHS, pentane, 5°C.	6.6	—	Incompletely soluble in methanol, acetone, and methyl ethyl ketone <sup>a</sup>
Poly(vinyl <i>n</i> -butyl ether)	AHS, benzene, 36°C.	6.7	6.50 <sup>b</sup>	Insoluble in methanol and acetone. Incompletely soluble in methyl ethyl ketone; insoluble fraction had a melting temperature of 68–69°C. (lit. value: 64°C.) <sup>c</sup>
Poly(vinyl isobutyl ether)	AHS, benzene, 36°C.	6.7	6.5 <sup>d</sup>	Insoluble in methanol and acetone. Incompletely soluble in methyl ethyl ketone, heptane, benzene, and tetrahydrofuran. Fractions insoluble in heptane, benzene, and tetrahydrofuran had melting temperatures of 141–143°C., 159°C., and 162°C., respectively. (lit. value: 165°C.) <sup>e</sup>
Poly(vinyl isopropyl ether)	AHS, pentane, 5°C.	36	35.5 <sup>e</sup>	Insoluble in methanol. Incompletely soluble in acetone and diethyl ketone. The fraction insoluble in diethyl ketone had a melting temperature of 175–180°C. (lit. value: 190°C.) <sup>e</sup>

<sup>a</sup> Solubility in methyl ethyl ketone was considerably greater than in methanol or acetone.

<sup>b</sup> Data of Dall'Asta and Bassi.<sup>21</sup>

<sup>c</sup> Data of Vandenberg et al.<sup>5</sup>

<sup>d</sup> Data of Natta et al.<sup>2</sup>

<sup>e</sup> Data of Dall'Asta and Oddo.<sup>22</sup>

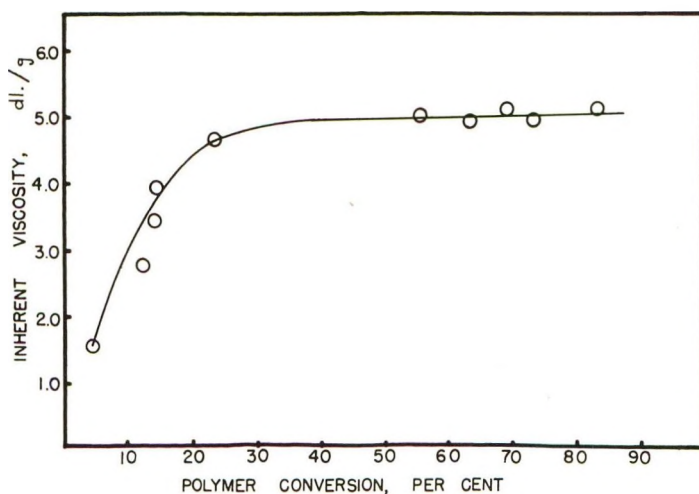


Fig. 2. Polymerization of vinyl *n*-butyl ether with AHS catalyst (suspension No. 1) at 50°C. in hexane. Dependence of inherent viscosity of the polymer on per cent conversion.

isobutyl ether) and poly(vinyl *n*-butyl ether) prepared with metal sulfate-sulfuric acid complex catalyst are also isotactic. The same is also true of our poly(vinyl ethyl ether) which has an identity period of 6.6 Å. The identity period of 36 Å. for the poly(vinyl isopropyl ether), prepared with the aluminum hydrosulfate, is also in agreement with the value of 35.5 Å. reported by Dall'Asta and Oddo<sup>22</sup> for isotactic poly(vinyl isopropyl ether).

The poly(vinyl isopropyl ether) prepared either with AHS or FHS catalyst was only partially soluble in acetone. This is in contrast to the complete solubility of the polymer in acetone at room temperature as reported by Dall'Asta and Oddo.<sup>22</sup> Presumably, the poly(vinyl isopropyl ether) prepared by these investigators was less crystalline than our polymer.

### Effect of Solvent during Polymerization

The nature of solvent employed in the polymerization of vinyl alkyl ether with metal sulfate-sulfuric acid complex catalyst is quite important. We have observed that the polymerization of vinyl *n*-butyl ether in benzene or toluene is considerably slower than in heptane. A comparison of the per cent insolubility of the polymer in various organic solvents showed that the polymer made in benzene had a greater insoluble fraction than the polymer prepared in heptane. For instance, a poly(vinyl *n*-butyl ether) sample prepared in benzene at 36°C. (inherent viscosity 3.4) contained 8% of a methyl ethyl ketone-insoluble, highly crystalline fraction, whereas another polymer sample (inherent viscosity 4.0) prepared in heptane under otherwise similar conditions had only 1-2% of a methyl ethyl ketone-insoluble fraction. Similarly, a poly(vinyl isobutyl ether) sample prepared in benzene at 36°C. had a benzene-insoluble fraction

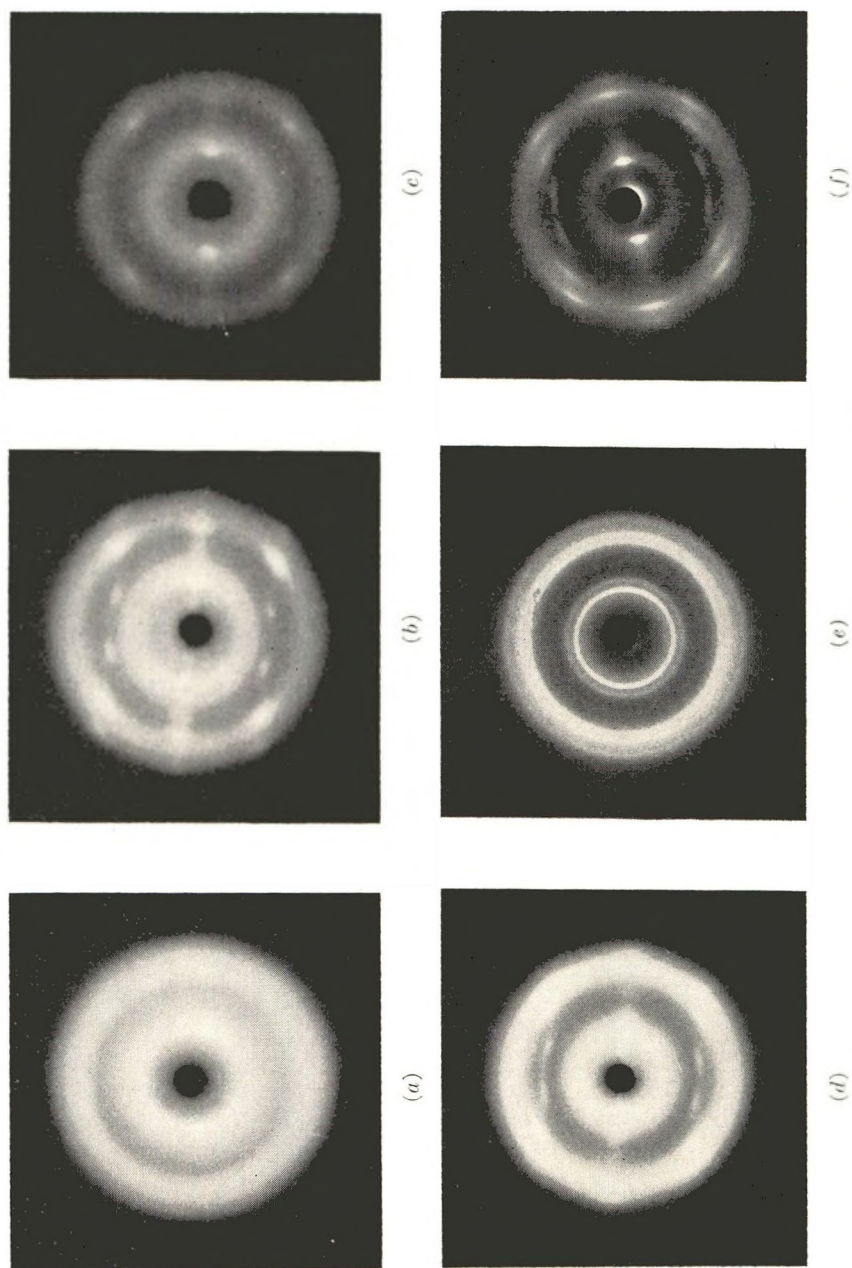


Fig. 3. X-ray diffraction patterns of poly(vinyl alkyl ethers): (a) unstretched poly(vinyl ethyl ether); (b) stretched poly(vinyl ethyl ether); (c) stretched poly(vinyl isobutyl ether); (d) stretched poly(vinyl *n*-butyl ether); (e) unstretched poly(vinyl isobutyl ether); (f) stretched poly(vinyl isobutyl ether). Polymer c was prepared with ferric hydrosulfate catalyst; the remaining polymers were prepared with aluminum hexahydrosulfate catalyst.

amounting to 25% as compared to 9% present in the polymer prepared in heptane. These benzene-insoluble fractions melted at 158.5–159.5°C. under a polarizing microscope. Dall'Asta and Bassi<sup>21</sup> have also reported that in contrast to aromatic hydrocarbons, such as toluene, the aliphatic hydrocarbons, such as heptane, give very weakly crystalline or absolutely amorphous poly(vinyl *n*-butyl ether) during polymerization with modified Friedel-Crafts catalysts at –78°C. As stated above, the rate of polymerization of vinyl *n*-butyl ether with AHS catalyst in benzene or toluene is slower than in heptane. This is in contrast to the marked increase in polymer conversion reported by Dall'Asta and Bassi when toluene was substituted for heptane.

### Effect of Monomer Structure on Polymerization Rate

The data in Table II indicate that vinyl alkyl ethers having linear as well as branched alkyl groups can be polymerized with the metal sulfate-sulfuric acid complexes. However, a vinyl ether having a linear alkyl group polymerizes considerably faster than the monomer having a branched alkyl group. As shown in Figure 4, under identical conditions the apparent first-order rate constant for the polymerization of vinyl *n*-butyl ether at 36°C. is about 25 times the corresponding value for vinyl isobutyl ether. This lower rate is partly due to the formation of threadlike agglomerates of the catalyst during the polymerization of vinyl isobutyl ether. The bulkiness of the isobutyl group of this monomer might also hinder the approach of the monomer to the reactive centers of the heterogeneous catalyst, thereby reducing the rate of its polymerization. The influence of the length of the linear alkyl group on the rate of polymerization of vinyl ethers is shown in Figures 4 and 5. Increasing the length of the alkyl group of the monomer from ethyl to *n*-hexyl caused a decrease in the rate of polymerization. Further increase in the length of the alkyl group from *n*-hexyl to *n*-octyl apparently did not affect the polymerization rate. The

TABLE IV  
Apparent First-Order Rate Constants for the Polymerization of Vinyl Alkyl Ethers with AHS Catalyst<sup>a</sup>

Alkyl group in monomer	Polymerization temp., °C.	Apparent first-order rate constant, min. <sup>-1</sup> × 10 <sup>3b</sup>
Ethyl	0.5	4.0
<i>n</i> -Butyl	0.5	0.55
<i>n</i> -Butyl	36	42
Isobutyl	36	1.7
<i>n</i> -Hexyl	36	0.54
<i>n</i> -Octyl	36	0.54

<sup>a</sup> Catalyst suspension No. 3 in mineral oil. The average particle size of the catalyst was about 5  $\mu$ . During polymerization of vinyl *n*-butyl ether, the catalyst particles remained unchanged in size.

<sup>b</sup> [M] = 0.71 mole/l.; [Cat.] =  $2.43 \times 10^{-5}$  mole/l.

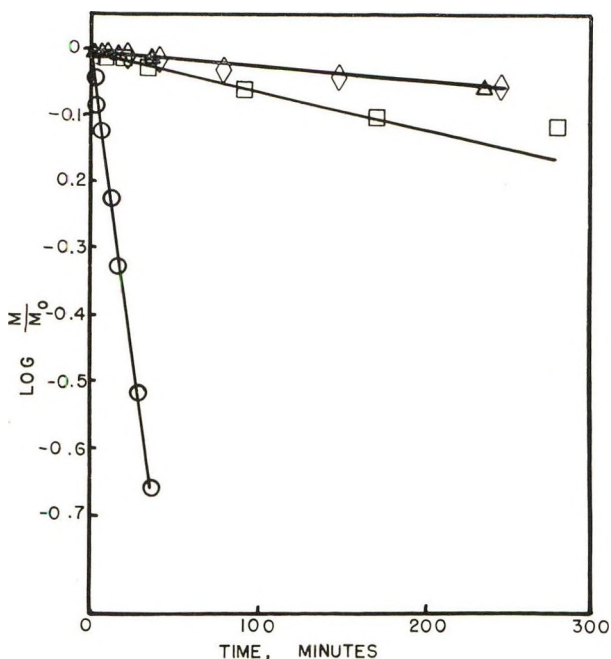


Fig. 4. Effect of length and shape of alkyl group on rate of polymerization of vinyl alkyl ethers at 36°C. in *n*-heptane; (O) *n*-butyl; (□) isobutyl; (▽) *n*-hexyl; (◇) *n*-octyl. [Monomer] = 0.71 mole/l.; [Cat.] =  $2.43 \times 10^{-3}$  mole/l.; AHS suspension No. 3.

apparent first-order rate constant values for the polymerization of these monomers with a particular catalyst suspension are given in Table IV and indicate the following sequence: vinyl ethyl ether > vinyl *n*-butyl ether > vinyl *n*-hexyl ether = vinyl *n*-octyl ether.

#### Effect of Temperature on Polymerization Rate

The overall activation energy for the polymerization of vinyl *n*-butyl ether in heptane with AHS catalyst in the temperature range of 30–58°C was found to be 9.7 kcal./mole (Fig. 6). In these experiments, the volume ratio of the solvent to the monomer was 10:1 and the molar ratio of the monomer to the catalyst was  $2.83 \times 10^4:1$ . Our value of the activation energy is of the same magnitude as the value of  $6.0 \pm 0.5$  kcal./mole reported by Coombes and Eley<sup>23</sup> for the polymerization of vinyl *n*-butyl ether in diethyl ether solvent using boron trifluoride–diethyl ether catalyst.

#### Mechanism of Polymerization

The exact mechanism of the polymerization of vinyl alkyl ethers with metal sulfate–sulfuric acid catalysts to form crystallizable polymers has not been elucidated. Steric considerations associated with the heterogeneous nature of the catalyst play a major role in determining the mode of

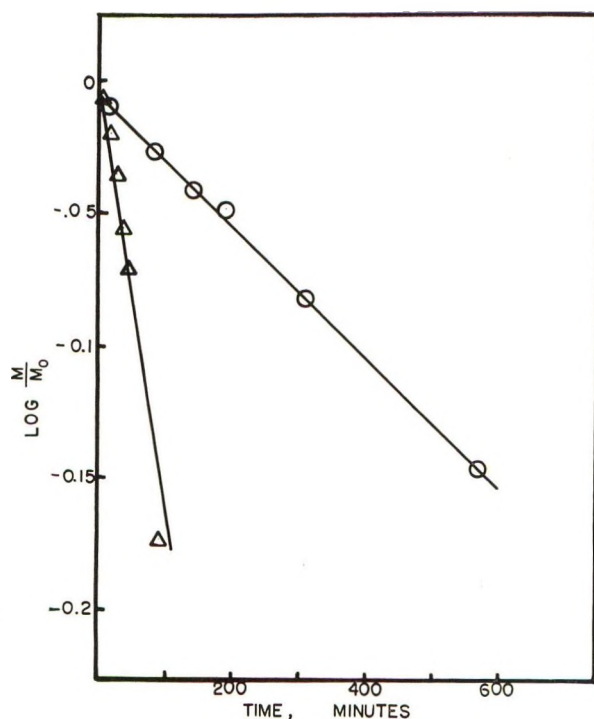
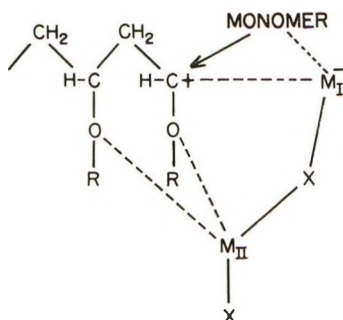


Fig. 5. Effect of length of *n*-alkyl group on rate of polymerization of vinyl alkyl ethers at 0.5°C. in *n*-heptane: (O) *n*-butyl; (Δ) ethyl. [Monomer] = 0.71 mole/l., [Cat.] =  $2.43 \times 10^{-5}$  mole/l.; AHS suspension No. 3.

insertion of the monomer between the heterogeneous anion and the growing polymer cation. Further steric control may be involved by coordination of the ether groups of the polymer with the catalyst centers (Fig. 7).

Furukawa<sup>24</sup> has proposed that such a complex catalyst should possess at least two coordination centers. If two adjacent ether groups near the chain end are linked to the second catalyst center, the isotactic polymer may be expected by the attack of the coordinating monomer, which adds to the chain end by entering from the opposite side of the polymer chain.



where  $M_{II}$   $M_{II}$  are metals and X is the ligand.

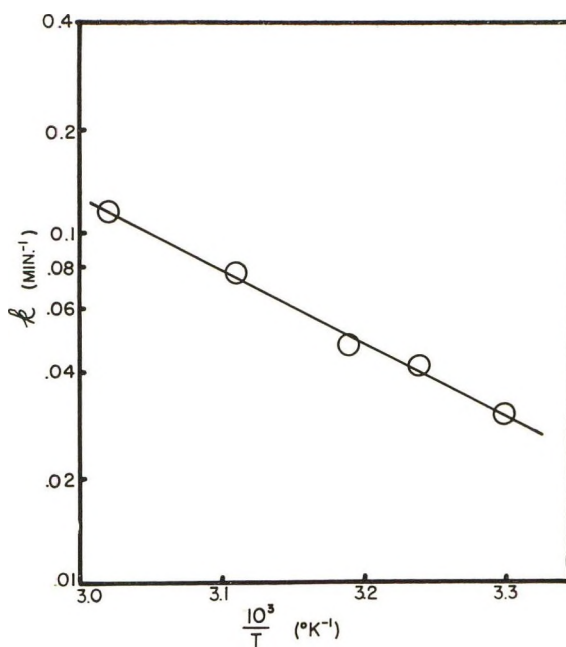


Fig. 6. Arrhenius plot for AHS-catalyzed polymerization of vinyl *n*-butyl ether in *n*-heptane. [Monomer] = 0.71 mole/l.; [Cat.] =  $2.43 \times 10^{-5}$  mole/l., AHS suspension No. 3.

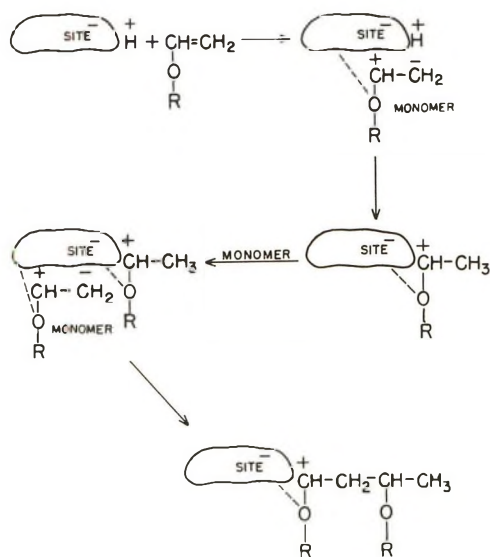


Figure 7.

### Copolymerization

We have copolymerized vinyl alkyl ethers with other suitable monomers using AHS catalyst. When vinyl *n*-butyl ether or vinyl ethyl ether was copolymerized with vinyl 2-chloroethyl ether, the copolymers could be vulcanized with ditertiary amines or polytertiary amines. The reactivity ratios of vinyl *n*-butyl ether and  $\beta$ -vinylloxyethyl methacrylate during

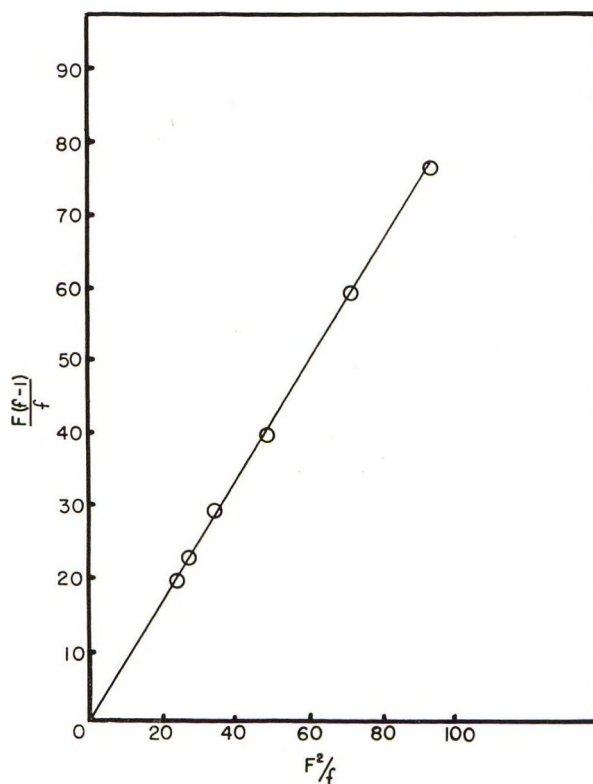


Fig. 8. Fineman-Ross plot for the copolymerization of vinyl *n*-butyl ether and  $\beta$ -vinylloxyethyl methacrylate with AHS catalyst at 26°C. in *n*-pentane.

copolymerization have been determined at 26°C. in the presence of AHS in pentane solvent. The copolymerizations were confined to the region of 1–5 mole-% VEM because we were primarily interested in synthesizing vulcanizable copolymers. Furthermore, a few copolymerizations using much higher mole per cent of VEM were quite sluggish. The reactivities of vinyl *n*-butyl ether ( $M_1$ ) and VEM ( $M_2$ ) were calculated by the method of Fineman and Ross.<sup>25</sup> The familiar copolymer equation

$$\frac{m_1}{m_2} = \frac{M_1}{M_2} \cdot \frac{M_1 r_1 + M_2}{M_2 r_2 + M_1} \quad (1)$$

can be rewritten as

$$\frac{F}{f} (f - 1) = \frac{r_1}{f} F^2 - r_2 \quad (2)$$

and

$$\frac{f - 1}{F} = r_1 - \frac{r_2 f}{F^2} \quad (3)$$

where  $f = m_1/m_2$  and  $F = M_1/M_2$ .  $M_1$  and  $M_2$  are the molar concentrations of the monomers in the monomer mixture,  $m_1$  and  $m_2$  are their molar concentrations in the copolymers, and  $r_1$  and  $r_2$  are their reactivity ratios according to the usual convention. The compositions of the monomer

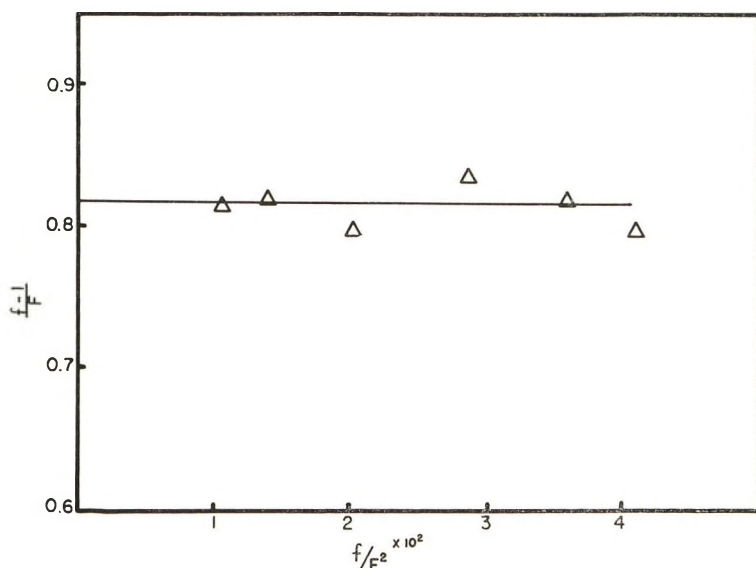


Fig. 9. Fineman-Ross plot for the copolymerization of vinyl *n*-butyl ether and  $\beta$ -vinylxyethyl methacrylate with AHS catalyst at 26°C. in *n*-pentane.

mixtures and their copolymers are shown in Table V. A plot of  $(F/f)(f - 1)$  against  $F^2/f$  [eq. (2)] gave the slope  $r_1$  and intercept  $-r_2$  as shown in Figure 8. From a linear least square fit of the data, values of  $r_1 = 0.816$  and  $r_2 = -0.16$  were obtained. Similarly a plot of  $(f - 1)/F$  against  $f/F^2$  [eq. (3)] gave from the intercept  $r_1 = 0.818$  and slope  $r_2 = 0.168$  as shown in Figure 9. The average values of  $r_1 = 0.817$  and  $r_2 = 0.004$  were thus obtained.

The copolymerization data were also treated according to the intersection method of Mayo and Lewis.<sup>26</sup> By substituting the values of  $M_1$ ,  $M_2$ ,  $m_1$ , and  $m_2$  in eq. (1) a simplified expression is obtained in which  $r_1$  and  $r_2$  are linearly related. From the enclosed circular area (Fig. 10), values of  $r_1 = 0.82$  and  $r_2 = 0.3$  were obtained.

TABLE V  
Copolymerization of Vinyl *n*-Butyl Ether ( $M_1$ ) with  $\beta$ -Vinylloxyethyl Methacrylate ( $M_2$ )  
(AHS Catalyst)<sup>a</sup>

Expt.	$M_2$	$m_2$	$f = m_1/m_2$	$F = M_1/M_2$
I	1.27	1.53	64.32	77.70
II	1.635	1.95	50.28	60.16
III	2.40	2.91	33.36	40.67
IV	3.20	3.67	26.25	30.25
V	4.02	4.65	20.50	23.88
VI	4.63	5.42	17.45	20.60

<sup>a</sup>  $M_1$  and  $M_2$  represent molar concentrations of vinyl *n*-butyl ether and  $\beta$ -vinylloxyethyl methacrylate in monomer mixtures and  $m_1$  and  $m_2$  are their molar concentrations in the copolymers.

The uncertainty in the value of  $r_2$  lies principally in the fact that the portion of the copolymer curve under investigation is extremely insensitive to the value of  $r_2$ . If copolymer composition data for higher mole per cent VEM were available, the value of  $r_2$  could be determined with greater

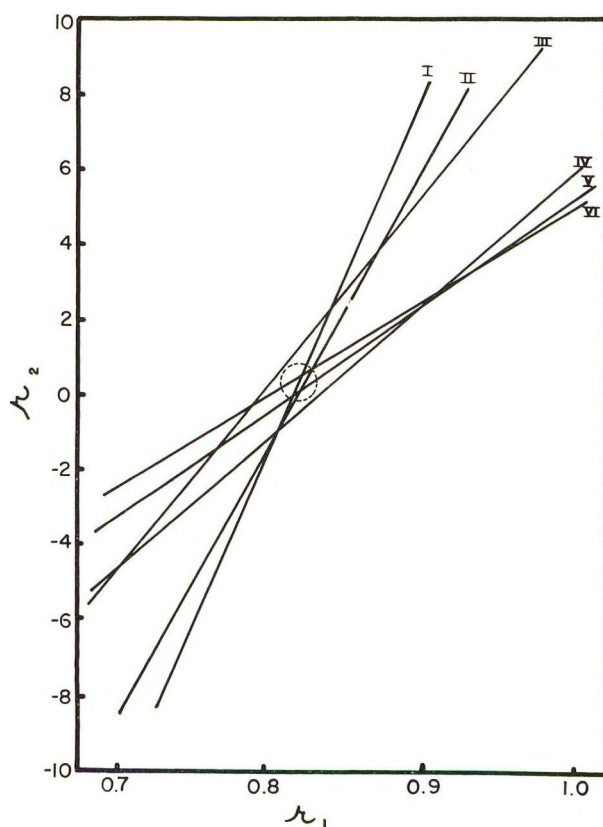


Fig. 10. Lewis-Mayo plot for the copolymerization of vinyl *n*-butyl ether with  $\beta$ -vinylloxyethyl methacrylate with AHS catalyst at 26°C. in *n*-pentane.

accuracy. As the concentration of VEM in the monomer mixture increases, the rate of polymerization slows down. This suggests a low value of  $r_2$ . Since AHS catalyst is insoluble in the polymerization medium, some steric considerations of the catalyst surface are presumably responsible for this extremely low value of  $r_2$ . The homopolymerization of VEM in pentane was extremely sluggish with AHS catalyst, ostensibly for the same steric factors. (The homopolymerization was quite rapid with soluble catalysts such as stannic chloride.)

The authors wish to express their thanks to the Goodyear Tire & Rubber Company and Dr. H. J. Osterhof for permission to publish this work, to Dr. K. W. Scott for helpful discussions, to Dr. E. P. Devlin for infrared analysis, and to Mr. D. J. Zimmerman for technical assistance.

### References

1. Schildknecht, C. E., S. T. Gross, H. R. Davidson, J. M. Lambert, and A. O. Zoss, *Ind. Eng. Chem.*, **40**, 2104 (1948).
2. Natta, G., P. Corradini, and I. W. Bassi, *Makromol. Chem.*, **18/19**, 455 (1956).
3. Lal, J., *J. Polymer Sci.*, **31**, 179 (1958).
4. Natta, G., G. Dall'Asta, G. Mazzanti, U. Giannini, and S. Cesca, *Angew. Chem.*, **71**, 205 (1959).
5. Vandenburg, E. J., R. F. Heck, and D. S. Breslow, *J. Polymer Sci.*, **41**, 519 (1959).
6. Roch, R. M., and J. Saunders, *J. Polymer Sci.*, **38**, 554 (1959).
7. Bogdanova, A. V., *Vysokomol. Soedin.*, **2**, 576 (1960).
8. Okamura, S., T. Higashimura, and I. Sakurada, *J. Polymer Sci.*, **39**, 507 (1959).
9. Mosley, S. A., U. S. Pat. 2,549,921 (April 24, 1951).
10. Herrle, K., H. Fikentscher, and H. P. Siebel, U. S. Pat. 2,825,719 (March 4, 1958).
11. Lal, J., U. S. Pat. 3,038,889 (June 12, 1962).
12. Lal, J., U. S. Pat. 2,984,656 (May 16, 1961); Brit. Pat. Specification 846,690 (August 31, 1960).
13. Lal, J., U. S. Pat. 3,062,789 (Nov. 6, 1962).
14. Okamura, S., T. Higashimura, and T. Watanabe, *Makromol. Chem.*, **50**, 137 (1961).
15. Chiang, R., U. S. Pat. 3,014,014 (Dec. 19, 1961).
16. Heck, R. F., U. S. Pat. 3,014,013 (Dec. 19, 1961).
17. Christman, D. L., and E. J. Vandenburg, U. S. Pat. 3,025,282 (March 13, 1962).
18. Heck, R. F., and E. J. Vandenburg, U. S. Pat. 3,025,283 (March 13, 1962).
19. Kray, R. J., *J. Polymer Sci.*, **44**, 264 (1960).
20. Watanabe, W. H., and L. E. Conlon, *J. Am. Chem. Soc.*, **79**, 2828 (1957).
21. Dall'Asta, G., and I. W. Bassi, *Chim. Ind. (Milan)*, **43**, 999 (1961).
22. Dall'Asta, G., and N. Odde, *Chim. Ind. (Milan)*, **42**, 1234 (1960).
23. Coombes, J. D., and D. D. Eley, *J. Chem. Soc.*, **1957**, 3700.
24. Furukawa, J., *Polymer*, **3**, 487 (1962).
25. Fineman, M., and S. D. Ross, *J. Polymer Sci.*, **5**, 259 (1950).
26. Mayo, F. R., and F. M. Lewis, *J. Am. Chem. Soc.*, **66**, 1594 (1944).

### Résumé

La polymérisation des éthers alcoyl-vinylés à température de chambre et au-dessus, pour fournir des polymères cristallisables, est d'un intérêt considérable tant au point de vue théorique que pratique. On étudie la polymérisation de ces monomères par des catalyseurs complexes d'acide sulfurique et de sulfate métallique à 0°C et au-dessus

produisant des polymères isotactiques de poids moléculaire élevé. On utilise comme catalyseur de l'hydrate d'hydrosulfate ferrique et de l'heptahydrate d'hexahydrosulfate d'aluminium (AHS). On trouve que la nature du solvant utilisé pendant la polymérisation avec ces catalyseurs hétérogènes est relativement importante au point de vue de la vitesse de polymérisation et de la stéréorégularité du polymère. Un éther vinylique ayant un groupement alcoylé linéaire polymérise considérablement plus vite qu'un monomère ayant un groupement alcoylé en ramification. Les valeurs des constantes de vitesse apparentes de premier ordre, pour la polymérisation par les catalyseurs AHS des éthers alcoylés vinyliques ayant des groupements *n*-alcoylés, présentent la séquence suivante: éthyle > *n*-butyle > *n*-hexyle = *n*-octyle. On trouve que dans le domaine de température de 30° à 58°C l'énergie d'activation globale pour la polymérisation des éthers vinyl-*n*-butylique dans l'heptane avec le catalyseur AHS est de 9.7 kcal./mole. L'éther *n*-butyl-vinylique est copolymérisé avec le méthacrylate de bêta-vinyloxyéthyle ( $M_2$ ) par le catalyseur AHS. On obtient les valeurs moyennes de  $r_1 = 0.82$  et  $r_2 = 0.004$ .

### Zusammenfassung

Die Polymerisation von Vinylalkyläthern bei Raumtemperatur oder darüber unter Bildung kristallisierbarer Polymerer ist von beträchtlichem theoretischen und praktischem Interesse. Es wurde die Polymerisation dieser Monomeren mit Metallsulfat-Schwefelsäure-Komplexen als Katalysatoren bei 0°C oder darüber unter Bildung hochmolekularer isotaktischer Polymerer untersucht. Als Katalysatoren wurden Eisen(III)-hydrosulfat-Hydrat und Aluminiumhexahydrosulfat-Heptahydrat (AHS) verwendet. Die Art des bei der Polymerisation mit diesen heterogenen Katalysatoren verwendeten Lösungsmittels ist sowohl für die Polymerisationsgeschwindigkeit als auch für die Stereoregularität des Polymeren von grosser Bedeutung. Vinyläther mit linearer Alkylgruppe polymerisieren bedeutend schneller als Monomere mit verzweigter Alkylgruppe. Die Werte der scheinbaren Geschwindigkeitskonstanten erster Ordnung für die AHS-katalysierte Polymerisation von Vinylalkyläthern mit *n*-Alkylgruppen nehmen in der Reihenfolge Äthyl > *n*-Butyl > *n*-Hexyl = *n*-octyl ab. Im Temperaturbereich von 30–58°C ist die Bruttoaktivierungsenergie der Polymerisation von Vinyl-*n*-butyläther in Heptan mit dem AHS-Katalysator 9,7 kcal./Mol. Vinyl-*n*-butyläther wurde unter Verwendung des AHS-Katalysators mit  $\beta$ -Vinyloxyäthylmethacrylat ( $M_2$ ) copolymerisiert. Es wurden mittlere Werte von  $r_1 = 0,82$  und  $r_2 = 0.004$  bestimmt.

Received March 8, 1963

Revised April 29, 1963

## Cyclopolymerization of $\alpha,\omega$ -Polymethylene Diisocyanates\*

YOSHIO IWAKURA, KEIKICHI UNO, and KIYOSHI ICHIKAWA,†  
*Department of Synthetic Chemistry, Faculty of Engineering,  
University of Tokyo, Bunkyo-ku, Tokyo, Japan*

### Synopsis

The study of polymerization of  $\alpha,\omega$ -polymethylene diisocyanates, tetramethylene, trimethylene, ethylene, and methylene diisocyanate, was carried out by the use of basic catalysts and polar solvents. Soluble polymers were obtained. Structures of the polymers were determined on the basis of solubility, infrared absorption, x-ray diffraction, and chemical reactions, especially aminolysis of the polymers. It was shown that these polymers contained heterocyclic recurring units (imidazolidone and imidazoline) in each polymer chain. Finally, a possible mechanism of this kind of cyclopolymerization is described.

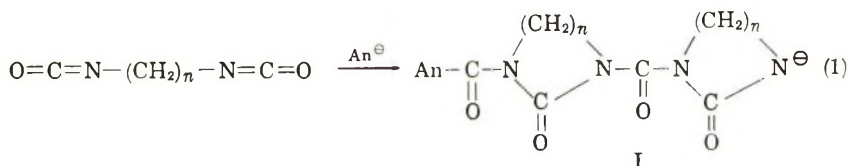
### INTRODUCTION

It has been generally accepted for many years that the organic isocyanates are converted to their dimers (1,3-disubstituted uretidinediones) and their trimers (1,3,5-trisubstituted isocyanurates) in the presence of various kinds of basic catalysts.<sup>1,2</sup> Recently, however, Shashoua<sup>3</sup> has shown that basic catalysts such as sodium cyanide in *N,N*-dimethylformamide are much effective for the polymerization of both aliphatic and aromatic isocyanates to yield linear high molecular weight polymers which should be structurally called "1-nylons." More recently, it has been reported by Natta<sup>4</sup> that crystalline polymers can be obtained by the polymerization of phenyl and *n*-butyl isocyanate in the presence of anionic catalysts such as lithium and sodium alkyls.

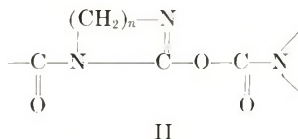
So, it was assumed that under some suitable conditions the anionic polymerization of  $\alpha,\omega$ -polymethylene diisocyanates might give linear polymers with cyclic recurring units in the main chain by an alternating intermolecular-intramolecular propagation mechanism, as shown in eq. (1), where  $An^{\ominus}$  is the initiating anion.

\* Presented, in part, at the 11th annual meeting of the Society of High Polymer Chemistry, Nagoya, Japan, May 27, 1962, and at the 12th annual meeting of the Society of High Polymer Chemistry, Tokyo, Japan, May 26, 1963.

† Present address: The Technical Research Laboratory, Asahi Chemical Industry Co., Ltd., Nakadai-cho, Itabashi-ku, Tokyo, Japan.



In our study the polymerizations of polymethylene diisocyanates ( $n = 1, 2, 3,^* 4$ ) were carried out, and, as results, linear soluble polymers containing cyclic recurring units in the main chain were obtained. The structures of the polymers obtained were determined. It was found that the polymers obtained had the recurring unit II in addition to those mentioned above.



The details and the mechanisms of the cyclopolymerization of polymethylene diisocyanates will be described below.

## RESULTS AND DISCUSSION

### Preparation of Polymers

Table I shows representative polymerization conditions and results for each of the polymers from  $\alpha,\omega$ -polymethylene diisocyanates ( $n = 1, 2, 3, 4$ ) used.

As a catalyst, sodium cyanide in a solution of *N,N*-dimethylformamide was used, because it has been found to be an effective initiator<sup>3</sup> for the homopolymerization of monoisocyanate. The others, pyridine, a useful catalyst<sup>1,2</sup> for the dimerization of isocyanates, and a trace of pyridine in epichlorohydrin, a more effective catalyst<sup>6</sup> for the trimerization, were also available only for the polymerization of ethylene diisocyanate ( $n = 2$ ), to yield a linear soluble polymer as shown in Table I. It is of interest that the  $\gamma$ -ray irradiation of ethylene diisocyanate gave a soluble polymer even in the solid state at  $-195^\circ\text{C}$ . and the structure of the polymer was the same as that of the polymer obtained from the catalytic polymerization in solvents. The radiation polymerization of isocyanates has not hitherto been reported in the literature.

Tetramethylene diisocyanate ( $n = 4$ ) gave only an insoluble gel-like polymer in the presence of a trace of pyridine in epichlorohydrin and on  $\gamma$ -ray irradiation at near room temperature. From the infrared spectrum of the gel-like polymer, it was found that this polymer had the same linkage as that of polyisocyanurate<sup>7</sup> and had no cyclic recurring unit in the polymer chain but unreacted isocyanate group in the side chain.

\* Miller and Black<sup>5</sup> also reported an example of cyclopolymerization of trimethylene diisocyanate.

Among the monomers used, methylene diisocyanate, the simplest member of  $\alpha,\omega$ -polymethylene diisocyanate, is essentially very unstable. It polymerized spontaneously during storage for a long period even in dry condition and violently on direct contact with *N,N*-dimethylformamide. The polymer thus formed was tough, transparent, and insoluble, and its real structure remained unknown. Toluene was accordingly used as a solvent in the polymerization of methylene diisocyanate, but the yield was poor. *N,N*-Dimethylformamide was mainly used for the other diisocyanates, and excellent yields were recorded. The rather low yield in the polymerization of methylene diisocyanate seemed due to the non-polarity of the solvent used. The polymerization of *n*-nonyl isocyanate was attempted in *N,N*-dimethylformamide and toluene under the same conditions. In the former solvent, *n*-nonyl 1-nylon having an intrinsic viscosity of 3.3 (in toluene at 30°C.) was obtained in quantitative yield, whereas in the latter solvent a polymer was obtained in only 4% yield and its intrinsic viscosity was 0.15.

### Some Properties of the Polymers

Table II lists some properties of the polymers prepared. All polymers obtained were in the form of white powders.

These polymers gave no apparent melting points, but began to decompose slowly at the temperatures shown in Table II. It was observed that polymers A, C, and D were more heat stable than polymer B. 1-Nylons have lower heat stabilities than the polymers obtained here.<sup>3</sup> It seems that the rather stable nature of these polymers is attributed to the cyclic structures in the polymer systems.

All polymers obtained were soluble in hot organic solvents as listed in Table II. In concentrated sulfuric acid at 30°C., it was observed that the intrinsic viscosities of the polymers were 0.07–0.08 for polymer D and 0.16 for polymer C at the time of the preparation of the solutions, but the viscosity of the former decreased to almost zero after four days, and that of the latter to 0.067 after eight days. This decrease in the viscosity shows degradation of the polymers in concentrated sulfuric acid.

### Structure of the Polymers

Infrared absorption data of the polymers and typical model compounds are shown in Figure 1 and Table III. Table IV summarizes the sources of the model compounds used, some of which are not hitherto reported in the literature. The compounds prepared were identified by their analytical data and infrared spectra.

All the polymers obtained in this work have essentially linear structures, for they are soluble in some organic solvents as mentioned above. The polymers gave no absorption bands characteristic of isocyanate group, except polymer A. The degree of cyclization of polymers B, C, and D appears to be nearly 100%, but not that of polymer A. Thus the recurring unit III

TABLE I  
Polymerization of  $\alpha,\omega$ -Polymethylene Diisocyanates

Sample No.	Catalyst	Solvent	Monomer concentration, moles/l.	Catalyst concentration $\times 10^{-2}$ g./100 ml.	Monomer, moles/mole catalyst	Temp., °C.		Yield, %	$[\eta]$ at 30°C., 100 ml./g.
						Initial	Max.		
Polymer A 1 <sup>a</sup>	NaCN	Toluene	0.660	1.25	259	23	23	92	
( <i>n</i> = 1) 2 <sup>a</sup>	NaCN	Toluene	0.410	1.5	133	-65	-64	53	
Polymer B 1 <sup>b</sup>	NaCN	DMF	0.178	1.5	58	-54	-46	80	0.08 <sup>c</sup>
( <i>n</i> = 2) 2 <sup>b</sup>	NaCN	DMF	0.178	1.5	58	-56	-49	85	
3 <sup>b</sup>	NaCN	DMF	0.268	1.5	88	-56	-46	63	
4 <sup>b</sup>	NaCN	DMF	0.134	0.75	88	-20	-10	80	
5 <sup>b</sup>	NaCN	DMF	0.268	1.5	88	23.5	35	53	
6 <sup>b</sup>	Pyridine	Epichlorohydrin	2.11	—	—	23.5	23.5	100	
7 <sup>b</sup>	Pyridine	Pyridine	0.536	—	—	23.5	—	80	
8 <sup>b</sup>	Pyridine	Pyridine	0.383	—	—	80	—	100	
9 <sup>b</sup>	$\gamma$ -ray <sup>d</sup>	—	Bulk	—	—	-195	—	6.7	

Polymer C 1 <sup>b</sup> ( <i>n</i> = 3)	NaCN	DMF	0.160	1.5	52	-56	-50	100	0.53 <sup>e</sup>
Polymer D 1 <sup>c</sup> ( <i>n</i> = 4)	NaCN	DMF	0.430	1.0	210	-56	-47	97	0.16 <sup>f</sup>
2 <sup>e</sup>	NaCN	DMF	0.430	0.5	420	-56	-50	80	0.07 <sup>f</sup>
3 <sup>e</sup>	NaCN	DMF	0.430	1.5	140	-50	-40	100	0.08 <sup>f</sup>
4 <sup>e</sup>	NaCN	DMF	0.215	1.5	70	-56	-52	100	
5 <sup>e</sup>	NaCN	DMF	0.430	1.5	140	-30	-27	100	
6 <sup>e</sup>	NaCN	DMF	0.110	0.75	70	-56	-53	53	
7 <sup>e</sup>	NaCN	DMF	0.110	1.5	35	-56	-53	100	
8 <sup>b</sup>	NaCN	DMF	0.110	1.5	35	-56	-53	100	
9 <sup>b</sup>	NaCN	DMF	0.110	1.5	35	-56	-53	100	

<sup>a</sup> Treated with benzene at the end of the reaction.<sup>b</sup> Treated with ether.<sup>c</sup> Measured in dimethylsulfoxide.<sup>d</sup> Solid monomer was irradiated with  $\gamma$ -rays from a Co<sup>60</sup> source ( $1.5 \times 10^5$  r/hr.) for 22.5 hr.<sup>e</sup> Measured in *m*-cresol.<sup>f</sup> Measured in concentrated sulfuric acid.<sup>g</sup> Treated with methanol.<sup>h</sup> Treated with di-*n*-butylamine.

TABLE II  
 Polymethylene Diisocyanate Polymers and Their Properties

	Decomposition temp., °C.	Soluble in
Polymer A ( $n = 1$ )	>350	Dimethyl sulfoxide, <i>N</i> -methylpyrrolidone (LiCl), H <sub>2</sub> SO <sub>4</sub>
Polymer B ( $n = 2$ )	270-280	Dimethylsulfoxide, H <sub>2</sub> SO <sub>4</sub>
Polymer C ( $n = 3$ )	>350	<i>m</i> -Cresol, H <sub>2</sub> SO <sub>4</sub>
Polymer D ( $n = 4$ )	>350	Ethylene carbonate, H <sub>2</sub> SO <sub>4</sub>

 TABLE III  
 Infrared Absorption of Polymers and Model Compounds<sup>a</sup>

Compound	Ring size	N=C=O band, cm. <sup>-1</sup>	C=O stretching (S), cm. <sup>-1</sup>		CH <sub>2</sub> rocking (m or w), cm. <sup>-1</sup>
			In ring	Between rings	
Polymer A	4	2280	Near 1720 (single broad band)		760
Polymer B	5		1773	1690	760
Polymer C	6		1720 (Shoulder)	1685	775
Polymer D	7		1716 (Shoulder)	1688	762
Imidazolidone-2	5		1660		767
<i>N</i> -Acetylimidazolidone-2 <sup>b</sup>	5		1751	1653	748
<i>N,N'</i> -Diacetylimidazolidone-2	5		1745	1690	750
<i>N</i> -Phenylcarbamoylimidazolidone-2	5		1727	1665	757 (746)
<i>N,N'</i> -Trimethyleneurea	6		1688 (1674)		783
<i>N,N'</i> -Diacetyltrimethyleneurea	6		1708 (Shoulder)	1692	753
<i>N,N'</i> -Tetramethyleneurea	7		1646		740
<i>N,N'</i> -Diacetyltetramethyleneurea	7		1726	1686	761
Tri- <i>n</i> -pentylisocyanurate	6		1692		
<i>n</i> -Pentyl-1-nylon	Linear			1693 <sup>c</sup>	

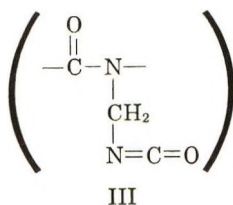
<sup>a</sup> Measurements were carried out in the solid state in Nujol mull.<sup>b</sup> Data of Hall and Zbinden.<sup>8</sup><sup>c</sup> In 1% benzene solution.

TABLE IV. Sources of Model Compounds

Compound	Preparation	Melting point, °C.	Formula	Analyses						Reference
				Calcd.			Found			
				C, %	H, %	N, %	C, %	H, %	N, %	
Imidazolidone-2		131	C <sub>3</sub> H <sub>4</sub> ON <sub>2</sub>	46.86	6.29	21.86	46.31	5.62	21.89	8, 9
N-Acetylimidazolidone-2	Imidazolidone-2, ketene (or acetylchloride)	183	C <sub>5</sub> H <sub>8</sub> O <sub>2</sub> N <sub>2</sub>							
N,N'-Diacetylimidazolidone-2	Imidazolidone-2, acetic anhydride	126	C <sub>7</sub> H <sub>10</sub> O <sub>4</sub> N <sub>2</sub>	49.41	5.92	16.46	49.16	6.30	16.08	10
N-Phenylcarbamoylimidazolidone-2	Imidazolidone-2, phenyl isocyanate	169	C <sub>10</sub> H <sub>11</sub> O <sub>2</sub> N <sub>3</sub>	58.53	5.40	20.48	58.40	5.49	20.52	
N,N'-Trimethyleneurea	Trimethylene diisocyanate, water	258	C <sub>4</sub> H <sub>8</sub> ON <sub>2</sub>							11
N,N'-Diacetyltrimethyleneurea	N,N'-Trimethyleneurea, acetic anhydride (or acetylchloride)	39	C <sub>8</sub> H <sub>12</sub> O <sub>4</sub> N <sub>2</sub>	52.16	6.57	15.21	52.49	6.60	15.08	
N,N'-Tetramethyleneurea	Tetramethylene diisocyanate, water	174	C <sub>3</sub> H <sub>10</sub> ON <sub>2</sub>							12
N,N'-Diacetyltetramethyleneurea	N,N'-Tetramethyleneurea, acetic anhydride	145	C <sub>9</sub> H <sub>16</sub> O <sub>4</sub> N <sub>2</sub>	54.53	7.11	14.13	54.70	6.85	13.96	
Tri-n-pentylisocyanurate <sup>b</sup>	n-Pentylisocyanate, sodium methylate	173 <sup>a</sup> 1 mm.	(C <sub>6</sub> H <sub>11</sub> ON) <sub>3</sub>	63.68	9.80	12.39			12.54	
n-Pentyl-1-nylon <sup>c</sup>	n-Pentylisocyanate, sodium cyanide	204	(C <sub>6</sub> H <sub>11</sub> ON) <sub>n</sub>	63.68	9.80	12.39	63.65	9.82	12.29	3

<sup>a</sup> Boiling point.

<sup>b</sup> The molecular weight by the cryoscopic method in nitrobenzene was found 351 (Calcd. for (C<sub>6</sub>H<sub>11</sub>ON)<sub>3</sub>, 339). A sample, showing the intrinsic viscosity 15.6 in toluene at 30°, was used.



is involved in the main chain of Polymer A.

The polymers gave two characteristic absorption bands at 1770–1710 and 1690  $\text{cm}^{-1}$ . Absorption data of model compounds in Table III show that  $\text{C}=\text{O}$  stretching bands of the cyclic ureas shift to a higher region on substitution of hydrogen atoms on nitrogen by acyl groups. The absorption band of the  $\text{C}=\text{O}$  linkage between rings in structure I would not be so much affected by the ring size and give nearly the same wave numbers as those of 1-nylons. From the facts mentioned above, the  $\text{C}=\text{O}$  stretching absorp-

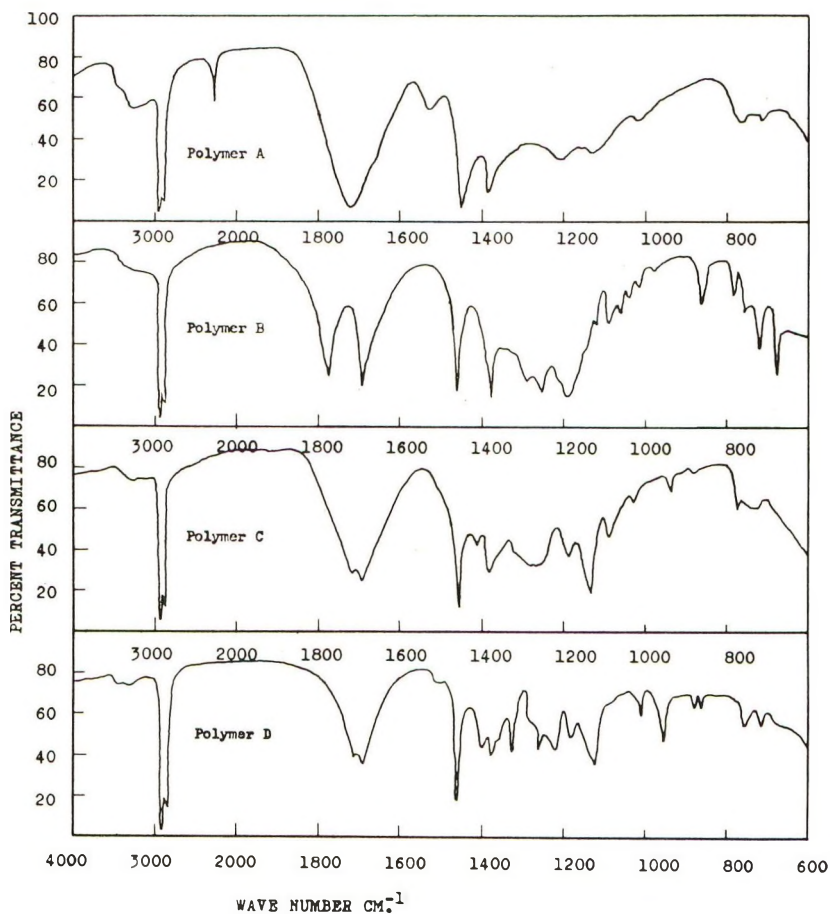


Fig. 1. Infrared spectra of the polymers.

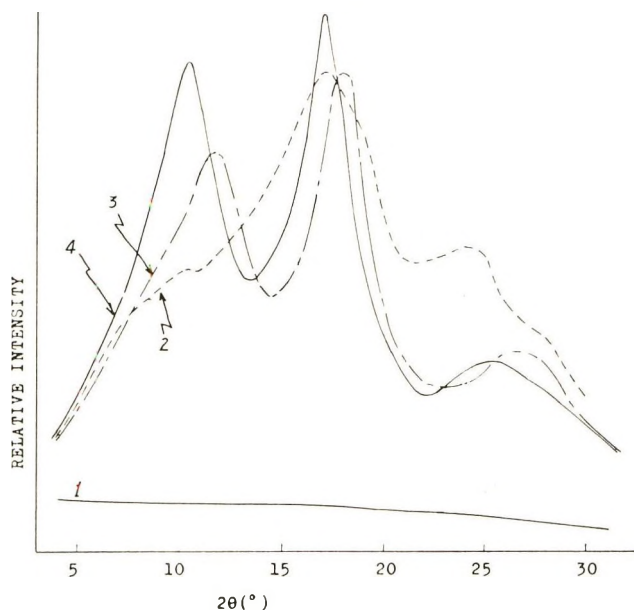
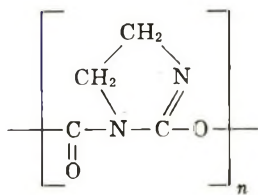


Fig. 2. X-ray diffraction curves of the polymers: (1) polymer A; (2) polymer B; (3) polymer C; (4) polymer D.

tion bands of polymers C and D may be assigned as follows: the bands in the higher region are those of the C=O in a ring structure and the bands in the lower region are those of C=O groups between rings. Polymer A gave an absorption band at  $2280\text{ cm.}^{-1}$  which was characteristic of the isocyanate group, and a single broad band in the C=O stretching region. Although two absorption bands were not recognized in that region in this case, it may be explained that those two bands overlap each other. So the polymer would have cyclic recurring units.

Polymer B gave two characteristic absorption bands at 1773 and  $1690\text{ cm.}^{-1}$ . It is shown in Table III that C=O absorption of imidazolidone at  $1660\text{ cm.}^{-1}$  shifts up to around  $1750\text{ cm.}^{-1}$  on acylation of the N-H group in cyclic urea. Then, the two absorption bands of polymer B might be assigned as follows: the band at higher wave number corresponds to C=O groups in a ring, and the other to C=O groups between rings.

In this polymerization, the formation of structure IV would be possible.



IV

The determination of the structure will be described later in this paper. In this case two absorption bands at  $1773$  and  $1690\text{ cm}^{-1}$  would correspond to the  $\text{C}=\text{O}$  and  $\text{C}=\text{N}$  stretching vibrations, respectively. The carbonyl group in structure IV is that of the urethane linkage which has the unsaturated substituents on nitrogen and oxygen atoms. The carbonyl absorption of urethanes may shift from the usual frequency region ( $1720\text{ cm}^{-1}$ ) to a higher one by such a substitution. The stretching absorption band of the  $\text{C}=\text{N}$  group usually appears at about  $1660\text{ cm}^{-1}$ , but in structure IV it should shift to a higher region by the same reason as the case of  $\text{C}=\text{O}$  stretching absorption. The assignment of these two bands in polymer B, therefore, is considered to be a reasonable one.

X-ray diffraction patterns are shown in Figure 2. This shows that polymers B, C, and D contain highly crystalline structure, and polymer A is amorphous. Presence of highly crystalline structure gives further evidence that these polymers appear essentially linear.

### Chemical Behavior of the Polymers

Aminolysis of the polymers was investigated with secondary di-*n*-butylamine. Consumption of di-*n*-butylamine was observed when the polymers were treated with excess amount of di-*n*-butylamine in *N,N*-dimethylformamide containing a catalytic amount of sodium cyanide. The amount

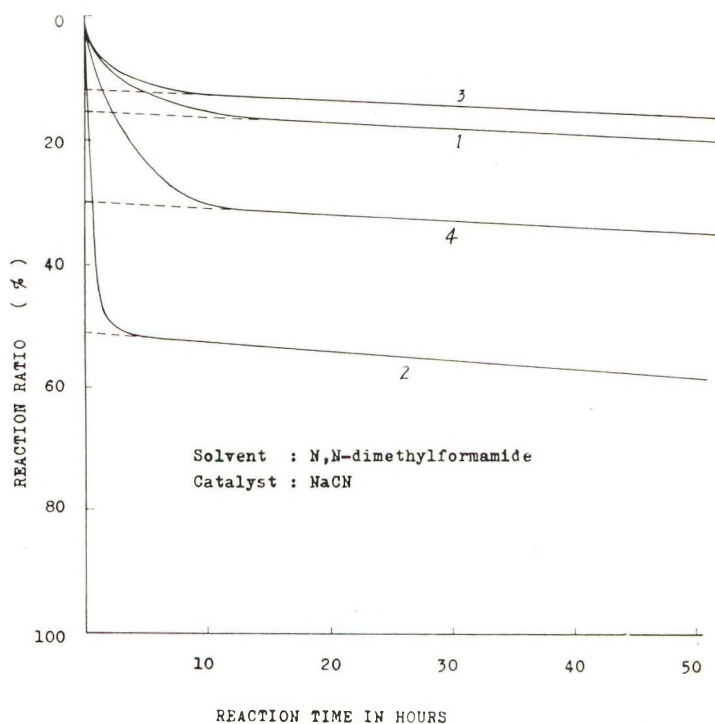


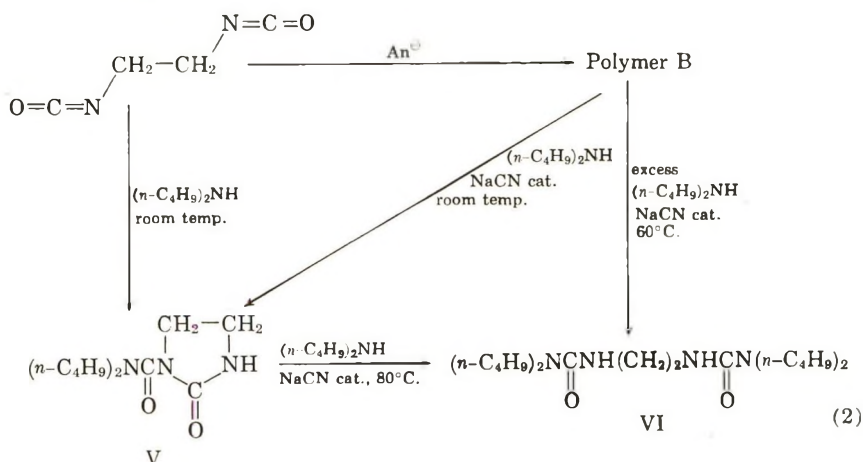
Fig. 3. Aminolysis reaction of the polymers: (1) polymer A; (2) polymer B; (3) polymer C; (4) polymer D.

of amine consumed was measured by titration with hydrochloric acid. Figure 3 shows the curves obtained on plotting the ratio of the reacted linkage in the polymers against the reaction time, it being assumed that the amine would react with equivalent moles of the linkage.

The aminolysis reactions of the polymers were carried out under the swollen states in *N,N*-dimethylformamide except polymer A, which was treated after drying. In the case of polymers A and B, the reaction mixtures became homogeneous after half reaction time had elapsed. From Figure 3 it is seen that two kinds of reactions are involved in aminolysis of the polymers: one is a relatively rapid reaction, and the other is a very slow one. In the latter, a linear relationship is observed between conversion and time. The intersections of the straight lines and vertical axis may give approximate amounts of linkages in the polymers which reacted with the amine. The results are summarized in Table V.

The aminolysis product of polymer A was viscous oil. The intrinsic viscosity of polymer C was reduced from 0.53 to 0.096 after the reaction. These results suggest that the aminolysis reaction occurs with scission of the main chain. In polymers A, C, and D, the aminolysis products gave the same infrared spectra as the parent polymers after sufficient reaction time; polymer B gave *N*-substituted imidazolidone. These facts indicate that the urea linkage is scarcely affected by the amine, and the rapid aminolysis reaction takes place at a linkage other than the urea.

Polymer B, unlike the others, reacted more easily with di-*n*-butylamine in *N,N*-dimethylformamide containing a catalytic amount of sodium cyanide to give 1-(*N,N*-di-*n*-butylcarbamoyl)-imidazolidone-2 (V) at room temperature and ethylenebis(*N,N,N',N'*-tetra-*n*-butyl)urea (VI) at 60°C. as shown in eq. (2).

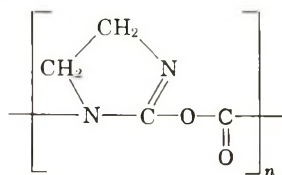


The aminolysis product of polymer B at room temperature is identified as V. Authentic compound V was prepared from ethylene diisocyanate and di-*n*-butylamine, according to the reaction<sup>9</sup> of ethylene diisocyanate

TABLE V  
 Aminolysis of Polymers with Di-*n*-butylamine

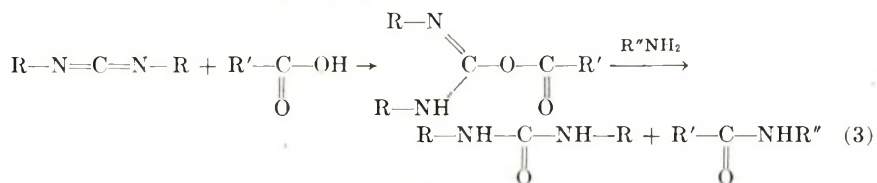
Polymer	Temp., °C.	Proportion of linkage reacted with the amine, %
Polymer A	30	17
Polymer B	23	52
Polymer C	30	12
Polymer D	30	30

and ammonia to yield *N*-carbamoyl imidazolidone-2. No further change was observed when V was treated with excess di-*n*-butylamine in the absence of catalyst, even at an elevated temperature. An apparent reaction, however, was observed on adding a trace of sodium cyanide at 80°C. The product obtained by this reaction is the same as that given in the aminolysis of polymer B at 60°C., and confirmed as VI. The titration result that 50% of the linkage reacted rapidly with the amine in polymer B, supports the formation of V. From these results, the structure of polymer B is considered to be VII:

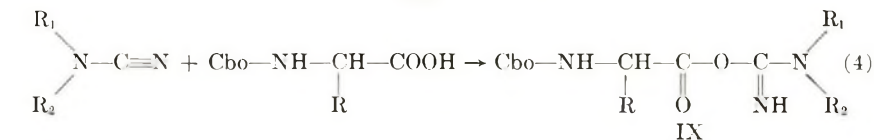


VII

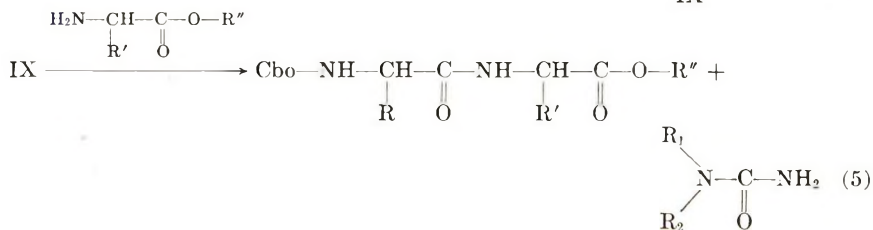
It has been reported that *N,N'*-disubstituted carbodiimides<sup>13</sup> and *N,N'*-dialkylcyanamides<sup>14</sup> react with carboxylic acids and amines to give amides and ureas as shown in eqs. (3)–(5).



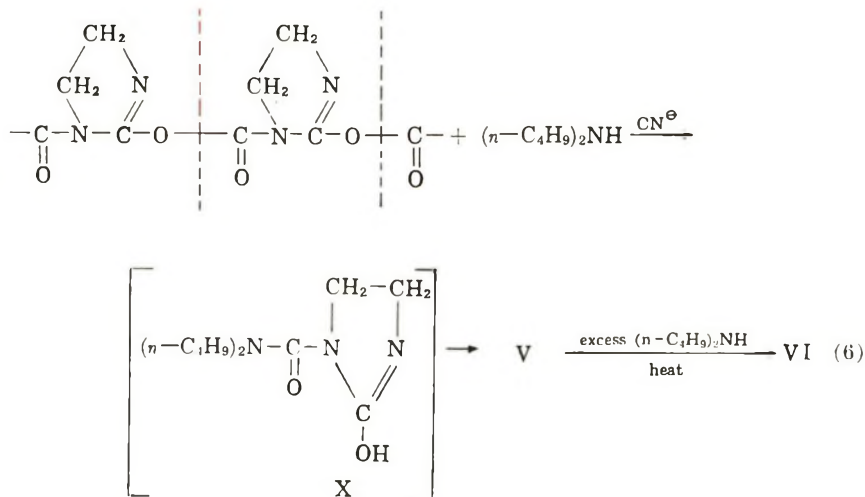
VIII



IX



The structures of intermediates VIII and IX are the same as that of VII. The large reactivity of these intermediates give additional evidence for structure VII. The aminolysis of polymer B can be described in the following eq. (6):



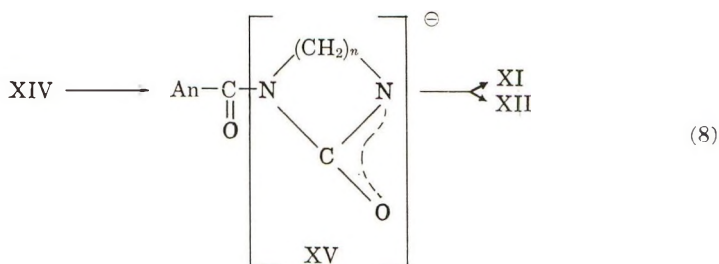
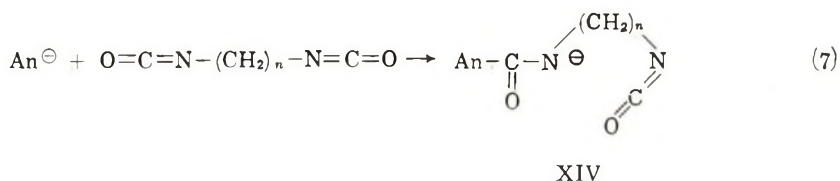
The cleavage of the single carbon-oxygen bond in the urethane linkage produces a pseudourea type intermediate (X) which rearranges into V, followed by the conversion into VI. The linkage in the other polymers A, C, and D which react rapidly with the amine would be the same as that of polymer B. Tentative average structures of the polymers are proposed in Table VI, mainly from the data of aminolysis.

TABLE VI  
Proposed Average Structures for the Polymers

	$  \left[ \begin{array}{c} \text{C}=\text{O} \\   \\ \text{N} \end{array} \begin{array}{c} \text{CH}_2 \\ \diagup \quad \diagdown \\ \text{CH}_2 \quad \text{N} \\ \diagdown \quad \diagup \\ \text{C}=\text{O} \end{array} \right]_x \left[ \begin{array}{c} \text{C}=\text{O} \\   \\ \text{N} \end{array} - \text{C} - \text{O} - \begin{array}{c} \text{CH}_2 \\ \diagup \quad \diagdown \\ \text{CH}_2 \quad \text{N} \\ \diagdown \quad \diagup \\ \text{C}=\text{O} \end{array} \right]_y \left[ \begin{array}{c} \text{N}=\text{C}=\text{O} \\   \\ \text{CH}_2 \\   \\ \text{C}=\text{O} \end{array} - \text{N} - \text{C} - \text{O} - \begin{array}{c} \text{CH}_2 \\ \diagup \quad \diagdown \\ \text{CH}_2 \quad \text{N} \\ \diagdown \quad \diagup \\ \text{C}=\text{O} \end{array} \right]_z  $		
	XI	XII	XIII
	$x, \%$	$y, \%$	$z, \%$
Polymer A	66		34
Polymer B	0	100	0
Polymer C	76	24	0
Polymer D	40	60	0

### Mechanism of the Polymerization

The mechanism of this cyclopolymerization would be considered as below. First, the initiation step proceeds by the attack of the catalyst anion against the carbon atom of the isocyanate group at one end of the diisocyanate to cause the opening of the carbon-nitrogen double bond, as shown in eq. (7). This initiation reaction is supported by the fact that the anionic polymerization of monoisocyanates gives 1-nylons.



Second, the intramolecular propagation may be the coordination of the nitrogen anion to the carbon atom of another isocyanate group in the same molecule with ring formation. In the cyclic intermediate XV the negative charge is delocalized over the nitrogen and the oxygen atom. The succeeding intermolecular propagation occurs by the additional opening of the carbon-nitrogen double bond of another diisocyanate molecule by the anion XV. When the nitrogen anion contributes more to the cyclic intermediate XV, structure XI will be formed predominantly, as seen in polymers C and D. When the oxygen anion contributes more, the formation of structure XII will result. Polymer B is supposed to be produced only through the opening of the carbon-oxygen double bond at the intramolecular propagation step.

### EXPERIMENTAL

All melting points and boiling points are uncorrected.

#### Synthesis of Monomers

The various  $\alpha,\omega$ -polymethylene diisocyanates used in this work were synthesized from the corresponding dicarboxylic dihydrazides and sodium nitrite through the Curtius rearrangement. The following method for the preparation of tetramethylene diisocyanate may be regarded as typical of

the reaction conditions used. All the monomers were freshly distilled just before any polymerization reaction.

**Tetramethylene Diisocyanate.** A 211-g. portion (1.21 mole) of adipoyl dihydrazide (m.p. 179°C.) was dissolved in 1.4 l. of aqueous hydrochloric acid containing 2.42 mole of the acid, and the solution was chilled to 0–5°C. with an ice-salt bath. To the cold solution, a solution of 173 g. (2.5 mole) of sodium nitrite in 200 ml. of water was added with good mechanical stirring at such a rate that the temperature did not rise above 8°C. Half-way along the operation 400 ml. of benzene was added. After the complete addition of the sodium nitrite solution, the benzene layer was separated and the aqueous layer was extracted twice with each 100 ml. of benzene. The extracts were collected and dried for 2 hr. over anhydrous calcium chloride. The benzene solution was heated slowly with good stirring, until no further nitrogen was evolved. The benzene was then removed under vacuum and the residue fractionated, yielding 86.8 g. of tetramethylene diisocyanate (51%), b.p. 112–113°C./19 mm., in a clear white liquid. The boiling points and the yields of other monomers were; trimethylene diisocyanate, 103°C./30 mm., 73%; ethylenediisocyanate, 81°C./20 mm., 74%; methylenediisocyanate, 39°C./17 mm., 27%. Methylene diisocyanate was prepared according to Roesh's method<sup>15</sup> and identified as a phenylurea derivative by its melting point (232°C.), infrared spectrum, and elementary analysis.

ANAL. Calcd. for  $C_{15}H_{16}O_2N_4$ : C, 63.36%; H, 5.67%; N, 19.71%. Found: C, 63.38%; H, 5.99%; N, 19.55%.

### Preparation of Catalysts

For the preparation of sodium cyanide solution, 30 ml. of *N,N*-dimethylformamide was distilled directly into a Schlenk tube in which 0.15 g. of sodium cyanide had been dried previously. This solution was stored under nitrogen. Pyridine used was dried over sodium hydroxide and then rectified, b.p. 115.5°C.

### Purification of Solvents

All of the solvents used in this work were dried and distilled before use. *N,N*-Dimethylformamide, commercially available, was first distilled with 10% volume of ethanol and then the middle fraction was stored over calcium hydride. Before the polymerization studies, the solvent was redistilled at 60°C./30 mm. and then used. Toluene was purified by rectification from phosphoric anhydride, b.p. 110°C. Epichlorohydrin was purified by fractionation. The fraction boiling at 116–117°C. was used for the polymerization studies.

### Polymer Preparation

Table I shows representative reaction conditions for each of the polymers prepared in this work. The following is a typical polymerization proce-

ture. A 200-ml., four-necked flask was equipped with a stirrer, Schlenk tube, and two side-arm adapters. One of these adapters had a calcium chloride tube and a dropping funnel containing the noted amount of the solvent, the other was fitted with a nitrogen inlet tube and a thermometer. The flask was then flamed out while being swept with nitrogen and dried by passing through the phosphoric anhydride tube. The monomer and the solvent were added, and the contents were cooled to the indicated temperature (Dry Ice-methanol bath for lower temperature). The initiator solution was added at once from the Schlenk tube with vigorous stirring. Usually the reaction proceeded exothermically, and the polymer precipitated at once. After stirring for 30 min., the reagent (Table I) was added. The polymer was filtered and washed with ether. The product obtained was dried at room temperature under vacuum.

### Characterization of Polymers

Viscosity measurements were carried out at 30°C. in an Ubbelohde-type viscometer, and the intrinsic viscosities were obtained. The infrared spectra were obtained in a double-beam Hitachi EPI-S2 infrared spectrophotometer on samples in Nujol mulls. The x-ray diffraction patterns were run on a Rigaku-Denki Geigerflex ( $\text{CuK}\alpha$ , Ni filter) for powdered samples of the polymers.

### Aminolysis of the Polymers

A mixture of about 2 g. of the polymer, 100 ml. of *N,N*-dimethylformamide, 3 ml. of the catalyst solution, and 10 ml. of di-*n*-butylamine was maintained at 30°C. (for polymers A, C, and D) or at 23°C. (for polymer B) in a well-controlled bath. The polymer sample was used in a swollen state (for polymers B, C, and D) or in a finely powdered state (for polymer A), since the reaction proceeded usually heterogeneously. Each 5 ml. of the reaction mixture, after dilution with 10 ml. of dioxane, was titrated at intervals with 0.25*N* hydrochloric acid, using bromophenol blue indicator. The ratio of the reaction was calculated from the titer. Results are shown in Table V and Figure 3.

**Aminolysis of Polymer B.** To a mixture of 4.056 g. of polymer B (corresponding to 0.0362 mole of ethylene diisocyanate unit), 150 ml. of *N,N*-dimethylformamide, and 4.5 ml. of the catalyst solution of sodium cyanide was added 4.68 g. of di-*n*-butylamine (0.0362 mole) and the mixture allowed to stand for two days. After the removal of the unreacted polymer by filtration, the filtrate was subjected to a distillation at 30–40°C. under reduced pressure, leaving a light yellow, viscous oil. The residual oil was treated with 50 ml. of ether to precipitate 1.6 g. of white solid (decomposition point, 155–190°C.) which was supposed to be an oligomer of low molecular weight. The ethereal filtrate was washed with water and dried over calcium chloride. The ether was evaporated off at room temperature, leaving 0.8 g. of a viscous oil which was identified

as 1-(*N,N*-di-*n*-butylcarbamoyl)-imidazolidone-2 (V) by comparing its infrared spectrum with that of an authentic sample. Principal bands observed were: 3340  $\text{cm}^{-1}$  (N-H stretching), 1727  $\text{cm}^{-1}$  (C=O in ring), 1666  $\text{cm}^{-1}$  (C=O between rings), 1530  $\text{cm}^{-1}$  (Amide II band), 751  $\text{cm}^{-1}$  ( $\text{CH}_2$  rocking in ring). Other peaks of remarkable strength were found at 1299  $\text{cm}^{-1}$ , 1255  $\text{cm}^{-1}$ , 1132  $\text{cm}^{-1}$ , 1098  $\text{cm}^{-1}$ , 1060  $\text{cm}^{-1}$ , some of which might be referred to C-N stretching vibration. The authentic sample was synthesized in an excellent yield, by the reaction of ethylene diisocyanate and di-*n*-butylamine in benzene.

ANAL. Calcd. for  $\text{C}_{12}\text{H}_{23}\text{O}_2\text{N}_3$ : C, 59.72%; H, 9.61%; N, 17.41%. Found: C, 59.38%; H, 9.51%; N, 16.54%.

Alternatively, a mixture of 4.0 g. of polymer B (corresponding to 0.036 mole of ethylene diisocyanate unit), 150 ml. of *N,N*-dimethylformamide, 4.5 ml. of catalyst solution of sodium cyanide, and 15 g. of di-*n*-butylamine (0.116 mole) was heated at 60°C. for 2 hr. The reaction medium became homogeneous immediately after the beginning of the reaction. On removal of volatile materials under reduced pressure, there remained oil which solidified on standing for a day. The residual product was recrystallized from *n*-hexane to give 2.8 g. of cottonlike needles, m.p. 102–103°C., which were identified as ethylenebis(*N,N,N',N'*-tetra-*n*-butyl)-urea (VI) by comparison of its melting point and infrared spectrum with those of an authentic sample. The infrared spectrum of this compound had representative bands at 3350  $\text{cm}^{-1}$  (N-H stretching), 1624  $\text{cm}^{-1}$  (C=O stretching), 1532  $\text{cm}^{-1}$  (Amide II band), and 1295  $\text{cm}^{-1}$  (Amide III band). The authentic sample was prepared from V and di-*n*-butylamine in *N,N*-dimethylformamide.

ANAL. Calcd. for  $\text{C}_{20}\text{H}_{42}\text{O}_2\text{N}_4$ : C, 64.82%; H, 11.42%; N, 15.12%. Found: C, 64.50%; H, 11.01%; N, 15.82%.

## References

1. Saunders, J. H., and R. J. Slocombe, *Chem. Revs.*, **43**, 203 (1948).
2. Arnold, R. G., J. A. Nelson, and J. J. Verbanc, *Chem. Revs.*, **57**, 47 (1957).
3. Shashoua, V. E., W. Sweeny, and R. F. Tietz, *J. Am. Chem. Soc.*, **82**, 866 (1960).
4. Natta, G., J. DiPietro, and M. Cambini, *Makromol. Chem.*, **56**, 200 (1962).
5. Miller, W. L., and W. B. Black, paper presented at the 142nd Meeting, American Chemical Society, Division of Polymer Chemistry, Atlantic City, N. J., September 1962.
6. Jones, J. I., and N. G. Savill, *J. Chem. Soc.*, **1957**, 4392.
7. Tsuzuki, R., K. Ichikawa, and M. Kase, *J. Org. Chem.*, **25**, 1009 (1960).
8. Hall, H. K., Jr., and R. Zbinden, *J. Am. Chem. Soc.*, **80**, 6428 (1958).
9. Naegeli, C., and P. Lendorff, *Helv. Chim. Acta*, **15**, 49 (1932).
10. Kirkwood, M. W., and G. F. Wright, *J. Am. Chem. Soc.*, **76**, 1836 (1954).
11. Iwakura, Y., *Kobunshi Kagaku*, **4**, 94 (1947).
12. Iwakura, Y., K. Uno, and K. Hamatani, *Nippon Kagaku Zasshi*, **78**, 1416 (1957).
13. Khorana, H. G., *Chem. Revs.*, **53**, 145 (1953).
14. Losse, G., and H. Weddige, *Ann.*, **636**, 144 (1960).
15. Roesh, R., and M. H. Gold, *J. Am. Chem. Soc.*, **73**, 2959 (1951).

### Résumé

Nous avons étudié la polymérisation des  $\alpha,\omega$ -diisocyanates polyméthyléniques, tétraméthylène-, triméthylène-, éthylène-, et méthylène-diisocyanate, en utilisant des catalyseurs basique et des solvants polaires. Les polymères obtenus étaient solubles dans les solvants organiques. On admet que les polymères sont constitués d'unités périodiques cycliques (imidazolidone ou imidazoline). Les structures des polymères sont montrés sur la base des solubilités, des spectres des infra-rouges, des diffractions des rayons-X, et de leur réactions chimiques. Enfin, on propose un mécanisme de la polymérisation cyclique des  $\alpha,\omega$ -diisocyanates polyméthyléniques.

### Zusammenfassung

Aus  $\alpha,\omega$ -Polymethylen-diisocyanaten (Tetramethylen-, Trimethylen-, Äthylen-, und Methylen-diisocyanat) wurden mit basischen Katalysatoren in polaren Lösungsmitteln lösliche Polymere hergestellt. Diese Polymeren enthielten in der Polymerkette heterocyclische (Imidazolin- und Imidazolidon-) Ringe. Die Struktur der Polymeren auf Grund von Löslichkeit, Infrarotabsorption, Röntgenbeugung und Aminolysereaktion wurde bestimmt. Ein für diese Art von Cyclopolymerisation möglicher Mechanismus wird angegeben.

Received June 17, 1963

Revised September 26, 1963

## Study of Epoxy Compounds. Part VI. Curing Reactions of Epoxy Resin and Acid Anhydride with Amine, Acid, Alcohol, and Phenol as Catalysts

YOSHIO TANAKA and HIROSHI KAKIUCHI, *Department of Applied Chemistry, Yokohama National University, Yokohama, Japan*

### Synopsis

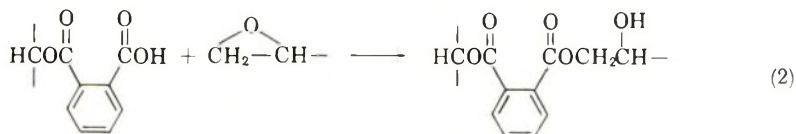
The curing reaction of an epoxy resin and acid anhydride with an amine and/or acid, alcohol, and phenol was studied kinetically by using commercial epoxy resins and acid anhydrides. No etherification reaction occurred at 70–140°C., even in the case of epoxide/acid anhydride/HA (acid, alcohol, or phenol) and of epoxide/acid anhydride tertiary amine/HA, and the initial reaction rate was proportional to the concentrations of epoxide, acid anhydride, and catalysts such as tertiary amine, acid, alcohol, and phenol. The apparent activation energy of the reaction system of Epikote 828/methylbicyclo(2,2,1)heptene-2,3-dicarboxylic anhydride/triethanol amine/HA was obtained as about 14.7 kcal./mole, and the low frequency factors and large negative entropies of activation for the reaction might confirm that the curing reaction of epoxy resins and anhydrides belongs to the type of nucleophilic bimolecular displacement reaction. The effects of the substituents, R, of acid, alcohol, and phenol as cocatalyst on the curing reaction of epoxy resin/acid anhydride/tertiary amine/HA were studied. The reaction constants,  $\rho$ , obtained positively for HA's, indicate that electron-withdrawing substituents of HA increase the rate of curing reaction of system of epoxide/acid anhydride/amine/HA. Differences in the catalytic and cocatalytic effects among benzoic acid, benzyl alcohol, and phenol in these reaction systems might be considered to depend on the donating power of hydrogen bond which is the important role rather than a general electrostatic interaction effect as solvent effects in nucleophilic substitution reactions. These results supported the proposed mechanisms reasonably.

### INTRODUCTION

The mechanism of the curing reaction of epoxide and acid anhydride has been somewhat obscure, but Fisch and Hofmann<sup>1,2</sup> have recently proposed a sequence of reactions which accounts for most of the observed facts. They studied carefully the uncatalyzed reaction and assumed that the primary step in the curing is reaction between anhydride and the secondary hydroxyl groups of the resin to produce monoester:



Next, the newly formed carboxyl group reacts with the epoxide group of another molecule to give a diester and a new secondary hydroxyl group which may itself react with the anhydride:



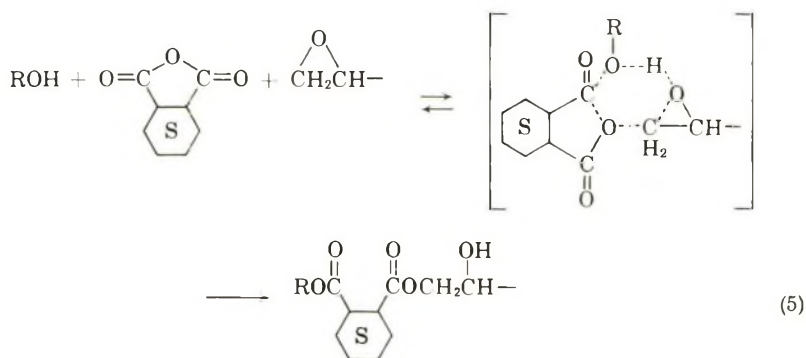
These reactions were confirmed by the evidence that the amounts of mono- and diester produced are stoichiometrically equivalent to the amount of anhydride which disappears, and that the initial rate of production of mono-ester parallels the rate of consumption of anhydride and is much faster than the rate of formation of diester. Analytical studies of the curing process gave the unexplained fact that in every case the epoxy groups decreased significantly faster than the diester groups increased, while, according to eq. (2), these two quantities should be equivalent. They suggested that etherification takes place between the epoxy and the hydroxyl groups under the catalytic influence of anhydride or carboxyl groups.



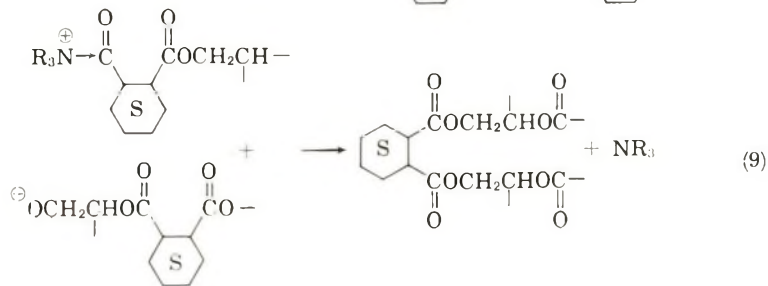
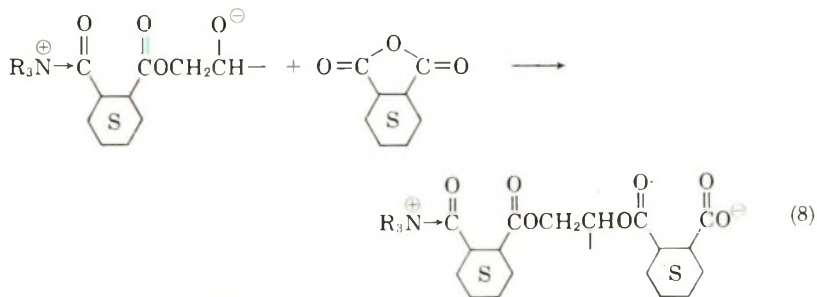
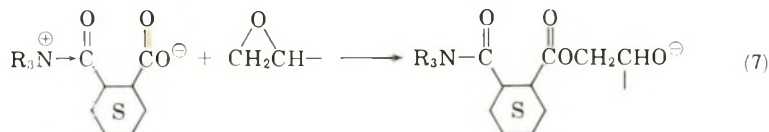
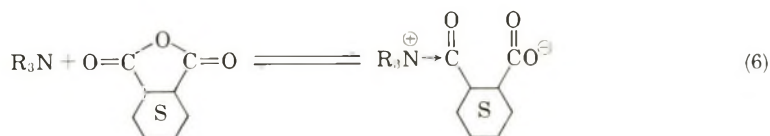
The acceleration of the curing rate of an epoxy resin (Epon-834)/phthalic anhydride system by addition of benzoic, succinic, and tricarballic acids was studied by Dearborn, Fuoss, and White,<sup>3</sup> who showed that carboxylic acids react directly with epoxide groups to produce secondary hydroxyl groups which in turn react with phthalic anhydride, regenerating carboxylic acid.



In a previous paper,<sup>4</sup> it was shown that no etherification occurs, at least up to the gelation time, from the unexpected evidence that there was no significant difference in consumption of epoxide and anhydride. The difference in gelation time between the systems of Epikote-828/hexahydrophthalic anhydride (HHPA)/amine and Epikote-1001/HHPA/amine might be due to the catalytic effect of hydroxyl groups of resin. The accelerating effect of a mixed catalyst of an amine and an alcohol appeared to be the sum of the effects of the amine and of the alcohol or hydroxyl group from the result that the relations of the initial concentration of the amine and the alcohol to the gelation time of these reaction systems run parallel to each other. The catalytic effect of the hydroxyl group was suggested as follows:



The evidence presented for the reactions of eq. (5) i.e., that this is a third-order reaction, that is, the reaction is first order with respect to epoxide, anhydride, and hydroxyl, and the  $\rho_P$  value for alcohols in the curing reaction was obtained positively, which indicates the electron-withdrawing substituents of alcohols increase the rate of the curing reaction. In this paper, the kinetic studies of these systems were carefully made. The catalytic



effect of the compounds having active hydrogen, including alcohol, on the curing reaction was quantitatively studied, and a new modified mechanism was proposed.

It has been shown that bases, such as tertiary amines, improve both the rate and course of the reaction between epoxides and anhydrides.<sup>3,5</sup> Recently Fischer<sup>6</sup> proposed the mechanisms shown in eqs. (6)–(9). These were confirmed by the result that, within certain limits, the reaction was zero order, i.e., independent of the concentrations of epoxide and anhydride, and proportional to the concentration of the catalyst.

In a preceding paper,<sup>4</sup> we studied kinetically the curing reaction of epoxy resin and acid anhydride, and proposed that the reaction of eq. (7) might be the rate-determining step in the curing reaction. This result is in general agreement with the observation that the reaction was third order, that is, first order with respect to epoxide, anhydride, and amine, respectively, and that the polar reaction constant,  $\rho_P$  for amines in the curing reaction was obtained negatively, which indicates that electron-repelling substituents of the amine,  $\text{NR}_3$ , increase the curing rate.

This paper deals with the kinetic studies of the curing reaction of epoxy resin and acid anhydride, and the catalytic and cocatalytic effects on the curing reaction of tertiary amines and other compounds having active hydrogen such as acid, alcohol, and phenol.

## EXPERIMENTAL

### Reagents

The epoxy resins were Shell Chemical Company Epikote 828 (E-828) and Epikote 1001 (E-1001); acid anhydrides were Allied Chemical and Dye Corporation hexahydrophthalic anhydride (HHPA) and methylbicyclo-[2,2,1]heptene-2,3-dicarboxylic anhydride (MNA) isomers. Some physical and chemical properties of MNA are shown in Table I; those of the other reagents were described in a previous paper.<sup>4</sup>

TABLE I  
Properties of MNA

$n_D^{25}$ (obsd.)	$d_4^{25}$		$\eta_{25}$ , cpoise		Acidity $\times 10^{-3}$ , equiv./g.	
	Obsd.	Lit.	Obsd.	Lit.	Obsd.	Calcd.
1.5041	1.227	1.2358 <sup>a</sup>	152	140 <sup>a</sup>	5.46	5.62

<sup>a</sup> Manufacturer's data.<sup>7</sup>

The reagents used as catalysts were all reagent grade and used after distillation or recrystallization.

### Procedure

The polymerization and analytical procedures have been adequately described previously.<sup>4</sup> The ratio of epoxy resin to acid anhydride and/or catalyst concentrations is the molar ratio in all cases given below.

The extent of reaction  $P$  is defined as:

$$P = (C_i - C_t)/C_i = 1 - C_t/C_i \quad (10)$$

where  $C_t$  and  $C_i$  are the concentrations of reagents in the reaction system at the time of measurement and initially respectively. The rate equation of the second-order reaction is obtained as:

$$P/(1 - P) = K_2 C_i t = K_2' t \quad (11)$$

where

$$K_2 C_i = K_2'$$

when the initial concentration of epoxide,  $C_i$ , is the same as that of acid anhydride.

## RESULTS

### Reaction Order

In the reactions of E-828 and HHPA or MNA with acid, alcohol, or phenol and with or without amine as catalysts, there were almost no differences in decreases of the concentration between epoxide and HHPA or MNA, as shown in Figures 1-3. When  $P/(1 - P)$  is plotted against the

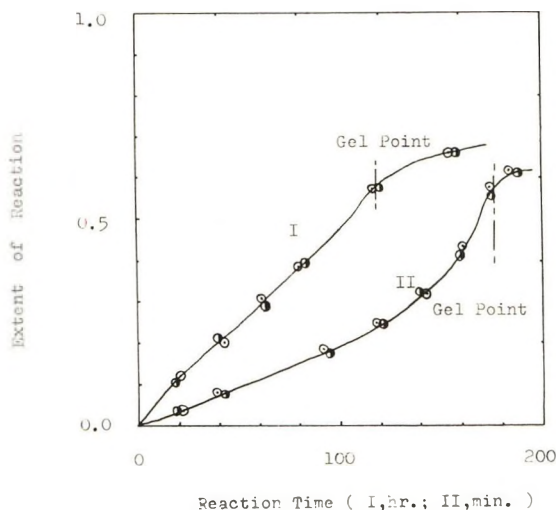


Fig. 1. Reaction of epoxy resin/acid anhydride/acid with or without amine at 100°C.; (○) epoxide; (●) MNA; (I) E-828/MNA/benzoic acid (0.2:0.2:0.02); (II) E-828/MNA/benzoic acid/triethanolamine (0.2:0.2:0.02:0.0034).

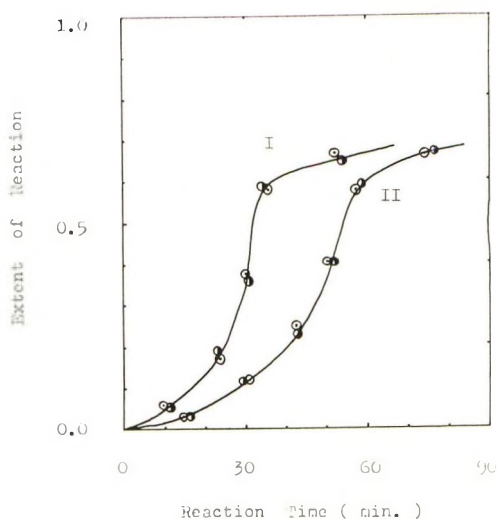


Fig. 2. Reaction of E-828/HHPA/methyl alcohol/triethanolamine (1:1:0.01) at 90°C.: (○) epoxide; (●) HHPA; (I)  $6.98 \times 10^{-5}$  mole/g.; (II)  $3.49 \times 10^{-5}$  mole/g.

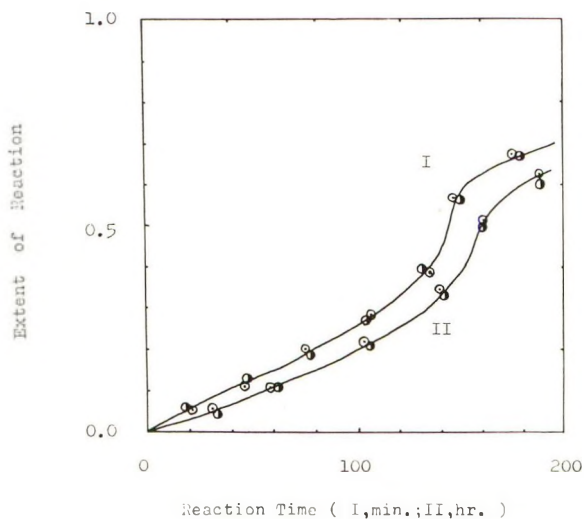


Fig. 3. Reaction of epoxy resin/acid anhydride/phenol (0.2:0.2:0.02) with or without amine (0.0034) at 100°C.: (○) epoxide; (●) acid anhydride; (I) E-828/MNA/phenol/triethanolamine; (II) E-828/MNA/phenol.

reaction time, the slope of the best line drawn through the points is  $K_2$ , the second order reaction rate coefficient. Figures 4-6 show the data of typical experiments to determine the reaction order. The curing reaction was second order with respect to the concentrations of epoxide and anhydride, as shown by eq. (11), that is, first order with respect to each reagent in these systems at the temperatures given, since the decrease of

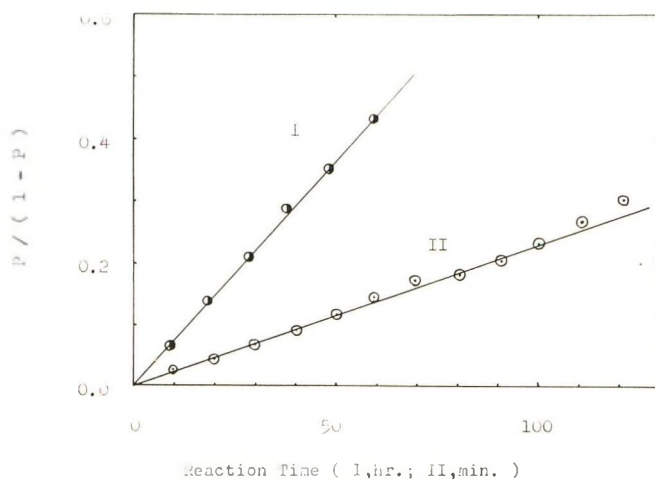


Fig. 4. Reaction of epoxy resin/acid anhydride/acid with or without amine at 100°C.: (I) E-828/MNA/benzoic acid; (II) E-828/MNA/benzoic acid/triethanolamine.

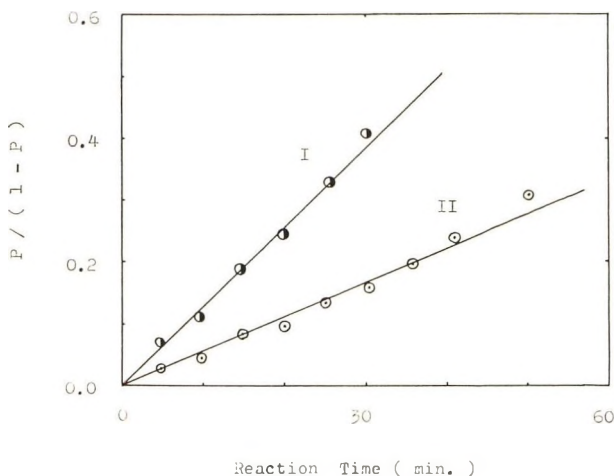


Fig. 5. Reaction of E-828/HHPA/methyl alcohol/triethanolamine at 90°C.; (I)  $6.98 \times 10^{-5}$  mole/g. of amine; (II)  $3.49 \times 10^{-5}$  mole/g. of amine.

epoxide was stoichiometrically equivalent to the amount of anhydride which disappeared. The rate equation of this curing reaction, therefore, is obtained as follows:

$$\begin{aligned} -d [\text{epoxide}]/dt &= -d [\text{acid anhydride}]/dt \\ &= K_A [\text{epoxide}][\text{acid anhydride}] \end{aligned} \quad (12)$$

where  $K_A$  is the observed second-order rate coefficient containing the concentration of the catalysts, and shown as  $K_A = K [\text{amine}]$ , in the system epoxide/anhydride/amine and  $K_A = K[\text{HA}]$ , in the system epoxide/

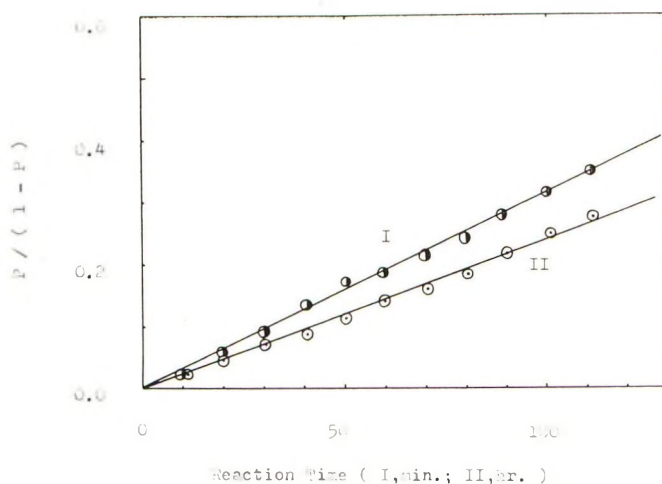


Fig. 6. Reaction of epoxy resin/acid anhydride/phenol with or without amine at 100°C.: (I) E-828/MNA/phenol/triethanolamine; (II) E-828/MNA/phenol.

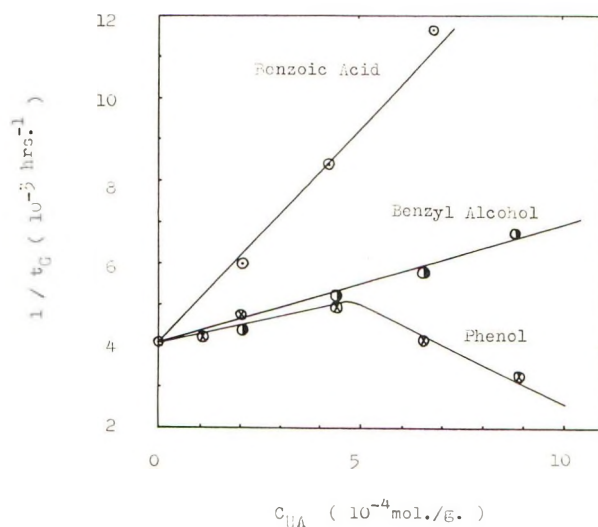


Fig. 7. Effect of concentration of HA (acid, alcohol, or phenol) on gel time  $t_g$  of the reaction system E-828/MNA (0.2:0.2) at 100°C.

anhydride/HA, HA being acid, alcohol, or phenol, and  $K_A = K[\text{amine}]/[\text{HA}]$ , in the system epoxide/anhydride/amine/HA.

### Effect of Acid

As shown in Figures 7 and 8, benzoic acid played an effective role as catalyst and as cocatalyst on the curing reaction of the systems E-828/

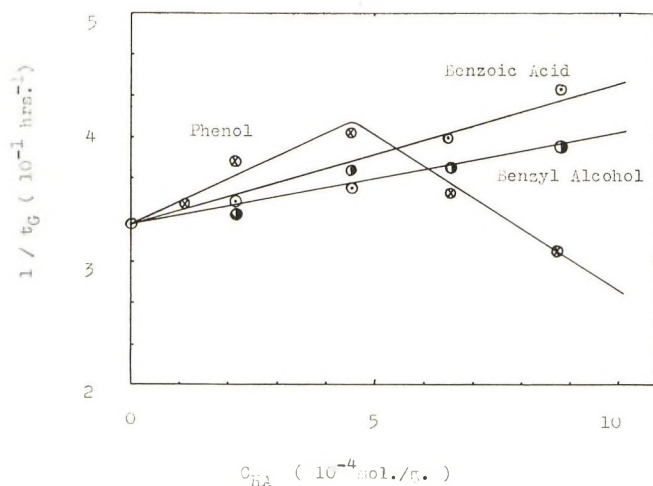


Fig. 8. Cocatalytic effect of HA (acid, alcohol, or phenol) on gel time  $t_G$  of the reaction systems E-828/MNA/triethanolamine (0.2:0.2:0.0034) at 100°C.

MNA and E-828/MNA/triethanolamine at 100°C., respectively, and there was a relationship, as shown by eq. 13, between the initial concentration of acid,  $C_{HA}$ , and gelation time,  $t_G$ , of the reaction system.

$$C_{HA} t_G = K \quad (13)$$

where  $K$  is a constant. These may support the definition of  $K_A$  in eq. (12). A plot of the logarithm of the gelation times against Hammett's sigma constants shows the usual linear relationship as shown in Figure 9 in which the cocatalytic effect of some acids on the curing reaction of the system E-828/MNA/triethanolamine (0.2:0.2:0.0034) at 100°C. is given.

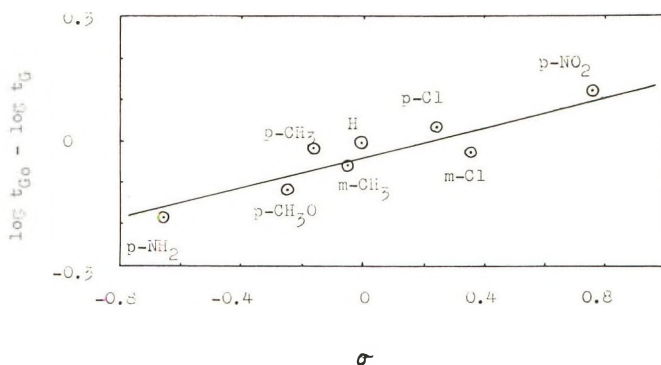


Fig. 9. Plot of  $(\log t_{G0} - \log t_G)$  vs.  $\sigma$  for the reaction of E-828/MNA/triethanolamine with various acids as cocatalysts. Parent acid,  $\text{RC}_6\text{H}_4\text{COOH}$ , is benzoic acid;  $\rho = +0.18$ .

### Effect of Alcohol

We discussed previously<sup>4</sup> the cocatalytic effect of alcohol on the curing reaction of E-828/HHPA/triethanolamine. If different values of the reciprocal,  $1/t_G$ , of the gelation time are plotted against the concentration of the alcohol, a set of linear plots is obtained (Figs. 7 and 8). These show the catalytic and cocatalytic effects of alcohol on the curing reactions of E-828/MNA and E-828/MNA/triethanolamine (0.2:0.2:0.0034) at 100°C., and indicate that the same relation as acid is obtained as shown by eq. (13). The cocatalytic effects of some alcohols are shown graphically in Figure 10.

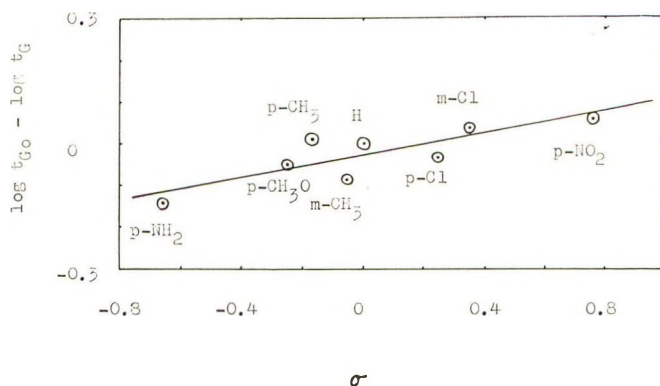


Fig. 10. Plot of  $(\log t_{G0} - \log t_G)$  vs.  $\sigma$  for the reaction of E-828/MNA/triethanolamine with various alcohols as cocatalysts. Parent alcohol,  $\text{RC}_6\text{H}_4\text{CH}_2\text{OH}$ , is benzyl alcohol;  $\rho = +0.13$ .

### Effect of Phenol

The catalytic and cocatalytic effects of phenol on the curing reactions of the systems E-828/MNA (0.2:0.2) and E-828/MNA/triethanolamine

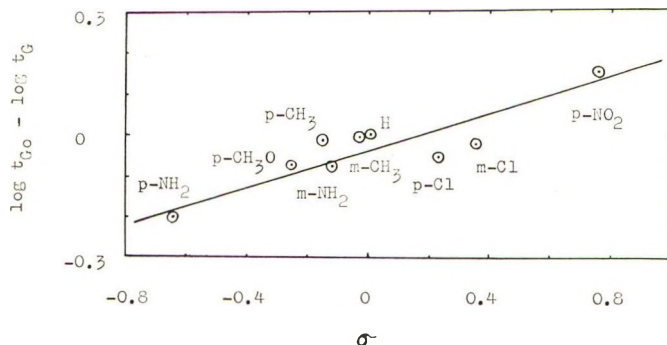


Fig. 11. Plot of  $(\log t_{G0} - \log t_G)$  vs.  $\sigma$  for the reaction of E-828/MNA/triethanolamine with various phenols as cocatalysts. Parent phenol,  $\text{RC}_6\text{H}_4\text{OH}$ , is phenol,  $\rho = +0.22$ .

(0.2:0.2:0.0034) at 100°C. are shown in Figures 7 and 8, which indicate that between the initial concentration of phenol,  $C_{HA}$ , and the gelation time,  $t_G$ , the relation of eq. (13) is obtained. ( $\log t_{G0}/t_G$ ) is plotted against Hammett's sigma constants for the curing reaction of the system E-828/MNA/triethanolamine (0.2:0.2:0.0034) at 100°C. The best straight line has been found in Figure 11, which shows the cocatalytic effects of some phenols on the reaction.

### Effect of Amine

The catalytic effect of amine is shown by the difference in  $t_G$  of the systems E-828/MNA/HA and E-828/MNA/HA/triethanolamine as given in Figures 7, 8, and 12; the latter shows the catalytic effects of triethanolamine on the curing reaction of E-828/HHPA and E-828/HHPA/methanol at 100°C. There was a relation, as shown by eq. (13), between the initial concentration of amine,  $C_A$ , and the gelation time,  $t_G$ , of the reaction systems, and this may support the definition of  $K_A$  in eq. (12).

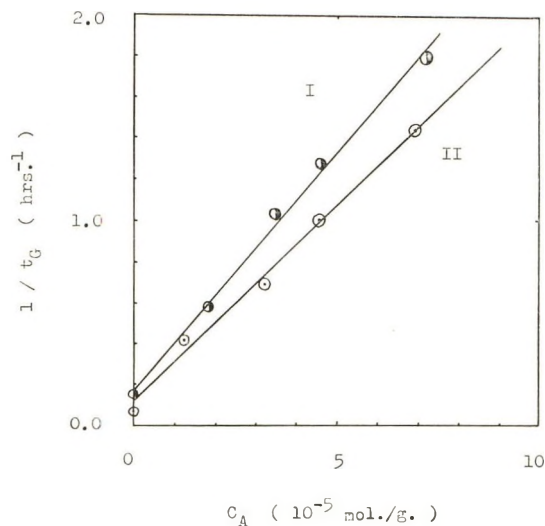


Fig. 12. Catalytic effect of triethanolamine on gel time  $t_G$  of the reaction systems (I) E-828/NHPA/ $\text{CH}_3\text{OH}$  at 100°C.; (II) E-828/HHPA at 100°C.

### Effect of Temperature

The temperature dependences of  $t_G$  in the reaction systems of E-828/MNA/HA/triethanolamine are shown in Figure 13, from which the apparent activation energies and the frequency factors  $A$  (pre-exponential factors of the Arrhenius equation) were obtained. The entropies of activation for these reactions were calculated and are given in Table II. A theoretical and experimental treatment was studied for a gel point method to estimate overall polymerization reactions according to Gough and Smith.<sup>8</sup>

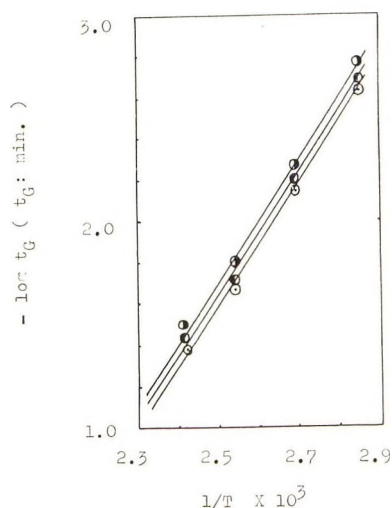


Fig. 13. Temperature dependence of curing reaction of E-828/MNA/triethanolamine/HA (0.2:0.2:0.0034:0.02) for various HA: (●) benzoic acid; (○) benzyl alcohol; (◐) phenol.  $E_A = 14.7$  kcal./mole.

TABLE II  
Activation Parameters for Curing Reaction of Epoxide/Anhydride/HA/Tertiary Amine<sup>a</sup>

HA	$E_A$ , kcal./mole	$\log A$ , min. <sup>-1</sup>	$\Delta S^*_{298}$ , e.u.
Benzoic acid	14.7	6.4	-35.0
Benzyl alcohol	"	6.2	-35.4
Phenol	"	6.3	-35.2

<sup>a</sup> The reaction system was E-828/MNA/HA/triethanolamine (0.2:0.2:0.02:0.0034).

## DISCUSSION

In a previous paper,<sup>4</sup> we showed that no etherification reaction occurred in the tertiary amine-catalyzed reaction systems of acid anhydride and epoxy resin having some or no OH groups in molecular structure. Moreover, Figures 1-3 show almost no differences in conversion between the epoxides and anhydrides within the conditions of this experiment, and implies the etherification reaction shown by eq. (3) did not occur up to the gelation point, even in the epoxide/acid anhydride/HA/tertiary amine systems having OH groups in the reaction system and the epoxide/acid anhydride/HA systems which has no amine catalyst. This disagrees with Fisch and Hoffmann's results,<sup>1,2</sup> which showed some epoxide homopolymerization occurs in the uncatalyzed reaction of epoxide and acid anhydride. We may suppose, therefore, that the etherification reaction occurs at least after the gelation.

The reaction mechanism was studied kinetically and the rate-determining step was previously<sup>4</sup> discussed for the reaction system epoxide/acid an-

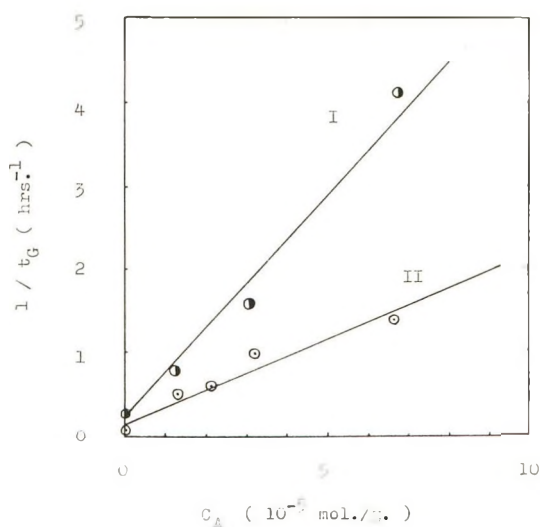
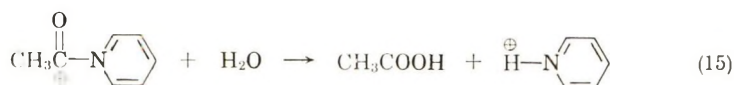
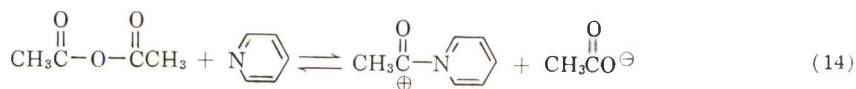


Fig. 14. Catalytic effects of triethanolamine on gel time  $t_g$  of the reaction systems of epoxy resin/HHPA: (I) E-1001 at 110°C.; (II) E-828 at 100°C.

hydride/amine. The reaction mechanism shown by eqs. (6) and (7) may be suggested analogously from that proposed for the hydrolysis of acid anhydrides,<sup>9-12</sup> for example, with acetic anhydride, the hydrolysis is:



It was found that the catalysis of amines is not confined to the acetylation of water, but that pyridine catalyzes the acetylation of *p*-chloroaniline and of ethanol, and that quinoline is inactive.<sup>9</sup> These differences in the catalytic efficiencies of various amine, as well as in the case of the reaction system epoxide/anhydride/amine in the preceding paper, may be due to the steric influences of amines and suggest a steric effect on the mechanism of catalysis. More significantly, the same influence of catalytic amines was observed in the decomposition of acetic formic anhydride in an aprotic solvent<sup>11</sup> where the only possible catalytic effect of the amine is by interaction with the anhydride. These results suggest that in the reaction of epoxide and anhydride, too, the catalysis is due to an interaction of amine and anhydride. Whatever the nature of this interaction, it fairly certainly does not produce an appreciable equilibrium concentration of a new species. All experiments to detect such a product have had negative results: The absorption spectra of pyridine and acetic anhydride in cyclo-

hexane over the range 2300–2800 Å., which is the chief absorption region of pyridine in the near ultraviolet, are strictly additive.<sup>10</sup> In the infrared absorption spectra of acetic anhydride and pyridine in carbon tetrachloride the intensity and position of the bands due to carbonyl vibrations (at 1769 and 1936  $\text{cm}^{-1}$ ) and COC skeletal vibrations (at 1124  $\text{cm}^{-1}$ ) of acetic anhydride are unaffected by the presence of pyridine. The electrical conductivities of mixtures of acetic anhydride and pyridine in dry acetone were not significantly higher than the sum of the conductivity of solutions of acetic anhydride and of pyridine in acetone;<sup>10</sup> the same result was obtained with benzoic anhydride and pyridine in 50% acetone–water at 0°C.<sup>10</sup> Depressions of the freezing point of benzene by acetic anhydride and pyridine are additive. Thus neither an association complex nor an ionic reaction product between an anhydride and pyridine are formed in analytically detectable amounts.

The view that the catalysis occurs via some association between amine and the whole or part of the anhydride molecule is strengthened by the known steric hindrance of  $\alpha$ -substituents on the rate and equilibria of association reactions of tertiary amines. The Menshutkin reactions of alkyl chlorides<sup>13</sup> and benzyl bromide<sup>14</sup> with heterocyclic amines proceed more slowly if the amine contains a blocked  $\alpha$ -position. The complex of 2-picoline with trimethylboron is much less stable than the analogous complexes of pyridine or 3- and 4-picoline<sup>5</sup> but more stable than the doubly substituted amine, 2,6-lutidine; similarly the complex of boron trifluoride with 2,6-lutidine is less stable than that with pyridine.<sup>16</sup>

The catalytic coefficient for pyridine according to the mechanism shown by eqs. (14) and (15) is given by<sup>12</sup>

$$k_p = k_1 k_2 [\text{H}_2\text{O}] / (k_{-1} [\text{OAc}^-] + k_2 [\text{H}_2\text{O}]) \quad (16)$$

The found relationship<sup>9–12</sup> of  $k_{-1} [\text{OAc}^-] > k_2 [\text{H}_2\text{O}]$  in this case implies a certain large selectivity of acetylpyridinium ion in its reaction with nucleophiles. Aromatic anhydrides are not incapable of ionic splitting, because benzoic anhydride,<sup>17</sup> but not ethyl benzote,<sup>18</sup> forms the oxocarbonium ion  $\text{ArCO}^+$  in concentrated sulfuric acid. It can safely be assumed, however, that the reaction belongs to the type of nucleophilic bimolecular displacement reactions with its analog in ester hydrolysis.<sup>19</sup> Meloche and Laidler<sup>20</sup> have recently outlined a general scheme for the hydrolysis of acid derivatives which can be applied also to the reaction of epoxide and anhydride, as was done to the hydrolysis of anhydride by Berliner and Altschul.<sup>21</sup>

The energies of activation and the frequency factors, as well as the

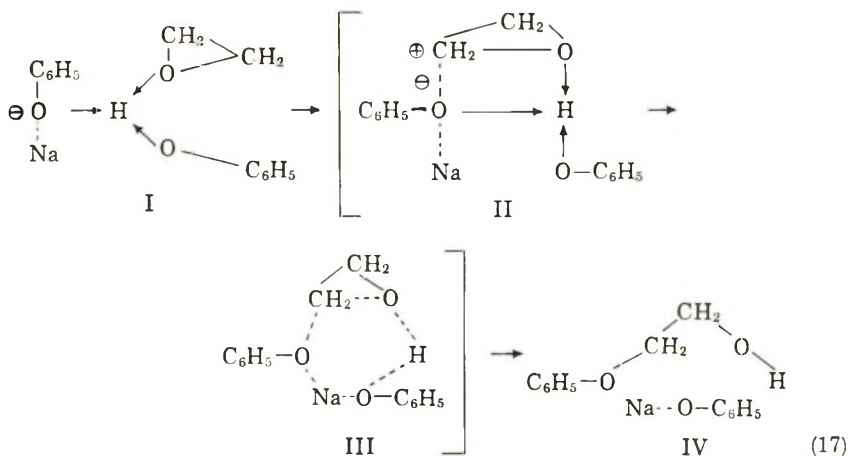
TABLE III  
Activation Parameters for Reaction of Epoxy Resin/HHPA/Triethanolamine

Epoxy Resin	$E_a$ , kcal./mole	$\log A$ , $\text{min}^{-1}$	$\Delta S^*_{298}$ , e.u.
E-828	14.1	6.69	–35.0
E-1001	14.4	6.76	–34.8

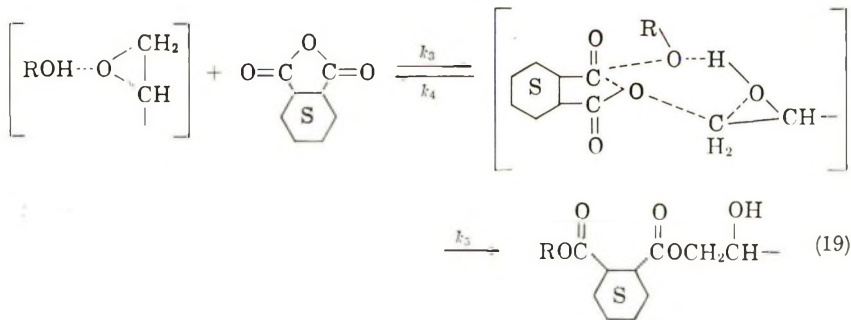
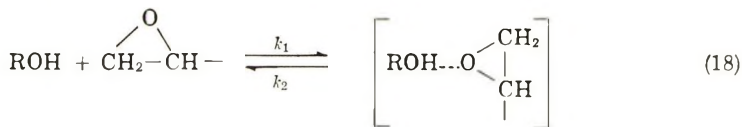
entropies of activation are listed in Table III for the curing reaction of epoxide/anhydride/amine (0.2:0.2:0.0034).

The low frequency factors and large negative entropies of activation for the reaction shown in Table III might support the idea that the curing reaction of epoxy resins and anhydrides belongs to the type of nucleophilic bimolecular displacement reactions.

The reaction mechanism proposed previously<sup>4</sup> for the system epoxide/acid anhydride/HA (alcohol), might be suggested analogously from the mechanism<sup>22</sup> for the ethylene oxide and phenol:



The proposed mechanism illustrated by equations involving a termolecular reaction would require a large negative entropy. There is a slight probability for such a postulation as described above but since no measurements were made, a more probable mechanism which would allow the same kinetic order but which is indistinguishable from that proposed in previous paper<sup>4</sup> on a purely kinetic basis is shown in eqs. (18) and (19).



For  $C_{HA}$ ,  $C_B$ ,  $C_D$ ,  $C_C$ , and  $C_E$  as the concentrations of alcohol, acid anhydride, epoxide, the activated complex of alcohol and epoxide shown by eq. (18) and the activated complex of alcohol, epoxide, and anhydride shown by eq. (19), respectively, the following equations are obtained:

$$dC_C/dt = k_1 C_{HA} C_D - k_2 C_C - k_3 C_C C_B + k_4 C_E \quad (20)$$

$$dC_E/dt = k_3 C_C C_B - k_4 C_E - k_5 C_E \quad (21)$$

Since no detectable amounts of intermediates are formed, we may apply the stationary state hypothesis,  $dC_C/dt = dC_E/dt = 0$ , and can obtain:

$$C_E = k_1 k_3 C_{HA} C_B C_D / (k_2 k_4 + k_2 k_5 + k_3 k_5 C_B) \quad (22)$$

The equation of reaction rate,  $v$ , takes the form

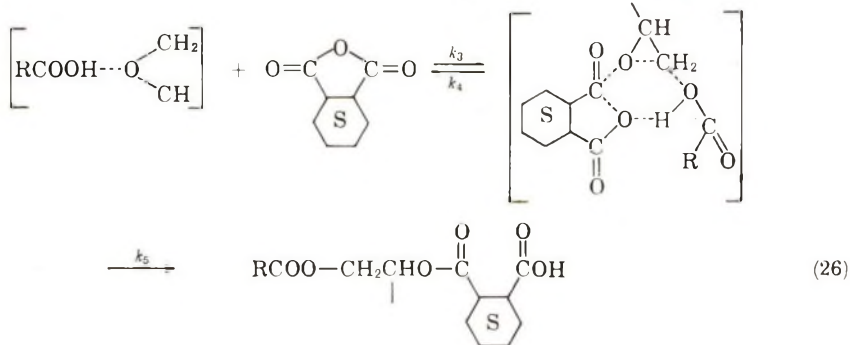
$$\begin{aligned} v &= -dC_B/dt = -k_5 C_E \\ &= -k_1 k_3 k_5 C_{HA} C_B C_D / (k_2 k_4 + k_2 k_5 + k_3 k_5 C_B) \end{aligned} \quad (23)$$

If  $k_1, k_2, k_3, k_4 \gg k_5$  and  $1 \gg C_B, C_D$ , we can obtain:

$$v = [-k_1 k_3 k_5 / k_2 (k_4 + k_5)] C_{HA} C_B C_D \quad (24)$$

and eq. (24) explains more reasonably the results of Figures 2, 5, and 7, which show that the reaction rate is proportional to the concentrations of alcohol, epoxide, and acid anhydride. The equation of reaction rate, therefore, may be shown experimentally by eq. (12), which supports the proposed mechanism, where  $K_A$  is equal to  $K[\text{alcohol}]$ . The equilibrium reaction shown by eq. (18) may be suggested from the observed electron donor ability of substituted ethylene oxides in hydrogen bonding toward chloroform and methanol- $d$ , although both the spectral data and the heats of mixing show that the three-membered ring ethers, propylene oxide, and the other substituted ethylene oxides, are much poorer donor molecules than the other cyclic ethers, the four-, five-, and six-membered ring ethers.<sup>23-25</sup>

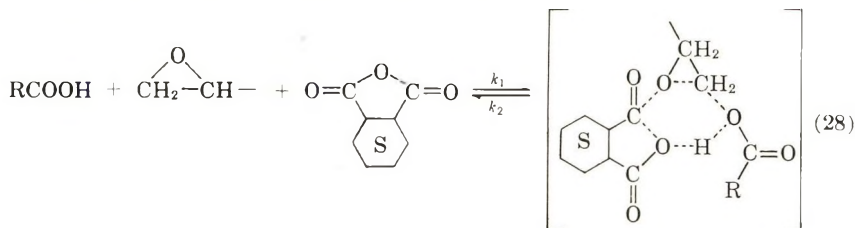
HA being acid, RCOOH, the following elementary reactions are assumed to occur:



For  $C_{HA}$ ,  $C_B$ ,  $C_D$ ,  $C_C$ , and  $C_E$  the concentrations of acid, acid anhydride, epoxide, the activated complex shown by eq. (25) and the activated complex shown by eq. (26), respectively, the following equation is obtained for the system epoxide/anhydride/alcohol:

$$\begin{aligned} v &= -\dot{a}C_{\text{B}}/dt = -dC_{\text{D}}/dt \\ &= -k_1k_3k_5C_{\text{HA}}C_{\text{B}}C_{\text{D}}/(k_2k_4 + k_2k_5) \end{aligned} \quad (27)$$

If the following termolecular reaction occurs

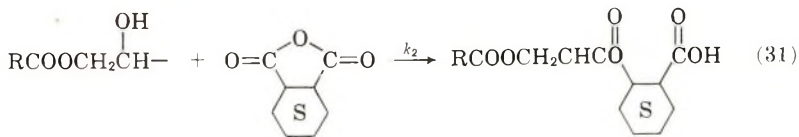


and is then accompanied by the reaction of eq. (26) the rate equation can be obtained as:

$$v = -k_1 k_5 C_{\text{HA}} C_{\text{B}} C_{\text{D}} / (k_2 + k_5) \quad (29)$$

The mechanism illustrated by eqs. (28) and (26) involves a reaction accompanied by a large negative entropy, but might be suggested analogously from the mechanism<sup>22</sup> for the reaction of ethylene oxide and phenol. Since no activation entropy was obtained, the mechanism shown by eqs. (25) and (26) may be a more probable mechanism which would allow the same kinetic order but which is indistinguishable from the mechanism illustrated by eqs. (26) and (28) and on purely kinetic basis. Equations (27) and (28) agree with the experimental eq. (12) obtained from Figures 1, 4, and 7.

Suppose the following reactions occur:



The reaction rate might be obtained as:

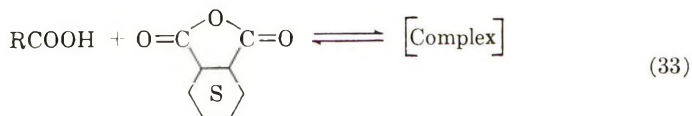
$$r = -dC_D/dt = -k_1 C_{HA} C_D \quad k_1 < k_2 \quad (32a)$$

$$= -dC_B/dt = -k_2 C_{HA} C_B \quad k_1 > k_2 \quad (32b)$$

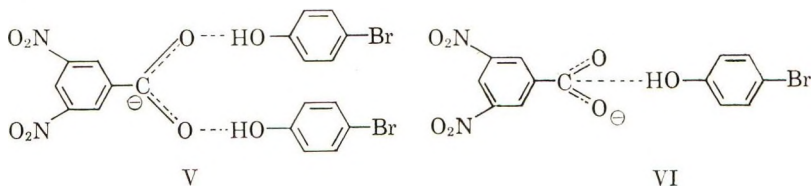
and disagrees with the experimental eq. (12) obtained from Figures 1, 4, and 7.

The equilibrium reaction shown by eq. (25) may be suggested from the observed electron-donor ability of epoxides in hydrogen bonding<sup>22-25</sup> and

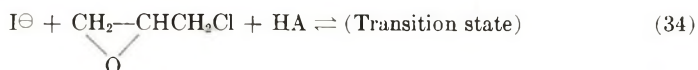
from the probability for the presence of the oxonium form of epoxide in acidified solutions.<sup>26,27</sup> The following equilibrium:



might be suggested also from the evidence<sup>28</sup> that the infrared spectra of mixtures of 3,5-dinitrobenzoate with *p*-bromophenol are accounted for by formation of 2:1 and 1:1 hydrogen-bonded complexes between *p*-bromophenol and 3,5-dinitrobenzoate anion, represented by structures V and VI:

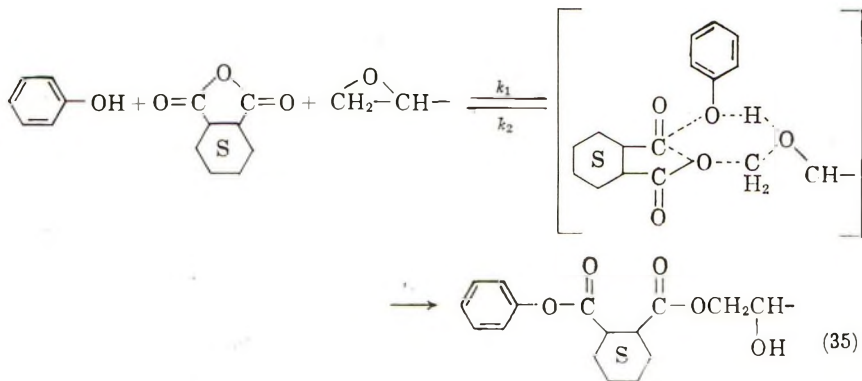


It is found, however, that acid catalysis in the hydrolysis of benzoic anhydride is relatively small, even in the presence of 0.1*N* hydrochloric acid.<sup>29-31</sup> Therefore, the catalytic effect of the complex shown by eq. (33) may be small or negligible for this reaction. Swain<sup>32</sup> studied the reaction of iodide ion with a substituted ethylene oxide (epichlorohydrin in water), and concluded that the reaction involves

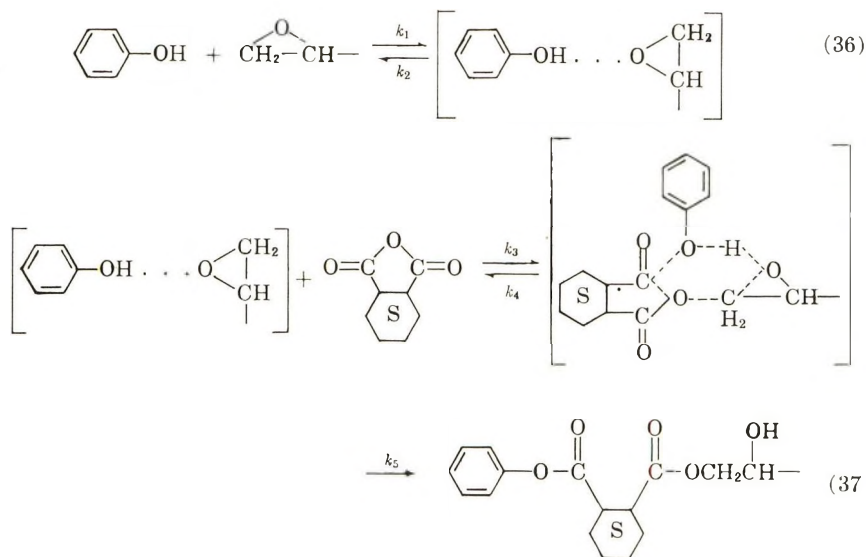


where HA may be H<sub>2</sub>O, HOAc, or H<sub>3</sub>O<sup>+</sup>. Thus no pre-equilibrium between oxide and the free (dissociated) oxonium salt of the oxide is involved in the main reaction which yields iodohydrin.

When HA is phenol, the following reaction mechanism might be suggested analogously from the mechanism<sup>22</sup> for the reaction of ethylene oxide and phenol as described above:

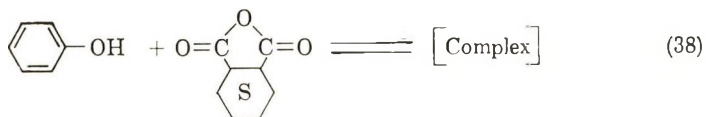


The equation of reaction rate,  $v$ , takes the same form of eq. (29) as shown in the case of the other HA's, alcohol and acid, and agrees with the experimental eq. (12). The mechanism illustrated by eq. (35) however, involves a reaction accompanied by a large negative entropy, and the mechanism shown by eqs. (36) and (37) may be a more probable one which would allow the same kinetic order.



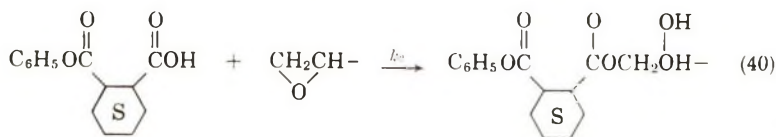
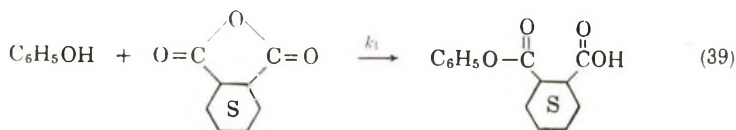
The reaction rate, then, is obtained as in the cases of the other HA's, alcohol and acid, and can explain the results in Figures 6 and 7.

The equilibrium reaction shown by eq. (36) is suggested from the observed electron donor ability of epoxides in hydrogen bonding<sup>23-25</sup> and from the probability<sup>26,27</sup> for the presence of the oxonium form of epoxides. The following equilibrium:

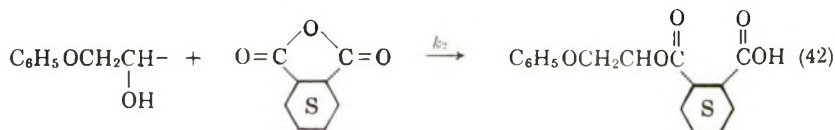
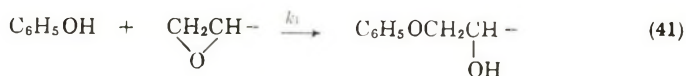


might be suggested also from the fact<sup>28</sup> that formation of 2:1 and 1:1 hydrogen-bonded complexes between *p*-bromophenol and 3,5-dinitrobenzoate anion represented by V and VI was observed with the infrared spectra. The catalytic efficiency of the complex indicated in eq. (38), however, may be smaller for this reaction because of poor acid catalysis in the hydrolysis of benzoic anhydride even in acidic solution.<sup>29-31</sup>

If the following reactions occur:



or



The reaction of eq. (39) is supported by the production<sup>33,34</sup> of phenyl esters, but the reaction rate as obtained as the same form of eqs. (32), disagrees with the experimental eq. (12) and cannot explain the results in Figures 6 and 7.

Shechter, Wynstra, and Kurkijy<sup>35</sup> and Kakurai and Noguchi<sup>36</sup> studied the accelerating and retarding effects of various compounds on the reaction of epoxide and amine, and proposed a push-pull mechanism, i.e., a termolecular "concerted displacement" for the reaction. Smith and Gough<sup>37,38</sup> studied the catalytic effects of additives on the curing reaction of epoxy resin and amine, and supported the mechanism of Shechter et al.<sup>35</sup> They<sup>37</sup> also showed that since acceleration might be associated with donation of hydrogen bonds in transition states, accelerators are capable of hydrogen bonding to an oxygen atom, and addition of a compound capable of acting as hydrogen bond acceptor might be expected to reduce the number of hydrogen-bonded epoxide groups and hence to reduce the curing rate.

If the catalytic effect of HA on the curing reaction of epoxide and acid anhydride may be shown by eqs. (18), (25), and (36), which show acceleration may be associated with donation of hydrogen bonds, we can attempt to predict the effect of added compounds on the curing reaction. A list of functional groups based on Gough and Smith<sup>37</sup> is shown in Table IV.

Differences in the catalytic effects among benzoic acid, benzyl alcohol, and phenol in the reaction system of epoxy resin/anhydride are considered to depend on the donating power of the hydrogen bond which is the important role rather than a general electrostatic interaction effect as solvent effects in nucleophilic substitution reactions.

TABLE IV  
 Catalytic Effects of Various Compounds

Accelerators	Retarders
—OH	—OR (R ≠ H)
—CO <sub>2</sub> H	—CO <sub>2</sub> R
—SO <sub>3</sub> H	—SO <sub>3</sub> R
—CONH <sub>2</sub>	—CONR <sub>2</sub>
—CONHR	—SO <sub>2</sub> NR <sub>2</sub>
—SO <sub>2</sub> NH <sub>2</sub>	—CO—
—SO <sub>2</sub> NHR	—CN
	—NO <sub>2</sub> (≠ CH <sub>3</sub> NO <sub>2</sub> )

It is clear from Table V and the results in Figure 7 that there is no relationship between the dielectric constants of additives and their effects on the rate of curing reactions. It has been shown that the  $pK_a$  values of organic bases may be correlated with their hydrogen bond-acceptor properties.<sup>39,40</sup> Schechter and Wynstra<sup>41</sup> showed that the order of the base-catalyzed reactions of the systems of epoxide/acid, epoxide/alcohol, and epoxide/phenol is alcohol > phenol > acid, and that this is also the order of increasing basicity of the anions derived from each of these compounds. Smith and Gough<sup>37</sup> showed, similarly, a correlation may be found between the  $pK_a$  values of acidic compounds and their hydrogen bond donor properties, as long as the compounds have similar structures and are free from varying steric effects.

 TABLE V  
 Physical Properties of Additives

Compounds	Dielectric constants <sup>c</sup>	$pK_a$ at 25°C. <sup>b</sup>	Association equilibrium constants $K$ at 25°C., l./mole <sup>a</sup>	
			In CCl <sub>4</sub>	In C <sub>6</sub> H <sub>6</sub>
Benzoic acid	<sup>d</sup>	4.2	1000–4000	170–550
Benzyl alcohol	13.1 (20°C.)		0.8–2.5	
Phenol	9.78 (60°C.)	9.9	0.7–2.3	0.57

<sup>a</sup> Data of Pimentel and McClellan.<sup>42b</sup>

<sup>b</sup> Data of Lange.<sup>43a</sup>

<sup>c</sup> Data of Lange.<sup>42b</sup>

<sup>d</sup> Acetic acid, 6.15 (20°C.); formic acid, 58.5 (16°C.); oleic acid, 2.46 (20°C.).

According to the above hypothesis, we might anticipate that phenol could be more effective than alcohol. No correlation, however, was found between the  $pK_a$  values of acid, alcohol, and phenol, and their catalytic effects on these curing reactions as shown in Table V and in Figure 7. Table V also shows some association equilibrium constants for the formation of hydrogen bonds written in this form:<sup>42a</sup>

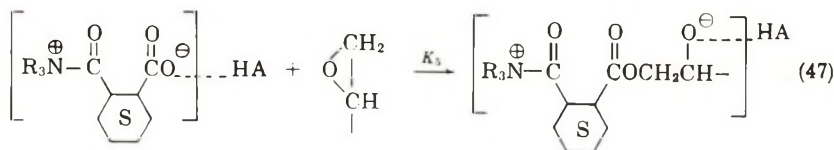
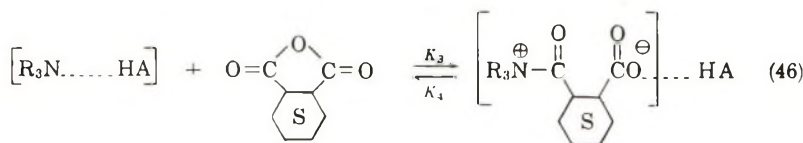


$$K = [A-H \cdots B]/[AH][B] \quad (44)$$

A correlation may be found easily between the equilibrium constants,  $K$ , for the formation of hydrogen bonds and their catalytic effects shown in Figure 7, and this must be consistent with the fact that accelerating effect of phenol was almost the same as that of alcohol with smaller concentration.

Although this is in qualitative agreement with the experimental results presented above, and strengthens the validity of the proposed mechanism shown by eqs. (18), (25), and (36), there are certain points worthy of further discussion. According to the above scheme, we might anticipate that the accelerating effect of phenol must be proportional to its concentration within this experiment as the other HA's. The fact that with larger concentration phenol had a retarding effect proportional to its concentration as shown in Figure 7, indicates that phenol plays both roles of accelerating and retarding the gelation of the reaction system of epoxy resin/acid anhydride. This, in turn, suggests that there are certain points worthy of further study for the catalytic effect of phenol and the reaction mechanism in the system of epoxide/anhydride/phenol.

In the reaction system of epoxide/anhydride/tertiary amine/HA, the following elemental reactions are assumed to occur:



where HA are acid, alcohol, or phenol. When  $C_A$ ,  $C_{HA}$ ,  $C_B$ ,  $C_D$ ,  $C_C$ , and  $C_E$  are the concentrations of tertiary amine, HA (acid, alcohol, or phenol), acid anhydride, epoxide, activated complex of amine, HA, and anhydride shown by eq. (46) and the complex of amine and HA shown by eq. (45), respectively, the following equations are obtained:

$$dC_E/dt = k_1 C_A C_{HA} - k_2 C_E - k_3 C_E C_B + k_4 C_C \quad (48)$$

$$dC_C/dt = k_3 C_E C_B - k_4 C_C - k_5 C_D C_C \quad (49)$$

since  $dC_C/dt = dC_E/dt = 0$  in the stationary state, we obtain:

$$C_C = k_1 k_3 C_A C_{HA} C_B / (k_2 k_4 + k_2 k_5 C_D + k_3 k_5 C_B C_D) \quad (50)$$

The equation of reaction rate,  $v$ , takes the form with the above eq. (50):

$$v = -dC_D/dt = -k_5 C_C C_D$$

$$= -k_1 k_3 k_5 C_A C_B C_D C_{HA} / (k_2 k_4 + k_2 k_5 C_D + k_3 k_5 C_B C_D) \quad (51)$$

If  $k_1 > k_2$ ,  $k_3, k_4 \gg k_5$ , and  $1 > C_B, C_D$ , we can obtain:

$$v = (-k_1 k_3 k_5 / k_2 k_4) C_A C_B C_D C_{HA} \quad (52)$$

and eq. (52) explains more reasonably the results of Figures 4-6, 8, and 12, and is consistent with the experimental equation of reaction rate, eq. (12). These might be also supported with the observed large negative entropies of activation for these reactions as shown in Table II.

The equilibrium reaction shown by eq. (45) is suggested from the facts that the formations of association products,  $R_3N(RCOOH)_n$ , where  $n > 2$ , or carboxylic acids and their 1:1 acid-amine salts in nonpolar media,<sup>44</sup> and the hydrogen-bonded complexes of tertiary amine with phenol<sup>45</sup> or alcohol.<sup>46</sup> have been detected experimentally by ultraviolet<sup>47</sup> and infrared<sup>48-50</sup> spectrophotometry. The important role of the complex shown by eq. (45) might be also suggested from a more detailed kinetic investigation showing the relative importance of the 1:1 and 2:1 salts or complexes of acid and amine as reactants in the amine-induced chloroacetylolysis of trityl chloride in carbon tetrachloride.<sup>44</sup>

Table VI shows the equilibrium constants for the formation of hydrogen bonds between a tertiary amine and HA written in those forms of eqs. (43) and (44), and makes us anticipate that the order of the complex concentration of tertiary amine and HA may be acid > phenol > alcohol. The fact that phenol was most effective of other HA's within certain concentration, suggests that if the curing reaction proceeds with eqs. (45)-(47), phenol might play most effective cocatalytic role on the elemental reaction shown by eq. (46) and that the complex of acid with amine is more stable or less reactive than that of phenol. Differences in the cocatalytic effects among benzoic acid, benzyl alcohol, and phenol in the reaction system of epoxide/anhydride/amine/HA are considered to depend on the donating

TABLE VI  
Equilibrium Constants for the Formation of  
Hydrogen Bonds between Amine and HA

Compounds	Amines	Solvents	Temp., °C.	$K$ , l./mole	Ref.
Acetic acid	Diethylamine	CCl <sub>4</sub>	25-30	2800	49
	"	CHCl <sub>3</sub>	"	3000	"
	Pyridine	CCl <sub>4</sub>	Room temp.	220	"
	"	CHCl <sub>3</sub>	"	70	"
Ethyl alcohol	Triethylamine	CCl <sub>4</sub>	—	2.9	51
Phenol	"	<i>n</i> -Heptane	25	83.8	52
	Trimethyl- amine	Cyclo- hexane	"	86	53
	Pyridine	CCl <sub>4</sub>	18-20	55	54

power of hydrogen bond with amine, which is the important role rather than an electrostatic interaction effect in these reaction systems, and on the reactivity of the complex of HA with amine.

Although this is in qualitative agreement with the experimental results presented above, and supports the validity of the proposed mechanism shown by eqs. (45)–(47), there are certain points worthy of further discussion. According to the above hypothesis, we might anticipate that the cocatalytic effect of phenol must be proportional to its concentration within this experiment as the other HA's. Phenol with larger concentration had a retarding effect proportional to its concentration shown in Figure 8, and this indicates that phenol has both effects of accelerating and retarding the gelation of the reaction system of epoxide/anhydride/amine. This, also, suggests that there are some points worthy of further investigation for the cocatalytic effect of phenol and the reaction mechanism in the system of epoxide/anhydride/tertiary amine/phenol.

Figures 12 and 14 suggest that the accelerating effect of mixed catalyst of amine and HA might not be the sum of the effect of amine and of HA, but the catalytic effect of complex of amine and HA, as shown by eq. (45), that is, HA has a cocatalytic effect in these mixed catalysts. Curves *I* and *II* in Figures 12 and 14 must run parallel to each other, if the acceleration of the mixed catalyst is the sum of each catalytic effect. For the catalytic effects of acid, alcohol, and phenol showed by eqs. (45) and (46), they may depend on the complex-forming powers of hydrogen atom of acid, alcohol, and phenol with amine, and the reactivity of the complex shown by eq. (45). In Figures 9–11 ( $\log t_{G0}/t_G$ ) is plotted against Hammett's sigma constants,  $\sigma$ ,<sup>55,56</sup> for the curing reactions of epoxy resin/acid anhydride/tertiary amine/HA at 100°C. The best straight lines have been found in these cases and, from slopes, are found to be +0.18, +0.13, and +0.22 for acid, alcohol, and phenol, respectively. The fact that  $\rho$  are all positive indicates that electron-withdrawing substituents of  $\text{RC}_6\text{H}_4\text{COOH}$ ,  $\text{RC}_6\text{H}_4\text{CH}_2\text{OH}$ , and  $\text{RC}_6\text{H}_4\text{OH}$  increase the reaction rate and that HA might play the cocatalytic role in the transition states shown by eqs. (46) and (47). The results in Figures 9–11 supported the proposed curing mechanisms of eqs. (45)–(47) better.

## References

1. Fisch, W., and W. Hofmann, *J. Polymer Sci.*, **12**, 497 (1954).
2. Fisch, W., W. Hofmann, and J. Koskikallio, *J. Appl. Chem.*, **6**, 429 (1956); *Chem. Ind. (London)*, **1956**, 756.
3. Dearborn, E. C., R. M. Fuoss, and A. F. White, *J. Polymer Sci.*, **16**, 201 (1955).
4. Tanaka, Y., and H. Kakiuchi, *J. Appl. Polymer Sci.*, **7**, 1063 (1963).
5. Wegler, R., *Angew. Chem.*, **67**, 582 (1955).
6. Fischer, R. F., *J. Polymer Sci.*, **44**, 155 (1960).
7. Allied Chemical & Dye Corporation, Tech. Bull., R92856.
8. Gough, L. J., and I. T. Smith, *J. Appl. Polymer Sci.*, **3**, 362 (1960).
9. Bafna, S. L., and V. Gold, *J. Chem. Soc.*, **1953**, 1406.

10. Gold, V., and E. G. Jefferson, *J. Chem. Soc.*, **1953**, 1409.
11. Gold, V., and E. G. Jefferson, *J. Chem. Soc.*, **1953**, 1416.
12. Johnson, S. L., *J. Phys. Chem.*, **67**, 495 (1963).
13. Long, F. S., *J. Chem. Soc.*, **1911**, 2164.
14. Baker, J. W., and W. S. Nathan, *J. Chem. Soc.*, **1935**, 519.
15. Brown, H. C., and G. K. Barbaras, *J. Am. Chem. Soc.*, **69**, 1137 (1947).
16. Brown, H. C., H. I. Schlesinger, and S. Z. Cardon, *J. Am. Chem. Soc.*, **64**, 325 (1942).
17. Gillespie, R. J., *J. Chem. Soc.*, **1950**, 2997.
18. Kuhn, L. P., and A. W. Gorwin, *J. Am. Chem. Soc.*, **70**, 3370 (1948).
19. Day, J. N. E., and C. K. Ingold, *Trans. Faraday Soc.*, **37**, 686 (1941).
20. Meloche, I., and K. Laidler, *J. Am. Chem. Soc.*, **73**, 1712 (1951).
21. Berliner, E., and I. H. Altschul, *J. Am. Chem. Soc.*, **74**, 4110 (1952).
22. Patat, F., and B. Wojtech, *Makromol. Chem.*, **37**, 1 (1960).
23. Searles, S., and M. Tamres, *J. Am. Chem. Soc.*, **73**, 3704 (1951).
24. Searles, S., M. Tamres, and E. R. Lippincott, *J. Am. Chem. Soc.*, **75**, 2775 (1953).
25. Gutowsky, H. S., R. L. Rutledge, M. Tamres, and S. Searles, *J. Am. Chem. Soc.*, **76**, 4242 (1954).
26. Parker, R. E., and N. S. Isaacs, *Chem. Revs.*, **59**, 737 (1959).
27. Zimakof, P. V., *Zhur. Fiz. Khim.*, **30**, 1904 (1956).
28. Kolthoff, I. M., and M. K. Chantooni, Jr., *J. Am. Chem. Soc.*, **85**, 2195 (1963).
29. Wilsdon, B. H., and N. V. Sidgwick, *J. Chem. Soc.*, **1913**, 103, 1959.
30. Olivier, S. C. J., and G. Berger, *Rec. Trav. Chim.*, **46**, 609 (1927).
31. Vles, S. E., *Rec. Trav. Chim.*, **52**, 809 (1933).
32. Swain, C. G., *J. Am. Chem. Soc.*, **74**, 4108 (1952).
33. Bader, A. R., and A. D. Kontowicz, *J. Am. Chem. Soc.*, **75**, 5416 (1953).
34. Nakazawa, K., and S. Baba, *J. Pharm. Soc. Japan*, **75**, 378 (1955).
35. Shechter, L., J. Wynstra, and R. P. Kurkijy, *Ind. Eng. Chem.*, **48**, 94 (1956).
36. Kakurai, T., and T. Noguchi, *Kogyo Kagaku Zasshi*, **63**, 294 (1960).
37. Gough, L. J., and I. T. Smith, *J. Oil Colour Chemists' Assoc.*, **43**, 409 (1960).
38. Smith, I. T., *Polymer*, **2**, 95 (1961).
39. Tamres, M., S. Searles, E. M. Leighly, and D. W. Mohrman, *J. Am. Chem. Soc.*, **76**, 3983 (1954).
40. Halleux, A., *Bull. Soc. Chim. Belges*, **68**, 381 (1959).
41. Shechter, L., and J. Wynstra, *Ind. Eng. Chem.*, **48**, 86 (1956).
42. Pimentel, G. C., and A. L. McClellan, *The Hydrogen Bond*, W. H. Freeman, San Francisco-London, 1960, (a) p. 349; (b) p. 365.
43. Lange, N. A., *Handbook of Chemistry*, 9th Ed., Handbook Publishers, Sandusky, Ohio, 1956, (a) p. 1198; (b) p. 1221.
44. Andrews, L. J., and R. M. Keefer, *J. Am. Chem. Soc.*, **84**, 2886 (1962).
45. Chandra, A. K., and S. Banerjee, *J. Phys. Chem.*, **66**, 952 (1962).
46. Stevenson, D. P., *J. Am. Chem. Soc.*, **84**, 2849 (1962).
47. Keefer, R. M., and L. J. Andrews, *J. Am. Chem. Soc.*, **84**, 941 (1962).
48. Barrow, G. M., and E. A. Yerger, *J. Am. Chem. Soc.*, **76**, 5211 (1954).
49. Yerger, E. A., and G. M. Barrow, *J. Am. Chem. Soc.*, **77**, 4475, 6206 (1955).
50. Barrow, G. M., *J. Am. Chem. Soc.*, **78**, 5802 (1956).
51. Barrow, G. M., *J. Am. Chem. Soc.*, **76**, 5247 (1954).
52. Nagakura, S., and M. Gouterman, *J. Chem. Phys.*, **26**, 881 (1957).
53. Denyer, R. L., A. Gilchrist, J. A. Pegg, J. Smith, T. E. Tomlinson, and L. E. Sutton, *J. Chem. Soc.*, **1955**, 3889.
54. Fuson, N., et al., *J. Chim. Phys.*, **55**, 454 (1958).
55. Jaffé, H. H., *Chem. Revs.*, **53**, 191 (1953).
56. Taft, R. W., in *Steric Effect in Organic Chemistry*, M. S. Newman, Ed., Wiley, New York, 1956, p. 556.

### Résumé

La réaction de vulcanisation d'une résine époxy et d'un anhydride acide avec une amine et/ou un acide, un alcool et un phénol a été étudiée cinétiquement en employant des résine époxy et des anhydrides acides commerciaux. La réaction d'éthérification ne se produit pas à 70–140°C. même dans le cas du mélange époxyde/anhydride acide/HA (acide, alcool ou phénol) et d'époxyde/anhydride acide/amine tertiaire/HA et la vitesse initiale de réaction est proportionnelle à la concentration en époxyde, en anhydride acide et en catalyseurs tels qu'une amine tertiaire, un acide, un alcool et un phénol. L'énergie d'activation apparente du système réactionnel Epikote 828/méthylbicyclo(2,2,1)-heptène-2,3-anhydride dicarboxylique/triéthanolamine/HA, obtenue est de 14.7 Kcal./mole et les faibles facteurs de fréquence ainsi que les entropies d'activation fortement négatives, pour la réaction, montrent que la réaction de vulcanisation des résines époxy et des anhydrides suit le type de réaction de substitution nucléophile. Les effets des substituants R, des acides, alcools et phénols comme cocatalyseurs sur la réaction de vulcanisation des résines époxy/anhydride acides/amine tertiaire/HA ont été étudiés. Les constantes de réaction  $\rho$  positives obtenues pour des HA indiquent que les substituants de HA capteurs augmentent la vitesse de réaction de vulcanisation du système époxyde/anhydride acide/amine/HA. Des différences dans les effets catalytiques et cocatalytiques entre l'acide benzoïque, l'alcool benzylique et le phénol dans ces systèmes de réaction peuvent être considérés comme dépendantes du pouvoir donneur du lien hydrogène dont le rôle est plus important qu'une interaction électrostatique générale comme des effets de solvant dans des réactions de substitution nucléophile. Ces résultats vérifient raisonnablement les mécanismes proposés.

### Zusammenfassung

Die Härtingsreaktion eines Epoxyharzes und Säureanhydrids mit einem Amin und einer Säure, einem Alkohol und Phenol wurde kinetisch unter Verwendung handelsüblicher Epoxyharze und Säureanhydride untersucht. Bei 70–140°C. trat selbst in den Systemen Epoxyd-Säureanhydrid-HA (Säure, Alkohol oder Phenol) und Epoxyd-Säureanhydrid-tertiäres Amin-HA keine Verätherung auf und die Anfangsreaktionsgeschwindigkeit war der Konzentration an Epoxyd, Säureanhydrid und Katalysatoren wie tertiäres Amin, Säure, Alkohol und Phenol proportional. Die scheinbar Aktivierungsenergie im System Epikote 828-Methylbicyclo-(2,2,1)-hepten-2,3-dicarbonsäureanhydrid-Triäthanolamin-HA wurde zu etwa 14,7 kcal./Mol erhalten; die niedrigen Frequenzfaktoren und grossen negativen Aktivierungsentropiewerte der Reaktion sprechen dafür, dass die Härtingsreaktion der Epoxyharze und Anhydride zum Typ der nucleophilen bimolekularen Verdrängungsreaktionen gehört. Der Einfluss der Substituenten R, an Säure, Alkohol und Phenol als Kokatalysator auf die Härtingsreaktion des Systems Epoxyharz-Säureanhydrid-tertiäres Amin-HA wurde untersucht. Die für die HA's positiv erhaltenen Reaktionskonstanten,  $\rho$ , zeigen, dass elektronenentziehende Substituenten an HA die Geschwindigkeit der Härtingsreaktion im System Epoxyd-Säureanhydrid-Amin-HA erhöhen. Unterschiede in der katalytischen und kokatalytischen Wirkung zwischen Benzoesäure, Benzylalkohol und Phenol in diesen Systemen scheinen von der Donorstärke der Wasserstoffbindung und nicht von einem allgemeinen elektrostatischen Wechselwirkungseffekt, wie Lösungsmittelleffekte bei nucleophilen Substitutionsreaktionen, abzuhängen. Die Ergebnisse bilden eine ausreichende Stütze für den angenommenen Mechanismus.

Received July 8, 1963

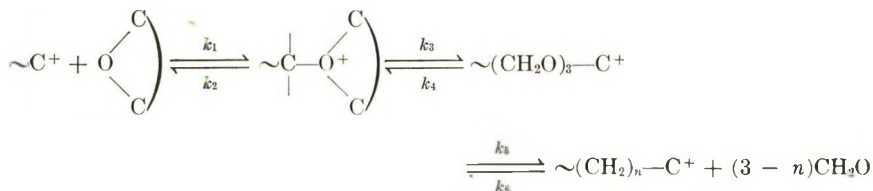
Revised October 11, 1963

## Kinetics of Polymerization of Molten Trioxane

MILOSLAV KUČERA and EDUARD SPOUSTA, *Research Institute of Macromolecular Chemistry, Brno, Czechoslovakia*

### Synopsis

Conversion curves of molten trioxane polymerization at temperatures between 70 and 90°C. have been measured. Their analysis has established that the rate-controlling step of the reaction



is the addition of a trioxane molecule to the active center. Values of the rate constants,  $k_1$  and  $k_3k_4/k_2$  as well as the rate constants of initiator deactivation  $k_6$  have been determined. Initiator deactivation causes premature leveling off of the conversion curves, especially at lower temperatures of polymerization (70–80°C.). The activation energies of the rate constants have been determined.

Cationic polymerization of heterocyclics is of considerable theoretical interest. As can be seen from the patent literature, interest is focused at present mainly on trioxane, which can be polymerized in solid<sup>1</sup> and liquid<sup>2,3</sup> phases and in solution<sup>2-7</sup> or suspension.<sup>2,3,5</sup>

Although the number of original papers published in the scientific literature and dealing with the polymerization of trioxane is not too large, they contain valuable information;<sup>8-11</sup> however, none of these deals with the polymerization of molten trioxane.

Very little is known regarding processes accompanying the transition from liquid trioxane into solid, high molecular-weight polyoxymethylene. In a previous communication of the present authors,<sup>12</sup> attention was drawn to certain phenomena caused by decreased concentration of active centers through deactivation. Since then it proved desirable to investigate the behavior of trioxane at different temperatures; results of such a study are reported in this paper.

### Experimental

Apparatus, materials, and procedure are as described earlier.<sup>12,13</sup>

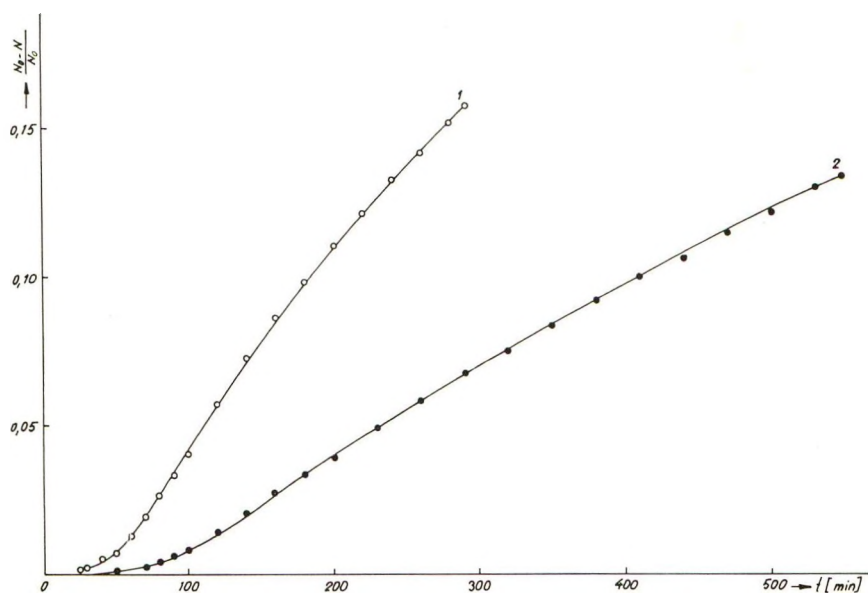


Fig. 1. Polymerization of trioxane at 70°C.: (1) initial initiator concentration  $I_0/G = 4.47$  mmoles  $kg.^{-1}$ ; (2) initial initiator concentration  $I_0/G = 2.19$  mmoles  $kg.^{-1}$ .

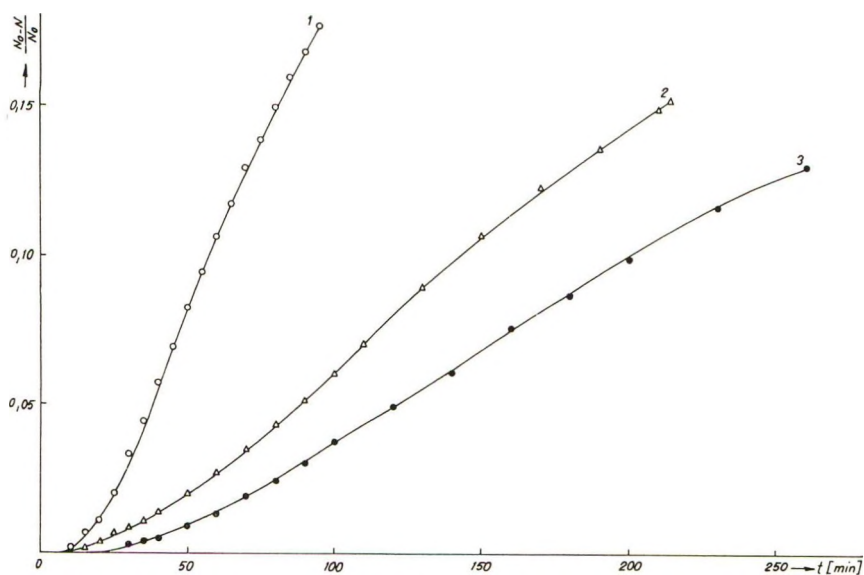


Fig. 2. Polymerization of trioxane at 80°C.: (1) initial initiator concentration  $I_0/G = 4.47$  mmoles  $kg.^{-1}$ ; (2) initial initiator concentration  $I_0/G = 2.19$  mmoles  $kg.^{-1}$ ; (3) initial initiator concentration  $I_0/G = 1.49$  mmoles  $kg.^{-1}$ .

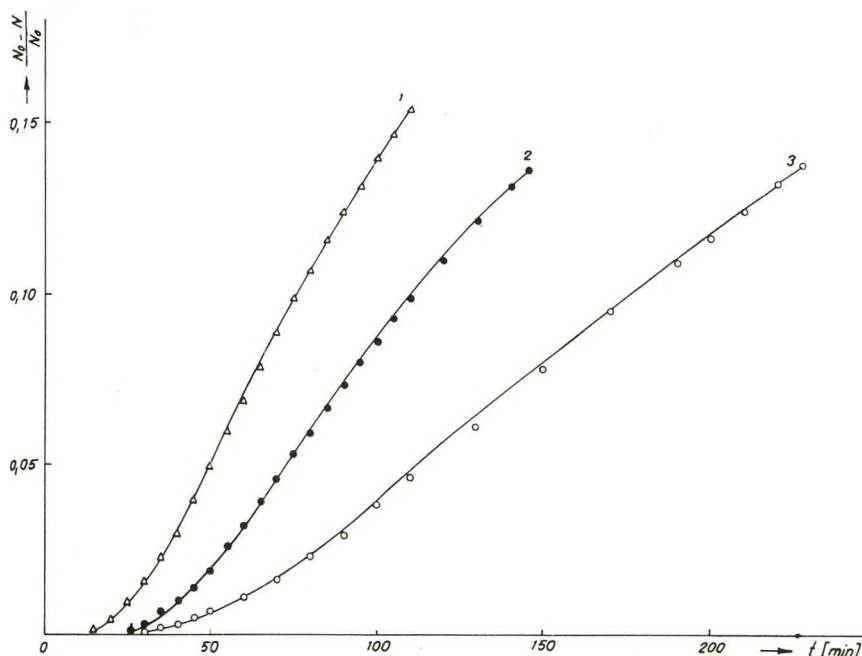


Fig. 3. Polymerization of trioxane at 85°C.: (1) initial initiator concentration  $I_0/G = 1.51$  mmoles  $\text{kg}^{-1}$ ; (2) initial initiator concentration  $I_0/G = 0.76$  mmoles  $\text{kg}^{-1}$ ; (3) initial initiator concentration  $I_0/G = 0.54$  mmoles  $\text{kg}^{-1}$ .

## Results

Conversion curves of trioxane polymerization at 70, 80, 85, and 90°C. are shown in Figures 1–4. In the previous paper, a relation was derived<sup>12</sup> for the polymerization of molten trioxane:

$$(1/G)(dN/dt) = k(N/G)(I_0/G)[1 - k_s(N_0 - N)] \quad (1)$$

where  $N_0$  and  $N$  are the number of moles of trioxane at zero time and time  $t$ , respectively,  $G$  is the weight of the liquid phase of the polymerizing system (in kilograms),  $I_0$  is the number of moles of initiator in the polymerization feed,  $k$  is the reaction rate constant (in kilograms per mole min.),  $k_s$  is the deactivation rate constant (per mole), and  $M$  is the molecular weight of trioxane (in kilograms per mole).

Equation (1) yields upon integration

$$(N_0 - N)/N_0 = (1 - e^{-(kk_s I_0/M)t})/k_s N_0 \quad (2)$$

which gives access to the constants  $k$  and  $k_s$ . The time dependence of  $\ln [1 - k_s(N_0 - N)]$  for various temperatures is shown in Figures 5–8.

## Discussion

Let us assume that the addition of a trioxane molecule to an active center proceeds through the mechanism shown in eq. (3). (Practically the

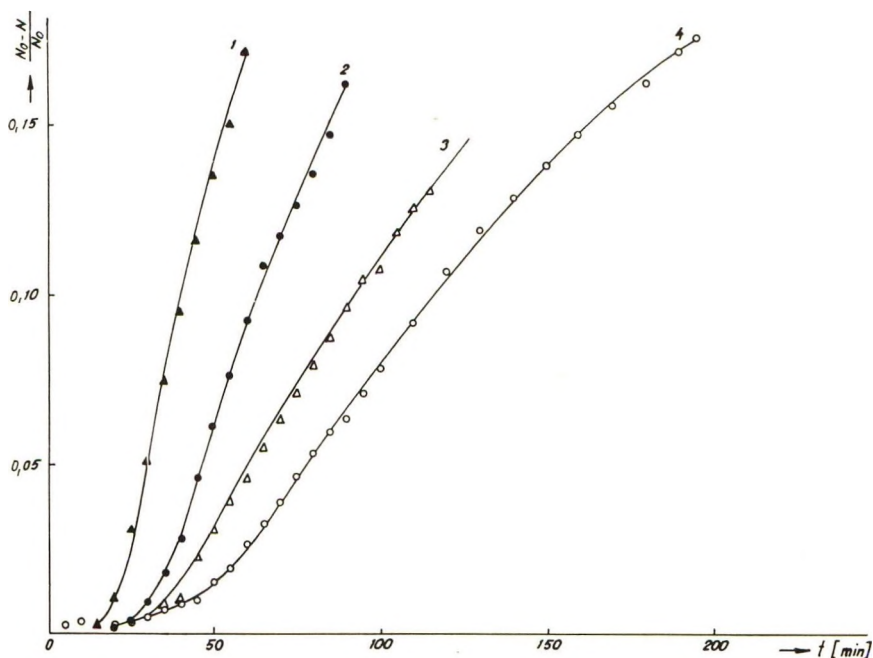


Fig. 4. Polymerization of trioxane at 90°C.: (1) initial initiator concentration  $I_0/G = 2.19$  mmoles  $\text{kg}^{-1}$ ; (2) initial initiator concentration  $I_0/G = 1.49$  mmoles  $\text{kg}^{-1}$ ; (3) initial initiator concentration  $I_0/G = 1.09$  mmoles  $\text{kg}^{-1}$ ; (4) initial initiator concentration  $I_0/G = 0.79$  mmoles  $\text{kg}^{-1}$ .

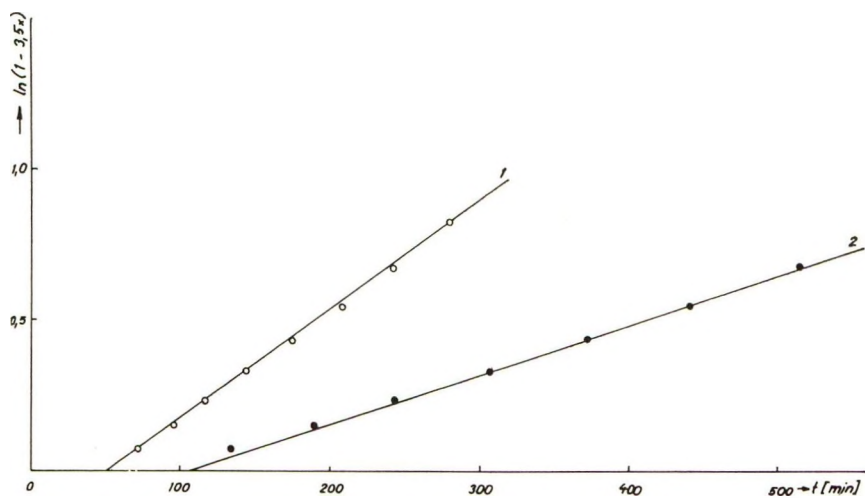
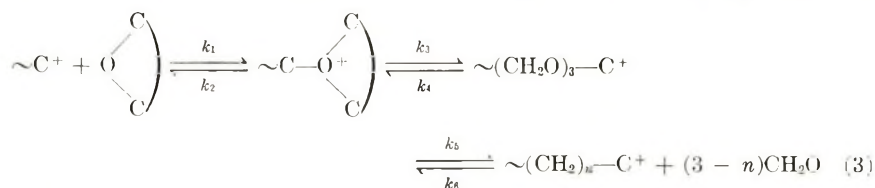


Fig. 5. Temperature dependence of  $\ln [1 - k_e(N_0 - N)]$  at 70°C. Symbols as in Fig. 1,  $x = N_0 - N/N_0$ .

same mechanism simplified by neglecting the reverse reactions from right to left in a few instances was assumed also by other workers, e.g., Jaacks.<sup>8)</sup>



The effect of the counterion is neglected in eq. (3).  $n$  stands for the number of formaldehyde molecules which prolong the polyoxymethylene chain upon trioxane addition; it may be 0, 1, 2, or 3.

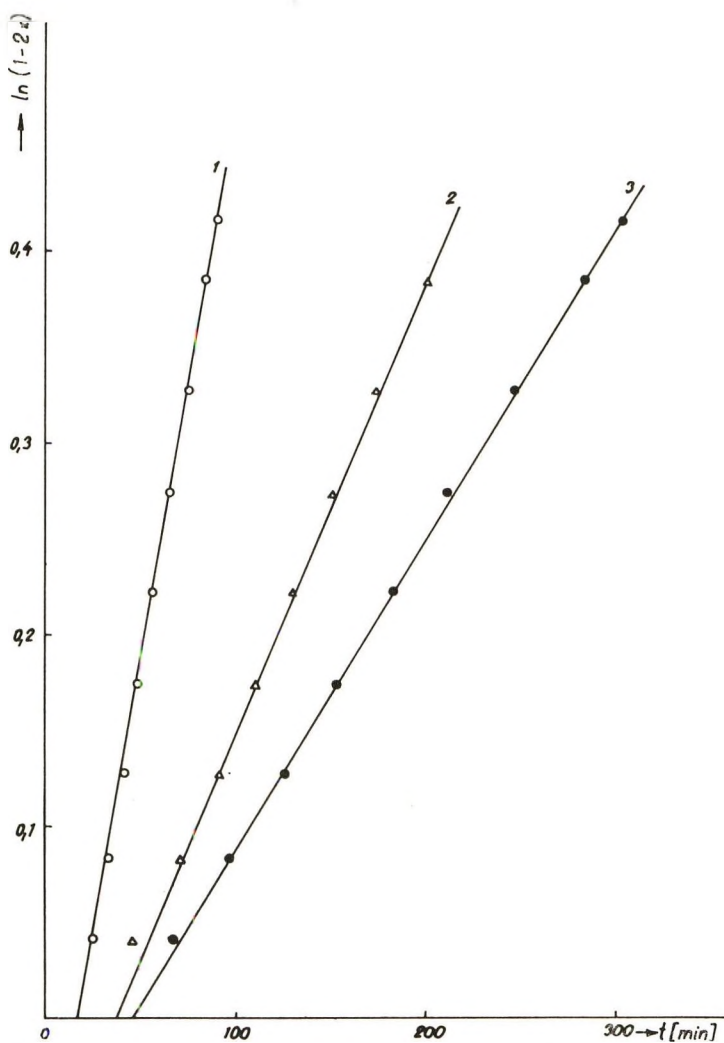


Fig. 6. Temperature dependence of  $\ln [1 - k_2(N_0 - N)]$  at 80°. Symbols as in Fig. 2.

Equation (1) which describes the course of trioxane polymerization is accurately obeyed under our experimental conditions although it cannot be used to determine unambiguously the rate-controlling step; this step can be either a bimolecular reaction of an active center with a trioxane molecule or the decomposition of a transitional complex.

The rate-controlling step can be determined by a more detailed analysis of eq. (3). If the initiation reaction is quick, the whole of the dosed initiator will react in the active centers; therefore the concentration of active centers in the liquid phase will be identical with the concentration of the initiator. To simplify notation let us write  $C$  for the concentration of active centers  $-C^+$ ,  $N$  for the number of molecules of trioxane, and  $O'$  for the number of molecules of transitional complex,  $C-O^+-C-C$ .

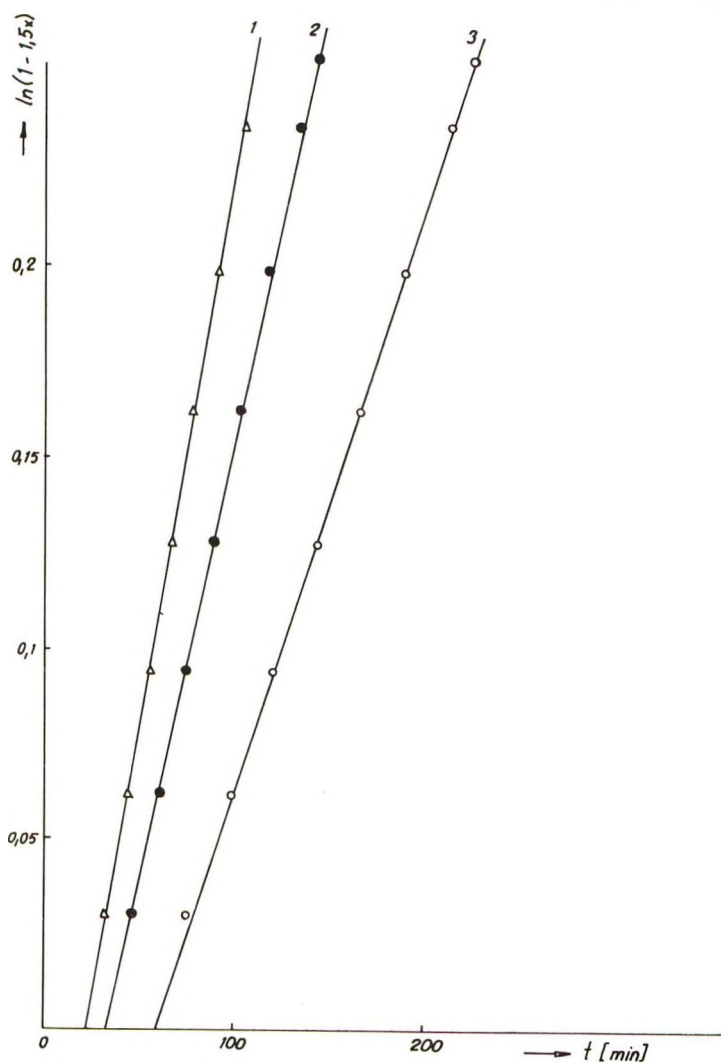


Fig. 7. Temperature dependence of  $\ln [1 - k_p(N_0 - N)]$  at 85°C. Symbols as in Fig. 3.

The rate of change of the number of moles of  $O'$  in the liquid phase of the polymerizing system is given by

$$\begin{aligned} (1/G)(dO'/dt) &= k_1(N/G)C + k_4C - (k_2 + k_3)(O'/G) \\ &= C[k_1(N/G) + k_4] - (k_2 + k_3)(O'/G) \end{aligned} \quad (4)$$

and using expressions derived earlier<sup>12</sup> for  $C$  and  $N$ , we have

$$\begin{aligned} (1/G)(dO'/dt) &= (I_0/G)[k_1(N/G) + k_4][1 - k_5(N_0 - N)] - \\ &\quad (k_2 + k_3)(O'/G) \end{aligned} \quad (5)$$

and

$$dO'/dt = [I_0(k_1 + k_4M)/M]e^{-(kk_5I_0/M)t} - (k_2 + k_3)O' \quad (6)$$

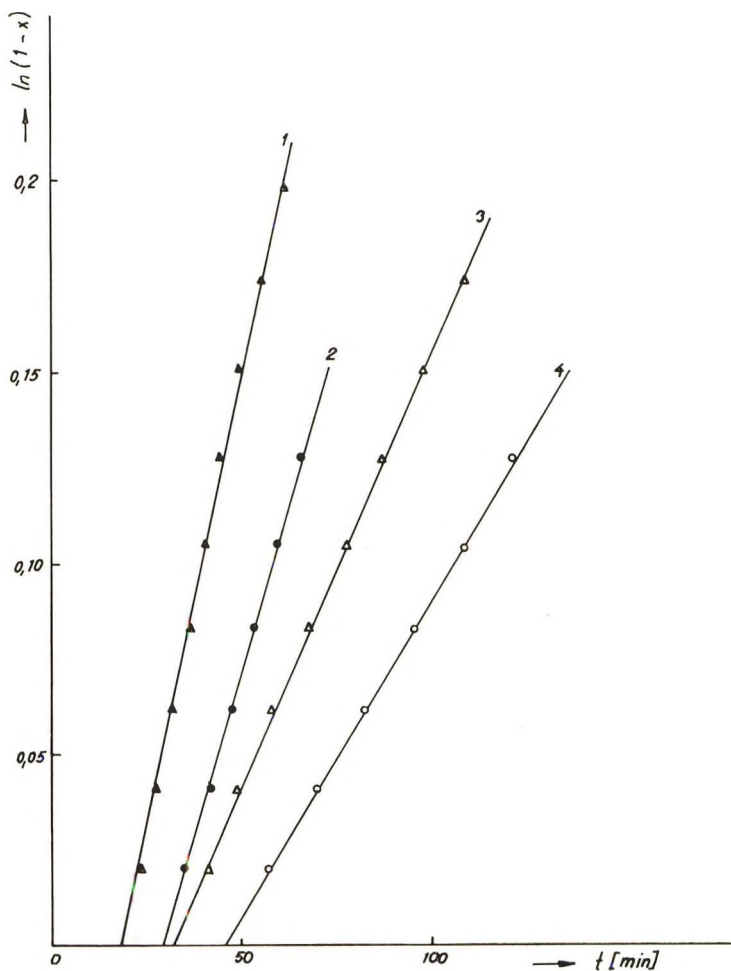


Fig. 8. Temperature dependence of  $\ln [1 - k_5(N_0 - N)]$  at  $90^\circ\text{C}$ . Symbols as in Fig. 4.

In deriving eq. (4) we make use of the assumption that starting from a certain low conversion the concentration of  $\text{CH}_2\text{O}$  in the liquid phase during the polymerization of trioxane is constant. This is in good agreement with published data.<sup>8</sup>

Integration of eq. (6) yields

$$O' = \frac{(k_1 + k_4M)I_0}{(k_2 + k_3)M - kk_sI_0} [e^{-(kk_sI_0/M)t} - e^{-(k_2 + k_3)t}] \quad (7)$$

Equation (7) has meaning only if  $(k_2 + k_3)M > kk_sI_0$ . Analysis of the expression  $(k_2 + k_3)M - kk_sI_0$  (substituting for  $k_3$  or  $k_1$ ) shows that the condition  $(k_2 + k_3)M \gg kk_sI_0$  is always fulfilled and accordingly

$$O' \doteq \frac{(k_1 + k_4M)I_0}{(k_2 + k_3)M} e^{-(kk_sI_0/M)t} \quad (7a)$$

The rate of decrease of  $N$  must be a function of the "equilibrium" concentration  $O'$ . The fact that polymer is formed proves that  $k_3O' > k_4C$ . Neglecting  $k_4C$  against  $k_3O'$  in the first approximation we have (as the polymerization of trioxane is a precipitation reaction—the product falls out as a solid phase—no great error seems to be introduced by neglecting the reverse reaction)

$$-(1/G)(dN/dt) = k_3(O'/G) \quad (8)$$

from which after substitution from eq. (7a) and integration with appropriate boundaries we obtain:

$$\frac{N_0 - N}{N_0} = \frac{k_3(k_1 + k_4M)}{(k_2 + k_3)kk_sN_0} [1 - e^{-(kk_sI_0/M)t}] \quad (9)$$

A comparison of eq. (9) with eq. (1) shows that

$$k = \frac{k_3(k_1 + k_4M)}{k_2 + k_3} \quad (10)$$

The number of moles of  $O'$  cannot at any moment of the polymerization exceed the number of initiator  $I_0$ . Since the expression

$$[e^{-(kk_sI_0/M)t} - e^{-(k_2 + k_3)t}]$$

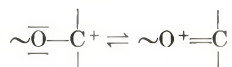
in eq. (7) assumes values near unity in a certain period of polymerization, the relation

$$\frac{k}{k_3} = \frac{k_1 + k_4M}{k_2 + k_3} < 1 \quad (11)$$

must hold, as a substitution from eq. (10) into eq. (7) proves; in other words,  $k < k_3$ . Accordingly the decomposition of the transitional complex  $O'$  cannot be the rate-controlling step. The rate constant of complex decomposition must be larger than the measured constant of the overall reaction rate.

It follows from the above consideration that the formation of the transitional complex  $O'$  is the controlling step. The empirical constant  $k$  from eq. (1) can therefore be identified with  $k_1$  from eq. (3) (i.e., when  $k_1NC \gg k_2O'$ ; the agreement of eqs. (1) and (2) with experiment bears out this assumption).

A further consequence of the above considerations are the inequalities  $k_1k_2 = a < 1$  and  $k_3k_4M = a < 1$ ; hence  $k_4M < k_2$ . This conclusion agrees with the assumptions made so far about the qualities of individual components taking part in the reaction. For one thing  $\sim C^+$  is probably stabilized by mesomery



Upon formation of the complex, the C—O—C bonds are being deformed, which requires a certain amount of energy. On the other hand the splitting of the complex can proceed smoothly: the energies due to internal strain of the cycle and to bond deformation through complex formation are liberated.

All of the above considerations hold true under the assumption that the initiation is very quick. This seems to contradict the conclusion just made, viz., that the rate of formation of the transitional complex is slow. Even during initiation such a complex ought to form slowly and active centers ought to form slowly too. This apparent disagreement can be explained away by the function of formaldehyde in the system. Discussion of this aspect will be published in a forthcoming paper.

Values of individual constants are summarized in Table I. Figure 9 shows the graphical dependence of rate constants on temperature. Activation energies are shown in Table II.

TABLE I  
Rate Constants of Initiator Deactivation  $k_s$ , Rate Constant of Interaction of Active Centers with Trioxane Molecules  $k_1$ , and Values of  $k_3k_4/k_2$

Temp. $t$ , °C.	$k_s$ , kg. mole <sup>-1</sup> min. <sup>-1a</sup>	$k_1$ , kg. mole <sup>-1</sup> min. <sup>-1</sup>	$k_3k_4/k_2$ , min. <sup>-1</sup>
70	0.346	0.215	2.39
75	0.345	0.560	6.22
80	0.181	0.570	6.43
85	0.135	1.720	19.10
90	0.090	2.180	24.20

<sup>a</sup>  $N_0 = 11.1$  mole. See Kucera and Spousta.<sup>12</sup>

TABLE II  
Activation Energies  $E$  of the Rate Constants

	$E$ , kcal. mole <sup>-1</sup>
$k_s$	$-6.5 \pm 2.2$
$k_1$	$28.3 \pm 4.8$
$k_3k_4/k_2$	$28.3 \pm 4.8$

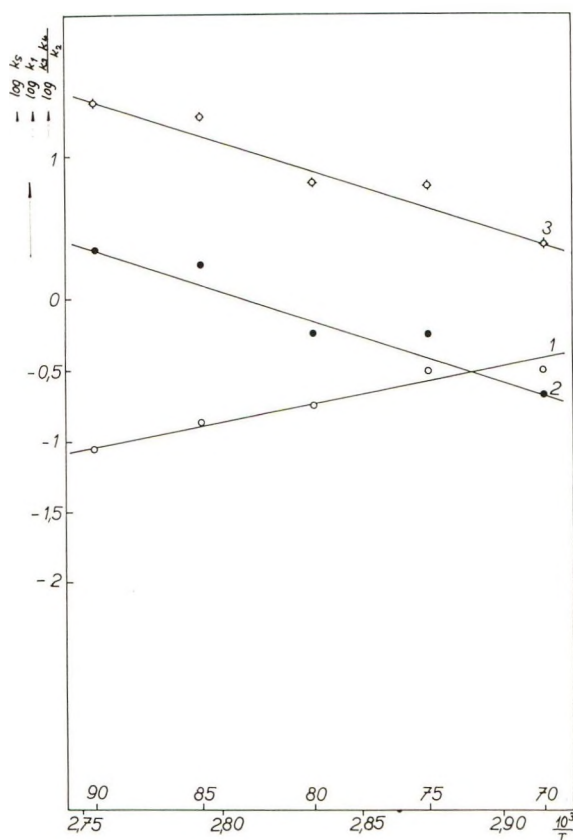


Fig. 9. Temperature dependence of the rate constants: (1) temperature dependence of  $k_a''$ ; (2) temperature dependence of  $k_1$ ; (3) temperature dependence of  $k_3k_4/k_2$ .

### Conclusion

Analysis of the course of conversion curves of molten trioxane polymerization has established the rate-controlling step, the magnitude of rate constants of interaction of trioxane molecules with the active centers, and the rate constants of initiator deactivation. Information concerning the mechanism and rate of initiation and rate constants of reversible processes which would complete the kinetic analysis is not available so far.

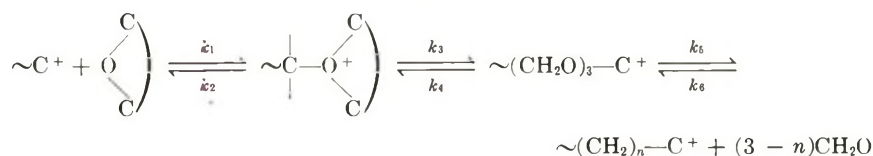
### References

1. Sack, H., Belg. Pat. 612,792 (Feb. 15, 1962).
2. Hudgin, D. E., Summit, and F. M. Berardinelli, U. S. Pat. 2,989,507 (June 20, 1961).
3. Hudgin, D. E., Summit, and F. M. Berardinelli, U. S. Pat. 2,989,506 (June 20, 1961).
4. Hudgin, D. E., Summit, and F. M. Berardinelli, U. S. Pat. 2,989,508 (June 20, 1961).

5. Hudgin, D. E., Summit, and F. M. Berardinelli, U. S. Pat. 2,989,505 (June 20, 1961).
6. Schneider, A. K., U. S. Pat. 2,795,571 (June 11, 1961).
7. Deutsche Gold- und Silber-Scheideanstalt, Fr. Pat. 1,260,237 (March 27, 1961).
8. Jaacks, V., Dissertation, Mainz, 1959.
9. Okamura, S., K. Hayashi, and J. Kitanishi, *J. Polymer Sci.*, **58**, 925 (1962).
10. Okamura, S., T. Higashimura, and K. Takeda, *Makromol. Chem.*, **51**, 217 (1962).
11. Kern, W., and V. Jaacks, *J. Polymer Sci.*, **48**, 399 (1960).
12. Kučera, M., and E. Spousta, in preparation.
13. Kučera, M., and E. Spousta, *Chem. Listy*, **57**, 842 (1963).

### Résumé

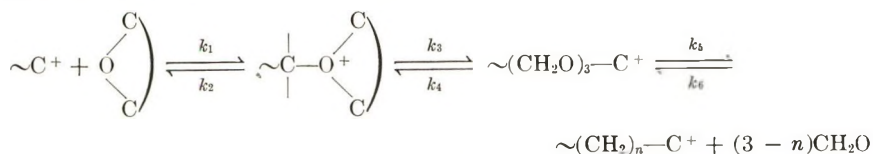
Des courbes de conversion de la polymérisation du trioxane à l'état fondu ont été obtenues à des températures se situant entre 70° et 90°C. Leur analyse a montré que l'étape déterminante de la vitesse de la réaction:



est l'addition d'une molécule de trioxane à un centre actif. Les valeurs des constantes de vitesse  $k_1$  et  $k_3k_4/k_2$  ainsi que les constantes de vitesse de désactivation de l'initiateur  $k_6$  ont été déterminées. La désactivation de l'initiateur provoque une déviation prématurée des courbes de conversion spécialement à des températures de polymérisation plus basses (70°–80°C.). Les énergies d'activation des constantes de vitesse ont été déterminées.

### Zusammenfassung

Die Umsatzkurven für die Polymerisation von geschmolzenem Trioxan wurden bei Temperaturen zwischen 70 und 90°C gemessen. Ihre Analyse hat gezeigt, dass der geschwindigkeitsbestimmende Schritt der Reaktion



die Addition eines Trioxanmoleküls an das aktive Zentrum ist. Es wurden sowohl Werte der Geschwindigkeitskonstanten  $k_1$  und  $k_3k_4/k_2$ , als auch die Geschwindigkeitskonstanten der Starterdesaktivierung  $k_6$  bestimmt. Die Starterdesaktivierung verursacht eine frühzeitige Krümmung der Umsatzkurven, besonders bei niedrigeren Polymerisationstemperaturen (70–80°C.). Die Aktivierungsenergie der Geschwindigkeitskonstanten wurden bestimmt.

Received August 29, 1963

## Initiation of the Bulk Polymerization of Trioxane

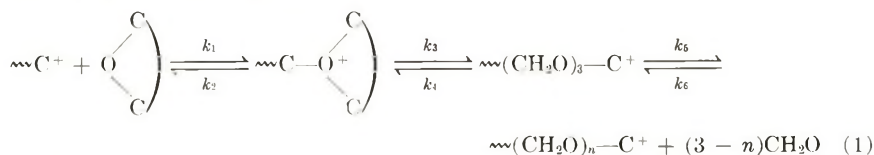
MILOSLAV KUČERA and EDUARD SPOUSTA,

*Research Institute of Macromolecular Chemistry, Brno, Czechoslovakia*

### Synopsis

Kinetic analysis of the induction periods of trioxane polymerization shows that although the interaction of the initiator with a trioxane molecule is slow, the reaction of the initiator with free formaldehyde (followed by the splitting of trioxane) is quick and yields active centers. Kinetic relations have been developed for the amount of free formaldehyde in the first stages of the reaction between the initiator and trioxane, for the rate of formation of active centers and for the time dependence of the conversion of trioxane during the induction period. Kinetic formulas are compared with experimental data.

In a previous communication the present authors<sup>1</sup> presented an analysis of the course of conversion curves of the bulk polymerization of molten trioxane. The chain growth of polyoxymethylene has been assumed to take place by the mechanism<sup>1</sup>



It has been proved that the rate-controlling step can be only a bimolecular interaction of an active center with a trioxane molecule. Assuming a high rate of initiation, kinetic relationships were derived and the overall rate constant was shown to be identical with  $k_1$ .

At first sight the above assumption seems incorrect. If the initiation were to take place according to eq. (1) ( $\sim C^+$  would be replaced by an initiating acid) this step could not be quick. To explain this apparent contradiction it is necessary to consider another factor, viz., the presence of free formaldehyde in the system. The importance of free formaldehyde in the polymerizing system has first been stressed by Jaacks.<sup>2</sup>

### Experimental

Trioxane was brought to temperature in a thermostatted reactor with bottom outlet and was mixed with a required quantity of  $\sim \text{Si}^+ \text{HSO}_4^-$  initiator dissolved in cyclohexane;<sup>1</sup> the mixture was stirred and samples were withdrawn at definite time intervals into beakers half filled with

water. Free formaldehyde in the trioxane-initiator system was determined iodometrically<sup>4</sup> in aqueous solution. Other details of experimental technique are being published.<sup>3</sup>

### Results

The time dependence of the concentration of free formaldehyde in the trioxane-initiator system at 70, 80, and 90°C. is shown in Figure 1. This concentration is directly proportional to time up to the moment when

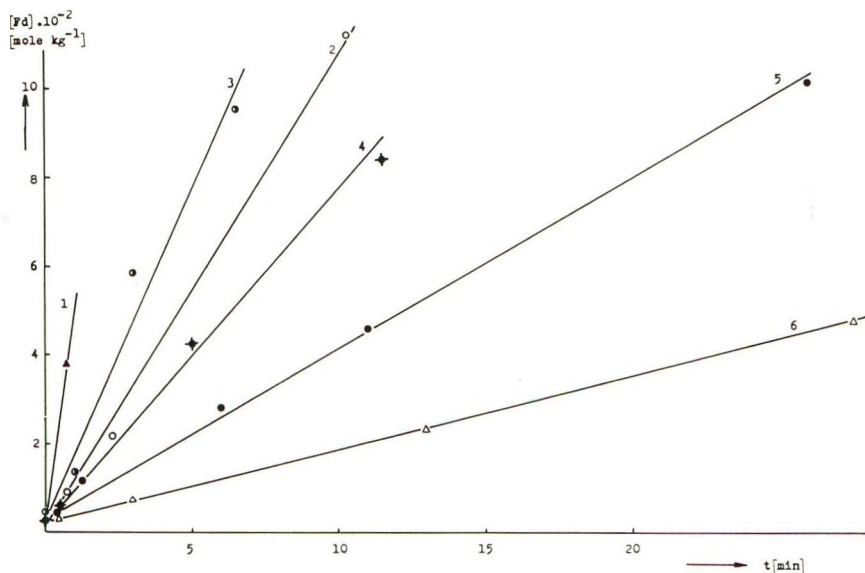


Fig. 1. Time dependence of the amount of formaldehyde liberated from trioxane at various initiator concentrations and temperatures: (1) 90°C., initiator concentration  $I_0/G = 5.1 \times 10^{-4}$  mole kg.<sup>-1</sup>; (2) 90°C.,  $I_0/G = 1.4 \times 10^{-4}$  mole kg.<sup>-1</sup>; (3) 80°C.,  $I_0/G = 4.3 \times 10^{-4}$  mole kg.<sup>-1</sup>; (4) 80°C.,  $I_0/G = 2.4 \times 10^{-4}$  mole kg.<sup>-1</sup>; (5) 70°C.,  $I_0/G = 2.7 \times 10^{-4}$  mole kg.<sup>-1</sup>; (6) 70°C.,  $I_0/G = 1.3 \times 10^{-4}$  mole kg.<sup>-1</sup>.

polymer settles out. The quantity of formaldehyde liberated from trioxane after equal time lapses is proportional to the initiator concentration, as is shown in Figure 2.

Analogous measurements were made also at 75 and 85°C. These results are in basic agreement with results mentioned above.

The rate of polymerization of trioxane reaches its maximum after a certain time, as is seen from the conversion curves.<sup>1</sup> We tried to find why this is so.

### Discussion

Jaacks has shown in his work<sup>2</sup> that polymerization of trioxane takes place only after a certain amount of formaldehyde has been set free. The concentration of free formaldehyde required for the polymerization to start

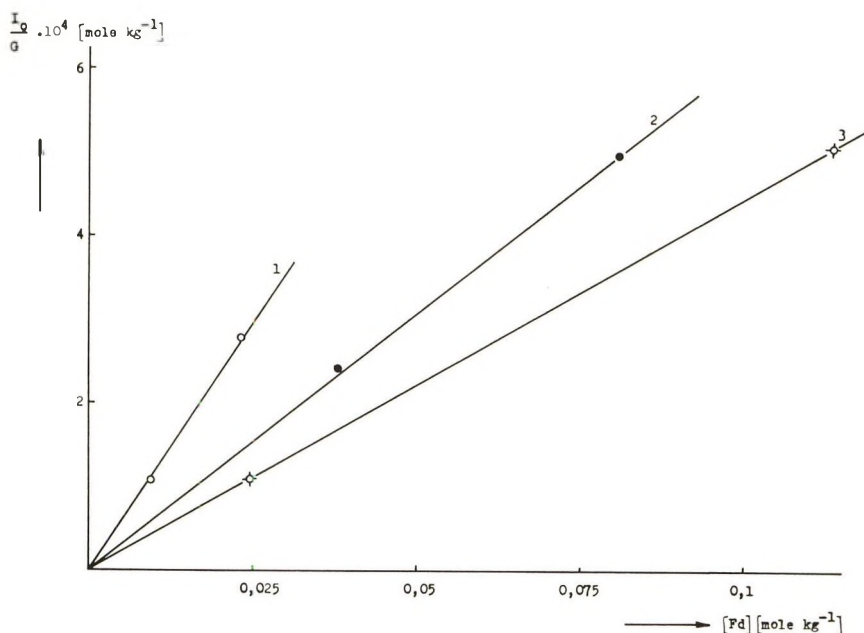
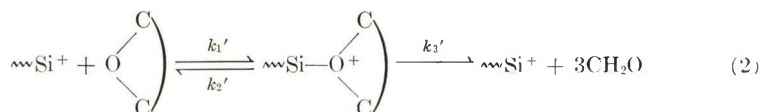


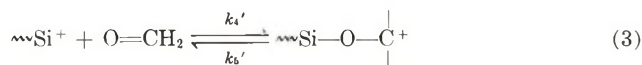
Fig. 2. Relation between the initial concentration of initiator and the amount of formaldehyde liberated from trioxane in constant time: (1) 70°C., 5 min.; (2) 80°C., 5 min.; (3) 90°C., 2.5 min.

is a function of thermodynamic factors of the reaction. Let us consider two stages of initiation:

First stage:



Second stage:



The first stage is slow; there is practically no polymerization in the initial stages, since  $\text{CH}_2\text{O}$  is not present in the necessary equilibrium concentration. While the concentration of formaldehyde increases, free  $\text{CH}_2\text{O}$  molecules react (one or more at a time) very quickly with  $\sim\text{Si}^+$  with the formation of an active center  $\sim\text{C}^+$ . The occurrence of complicated processes in the initial stages of the polymerization results in a dynamic equilibrium between  $\sim\text{Si}^+$ ,  $\sim\text{Si}-\text{O}^+-\text{C}-\text{C}$ ,  $\text{CH}_2\text{O}$ ,  $\sim\text{C}^+$ ,

$\sim\text{C}-\text{O}^+-\text{C}-\text{C}$ , and later on, polymer.

Let us introduce the symbol  $\text{O}'$  for  $\sim\text{Si}-\text{O}^+-\text{C}-\text{C}$  and let us examine

the rate of change of  $O'$  with time ( $G$  is the weight of the liquid phase of the system; since initiation occurs practically in homogeneous phase,  $G = \text{constant} = 1 \text{ kg.}$ ; it is being used for the sake of dimensional homogeneity). Molecules of trioxane are designated as  $N$ , the molecular weight of trioxane as  $M$  (in kilograms/mole) and the initial number of moles of initiator as  $I_0$ .

Then

$$(dO'/Gdt) = k_1'(I_0/G)(N/G) - (k_2' + k_3')(O'/G) \quad (4)$$

Integration of eq. (4) yields

$$O' = [k_1'I_0/(k_2' + k_3')M](1 - e^{-(k_2' + k_3')t}) \quad (5)$$

The number of moles of liberated formaldehyde ( $F$ ) is given by

$$dF/dt = 3k_3'O' \quad (6)$$

from which, after substitution from eq. (5) and integration, there is obtained

$$\begin{aligned} F &= \frac{3k_3'k_1'I_0}{(k_2' + k_3')M} \left[ t - \frac{1}{k_2' + k_3'} + \frac{e^{-(k_2' + k_3')t}}{k_2' + k_3'} \right] \\ &\doteq \frac{3k_3'k_1'I_0}{(k_2' + k_3')M} \left( t - \frac{1}{k_2' + k_3'} \right) \\ &\doteq \lambda \left( t - \frac{1}{k_2' + k_3'} \right) \frac{I_0}{M} \end{aligned} \quad (7)$$

(for  $1/(k_2' + k_3') < t < t_{\text{induction}}$ ).

Therefore the quantity of formaldehyde liberated upon addition of the initiator in the initial stages (before reactions leading to its loss through polymerization become important) is proportional to the initial number of moles of initiator and to time. Figures 1 and 2 show that this is the case.

Equation (3) leads to the dependence of the moles of active centers  $A$  on time as follows (see also Kučera and Spousta<sup>3</sup>); the loss of active centers through their deactivation is neglected):

$$dA/Gdt = k_4'(I_0/G)(F/G) - k_5'(A/G) \quad (8)$$

and after integration and rearrangement

$$A = \frac{k_4'I_0^2\lambda}{MGk_5'} \left[ \frac{(k_2' + k_3') - k_5'}{(k_2' + k_3')k_5'} (e^{-k_5't} - 1) + t \right] \quad (9)$$

For

$$\frac{k_2' + k_3' - k_5'}{(k_2' + k_3')k_5'} (e^{-k_5't} - 1) \ll t$$

there is obtained

$$A \doteq \frac{k_4'I_0^2\lambda}{Gk_5'M} t \doteq \frac{\alpha I_0^2}{GM} t \doteq \frac{3k_1'k_3'k_4'I_0^2}{G(k_2' + k_3')Mk_5'} t \quad (9a)$$

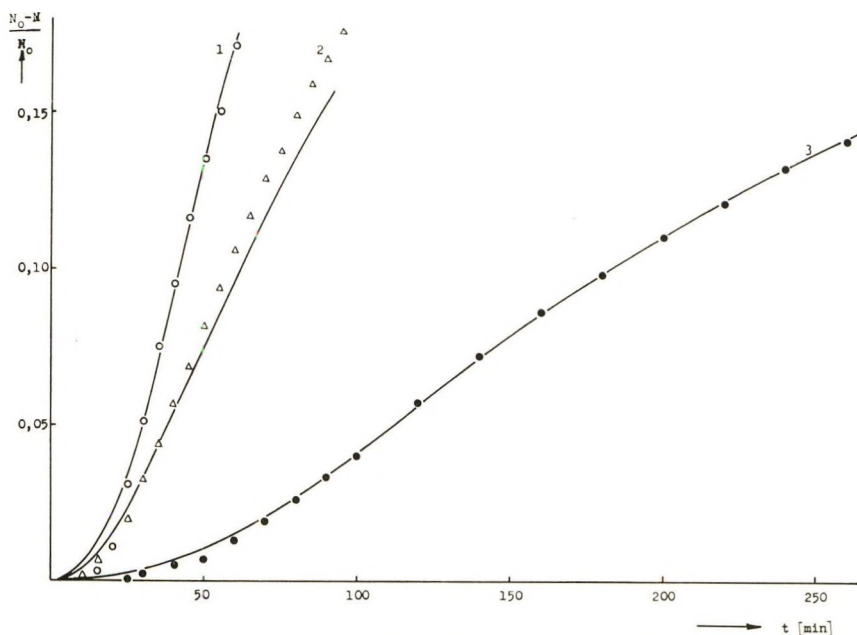


Fig. 3. Comparison of (O, ●, △) experimentally determined conversion curves with (—) the theoretical course: (1) at 90°C.,  $I_0/G = 2.19$  mmole kg.<sup>-1</sup>; (2) 80°C.,  $I_0/G = 4.47$  mmole kg.<sup>-1</sup>; (3) 70°C.,  $I_0/G = 4.47$  mmole kg.<sup>-1</sup>.

Equation (9) is valid only for the induction period, since the validity of eq. (7) used in the derivation is limited to this interval; this is why the actual dependence  $A = f(t)$  does not go through a maximum as eq. (9) would imply.

Substitution of  $A$  from eq. (9a) into a relation describing the change of number of moles of trioxane with time<sup>3</sup> yields

$$-dN/Gdt = k_1(N/G)(A/G) = k_1(A/GM) \quad (10)$$

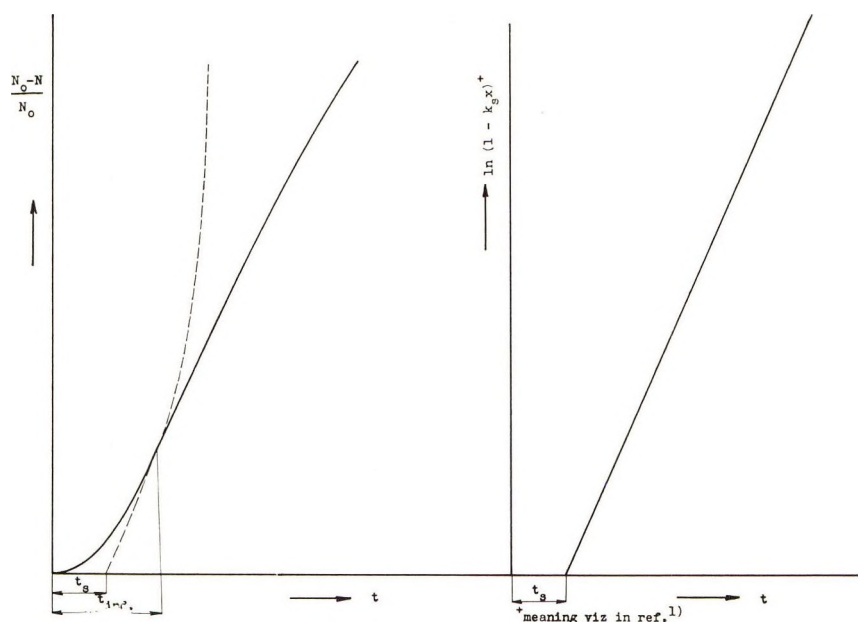
$$-dN/dt = k_1(I_0/M)^2(\alpha/G)t$$

Upon integration we obtain eq. (11) expressing the rate of trioxane disappearance during the induction period as a function of time ( $0 < t < t_{\text{induction}}$ )

$$(N_0 - N)/N_0 = (I_0^2 \alpha / 2G^2 M) k_1 t^2 \quad (11)$$

The value of  $\alpha$  can be estimated with good accuracy from the conversion curves;  $k_4'/k_5'$  can be calculated from eqs. (7), (9), and (11).

The measured value of  $k_4'/k_5' = K_2$  of the second stage of initiation, [eq. (3)] may be only an apparent equilibrium constant. The measured value may also be influenced by thermodynamic factors so far not taken into account, especially at low formaldehyde concentrations (effect of the ceiling temperature). Therefore the actual value of the  $K_2$  constant may be higher than indicated.

Fig. 4. Characterization of  $t_{\text{induction}}$  and  $t_s$ .

The extent to which the above assumptions are fulfilled and simplifications justified is illustrated in Figures 3 and 4, which show the experimental conversion data and the derived theoretical curves as a function of time. For  $0 < t < t_{\text{induction}}$  theoretical curve is based on eq. (11), while for  $t > t_{\text{induction}}$  it is based on the relation:<sup>1</sup>

$$(N_0 - N)/N_0 = (1 - e^{-(k_1 k_2 I_0 / M)t'})/k_s N_0 \quad (12)$$

where

$$t' = t - t_s$$

The range of validity of eqs. (11) and (12) is well visible in Figure 4.

Table I summarizes the constants found.

TABLE I  
Constants of Initiation Reactions<sup>a</sup>

Temp. $t$ , °C.	$\lambda = \frac{k_1' k_3'}{k_2' + k_3'}$ , kg. mole <sup>-1</sup> min. <sup>-1</sup>	$K_s = \frac{k_4'}{k_5'}$ , kg. mole <sup>-1</sup>	$\alpha = \lambda K_s$ , kg. <sup>2</sup> mole <sup>-2</sup> min. <sup>-1</sup>
70	0.39	0.13	0.05
75	0.40	0.70	0.28
80	0.94	0.19	0.18
85	1.47	0.35	0.51
90	2.29	0.14	0.32

<sup>a</sup> The temperature dependence of  $\lambda$  is  $E_\lambda = 23.7 \pm 3.25$  kcal. mole<sup>-1</sup>.

The value of  $\lambda$  and its changes with temperature are practically identical with the  $k_1$  values.<sup>3</sup> This may indicate that  $k_2'$  is very small; i.e., the decomposition of the complex into original components—viz. eq. (2)—is practically negligible, and then  $k_1'$  would nearly approach the value of  $k_1$  [eq. (1)].

### Conclusion

The active part played by formaldehyde in initiation reactions can help to explain the existence of the induction period in trioxane polymerization. The formation of active centers by a quick reaction between formaldehyde and the initiator explains the apparent contradiction between an assumed quick initiation on the one hand and a slow interaction of active centers with trioxane, derived from kinetic considerations, on the other hand.

Kinetic evidence supports this view. The initiation of trioxane polymerization differs from that of other heterocycles of the tetrahydrofuran, oxycyclobutane, etc. type by its high speed. The above considerations explain why polymerization of heterocycles in which no formaldehyde liberated is slow and why the kinetics of such processes is complicated. The presence of a small amount of formaldehyde (or other substances quickly reacting with acids, e.g., ethylene oxide) accelerates the polymerization of heterocycles.<sup>5</sup> These conclusions are of general validity.

### References

1. Kučera, M., and E. Spousta, *J. Polymer Sci.*, **A2**, 3431 (1964).
2. Jaacks, V., Dissertation, Mainz (1959).
3. Kučera, M., and E. Spousta, in preparation.
4. Goldman, F. G., and H. Yagoda, *Ind. Eng. Chem. Anal. Ed.*, **15**, 376 (1943).
5. Saegusa, T., M. Imai, and J. Furukawa, *Makromol. Chem.*, **54**, 218 (1962).

### Résumé

Une analyse cinétique des périodes d'induction dans la polymérisation du trioxane montre que l'interaction de l'initiateur avec les molécules de trioxane est lente, tandis que la réaction de l'initiateur avec le formaldéhyde libre (suivie de la désintégration du trioxane) est rapide et donne des centres actifs. Des relations cinétiques ont été développées pour déterminer la quantité de formaldéhyde libre dans les premières phases de la réaction entre l'initiateur et le trioxane pour la vitesse de formation des centres actifs et pour la dépendance vis-à-vis du temps de conversion du trioxane pendant la période d'induction. Des formules cinétiques sont comparées avec des données expérimentales.

### Zusammenfassung

Die kinetische Analyse der Induktionsperiode der Trioxanpolymerisation zeigt, dass die Reaktion des Starters mit freiem Formaldehyd (gefolgt von der Aufspaltung von Trioxan) trotz langsamer Wechselwirkung zwischen Starter und Trioxanmolekül schnell erfolgt und aktive Zentren erzeugt. Es wurden kinetische Beziehungen für den Anteil an freiem Formaldehyd in den ersten Stufen der Reaktion zwischen dem Starter und Trioxan, für die Bildungsgeschwindigkeit der aktiven Zentren und die Zeitabhängigkeit der Trioxanumwandlung während der Induktionsperiode entwickelt. Die kinetischen Formeln wurden mit den Versuchsergebnissen verglichen.

Received August 29, 1963

## A Method of Estimating Molecular Weight Distributions of Polymer Fractions

HIROSHI OKAMOTO, *The Electrical Communication Laboratory, Nippon Telegraph and Telephone Public Corporation, Musashino-shi, Japan*

### Synopsis

A method of estimating molecular weight distributions of polymer fractions which was proposed previously is investigated. The distribution curves calculated by the proposed method are compared to the experimental curves. Several numerical experiments are also carried out to discuss a nonsystematic change of the fractionation parameters.

### Introduction

In the study of polymer properties, molecular weight distribution is very important. Polymer samples are usually separated into fractions to reduce their polydispersity. However, a monodisperse sample can never be obtained by the usual fractionation procedures. Therefore, the polydispersity of polymer fractions has always been an important factor in the various polymer studies.

In a previous paper, a method of estimating molecular weight distributions of polymer fractions was proposed by Okamoto and Sekikawa<sup>1</sup> from their study of phase equilibria of polydisperse polymer solutions. The proposed method has been tried, and the results are described in this paper.

### Brief Description of the Method

Consider a two-phase equilibrium (liquid-liquid) of a polydisperse polymer solution. The molecular weight distribution of the polymer is known as  $f_0(x)$ . The weight fraction of the polymer in the concentrated phase is  $W$ . The ratio of the volume of the dilute phase to that of the concentrated phase is  $R$ . It was found that the molecular weight distribution of the polymer in the dilute phase  $f_{a,1}(x)$  is given by<sup>1</sup>

$$f_{a,1}(x) = \left( \frac{1}{1-W} \right) \frac{R \exp \{ -\sigma x^\alpha \}}{1 + R \exp \{ -\sigma x^\alpha \}} f_0(x) \quad (1)$$

and  $f_{b,1}(x)$  that of the polymer in the concentrated phase or the first fraction

$$f_{b,1}(x) = \left( \frac{1}{W} \right) \frac{1}{1 + R \exp \{ -\sigma x^\alpha \}} f_0(x) \quad (2)$$

where  $\alpha$  and  $\sigma$  are unknown fractionation parameters. In the case where  $\alpha = 1$ , the above relations reduce to those obtained by Flory.<sup>2</sup> From eq. (2), the weight fraction  $W$  and the weight-average molecular weight  $\bar{x}$  of the polymer in the concentrated phase or of the first fraction are given by

$$W = \int_0^\infty \frac{f_0(x)}{1 + R \exp \{-\sigma x^\alpha\}} dx \quad (3)$$

and

$$\bar{x} = \frac{1}{W} \int_0^\infty \frac{x f_0(x)}{1 + R \exp \{-\sigma x^\alpha\}} dx \quad (4)$$

In eqs. (3) and (4),  $W$ ,  $\bar{x}$ , and  $R$  are experimentally obtainable quantities, and  $f_0(x)$  is assumed to be known; therefore, these equations can be regarded as a simultaneous equation with two unknowns  $\alpha$  and  $\sigma$  and can be solved by numerical calculations. The molecular weight distributions  $f_{a,1}(x)$  and  $f_{b,1}(x)$  can be calculated by substituting the solved values of  $\alpha$  and  $\sigma$  into eqs. (1) and (2). When the dilute solution phase is further fractionated, the distribution of the second fraction  $f_{b,2}(x)$  can be calculated in a similar way by the replacement of  $f_0(x)$  with  $f_{a,1}(x)$ . Further repetition of the above procedure yields the distribution of any fraction.

Linear polyethylene (Marlex 6009) was successively fractionated into 11 fractions. The first, the fourth, the fifth, and the last fraction were further fractionated to determine their molecular weight distributions. The distributions were also calculated by the proposed method, and the two distributions were compared.

### Experimental

The fractionation apparatus used is shown in Figure 1. The whole apparatus was immersed in an oil bath at  $120 \pm 0.1^\circ\text{C}$ . About 0.5 g./100 ml.

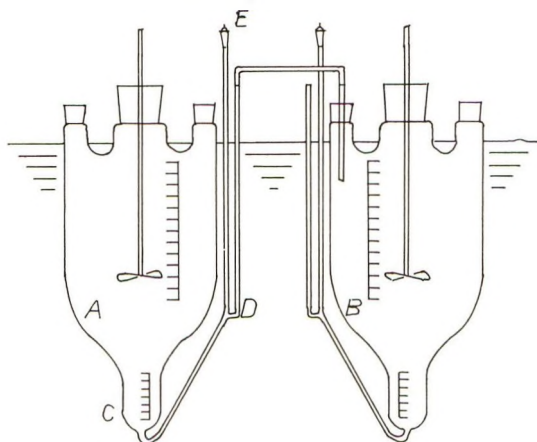


Fig. 1. Schematic diagram of the fractionation apparatus.

solution of linear polyethylene Marlex 6009 in xylene was prepared in flask A. Polyethylene glycol of molecular weight 400, which is nonsolvent, was added slowly until an appropriate amount of concentrated phase was produced. After a vigorous agitation of the solution, equilibrium was considered to be attained. The concentrated phase settled at the top of the solution. The total volume of the solution was measured by a mark on the wall of the flask. The dilute phase was then drained through the glass tube D into the neighbor flask B by suction. When the boundary between the dilute and the concentrated phase reached the bottom of the flask A, the plug E was opened; thus the concentrated phase remained in the narrow part C of the flask. The volume of the concentrated phase was measured in this stage. Discrimination of the boundary between the

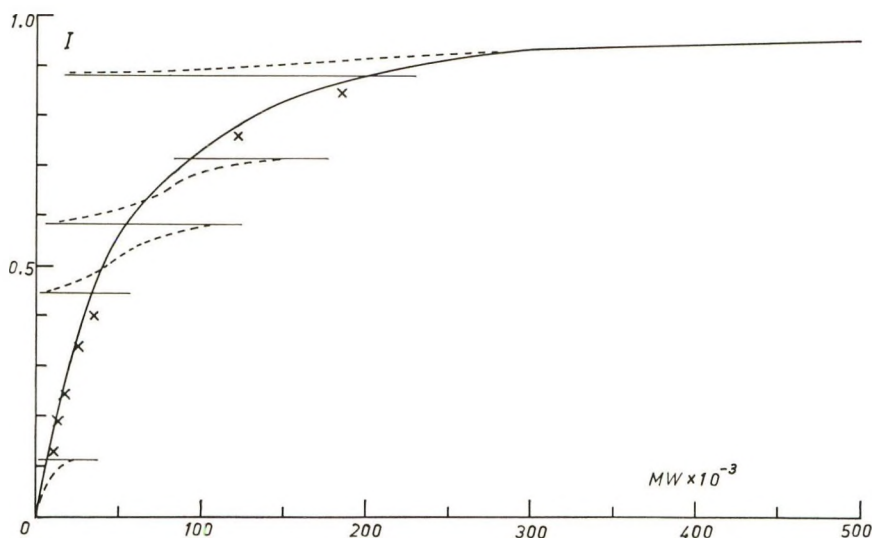


Fig. 2. Integral molecular weight distribution of Marlex 6009; (—) obtained by combining fractionation data (X) and refractionation data (---).

two phases is often difficult. Addition of a very small amount of dye, Sudan Black, when nearly all the dilute solution was transferred to B, was very convenient. The dilute phase was colored by the dye but the concentrated phase was not; the boundary could then be clearly observed. The concentrated phase was redissolved in xylene and then poured into a large amount of methanol. The polymer precipitated from methanol was filtered, washed repeatedly with methanol, vacuum-dried, and then weighed as the first fraction. Further fractionation consisted of repetition of the above procedure for the remaining dilute phase. The second, the third, . . . , and the tenth fraction were obtained successively. The residual solution was the last fraction. The first, the fourth, the fifth, and the last fraction were refractionated to obtain their distributions.

The molecular weight of every fraction was determined through solu-

tion viscosity measurement. The solvent was tetralin at 130°C. The intrinsic viscosity-molecular weight relation derived by Tung<sup>3</sup> was used:

$$[\eta] = 4.6 \times 10^{-4} M^{0.725} \quad (5)$$

The integral molecular weight distribution of the unseparated polymer  $I_0(x)$ , which is shown in Figure 2, was evaluated by combining the first fractionation data shown in Table I and the experimental refractionation data. They are represented by crosses and dotted lines in Figure 2.

TABLE I  
Fractionation Data of Marlex 6009

Fraction No.	$w^a$	$\bar{M}$	$R$	$\alpha$	$\sigma$
1	0.122	547,000	88	1.62	$3.55 \times 10^{-11}$
2	0.073	188,000	182	2.33	$1.52 \times 10^{-14}$
3	0.087	125,000	191	2.00	$1.74 \times 10^{-12}$
4	0.136	71,500	161	0.911	$8.33 \times 10^{-7}$
5	0.131	50,400	204	1.08	$2.18 \times 10^{-7}$
6	0.098	35,200	330	1.56	$2.57 \times 10^{-9}$
7	0.075	22,400	593	1.06	$6.88 \times 10^{-7}$
8	0.063	17,300	841	0.957	$2.64 \times 10^{-6}$
9	0.048	12,600	927	0.699	$3.84 \times 10^{-5}$
10	0.050	9,600	1500	0.488	$3.37 \times 10^{-5}$
11	0.119	6,200			

<sup>a</sup> The ratio of the fraction weight to the total polymer weight. This is not  $W$  in the text.

Though the refractionation of the selected fractions was carried out by the usual procedure, some of the "refractions" were too large (in quantity) and were further fractionated. The distributions of the first and the fourth fraction were evaluated by combining these data as shown in Figures 3 and 4.

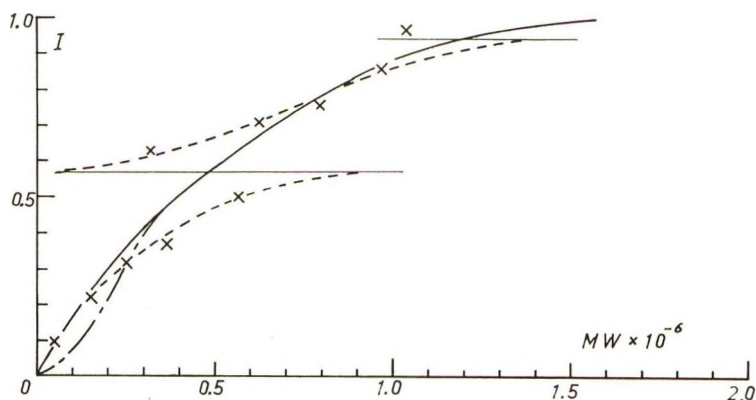


Fig. 3. Comparison of the integral distributions: (—) calculated for the first fraction and (—) the experimental obtained by combining fractionation  $\times$  and refractionation data (—X—).

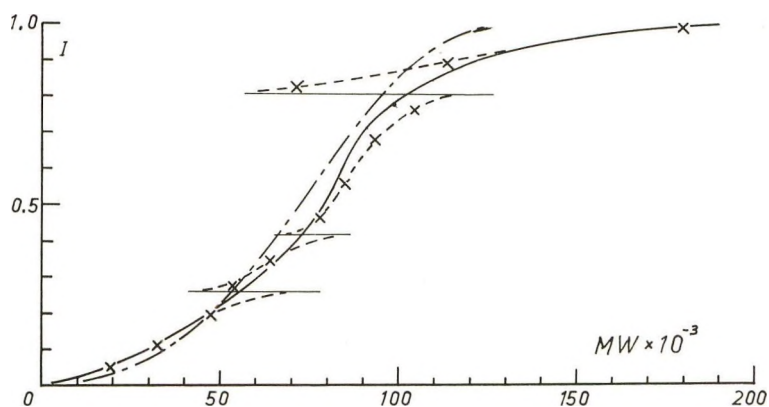


Fig. 4. Comparison of integral distributions: (—) calculated for the fourth fraction and (—) the experimental obtained by combining (X) fractionation, and (- -X - -) refractometry data.

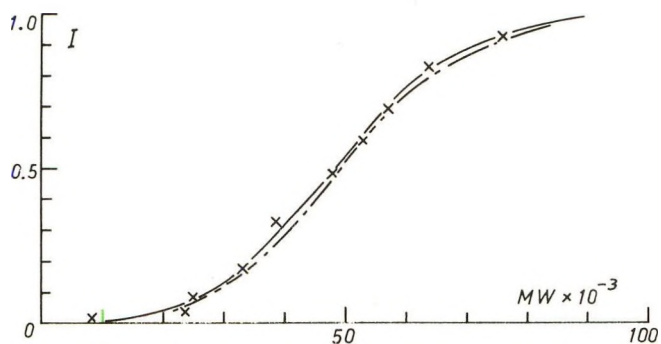


Fig. 5. Integral distributions: (—) calculated for the fifth fraction and (—X—) the experimental distribution.

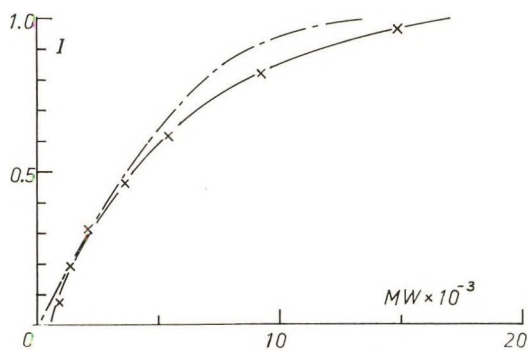


Fig. 6. Comparison of the integral distributions: (—) calculated for the last fraction and (—X—) the experimental.

The other distributions were evaluated by the usual method and are shown in Figures 5 and 6.

### Numerical Calculations

All the distribution curves were handled in integral forms to avoid the errors inherent in graphical differentiation. Equations (3) and (4) for the  $i$ th fractionation step are rewritten in integral forms by using appropriate subscripts  $i$  and  $(i-1)$ :

$$W_i = 1 - R_i \alpha_i \sigma_i \int_0^\infty \frac{x^{\alpha-1} \exp \{ -\sigma_i x^\alpha \} I_{a,i-1}(x)}{[1 + R_i \exp \{ -\sigma_i x^\alpha \}]^2} dx \quad (6)$$

$$\bar{x}_{b,i} = \frac{\bar{x}_{a,i-1}}{W_i} - \frac{R_i \alpha_i \sigma_i}{W_i} \int_0^\infty \frac{x^{\alpha-1} \exp \{ -\sigma_i x^\alpha \} J_{a,i-1}(x)}{[1 + R_i \exp \{ -\sigma_i x^\alpha \}]^2} dx \quad (7)$$

where  $i = 1, 2, 3, \dots$ , and  $I_{a,i-1}(x)$  is the integral distribution of the polymer in the  $(i-1)$ th dilute phase,  $\bar{x}_{a,i-1}$  is its weight-average molecular weight, and  $J_{a,i-1}(x)$  is defined by

$$J_{a,i-1}(x) = \int_0^x x f_{a,i-1}(x) dx \quad (8)$$

and the subscripts  $i$  for  $\alpha$  in the exponent are omitted.

The numerical solutions of  $\alpha_i$  and  $\sigma_i$  of the simultaneous equation were substituted into eq. (9), the rewritten integral form of eq. (2).

$$I_{b,i}(x) = \frac{1}{W_i} \left( \frac{I_{a,i-1}(x)}{1 + R_i \exp \{ -\sigma_i x^\alpha \}} - R_i \alpha_i \sigma_i \int_0^x \frac{x^{\alpha-1} \exp \{ (-\sigma_i x^\alpha) \} I_{a,i-1}(x)}{[1 + R_i \exp \{ -\sigma_i x^\alpha \}]^2} dx \right) \quad (9)$$

All the calculations were made by an electronic computer. The comparison of the experimental and the calculated curves is shown in Figures 3-6. The agreement is fairly good. The best agreement was obtained for the fifth fraction. The number-average molecular weight of the fourth fraction from the calculated curves is 52,000 and 60,000 from an osmotic measurement. The values of the calculated  $\alpha_i$  and  $\sigma_i$  are listed in Table I.

As the fractionation step proceeded, a systematic change of the values of  $\alpha_i$  and  $\sigma_i$  was at first expected. Contrary to this expectation, the results were quite nonsystematic. These results will be discussed later.

### Discussion

The possible errors of the calculated distributions of the proposed method consist of two parts. The one is due to the reliability of the fundamental equations, eqs. (1) and (2), and the other is due to the errors in the measurements of  $W$ ,  $\bar{x}$ ,  $R$ , and  $f_0(x)$ . The former problem is fundamental and very important; the accumulation of much more experimental results

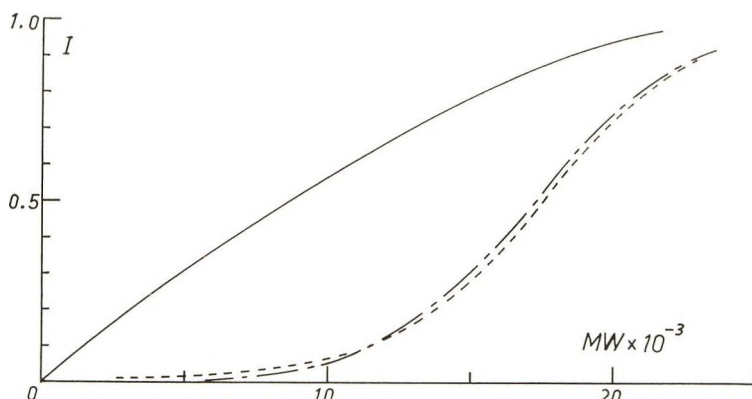


Fig. 7. Calculated integral distributions: (—) the eighth fraction for  $R = 841$  (---) calculated that for  $R = 84$  together with (—) the calculated integral distribution of the polymer in the dilute phase of the seventh fractionation step.

may be still needed. The latter problem is considered here by numerical calculations. It is adventurous to deduce a general conclusion from a limited number of numerical calculations, but it is certain that the results obtained reflect the complicated problem.

In Figure 7, the calculated integral distribution of the eighth fraction is compared with that calculated for one-tenth volume ratio of the measured value. The difference of the two distributions is very small. It can be said that no accurate measurement of  $R$  is probably needed (for the case  $R > 100$ ). The obtained values of  $\alpha$  and  $\sigma$  in the two cases are listed in Table II.

TABLE II  
Relation between the Change in the Volume Ratio and in the Fractionation Parameters Calculated in the Eighth Fractionation Step

$R$	$\alpha$	$\sigma$
841	0.957	$2.64 \times 10^{-6}$
84	1.79	$5.50 \times 10^{-10}$

The effects of the errors in molecular weight measurements were investigated by a model distribution of the unfractionated polymer assumed as shown in Figure 8. Two distributions of the first fraction of the model polymer were calculated for  $\bar{x} = 187,000$  and  $169,000$  under the condition  $W = 0.1$  and  $R = 300$ . The other two distributions of the first fraction of the model polymer were calculated for  $\bar{x} = 151,000$  and  $136,000$  under the condition  $W = 0.4$ ,  $R = 200$ .

These calculated curves are shown in Figure 8. A difference of molecular weight of about 10% affects the broadness of distribution. In the case of  $W$  small ( $= 0.1$ ), the integral distribution curve for the higher average-molecular weight crosses the curve for the lower molecular weight

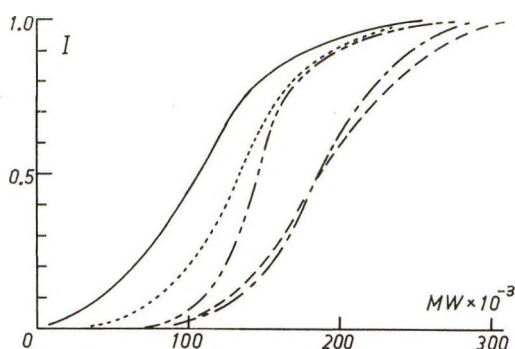


Fig. 8. Integral molecular weight distributions: (—) for the model polymer and these of the first fraction calculated under various conditions: (---)  $W = 0.1$ ,  $R = 300$ ,  $\bar{x} = 187,000$ ; (---)  $W = 0.1$ ,  $R = 300$ ,  $\bar{x} = 169,000$ ; (---)  $W = 0.4$ ,  $R = 200$ ,  $\bar{x} = 151,000$ ; (---)  $W = 0.4$ ,  $R = 200$ ,  $\bar{x} = 136,000$ .

at the intermediate point of the molecular weight range. The former distribution is sharper than the latter. In the case of  $W$  large ( $= 0.4$ ), the two curves never cross, and the lower curve belongs to that calculated for the higher molecular weight. The difference of the two curves is large in the lower molecular weight region and small in the higher molecular weight region. In any case, corresponding changes of  $\alpha$  and  $\sigma$  are large, as are shown in Table III. The aforementioned nonsystematic changes of  $\alpha$  and  $\sigma$  are probably due to errors in the volume ratios and the molecular weight measurements.

The error in weight fraction measurement is so small that calculations to investigate its effect were not undertaken.

Also the study of the effect of the errors in the initial distribution  $f_0(x)$  was not undertaken. The study appears to be rather a complicated problem to treat in a simple form.

It was at first expected that the agreement was best in the first fraction and gradually became worse as the errors in each step were accumulated.

Contrary to this expectation, the best agreement was obtained in the fifth step, as described before. A more accurate original distribution  $f_0(x)$  may be necessary to estimate an accurate distribution of every fraction. An investigation on a smaller number of fractionation steps may be desirable to elucidate this problem.

TABLE III  
Relation between the Change in Molecular Weight and in the Fractionation Parameters. (Calculations Made for the Model Polymer in Fig. 8.)

$W$	$R$	$\bar{x}$	$\alpha$	$\sigma$
0.1	300	187,000	2.50	$9.27 \times 10^{-16}$
0.1	300	169,000	1.22	$1.79 \times 10^{-8}$
0.4	200	151,000	2.50	$2.29 \times 10^{-14}$
0.4	200	136,000	0.574	$3.72 \times 10^{-6}$

### Conclusion

Though some problematical points remain as discussed in the preceding section, the results shown in Figures 3-6 indicate that the proposed method is useful for estimating molecular weight distributions of polymer fractions.

The author wishes to express his thanks to Dr. A. Nishioka for his encouragement and to Mr. S. Tanaka for his help in the experimental work.

### References

1. Okamoto, H., and K. Sekikawa, *J. Polymer Sci.*, **55**, 597 (1961).
2. Flory, P. J., *Principles of Polymer Chemistry*, Cornell Univ. Press, Ithaca, N. Y., 1953.
3. Tung, L. H., *J. Polymer Sci.*, **36**, 287 (1959).

### Résumé

L'auteur étudie une méthode qui permet estimer la distribution des poids moléculaires dans chaque fraction de polymère. Les distributions calculées par cette méthode sont comparées avec les valeurs mesurées. Pour étudier le changement nonsystematique des paramètres de fractions quelques calculs numériques on a effectué.

### Zusammenfassung

Die schon früher vorgeschlagene Methode zur Bestimmung der Molekulargewichtsverteilung von Fraktionen wird untersucht. Die berechneten Verteilungen werden mit den experimentellen verglichen. Um die beobachteten, nichtsystematischen Änderungen der Fraktionsparameter zu diskutieren, werden einige numerische Berechnungen durchgeführt.

Received July 9, 1963

Revised October 11, 1963

## Some Aspects of Thermal Decomposition of Polyoxymethylene and Irradiated Polyoxymethylene

SADAO TORIKAI, *Central Research Laboratories, Toyo Rayon Co., Ltd.,  
Otsu, Shiga, Japan*

### Synopsis

The thermal decomposition of polyoxymethylene and irradiated polyoxymethylene in vacuum was carried out and the kinetic aspects of thermal decomposition discussed. Although decomposition of low viscosity polyoxymethylene followed a pattern in which  $\log$  (polymer residue) was roughly linear with decomposition time, the high-viscosity polyoxymethylene which was obtained by the post-polymerization of irradiated solid formaldehyde showed the two components different in stability. However the concentrations of the components depended on the decomposition temperature. After the thermal decomposition, the sample could not be further stabilized by acetylation, while this initial polymer could be highly stabilized by acetylation. The irradiated polymer also could not be thermally stabilized by acetylation, though the first component of the irradiated polyoxymethylene disappeared after acetylation. The components of the polymer irradiated at 100°C.,  $\sim 4$  Mr ( $\eta_{sp}/c = 0.23$ ) showed three components the concentrations of which are independent of decomposition temperature. In irradiation at room temperature, or in the case of irradiation by the electron beams from a Van de Graaf generator at a high dose rate, the evacuation at 100°C. of the irradiated sample after irradiation disclosed the clear dependence of formation of stable polymer on dose, and the formation of three components which are independent of the decomposition temperature.

### INTRODUCTION

Kern and others reported the mechanisms of the thermal decomposition of polyoxymethylene according to which decomposition starts at the polymer ends and main-chain scission hardly occurs under 270°C.<sup>1,2</sup> The thermal decomposition of polyoxymethylene, however, exhibits complicated features in some cases, where the thermal stability of the sample seems to be changed during thermal decomposition. The termination of depolymerization, main-chain scission, and other miscellaneous phenomena might change the stability of the polymer in the process of decomposition.

The change in stability on irradiation with  $\gamma$ -rays at room temperature was studied in our previous paper.<sup>3</sup> The three components of irradiated polyoxymethylene different in stability were dependent slightly on the decomposition temperatures, and the concentrations of the three components could not be definitely decided.

The present paper deals primarily with the thermal decomposition of polyoxymethylene and irradiated polyoxymethylene, undertaken with a

view to elucidating the effect of thermal decomposition and decomposition by irradiation on the thermal stability of the polymer. It also supplements some results and discussion to our previous paper.

## EXPERIMENTAL

Polyoxymethylene dihydrate was prepared by introducing anhydrous formaldehyde gas into stirred *n*-heptane which contained dimethylformamide as initiator. High viscosity polyoxymethylene was also obtained by the post-polymerization of irradiated solid formaldehyde.<sup>4-6</sup> The viscosity number of this polymer was estimated to be 5-6.<sup>3</sup>

Acetylation of polyoxymethylene was carried out by using boiled acetic anhydride in the presence of sodium acetate in nitrogen gas for 2 hr. Polyoxymethylene was irradiated by  $\gamma$ -rays from a Co<sup>60</sup> source at a dose rate of  $0.83 \times 10^4$  r/hr., or by electron beams from a Van de Graaff-type generator at a dose rate of  $0.77 \times 10^7$  rad/min., at room temperature and 100°C. in vacuum, an *n*-shaped glass ampule, of which one end was immersed in liquid nitrogen during irradiation, being used.

Thermal decomposition of the sample was measured in vacuum (ca.  $10^{-5}$  mm. Hg) by the same method as described in our previous paper. It took 4-12 min. for the temperature of the sample to rise to 150-300°C., respectively. Viscosity number was measured at 60°C. in *p*-chlorophenol containing 2% of  $\alpha$ -pinene at a concentration of 0.5 g. polymer/100 cc. solvent, after dissolving the polymer in the solvent at 110-120°C. for 1 hr.

## RESULTS

### Thermal Decomposition of Polyoxymethylene Dihydrate and Polyoxymethylene Diacetate

Several kinds of polyoxymethylene were decomposed in vacuum at various temperatures from 150 to 200°C.

Figure 1A shows the result of decomposition of polyoxymethylene dihydrate which was polymerized by dimethylformamide as initiator. Each of the curves in Figure 1A follows approximately a first-order decomposition. Polyoxymethylene dihydrate having a viscosity number not exceeding about 2 usually decomposes in this manner.

On the other hand, polyoxymethylene obtained from irradiated solid formaldehyde decomposes in a complicated manner. This is illustrated in Figure 1B. The decomposition curves of this polymer might be divided into two components each of which roughly follows a first-order decomposition. The concentrations of two components, however, would differ markedly from one another depending on the decomposition temperature.

In spite of this queer aspect of decomposition, the polymer obtained from irradiated solid formaldehyde could be highly stabilized by acetylation,

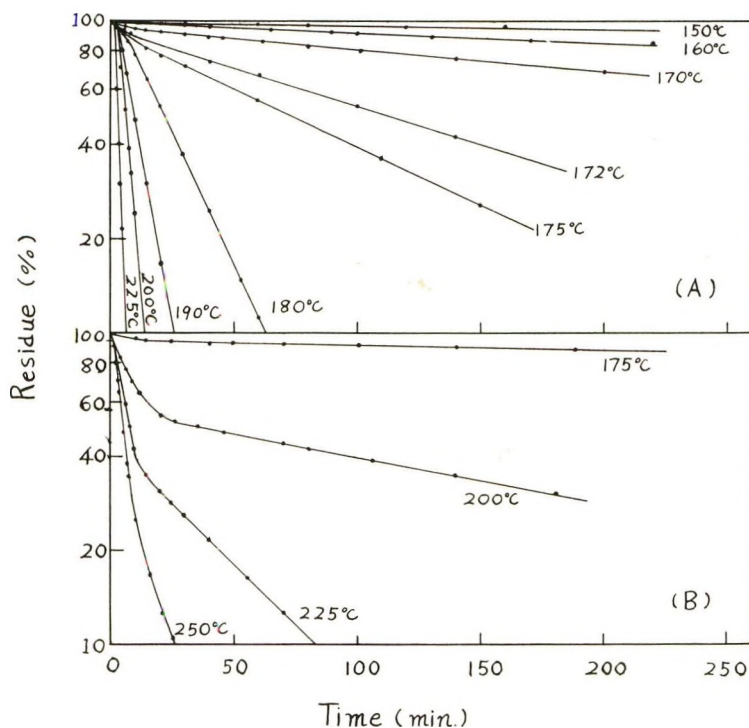


Fig. 1. Thermal decomposition of polyoxymethylene dihydrate in vacuum: (A) polymer polymerized with dimethylformamide as initiator,  $\eta_{sp}/c = 1.68$ ; (B) polymer from irradiated solid formaldehyde,  $\eta_{sp}/c$  estimated to be 5-6.

just as polyoxymethylene dihydrate polymerized by dimethylformamide as shown in Figure 2.

#### Thermal Decomposition of Irradiated Polyoxymethylene Polymerized by Dimethylformamide as Initiator

It was found that in the case of irradiation at high temperatures, the irradiated polyoxymethylene shows definite concentrations of the different components which are independent of the decomposition temperature. This is illustrated in Figures 3A and 3B, where the polymer was irradiated at 100°C. in vacuum. Direct comparison of the concentrations with the results of irradiation at room temperature seems to be complicated, as ca. 14% of the sample was decomposed during irradiation at 100°C.

In some cases of irradiation at room temperature, the dependence of the concentrations of the components on the decomposition temperature was large, as shown in Figure 4A. In this case, evacuation at 100°C. of the polymer which was irradiated at room temperature afforded some distinctness to the concentrations of the three components. This is illustrated in Figure 4B.

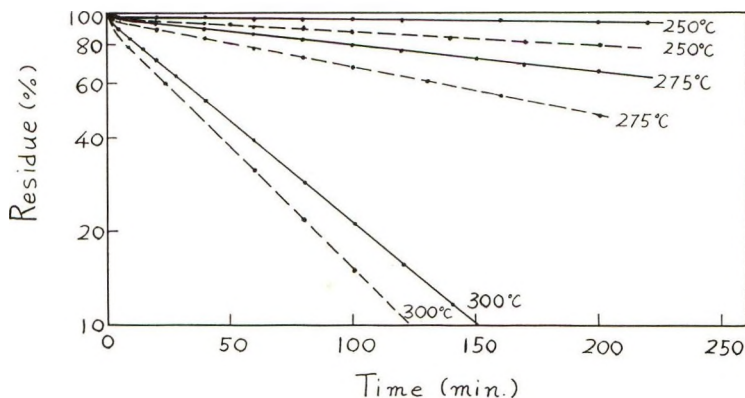


Fig. 2. Thermal decomposition of polyoxymethylene diacetate in vacuum: (—) polymer from irradiated solid formaldehyde; (---) polymer polymerized by dimethylformamide.

Similar results were also obtained in the case of irradiation at a high dose rate by electron beams from a Van de Graaff generator. The thermal stabilization, in this case, was obscure and the formation of stable polymer did not depend clearly on irradiation dose. However, evacuation at 100°C. after the irradiation by electron beams disclosed clearly the dependence of the formation of stable polymer on irradiation dose. This is shown in Figure 5.

#### Change in Thermal Stability of Polyoxymethylene Obtained from Irradiated Solid Formaldehyde by Irradiation and by Thermal Decomposition

In Figure 6 are shown the thermal decomposition curves at 250°C. of the samples derived from polyoxymethylene from irradiated solid formaldehyde. These curves indicate the similarities and differences in the stability change resulting from irradiation decomposition and thermal decomposition.

The acetylation of the initial polymer gave the most stable derivatives (Fig. 6, curves 5 and 5'). It is evident in Figure 6 that the viscosity of the sample does not have as important an effect on the stability as the kind of endgroups.

When the initial polymer was at first decomposed at 180°C. for 5 hr. to 82% residue, the thermal decomposition at 250°C. of the polymer was obviously changed, especially at the initial stage of the decomposition at 250°C., as shown in Figure 6 (curve 3).

On the other hand, irradiated polyoxymethylene showed three components apparently different in their stability (Fig. 6, curve 2). When the irradiated polyoxymethylene was heated at 180°C. for 5 hr. the first components of the irradiated polyoxymethylene formed disappeared in subsequent decomposition at 250°C., just as the first component had decomposed in the first decomposition at 180°C. (Fig. 6, curve 4).

One of the most important results in Figure 6 is that neither the irradiated polymer nor the polymer preheated at 180°C. could be stabilized so well by acetylation as polyoxymethylene dihydrate or initial polymer (Fig. 6, curves 6-8). (Acetylation of the treated polyoxymethylene improved the thermal stability to some extent, but the rate of decomposition

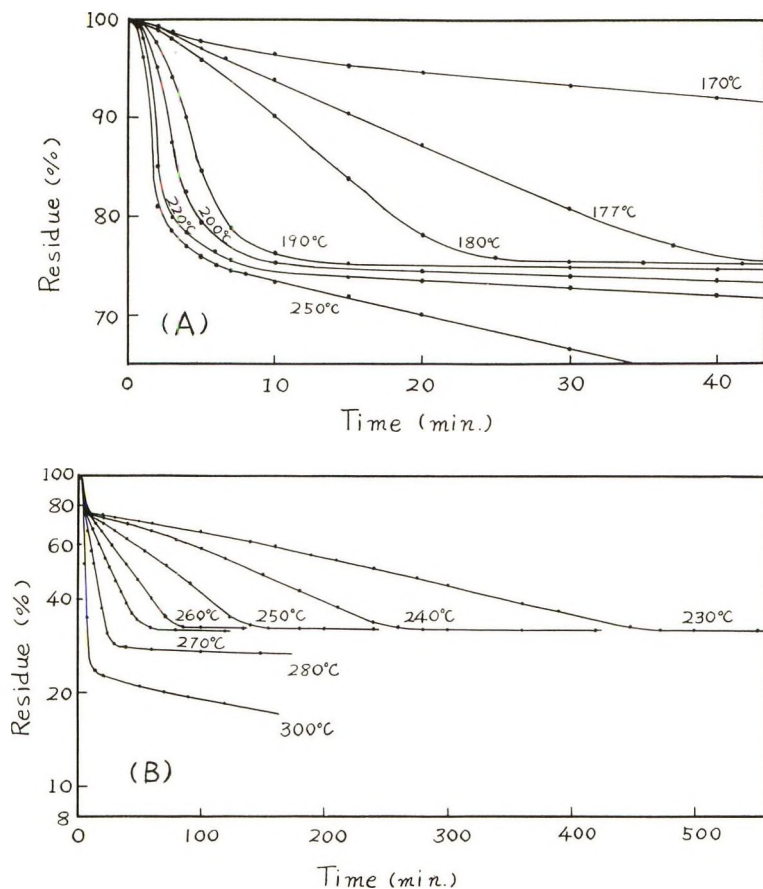


Fig. 3. Thermal decomposition of polyoxymethylene irradiated with  $\gamma$ -rays at 100°C. in vacuum: (A) per cent residue at first inflection points; (B) per cent residue at second inflection points. Initial polymer obtained by polymerization in the presence of dimethylformamide,  $\eta_{sp}/c = 1.68$ ; irradiation dose 4 Mr; irradiated polymer  $\eta_{sp}/c = 0.23$ .

was the order of the second component of the irradiated polyoxymethylene.)

Non-irradiated sample (excluding the part obtained by acetylation) seemed to lack the component corresponding to the third component of the irradiated sample.

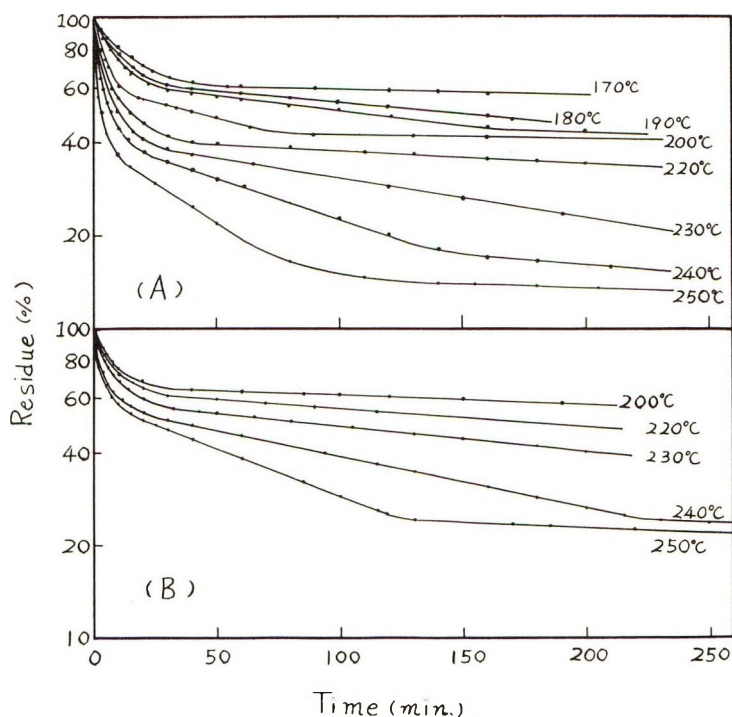


Fig. 4. Thermal decomposition of polyoxymethylene irradiated at 20°C. in vacuum: (A) direct decomposition after irradiation; (B) decomposition after evaluation of the irradiated sample at 100°C. for 5 hr. (4% decrease in weight during evacuation). Initial polymer obtained by polymerization in the presence of dimethylformamide,  $\eta_{sp}/c = 1.68$ ; irradiation dose 10 Mr, irradiated polymer  $\eta_{sp}/c = 0.33$ .

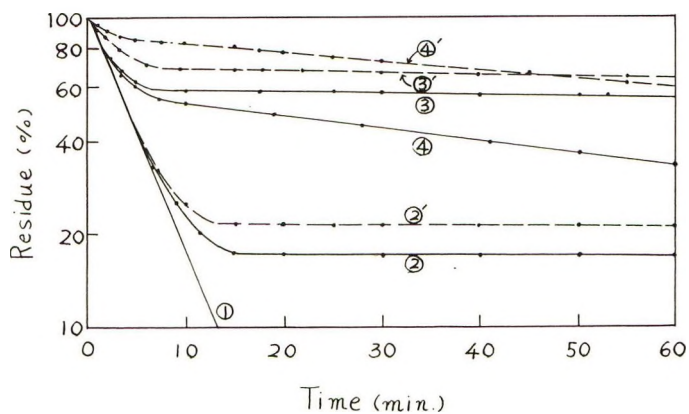


Fig. 5. Thermal decomposition at 200°C. of polyoxymethylene irradiated at room temperature by electron beams from a Van de Graaff generator: (1) initial polymer,  $\eta_{sp}/c = 1.68$ ; (2) irradiated with 1 Mrad; (2') irradiated with 1 Mrad, then evacuated at 100°C. for 16 hr.; (3) irradiated with 10 Mrad; (3') irradiated with 10 Mrad, then evacuated at 100°C. for 5 hr.; (4) irradiated with 50 Mrad; (4') irradiated with 50 Mrad, then evacuated at 100°C. for 5 hr.

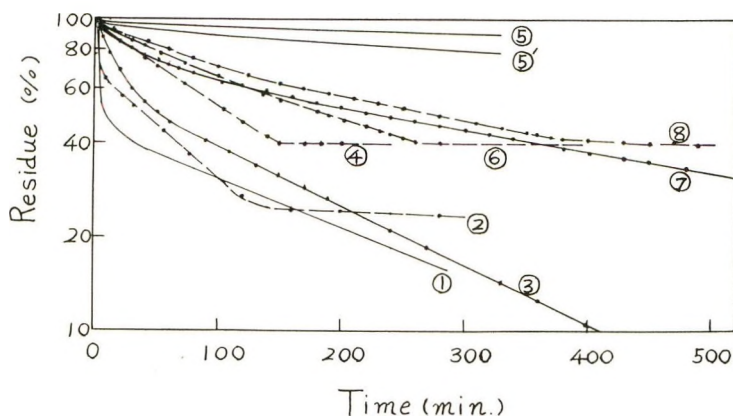


Fig. 6. Thermal decomposition at 250°C. of polyoxymethylene derived by irradiation, thermal decomposition, or acetylation: (1) initial polymer, from irradiated solid formaldehyde,  $\eta_{sp}/c = 5-6$ ; (2) irradiated with 0.5 Mrad at room temperature,  $\eta_{sp}/c = 1.10$ ; (3) decomposed thermally at 180°C. for 5 hr. (18% decrease in weight during thermal treatment); (4) 2 thermally decomposed at 180°C. for 5 hr. (16% decrease in weight during thermal treatment),  $\eta_{sp}/c = 1.07$ ; (5) acetylated (4% decrease in weight during acetylation); (5') polyoxymethylene dihydrate with viscosity of 1.68 acetylated (3% decrease in weight during acetylation),  $\eta_{sp}/c = 1.70$ ; (6) 2 acetylated (10% decrease in weight during acetylation),  $\eta_{sp}/c = 1.15$ ; (7) 3 acetylated (2% decrease in weight during acetylation); (8) 4 acetylated (10% decrease in weight during acetylation),  $\eta_{sp}/c = 1.08$ .

## DISCUSSION

As far as the results here are concerned, the decomposition curves might be taken to indicate that the components follow a first-order decomposition. No fundamental basis for this kinetic aspect of thermal decomposition is known. However, it seems that the separation of the components different in the stability should be due to either of the following reasons: (a) the initial sample consists of components differing in stability; (b) the stability changes during the process of thermal decomposition in vacuum (as a result of the nature of the sample or the nature of the decomposition).

The discrimination between (a) and (b) might be achieved by the examination of the dependence of the component concentration on the decomposition temperature.

As for this point, the polyoxymethylene irradiated at 100°C. ( $\eta_{sp}/c = 0.23$ ) showed components of which the concentrations were independent of the decomposition temperature. So, in this case, the thermal decomposition itself did not affect the stability, and the three components had been evidently produced during irradiation.

On the other hand, in the case of the polyoxymethylene of high viscosity which was obtained by polymerization of irradiated solid formaldehyde, the concentrations of the components were extremely dependent on the decomposition temperature. So the stability seems to be changed during the process of thermal decomposition. As long as this polyoxymethylene could

be stabilized by acetylation, this initial polymer might well be taken as polyoxymethylene dihydrate. No viscosity decrease seemed to occur during the acetylation reaction, for the acetylated polymer did not dissolve in *p*-chlorophenol at 120°C. and its viscosity decreased by irradiation almost to the same degree as the initial polymer. After thermal decomposition, the polymer showed fairly stabilized thermal decomposition (less stable than the acetylated polymer, almost equally stable as the second component of the irradiated polymer).

This thermally treated polymer could not be further stabilized by acetylation. Thus, the thermally treated polyoxymethylene from irradiated solid formaldehyde seems to have mainly other kinds of endgroups than hydroxy endgroups. (The ineffectiveness of acetylation of the irradiated polymer was also observed, although the first component disappeared after acetylation.) In principle, the reactions after the main-chain scission or the terminations of depolymerization seem to be able to produce such endgroups as methoxy, formyloxy, and hydroxy. The possibility of crosslinking during thermal decomposition might be also considerable. (The viscosity change during the thermal decomposition showed some complicated features.<sup>7,8</sup>) Polyoxymethylene dihydrate showed a slight increase in viscosity during the thermal decomposition at 175–200°C. There was a slight decrease in viscosity of polyoxymethylene diacetate beginning from 250°C. No decrease in viscosity of polyoxymethylene diacetate was observed in the thermal decomposition below 225°C.

Here, it should be noted that the stability change during the thermal decomposition was shown clearly only in the case of the polymer of high viscosity and that no apparent viscosity decrease during the thermal treatment could be observed. The accumulation of experiments seems to be necessary to permit the mechanisms of the stability change to be deduced.

As for the dependence of the concentrations of the components on the decomposition temperatures, polyoxymethylene irradiated at room temperature showed the less dependent concentrations of the components after evacuation at 100°C. Polyoxymethylene irradiated by a Van de Graaff generator also indicated the clear dependence of stable polymer formation on irradiation dose after evacuation at 100°C. The effects of the evacuation at 100°C. seem to be due to the exclusion of the low molecular weight substances and such substances as would accelerate the decomposition.

The author is greatly indebted to the Director of the Laboratories, Dr. H. Kobayashi, and to Drs. E. Mukoyama and Y. Shinohara for suggestions and interest in this study. He is also indebted to Mr. S. Saito and Mr. H. Mekata for the collaborations in the experiments.

## References

1. Kern, W., and H. Cherdron, *Makromol. Chem.*, **40**, 101 (1960).
2. Kern, W., H. Cherdron, and V. Jaaks, *Angew. Chem.*, **73**, 177 (1961).
3. Torikai, S., *J. Polymer Sci.*, in press.
4. Chachaty, C., M. Magot, and L. T. Minassain, *J. Polymer Sci.*, **48**, 139 (1960).
5. Magat, M., *J. Polymer Sci.*, **48**, 379 (1960).
6. Tsuda, Y., *J. Polymer Sci.*, **49**, 369 (1961).
7. Torikai, S., *Kobunshi Kagaku*, in press.
8. Torikai, S., paper presented at the 11th Symposium of High Polymers, Japan, 1962.

## Résumé

On a effectué la décomposition thermique du polyoxyméthylène et du polyoxyméthylène irradié sous vide et une discussion qualitative a été faite à partir des aspects cinétiques de la décomposition thermique. Bien que le polyoxyméthylène de faible viscosité se décompose approximativement d'une façon linéaire entre le log du résidu polymérique et le temps de décomposition, le polyoxyméthylène qui a été obtenu par la post-polymérisation du formaldéhyde solide irradié présente les deux composants différents de stabilité. Cependant les concentrations des composants dépendent fortement de la température de décomposition. Après la décomposition thermique l'échantillon ne peut plus être stabilisé par acétylation, tandis que ce polymère initial peut-être fortement stabilisé par acétylation. Le polymère irradié ne peut pas non plus être stabilisé par acétylation, bien que le premier composant du polyoxyméthylène irradié disparaisse après acétylation. Les composants du polymère irradié à 100°C. ( $\eta_{sp}/c = 0.2$ ,  $\sim 4$  Mr) montrent les trois composants qui sont indépendants des températures de décomposition. Dans certains cas d'irradiation à température de chambre, ou dans le cas d'irradiation par un faisceau d'électrons provenant d'un générateur de Van der Graaf à une vitesse de dose élevée, l'évacuation à 100°C. de l'échantillon irradié, révèle après irradiation la nette dépendance de la formation de polymère stable vis-à-vis de la dose et les trois composants qui sont indépendants de la température de décomposition.

## Zusammenfassung

Die thermische Zersetzung von Polyoxymethylen und bestrahltem Polyoxymethylen im Vakuum wurde untersucht und die kinetischen Aspekte der thermischen Zersetzung einer qualitativen Diskussion unterzogen. Niederviskoses Polyoxymethylen zersetzte sich zwar angenähert nach einer linearen Beziehung zwischen  $\log(\text{Polymerrückstand})$  und Zersetzungsdauer, das hochviskose, durch Nachpolymerisation von bestrahltem festen Formaldehyd erhaltene Polyoxymethylen besass jedoch zwei Komponenten verschiedener Stabilität. Die Konzentration der Komponenten zeigte eine extreme Abhängigkeit von der Zersetzungstemperatur. Nach der thermischen Zersetzung konnte die Probe durch Acetylierung nicht mehr stabilisiert werden, während beim Ausgangspolymeren auf diese Weise eine hochgradige Stabilisierung erreicht wurde. Das bestrahlte Polymere konnte ebenfalls durch Acetylierung nicht thermisch stabilisiert werden, obgleich die erste Komponente des bestrahlten Polyoxymethylens nach der Acetylierung verschwand. Das bei 100°C. bestrahlte Polymere ( $\eta_{sp}/c = 0,23$ ,  $\sim 4$  Mr) zeigte drei von der Zersetzungstemperatur unabhängige Komponenten. Bei manchen Bestrahlungen bei Raumtemperatur oder bei der Bestrahlung mit Elektronen eines Van de Graaf-Generators bei hoher Dosisleistung liess die Evakuierung der bestrahlten Probe nach der Bestrahlung bei 100°C. klar die Abhängigkeit der Bildung des stabilen Polymeren von der Dosis sowie die drei von der Zersetzungstemperatur unabhängigen Komponenten erkennen.

Received July 9, 1963

Revised October 20, 1963

## Coupled Vinyl and Acetal Ring-Opening Polymerization

MURRAY GOODMAN and AKIHIRO ABE, *Polymer Research  
Institute, Polytechnic Institute of Brooklyn, Brooklyn, New York*

### Synopsis

4-Methylene-1,3-dioxolane and its derivatives were polymerized by cationic catalysts. Infrared and ultraviolet studies showed that the polymers of 2,2-dimethyl- or 2-methyl-1,3-dioxolane possess appreciable carbonyl content. This indicates that the polymerization takes place in such a manner that the carbon-carbon double bond opening is coupled with a concurrent acetal ring rearrangement in the propagation step to give "ketoether" sequences. 4-Methylene-1,3-dioxolane, on the other hand, was found to polymerize mostly at the carbon-carbon double bond. Copolymerization of these monomers with acrylonitrile under ultraviolet irradiation was also studied.

### INTRODUCTION

The ring-opening polymerization of cyclic formals was first studied by Hill and Carothers.<sup>1</sup> They reported that while seven- and eight-membered rings are polymerizable with cationic catalyst systems, six-membered ring formals are unreactive. The polymerizations of dioxolane, other higher formals and their derivatives have also been reported.<sup>1-7</sup> In addition to these simple ring-opening reactions, a double ring-opening polymerization was observed by Bodenbenner.<sup>8</sup>

On the other hand, the polymerization of ketene acetals<sup>9-11</sup> was known to proceed primarily by the carbon-carbon double bond addition route with cationic catalysts.

Recently the preparation and polymerization of 1,3-dioxole and 2,2-dimethyl-1,3-dioxole was reported by Field.<sup>12</sup> Vinyl polymerization was observed with boron trifluoride at Dry Ice-acetone temperatures. An alternating copolymer with maleic anhydride was obtained by use of a free radical initiator.

The compound 4-methylene-1,3-dioxolane and its derivatives also polymerize by Friedel-Craft catalysts at about room temperature.<sup>13,14</sup> Although the pure monomers are essentially indifferent to radical initiators,<sup>15</sup> they copolymerize with some vinyl compounds in the presence of radical catalysts. However, in this report we present data on the polymerization mechanisms and polymer structures which have heretofore not been elucidated.

TABLE I. Polymerization of 2,2-Dimethyl-4-methylene-1,3-dioxolane

Catalyst used	Reaction temp., °C.	Monomer, g.	Solvent	Monomer concn., %	Amt. catalyst	Reaction time, hr.	Polymer yield, %	Soft. temp., °C.	Viscosity $[\eta]$ , (100 ml./g.)
BF <sub>3</sub> ·Et <sub>2</sub> O (48%)	-78	4.7	Ether	37	0.2 ml.	36	64 <sup>a</sup>	85-90	0.16 <sup>b</sup>
AlCl <sub>3</sub>	-78	2.8	Ether	47	0.3 g.	240	5 <sup>a</sup>	100-110	—
AlCl <sub>3</sub>	25	2.8	Ether	47	0.3 g.	36	7	70-80	—
Molecular sieves	30	—	—	—	—	—	—	70-80	0.04 <sup>b</sup>

<sup>a</sup> Anal. Calcd. for (C<sub>6</sub>H<sub>10</sub>O<sub>2</sub>)<sub>n</sub>: C, 63.14%; H, 8.83%. Found: C, 63.36%; H, 9.05%.<sup>b</sup> In chloroform at 26.8°C.<sup>c</sup> Anal. Found: C, 62.96%; H, 9.05%.

TABLE II. Polymerization of 2-Methyl-4-methylene-1,3-dioxolane

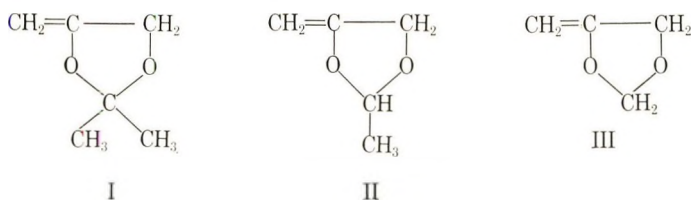
Catalyst used	Reaction temp., °C.	Monomer, g.	Solvent	Monomer concn., %	Amt. catalyst	Reaction time, hr.	Polymer yield, %	Soft. temp., °C.	Viscosity $[\eta]$ , (100 ml./g.)
BF <sub>3</sub> ·Et <sub>2</sub> O (48%)	-78	4.9	Ether	49	0.25 ml.	48	71 <sup>a</sup>	75-85	0.17 <sup>b</sup>
BF <sub>3</sub> ·Et <sub>2</sub> O (48%)	-78	1.9	Ether	48	0.1 ml.	3.5	47	75-85	0.29 <sup>b</sup>
AlCl <sub>3</sub>	-78	1.9	Methylene chloride	48	0.3 g.	240	58	75-85	0.04 <sup>b</sup>
H <sub>2</sub> SO <sub>4</sub> (conc.)	-78	1.9	Ether	48	0.15 ml.	48	11	75-85	—
AlCl <sub>3</sub>	25	1.0	Benzene	49	0.2 g.	48	5	75-85	0.66 <sup>c</sup>
Molecular sieves	>25	—	—	—	—	—	~70 <sup>d</sup>	65-70	0.04 <sup>e</sup>

<sup>a</sup> Anal. Calcd. for (C<sub>7</sub>H<sub>10</sub>O<sub>2</sub>)<sub>n</sub>: C, 59.96%; H, 8.05%. Found: C, 58.66%; H, 7.84%, corresponding to 2 mole-% of trapped chloroform.<sup>b</sup> In benzene at 26.8°C.<sup>c</sup> In chloroform at 26.8°C.<sup>d</sup> Anal. Found: C, 60.13%; H, 8.13%.<sup>e</sup> ( $\eta_{sp}/c$ ) at  $c = 0.526$  g./100 ml. in benzene at 26.8°C.

## RESULTS

## Polymerization and Copolymerization

The monomers, 2,2-dimethyl-4-methylene-1,3-dioxolane (I), 2-methyl-4-methylene-1,3-dioxolane (II), and 4-methylene-1,3-dioxolane (III) were prepared by acetal formation as follows: (1) acetone was allowed to react with epichlorohydrin; (2) acetaldehyde was allowed to react with epichlorohydrin; and (3) trioxane was allowed to react with 3-chloro-1,2-propanediol. These chlorinated dioxolanes were dehydrohalogenated with potassium hydroxide.



Polymerizations of these monomers take place easily with typical cationic catalysts at Dry Ice-acetone temperatures. While aluminum trichloride catalyst gave white or slightly yellowish polymers at room temperature, the polymers with boron trifluoride etherate at this temperature were black and completely insoluble. It was also found fortuitously that molecular sieves were able to initiate the cationic polymerization of these monomers. The results of the polymerization are summarized in Tables I-III.

Most of the polymers were observed to be very soluble in benzene, chloroform, *p*-dioxane, acetone, and even partially soluble in methanol. They are insoluble in *n*-pentane or *n*-hexane. When the polymers of 2,2-dimethyl- or 2-methyl-4-methylene-1,3-dioxolane contain a small amount of solvent, they exhibit sizable adhesive properties, and they become fairly brittle when completely dry. Poly-4-methylene-1,3-dioxolane, on the other hand, is somewhat more brittle under the same conditions. All of the polymers were shown to be amorphous by x-ray examination. Viscosity measurements were carried out using an Ubbelohde-type viscometer. The intrinsic viscosities in benzene or chloroform are shown in Tables I-III. The softening temperatures of the polymers were observed by the capillary method. These are the temperatures at which the polymers become viscous liquids. The polymers are very sensitive to acid, the color becoming variously yellow, green, or black, under these conditions.

The polymerizations of the saturated analogs, 2,4-dimethyl-1,3-dioxolane and 2-methyl-4-chloromethyl-1,3-dioxolane, were also attempted. Although some viscosity increase was observed at room temperature, no recognizable reaction was observed at Dry Ice-acetone temperatures with the cationic catalysts mentioned above.

While pure 4-methylene-1,3-dioxolane derivatives are essentially insensitive to ultraviolet irradiation, they smoothly copolymerize with vinyl

TABLE III. Polymerization of 4-Methylene-1,3-dioxolane

Catalyst used	Reaction temp., °C.	Monomer, g.	Solvent	Monomer concn., %	Amt. catalyst	Reaction time, hr.	Polymer yield, %	Soft. temp., °C.	Viscosity $[\eta]$ , (100 ml./g.)
BF <sub>3</sub> ·Et <sub>2</sub> O (45%)	-78	3.1	Ether	24	0.15 ml.	45	10 <sup>a</sup>	125-130	0.22 <sup>b</sup>
BF <sub>3</sub> ·Et <sub>2</sub> O (45%)	-78	2.1	Ether	10	0.15 ml.	40	12	125-130	—
AlCl <sub>3</sub>	-78	5.2	Ether	52	0.3 g.	48	5 <sup>c</sup>	125-130	—
AlCl <sub>3</sub>	25	3.1	Benzene	39	0.3 g.	24	16 <sup>d</sup>	— <sup>e</sup>	—

<sup>a</sup> Anal. Calcd. for (C<sub>4</sub>H<sub>6</sub>O<sub>2</sub>)<sub>n</sub>: C, 55.81%; H, 7.03%. Found: C, 55.99%; H, 7.27%.<sup>b</sup> In chloroform at 25.0°C.<sup>c</sup> Anal. Found: C, 56.07%; H, 7.09%.<sup>d</sup> Insoluble in conventional organic solvents.<sup>e</sup> The color changes gradually to brown-black (>150°C.), but no apparent softening is observed.

TABLE IV. Copolymerizations of 4-Methylene-1,3-dioxolane Derivatives with Acrylonitrile by Ultraviolet Irradiation

Monomer	Reaction temp., °C.	Monomer, g.	Acrylonitrile, g.	Reaction time, hr.	Polymer yield, g.	Softening temp., °C.	Viscosity $[\eta]$ , 100 ml./g.
2,2-Dimethyl-4-methylene-1,3-dioxolane	35	1.1	0.8	16	1.0 <sup>a</sup>	140-150	0.31 <sup>b</sup>
2-Methyl-4-methylene-1,3-dioxolane	35	1.0	0.8	12	1.7 <sup>c</sup>	>250 <sup>d</sup>	0.28 <sup>b</sup>
4-Methylene-1,3-dioxolane	35	1.6	1.0	25	1.5 <sup>e</sup>	>230 <sup>d</sup>	0.94 <sup>f</sup>

<sup>a</sup> Anal. Calcd. for (1:1) copolymer (C<sub>9</sub>H<sub>13</sub>NO<sub>2</sub>)<sub>n</sub>: C, 64.65%; H, 7.84%; N, 8.38%. Found: C, 64.43%; H, 7.95%; N, 8.61%.<sup>b</sup> In chloroform at 26.8°C.<sup>c</sup> Anal. Calcd. for (1:1.3) copolymer (acrylonitrile excess): C, 63.23%; H, 7.09%; N, 10.77%. Found: C, 63.07%; H, 6.88%; N, 10.83%.<sup>d</sup> The color changes gradually to brown-black.<sup>e</sup> Anal. Calcd. for (1:1) copolymer (C<sub>7</sub>H<sub>9</sub>NO<sub>2</sub>)<sub>n</sub>: C, 60.42%; H, 6.52%; N, 10.07%. Found: C, 60.85%; H, 6.47%; N, 10.30%.<sup>f</sup> In *N,N*-dimethylformamide at 25.0°C.

compounds carrying an electron-attracting substituent such as acrylonitrile under irradiation. The resulting copolymers with acrylonitrile are soluble in both chloroform and *N,N*-dimethylformamide, and can be reprecipitated from these solutions by addition of *n*-pentane or methanol. These polymers are also found to be amorphous by x-ray examination. Viscosities and softening temperatures were measured in the same manner as described above, and are tabulated in Table IV. When the copolymer of 2-methyl-4-methylene-1,3-dioxolane with acrylonitrile is heated in concentrated hydrochloric acid, it dissolves completely. Addition of methanol to this solution gives a white polymer which shows a characteristic carboxyl absorption in infrared. At the same time the nitrile peak at  $2240\text{ cm}^{-1}$  and the acetal peaks at  $1200\text{--}1050\text{ cm}^{-1}$  disappear. This is probably due to complete hydrolysis of nitrile and acetal groups in the polymer. As expected, this polymer is very soluble in aqueous sodium hydroxide solution.

### Infrared and Ultraviolet Absorption Studies and the Elucidation of the Homopolymer Structures

Infrared absorption measurements were carried out with the use of Perkin-Elmer Model 21 and Infracord instruments. Most of the polymer samples were prepared by casting films from chloroform or benzene solution. Typical examples of the spectra of the monomer, its saturated analog, and polymer are shown in Figures 1–5.

Some remarkable differences are recognized in the fingerprint region of the infrared spectra of the polymers from those of the monomers resulting from the disappearance of the carbon-carbon double bonds ( $1690$ ,  $1250\text{--}1290$ ,  $940\text{--}960$ , and  $800\text{--}810\text{ cm}^{-1}$ ) during polymerization. Chemical tests on poly-2-methyl-4-methylene-1,3-dioxolane also indicate that no sizable amount of carbon-carbon double bonds remains in the polymer. The tests on which these conclusions are based are summarized below.

(a) Hydrogenation of the polymer was attempted with 5% palladium on charcoal or platinum oxide in dioxane under 40 psi pressure at room temperature for several hours. The polymer after such treatment was shown to be exactly the same as the original polymer.

(b) The polymer solution in acetone did not decolorize added dilute potassium permanganate solution at room temperature. At an elevated temperature, the color changed from the permanganate purple to deep red.

(c) Addition of a small amount of bromine solution in carbon tetrachloride to a polymer solution in the same solvent gave a very insoluble black precipitate.

In the case of poly-2,2-dimethyl-4-methylene-1,3-dioxolane and poly-2-methyl-4-methylene-1,3-dioxolane, fairly sharp absorptions are observed at  $1730\text{ cm}^{-1}$  (Figs. 3 and 4), suggesting the presence of a carbonyl group. The intensities of these peaks remain constant after repeated reprecipitation from chloroform or benzene solution by *n*-pentane. It was, however, observed that the intensity of the carbonyl absorption in the infrared varied appreciably depending upon the catalyst system and polymerization

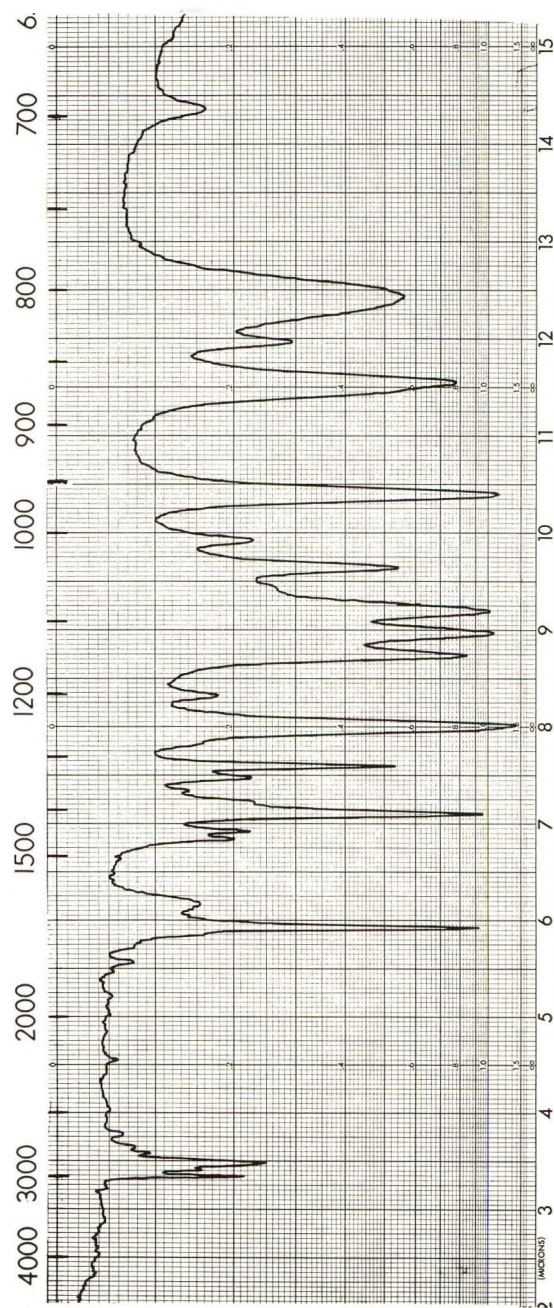


Fig. 1. Infrared spectrum of 2-methyl-4-methylene-1,3-dioxolane (monomer).

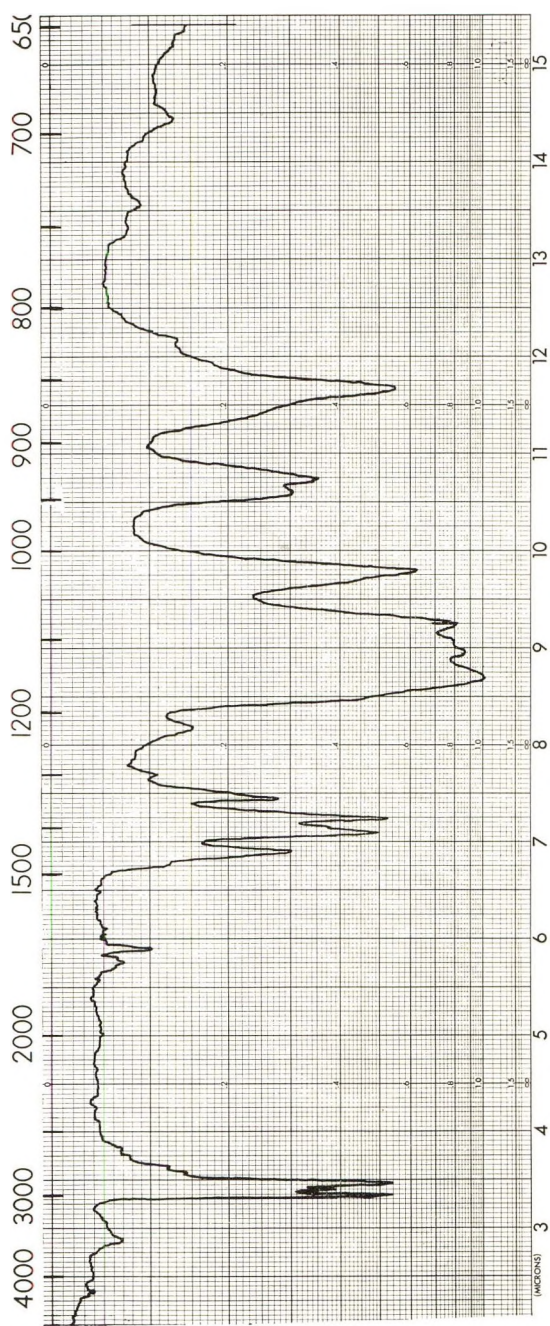


Fig. 2. Infrared spectrum of 2,4-dimethyl-1,3-dioxolane (saturated analog).

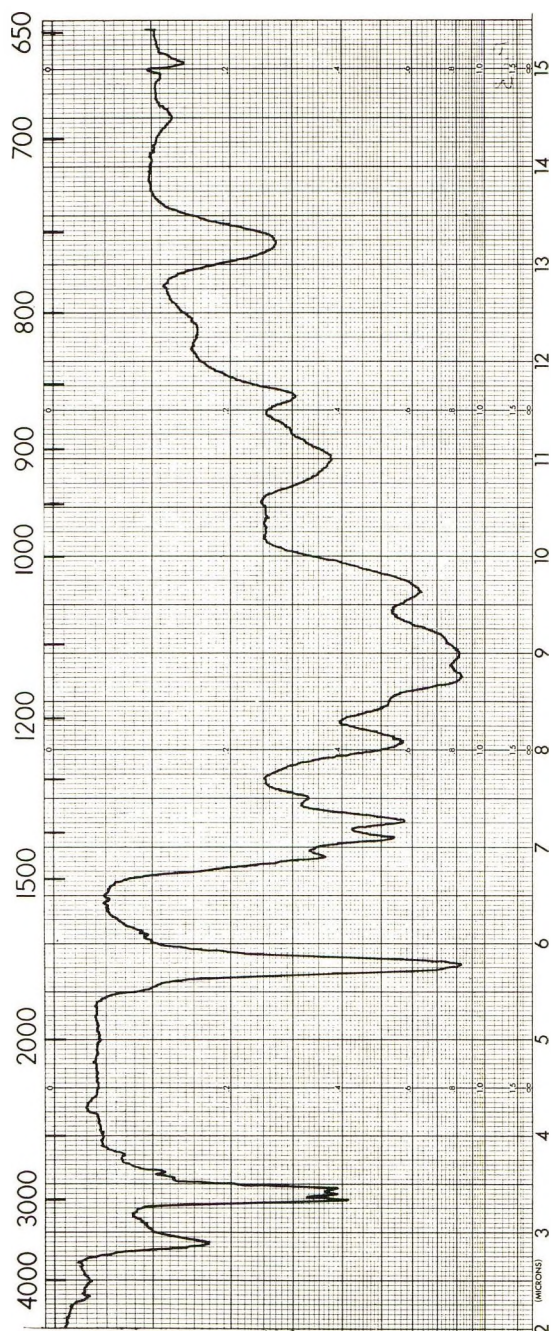


Fig. 3. Infrared spectrum of poly-2-methyl-4-methylene-1,3-dioxolane prepared by  $\text{BF}_3 \cdot \text{Et}_2\text{O}$  catalyst (film cast from chloroform).

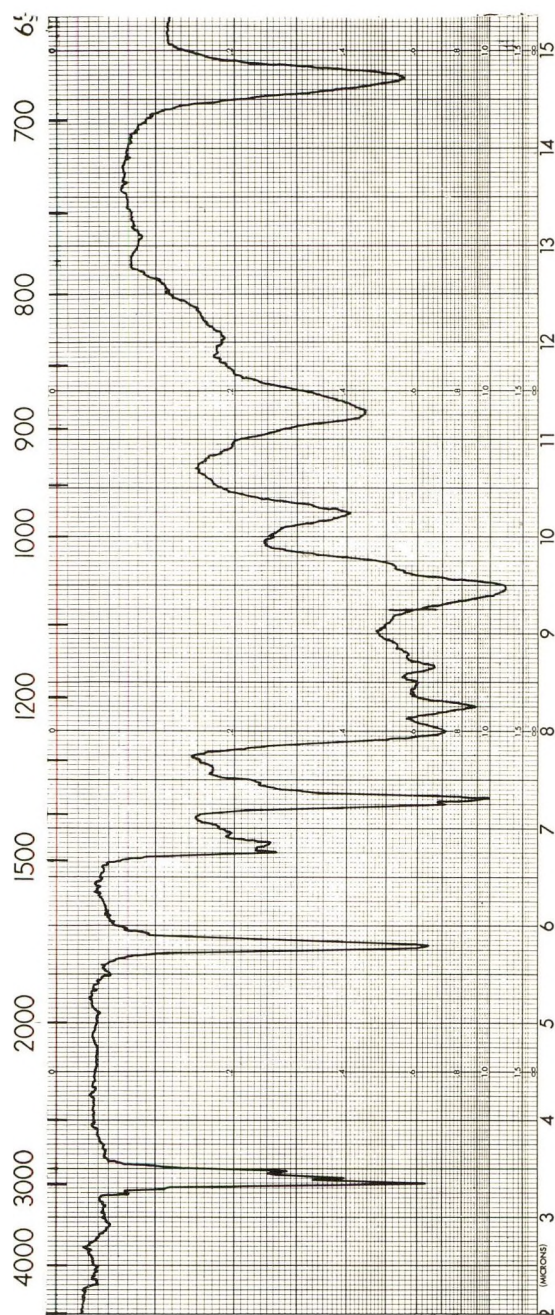


Fig. 4. Infrared spectrum of poly-2,2-dimethyl-4-methylene-1,3-dioxolane prepared by  $\text{BF}_3 \cdot \text{Et}_2\text{O}$  catalyst (film cast from benzene).

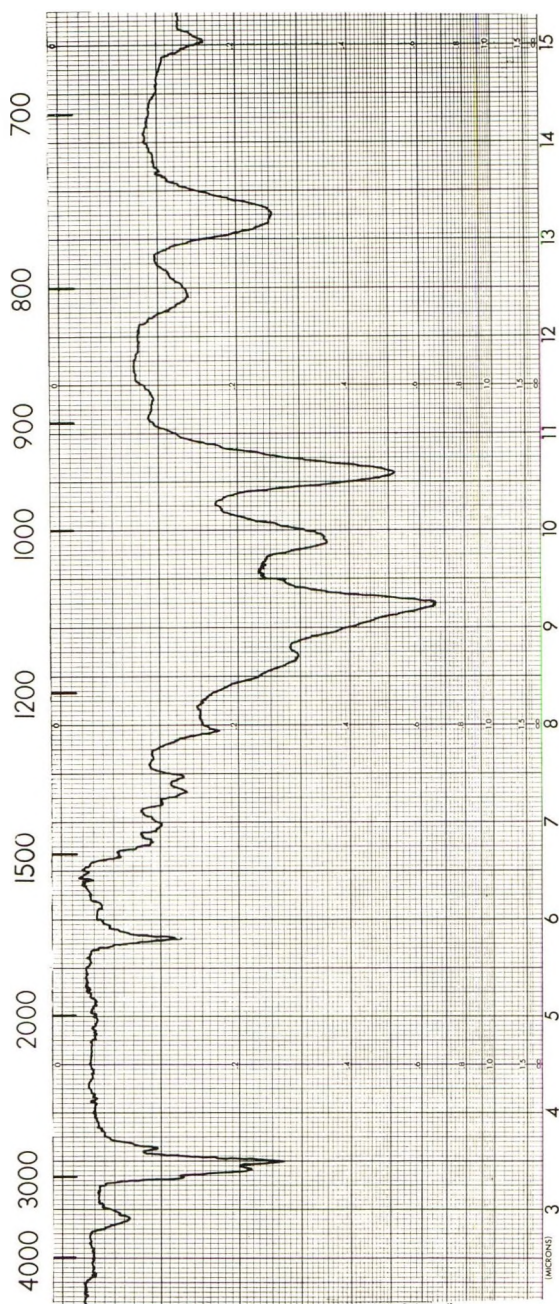


Fig. 5. Infrared spectrum of poly-4-methylene-1,3-dioxolane prepared by  $\text{BF}_3 \cdot \text{Et}_2\text{O}$  catalyst (film cast from chloroform).

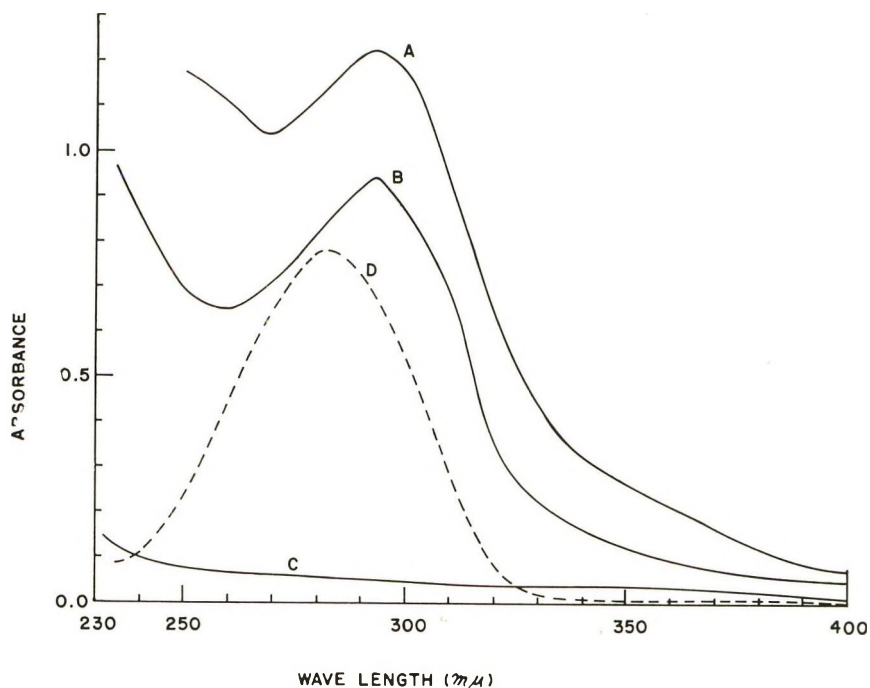
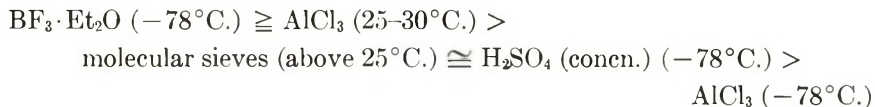


Fig. 6. Ultraviolet absorption of the polymers and the model compound ( $c = 0.050$  mole/l. in methylene chloride): (A) poly-2,2-dimethyl-4-methylene-1,3-dioxolane prepared by  $\text{BF}_3 \cdot \text{Et}_2\text{O}$  catalyst; (B) poly-2-methyl-4-methylene-1,3-dioxolane prepared by  $\text{BF}_3 \cdot \text{Et}_2\text{O}$  catalyst; (C) poly-4-methylene-1,3-dioxolane prepared by  $\text{BF}_3 \cdot \text{Et}_2\text{O}$  catalyst; (D) 1-methoxy-2-propanone.

temperature employed. While the polymers obtained using boron trifluoride etherate as a catalyst at Dry Ice-acetone temperatures show the strongest carbonyl absorption, those derived from the aluminum trichloride catalyst possess the weakest. The carbonyl absorptions of both polymers derived from 2,2-dimethyl- and 2-dimethyl-4-methylene-1,3-dioxolane diminish in the following order:



As shown in Figure 5, on the other hand, poly-4-methylene-1,3-dioxolane possesses an extremely weak carbonyl absorption, even when it was formed by using boron trifluoride etherate at Dry Ice-acetone temperatures. Ultraviolet absorption studies supply additional proof of the structures of the polymers. All of the samples were freshly prepared by reprecipitating from the solvent which was used in the ultraviolet absorption measurements, and dried completely under reduced pressure. The measurements were carried out with a Cary Model 14 spectrophotometer. As is clearly

TABLE V  
Ultraviolet Absorption of Polymers and Related Low Molecular Weight Compounds

Polymers and related compounds	Polymerization system		$\lambda_{\max}$ , m $\mu$	$\epsilon_{\max}^a$	Net $\epsilon_{\max}^b$	Solvent
	Catalyst	Temp., °C.				
Poly-2,2-dimethyl-4-methylene-1,3-dioxolane	BF <sub>3</sub> ·Et <sub>2</sub> O	-78	293	24.3	12	Methylene chloride
	BF <sub>3</sub> ·Et <sub>2</sub> O	-78	292	23.4	11	Diethyl ether
	AlCl <sub>3</sub>	-78	290	12.5	6	Methylene chloride
Poly-2-methyl-4-methylene-1,3-dioxolane	BF <sub>3</sub> ·Et <sub>2</sub> O	-78	293	18.8	14	Methylene chloride
	AlCl <sub>3</sub>	-78	294	13.5	6	Methylene chloride
	Molecular sieves	>25	295	24.5	9	Methylene chloride
1-Methoxy-2-propanone	—	—	282.5	15.6	—	Methylene chloride
Acetone <sup>c</sup>	—	—	275	—	—	Methylene chloride
Acetaldehyde <sup>d</sup>	—	—	286	—	—	Methylene chloride

<sup>a</sup> Calculated value based on the monomer residue weight.

<sup>b</sup> Estimated carbonyl absorption by subtracting neighboring absorption.

<sup>c</sup> Literature value;<sup>16</sup>  $\lambda_{\max} = 277$  m $\mu$ ,  $\epsilon_{\max} = 17$  (chloroform).

<sup>d</sup> Literature value;<sup>17</sup>  $\lambda_{\max} = 289.9$  m $\mu$ ,  $\epsilon_{\max} = 17.0$  (*n*-heptane).

seen in Figure 6, while the polymers of 2,2-dimethyl- and 2-methyl-4-methylene-1,3-dioxolane obtained with boron trifluoride etherate catalyst at Dry Ice-acetone temperatures exhibit appreciable absorptions at 290–295  $m\mu$ , the polymer derived from 4-methylene-1,3-dioxolane under the similar conditions does not show any absorption in this region. The observed values for the polymers and related compounds are listed in Table V. While the polymers show absorption maxima at 290–295  $m\mu$ , a simple aldehyde or ketone possesses an absorption maximum at lower wavelength in the same solvent. Since none of the polymers shows the infrared absorption attributable to an aldehyde residue at 2750  $\text{cm}^{-1}$ , it is reasonable to assume that the carbonyl absorption is attributable to a ketone group. From the data shown in Table V, it is also reasonable to assume that large portions of the monomeric units of the polymer derived from either 2,2-dimethyl- or 2-methyl-4-methylene-1,3-dioxolane by use of boron trifluoride etherate contain a carbonyl group.

Infrared absorptions of these polymers in the ether region (C–O–C stretching, 1200–1000  $\text{cm}^{-1}$ ) show only slight differences from the spectra of the corresponding monomer (Fig. 1), the saturated analog (2,4-dimethyl-1,3-dioxolane) (Fig. 2), and the copolymer with acrylonitrile. As will be discussed later, this is probably due to the copolymer nature of the polymer sequences.

### Infrared Absorption Studies of the Copolymer with Acrylonitrile

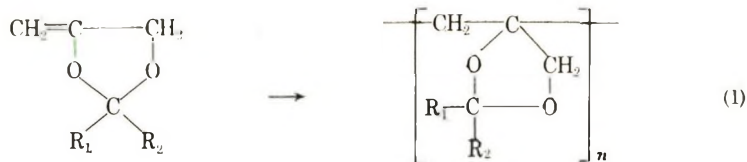
An example of the infrared spectra is shown in Figure 7. A sharp absorption peak at 2240  $\text{cm}^{-1}$  is assignable to a nitrile group. From the fact that there are no detectable carbonyl or carbon-carbon double bond absorption bands, we conclude that the monomers (4-methylene-1,3-dioxolane derivatives) copolymerize with acrylonitrile only by carbon-carbon double bond addition reactions.

From chemical analyses (Table IV) and the fact that pure 4-methylene-1,3-dioxolane derivatives are stable to ultraviolet irradiation and radical initiators,<sup>15</sup> it is most reasonable to assume almost alternating structures for the copolymers. The exact structures of these copolymers are still unknown, however.

## DISCUSSION

The three polymerization routes shown in eqs. (1)–(3) are conceivable for polymerization of 4-methylene-1,3-dioxolane derivatives with cationic catalysts.

Vinyl Polymerization:



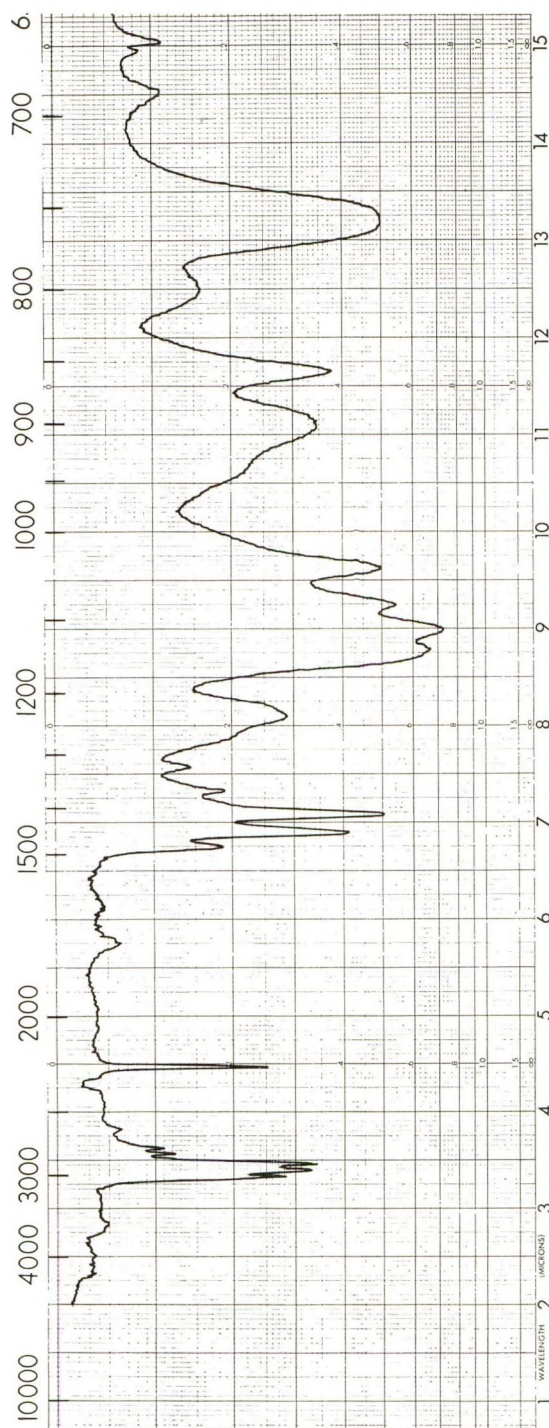
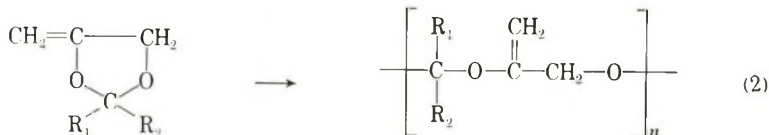


Fig. 7. Infrared spectrum of copolymers of 2-methyl-4-methylene-1,3-dioxolane with acrylonitrile prepared by ultraviolet irradiation (film cast from chloroform).

## Ring-Opening Polymerization:



## Coupled Vinyl and Ring-Opening Polymerization:



As we have seen above, when the polymers of 2,2-dimethyl- and 2-methyl-4-methylene-1,3-dioxolane are prepared by boron trifluoride etherate at Dry Ice-acetone temperatures or by aluminum trichloride at room temperature, large portions of the monomeric units of the polymers contain ketonic groups. This fact can be explained only by assuming that route (3) is important, i.e., the double bond opening by cationic catalyst is coupled with the acetal ring rearrangement to a ketone. This generates another electron-deficient site which is attacked by additional monomer. This structure is also consistent with the other observations cited above. 1-Methoxy-2-propanone was prepared as a model compound for this polymer structure. As shown in Table V, this compound possesses an absorption maximum at  $282.5 \text{ m}\mu$  in methylene chloride, which is higher than that observed for acetone ( $275 \text{ m}\mu$ ) in the same solvent. It is, therefore, seen that an alkoxy substitution as well as an alkyl group<sup>18</sup> at the position  $\alpha$  to the carbonyl group shifts the absorption maximum to a higher wavelength.

The fact that the intensity of the carbonyl absorption in infrared is more or less variable depending upon the catalyst system and polymerization temperature employed is probably due to partial polymerization via route (1), that is, a simple vinyl polymerization. By taking the molar extinction coefficient of 1-methoxy-2-propanone as a standard, conversion to the above-mentioned ketoether type sequence during cationic polymerization is estimated to be between 40 and 90% (Table V).

In the case of 4-methylene-1,3-dioxolane, polymerization takes place mostly at the carbon-carbon double bond. It can be explained in terms of the difficulty of forming the primary carbonium ion, which would be produced if the polymerization were accompanied by acetal ring rearrangement.

In summary, we conclude that cationic polymerization of 2,2-dimethyl- or 2-methyl-4-methylene-1,3-dioxolane under certain conditions mainly takes place by a coupled vinyl and acetal ring opening to give a "poly-ketoether." It is interesting to note that although the polymerization of 1,3-dioxoles may be considered to proceed through a similar transition state,

only vinyl-type polymerization was reported.<sup>12</sup> In the present case, it is reasonable to assume that the polymerization involves concurrent acetal ring rearrangement in a large portion of the propagation steps. In this respect, we may find some analogy to the polymerization of 1,4,6-trioxaspiro-[4,4]-nonane,<sup>8</sup> which yields a type of 1:1 copolymer of ethylene oxide and  $\gamma$ -butyrolactone by a double ring opening.

## EXPERIMENTAL

The chemical analyses were carried out by Schwarzkopf Microanalytical Laboratory.

### Syntheses of the Monomers and Model Compounds

**2,2-Dimethyl-4-chloromethyl-1,3-dioxolane.**<sup>19</sup> An ice-cooled mixture of acetone (127 g., 2.19 mole) and epichlorohydrin (198.5 g., 2.16 mole) in 350 ml. of methylene chloride was slowly added to a cold solution of stannic chloride (20.1 g., 0.077 mole) in 50 ml. of methylene chloride. The solution was stirred and the addition was continued at such a rate that the temperature did not rise above 25°C. The resulting orange-brown solution was poured into 300 ml. of a 10% sodium carbonate solution to remove the catalyst. The organic layer was separated, washed with water, and dried over anhydrous sodium sulfate overnight. This solution was more rigorously dried with molecular sieves for 5 hr. before distillation.

The desired acetal was thus obtained: 216 g.; 66.7%; b.p. 54–55°C./15 mm. Hg.

**2,2-Dimethyl-4-methylene-1,3-dioxolane.**<sup>20</sup> Commercial potassium hydroxide pellets (350 g.) were heated to 250°C. in a copper flask with stirring under reduced pressure (2–3 mm. Hg). The molten potassium hydroxide began to resolidify after 30–60 min. or heating. Completely solidified potassium hydroxide was allowed to cool to room temperature. The reactant, 2,2-dimethyl-4-chloromethyl-1,3-dioxolane (200 g., 1.33 mole) obtained above, was decanted onto this solid potassium hydroxide at atmospheric pressure. After refluxing for 30 min. on a sand bath, the product was collected by distillation (100–150°C.) at atmospheric pressure and finally under the reduced pressure (3 mm. Hg). The resulting product was washed with a small amount of water and dried over anhydrous sodium sulfate overnight. It was more rigorously dried with a small amount of molecular sieves for 5 hr. before distillation. It is important not to use too much because of polymerization, (see later section). Pure product was obtained by distillation under nitrogen. Some of the starting acetal (79.6 g., b.p. 56–59°C./17 mm. Hg) was also recovered. The product was obtained in 55.2 g. yield (60.3%); b.p. 110–111°C.;  $n_D^{23}$  1.4272 (Lit. value:<sup>20</sup>  $n_D^{20}$  1.4221);  $d_4^{26}$  0.9360.

ANAL. Calcd. for (C<sub>6</sub>H<sub>10</sub>O<sub>2</sub>): C, 63.14%; H, 8.83%. Found: C, 63.02%; H, 9.04%.

**2-Methyl-4-chloromethyl-1,3-dioxolane.** Acetaldehyde (100 g., 2.3 mole) and epichlorohydrin (200 g., 2.2 mole) were treated with stannic chloride (24 g., 0.092 mole) in a similar manner as described in the previous section. Carbon tetrachloride was employed as a reaction solvent. A fraction boiling at 45–47°C./12 mm. Hg was collected; yield 140 g. (46.8%).

ANAL. Calcd. for ( $C_4H_9ClO_2$ ): C, 43.95%; H, 6.64%; Cl, 25.97%. Found: C, 43.74%; H, 6.60%; Cl, 25.76%.

**2-Methyl-4-methylene-1,3-dioxolane.** Dehydrohalogenation of 2-methyl-4-chloromethyl-1,3-dioxolane (62 g., 0.46 mole) was carried out in the same manner as described above. Potassium hydroxide pellets (160 g.) were used. The pure product (13.0 g.) and unreacted starting acetal (22.2 g.) were obtained by distillation under nitrogen; yield 44.4%; b.p. 95–97°C.;  $n_D^{25}$  1.4304;  $d_4^{25}$  0.9707.

ANAL. Calcd. for ( $C_5H_8O_2$ ): C, 59.96%; H, 8.06%. Found: C, 60.01%; H, 8.05%.

**4-Chloromethyl-1,3-dioxolane.** To a mixture of trioxymethylene (60.0 g., 0.667 mole) and stannic chloride (55.8 g., 0.214 mole) in 300 ml. of carbon tetrachloride was added 3-chloro-1,2-propanediol (220 g., 2.00 mole). The mixture was refluxed with stirring for 5 hr. The resulting solution was poured into 500 ml. of a 20% sodium carbonate solution to remove the catalyst. The organic layer was separated, washed with water, and dried over anhydrous sodium sulfate overnight. This solution was more rigorously dried with molecular sieves for several hours before distillation. After removal of the solvent, the desired product was obtained by distillation under reduced pressure; yield 121.5–130.0 g. (49.8–53.3%); b.p. 45–47°C./10 mm. Hg.

**4-Methylene-1,3-dioxolane.** 4-Chloromethyl-1,3-dioxolane (200 g., 1.64 mole) was treated with potassium hydroxide pellets (400 g.) according to the procedure described above. A crude product (60 ml.) boiling at 85–100°C. and a portion (90.0 g.) of unreacted starting acetal were obtained by distillation. Redistillation under a nitrogen atmosphere gave pure 4-methylene-1,3-dioxolane; yield 40.5 g. (52.2%); b.p. 88.5–89°C.;  $n_D^{22}$  1.4372;  $d_4^{24.5}$  1.0397.

ANAL. Calcd. for ( $C_4H_6O_2$ ): C, 55.81%; H, 7.03%. Found: C, 55.62%; H, 7.03%.

**1-Methoxy-2-propanone.** 1-Methoxy-2-propanol (228 g., 2.53 mole) was oxidized with sodium dichromate by the procedure given by Mariella and Leech.<sup>21</sup> The pure product (32.7 g.) and unreacted alcohol (15 g.) were obtained; yield 15.7%; b.p. 114.0–114.3°C.,  $n_D^{27}$  1.3982 (Lit. value<sup>21</sup>:  $n_D^{20}$  1.3982).

ANAL. Calcd. for ( $C_4H_8O_2$ ): C, 54.53%; H, 9.15%. Found: C, 54.53%; H, 9.32%.

**2,4-Dimethyl-1,3-dioxolane.** The saturated analog of 2-methyl-4-methylene-1,3-dioxolane was prepared from acetaldehyde and propylene oxide in a similar manner as described for the preparation of 2,2-dimethyl-4-chloromethyl-1,3-dioxolane. Acetaldehyde (44 g., 1.0 mole) and propylene oxide (58 g., 1.0 mole) were treated with stannic chloride (6 g., 0.023 mole) in methylene chloride as a solvent. Distillation under nitrogen gave about 40 ml. of a crude product (b.p. 90–120°C.) which was redistilled under a nitrogen atmosphere. A fraction boiling between 97 and 100°C. was collected; yield 18 g. (17.6%);  $n_D^{25}$  1.4048;  $d_4^{24}$  0.9390.

ANAL. Calcd. for ( $C_5H_{10}O_2$ ): C, 58.78%; H, 9.87%. Found: C, 58.79%; H, 9.72%.

### Polymerization

**Polymerization at Low Temperatures.** Polymerizations were carried out at Dry Ice–acetone temperatures in glass ampules which were thoroughly dried and swept with dry prepurified nitrogen. Typical cationic catalysts were found to be effective for all of the monomers prepared.

In the case of boron trifluoride etherate, the polymerization took place in ether solution instantaneously after the introduction of a few drops of catalyst yielding a white polymer. With concentrated sulfuric acid, the reaction also took place very rapidly. However, the resulting polymer was colored because the acid attacked the formed polymer.

When aluminum trichloride was used as a catalyst, the polymerization in both ether and methylene chloride proceeded very slowly. The viscosity increase of the system was clearly observed after about 20 hr.

In the case of boron trifluoride etherate and concentrated sulfuric acid, the catalysts were destroyed by the addition of a small portion of either sodium ethylate in methanol or more efficiently, ammoniacal methanol solution. The polymers obtained were repeatedly reprecipitated by employing a chloroform (good solvent)–*n*-pentane (poor solvent) or benzene (good solvent)–*n*-pentane (poor solvent) system. On the other hand, aluminum trichloride was removed by filtration from the diluted ether or methylene chloride solution as quickly as possible. After a small portion of ammoniacal methanol solution was added to remove the remaining catalyst, the addition of *n*-pentane gave a white or slightly yellowish polymer.

The purified polymers thus obtained were dried either at room temperature under reduced pressure (1–2 mm. Hg) for 20–40 hr. or by freeze-drying from benzene solution. The complete removal of the trapped solvent was achieved only by the latter technique. Some typical examples are shown in Tables I–III.

**Polymerization with Aluminum Trichloride at Room Temperature.** Polymerization was carried out in a glass ampule at room temperature. Aluminum trichloride was added to the monomer solution in ether or in benzene under a dry nitrogen atmosphere. Two days later, the resulting

yellow viscous solution was diluted with an equal volume of solvent, and aluminum trichloride was removed by filtration. The removal of the catalyst was completed by addition of a small portion of ammoniacal methanol solution. Addition of *n*-pentane yielded a slightly yellowish polymer. The resulting polymer was purified and dried in a similar manner as described above. In the case of 4-methylene-1,3-dioxolane, however, the polymer was formed on an aluminum trichloride surface and was insoluble in conventional organic solvents. The exact reaction conditions and results are shown in Tables I-III. At room temperature with boron trifluoride etherate, the polymerization system immediately became black.

**Fortuitous Polymerization with Molecular Sieves.** 2,2-Dimethyl-4-methylene-1,3-dioxolane (about 50 g.) in ether (40 ml.) was kept over molecular sieves (4 Å.) (about 10 g.) for a month. After the molecular sieves were removed by filtration, the solution was submitted to distillation. Pure 2,2-dimethyl-4-methylene-1,3-dioxolane (32 g.) boiling at 110-111°C. was obtained. On the other hand, the distillation residue was diluted with benzene to reduce the viscosity of the system. After the filtration, addition of *n*-pentane gave a white polymer (2.5 g.) (see Table I).

2-Methyl-4-chloromethyl-1,3-dioxolane (37.0 g.) was dehydrohalogenated by the procedure described above. The resulting crude product (about 30 ml.) was washed with a small portion of water. When molecular sieves (5 Å.) (about 4 g.) were added to this solution, some heat was instantaneously evolved probably due to the water present and, at the same time, viscosity increase of the system was observed. About an hour later, the resulting viscous gel was dissolved in benzene. After the molecular sieves were removed by filtration, a white polymer (6.1 g.) was obtained by addition of *n*-pentane. On the assumption of an average yield for the dehydrohalogenation step, the polymer yield is estimated at about 70% (see Table II).

**Copolymerization with Acrylonitrile by Ultraviolet Irradiation.** A mixture of a 4-methylene-1,3-dioxolane derivative and acrylonitrile was placed in a Pyrex glass ampule and irradiated by ultraviolet light (Hanovia lamp, Type SH). In the case of the 2,2-dimethyl- or 2-methyl- derivative, the resulting hard, clear solid was dissolved in chloroform and reprecipitated by addition of *n*-pentane or methanol to give a white polymer. It was dried under 1-2 mm. Hg pressure at 60°C. for 24 hr. When 4-methylene-1,3-dioxolane was used as a component, the copolymer was soluble only in *N,N*-dimethylformamide and reprecipitated by addition of methanol. The resulting polymer was thoroughly washed by methanol and dried at 40°C. under 0.5-1.0 mm. Hg pressure for 16 hr. The results are shown in Table IV.

The pure monomers of 4-methylene-1,3-dioxolane derivatives did not show any tendency to polymerize under the same conditions.

We wish to acknowledge the support via a predoctoral fellowship granted by the United Carbon Company of Houston, Texas.

## References

1. Hill, J. W., and W. H. Carothers, *J. Am. Chem. Soc.*, **57**, 925 (1935).
2. Vaala, G. T., and R. B. Carlin, U. S. Pat. 2,385,661 (1945).
3. Gresham, W. F., U. S. Pat. 2,394,910 (1946).
4. Strepikheev, A. A., and A. V. Volokhina, *Dokl. Akad. Nauk SSSR*, **99**, 407 (1954).
5. Frommelt, H., *Angew. Chem.*, **69**, 148 (1957).
6. Muetterties, E. L., U. S. Pat. 2,856,370 (1958).
7. Pattison, D. B., U. S. Pat. 2,870,097 (1959).
8. Bodenbenner, K., *Ann.*, **623**, 183 (1959).
9. Johnson, P. R., H. M. Barnes, and S. M. McElvain, *J. Am. Chem. Soc.*, **62**, 964 (1940).
10. McElvain, S. M., and M. J. Curry, *J. Am. Chem. Soc.*, **70**, 3781 (1948).
11. McElvain, S. M., *Chem. Revs.*, **45**, 453 (1949).
12. Field, N. D., *J. Am. Chem. Soc.*, **83**, 3504 (1961).
13. Radcliffe, M. R., and W. G. Mayes, U. S. Pat. 2,445,733 (1948).
14. Dynamit A.-G., vorm. Alfred Nobel and Co., Ger. Pats. 906,514 (1954), 926,937 (1955).
15. Kenyon, W. O., and T. F. Murray, Jr., U. S. Pat. 2,415,638 (1947).
16. Scheibe, G., *Ber.*, **58**, 586 (1925).
17. Herold, W., and K. L. Wolf, *Z. Physik. Chem.*, **B12**, 165 (1931).
18. Dimroth, K., *Angew. Chem.*, **52**, 545 (1939).
19. Willfang, G., *Ber.*, **74**, 145 (1941).
20. Fisher, H. O. L., E. Baer, and L. Feldmann, *Ber.*, **63**, 1732 (1930).
21. Mariella, R. P., and J. L. Leech, *J. Am. Chem. Soc.*, **71**, 3558 (1949).

Received January 28, 1964

## Résumé

On a polymérisé le 4-méthylène-1,3-dioxolane et ses dérivés avec des catalyseurs cationiques. Au moyen d'études infrarouges et ultraviolettes, on a trouvé que les polymères de 2,2-diméthyl- ou 2-méthyl-1,3 dioxolane contiennent encore beaucoup de carbonyles. Ceci indique que la polymérisation prend place de telle manière que l'ouverture de la double liaison carbone-carbone est couplée avec un réarrangement concurrent d'un cycle acétalique en cours de propagation pour donner des séquences cétoesters. Pour le 4-méthylène-1,3-dioxolane, on a trouvé que la polymérisation prend place surtout à la double liaison carbone-carbone. On a étudié aussi la copolymérisation de ces monomères avec l'acrylonitrile sous l'influence de rayons ultraviolets.

## Zusammenfassung

4-Methylen-1,3-dioxolan und seine Derivate wurden mit kationischen Katalysatoren polymerisiert. Nach Infrarot- und Ultraviolettuntersuchungen besitzen die 2,2-Dimethyl- und 2-Methyl-1,3-dioxolanpolymeren einen beträchtlichen Gehalt an Carbonylgruppen. Das beweist, dass die Polymerisation in der Weise erfolgt, dass die Öffnung der Kohlenstoff-Kohlenstoffdoppelbindung beim Wachstumsschritt mit einer gleichzeitig verlaufenden Acetalringumlagerung unter Bildung von "Ketoäther"-sequenzen gekoppelt ist. Andererseits polymerisiert 4-Methylen-1,3-dioxolan bevorzugt an der Kohlenstoff-Kohlenstoffdoppelbindung. Auch die Copolymerisation dieser Monomeren mit Acrylnitril bei Ultraviolettbestrahlung wurde untersucht.

## Optically Active Polymers: Cyclopolymerization of the Divinylacetal of (*R*)(+)-3,7- Dimethyloctanal

AKIHIRO ABE and MURRAY GOODMAN, *Polymer Research Institute,  
Polytechnic Institute of Brooklyn, Brooklyn, New York*

### Synopsis

The divinylacetal of (*R*)(+)-3,7-dimethyloctanal was polymerized by radical and cationic initiators. Radical initiation gave only viscous liquid polymers, while cationic systems gave solid products. Optical rotatory dispersions of these polymers fit simple Drude plots. The polymer prepared by boron trifluoride etherate exhibits negative optical rotations, while both the polymer obtained by azobisisobutyronitrile and the model compound show positive rotations. From these observations, it is suggested that the polymers might differ from each other in stereoregularity.

### INTRODUCTION

Cyclopolymerization of divinylacetal has been reported by Matsuyan et al.<sup>1-3</sup> They prepared a variety of soluble polymers carrying different aldehyde residues by radical initiation. Cationic polymerization, however, gave only insoluble polymers.

We prepared a divinylacetal derived from (*R*)(+)-3,7-dimethyloctanal, which yields soluble polymers either by radical or cationic initiation under certain conditions. Our original attempt to study the radical polymerization kinetics by optical rotatory technique<sup>4-6</sup> was unsuccessful because of the small differences in the optical rotatory power between the monomer and polymer. It was, however, found that the optical activity of the polymer is opposite in sign when a cationic catalyst is employed in the polymerization.

### RESULTS

The monomer, divinylacetal of (*R*)(+)-3,7-dimethyloctanal, was prepared from (*R*)(+)-citronellal\* by a synthesis involving the following steps: (a) hydrogenation of the carbon-carbon double bond, (b) acetal formation with 2-chloroethanol, followed by dehydrohalogenation.

The results of the polymerization are summarized in Table I.

\* This aldehyde was obtained by purification of commercial citronellal<sup>7</sup> and possesses  $[\alpha]_D^{26} = 12.9^\circ$ . Optical purity of this material appears to be about 80%.<sup>8</sup>

TABLE I  
Polymerization of Divinylacetal of (*R*)(+)-3,7-Dimethyloctanal

Initiator used	Reaction temp., °C.	Solvent and amt., ml.	Monomer, g.	Amt. initiator	Reaction time, hr.	Polymer yield, %	Viscosity $[\eta]$ , (100 ml./g.)
BF <sub>3</sub> ·OEt <sub>2</sub> (48%)	-78	Ether, 250	8.5	1.5 ml.	30	39.8 <sup>a</sup>	0.24 <sup>b</sup>
AlCl <sub>3</sub>	-78	Ether, 5	0.85	0.3 g.	240	11.7	—
AIBN	80	Bulk	2.6	0.027 g.	24	50.8 <sup>c</sup>	—
AIBN	76	Benzene, 5	4.3	0.035 g.	20	46.8	—

<sup>a</sup> Anal. Calcd. for (C<sub>14</sub>H<sub>26</sub>O<sub>2</sub>): C, 74.27%; H, 11.59%. Found: C, 74.53%; H, 11.76%.

<sup>b</sup> In chloroform at 25.5°C.

<sup>c</sup> Anal. Calcd. for (C<sub>14</sub>H<sub>26</sub>O<sub>2</sub>): C, 74.27%; H, 11.59%. Found: C, 74.37%; H, 11.62%.

TABLE II  
Optical Rotatory Properties of Poly[divinylacetal of (*R*)(+)-3,7-Dimethyloctanal] and its Model Compound

Model compound ( <i>R</i> )(+)-2-[2,6-Dimethylheptyl]-1,3-dioxane Polymer (polymerization initiated by AIBN in bulk) Polymer (polymerization initiated by AIBN in benzene) Polymer (polymerization initiated by BF <sub>3</sub> ·OEt <sub>2</sub> )	Solvent	Concentration, g./ml.	Optical activity			Drude constants	
			$[\alpha]_{450}^{25}$	$[\alpha]_{589}^{25}$	$[M]_{589}^{25}$	$K \times 10^{-5}$	$\lambda_c, m\mu$
	Benzene	0.20256	0.790	0.434	0.929	1.40	161
	Chloroform	0.19298	4.72	2.48	5.31	7.71	195
	Benzene	0.03987	3.41	1.71	3.86	5.10	222
	Chloroform	0.05450	6.13	3.18	7.19	10.2	187
	Chloroform	0.03852	5.06	2.82	6.37	8.06	206
	Benzene	0.04818	-14.21	-7.56	-17.09	-23.4	193
	Chloroform	0.07144	-12.34	-6.78	-15.32	-21.8	160

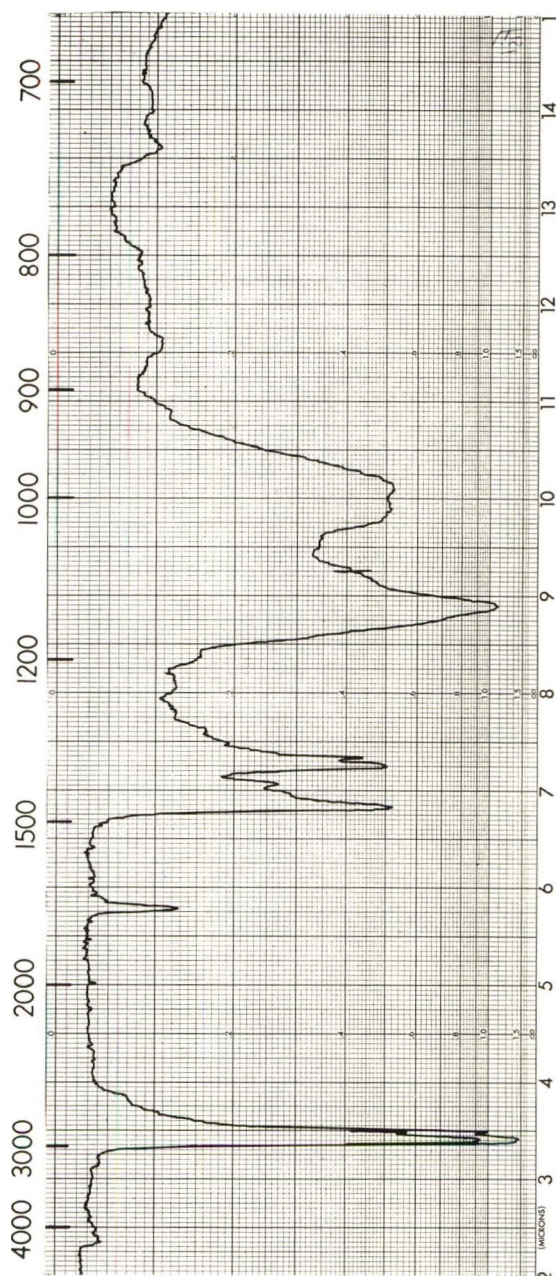


Fig. 1. Infrared spectrum of poly[divinylacetal of (*R*)(+)-3,7-dimethyloctanal] prepared by AIBN initiator (film).

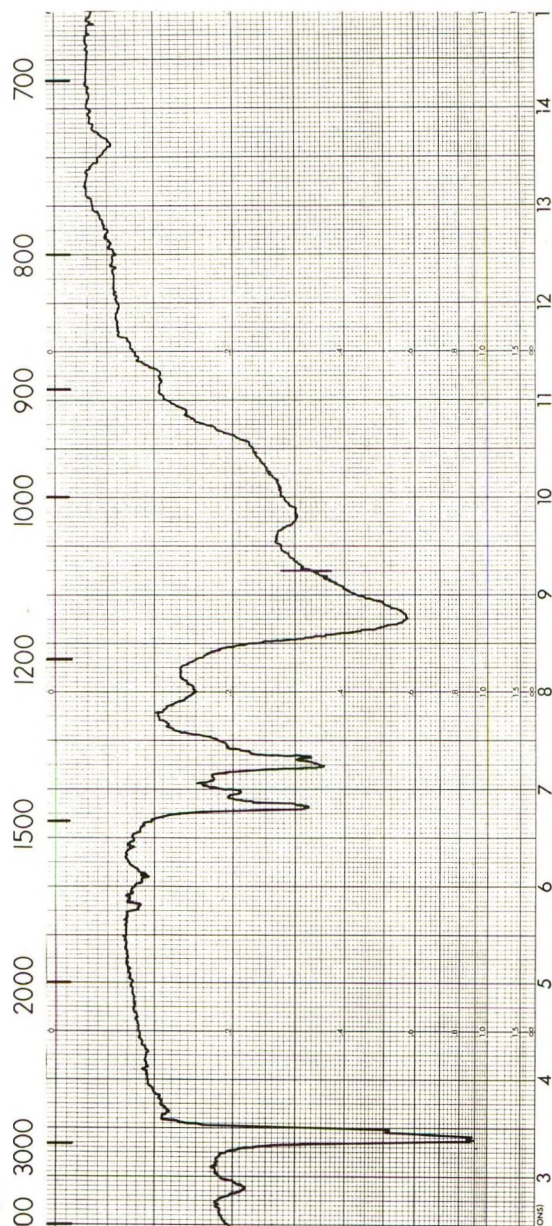


Fig. 2. Infrared spectrum of poly[divinylacetal of (R)(+)-3,7-dimethyloctanal] prepared by  $\text{BF}_3 \cdot \text{OEt}_2$  catalyst (KBr disk).

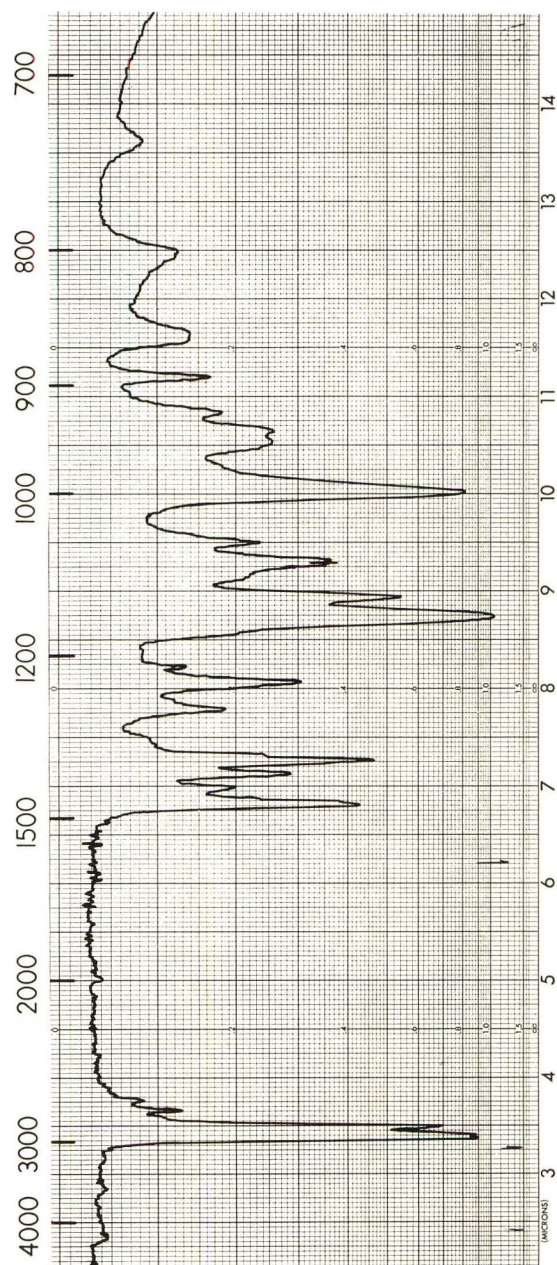


Fig. 3. Infrared spectrum of (R)(+)-2-[2,6-dimethylheptyl]-1,3-dioxane (liquid).

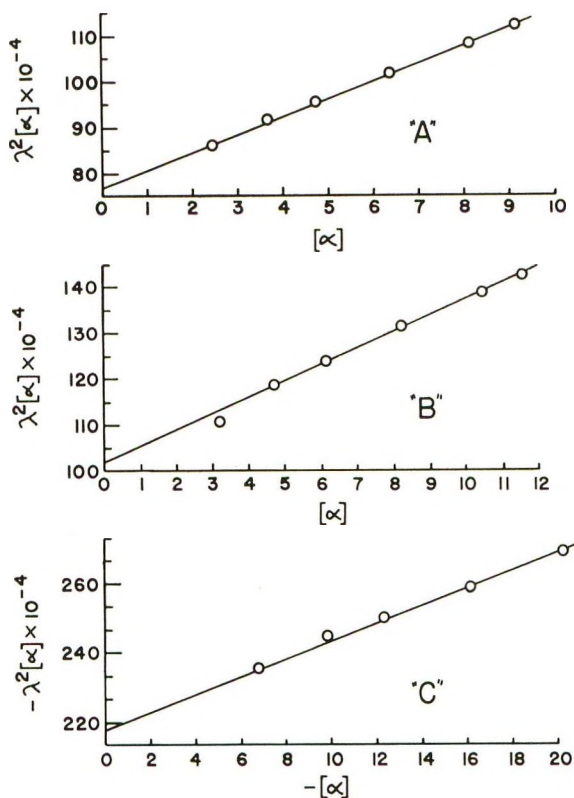


Fig. 4. Drude dispersions of poly[divinylacetal of (*R*)(+)-3,7-dimethyloctanal] and its model compound (in chloroform at 25°C.): (A) model compound; (B) polymer prepared by AIBN initiator; (C) polymer prepared by  $\text{BF}_3 \cdot \text{OEt}_2$  catalyst.

Radical polymerization with azobisisobutyronitrile as an initiator gave only extremely viscous liquid either in bulk or in solution. The polymer is soluble in benzene or in chloroform and insoluble in methanol.

Cationic polymerization initiated by boron trifluoride etherate or aluminum trichloride yielded solid polymers. Soluble solid polymer was obtained only when the polymerization was carried out at very high dilution. At higher concentration of the monomer, the polymers were completely or partially insoluble, probably because of crosslinking side reactions. The soluble polymer thus obtained can be reprecipitated from benzene or chloroform solution by addition of methanol. The polymer is amorphous on x-ray examination, and it turns to a viscous liquid at 120–130°C.

Infrared spectra of the polymers prepared by azobisisobutyronitrile and boron trifluoride etherate as initiators are shown in Figures 1 and 2, respectively. In spite of the fact that one was taken as a film and the other as a potassium bromide pellet, they are quite similar to each other except in the region of  $1000 \text{ cm}^{-1}$ , where the polymer prepared by azobisisobutyronitrile possesses a double peak ( $1010$  and  $990 \text{ cm}^{-1}$ ) and that initiated by

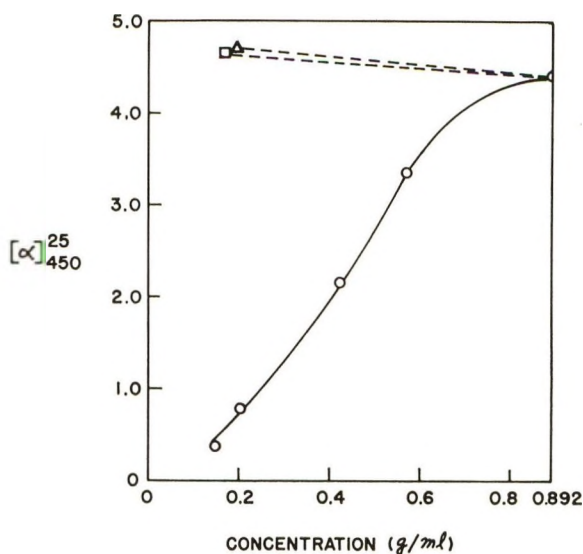


Fig. 5. Concentration effect on the optical rotatory power of (*R*)(+)-2-(2,6-dimethylheptyl)-1,3-dioxane: (Δ) chloroform; (□) dioxane; (○) benzene.

boron trifluoride etherate shows a broad peak ( $1020\text{ cm}^{-1}$ ). For comparison purposes, a low molecular weight model compound, an acetal derived from (*R*)(+)-3,7-dimethyloctanal and 1,3-propanediol, was also prepared. The infrared spectrum of the model compound (Fig. 3) is quite different from those of the polymers.

Optical rotatory properties of the polymers and model compounds were studied by using a Rudolph polarimeter equipped with a xenon-mercury lamp and a photoelectric read-out system. The results are shown in Table II. As shown in Figure 4, optical rotatory dispersions of both polymers and model compounds fit simple Drude plots:<sup>9</sup>

$$[\alpha] = K/(\lambda^2 - \lambda_c^2)$$

the constants of which are also summarized in Table II. While the polymer obtained by radical initiation possesses the same sign (positive) and the same order of magnitude of the rotation of the model compound, the polymer prepared by cationic catalyst exhibits a negative optical rotation.

As shown in Figure 5, while the model compound shows a very large concentration effect on its optical rotatory power in benzene, there is little effect on the polymers in the observed range of concentrations (3–16% of solute). It is, however, interesting to note that while the model compound and the polymer prepared by azobisisobutyronitrile show lower optical rotations in benzene than in chloroform, the polymer prepared by boron trifluoride etherate possesses higher absolute values of rotation in benzene (Table II). In other words, the optical rotatory powers of all the compounds shift in the negative direction in benzene. A similar solvent effect

TABLE III  
Concentration Effect on the Optical Rotatory Powers of Cyclic and Open-Chain Acetals

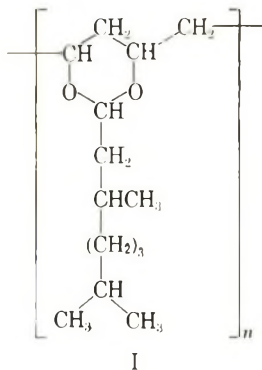
	Solvent	Concentration, g./ml.	Optical activity		Drude constants	
			$[\alpha]_{450}^{25}$	$[\alpha]_D^{25}$	$K \times 10^{-6}$	$\lambda_c$ m $\mu$
<i>(R)</i> (+)-2-[2,6-Dimethylheptyl]-1,3-dioxane (cyclic acetal)	Bulk	—	4.41	2.35	7.41	185
	Benzene	0.5905	3.36	1.84	5.86	168
	"	0.42373	2.16	1.18	3.76	163
	"	0.20256	0.790	0.434	1.40	161
	Chloroform	0.19298	4.72	2.48	7.71	195
	Dioxane	0.16745	4.67	2.46	7.85	185
Diethylacetal of <i>(R)</i> (+)-citronellal	Bulk	—	7.69	3.91	11.6	226
	Benzene	0.14822	6.41	3.29	9.50	235
	Chloroform	0.17856	9.29	4.76	14.1	224

has been observed for poly-L-propylene oxide by Price and Osgan.<sup>10</sup> As shown in Table III, however, an open chain acetal, the diethyl acetal of (*R*)(+)-citronellal,<sup>7</sup> does not exhibit as large a concentration effect in benzene as that observed on the above cyclic acetal.

Because of the small optical activity difference between the monomer and the polymer prepared by radical initiators, we could not carry out satisfactory kinetic studies on the cyclopolymerization by the optical rotation method.<sup>4-6</sup> When the monomer concentration was low, the optical activity change resulting from polymerization was too small to follow. At a high monomer concentration (1.54 mole/l. in dioxane), only zero-order rate was observed. The polymerization was initiated by benzoyl peroxide (1.6 mole-% of the monomer) at 54°C.

### DISCUSSION

Complete disappearance of the carbon-carbon double bond (1650, 944, and 843 cm.<sup>-1</sup>) on polymerization (Figs. 1 and 2) and fairly high solubilities of the polymers suggest that the polymers possess mainly linear polyvinylacetal structures(I):



As mentioned above, the following differences are recognized between the polymers obtained by radical and cationic initiators: (1) molecular weight (one is a viscous liquid, while the other is solid), (2) infrared spectra in the region about 1000 cm.<sup>-1</sup>, (3) optical rotatory properties. The molecular weight of the polymer prepared with azobisisobutyronitrile is apparently much lower than that of the polymer obtained with boron trifluoride etherate. We recognize that this is a factor in some differences in properties noted above. These differences may reside, however, in the stereoregularities of the polymers, a possibility now under active investigation in our laboratories. At this stage, however, we favor the latter explanation based on related work with optically active polyolefins, polyaldehydes, and polyethers.

It has been demonstrated<sup>7,11-14</sup> that optically active vinyl or acetal polymers carrying asymmetric sites in their side chains can show optical

activity enhancements over corresponding monomers or low molecular weight model compounds only when the asymmetric site is sufficiently close to the main chain of the polymer to limit the number of allowed conformations.<sup>15</sup> Following this line of reasoning, the difference in the optical rotatory power between the model compound and the divinyl acetal polymer prepared by boron trifluoride etherate, can arise from the stereoregular structure of this polymer. It is also reasonable to expect stereoregularity in such ionic polymerization at low temperatures. If all of the carbon-carbon bonds of the main chain are exclusively either equatorial or axial with reference to the corresponding six-membered acetal rings (assuming the same conformation for all of the acetal rings), the main chain structure must be isotactic. If they are alternatively equatorial and axial, on the other hand, a syndiotactic polymer results.

At this point, we must consider another possibility, that is, an asymmetric induction during polymerization. As we can see from structure I, each of the methinyl carbons in the main chain is truly asymmetric in its immediate vicinity, because the two methylene groups on either side are not identical, since one is in the ring, while the other bridges the ring system. If the polymer possesses an isotactic sequence, however, any adjacent asymmetric centers in the main chain are opposite in their configuration with reference to the acetal ring. In other words, internal compensation of the optical activity takes place in an isotactic polymer chain. On the other hand, a syndiotactic polymer contains only asymmetric centers of the same configuration. Therefore, if the polymerization proceeds under the influence of the asymmetric sites in the side chain<sup>16-18</sup> and if the resulting polymer favors a syndiotactic structure, we may expect some optical activity contribution from these newly induced asymmetric centers in the main chain. We are now actively engaged in a structural investigation to test this hypothesis.

## EXPERIMENTAL

The chemical analyses were carried out by Schwarzkopf Microanalytical Laboratory.

### Syntheses of the Monomer and Model Compound

**(*R*)(+)-3,7-Dimethyloctanal.** Palladium (5%) on charcoal (1.5 g.) was added to freshly distilled (*R*)(+)-citronellal (60.0 g., 0.39 mole) in methanol (150 ml.) under a nitrogen atmosphere. Hydrogenation was carried out under 40 psi hydrogen pressure using a Parr apparatus at room temperature. Hydrogen absorption ceased in 3 hr. after a quantitative amount of hydrogen was absorbed. The catalyst was removed by filtration. Pure (*R*)(+)-3,7-dimethyloctanal (55.4 g.) was obtained by distillation under reduced pressure; yield 91.0%; b.p. 50°C./1.2 mm. Hg;  $[\alpha]_D^{24} = +10.0^\circ$  ( $c = 4.550$  benzene).

**Divinylacetal of (*R*)(+)-3,7-dimethyloctanal.** A mixture of (*R*)(+)-3,7-dimethyloctanal (78.0 g., 0.5 mole), 2-chloroethanol (80.0 g., 1 mole), and *p*-toluenesulfonic acid monohydrate (4 g.) in benzene (150 ml.) was refluxed in a flask equipped with a Dean-Stark trap. In 5 hr., an almost theoretical amount (9 ml., 0.5 mole) of water was separated. The reaction mixture was poured into 10% sodium carbonate solution (200 ml.) to remove the catalyst. The organic layer was separated, washed by water, and dried over anhydrous sodium sulfate overnight. After the solvent (benzene) was removed by distillation under reduced pressure, the red-brown liquid was submitted to alkali fusion without further purification.

Commercial potassium hydroxide pellets (300 g.) were placed in a three-necked copper flask and heated to 250°C. with stirring under reduced pressure (3 mm. Hg). After 1 hr. of heating, solidified potassium hydroxide was allowed to cool to room temperature. The crude acetal obtained above was added to this solid potassium hydroxide at atmospheric pressure. The mixture was again heated until the potassium hydroxide melted. The product was collected by distillation under reduced pressure (70–120°C./3 mm. Hg), washed with water, and dried over anhydrous sodium sulfate overnight. Pure divinylacetal of (*R*)(+)-3,7-dimethyloctanal (17.0 g.) was obtained by distillation under reduced pressure; yield 15.0% (based on the starting aldehyde); b.p. 77–80°C./2.8 mm. Hg;  $n_D^{24}$  1.4489,  $d_4^{24}$  0.8542,  $[\alpha]_D^{26} = +3.04^\circ$  ( $c = 10.703$  chloroform).

ANAL. Calcd. for ( $C_{14}H_{26}O_2$ ): C, 74.27%, H, 11.59%. Found: C, 74.49%, H, 11.64%.

**(*R*)(+)-2-[2,6-Dimethylheptyl]-1,3-dioxane (Model Compound).** A mixture of (*R*)(+)-3,7-dimethyloctanal (78.0 g., 0.5 mole) and 1-3-propanediol (38.0 g., 0.5 mole) in benzene (150 ml.) was refluxed in the presence of *p*-toluenesulfonic acid monohydrate (4 g.). Water formed (9 ml., 0.5 mole) was removed with the use of a Dean-Stark trap. After 5 hr., the reaction mixture was decanted into 10% sodium carbonate solution (300 ml.) to remove the catalyst. The organic layer was separated, washed with water, and dried over anhydrous sodium sulfate overnight. After the removal of the solvent, the product (75.6 g.) was obtained by distillation under reduced pressure; yield 70.7%; b.p. 85.5–86.0°C./1.3 mm. Hg;  $n_D^{21}$  1.4482;  $d_4^{24}$  0.8920;  $[\alpha]_D^{25} = +2.48^\circ$  ( $c = 19.298$  chloroform).

ANAL. Calcd. for ( $C_{19}H_{36}O_2$ ): C, 72.84%, H, 12.23%. Found: C, 72.73%, H, 12.46%.

## Polymerization

**Radical Polymerization.** The monomer, divinylacetal of (*R*)(+)-3,7-dimethyloctanal was polymerized by azobisisobutyronitrile at 80.0°C. in a sealed Pyrex glass tube under a nitrogen atmosphere. After 24 hr., the resulting viscous liquid was washed with methanol and dissolved in benzene. After filtration, the polymer was obtained by addition of methanol. The

polymer was reprecipitated several times in the same manner and dried at 40°C. under reduced pressure (2 mm. Hg) for 24 hr. A transparent viscous liquid was obtained.

Solution polymerization in benzene was also carried out in a similar manner as described above.

The results are shown in Table I.

**Cationic Polymerization.** Polymerization with an aluminum trichloride catalyst was carried out in diethyl ether as a solvent in a glass tube at Dry Ice-acetone temperatures under a nitrogen atmosphere. The reaction mixture was washed by ammoniacal methanol to destroy the catalyst. The polymer formed was purified by reprecipitation with a benzene-methanol system and dried at 40°C. under 2 mm. Hg pressure for 24 hr.

A soluble polymer was also prepared with the use of boron trifluoride etherate (48%) as a catalyst. Polymerization was carried out in a three-necked flask under nitrogen at the temperature of Dry Ice-acetone. During the polymerization, stirring was continued and the resulting polymer was treated in a similar manner as described above. A white polymer was obtained by freeze-drying from benzene solution. The exact conditions and results are summarized in Table I.

The authors gratefully acknowledge the financial support of the United Carbon Company for this work.

## References

1. Matsoyan, S. G., and M. G. Avetyan, *J. Gen. Chem. USSR (Eng. Transl.)*, **30**, 697 (1960).
2. Matsoyan, S. G., M. G. Avetyan, and M. G. Voskanyan, *Vysokomolekul. Soedin.*, **2**, 314 (1960).
3. Matsoyan, S. G., *J. Polymer Sci.*, **52**, 189 (1961).
4. Marvel, C. S., J. Dec, and H. G. Cooke, Jr., *J. Am. Chem. Soc.*, **62**, 3499 (1940).
5. Price, C. C., and R. W. Kell, *J. Am. Chem. Soc.*, **63**, 2798 (1941).
6. Marvel, C. S., and C. G. Overberger, *J. Am. Chem. Soc.*, **66**, 475 (1946).
7. Abe, A., and M. Goodman, *J. Polymer Sci.*, **A1**, 2193 (1963).
8. Pino, P., et al., to be published.
9. Djerassi, C., *Optical Rotatory Dispersion*, McGraw-Hill, New York, 1960.
10. Price, C. C., and M. Osgan, *J. Am. Chem. Soc.*, **78**, 4787 (1956).
11. Pino, P., F. Ciardelli, G. P. Lorenzi, and G. Montagnoli, *Makromol. Chem.*, **61**, 207 (1963).
12. Bailey, W. J., and E. T. Yates, *J. Org. Chem.*, **25**, 1800 (1960).
13. Nozakura, S., S. Takeuchi, H. Yuki, and S. Murahashi, *Bull. Chem. Soc. Japan*, **34**, 1673 (1961).
14. Goodman, M., M. A. Stake, A. Abe, and K. J. Clark, *Makromol. Chem.*, **72**, 131 (1964).
15. Brewster, J. H., *J. Am. Chem. Soc.*, **81**, 5475 (1959).
16. Beredjick, N., and C. Schuerch, *J. Am. Chem. Soc.*, **78**, 2646 (1956); **80**, 1933 (1958).
17. Schmitt, G. J., and C. Schuerch, *J. Polymer Sci.*, **45**, 313 (1960).
18. Pino, P., F. Ciardelli, G. P. Lorenzi, and G. Natta, *J. Am. Chem. Soc.*, **84**, 1487 (1962).

### Résumé

Le divinyl-acétal du (*R*)(+)-3,7-diméthyl-octanal a été polymérisé au moyen d'initiateurs radicalaires et cationiques. Les initiateurs radicalaires ne donnent que des polymères visqueux et liquides, tandis que les systèmes cationiques donnent des produits solides. Les dispersions optiques rotatoires de ces polymères donnent des diagrammes de Drude simples. Le polymère préparé avec l'éthérate du trifluorure de bore montre des rotations optiques négatives, tandis que les polymères obtenus avec l'azo-bis-isobutyronitrile et le composé modèle montrent des rotations positives. À partir de ces observations, on suggère que les polymères possèdent une stéréorégularité différente.

### Zusammenfassung

Das Divinylacetal von (*R*)(+)-3,7-Dimethyloctanal wurde mit radikalischen und kationischen Startern polymerisiert. Radikalstart lieferte nur viskose flüssige Polymere während kationische Systeme zu festen Produkten führten. Die optische Rotationsdispersion dieser Polymeren gehorchte der einfachen Drude-Beziehung. Das mit Bortrifluorid-Ätherat hergestellte Polymere zeigt negative optische Drehung während sowohl das mit Azoisobutyronitril erhaltene Polymere als auch die Modellverbindung positive Drehung zeigen. Aus diesen Beobachtungen wird geschlossen, dass sich die Polymeren in ihrer Stereoregularität unterscheiden.

Received January 28, 1964

## Thermal Decomposition of Model Compounds of Polyvinyl Chloride. I. Gaseous Thermal Decomposition of Model Compounds Having Secondary and Tertiary Chlorine

MITSUO ASAHINA and MITSUO ONOZUKA, *Tokyo Laboratory, Kureha Kagaku Company, Ltd., Tokyo, Japan*

### Synopsis

The thermal stabilities of branched model compounds of poly(vinyl chloride) are studied in the gaseous state. The compounds containing tertiary chlorine, i.e., 2-methyl-2-chloropropane and 3-ethyl-3-chloropentane, are compared with those containing a secondary chlorine, i.e., 2-chloropropane and 2,4-dichloropentane. The results of gaseous thermal decomposition show that the tendency of C-Cl cleavage depends on the electronegativity of carbon bonded chloride. The decomposition temperature  $T_D$  can be used for the evaluation of the thermal stabilities of various model compounds.

### INTRODUCTION

The thermal dehydrochlorination of polyvinyl chloride has been studied extensively.<sup>1-7</sup> Druesdow and Gibbs<sup>8</sup> suggested that the first hydrogen chloride is lost from a position which is inherently unstable due to some structural abnormality such as tertiary chlorine and allyl type chlorine. Baum and Wartman,<sup>9</sup> from their experimental results on low molecular weight models of polyvinyl chloride, considered the sites for initiation to be unsaturated chain ends at about 150°C. and tertiary chlorine at about 190°C. However, the mechanism of dehydrochlorination of polyvinyl chloride is a very complicated process, and there are many problems which remain to be solved.

It is a matter of course to consider that the thermal stability should be different for each kind of abnormal structure, e.g., branched chain, unsaturated bond, or catalyst fragment at chain end.

The use of model compounds is a convenient way to elucidate the decomposition of polyvinyl chloride in relation to the abnormal structures in the molecular chain. Thus, we carried out experimental studies on the gaseous thermal decomposition of some low molecular weight chloride, which are considered the models of abnormal structures in polyvinyl chloride.

The present communication deals with the experimental results on the models of secondary chloride and tertiary chloride.

## EXPERIMENTAL

### A. Preparation of Model Compounds

The model compounds used in this work were purified by gas chromatography after distillation. Pure compounds were readily separated from impurities in this way and were analyzed by infrared spectrometry as well as gas chromatography and also by elemental analysis for carbon, hydrogen, and chlorine. Refractive indices close to the literature values were obtained for all samples.

**2-Chloropropane.** 2-Chloropropane was prepared by chlorination of 2-hydroxypropane. Purified sample showed  $n_D^{20}$ , 1.377; lit.,<sup>10</sup> 1.377.

ANAL. Calcd. for  $C_3H_7Cl$ : C, 45.8%; H, 8.9%; Cl, 45.2%. Found: C, 45.1%; H, 8.9%; Cl, 44.9%.

**2,4-Dichloropentane.** 2,4-Dichloropentane was prepared by chlorination of 2,4-dihydroxypentane which was obtained by hydrogenation of acetyl acetone with Raney nickel catalyst. Purified sample showed  $n_D^{20}$ , 1.4345–55; lit.,<sup>10</sup> 1.4360.

ANAL. Calcd. for  $C_5H_{10}Cl_2$ : C, 42.7%; H, 7.1%; Cl, 50.3%. Found: C, 43.2%; H, 7.3%; Cl, 49.9%.

**2-Methyl-2-chloropropane.** 2-Methyl-2-chloropropane was prepared by chlorination of *tert*-butyl alcohol. Purified sample showed  $n_D^{20}$ , 1.3820; lit.,<sup>10</sup> 1.3853.

ANAL. Calcd. for  $C_4H_9Cl$ : C, 51.8%; H, 9.7%; Cl, 38.4%. Found: C, 51.6%; H, 9.7%; Cl, 38.0%.

**3-Ethyl-3-chloropentane.** 3-Ethyl-3-chloropentane was prepared by chlorination of 3-ethyl-3-hydroxypentane which was obtained by reaction of diethyl ketone with ethyl Grignard reagent. Purified sample showed  $n_D^{20}$ , 1.436; lit.,<sup>10</sup> 1.4329.

ANAL. Calcd. for  $C_7H_{15}Cl$ : C, 62.4%; H, 11.1%; Cl, 26.4%. Found: C, 62.5%; H, 11.4%; Cl, 26.2%.

### B. Apparatus for Thermal Decomposition

The decompositions of the model compounds of polyvinyl chloride were studied in a static system by means of infrared spectrometry. A diagram of the apparatus is given in Figure 1. The gaseous sample used was adjusted by the stopcock  $K_1$  under a pressure from 10 to 200 mm. Hg, and the reaction vessel G was heated by a Nichrome coil at a temperature slightly higher than that at which the decomposition just takes place.

The reaction vessel was a gas cell, approximately 25 mm. long and 50 mm. in diameter, and completely enclosed in a box V which was heated by a Nichrome coil. The temperature of the reaction vessel was indicated by the thermometer T. During the reaction, the temperature of the reaction vessel was regulated so as to maintain the desired temperature, and could be kept constant almost indefinitely to within 1°C.

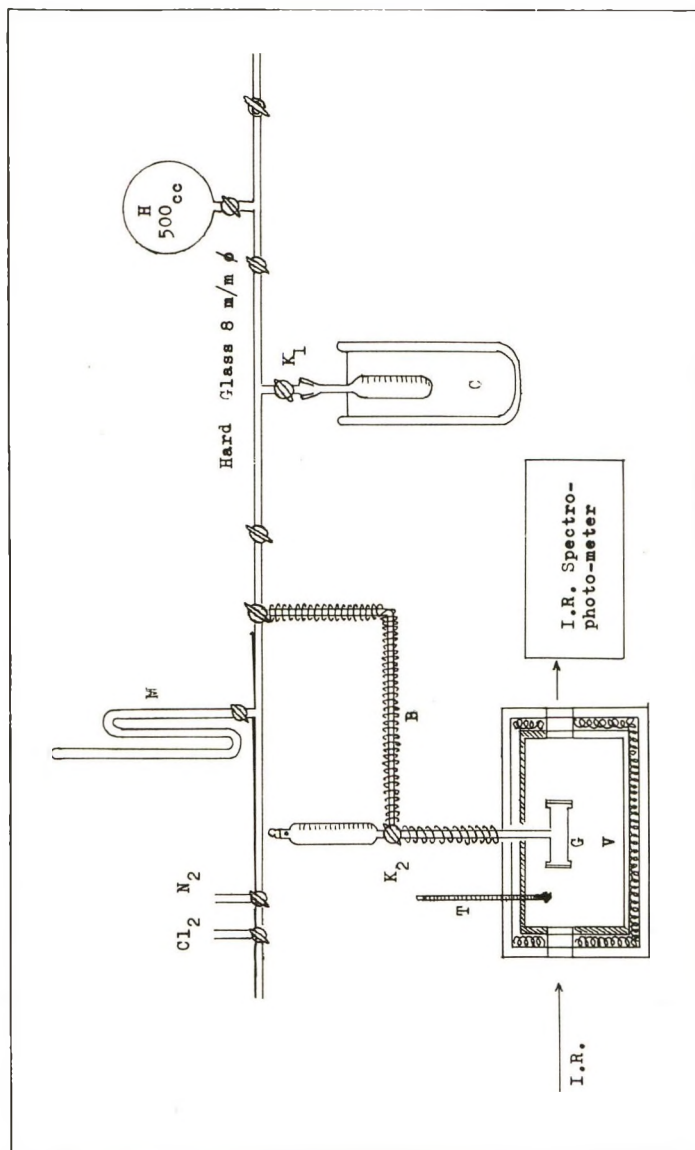


Fig. 1. Pyrolysis apparatus: (M) manometer; (H) gas reservoir; (B) band heater; (C) condenser; (T) thermometer; (G) gas cell

When the samples of high boiling point (e.g., 2,4-dichloropentane, 3-ethyl-3-chloropentane) were used, these samples were introduced through a stopcock  $K_2$ .

Before the pyrolysis the reaction vessel was evacuated and was flushed several times with nitrogen.

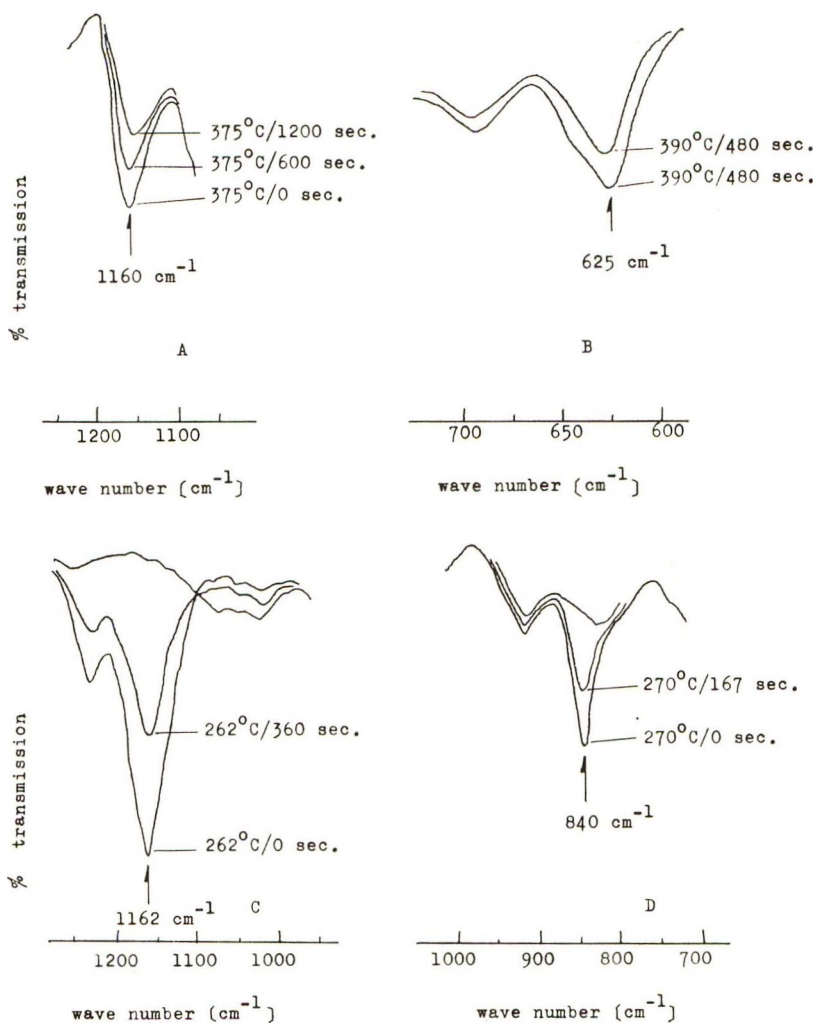


Fig. 2. Absorption spectra: (A) 2-chloropropane; (B) 2,4-dichloropentane; (C) 2-methyl-2-chloropropane; (D) 3-ethyl-3-chloropentane.

The reacted samples were analyzed by infrared spectrometry and the rate constant of decomposition for each sample was calculated on the basis of the decreasing absorption of key bands at 1160, 625, 1162, and  $840 \text{ cm}^{-1}$  for 2-chloropropane, 2,4-dichloropentane, 2-methyl-2-chloropropane, and 3-ethyl-3-chloropentane, respectively, as shown in Figure 2.

For gas chromatographic analysis of the decomposition products, 13 mm.  $\times$  3 m. steel columns packed with 40–60 mesh Shimalite brick containing 30% dioctyl phthalate and helium carrier gas were used. The products of thermal decomposition were put through the column at 20–120°C. at a flow rate of 70 ml./min.

## RESULTS AND DISCUSSION

The thermal decomposition of these model compounds was investigated over the temperature range of 230–380°C. The analytical results of decomposed samples showed that the decomposition products were hydrogen chloride and olefins, and the reaction should be a unimolecular dissociation process. It is readily understood from the results that the decomposition of model compounds is a first-order homogeneous gas reaction.

TABLE I  
Rate Constants at Various Temperatures of Model Compounds Containing Secondary and Tertiary Chlorines

Compound	Temperature, °C.	$k \times 10^4$ , sec. <sup>-1</sup>
2-Chloropropane	350	1.39
	362	3.04
	375	5.22
2,4-Dichloropentane	366	0.93
	376	1.26
	384	5.37
	392	8.26
2-Methyl-2-chloropropane	231	2.7
	240	8.1
	262	17.7
	280	89.4
3-Ethyl-3-chloropentane	230	3.8
	250	11.5
	262	21.5
	270	37.0

TABLE II  
Frequency Factors and Activation Energies of Samples

Model compound	Frequency factor $A$ , sec. <sup>-1</sup>	Activation energy $E_a$ , kcal./mole
2-Chloropropane	$1.1 \times 10^{11}$	42.4
2,4-Dichloro- pentane	$8.4 \times 10^{19}$	69.9
2-Methyl-2-chloro- propane	$7.9 \times 10^{12}$	41.6
3-Ethyl-3-chloro- pentane	$1.1 \times 10^{10}$	31.0

The unimolecular rate constant is given by

$$k = A \exp \{ -E_a/RT \} \quad (1)$$

The variation of the rate constant over the whole temperature range of 230–380°C. is shown in Table I. The activation energies are calculated from the plots of  $\log k$  against  $1/T$  are shown in Table II.

### A. Decomposition Temperatures

It is possible to evaluate the thermal stability of these model compounds by measuring the decomposition temperatures,  $T_D$ ,<sup>11</sup> which are defined as the measure of the temperature of initiation of decomposition.

When the reaction is reversible, the decomposition temperature may be obtained thermodynamically. But the thermal decompositions of these model compounds are irreversible reactions. Thus, we determined the  $T_D$  temperatures graphically as illustrated in Figure 3; the results are summarized in Table III.

TABLE III  
 $T_D$  of Model Compounds

Compound	$T_D$ , °C.
2-Chloropropane	340
2,4-Dichloropentane	360
2-Methyl-2-chloropropane	240
3-Ethyl-3-chloropropane	180

### B. Thermodynamics Factors

We tried to obtain the relation between  $T_D$  and the free energy of activation by using the absolute rate theory of Eyring.<sup>12</sup> The entropies of activation,  $\Delta S^*$ , at  $T_D$  were calculated according to Eq. (2).<sup>13</sup>

$$A = \kappa e(k_B T/h) \exp \{ \Delta S^*/R \} \quad (2)$$

where  $k_B$  is the Boltzmann constant ( $= 1.381 \times 10^{-16}$  erg./deg.);  $h$  is the Planck constant ( $= 6.624 \times 10^{-27}$  erg. sec.);  $\kappa$  is the transition coefficient, (assumed to be one);  $\Delta S^*$  is the entropy of activation (in calories/degree mole); and  $A$  is the frequency factor in the Arrhenius equation. The free energies of activation at  $T_D$  were calculated as follows

$$E_a = \Delta H^* - RT \quad (3)$$

$$\Delta F^* = \Delta H^* - T\Delta S^* \quad (4)$$

The results are shown in Table IV. From Eq. (5), it is readily seen that the rate constant,  $k$ , can be expressed by the free energy of activation

$$k = (k_B T/h) k_e^* = (k_B T/h) e^{-\Delta F^*/RT} \quad (5)$$

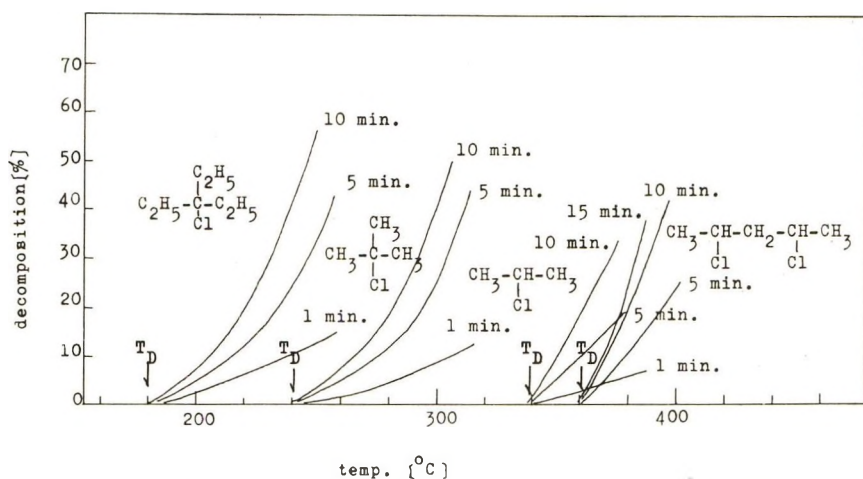


Fig. 3. Dependence of per cent decomposition on temperature and  $T_D$ .

where  $k_e^*$  is the constant for equilibrium between the ground state and transition state.

The contributions of the entropy term in the temperature interval of  $200^\circ$  which is the difference between the maximum and minimum values of

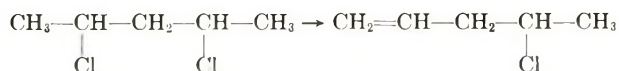
TABLE IV  
Thermodynamic Factors

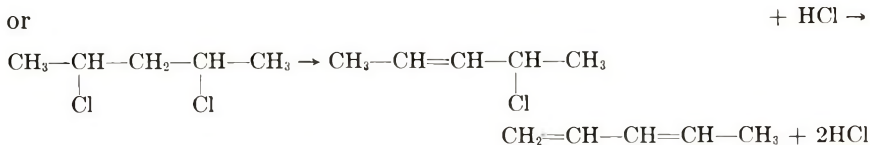
Model compound	$T_D$ , °K.	$E_a$ , kcal./mole	$\Delta H^*$ , kcal./mole	$\Delta S^*$ , e.u./mole	$\Delta F^*$ , kcal./mole
2-Chloropropane	613.2	42.4	41.1	-11.5	48.2
2,4-Dichloro- pentane	633.2	69.9	68.6	+29.2	50.2
2-Methyl-2-chloro- propane	513.2	41.6	40.6	-2.6	41.9
3-Ethyl-3-chloro- pentane	453.2	31.0	30.1	-15.4	37.1

$T_D$  among the samples are small enough so as not to affect the order of the results, that the free energy of activation at  $T_D$  could be used as a measure of thermal stability like  $T_D$ .

### C. Dehydrochlorination Mechanism and Relationships of Chemical Structure and Thermal Stability

The two possible decompositions lead to the same final products of reaction, e.g.,





As mentioned above, the mechanism of gas phase dehydrochlorination of the compounds is a unimolecular dissociation process and not a radical chain mechanism. If the decomposition takes place by a radical chain mechanism, the reaction should be affected extraordinarily by the presence of a radical scavenger such as propylene or the surface of the reaction vessel. In order to detect the wall effect, we carried out the experiments under various partial pressures of compound, but we could not observe any effect on the first-order rate constant. The absence of any inhibiting effect by propylene and wall effect in these decomposition are well proved by our experiments.

The model compounds (2-chloropropane and 2,4-dichloropentane) having the secondary chlorine showed the higher free energy of activation and higher decomposition temperature  $T_D$  than those (2-methyl-2-chloropropane and 3-ethyl-3-chloropentane) having the tertiary chlorine.

These results are consistent with the well recognized fact that the tendency of C-Cl cleavage depends upon the electronegativity of the carbon-bonded chlorine, and secondary chlorine is more stable than tertiary chlorine.

The mechanism of thermal dehydrochlorination of polyvinyl chloride is not so simple, because there are many kinds of weak points to initiate the decomposition, e.g., the unsaturated double bond at a chain end, tertiary chlorine of a branched chain, catalyst fragment at a chain end, and so on. Further work is in progress on the gaseous thermal decomposition of model compounds with an unsaturated chain end.

Thanks are given to Mr. Masao Koguro and Mr. Kazuo Sasaki for their assistance in the experimental work.

### References

1. Fox, V. W., J. G. Hendricks, and H. J. Ratti, *Ind. Eng. Chem.*, **41**, 1774 (1949).
2. Arlman, E. J., *J. Polymer Sci.*, **12**, 543, 547 (1954).
3. Bersch, C. F., M. R. Harvey, and B. G. Achhammer, *J. Res. Natl. Bur. Std.*, **60**, No. 5, 481 (1958).
4. Winkler, D. E., *J. Polymer Sci.*, **35**, 3 (1959).
5. Stromberg, R. R., S. Straus, and G. Achhammer, *J. Polymer Sci.*, **35**, 355 (1959).
6. Frye, A. H., and R. W. Horst, *J. Polymer Sci.*, **40**, 419 (1959); *ibid.*, **45**, 1 (1960).
7. Grassie, N., *J. Polymer Sci.*, **48**, 79 (1960).
8. Druesdow, D., and C. F. Gibbs, *Modern Plastics*, **30**, 123 (1953).
9. Baum, B., and L. H. Wartman, *J. Polymer Sci.*, **28**, 537 (1958).
10. Huntress, E. H., *Organic Chlorine Compounds*, Wiley, New York, 1948.
11. Hamman, W. C., *W.A.D.C. Tech. Rept.*, **57**, 158 (1958).
12. Glasstone, S., K. J. Laidler, and H. Eyring, *The Theory of Rate Processes*, McGraw-Hill, New York, 1941, p. 199.
13. Gerberich, H. R., and W. D. Walters, *J. Am. Chem. Soc.*, **83**, 4884 (1961).

### Résumé

Les stabilités thermiques de composés modèles ramifiés du chlorure de polyvinyle ont été étudiées à l'état gazeux. Les composés contenant un chlore tertiaire, c.à.d. le 2-méthyl-2-chloropropane et le 3-éthyl-3-chloropentane, ont été comparés avec ceux contenant un chlore secondaire comme le 2-chloropropane et le 2,4-dichloropentane. Les résultats de la décomposition thermique gazeuse montrent que la tendance à la rupture de C-Cl dépend de l'électronégativité du lien Carbone-chlore. La température de décomposition,  $T_D$ , peut être utilisée pour l'évaluation des stabilités thermiques de différents composés modèles.

### Zusammenfassung

Die thermische Stabilität verzweigter Modellverbindungen für Polyvinylchlorid wird in Gasphase untersucht. Verbindungen mit tertiärem Chlor, nämlich 2-Methyl-2-chlorpropan und 3-Äthyl-3-chlorpentan, werden mit solchen mit sekundärem Chlor, nämlich 2-Chlorpropan und 2,4-Dichlorpentan, verglichen. Die Ergebnisse der thermischen Zersetzung im Gaszustand zeigen, dass die Spaltungstendenz von C—Cl von der Elektronegativität des kohlenstoffgebundenen Chlors abhängt. Die Zersetzungstemperatur,  $T_D$ , kann zur Beurteilung der thermischen Stabilität verschiedener Modellverbindungen herangezogen werden.

Received July 15, 1963

Revised October 1, 1963

## Thermal Decomposition of Model Compounds of Polyvinyl Chloride. II. Gaseous Thermal Decomposition of Unsaturated Chain End Model Compounds

MITSUO ASAHINA and MITSUO ONOZUKA, *Tokyo Laboratory, Kureha Kagaku Company, Ltd., Tokyo, Japan*

### Synopsis

The gaseous thermal decomposition of model compounds with unsaturated chain ends which correspond to abnormal structures in polyvinyl chloride is studied. The allyl type chloride which is located in the main chain, but not at the end of polymer is more unstable than all kinds of abnormal structures present at the end of the polymer chain. Thus, it may be supposed that the sites of initiation of decomposition are formed during polymerization with chain transfer to polymer.

### INTRODUCTION

The previous paper<sup>1</sup> dealt with the difference in thermal stabilities between ideal structure and branched structure of polyvinyl chloride. This paper presents experimental results and some interpretations of the thermal stabilities of 4-chlorohexene-1, 3-chloropentene-1, 3-chloropentene-2, and 4-chlorohexene-2 which correspond to the abnormal structures in polyvinyl chloride having double bonds. One of the compounds, 4-chlorohexene-2, has already been studied by Baum and Wartman.<sup>2</sup> They suggested that the double bond at the chain end makes the adjacent chlorine labile. However, 4-chlorohexene-2 seems to be inappropriate as a model of chain end double bond structure of polyvinyl chloride from the kinetic theory of polymerization. Therefore, we carried out experiments of gaseous thermal dehydrochlorination of these compounds in order to get some clue to the thermal stability of polyvinyl chloride in relation to the various chain end structures.

### EXPERIMENTAL

#### A. Preparation of Model Compounds

**4-Chlorohexene-1.** 4-Chlorohexene-1 was prepared by chlorination of 4-hydroxyhexene-1 which was obtained by hydrogenation of propionic aldehyde by use of a Grignard reagent. After distillation, pure 4-chloro-

hexene-1 was separated from the trace impurities by gas chromatography. The purified sample showed  $n_D^{20}$  1.4280.

ANAL. Calcd. for  $C_6H_{11}Cl$ : C, 60.7%; H, 9.5%; Cl, 29.9%. Found: C, 61.7%; H, 9.5%; Cl, 28.1%.

**3-Chloropentene-1.** 3-Chloropentene-1 was prepared by chlorination of 3-hydroxypentene-1. A mixture of 3-chloropentene-1 and its isomer 1-chloropentene-2 was obtained by this method.<sup>3</sup> Pure 3-chloropentene-1 could not be separated from the isomer by gas chromatography, so we employed the mixture for experiments. The characteristic band,  $690\text{ cm}^{-1}$ , of 3-chloropentene-1 was not affected by the fact that both isomers were present. The purified mixture showed  $n_D^{20}$  1.4267.

ANAL. Calcd. for  $C_5H_9Cl$ : C, 57.4%; H, 8.6%; Cl, 34.0%. Found: C, 57.4%; H, 8.6%; Cl, 32.7%.

**3-Chloropentene-2.** 3-Chloropentene-2 was prepared by thermal dehydrochlorination of 3,3-dichloropentane which was obtained by means of chlorination of diethyl ketone. After purification it showed  $n_D^{20}$  1.4280.

ANAL. Calcd. for  $C_5H_9Cl$ : C, 57.4%; H, 8.6%; Cl, 34.0%. Found: C, 57.2%; H, 8.6%; Cl, 32.5%.

**4-Chlorohexene-2.** 4-Chlorohexene-2 was prepared by means of chlorination of the corresponding alcohol. After purification it showed  $n_D^{20}$  1.4387, lit.<sup>3</sup> 1.4385.

ANAL. Calcd. for  $C_6H_{11}Cl$ : C, 60.7%; H, 9.3%; Cl, 29.9%. Found: C, 60.2%; H, 9.2%; Cl, 29.1%.

## B. Apparatus for Thermal Decomposition

The apparatus for thermal decomposition of these compounds was the same as described in the previous paper.<sup>1</sup> The compounds were subjected to pyrolysis under reduced pressure at various constant temperatures in the range of  $160\text{--}380^\circ\text{C}$ . for about 3 hr. The degree of decomposition was measured by the rate of decreasing intensity of absorption bands at 685, 690,  $1600\text{--}600$ , and  $1218\text{ cm}^{-1}$ , for 4-chlorohexene-1, 3-chloropentene-1, 3-chlorohexene-2, and 4-chlorohexene-2, respectively, as shown in Figure 1.

## RESULTS

The thermal decomposition of these compounds is a unimolecular process in which hydrogen chloride and olefin are the main products of the decomposition. The gaseous products were analyzed by gas chromatography. From the results of these measurements, it was proved that 3-chloropentene-2 and 1-chloropentene-2 did not decompose at all at temperatures up to  $380^\circ\text{C}$ .; however, the others decomposed easily at rather lower temperature and showed a linear relation between the reciprocal of the absolute temperature and the logarithm of the per cent of undecom-

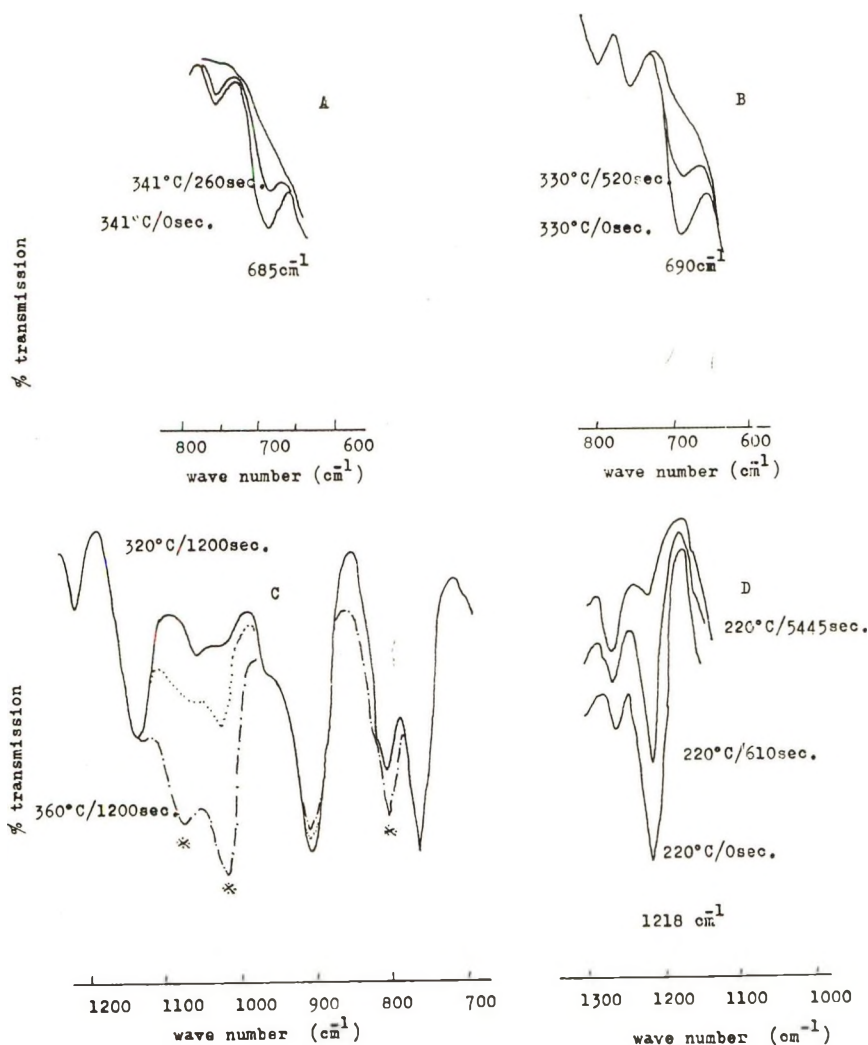


Fig. 1. Absorption spectra: (A) 4-chlorohexene-1; (B) 3-chloropentene-1; (C) 3-chlorohexene-2; (D) 4-chlorohexene-2.

posed substance. The rate constants obtained from the infrared spectra are shown in Table I, which gives the dependence of the rate constant on the temperatures. According to Eyring's theory, the rate constant is given by eq. (1):

$$k = e\kappa(k_B T/h) \exp \{ \Delta S^*/R \} \exp \{ -E_a/RT \} \quad (1)$$

where  $\Delta S^*$  is the entropy of activation,  $E_a$  is the energy of activation,  $\kappa$  is the transition coefficient,  $k_B$  is the Boltzmann constant, and  $h$  is the Planck constant.

From eq. (1), we calculated the free energies of activation at the decomposition temperatures which are indicated in Table II.

TABLE I  
Rate Constant at Various Decomposition Temperatures of Model Compounds

Compound	Temperature, °C.	$k \times 10^4$ , sec. <sup>-1</sup>
4-Chlorohexene-1	360	8.49
	367	6.79
3-Chloropentene-1	302	1.70
	330	7.20
	340	10.7
	349	16.1
4-Chlorohexene-2	195	1.42
	225	2.90
	245	6.64
	265	18.0
3-Chloropentene-2	360	0.0
	380	0.0

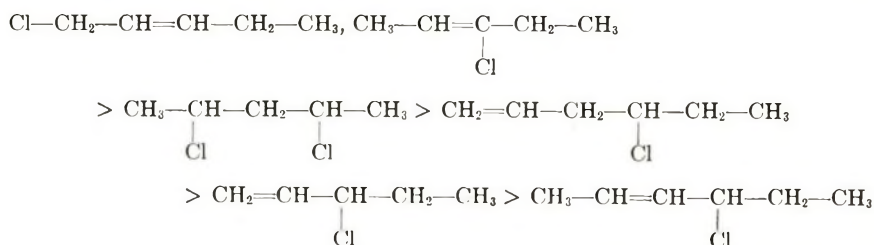
TABLE II  
Thermodynamic Factors

Model compound	$T_D$ , °C.	$E_a$ , kcal./mole	$\Delta H^*$ , kcal./mole	$\Delta S^*$ , e.u./mole	$\Delta F^*$ , kcal./mole
4-Chlorohexene-1	325	38.4	39.2	-16.5	47.0
3-Chloropentene-1	280	34.0	32.9	-19.8	43.9
4-Chlorohexene-2	160	28.5	27.6	-20.9	36.7
3-Chloropentene-2	400	—	—	—	—

## DISCUSSION

### A. Decomposition Temperature of Various Model Compounds

The decomposition temperatures  $T_D$  were obtained graphically as shown in Figure 2. These temperatures were defined in the preceding paper<sup>1</sup> as measures of the thermal stabilities of these compounds. We may estimate the stabilities from the decomposition temperatures and the calculated free energies of activation, both of which are shown in Table II. The order of thermal stabilities is as follows:



It seems that the unsaturated double bond does not have so much effect upon the cleavage of chlorine when there is a shielding effect on the allyl resonance by a methylene group, or when the hydrogen of the vinyl group is not replaced by a methyl group that is considered to be an electron donor

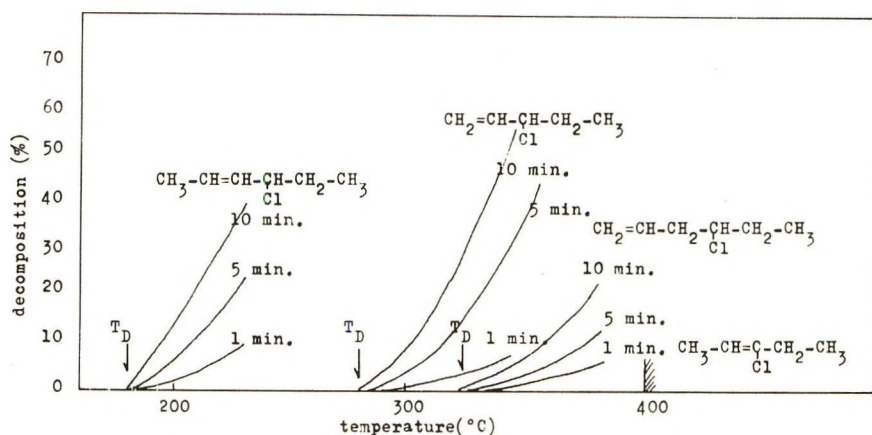


Fig. 2. Dependence of per cent decomposition on temperature and  $T_D$ .

and is capable of causing hyperconjugation as in 4-chlorohexene-2. Besides, it can be easily understood that 1-chloropentene-2, having the primary chlorine, is very stable and does not decompose at temperatures up to  $400^\circ\text{C}$ . It is conspicuous that 3-chloropentene-2, in which the chlorine is bound directly to the unsaturated carbon also does not decompose.

Many authors suggest that the unsaturated chain end is the site for initiation of thermal dehydrochlorination, but no experimental work on the instabilities of various chain end structures has been reported.

Considering the cause of formation of unsaturated chain end structure in polyvinyl chloride, there are two cases of chain transfer to monomer or polymer and of termination reaction with disproportionation, as shown in Table III.

From our results, it seems unlikely that the site for initiation of dehydrochlorination is the  $\beta$ -chlorine in the chain end which is formed by the disproportionation reaction (Table III).

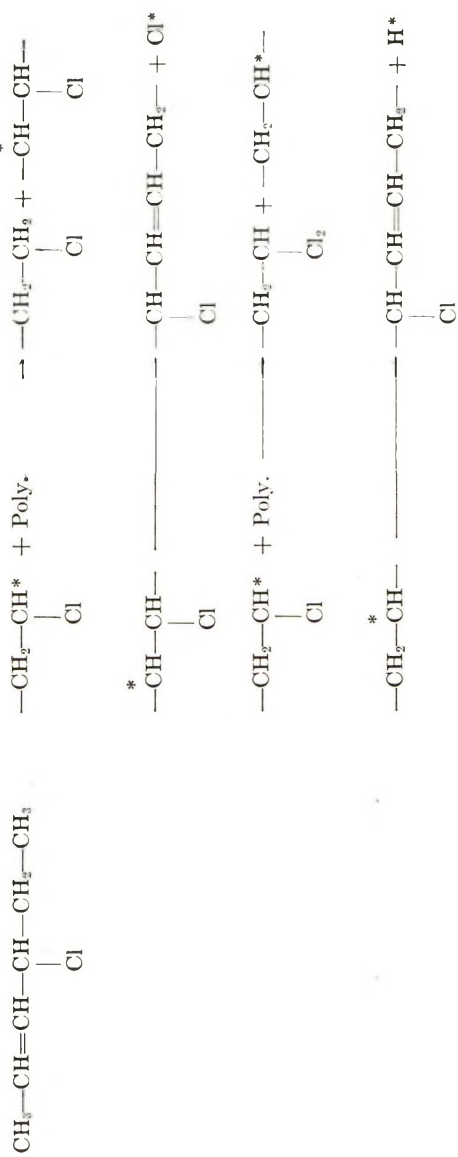
### B. Thermal Stabilities of Abnormal Structures in Polyvinyl Chloride

According to Baum and Wartman,<sup>2</sup> the prototype of an ester chain end in polyvinyl chloride, 2-chloropropyl acetate, seems to be rather stable compared with the models having unsaturated chain end structures. Our results show that 3-chloropentanone-2 is very stable at temperatures up to  $400^\circ\text{C}$ . From this, it is concluded that dehydrochlorination can hardly occur by the mechanism of intramolecular decomposition when the substituent vicinal to chlorine is an electron acceptor.

According to Bengough and Norrish,<sup>4</sup> chain transfer to monomer is considered to be a predominant termination process in the polymerization of vinyl chloride. Although unsaturated chain end structures were expected from termination reactions, it is unlikely that the "zipper"-type dehydrochlorination of polyvinyl chloride takes place from these defects in the chain end. The weak points which are considered as the initiators of the de-



## 4-Chloropentene-2



composition are the allyl type chlorine and the tertiary chlorine of a branched structure which exist in the main chain of polyvinyl chloride. 2-Chloropropane and 2,4-dichloropentane, which are considered to be models of ideal structure of polyvinyl chloride, show high thermal stabilities, having decomposition temperatures of over 300°C.

## CONCLUSIONS

From the experiments of gaseous pyrolysis of unsaturated chain end model compounds it seems reasonable to assume that the weak point structures which initiate zipper-type dehydrochlorination are allyl type chlorine and tertiary chlorine in the main chain structure caused by chain transfer to polymer, but the abnormal structures at the chain ends are rather stable.

## References

1. Asahina, M., and M. Onozuka, *J. Polymer Sci.*, **A2**, 3505 (1964).
2. Baum, B., and L. H. Wartman, *J. Polymer Sci.*, **28**, 537 (1958).
3. Lauer, W. M., and W. F. Filbert, *J. Am. Chem. Soc.*, **58**, 1388 (1936).
4. Bengough, W. I., and R. G. W. Norrish, *Proc. Roy. Soc. (London)*, **A200**, 301 (1950).

## Résumé

On étudie la décomposition thermique à l'état gazeux de composées modèles possédant des fins de chaîne insaturées, qui correspondent à des structures anormales du chlorure de polyvinyle. Le chlorure du type allylique, situé dans la chaîne principale et non pas à la fin du polymère, est plus instable que toutes les structures anormales situées à la fin de la chaîne polymérique. On peut donc supposer que les endroits où a lieu l'initiation de la décomposition sont formés au cours de la polymérisation par transfert de chaîne sur polymère.

## Zusammenfassung

Die thermische Zersetzung ungesättigter Modellverbindungen für das Kettenende, entsprechend der abnormalen Polyvinylchloridstruktur, wird in Gasphase untersucht. Das innerhalb der Hauptkette liegende Chlorid vom Allyltyp, aber nicht dasjenige am Ende der Polymerkette befindlichen abnormalen Strukturen. Es kann daher angenommen werden, dass die Stellen, an denen die Zersetzung beginnt durch Kettenübertragung während der Polymerisation vorbereitet werden.

Received July 15, 1963

Revised October 1, 1963

## Lattice Modes of Polyethylene

S. ENOMOTO and M. ASAHINA, *Tokyo Laboratory, Kureha Chemical Industry Company, Tokyo, Japan*

### Synopsis

A modified Urey-Bradley type force field was adopted to study the lattice modes of polyethylene by the GF matrices method with the intermolecular force constants which were estimated from the intermolecular potential function of methane. The frequencies of the modes were calculated at intervals of  $30^\circ$  for the phase differences along the  $a$  axis and the  $b$  axis. The elastic moduli of polyethylene crystal along both axes were also obtained from the intermolecular potential function.

### INTRODUCTION

The intramolecular potentials and intramolecular vibrations of high polymers have been well studied,<sup>1-7</sup> and the results were applied successfully to calculate the elastic moduli along the molecular chain.<sup>8-11</sup> However, the studies of the lattice modes of high polymers lag behind those of the intramolecular vibrations because of the incomplete understanding of intermolecular forces in high polymers and the difficulties involved in observing the lattice modes spectroscopically. Recently, the specific heat of polyethylene at low temperature has been studied in detail,<sup>12</sup> and the observed values in the range of 0–10°K. deviate considerably from the ones calculated on the basis of the intramolecular motions.<sup>12,13</sup> This suggests to us that the specific heats at low temperature are probably due to the lattice modes. A simplified general model of a linear high polymer was treated by Stockmayer and Hecht<sup>14</sup> to calculate the frequency spectrum and the specific heat; however, a better result can be obtained if the more exact intermolecular and intramolecular-potential functions are given. The effect of the intermolecular force on the intramolecular vibrations of polyethylene in crystalline region, say, the CH<sub>2</sub> rocking and bending modes, was first explained by Krimm, Liang, and Sutherland<sup>15</sup> and Stein.<sup>16</sup> Snyder showed that the intermolecular forces of  $n$ -paraffins were mainly occupied with Van der Waals forces, and the dipole-dipole coupling could be neglected.<sup>17</sup> As he took into account only the change of intermolecular H–H distance caused by the CH<sub>2</sub> rocking modes, the intermolecular motion or lattice vibration of polyethylene is not determined from his treatment. Shimanouchi and his co-workers calculated optically active lattice modes for an ionic crystal by the customary GF matrix method.<sup>18,19</sup>

The present authors have calculated the lattice modes of polyethylene at various phase differences along the  $a$  and the  $b$  axis, and also calculated the elastic moduli along both axes by using the intermolecular potential function.

## INTERMOLECULAR POTENTIAL FUNCTION OF POLYETHYLENE IN CRYSTALLINE REGION

### Intermolecular Forces between the $\text{CH}_2$ Groups of Polyethylene

The  $\text{CH}_2$  group is treated as one unit for the sake of simplicity, and the intermolecular forces between them in the crystalline region are calculated approximately from the Lenard-Jones potential function of methane given in eq. (1):<sup>29,30</sup>

$$U(r) = U_0[(r_0/r)^{12} - 2(r_0/r)^6] \quad (1)$$

where  $U_0$  is the dissociation energy (300 cal./mole),  $r_0$  is the intermolecular distance at minimum potential energy (4.30 Å), and the force constant  $K$  is given by eq. (2):

$$K = d^2U/dr^2 = 12(U_0/r_0^2)[13(r_0/r)^{14} - 7(r_0/r)^8] \quad (2)$$

The relation between the intermolecular force constant  $K$  and the intermolecular distance  $r$  is shown in Figure 1.

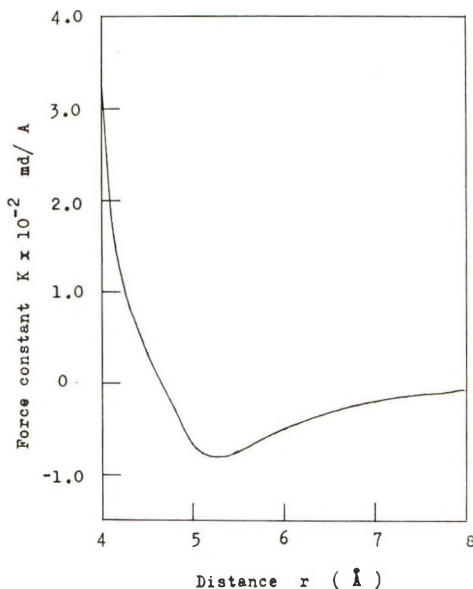


Fig. 1. Intermolecular force constant.

In case of polyethylene, the nearest intermolecular  $\text{CH}_2\text{-CH}_2$  distance  $R_1$  is 4.12 Å, and the next one  $R_2$  is 4.18 Å. The  $R_1$  and  $R_3$  are between the nearest molecules  $i$  and  $j$  (see Fig. 2). The third one  $R_3$  (4.51 Å) is between the closest neighboring molecules along the  $b$  axis. As shown in Figure 1, the intermolecular force becomes zero when the intermolecular  $\text{CH}_2\text{-CH}_2$  distance reaches about 4.7 Å, and the other intermolecular force constants between the  $\text{CH}_2$  groups in the polyethylene lattice can be neglected because the distance between them exceeds 4.7 Å. The value of the force constants are  $1.8 \times 10^{-2}$ ,  $1.4 \times 10^{-2}$ , and  $0.3 \times 10^{-2}$  mdyne/Å. for the  $R_1$ ,  $R_2$ , and  $R_3$ , respectively.

### Potential Function

The crystal structure of polyethylene is shown in Figure 2,<sup>20</sup> and the two closest neighboring molecules  $i$  and  $j$  make a Bravais lattice. The

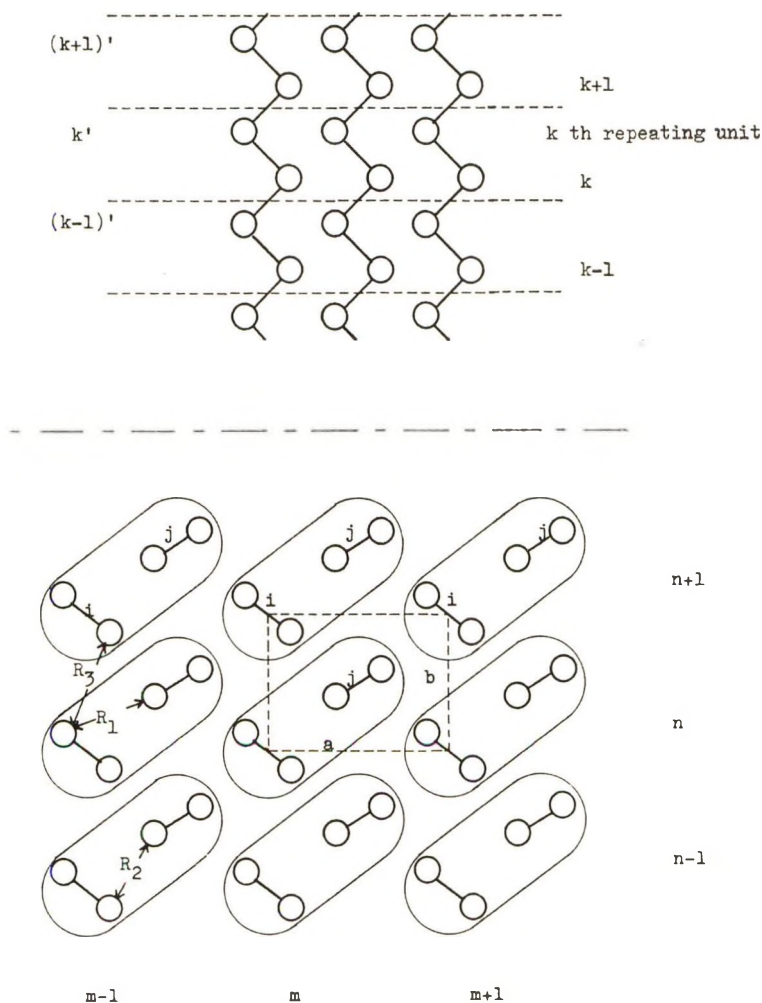


Fig. 2. Crystal of polyethylene.

numbers of the Bravais lattices are  $N_a$  and  $N_b$  along the  $a$  axis and the  $b$  axis, and there are  $N_c$  repeating units along the  $c$  axis in the crystalline region.

The potential function of the whole crystalline region can be expressed in eq. (3):<sup>21</sup>

$$\begin{aligned}
 V_T = & \sum_{m=1}^{N_a} \sum_{n=1}^{N_b} V_{i(m,n)}^0 + \sum_m \sum_n V_{j(m,n)}^0 + \sum_m \sum_n V_{i(m,n)j(m,n)} \\
 & + \sum_m \sum_n V_{i(m,n)j(m-1,n-1)} + \sum_m \sum_n V_{i(m,n)j(m-1,n)} \\
 & + \sum_m \sum_n V_{i(m,n)j(m,n-1)} + \sum_m \sum_n V_{i(m,n-1)i(m,n)} + \sum_m \sum_n V_{j(m,n-1)j(m,n)} \quad (3)
 \end{aligned}$$

where  $V_{i(m,n)}^0$  is the intramolecular potential function of the  $i$ th molecule in the  $(m,n)$ th Bravais lattice and  $V_{i(m,n)j(m',n')}$  is the intermolecular one between the  $i$ th molecule in the  $(m,n)$ th lattice and the  $j$ th molecule in the  $(m',n')$ th lattice, and only the three near-neighbor interactions mentioned in the previous section are considered.

A modified Urey-Bradley type force field<sup>31</sup> is used to express the intramolecular potential functions and the intermolecular ones. Bond distance, bond angle, and nonbonded distance are generally used in the Urey-Bradley type potential function; however, a Cartesian coordinate system is more convenient for understanding of the lattice modes.<sup>18,19</sup>

We set a system of the cartesian coordinates to express the intermolecular potential functions; the  $x$  axis is taken along the  $a$  axis, the  $y$  axis along the  $b$  axis and the  $z$  axis along the  $c$  axis. The Cartesian coordinates of a given  $\text{CH}_2$  group of the  $i$ th molecule in the  $(m,n)$ th Bravais lattice and the  $k$ th repeating unit are  $(x_k^{i(m,n)}, y_k^{i(m,n)}, z_k^{i(m,n)})$  or  $(x_{k'}^{i(m,n)}, y_{k'}^{i(m,n)}, z_{k'}^{i(m,n)})$ , where  $k$  and  $k'$  are used to distinguish the first  $\text{CH}_2$  group ( $k$ ) and the second one ( $k'$ ) of the two  $\text{CH}_2$  groups in the same  $k$ th repeating unit along the  $c$  axis.

The following notations are used for the intramolecular bond distances, the nonbonded ones, and intermolecular distances:  $r_k^{i(m,n)}$  is the intramolecular bond distance between the two  $\text{CH}_2$  groups of the  $k$ th repeating unit of the  $i$ th molecule in the  $(m,n)$ th lattice;  $r_{k-1/2}^{i(m,n)}$  is the intramolecular bond distance between the  $k$ th  $\text{CH}_2$  and the  $(k-1)$ 'th  $\text{CH}_2$  in the same molecule;  $q_{k-1/2}^{i(m,n)}$  is the intramolecular nonbonded distance between the  $k$ th  $\text{CH}_2$  and the  $(k-1)$ th  $\text{CH}_2$  in the same molecule;  $R_{i(m,n,k)j(m',n',k')}$  is the intermolecular distance between the  $k$ th  $\text{CH}_2$  group of the  $i$ th molecule in the  $(m,n)$ th lattice and the  $k'$ th  $\text{CH}_2$  of the  $j$ th molecule in the  $(m',n')$ th lattice.

The potential functions are given in eqs. (3'):

$$\begin{aligned}
 2V_{i(m,n)}^0 = & K_\infty \sum_k (\Delta r_{k-1/2}^{i(m,n)})^2 + K_\infty \sum_k (\Delta r_k^{i(m,n)})^2 \\
 & + K_\infty' \sum_k (\Delta q_{k-1/2}^{i(m,n)})^2 + K_\infty' \sum_k (\Delta q_{k-1/2}^{i(m,n)})^2
 \end{aligned}$$

$$\begin{aligned}
2V_{i(m,n)j(m,n)} &= K_1 \sum_k (\Delta R_{i(m,n,k')j(m,n,k')})^2 \\
&+ K_2 \sum_k (\Delta R_{i(m,n,k)j(m,n,k')})^2 \\
&+ K_2 \sum_k (\Delta R_{i(m,n,k)j(m,n,k-1')})^2 \\
2V_{i(m,n-1)i(m,n)} &= K_3 \sum_k (\Delta R_{i(m,n,k)i(m,n-1,k')})^2 + \\
&K_3 \sum_k (\Delta R_{i(m,n,k)i(m,n-1,k-1')})^2 \quad (3')
\end{aligned}$$

and the intramolecular distances and the intermolecular ones are easily given by eq. (3'):

$$\begin{aligned}
(r_{k-1/2}^{i(m,n)})^2 &= (x_k^{i(m,n)} - x_{(k-1)'}^{i(m,n)})^2 + (y_k^{i(m,n)} - y_{(k-1)'}^{i(m,n)})^2 + (z_k^{i(m,n)} - z_{(k-1)'}^{i(m,n)})^2 \\
(q_{k-1/2}^{i(m,n)})^2 &= (x_k^{i(m,n)} - x_{(k-1)}^{i(m,n)})^2 + (y_k^{i(m,n)} - y_{(k-1)}^{i(m,n)})^2 + (z_k^{i(m,n)} - z_{(k-1)}^{i(m,n)})^2 \\
(R_{i(m,n,k)j(m',n',k')})^2 &= (x_{k'}^{j(m',n')} - x_k^{i(m,n)})^2 \\
&+ (y_{k'}^{j(m',n')} - y_k^{i(m,n)})^2 + (z_{k'}^{j(m',n')} - z_k^{i(m,n)})^2 \quad (3'')
\end{aligned}$$

Then eq. (3') is rewritten in eqs. (3'''):

$$\begin{aligned}
2V_{i(m,n)}^0 &= K_\infty \sum_{k=1}^{N_c} [c_0(\Delta x_k^{i(m,n)} - \Delta x_{(k-1)'}^{i(m,n)}) - s_0(\Delta y_k^{i(m,n)} - \Delta y_{(k-1)'}^{i(m,n)}) \\
&+ t_0(\Delta z_k^{i(m,n)} - \Delta z_{(k-1)'}^{i(m,n)})]^2 + K_\infty \sum_k [-c_0(\Delta x_{k'}^{j(m,n)} - \Delta x_k^{i(m,n)}) \\
&+ s_0(\Delta y_{k'}^{j(m,n)} - \Delta y_k^{i(m,n)}) + t_0(\Delta z_{k'}^{j(m,n)} - \Delta z_k^{i(m,n)})]^2 \\
&+ K_\infty' \sum_k [(\Delta z_k^{i(m,n)} - \Delta z_{k-1}^{i(m,n)})]^2 + K_\infty' \sum_k [(\Delta z_{k'}^{j(m,n)} - \Delta z_{(k-1)'}^{i(m,n)})]^2 \quad (3''')
\end{aligned}$$

where  $K_\infty$  is the intramolecular force constant of the  $\text{CH}_2\text{—CH}_2$  bond and  $K_\infty'$  is that of the nonbonded adjacent  $\text{CH}_2\text{—CH}_2$  distance.

$$\begin{aligned}
2V_{i(m,n)j(m,n)} &= K_1 \sum_{k=1}^{N_c} [c_1(\Delta x_{k'}^{j(m,n)} - \Delta x_k^{i(m,n)}) + s_1(\Delta y_{k'}^{j(m,n)} - \Delta y_k^{i(m,n)})]^2 \\
&+ K_2 \sum_k [c_2(\Delta x_{k'}^{j(m,n)} - \Delta x_k^{i(m,n)}) + s_2(\Delta y_{k'}^{j(m,n)} - \Delta y_k^{i(m,n)}) \\
&+ t_2(\Delta z_{k'}^{j(m,n)} - \Delta z_k^{i(m,n)})]^2 + K_2 \sum_k [c_2(\Delta x_{(k-1)'}^{j(m,n)} - \Delta x_k^{i(m,n)}) \\
&+ s_2(\Delta y_{(k-1)'}^{j(m,n)} - \Delta y_k^{i(m,n)}) - t_2(\Delta z_{(k-1)'}^{j(m,n)} - \Delta z_k^{i(m,n)})]^2 \quad (3'''\text{b}) \\
2V_{i(m,n-1)i(m,n)} &= K_3 \sum_k [c_3(\Delta x_k^{i(m,n)} - \Delta x_{k'}^{i(m,n-1)}) \\
&+ s_3(\Delta y_k^{i(m,n)} - \Delta y_{k'}^{i(m,n-1)}) - t_3(\Delta z_k^{i(m,n)} - \Delta z_{k'}^{i(m,n-1)})]^2 \\
&+ K_3 \sum_k [c_3(\Delta x_k^{i(m,n)} - \Delta x_{(k-1)'}^{i(m,n-1)}) + s_3(\Delta y_k^{i(m,n)} - \Delta y_{(k-1)'}^{i(m,n-1)}) \\
&+ t_3(\Delta z_k^{i(m,n)} - \Delta z_{(k-1)'}^{i(m,n-1)})]^2 \quad (3'''\text{c})
\end{aligned}$$

where

$$\begin{aligned}
 c_0 &= 2\alpha/r \cos \phi/2 \\
 s_0 &= 2\beta/r \cos \phi/2 \\
 t_0 &= \sin \phi/2 \\
 c_1 &= a/2R_1 \\
 s_1 &= (b - 4\beta)/2R_1 \\
 c_2 &= (a - 4\alpha)/2R_2 \\
 s_2 &= b/2R_2 \\
 t_2 &= \gamma/2R_2 \\
 c_3 &= 2\alpha/R_3 \\
 s_3 &= (b - 2\beta)/R_3 \\
 t_3 &= \gamma/2R_3 \\
 \alpha &= (r/2) \cos (\phi/2) \cos \varphi \\
 \beta &= (r/2) \cos (\phi/2) \sin \varphi \\
 \gamma &= r \sin (\phi/2) \\
 R_1^2 &= a^2/4 + (b/2 - 2\beta)^2 \\
 R_2^2 &= (a/2 - 2\alpha)^2 + b^2 \\
 R_3^2 &= 4\alpha^2 + (b - 2\beta)^2 + \gamma^2
 \end{aligned}$$

and where  $r$  is the C—C bond length,  $\phi$  is the C—C—C bond angle,  $a$  and  $b$  are the dimension of the unit cell, and  $\varphi$  is the angle between a molecule and the  $a$  axis.

Three phase differences are considered for the intramolecular vibrations and the intermolecular vibrations.<sup>14</sup> As discussed in Appendix A, each CH<sub>2</sub> group of a polyethylene molecule vibrates at the same phase along the chain (the  $c$  axis) and only the two phase differences along the  $a$  and  $b$  axes are needed for the lattice modes. When each CH<sub>2</sub> group of the same chain vibrates at a different phase along the chain, this mode is an intramolecular vibration. The potential energy matrix of the whole crystalline region derived from eq. (3')  $\mathbf{F}_T$  can be given in eqs. (5) by using the new coordinate system given in eqs. (4), as the phase difference along the chain is zero.

$$\begin{aligned}
 \Delta x_{i(m,n)} &= (2/N_c^{1/2}) \sum_{k=1}^{N_c} \Delta x_k^{i(m,n)} & \Delta x'_{i(m,n)} &= (2/N_c^{1/2}) \sum_k \Delta x_k^{i(m,n)} \\
 \Delta y_{i(m,n)} &= (2/N_c^{1/2}) \sum_k \Delta y_k^{i(m,n)} & \Delta y'_{i(m,n)} &= (2/N_c^{1/2}) \sum_k \Delta y_k^{i(m,n)} \\
 \Delta z_{i(m,n)} &= (2/N_c^{1/2}) \sum_k \Delta z_k^{i(m,n)} & \Delta z'_{i(m,n)} &= (2/N_c^{1/2}) \sum_k \Delta z_k^{i(m,n)}
 \end{aligned} \quad (4)$$

The new transformed  $\mathbf{F}$  matrix of the whole crystalline region consists of only the intermolecular  $\mathbf{F}$  matrices and

$$\begin{aligned} \mathbf{F}_T = & \sum_m \sum_n \mathbf{F}_{i(m,n)j(m,n)} + \sum_m \sum_n \mathbf{F}_{i(m,n)j(m-1,n-1)} \\ & + \sum_m \sum_n \mathbf{F}_{i(m,n)j(m,n-1)} + \sum_m \sum_n \mathbf{F}_{i(m,n)j(m-1,n)} \\ & + \sum_m \sum_n \mathbf{F}_{i(m,n)i(m,n-1)} + \sum_m \sum_n \mathbf{F}_{j(m,n)j(m,n-1)} \quad (5) \end{aligned}$$

$\mathbf{F}_T$  is also written in another form to calculate the elastic moduli of polyethylene along the  $a$  and  $b$  axes; this is discussed in Appendix B.

We define the  $\mathbf{F}$  matrix of the  $(m,n)$ th Bravais lattice as  $\mathbf{F}_{0,0}$  and the  $\mathbf{F}$  matrix of the interaction between the  $(m,n)$ th lattice and the  $(m+m',n+n')$ th lattice as  $\mathbf{F}_{m'n'}$ .

$$\begin{aligned} \mathbf{F}_{0,0} &= \mathbf{F}_{i(m,n)j(m,n)} \\ \mathbf{F}_{0,\bar{1}} &= \mathbf{F}_{i(m,n)j(m,n-1)} + \mathbf{F}_{i(m,n-1)i(m,n)} + \mathbf{F}_{j(m,n-1)j(m,n)} \\ \mathbf{F}_{0,1} &= \mathbf{F}_{i(m,n+1)j(m,n)} + \mathbf{F}_{i(m,n)i(m,n+1)} + \mathbf{F}_{j(m,n)j(m,n+1)} \\ \mathbf{F}_{\bar{1},0} &= \mathbf{F}_{i(m,n)j(m-1,n)} \\ \mathbf{F}_{1,0} &= \mathbf{F}_{i(m+1,n)j(m,n)} \\ \mathbf{F}_{\bar{1},\bar{1}} &= \mathbf{F}_{i(m,n)j(m-1,n-1)} \\ \mathbf{F}_{1,1} &= \mathbf{F}_{i(m+1,n+1)j(m,n)} \quad (6) \end{aligned}$$

Then  $\mathbf{F}_T$  is written in eqs. (7)

$$\mathbf{F}_T = \begin{pmatrix} \dots & m-2 & m-1 & m & m+1 & \dots \\ & \mathbf{F}_0 & \mathbf{F}_{-a} & & & \\ & \mathbf{F}_a & \mathbf{F}_0 & \mathbf{F}_a & 0 & \\ & & \mathbf{F}_a & \mathbf{F}_0 & \mathbf{F}_{-a} & \\ & & & \mathbf{F}_a & \mathbf{F}_0 & \\ & 0 & & & & \mathbf{F}_a \end{pmatrix} \quad (7)$$

where

$$\mathbf{F}_j = \begin{pmatrix} & & (m) & & \\ n-2 & n-1 & n & n+1 & \dots \\ & \mathbf{F}_{0,0} & \mathbf{F}_{0,\bar{1}} & 0 & \\ & \mathbf{F}_{0,1} & \mathbf{F}_{0,0} & \mathbf{F}_{0,\bar{1}} & \\ & & \mathbf{F}_{0,1} & \mathbf{F}_{0,0} & \mathbf{F}_{0,\bar{1}} \\ & 0 & & \mathbf{F}_{0,1} & \mathbf{F}_{0,0} \end{pmatrix} \begin{matrix} n-2 \\ n-1 \\ n \\ n+1 \\ n+2 \end{matrix} \quad (m) \quad (7a)$$

$$\begin{array}{c}
 \begin{array}{cccc}
 & & (m) & \\
 & n-2 & n-1 & n & n+1 \\
 \mathbf{F}_{-a} = & \left[ \begin{array}{cccc}
 \mathbf{F}_{\bar{1},\bar{1}} & & & \\
 \mathbf{F}_{\bar{1},0} & \mathbf{F}_{\bar{1},\bar{1}} & & 0 \\
 & \mathbf{F}_{\bar{1},0} & \mathbf{F}_{\bar{1},\bar{1}} & \\
 0 & & \mathbf{F}_{\bar{1},0} & \mathbf{F}_{\bar{1},\bar{1}} \\
 & & & \mathbf{F}_{\bar{1},0}
 \end{array} \right] & \begin{array}{c}
 n-3 \\
 n-2 \\
 n-1 \\
 n \\
 n+1
 \end{array}
 \end{array}
 \end{array}
 \quad (m-1) \quad (7b)$$

and

$$\begin{array}{c}
 \begin{array}{cccc}
 & & (m) & \\
 & n-2 & n-1 & n & n+1 \\
 \mathbf{F}_a = & \left[ \begin{array}{cccc}
 \mathbf{F}_{1,0} & & & 0 \\
 \mathbf{F}_{1,1} & \mathbf{F}_{1,0} & & \\
 & \mathbf{F}_{1,1} & \mathbf{F}_{1,0} & \\
 0 & & \mathbf{F}_{1,1} & \mathbf{F}_{1,0} \\
 & & & \mathbf{F}_{1,1}
 \end{array} \right] & \begin{array}{c}
 n-2 \\
 n-1 \\
 n \\
 n+1 \\
 n+2
 \end{array}
 \end{array}
 \end{array}
 \quad (m+1) \quad (7c)$$

Let  $\Theta$  be the phase difference of the lattice modes between the  $(m,n)$ th lattice and the  $(m+1,n)$ th one and  $\Phi$  be that between the  $(m,n)$ th one and the  $(m,n+1)$ th one. The transformation matrices of the lattice modes along the  $a$  axis and the  $b$  axis are given in eqs. (8):

$$\mathbf{U}_a = (2/N_a)^{1/2} [ \dots \cos(m-1)\Theta \cos m\Theta \cos(m+1)\Theta \dots ]$$

$$\mathbf{U}_b = (2/N_b)^{1/2} [ \dots \cos(n-1)\Phi \cos n\Phi \cos(n+1)\Phi \dots ] \quad (8)$$

Application of eqs. (8) to eq. (7) reduces  $\mathbf{F}_T$  to the  $\mathbf{F}$  matrix of a single Bravais lattice given in eq. (9) for large  $N_a$  and  $N_b$ ,

$$\begin{aligned}
 \mathbf{F}_{ij} &= \mathbf{U}_a (\mathbf{U}_b \mathbf{F}_T \mathbf{U}_b^{\dagger}) \mathbf{U}_a^{\dagger} \\
 &= \mathbf{F}_{0,0} + (\mathbf{F}_{0,1} + \mathbf{F}_{0,\bar{1}}) \cos \Phi + (\mathbf{F}_{1,0} + \mathbf{F}_{1,\bar{0}}) \cos \Theta \\
 &\quad + (\mathbf{F}_{1,1} + \mathbf{F}_{\bar{1},\bar{1}}) \cos \Phi \cos \Theta \quad (9)
 \end{aligned}$$

From the above procedure, the complicated potential function of the whole crystalline region is reduced by the transformations of  $\mathbf{U}_a$  and  $\mathbf{U}_b$  to the simple form which contains only the interaction between the  $i$ th molecule and the  $j$  in an arbitrary lattice and the  $z$ -component of the  $\mathbf{F}_{ij}$  is separated from the  $x$ -component and the  $y$ -component.

### MATRIX AND SECULAR EQUATION

The  $\text{CH}_2\text{—CH}_2$  bond of polyethylene can be treated as a very rigid one because the force constant of the  $\text{CH}_2\text{—CH}_2$  bond is about 4.3 mdyne/A. and the intermolecular ones are very small compared to the former ( $10^{-2}$  mdyne/A.). The cartesian coordinates of the  $i$ th and the  $j$ th molecules in a Bravais lattice are given in eqs. (10), where  $\tau$  is the torsional angle around a C—C bond, and  $(X_i, Y_i, Z_i)$  are the cartesian coordinates of the center of the  $i$ th molecule (Fig. 3).

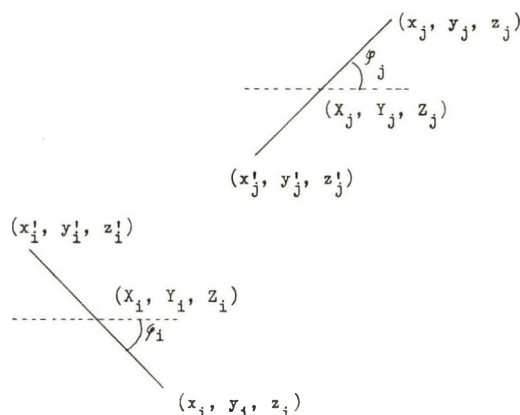


Fig. 3. Cartesian coordinates of the  $\text{CH}_2$  groups of the  $i$ th and the  $j$ th molecules in the Bravais lattice of polyethylene.

$$\begin{aligned}
 x_i &= X_i + \rho_i \cos \varphi_i \\
 x_i' &= X_i - \rho_i \cos \varphi_i \\
 y_i &= Y_i - \rho_i \sin \varphi_i \\
 y_i' &= Y_i + \rho_i \sin \varphi_i \\
 z_i &= Z_i - (r_i/2)(\sin \phi_i/2) \\
 z_i' &= Z_i + (r_i/2)(\sin \phi_i/2) \\
 2\rho_i &= r_i(\cos \phi_i/2)/[1 - (\cos^2 \tau_i/2)(\sin^2 \phi_i/2)] \\
 x_j &= X_j + \rho_j \cos \varphi_j \\
 x_j' &= X_j - \rho_j \cos \varphi_j \\
 y_j &= Y_j + \rho_j \sin \varphi_j \\
 y_j' &= Y_j - \rho_j \sin \varphi_j \\
 z_j &= Z_j - (r_j/2)(\sin \phi_j/2) \\
 z_j' &= Z_j + (r_j/2)(\sin \phi_j/2) \\
 2\rho_j &= r_j(\cos \phi_j/2)/[1 - (\cos^2 \tau_j/2)(\sin^2 \phi_j/2)] \quad (10)
 \end{aligned}$$

The displacement of each  $\text{CH}_2$  group consists of the intramolecular displacement and the center of the molecule, and this relation can be shown by the  $\mathbf{B}$  matrix<sup>22</sup> which is easily obtained from eqs. (10).

As this  $\mathbf{B}$  matrix is divided into the intramolecular  $\mathbf{B}$  matrix ( $\mathbf{B}_1$ ) and the intermolecular one ( $\mathbf{B}_2$ ),

$$\bar{\mathbf{B}}\mathbf{F}_{ij}\mathbf{B} = \begin{pmatrix} \bar{\mathbf{B}}_1\mathbf{F}_{ij}\mathbf{B}_1 & \mathbf{B}_2\bar{\mathbf{F}}_{ij}\bar{\mathbf{B}}_1 \\ \bar{\mathbf{B}}_2\mathbf{F}_{ij}\mathbf{B}_1 & \bar{\mathbf{B}}_2\mathbf{F}_{ij}\bar{\mathbf{B}}_2 \end{pmatrix} \quad (11)$$

where  $\bar{\mathbf{B}}_1\mathbf{F}_{ij}\mathbf{B}_1$  is the contribution of the intermolecular potential to the intramolecular potential,  $\bar{\mathbf{B}}_2\mathbf{F}_{ij}\mathbf{B}_1$  is the interaction between the inter-

molecular potential and the intramolecular one, and  $\mathbf{B}_2\mathbf{F}_i\mathbf{B}_2$  is the pure intermolecular potential function.

The customary  $\mathbf{GF}$  matrix method is generally used to calculate frequencies;<sup>23,24</sup> however, in case of the intermolecular vibration of polyethylene we use the mass-adjusted  $\mathbf{B}$  matrix instead of the customary method. The translation along the  $z$  axis and the rotations around the  $x$  and  $y$  axes can be neglected in the mass-adjusted  $\mathbf{B}$  matrix because the mass components and their moments of inertia can be treated as infinite, and the mass-adjusted intermolecular  $\mathbf{B}$  matrix ( $\mathbf{B}_{2M}$ ) is obtained from the  $\mathbf{B}_2$  in eq. (10) and the above consideration:

$$\mathbf{B}_{2M} = \begin{pmatrix} \Delta X_i & \Delta Y_i & \Delta \varphi_i & \Delta X_j & \Delta Y_j & \Delta \varphi_j \\ \left[ \begin{array}{ccc|cc} 1/M^{1/2} & 0 & \beta/I^{1/2} & & \\ 1/M^{1/2} & 0 & -\beta/I^{1/2} & & 0 \\ 0 & 1/M^{1/2} & \alpha/I^{1/2} & & \\ 0 & 1/M^{1/2} & -\alpha/I^{1/2} & & \\ & 0 & & 1/M^{1/2} & 0 & -\beta/I^{1/2} \\ & & & 1/M^{1/2} & & \beta/I^{1/2} \\ & & & 0 & 1/M^{1/2} & \alpha/I^{1/2} \\ & & & 0 & 1/M^{1/2} & -\alpha/I^{1/2} \end{array} \right] \end{pmatrix} \quad (12)$$

where  $M = 2m$ ,  $I = M/4(r \cos \phi/2)^2$ , and  $m$  is the mass of  $\text{CH}_2$  unit. The lattice modes of the  $i$  and  $j$  molecules in a single Bravais lattice is related to the displacements ( $\Delta X_i, \Delta Y_i, \Delta \varphi_i, \Delta X_j, \Delta Y_j$ , and  $\Delta \varphi_j$ ) by the  $\mathbf{B}_{2M}$ , and

$$\begin{pmatrix} T_{xi} \\ T_{yi} \\ R_{zi} \\ T_{xj} \\ T_{yj} \\ R_{zj} \end{pmatrix} = \mathbf{B}_{2M} \begin{pmatrix} \Delta X_i \\ \Delta Y_i \\ \Delta \varphi_i \\ \Delta X_j \\ \Delta Y_j \\ \Delta \varphi_j \end{pmatrix} \quad (13)$$

where  $T_{xi}$  is the translation of the  $i$ th molecule along the  $x$  axis and  $R_{zi}$  is the rotation around its chain axis, and so on (Fig. 4). As these lattice modes couple between both molecules in the lattice, the lattice modes of polyethylene are classified to two translation modes  $T_x, T_y$ , and two vibration modes  $T'_x, T'_y$ , along the  $a$  axis and the  $b$  axis, and one rotation mode  $R_z$  and one rotatory mode  $R'_z$  around the  $c$  axis. This relation is shown in eq. (14):

$$\begin{pmatrix} T_x \\ T_y \\ T'_x \\ T'_y \\ R_z \\ R'_z \end{pmatrix} = \begin{pmatrix} 2^{-1/2} & 0 & 0 & 2^{-1/2} & 0 & 0 \\ 0 & 2^{-1/2} & 0 & 0 & 2^{-1/2} & 0 \\ 2^{-1/2} & 0 & 0 & -2^{-1/2} & 0 & 0 \\ 0 & 2^{-1/2} & 0 & 0 & -2^{-1/2} & 0 \\ 0 & 0 & 2^{-1/2} & 0 & 0 & 2^{-1/2} \\ 0 & 0 & 2^{-1/2} & 0 & 0 & -2^{-1/2} \end{pmatrix} \begin{pmatrix} T_{xi} \\ T_{yi} \\ R_{zi} \\ T_{xj} \\ T_{yj} \\ R_{zj} \end{pmatrix} \quad (14)$$

and the square matrix is defined as  $\mathbf{U}$ .

The secular equation of the lattice modes is set up from eqs. (9), (12), and (14):

$$\begin{aligned} |\mathbf{H} - \mathbf{E}\lambda| &= 0 \\ \mathbf{H} &= \mathbf{U}(\mathbf{B}_{2M}\mathbf{F}_i\mathbf{B}_{2M})\mathbf{U} \end{aligned} \quad (15)$$

and the detail of  $\mathbf{H}$  is given in eq. (16) (see page 3534) where

$$A_1 = 4(c_1^2 K_1 + 2c_2^2 K_2)/M$$

$$A_1' = 8c_3^2 K_3/M$$

$$A_2 = 4(s_1^2 K_1 + 2s_2^2 K_2)/M$$

$$A_2' = 8s_3^2 K_3/M$$

$$B = -4(c_1 s_1 k_1 + 2c_2 s_2 k_2)/M$$

$$B' = 8c_3 s_3 k_3/M$$

$$C_1 = 4(c_1^2 \sin^2 \varphi K_1 + 2s_2^2 \cos^2 \varphi K_2)/M$$

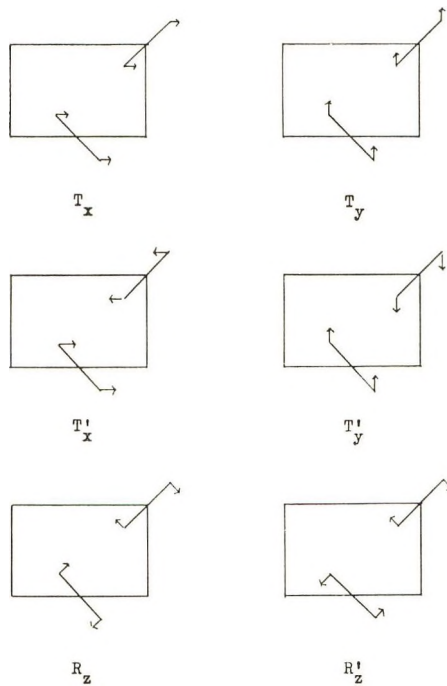


Fig. 4. Lattice modes of polyethylene.

$$\mathbf{H} = \begin{pmatrix} T_x & T_y & T_x' & T_y' & R_z & R_z' \\
 \begin{pmatrix} A_1[1 - (\cos^2 \Theta/2)] \\ (\cos^2 \Phi/2)] \\ + A_1'(\sin^2 \Phi/2) \\ B(\sin^2 \Theta/2)(\sin^2 \Phi/2) \end{pmatrix} & A_2[1 - (\cos^2 \Theta/2)] \\ (\cos^2 \Phi/2)] \\ + A_2'(\sin^2 \Phi/2) \\ B'(\sin^2 \Phi/2) \\ 0 \\ B'(\sin^2 \Phi/2) \\ D_1(\sin^2 \Theta/2) \\ (\cos^2 \Phi/2) \\ D_2(\cos^2 \Theta/2) \\ (\sin^2 \Phi/2) \\ \hline
 \begin{pmatrix} A_1[1 + (\cos^2 \Theta/2)] \\ (\cos^2 \Phi/2)] \\ + A_1'(\sin^2 \Phi/2) \\ - B(\sin^2 \Theta/2) \\ (\sin^2 \Phi/2) \\ - D_2(\cos^2 \Theta/2) \\ (\sin^2 \Phi/2) \\ - D_4(\sin^2 \Theta/2) \\ (\cos^2 \Phi/2) \\ \hline
 \begin{pmatrix} A_2[1 + (\cos^2 \Theta/2)] \\ (\cos^2 \Phi/2)] \\ + A_2'(\sin^2 \Phi/2) \\ - D_4(\sin^2 \Theta/2) \\ (\cos^2 \Phi/2) \\ - D_3(\cos^2 \Theta/2) \\ (\sin^2 \Phi/2) \\ \hline
 \begin{pmatrix} C_1 + C_2 + (C_1 - C_2) \\ (\cos^2 \Theta/2) \\ + C''(\cos^2 \Phi/2) \\ \hline
 \begin{pmatrix} C_1 + C_2 - (C_1 - C_2) \\ (\cos^2 \Theta/2) \\ + C'(\cos^2 \Phi/2) \end{pmatrix} \end{pmatrix} \end{pmatrix} \quad (16)$$

$$\begin{aligned}
C_2 &= 4(s_1^2 \cos^2 \varphi K_1 + 2c_2^2 \sin^2 \varphi K_2)/M \\
C' &= 8(c_3 \sin \varphi + s_3 \cos \varphi)^2 K_3/M \\
D_1 &= 4(c_1 s_1 k_1 \cos \varphi - 2c_2^2 K_2 \sin \varphi)/M \\
D_2 &= 4(c_1^2 K_1 \sin \varphi - 2c_2 s_2 K_2 \cos \varphi)/M \\
D_3 &= 4(s_1^2 k_1 \cos \varphi - 2c_2 s_2 K_2 \sin \varphi)/M \\
D_4 &= 4(c_1 s_1 K_1 \sin \varphi - 2s_2^2 K_2 \cos \varphi)/M
\end{aligned} \tag{17}$$

## RESULTS

According to the factor group analysis the six lattice modes of polyethylene,  $T_z$ ,  $T_x'$ ,  $T_y$ ,  $T_y'$ ,  $R_z$ , and  $R_z'$  were thought to be uncoupled from each other;<sup>15</sup> however, this case occurs at only  $\Theta = 0$  and  $\Phi = 0$ . Equation (16) suggests that the lattice modes couple each other in the general case and that special cases can be expected to occur at the following phase differences;

$$\begin{array}{llll}
\Theta = 0 & \Phi = 0 & T_z, T_y, R_z, & T_x', T_y', R_z' \\
\Theta = 0 & \Phi \neq 0 & (T_z, T_y', R_z'), & (T_x', T_y, R_z) \\
\Theta \neq 0 & \Phi = 0 & (T_z, T_y', R_z), & (T_x', T_y, R_z') \\
\Theta = \pi & \Phi = \pi & (T_z, T_y, T_x', T_y'), & (R_z, R_z')
\end{array}$$

The frequencies of the six modes are calculated for the variations of the two phase differences  $\Theta$  and  $\Phi$  at the interval of  $30^\circ$  and the results are

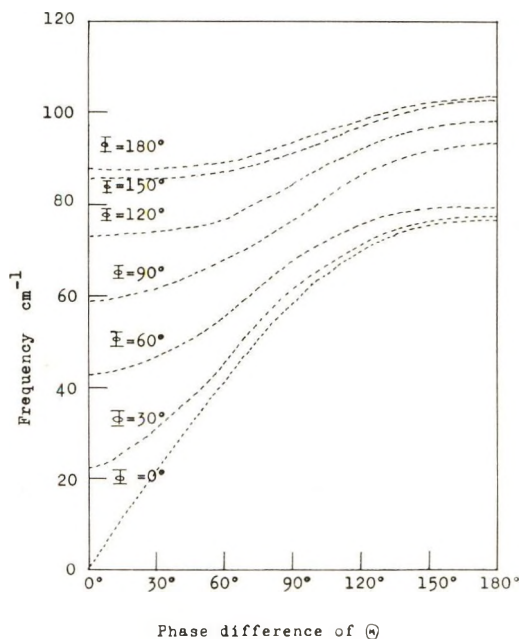
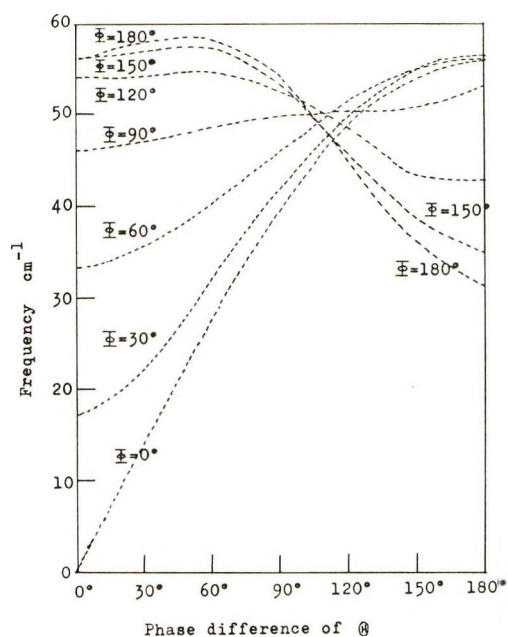
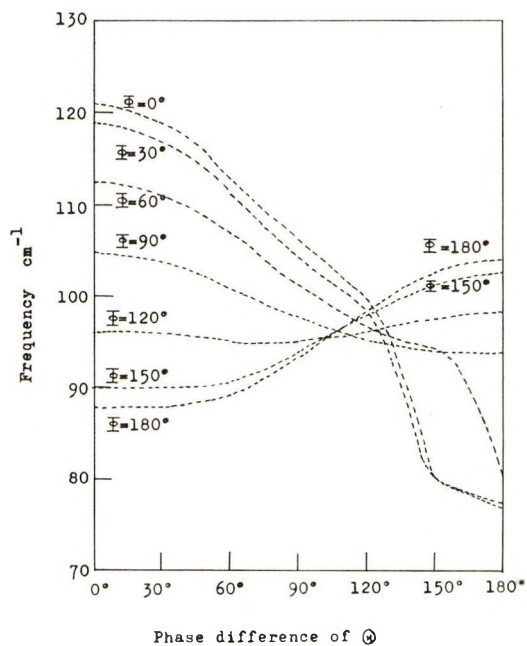
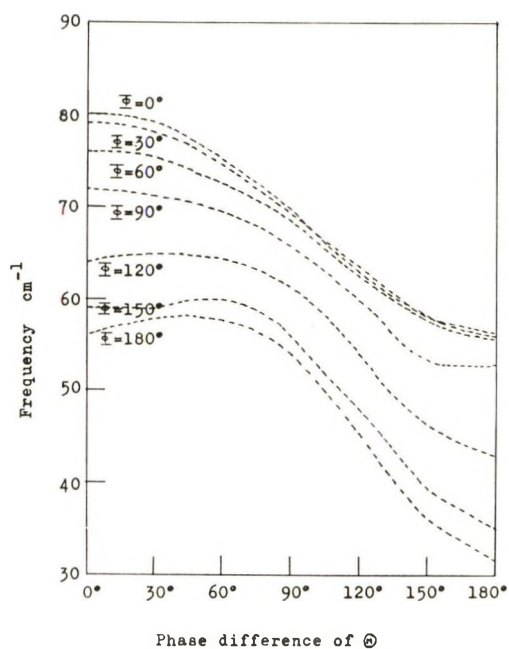
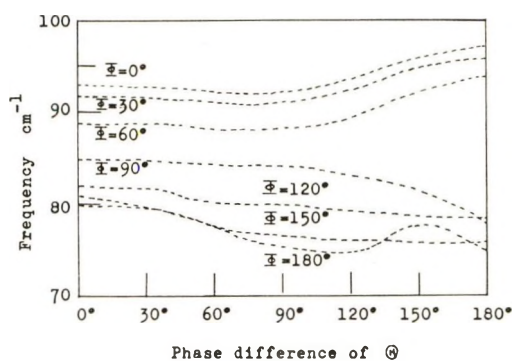
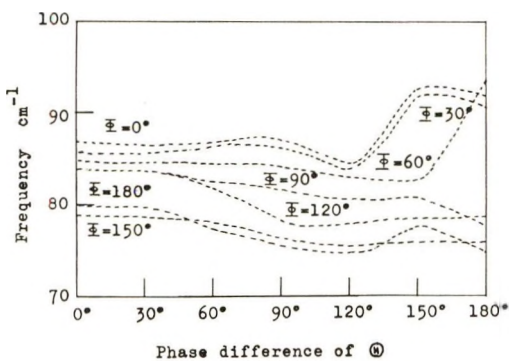


Fig. 5. Frequency of  $T_x$  mode.

Fig. 6. Frequency of  $T_y$  mode.Fig. 7. Frequency of  $T_z'$  mode.

Fig. 8. Frequency of  $T_y'$  mode.Fig. 9. Frequency of  $R_z'$  mode.Fig. 10. Frequency of  $R_z'$  mode.

shown in Figures 5-10. The frequency of the  $T_z$  mode increases from 0 to 104  $\text{cm}^{-1}$  as the phase differences increase from 0 to  $180^\circ$ . The frequency of the  $T_y$  mode increases as the  $\Phi$  increases from 0 to  $180^\circ$  when  $\Theta$  is in the range of about  $0-110^\circ$ ; however, when the  $\Theta$  is above this value, the frequency stays at near 55  $\text{cm}^{-1}$  in the range of the  $\Phi = 0-60^\circ$  and then decreases as the  $\Phi$  increases from  $60^\circ$  to  $180^\circ$ . The frequency of  $T_z'$  decreases when  $\Theta$  is from  $0^\circ$  to about  $100^\circ$  and  $\Phi$  is  $0-180^\circ$ , but for  $\Theta$  above  $120^\circ$ , it goes up from about 80 to 104  $\text{cm}^{-1}$  as  $\Phi$  increases from  $0^\circ$  to  $180^\circ$ . The frequency of  $T_y'$  decreases from 80 to 32  $\text{cm}^{-1}$  as  $\Theta$  and  $\Phi$  increase from  $0^\circ$  to  $180^\circ$ . The frequency changes continuously with the variations of the phase differences. On the other hand, the frequencies of  $R_z$  and  $R_z'$  change irregularly, and some singular points which were reported by Genensky and Newell<sup>25</sup> may correspond to these modes. In case of  $\Theta = 180^\circ$  or  $\Phi = 180^\circ$ ,  $T_z$  and  $T_z'$  give the same frequency, and this is valid for the other groups ( $T_y, T_y'$ ) and ( $R_z, R_z'$ ).

## DISCUSSION

In order to know whether the intermolecular force constants used in this calculation of the polyethylene lattice modes are reasonable or not, we have to get the experimental results, but this is quite difficult experimental work, because most of the modes are optically inactive. Measurement of the specific heat at various temperatures is also quite interesting for an understanding of the intermolecular forces, as the specific heat can be calculated if the frequency spectrum is obtained. For this treatment, there is a question whether or not the coupling between the torsional mode and the lattice modes of polyethylene occurs, because the values of their force constants are quite near each other. The answer is given if the matrix  $\mathbf{B}_1$  in eq. (11) is obtained. By using the relation between internal coordinates and helical parameters for a high polymer,<sup>26,27</sup> the  $\mathbf{B}_1$  is easily calculated, and the relation between the cartesian coordinates and the internal coordinates for the  $\text{CH}_2$  groups in polyethylene Bravais cell is given in eq. (18).

$$\begin{bmatrix} \Delta x_i \\ \Delta x_i' \\ \Delta y_i \\ \Delta y_i' \\ \Delta z_i \\ \Delta z_i' \end{bmatrix} = \begin{bmatrix} b_{z\tau} & b_{x\phi} & & & & \\ -b_{z\tau} & -b_{x\phi} & & & & \\ & b_{y\tau} & b_{y\phi} & & 0 & \\ -b_{y\tau} & -b_{y\phi} & & & & \\ b_{z\tau} & b_{z\phi} & & & & \\ -b_{z\tau} & -b_{z\phi} & & & & \end{bmatrix} \begin{bmatrix} \Delta r_i \\ r\Delta\phi_i \\ \Delta r_j \\ r\Delta\phi_j \end{bmatrix}$$

$$\begin{bmatrix} \Delta x_j \\ \Delta x_j' \\ \Delta y_j \\ \Delta y_j' \\ \Delta z_j \\ \Delta z_j' \end{bmatrix} = \begin{bmatrix} & & b_{z\tau} & b_{x\phi} & & \\ & & -b_{z\tau} & -b_{x\phi} & & \\ & 0 & b_{y\tau} & b_{y\phi} & & \\ & & -b_{y\tau} & -b_{y\phi} & & \\ & & b_{z\tau} & b_{z\phi} & & \\ & & -b_{z\tau} & -b_{z\phi} & & \end{bmatrix} \begin{bmatrix} \Delta r_i \\ r\Delta\phi_i \\ \Delta r_j \\ r\Delta\phi_j \end{bmatrix} \quad (18)$$

where

$$\begin{aligned}
 b_{x\tau} &= \frac{1}{2}(\cos \phi/2)(\cos \varphi) \\
 b_{y\tau} &= -\frac{1}{2}(\cos \phi/2)(\sin \varphi) \\
 b_{z\tau} &= -\frac{1}{2}(\sin \phi/2) \\
 b_{x\phi} &= -\frac{1}{4}(\sin \phi/2)(\cos \varphi) \\
 b_{y\phi} &= \frac{1}{4}(\sin \phi/2)(\sin \varphi) \\
 b_{z\phi} &= -\frac{1}{4}(\cos \phi/2)
 \end{aligned} \tag{19}$$

Equation (18) explains clearly that the lattice modes do not couple with the torsional mode for polyethylene which has planar zigzag chain configuration ( $\tau = 180^\circ$ ). When a polymer has a certain helical structure, we must take into account the coupling between its torsional mode and the lattice modes.

The frequency distribution of the lattice modes of polyethylene may be obtained from the results to calculate the specific heat with the distribution of the intramolecular modes,<sup>3,12</sup> and this will be useful for understanding more completely the intermolecular potential function of polyethylene. However, in order to obtain a better frequency distribution we have to determine the numbers of the group of  $\Theta$  and  $\Phi$  which give a fixed eigenvalue after putting the eigenvalue in eq. (15), because many combinations of the phase differences give the same frequency.

Another possible method for determining the reliability of the intermolecular force constants used in this study is to calculate the elastic moduli along the  $a$  axis and the  $b$  axis for polyethylene by the intermolecular potential function. The treatment for the elastic moduli is mentioned in detail in the appendix, and the calculated values are  $E_a = 2.1 \times 10^{10}$  dyne/cm.<sup>2</sup> (elastic modulus along  $a$  axis);  $E_b = 2.1 \times 10^{10}$  dyne/cm.<sup>2</sup> (elastic modulus along  $b$  axis).

Sakurada and Itoh<sup>28</sup> reported that the observed value by x-ray diffraction technique is about 2.9–3 dyne/cm.<sup>2</sup> and could not find any significant difference between  $E_a$  and  $E_b$ . The fact that our calculated result is not far from their experimental values supports the internal force constants used for the calculation of polyethylene lattice modes.

## APPENDIX A

### Phase Difference along Polyethylene Chain in Bravais Lattice

For the sake of simplicity, the treatment is limited to the  $(m,n)$ th Bravais lattice and the same procedure can be applied to the other lattices. The potential energy matrix of this lattice  $\mathbf{F}_{(m,n)}$  is given in eq. (A-1).

$$\begin{aligned}
 \mathbf{F}_{(m,n)} &= \mathbf{F}_{i(m,n)}^0 + \mathbf{F}_{j(m,n)}^0 + \mathbf{F}_{i(m,n)j(m,n)} \\
 &\quad i \qquad \qquad j \\
 &= \begin{bmatrix} \mathbf{F}_i^0 + \mathbf{F}_i & \mathbf{F}_{ij} \\ \mathbf{F}_{ij} & \mathbf{F}_j^0 + \mathbf{F}_j \end{bmatrix} \quad (\text{A-1})
 \end{aligned}$$

where  $\mathbf{F}_i^0$  and  $\mathbf{F}_j^0$  are the intramolecular  $\mathbf{F}$  matrices of the  $i$  and  $j$  molecules, and  $\mathbf{F}_i$ ,  $\mathbf{F}_j$ , and  $\mathbf{F}_{ij}$  are the intermolecular ones between them. When the chain is infinite, the matrices are reduced to the simple form under the operation of  $\mathbf{U}_c$  in eq. (A-2).<sup>3</sup>

$$\mathbf{U}_c = \begin{bmatrix} \mathbf{U}_i & 0 \\ 0 & \mathbf{U}_j \end{bmatrix} \quad (\text{A-2})$$

$$\mathbf{U}_i = (2/N_c)^{1/2} \begin{bmatrix} \dots \cos(k-1)\delta_i \cos k\delta_i \cos(k+1)\delta_i \dots \\ \dots \sin(k-1)\delta_i \sin k\delta_i \sin(k+1)\delta_i \dots \end{bmatrix} \quad (\text{A-2}')$$

where  $\delta_i$  is the phase difference of the intramolecular vibration of the  $i$ th molecule along the chain and  $k$  is the number of the repeating unit. From eqs. (A-1) and (A-2)

$$\mathbf{U}_c \mathbf{F}_{(m,n)} \bar{\mathbf{U}}_c = \begin{bmatrix} \mathbf{U}_i(\mathbf{F}_i^0 + \mathbf{F}_i) \bar{\mathbf{U}}_i & \mathbf{U}_i \mathbf{F}_{ij} \bar{\mathbf{U}}_j \\ \mathbf{U}_j \mathbf{F}_{ij} \bar{\mathbf{U}}_i & \mathbf{U}_j(\mathbf{F}_j^0 + \mathbf{F}_j) \bar{\mathbf{U}}_j \end{bmatrix} \quad (\text{A-3})$$

The  $\mathbf{F}$  matrices are written as follows

$$\mathbf{F}_i = \mathbf{F}_j^0 = \begin{bmatrix} \dots & k-1 & k & k+1 & \dots \\ & \mathbf{f}_1^0 & & 0 & \\ & \mathbf{f}_0^0 & \mathbf{f}_1^0 & & \\ & \mathbf{f}_1^0 & \mathbf{f}_0^0 & \mathbf{f}_1^0 & \\ & & \mathbf{f}_1^0 & \mathbf{f}_0^0 & \\ 0 & & & & \end{bmatrix} \quad (\text{A-4a})$$

$$\mathbf{F}_i = \begin{bmatrix} \dots & k-1 & k & k+1 & \dots \\ & \mathbf{f}_{i,0} & & 0 & \\ & & \mathbf{f}_{i,0} & & \\ 0 & & & \mathbf{f}_{i,0} & \end{bmatrix} \quad (\text{A-4b})$$

$$\mathbf{F}_j = \begin{bmatrix} & \mathbf{f}_{j,0} & & 0 & \\ & & \mathbf{f}_{j,0} & & \\ 0 & & & \mathbf{f}_{j,0} & \end{bmatrix} \quad (\text{A-4c})$$

$$\mathbf{F}_{ij} = \begin{bmatrix} k-1 & k & k+1 \\ \mathbf{f}_{ij,\bar{1}} & & 0 \\ \mathbf{f}_{ij,0} & \mathbf{f}_{ij,\bar{1}} & \\ \mathbf{f}_{ij,1} & \mathbf{f}_{ij,0} & \mathbf{f}_{ij,\bar{1}} \\ & \mathbf{f}_{ij,1} & \mathbf{f}_{ij,0} \\ 0 & & \mathbf{f}_{ij,1} \end{bmatrix} \quad (\text{A-4d})$$

where  $\mathbf{f}_0^0$  is the intramolecular  $\mathbf{F}$  matrix element of the  $k$ th repeating unit;  $\mathbf{f}_1^0$  is the intramolecular  $\mathbf{F}$  matrix element of the interaction between the  $k$ th and the  $(k + 1)$ th unit;  $\mathbf{f}_1^0$  is the transpose matrix of  $\mathbf{f}_1^0$ ;  $\mathbf{f}_{i,0}$  is the intermolecular  $\mathbf{F}$  matrix element of the  $k$ th repeating unit of the  $i$ th molecule;  $\mathbf{f}_{ij,0}$  is the intermolecular  $\mathbf{F}$  matrix element of the interaction between the  $k$ th repeating unit of the  $i$ th molecule and the same unit of the  $j$ th molecule;  $\mathbf{f}_{ij,1}$  is the intermolecular  $\mathbf{F}$  matrix element of the interaction between the  $k$ th repeating unit of the  $i$ th molecule and the  $(k + 1)$ th unit of the  $j$ th molecule.

Equation (A-3) is calculated from eqs. (A-2') and (A-4).

$$\begin{aligned} \mathbf{U}_i \mathbf{F}_{ij} \bar{\mathbf{U}}_i &= \mathbf{f}_{ij,0} + (\mathbf{f}_{ij,1} + \mathbf{f}_{ij,1}) \cos \delta_i & \delta_i &= \delta_j \\ &= 0 & \delta_i &\neq \delta_j \end{aligned} \quad (\text{A-5})$$

$$\begin{aligned} \mathbf{U}_i (\mathbf{F}_i^0 + \mathbf{F}_i) \mathbf{U}_i &= \mathbf{f}_0^0 + (\mathbf{f}_1^0 + \mathbf{f}_1^0) \cos \delta_i + \mathbf{f}_{i,0} & \delta_i &\neq 0 \\ &= \mathbf{f}_{i,0} & \delta_i &= 0 \end{aligned} \quad (\text{A-6})$$

Equation (A-5) shows that the intermolecular interaction does not occur between the  $i$ th molecule and the  $j$ th molecule in the Bravais lattice when their phase differences along the chain are different and their interaction occurs only when their phase differences are the same.

As shown in eq. (A-6), the intramolecular  $\mathbf{F}$  matrix  $\mathbf{f}_0^0 + (\mathbf{f}_1^0 + \mathbf{f}_1^0) \cos \delta_i$  becomes zero, and only the intermolecular ones remain for the lattice modes in which the phase difference  $\delta_i$  is zero.

## APPENDIX B

### Elastic Moduli in Perpendicular Directions of Polyethylene Chain

The following notations are used to get the modified potential function.  $R_{(m+m')/2, (n+n')/2}$  is the distance between the center of the  $i$ th molecule in the  $(m, n)$ th Bravais lattice and the  $j$ th molecule in the  $(m', n')$ th Bravais lattice.  $\theta_{(m+m')/2, (n+n')/2}$  is the angle between  $R_{(m+m')/2, (n+n')/2}$  and the  $a$  axis.  $X_{(m+m')/2, (n+n')/2}$  is the distance along the  $a$  axis between the centers of the both molecules, and  $Y_{(m+m')/2, (n+n')/2}$  is that along the  $b$  axis.

The interactions between the  $i$ th molecules or the  $j$ th molecules along the  $b$  axis can be neglected, as the force constant  $K_3$  between them is very small, and the  $Z$  components of the potential function can be omitted from the potential function to calculate the elastic moduli along the  $a$  axis and the  $b$  axis. The potential function given in eq. (5) is simplified to eq. (B-1):

$$\begin{aligned} 2V_T &= \sum_{m,n} \sum K_r [\Delta R_{m,n}^2 + \Delta R_{(m,n-1/2)}^2 + \Delta R_{(m-1/2,n-1/2)}^2 \\ &\quad + \Delta R_{(m-1/2,n)}^2] + \sum_{m,n} \sum K_\theta [\Delta \theta_{(m,n)}^2 + \Delta \theta_{(m,n-1/2)}^2 \\ &\quad + \Delta \theta_{(m-1/2,n-1/2)}^2 + \Delta \theta_{(m-1/2,n)}^2] + \sum_{m,n} \sum K_\varphi [\Delta \varphi_{i(m,n)}^2 + \Delta \varphi_{j(m,n)}^2] \\ &\quad + 2 \sum_{m,n} \sum K_{r\theta} [\Delta R_{(m,n)} \Delta \theta_{(m,n)} + \Delta R_{(m,n-1/2)} \Delta \theta_{(m,n-1/2)}] \end{aligned}$$

$$\begin{aligned}
& + \Delta R_{(m-1/2, n-1/2)} \Delta \theta_{(m-1/2, n-1/2)} + \Delta R_{(m-1/2, n)} \Delta \theta_{(m-1/2, n)} ] \\
& + 2 \sum \sum K_{\tau\varphi} [\Delta R_{(m, n)} \Delta \varphi_{i(m, n)} + \Delta R_{(m, n-1/2)} \Delta \varphi_{j(m, n-1/2)} \\
& \quad + \Delta R_{(m-1/2, n-1/2)} \Delta \varphi_{i(m, n)} + \Delta R_{(m-1/2, n)} \Delta \varphi_{j(m-1, n)}] \\
& + 2 \sum \sum K'_{\tau\varphi} [\Delta R_{(m, n)} \Delta \varphi_{j(m, n)} + \Delta R_{(m, n-1/2)} \Delta \varphi_{i(m, n)} \\
& \quad + \Delta R_{(m-1/2, n-1/2)} \Delta \varphi_{j(m-1, n-1)} + \Delta R_{(m-1/2, n)} \Delta \varphi_{i(m, n)}] \\
& + 2 \sum \sum K_{\theta\varphi} [\Delta \theta_{(m, n)} \Delta \varphi_{i(m, n)} + \Delta \theta_{(m, n-1/2)} \Delta \varphi_{j(m, n-1)} \\
& \quad + \Delta \theta_{(m-1/2, n-1/2)} \Delta \varphi_{i(m, n)} + \Delta \theta_{(m-1/2, n)} \Delta \varphi_{j(m-1, n)}] \\
& + 2 \sum \sum K'_{\theta\varphi} [\Delta \theta_{(m, n)} \Delta \varphi_{j(m, n)} + \Delta \theta_{(m, n-1/2)} \Delta \varphi_{i(m, n)} \\
& \quad + \Delta \theta_{(m-1/2, n-1/2)} \Delta \varphi_{j(m-1, n-1)} + \Delta \theta_{(m-1/2, n)} \Delta \varphi_{i(m-1, n)}] \\
& + 2 \sum \sum K_{\varphi\varphi} [\Delta \varphi_{i(m, n)} \Delta \varphi_{j(m, n)} + \Delta \varphi_{i(m, n)} \Delta \varphi_{j(m, n-1)} \\
& \quad + \Delta \varphi_{i(m, n)} \Delta \varphi_{j(m-1, n-1)} + \Delta \varphi_{i(m, n)} \Delta \varphi_{j(m-1, n)}] \quad (\text{B-1})
\end{aligned}$$

where

$$\begin{aligned}
K_{\tau} &= a_{\tau}^2 K_1 + 2b_{\tau}^2 K_2 \\
K_{\theta} &= a_{\theta}^2 K_1 + 2b_{\theta}^2 K_2 \\
K_{\varphi} &= a_{\varphi}^2 K_1 + 2b_{\varphi}^2 K_2 \\
K_{\tau\theta} &= a_{\tau} a_{\theta} K_1 + 2b_{\tau} b_{\theta} K_2 \\
K_{\tau\varphi} &= a_{\tau} a_{\varphi} K_1 + 2b_{\tau} b_{\varphi} K_2 \\
K'_{\tau\varphi} &= a_{\tau} a_{\varphi}' K_1 + 2b_{\tau} b_{\varphi}' K_2 \\
K_{\theta\varphi} &= a_{\theta} a_{\varphi} K_1 + 2b_{\theta} b_{\varphi} K_2 \\
K'_{\theta\varphi} &= a_{\theta} a_{\varphi}' K_1 + 2b_{\theta} b_{\varphi}' K_2 \\
K_{\varphi\varphi} &= a_{\varphi} a_{\varphi}' K_1 + 2b_{\varphi} b_{\varphi}' K_2 \quad (\text{B-2})
\end{aligned}$$

and

$$\begin{aligned}
a_{\tau} &= (R - 2\rho \sin \varphi \sin \theta)/R_1 \\
a_{\theta} &= (-2R\rho \sin \varphi \sin \theta)/R_1 \\
a_{\varphi} &= [-R\rho \sin (\theta + \varphi) + \rho^2 \sin 2\varphi]/R_1 \\
a_{\varphi}' &= [R\rho \sin (\varphi - \theta) + \rho^2 \sin 2\varphi]/R_1 \\
b_{\tau} &= (R - 2\rho \cos \varphi \cos \theta)/R_2 \\
b_{\theta} &= (2R\rho \cos \varphi \sin \theta)/R_2 \\
b_{\varphi} &= [R\rho \sin (\varphi + \theta) - \rho^2 \sin 2\varphi]/R_2 \\
b_{\varphi}' &= [R\rho \sin (\varphi - \theta) - \rho^2 \sin 2\varphi]/R_2 \\
R^2 &= (a^2 + b^2)/4 \quad (\text{B-3})
\end{aligned}$$

When a force  $F_x$  or  $F_y$  acts on a crystal of polyethylene along the  $a$  axis or the  $b$  axis, the intermolecular distance between the adjacent molecules should be equal, and rotations around the chain axis do not occur. The changes of  $\Delta R$  and  $\Delta\theta$  are obtained by differentiating eq. (B-1) with  $\Delta R$  and  $\Delta\theta$ ,

$$K_r \Delta R + K_{r\theta} \Delta\theta = f_r \quad (\text{B-4})$$

$$K_{r\theta} \Delta R + K_\theta \Delta\theta = f_\theta$$

For  $F_x$  where the crystal is stretched along the  $a$  axis,

$$\begin{aligned} f_r &= F_x(R/b) \sin 2\theta \\ f_\theta &= F_x(R^2/b) \cos 2\theta \end{aligned} \quad (\text{B-5})$$

$$\Delta X = 4(R/b) \sin 2\theta \Delta R + 4(R^2/b) \cos 2\theta \Delta\theta$$

and for  $F_y$  where the crystal is stretched along the  $b$  axis,

$$\begin{aligned} f_r &= F_y(R/a) \sin 2\theta \\ f_\theta &= F_y(R^2/a) \cos 2\theta \end{aligned} \quad (\text{B-6})$$

$$\Delta Y = 4(R/a) \sin 2\theta \Delta R + 4(R^2/a) \cos 2\theta \Delta\theta$$

The elastic moduli are

$$E_a = (F_x/A_a)/(\Delta X/X) = 2.09 \times 10^{10} \text{ dyne/cm.}^2 \quad (\text{B-7})$$

$$E_b = (F_y/A_b)/(\Delta Y/Y) = 2.11 \times 10^{10} \text{ dyne/cm.}^2$$

where  $A_a$  and  $A_b$  are the cross-sectional areas perpendicular to the  $b$  axis or the  $a$  axis and the numerical values used are as follows:  $r = 1.54 \text{ \AA.}$ ,  $\varphi = 48^\circ 40'$ ,  $\phi = 109^\circ 28'$ ,  $a = 7.4 \text{ \AA.}$ ,  $b = 4.93 \text{ \AA.}$ ,  $K_1 = 1.80 \times 10^{-2} \text{ mdyne/\AA.}$ ,  $K_2 = 1.4 \times 10^{-2} \text{ mdyne/\AA.}$

We are greatly indebted to Prof. Shimanouchi for his helpful discussion and encouragement during this study.

## References

1. Shimanouchi, T., *J. Chem. Phys.*, **17**, 734 (1949).
2. Miyazawa, T., *J. Chem. Phys.*, **35**, 693 (1961).
3. Tasumi, M., T. Shimanouchi, and T. Miyazawa, *J. Spectroscopy*, **9**, 261 (1962).
4. Shimanouchi, T., and M. Tasumi, *Bull. Chem. Soc. Japan*, **34**, 359 (1961).
5. Tadokro, H., *J. Chem. Phys.*, **33**, 1558 (1960); *ibid.*, **35**, 1050 (1961).
6. Tadokro, H., M. Kobayashi, Y. Kawaguchi, T. Kobayashi, and S. Murahashi, *J. Chem. Phys.*, **38**, 703 (1963).
7. Miyazawa, T., K. Fukushima, and Y. Ideguchi, *J. Chem. Phys.*, **37**, 2764 (1962).
8. Shimanouchi, T., M. Asahina, and S. Enomoto, *J. Polymer Sci.*, **59**, 93 (1962).
9. Asahina, M., and S. Enomoto, *J. Polymer Sci.*, **59**, 101 (1962).
10. Enomoto, S., and M. Asahina, *J. Polymer Sci.*, **59**, 113 (1962).
11. Enomoto, S., and S. Krimm, *Biophys. J.*, **2**, 317 (1962).
12. Wunderlich, B., *J. Chem. Phys.*, **37**, 1203 (1962).
13. Wunderlich, B., *J. Polymer Sci.*, **C1**, 41 (1963).
14. Stockmayer, W. H., and C. E. Hecht, *J. Chem. Phys.*, **21**, 1954 (1953).

15. Krimm, S., C. Y. Liang, and G. B. B. M. Sutherland, *J. Chem. Phys.*, **25**, 549 (1956).
16. Stein, R. S., *J. Chem. Phys.*, **23**, 734 (1955).
17. Snyder, R. G., *J. Mol. Spectroscopy*, **7**, 116 (1961).
18. Shimanouchi, T., M. Tsuboi, and T. Miyazawa, *J. Chem. Phys.*, **35**, 1597 (1961).
19. Tsuboi, M., M. Terada, and T. Shimanouchi, *J. Chem. Phys.*, **36**, 1301 (1962).
20. Bunn, C. W., *Trans. Faraday Soc.*, **35**, 482 (1939).
21. Dows, D. A., *J. Chem. Phys.*, **32**, 1342 (1960).
22. Mizushima, S., and T. Shimanouchi, *Sekigaisen Kyushu to Raman Koka*, Kyoritsu Shupan, Tokyo, 1962.
23. Wilson, E. B., *J. Chem. Phys.*, **7**, 1047 (1939).
24. Wilson, E. B., *J. Chem. Phys.*, **9**, 76 (1941).
25. Genensky, S. M., and G. F. Newell, *J. Chem. Phys.*, **26**, 486 (1957).
26. Shimanouchi, T., and S. Mizushima, *J. Chem. Phys.*, **23**, 707 (1955).
27. Miyazawa, T., *J. Polymer Sci.*, **55**, 215 (1961).
28. Itohō, T., and I. Sakurada, paper presented at the 11th Annual Meeting of the Society of Polymer Science, Japan, 1962.
29. Fowler, R. H., and E. A. Guggenheim, *Statistical Thermodynamics*, University Press, Cambridge, England (1939).
30. Hill, T. L., *J. Chem. Phys.*, **16**, 399 (1948).
31. Urey, H. C., and C. A. Bradley, *Phys. Rev.*, **38**, 1969 (1930).

### Résumé

Un champ de force du type Urey-Bradley modifié est adopté pour l'étude de la configuration du réseau du polyéthylène par la méthode des matrices GF avec des constantes de force intermoléculaire, estimées à partir de la fonction potentielle intermoléculaire du méthane. Les fréquences des modes sont calculées à des intervalles de  $30^\circ$  pour des différences de phase le long de l'axe  $a$  et  $b$ . Les modules d'élasticité du cristal de polyéthylène le long des deux axes sont ainsi obtenus à partir de la fonction potentielle intermoléculaire.

### Zusammenfassung

Ein modifiziertes Kraftfeld vom Urey-Bradley-Typ wurde mit den aus der intermolekularen Potentialfunktion von Methan bestimmten intermolekularen Kraftkonstanten zur Untersuchung der Gitterschwingungen von Polyäthylen nach der GF-Matrizenmethode herangezogen. Die Schwingungsfrequenzen wurden in Abständen von  $30^\circ$  für die Phasenunterschiede längs der  $a$ -Achse und der  $b$ -Achse berechnet. Die Elastizitätsmoduln eines Polyäthylenkristalls für die beiden Achsen wurden ebenfalls aus der intermolekularen Potentialfunktion erhalten.

Received July 17, 1963

Revised October 1, 1963

## Dilute Solution Properties of Partly Urethanized Polyvinyl Alcohol

ICHIRO SAKURADA, AKIO NAKAJIMA, and KYOICHIRO SHIBATANI, *Department of Polymer Chemistry, Kyoto University, Kyoto, Japan*

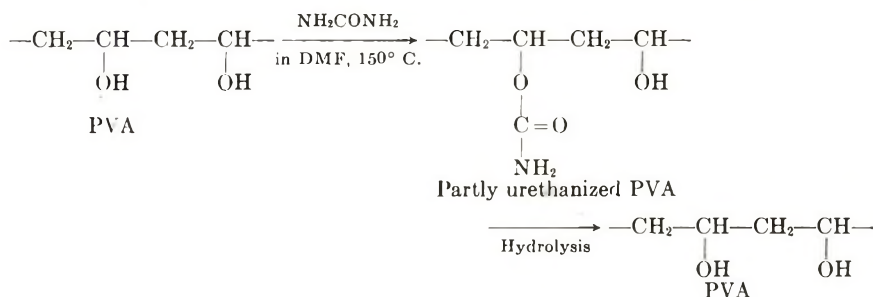
### Synopsis

Partly urethanized polyvinyl alcohol samples, in a range of degree of urethanization up to about 10 mole-%, were prepared by treatment of polyvinyl alcohol with urea. These were fractionated in a water-*n*-propanol system into fractions, each having nearly the same nitrogen content. The degree of polymerization of the partly urethanized polyvinyl alcohol was estimated from the intrinsic viscosity of polyvinyl alcohol obtained by hydrolysis of the corresponding urethanized polymer. The effects of introduced urethane residue on solubility and dissolved state of polymer were investigated in water and theta solvents. Further, some thermodynamic parameters in water were discussed in relation to those of partly acetylated polyvinyl alcohol.

### INTRODUCTION

Polyvinyl alcohol (PVA) with its free hydroxyl groups offers considerable latitude for chemical transformations such as esterification, etherification, and acetalization. Partly urethanized polyvinyl alcohol can be obtained<sup>1</sup> by treatment of polyvinyl alcohol with urea. The solubility of this polymer in water is a function of the degree of substitution: highly substituted polymer is soluble in organic solvents, but less substituted polymer is soluble in water, giving a stable solution.

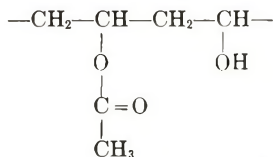
Studies by Mashio and others<sup>2-4</sup> have disclosed the following reactions:



Polyvinyl alcohol is readily urethanized by urea in dimethylformamide (DMF) at 150°C.; the reaction is accompanied by some chain cleavage. However, in the hydrolysis of partly urethanized PVA, no chain cleavage seems to occur. Accordingly, one can estimate the degree of polymeriza-

tion of partly urethanized PVA from that of the hydrolyzed products (PVA).

Previously,<sup>5,6</sup> we pointed out that partly acetylated (up to 15 mole-%) PVA



forms an exothermic solution in water and presents characteristic thermodynamic behavior. These two PVA derivatives differ from each other in structure in the  $\text{CH}_3$  and  $\text{NH}_2$  groups, respectively. The  $\text{CH}_3$  residue in acetylated PVA is hydrophobic in character, whereas the  $\text{NH}_2$  residue in urethanized PVA can form hydrogen bonds with the  $\text{C=O}$  groups. In aqueous solution, of course, OH groups in the polymer and water molecule are also involved in the formation of hydrogen bonds.

The purpose of this work is to investigate the effects of the introduced urethane groups, in the range of the degree of substitution up to about 10 mole-%, on solubility and dissolved state of the polymer, in comparison with the results on partly acetylated PVA. Further, we also expect more information about the dissolved state of PVA in aqueous solution by extrapolating the data on urethanized PVA to zero degree of substitution.

## EXPERIMENTAL

Partly urethanized PVA was prepared by treating urea with PVA having a degree of polymerization of 1320 in dimethylformamide at about  $150^\circ\text{C}$ . In a three-necked flask equipped with a stirrer, a condenser, and a thermometer were placed, for example, 20 g. of PVA, 100 g. of DMF, and 27.3 g. (1 mole urea to 1 base mole PVA) of urea. The vessel was maintained at a temperature of  $148\text{--}152^\circ\text{C}$ . The reaction mixture became homogeneous within a short time and the reaction proceeded, accompanied by evolution of gas. After definite times of reaction, the resulting polymer was precipitated into methanol, purified twice in excess methanol, then dried *in vacuo*. The nitrogen content ( $\text{N}\%$ ) of the thus obtained partly urethanized PVA samples was determined by semimicro Kjeldahl method.  $\text{N}\%$  was then converted to the degree of urethanization DU (in mole-%) by the following relation:

$$\text{DU} = 44(\text{N}\%) / (14 - 43(\text{N}\%) \times 10^{-2})$$

The degree of polymerization of partly urethanized PVA was determined from the intrinsic viscosity of PVA obtained by hydrolysis of corresponding urethanized polymer. For such a purpose, the urethanized PVA was hydrolyzed in a 5% aqueous solution by reacting sodium hydroxide (5 moles  $\text{NaOH}$ /1 mole urethan residue) for 5 hr. at  $85^\circ\text{C}$ . The polymer thus obtained was purified by dialysis, reprecipitation in methanol, and Soxhlet

extraction with methanol, and dried. The nitrogen content of the hydrolyzed products is zero, as shown in Table I. The degree of polymerization  $P$  of PVA was calculated from the intrinsic viscosity in water at 30°C. according to the equation<sup>7</sup>

$$[\eta] = 7.50 \times 10^{-3} P^{0.64}$$

Table I shows the time of reaction, the degree of urethanization, the intrinsic viscosity in water at 30°C., and the degree of polymerization for six samples.

TABLE I  
Characterization of Partly Urethanized PVA Samples

Sample	Reaction time, hr.	Partly urethanized PVA			Hydrolyzed product		
		N, %	DU, mole-%	$[\eta]$ , dl./g.	N, %	$[\eta]$ , dl./g.	$P$
K-1	3.0	2.3	7.8	0.675	0	0.685	1160
K-2	4.5	3.6	12.8	0.630	0	0.640	1050
K-3	6.0	3.7	13.0	0.580	0	0.600	950
K-5	3.0	3.10	11.5	0.590			
K-6	2.0	2.33	8.1	0.605			
K-7	1.0	1.50	4.9	0.640			

In cases of samples K-1 to K-3, the reactants used were 20 g. PVA, 100 g. DMF, and 27.3 g. urea; and those of samples K-5 to K-7 were 80 g. PVA, 400 g. DMF, and 109.2 g. urea.

Samples K-5 to K-7 were fractionated with the use of water as solvent and *n*-propanol as precipitant, because this system was found to bring about favorable liquid-liquid phase separation. Fractionation was carried out by fractional precipitation by adding *n* propanol to a 3% aqueous polymer solution at 30°C. As is obvious from Table II, the nitrogen content of every fraction was the same, within experimental error, for each series.

TABLE II  
Nitrogen Content and Degree of Polymerization  $P$  of Partly Urethanized PVA Fractions

Fraction no.	K-5		K-6		K-7	
	N, %	$P$	N, %	$P$	N, %	$P$
2	3.10	1860	2.42	1870	1.43	2040
3	3.03	1975	2.37	1950	1.45	2030
4	3.05	1940	2.27	1920	1.44	1850
5	3.12	1900	2.30	1830	1.51	1630
6	3.08	1820	2.32	1770	1.52	1610
7	3.07	1620	2.35	1650	1.51	1450
8	3.21	1470	2.38	1540	1.52	1340
9	3.09	1240	2.33	1260	1.50	1300
10	3.14	1070	2.35	970	1.56	900
11	3.05	680	2.21	710	1.54	770

This indicates that the composition distribution is very uniform and one can regard the fractions of each sample as a polymer homologous series.

## RESULTS

### Relation between Intrinsic Viscosity in Water and Degree of Polymerization

The intrinsic viscosity  $[\eta]$  of partly urethanized PVA was measured in water at 30°C. in a modified Ostwald-type viscometer. The intrinsic viscosities are plotted against the degrees of polymerization  $P$  in Figure 1. The observed relationships are of the type

$$[\eta] = K'P^a \quad (1)$$

The constants  $K'$  and  $a$  for three sample series used are given in Table III, together with those for PVA.<sup>7</sup> In the table, the average molecular weight  $M_0$  per monomeric unit is also shown.

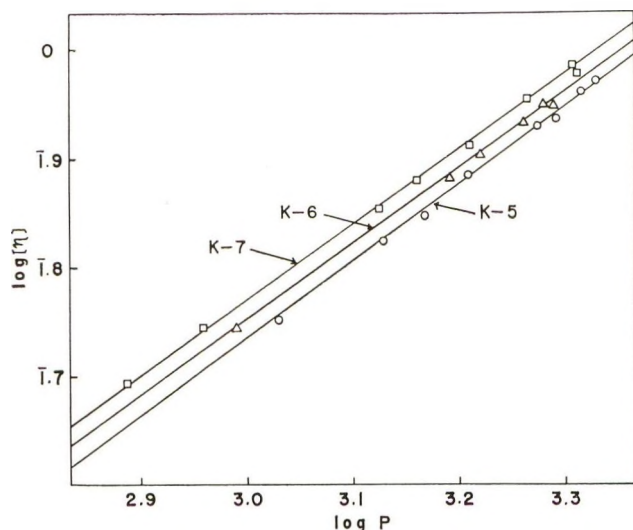


Fig. 1. Relation of intrinsic viscosity in water at 30°C. to degree of polymerization for partly urethanized polyvinyl alcohol.

TABLE III  
Constant  $K'$  and  $a$  in  $[\eta] = K'P^a$  for Partly Urethanized PVA in Water at 30°C.

Sample	DU, mole-%	$M_0$	$K' \times 10^3$	$a$
K-5 series	11.5	48.7	3.9	0.72
K-6 series	8.1	47.4	4.5	0.70
K-7 series	4.9	46.2	4.8	0.69
PVA	0	44.0	7.5	0.64

### Determination of $\Theta$ Solvent and Intrinsic Viscosity in $\Theta$ Solvent

Several trials to find the  $\Theta$  temperature from the critical miscibility temperature measurements proposed by Flory<sup>8</sup> did not succeed, at least in the present polymer systems. Alternatively, the method proposed by Elias,<sup>9</sup>

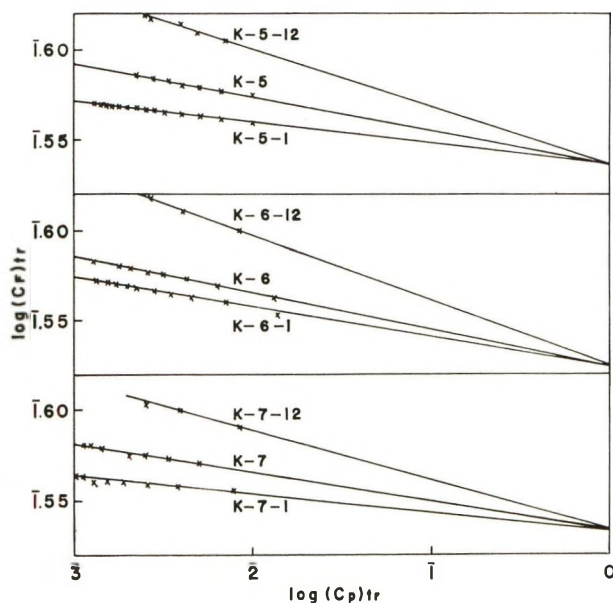


Fig. 2. Determination of  $\Theta$  composition at 30°C. in water-*n*-propanol system by plotting precipitant concentration  $(C_F)_{tr}$  against polymer concentration  $(C_P)_{tr}$  at precipitation point.

which determines the composition of the  $\Theta$  medium at a constant temperature by using a solvent-precipitant mixture, was used here. According to Elias, precipitant concentration at the precipitation point,  $(C_F)_{tr}$ , is related to polymer concentration at the precipitation point,  $(C_P)_{tr}$ , by the equation

$$\log(C_F)_{tr} = K_1 - k (\log(C_P)_{tr}) \quad (2)$$

where  $K_1$  and  $k$  are constants, and the  $(C_F)_{tr}$  value extrapolated to  $C_P \rightarrow 1$  is constant independent of molecular weight and molecular weight distribu-

TABLE IV  
 $\Theta$  Composition Given by *n*-Propanol-Water Volume Ratio

Sample	<i>n</i> -Propanol/water (volume ratio)	
	30°C.	60°C.
K-5	30/40	4/5
K-6	30/41	4/5
K-7	30/40	4/5

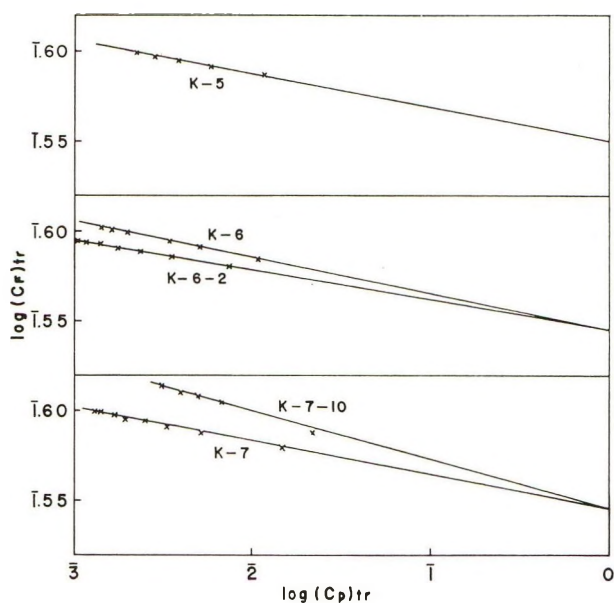


Fig. 3. Determination of  $\Theta$  composition at  $60^\circ\text{C}$ . in water-*n*-propanol system by plotting  $(C_F)_{tr}$  against  $(C_P)_{tr}$ .

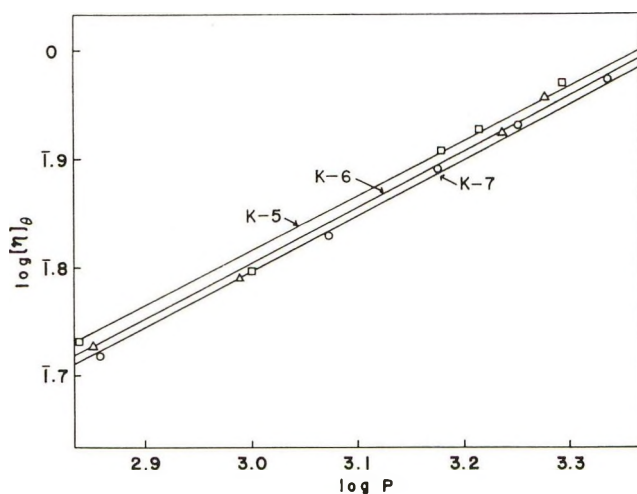


Fig. 4. Relation of intrinsic viscosity in  $\Theta$  solvent at  $30^\circ\text{C}$ . to degree of polymerization for partly urethanized polyvinyl alcohol.

tion of the polymer, and represents the  $\Theta$  conditions at that temperature. Here, experiments to determine the  $\Theta$  solvent were carried out in the water-*n*-propanol system at  $30^\circ\text{C}$ . and  $60^\circ\text{C}$ . The results are shown in Figures 2 and 3, from which the precipitant concentration in  $\Theta$  solvent was determined as shown in Table IV.

TABLE V  
Intrinsic Viscosities at 60°C. in  $\Theta$  Solvent and in Water

Fraction	$P$	Viscosity, dl./g.	
		$\eta_{60^\circ\text{water}}$	$\eta_{60^\circ\theta}$
K-5-3	1975	0.855	0.880
K-5-7	1620	0.667	0.789
K-5-10	1070	0.573	0.607
K-6-5	1830	0.692	0.898
K-6-7	1650	0.638	0.724
K-6-10	970	0.434	0.460
K-7-3	2030	0.783	0.869
K-7-6	1610	0.700	0.793
K-7-9	1300	0.545	0.648

TABLE VI  
Solubility of Partly Urethanized PVA (K-3)

Solvent	Solubility <sup>a</sup>		
	30°C. 7 days	60°C. 2 days	100°C. 10 hr.
Decalin	×		
Acetone	×	×	×
Methyl ethyl ketone	×	×	×
Dioxane	×	×	×
Cyclohexanone	×	×	
Ethyl acetate	×	×	×
Acetic acid	△	△	△
Dichloroacetic acid	○		
Water	○		
Pyridine	×	×	×
Dimethylformamide	○		
Dimethyl sulfoxide	○		
Carbon tetrachloride	×		
Carbon disulfide	×		
Acetonitrile	×	×	×
Benzene	×	×	×
Methanol	×		
Ethanol	×	×	×
<i>n</i> -Propanol	×	×	
Ethylene glycol	○		
Toluene	×	×	×
Nitrobenzene	×	×	×
Chlorobenzene	×	×	×
<i>o</i> -Dichlorobenzene	×	×	×

<sup>a</sup> Solubility: (○) soluble, (△) swell, (×) insoluble.

The relation between the intrinsic viscosity in the  $\Theta$  solvent given in Table IV and the degree of polymerization is shown in Figure 4, from which constants  $K'$ ,  $K$ , and  $a$  in eqs. (3) and (4) were obtained.

$$[\eta]_{\theta} = K'P^a \quad (3)$$

$$[\eta]_{\theta} = KM^a \quad (4)$$

These are shown in Table VII as  $K'(\text{obs})$ ,  $K(\text{obs})$ , and  $a(\text{obs})$ .

The intrinsic viscosities in  $\theta$  solvent at 60°C.,  $[\eta]_{60^\circ\theta}$ , and in water at 60°C.,  $[\eta]_{60^\circ\text{water}}$ , are given in Table V.

The solubility of the partly urethanized PVA in various solvents was qualitatively examined with 10 mg. polymer and 1 ml. solvent sealed in a glass tube. The results, for example, obtained with sample K-3, are shown in Table VI.

## DISCUSSION

As is obvious from Table VI, partly urethanized PVA is more soluble than PVA in solvents such as water, dimethylformamide, and dimethyl sulfoxide at room temperature. Moreover, the aqueous solution of partly urethanized PVA is more stable than an aqueous solution of PVA. Such a change in solubility may be due to the irregularity in the chain structure owing to the introduction of bulky O-CO-NH<sub>2</sub> residue. C=O and NH in the side residue are capable of forming hydrogen bonds with NH and C=O, respectively, in addition to hydrogen bonds originating from OH groups. Accordingly, in more highly urethanized PVA, C=O may strongly be hydrogen bonded to NH of the same or different polymer chain; thus the solubility in water may be remarkably reduced.

The constant  $a$  in eq. (4), given in Table VII, was nearly constant but slightly larger than the theoretically expected value (0.5). The method<sup>10</sup> of determining unperturbed chain dimensions from intrinsic viscosity-

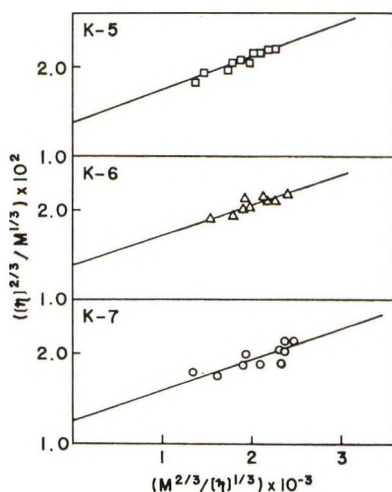


Fig. 5. Determination of  $K$  by eq. (5) from data obtained for aqueous solutions at 30°C.

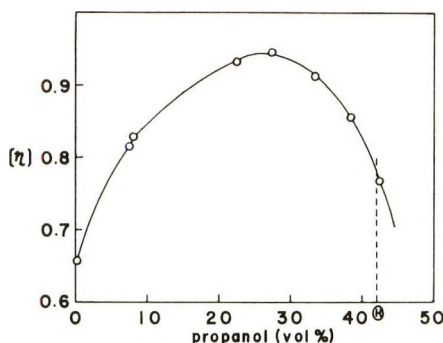


Fig. 6. Intrinsic viscosity of samples K-6-9 at 30°C. in water-*n*-propanol mixtures.

molecular weight data by eq. (5) in any solvent may occasionally be useful especially for polar polymers.

$$[\eta]^{2/3}/M^{1/3} = K^{2/3} + C'' (M^{2/3}/[\eta]^{1/3}) \quad (5)$$

$[\eta]^{2/3}/M^{1/3}$  should be a linear function of  $M^{2/3}/[\eta]^{1/3}$ , with an ordinate intercept equal to  $K^{2/3}$ . The unperturbed end-to-end distance of the chain,  $\langle R_0^2 \rangle^{1/2}$ , is then obtained from

$$K = \Phi(\langle R_0^2 \rangle / P)^{1/2} (1/M_0^{1/2}) \quad (6)$$

where  $\Phi$  is the universal constant<sup>8b</sup> and  $P$  is the degree of polymerization.  $K$  thus obtained corresponds to that given by eq. (4) with  $a = 0.5$ . The experimental results from the intrinsic viscosities measured in water at 30°C. are shown in Figure 5.  $K$  values obtained from Figure 5 and unperturbed chain dimension per monomer unit are listed as  $K(\text{calc.})$  and  $[\langle R_0^2 \rangle / P] (\text{calc.})$  in Table VII.

TABLE VII  
Constants  $K'$ ,  $K$ , and  $a$  in the Equations  $[\eta]_\theta = K'P^a$  and  $[\eta]_\theta = KM^a$  for Partly Urethanized PVA in  $\Theta$  Solvents at 30°C.

Sample	DU, mole-%	$K' \times 10^2$ (obs.)	$a$ (obs.)	$K \times 10^3$		$\Phi[(R_0^2)^{1/2} \times 10^2]$	
				(obs.)	(calc.)	(obs.)	(calc.)
K-5	11.5	1.93	0.51	2.66	1.87	94.0	63.6
K-6	8.1	1.88	0.51	2.62	1.87	89.1	61.0
K-7	4.9	1.69	0.52	2.29	1.66	78.0	52.1
	lim 0	1.5		1.9		67	
PVA (in H <sub>2</sub> O, 80°C.) <sup>a</sup>	0				1.65		48.2

<sup>a</sup> Data of Matsuo and Inagaki.<sup>11</sup>

In Table VII, the values extrapolated to DU = 0 and the values for PVA in water at 80°C. obtained by Matsuo and Inagaki<sup>11</sup> are also shown. Inagaki<sup>11</sup> pointed out that aqueous solution of PVA at 80°C. is approximately in the  $\Theta$ -condition. The results given in Table VII suggest that the

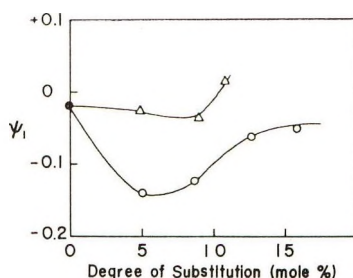


Fig. 7. Entropy parameter  $\psi_1$  of partly substituted polyvinyl alcohols in water at 30°C.: (O) partly acetylated polyvinyl alcohol; ( $\Delta$ ) partly urethanized polyvinyl alcohol.

unperturbed chain dimension per monomeric unit increases slightly with increasing degree of urethanization within the range studied here. The difference in numerical values between calculated and observed values of  $\Phi[\langle R_0^2 \rangle / P]^{1/2}$  may be due to a slightly higher value for  $a$  compared with the theoretical value,  $a = 0.5$ . The intrinsic viscosity in water is lower than that in the  $\Theta$  solvent both at 30 and 60°C., as shown in Table V and Figures 1 and 4. This may also be obvious from Figure 6, in which the intrinsic viscosity is plotted against solvent composition.

The thermodynamic parameters  $\psi_1$ ,  $\kappa_1$ , and  $\Theta$  defined by Flory<sup>8b</sup> were estimated for aqueous solution of the partly urethanized PVA, using the well-established equations of Flory:<sup>8b</sup>

$$[\eta]/[\eta]_{\theta} = \alpha^3 \quad (7)$$

$$\alpha^5 - \alpha^3 = 2C_M \psi_1 [1 - \Theta/T] M^{1/2} \quad (8)$$

$$\kappa_1 = \psi_1 \Theta / T \quad (9)$$

where

$$C_M = (27/2^{3/2} \pi^{3/2}) (v^2 / N_A V_1) (\langle R_0^2 \rangle / M)^{-3/2} \quad (10)$$

$C_M$  is a function of the partial specific volume of polymer  $v$ , mole volume of solvent  $V_1$ , and unperturbed polymer dimension  $\langle R_0^2 \rangle$ . Assuming that  $C_M$  is a constant independent of temperature,  $\kappa_1$ ,  $\psi_1$ , and  $\Theta$  were calculated for aqueous solutions from the experimental results obtained at 30 and 60°C. Data obtained are summarized in Table VIII and compared in Figure 7 with those<sup>5</sup> for partly acetylated PVA.

TABLE VIII  
Thermodynamic Parameters for Aqueous Solution of Partly Urethanized PVA

Sample	$\psi_1 \times 10^2$	$\kappa_1 \times 10^2$		$\Theta$ , °K.
		30°C.	60°C.	
K-5	+1.5	+1.8	+1.7	366
K-6	-3.5	-3.3	-3.0	292
K-7	-2.7	-2.9	-2.4	287
PVA <sup>5</sup>	-2.4	-3.2		410

The experimental results suggest that the aqueous solution of slightly urethanized PVA is an exothermic solution but that of polymer of  $DU = 12$  mole-% is endothermic in nature. The entropy parameter  $\psi_1$  decreases slightly with increasing  $DU$ , then passes through a minimum at about  $DU = 8$  mole-%, increases, and changes sign from minus to plus at about  $DU = 11$  mole-%. Such behavior is similar to that of partly acetylated PVA. However, the absolute values of  $\psi_1$  and  $\kappa_1$  of partly urethanized PVA are much smaller than those of partly acetylated PVA in water. The exothermic character for samples of lower  $DU$  may mainly be attributed to the steric effect of the bulky  $O \cdot CO \cdot NH_2$  group introduced on the chain. However, with increasing  $DU$ , the hydrogen bonds, presumably formed between  $CO$  and  $NH$  group, may play an important role to form endothermic solution ( $\kappa_1 > 0$ ). The positive  $\kappa_1$  obtained for samples of comparatively higher  $DU$  may be explained by assuming a mechanism similar to the formation of urea dimers in aqueous urea solution,<sup>12,13</sup> in which the enthalpy parameter  $\kappa_1$  is positive. The larger negative value of  $\kappa_1$  at the minimum point for partly acetylated PVA may be due to more than the hydrophobic nature of  $CH_3$  group compared with  $NH_2$  group in partly urethanized PVA.

### References

1. Paquin, A., *Z. Naturforsch.*, **1**, 518 (1946).
2. Mashio, F., Rept. of Poval Committee, No. 36, Kyoto, Japan (Dec. 1959).
3. Mashio, F., K. Watanabe, and Y. Morii, Rept. of Poval Committee, No. 38, Kyoto, Japan (Feb. 1960).
4. Mashio, F., K. Watanabe, T. Morii, and T. Iida, Rept. of Poval Committee, No. 39, Kyoto, Japan (June 1961).
5. Sakurada, I., A. Nakajima, and H. Takita, *Kobunshi Kagaku*, **12**, 15 (1955).
6. Sakurada, I., Y. Sakaguchi, and Y. Ito, *Kobunshi Kagaku*, **14**, 41 (1957).
7. Nakajima, A., and K. Hurutachi, *Kobunshi Kagaku*, **6**, 460 (1949).
8. Flory, P. J., *Principles of Polymer Chemistry*, Cornell Univ., Press, Ithaca, N. Y., 1953, (a) Chap. 13; (b) Chap. 14.
9. Elias, H. G., *Makromol. Chem.*, **33**, 140 (1959); *ibid.*, **50**, 1 (1961); H. G. Elias et al., *J. Polymer Sci.*, **46**, 264 (1960).
10. Kurata, M., W. H. Stockmayer, and A. Roig, *J. Chem. Phys.*, **33**, 151 (1960).
11. Matsuo, M., and H. Inagaki, *Makromol. Chem.*, **55**, 150 (1962).
12. Schellman, J. A., *Compt. Rend. Trav. Lab. Carlsberg, Ser. Chim.*, **29**, 223 (1955).
13. Gucker, F., and W. Pickard, *J. Am. Chem. Soc.*, **26**, 1464 (1940).

### Résumé

On a préparé des échantillons d'alcool polyvinylique partiellement transformé en uréthane par un traitement de l'alcool polyvinylique avec l'urée, avec un degré de transformation jusqu'à 10 mole pour cent. Les échantillons sont fractionnés dans un système eau-*n*-propanol; chaque fraction contient à peu près le même quantité d'azote. Le degré de polymérisation de l'alcool polyvinylique partiellement transformé en uréthane est estimé par mesure de la viscosité intrinsèque de l'alcool polyvinylique obtenu par l'hydrolyse du polymère uréthanisé correspondant. On a étudié les effets de l'introduction d'uréthane sur la solubilité et l'état de la solution du polymère en employant de l'eau

et des solvants  $\theta$ . On a discuté en outre quelques paramètres thermodynamiques dans l'eau en relation, avec ceux de l'alcool polyvinylique partiellement acétylé.

### Zusammenfassung

Teilweise urethanisierte Polyvinylalkoholproben wurden in einem Bereich bis zu etwa 10 Mol% Urethanisierung durch Behandlung von Harnstoff mit Polyvinylalkohol dargestellt. Sie wurden mit dem Wasser-*n*-Propanol-System in Fraktionen mit annähernd dem gleichen Stickstoffgehalt zerlegt. Der Polymerisationsgrad von teilweise urethanisiertem Polyvinylalkohol wurde aus der Viskositätszahl des durch Hydrolyse des entsprechenden urethanisierten Polymeren erhaltenen Polyvinylalkohols berechnet. Der Einfluss der Urethanreste auf die Löslichkeit und den gelösten Zustand des Polymeren wurde in Wasser und  $\theta$ -Lösungsmitteln untersucht. Weiters wurde die Beziehung der thermodynamischen Parameter in Wasser zu denjenigen von teilweise acetylierten Polyvinylalkohol diskutiert.

Received July 16, 1963

## The Influence of Molecular Weight Distribution on Some Properties of Polystyrene Melt

RICHARD L. BALLMAN and ROBERT H. M. SIMON, *Plastics Division, Monsanto Chemical Company, Springfield, Massachusetts*

### Synopsis

The viscosities of a number of monodisperse polystyrene melts have been measured using a capillary rheometer. The materials covered a molecular weight range of 43,000-460,000. Shear rates of 1.54-1540  $\text{sec}^{-1}$  and temperatures of 350-450°F. were studied. The effect of molecular weight distribution of polydisperse polystyrene was also measured. It was found that while low shear viscosity was dependent on  $\bar{M}_w$ , higher shear melt viscosities depended on averages between  $\bar{M}_w$  and  $\bar{M}_n$  until at 1000-2000  $\text{sec}^{-1}$ ,  $\bar{M}_n$  controlled viscosity. Agreement with the 3.4-power dependence of zero shear viscosity was good. Similar exponential relationships were found, with higher rates of shear, corresponding to smaller values of the exponent. Constant values of the exponent were found at constant shear stress but not at constant shear rate. Agreement with the constancy of the activation energy for viscous flow for various molecular weights and distributions at constant shear stress was good. However at constant shear rate,  $\Delta E$  decreased as the molecular weight average increased and as the distribution broadened. Viscosity versus shear rate master curves were constructed by using the Bueche-Harding procedure. All monodisperse polystyrenes showed excellent fit with the master curve. Other molecular weight distributions did not. Master curves also were constructed for measurements of dynamic viscosity versus frequency for monodisperse polystyrene. These curves when compared to steady state viscosities failed to confirm the correspondence of  $\eta_a$  to either  $|\eta^*|$  or to  $\eta'$ .

### INTRODUCTION

The advent of anionic polymerization has for the first time made easily available large amounts of essentially monodisperse polymers. Previous work has been reported on the evaluation of mechanical properties of such anionic polystyrenes by McCormick, Brower, and Kin<sup>1</sup> and on the melt flow properties by Rudd<sup>2,3</sup> and Cox and Ballman.<sup>4</sup> The work reported here on our evaluation of the melt properties of anionic polystyrenes confirms the findings of the above authors and, in addition, presents some findings on the effect of molecular-weight average and distribution on melt properties of polystyrene.

It was of interest to consider our data with reference to the molecular theory of F. Bueche<sup>5</sup> and its application to the Bueche-Harding<sup>6</sup> "universal curve" for depicting the influence of shear on the viscosity of concentrated

polymer solutions. This would provide a means of consolidating all the viscosity information for a linear homopolymer in a single curve.

It was also hoped that the master curve thus constructed for steady state viscosity could be compared to those derived from the dynamic measurements of Cox.<sup>7</sup> As the master curves cover a great range of shear, there should be sufficient portions of the curve in common to make good comparisons.

Lastly, it was hoped to investigate the region of the flow curve in which the product of the shear rate or frequency and the terminal relaxation time is unity. The uniqueness of this point of maximum molecular response to shear should prove valuable in understanding the mechanism of flow as revealed in the several experimental procedures used in this study.

## EXPERIMENTAL

### Preparation of Polymers

**Reagents.** 1,2-Dimethoxyethane (DME) was purified by distilling over calcium hydride. The distillate was refluxed with fresh sodium ribbon and 0.2 wt.-% of benzophenone until the blue color of sodium benzophenone ketyl formed. DME suitable for use was distilled from this mixture and stored under nitrogen.

Styrene was distilled over calcium hydride under nitrogen at 40 mm. An 80% heart cut of the distillate was stored under nitrogen for further use.

Naphthalene (recrystallized from alcohol) was used as received.

**Initiator Preparation.** A 6.4 g. portion of naphthalene was dissolved in a flask under nitrogen in 45 ml. DME. Approximately 1.5 g. of bright sodium chips was added and the mixture was agitated for about 1 hr. at room temperature. This solution of sodium naphthalene, approximately 1*M*, stored under nitrogen at 0°C., is stable for at least 10 days.

**Polymerization.** A 10–15 wt.-% solution of styrene in DME was transferred under nitrogen to a well agitated flask at room temperature equipped with a rubber serum cap over one neck. By means of a hypodermic syringe, initiator solution was rapidly introduced to the flask through the serum cap. The quantity of initiator solution required was based on the desired polymer molecular weight according to the following approximation:

$$\text{Moles sodium naphthalene} \cong \frac{2.5 (\text{g. styrene})}{\bar{M}_n}$$

On completion of initiator addition, the active chains were terminated with methanol. Polymer was precipitated from the resulting syrup with methanol and dried to constant weight in a vacuum oven at 70°C.  $\bar{M}_w/\bar{M}_n$  values obtained from polymer samples thus prepared varied in the range 1.04–1.07.

**Polystyrene Samples.** Monodisperse polystyrenes, having molecular weights of  $M = 460,000$ ,  $M = 180,000$ ,  $M = 127,000$ ,  $M = 107,000$ ,  $M = 62,000$ , and  $M = 43,000$  were used; for all of these,  $\bar{M}_w/\bar{M}_n < 1.1$ . Two blends were prepared: blend A (50%  $M = 550,000$  + 50%  $M = 48,000$ ) had  $\bar{M}_w = 299,000$ ,  $\bar{M}_n = 88,000$ ; blend B (30%  $M = 550,000$  + 70%  $M = 48,000$ ) had  $\bar{M}_w = 199,000$ ,  $\bar{M}_n = 66,000$ . Sample RL-35A, having  $\bar{M}_w = 231,000$ ,  $\bar{M}_n = 124,000$  was also used.

### Apparatus

The capillary viscometer used for this work has been described by Merz and Colwell<sup>8</sup> and its method of standard operation by Ballman and Brown.<sup>9</sup> The capillary used was 2.00 in. long, 0.0625 in. in diameter, and had a 90° entrance angle.

The temperature of the rheometer was controlled to  $\pm 1^\circ\text{F}$ . except for the material at the very top of the heating chamber, which was initially  $10^\circ\text{F}$ . lower. As the pressure drop in the rheometer barrel was quite small compared to the pressure drop in the capillary, the error introduced by this cold region was negligible.

At high shear rate, viscous heating in the capillary caused the polymer temperature to rise above the desired point. This was uncorrected and must be considered a source of increasing error in the data reported above a shear rate of 500  $\text{sec.}^{-1}$ .

The dynamic viscosity data of Cox were previously obtained on the elastoviscometer. This instrument has been described by Cox, Nielsen, and Keeney.<sup>10</sup>

### Error

The initial results from the capillary rheometer are not corrected for non-Newtonian flow except as indicated in Figure 12, where the effect of the Rabinowitsch correction<sup>11</sup> on the master flow curve is shown for comparison with the uncorrected curve. As indicated, the effect of this correction is small and does not influence the conclusions to be drawn from the data.

The error caused by the nonlinearity of the pressure drop across the capillary entrance is not great in the 32/1  $L/D$  capillary used, except at high rates of shear. Measurement of this error by the Bagley<sup>12</sup> technique shows it to be about 10% in the reduced shear region of  $10^4$ – $10^5 \text{ sec.}^{-1}$ .

For purposes of calculating the shear rate at the capillary wall, the polymer was assumed to be incompressible.

The effect of hydrostatic pressure on viscosity, while uncorrected, was not felt to seriously affect the general form of the data.

The reproducibility of data from the capillary rheometer is within 2% for one temperature setting or within 5% for repeated temperature settings.

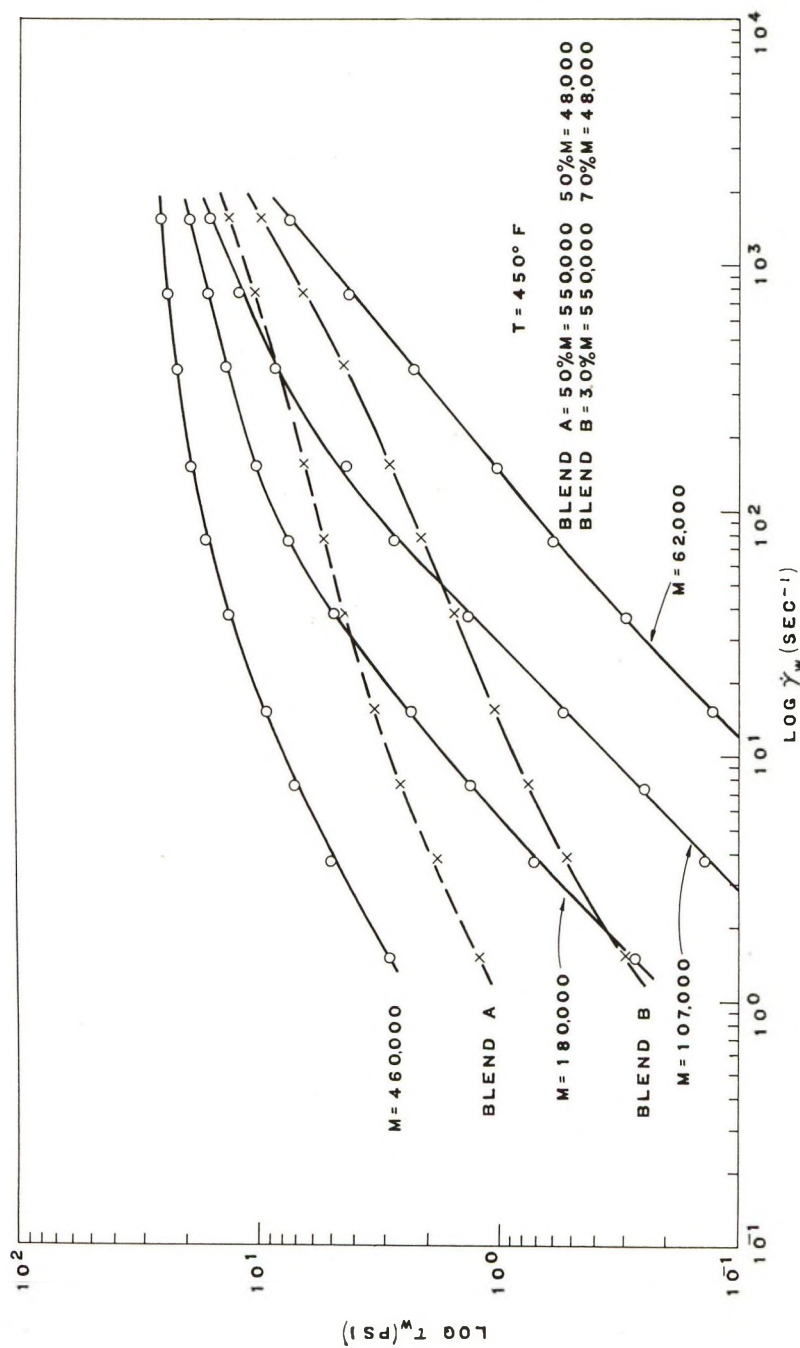


Fig. 1. Plots of log shear rate vs. log shear stress for narrow molecular weight distribution polystyrene.

## RESULTS

Typical flow data for monodisperse polystyrenes are plotted as log shear stress  $\tau_w$  versus log (apparent) shear rate  $\dot{\gamma}_w$  in Figure 1. Flow curves for other temperatures are not shown but are similar in form. Results for two of the polystyrene blends are shown on the same plot for comparison.

Zero shear viscosities  $\eta_0$  obtained from these data are plotted versus molecular weight  $M$  at various temperatures in Figure 2. A slope of 3.4 is also shown here.

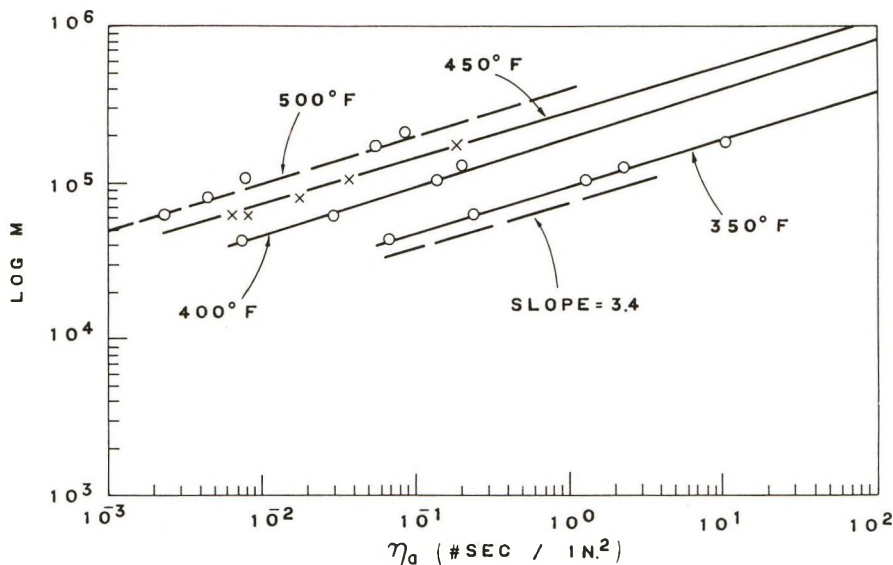


Fig. 2. Plots of zero shear apparent melt viscosity vs. molecular weight of narrow distribution polystyrene.

The dependence of the molecular weight-viscosity relationship on the amount of shear has been pointed out by Bagley<sup>13</sup> and studied extensively by Porter and Johnson<sup>14</sup> on other polymers. Monodisperse polystyrenes are compared in the same manner as shown in Figure 3, where  $\log \dot{\gamma}$  versus  $M$  is shown at various shear stress levels. The effect of the stress level on the slope of these curves is shown in Figure 4, where the ordinate intercept is seen to be  $\sim 3.3$  for zero shear. The data in Figure 4 can be represented by

$$-d \ln \dot{\gamma}_w / d \ln M = 3.31 - 0.0644 \tau_w$$

The effect of melt temperature on viscosity can be expressed at constant shear stress or at constant shear rate with widely different results. Figure 5 shows results at constant stress whereas data at constant shear rate are given in Figures 6 and 7. The shear rate level in Figure 6 is 10  $\text{sec.}^{-1}$  and in Figure 7 is 100  $\text{sec.}^{-1}$ . Data for two blends are included for comparison with the monodisperse materials.

## DISCUSSION

## Effect of Molecular Weight and Distribution

The typical flow data given in Figure 1 show the well-known transition from the initial low shear region of Newtonian viscosity to the region of rapidly decreasing viscosity at higher shear rates. At 450°F. this is particularly well shown by the 180,000 molecular weight polymer. It is

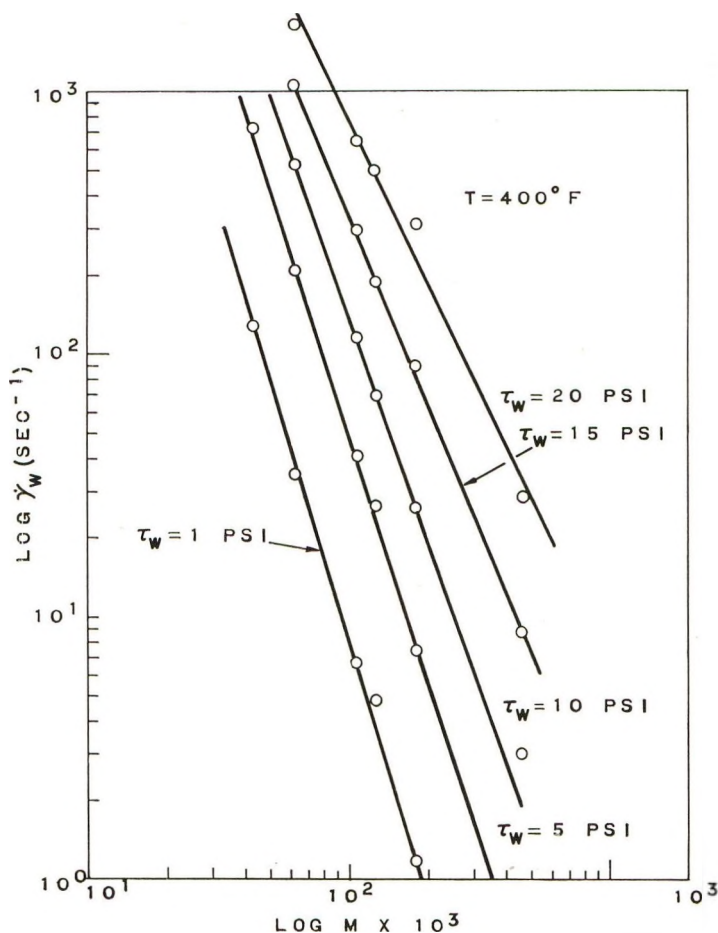


Fig. 3. Effect of shear stress on the molecular weight dependence of viscosity of narrow distribution polystyrene.

apparent that as the molecular weight increases, the transition from Newtonian to non-Newtonian flow occurs at ever lower rates of shear, similarly to the effect observed with a single material by lowering its temperature.

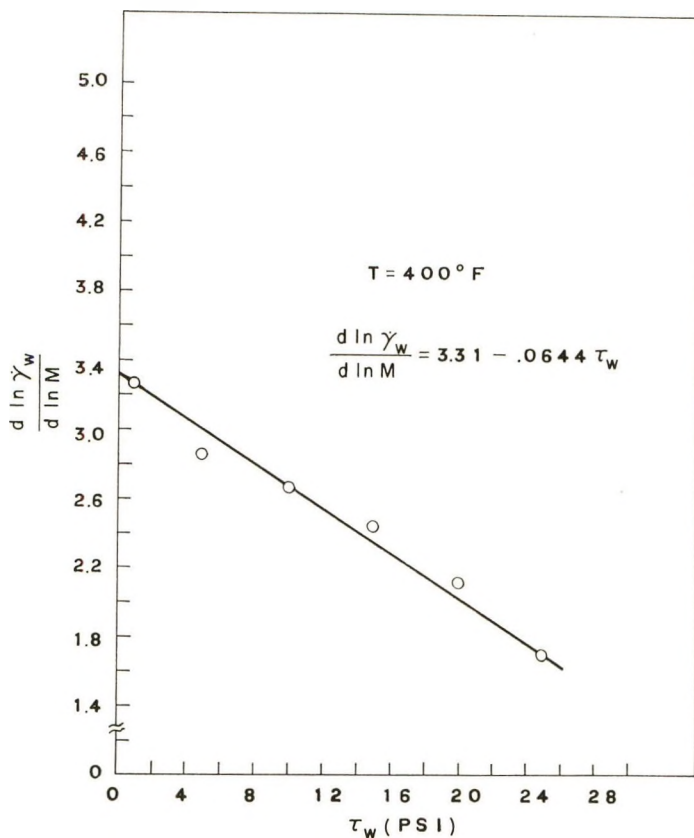


Fig. 4. Change in molecular weight dependence of viscosity with shear stress for narrow distribution polystyrene.

The convergence of the flow lines of Figure 1 with increasing shear is reflected in the diminishing of the exponent relating viscosity to molecular weight

$$\eta_a = KM^b$$

where  $\eta_a$  is the apparent viscosity ( $=\tau_w/\dot{\gamma}_w$ ). At zero shear, Fox and Flory<sup>15</sup> give a value of 3.4 for  $b$  for polystyrene fractions at 217°C., whereas Rudd<sup>2</sup> obtains 3.14 for his anionic polystyrenes at 227°C. Figure 2 shows that the value for  $b$  is about 3–3.4 for the entire temperature range 350 to 500°F. At higher shear stress an exponential relationship between viscosity and molecular weight still holds, as shown in Figure 3, but the value of  $b$  is no longer 3–3.4 and has decreased in proportion to the applied stress as shown in Figure 4. At a stress of 10.15 psi Rudd obtained a value of  $b = 2.54$  for monodisperse polystyrenes at  $\sim 400^{\circ}\text{F}$ . Figure 4 gives about 2.65 for  $b$  at 400°F.

The linear decrease of  $b$  with increasing stress indicates, if the linear change in  $b$  should continue, that apparent viscosity should be independent

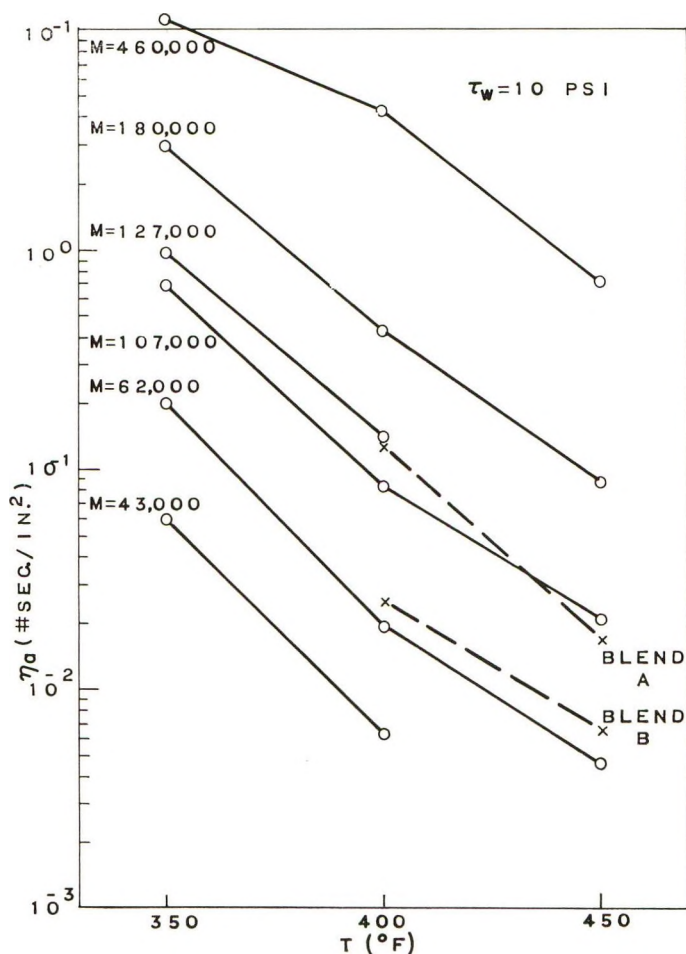


Fig. 5. Temperature dependence of apparent melt viscosity of narrow molecular weight distribution of polystyrene at constant shear stress.

of molecular weight when the shear stress reaches  $3.31/0.0644 = 51.4$  psi. Measurements in this region (not shown) do indeed indicate anomalous crossings-over of the flow curves of various molecular weight materials. However, the experimental difficulties in maintaining isothermal conditions, etc. in this region do not lend credence to these results. The predictions of Porter and Johnson indicate that the plot of  $b$  versus  $\tau_w$  probably levels out to a constant value of  $b$  at higher shear.

The flow curves of the two polystyrene blends shown in Figure 1 indicate that these materials follow the empirical "power law" expression

$$\tau_w = K\dot{\gamma}_w^n$$

much better than do the monodisperse materials. In exhibiting this constancy of slope, these flow curves necessarily cross the curves for the

monodisperse materials so that at different rates of shear the blends behave as if they have different molecular-weight averages. The calculated  $\bar{M}_w$  for blend A is 299,000 and for blend B is 199,000. Although the Newtonian region has not been reached for either material, at the lowest shear values measured in this work, their curves fall into position among the curves of the monodisperse materials roughly as  $\bar{M}_w$ . The calculated  $\bar{M}_n$  for

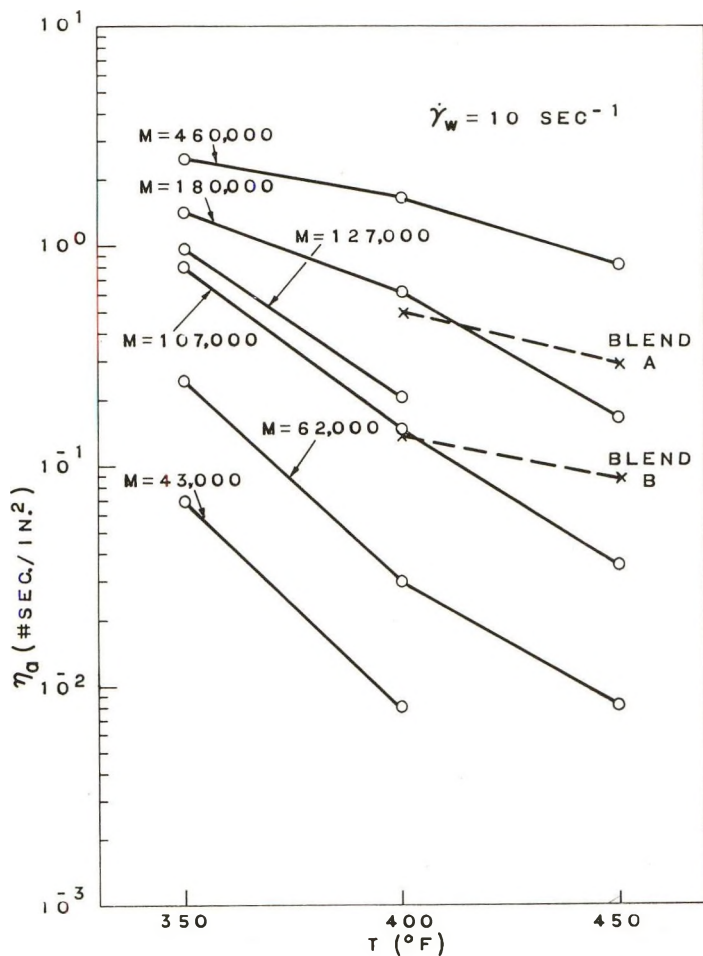


Fig. 6. Temperature dependence of apparent melt viscosity of narrow molecular-weight distribution of polystyrene at constant shear rate of 10 sec.<sup>-1</sup>.

blend A is 88,000 and for blend B is 66,000. It will be noted that the position of the flow lines for these materials in the high shear region of 1000-2000 sec.<sup>-1</sup> roughly fits these values. Therefore the conclusions may be drawn that the melt viscosity of polydisperse polystyrene depends on the weight-average molecular weight at low shear rates and on the number-average molecular weight at high rates of shear.

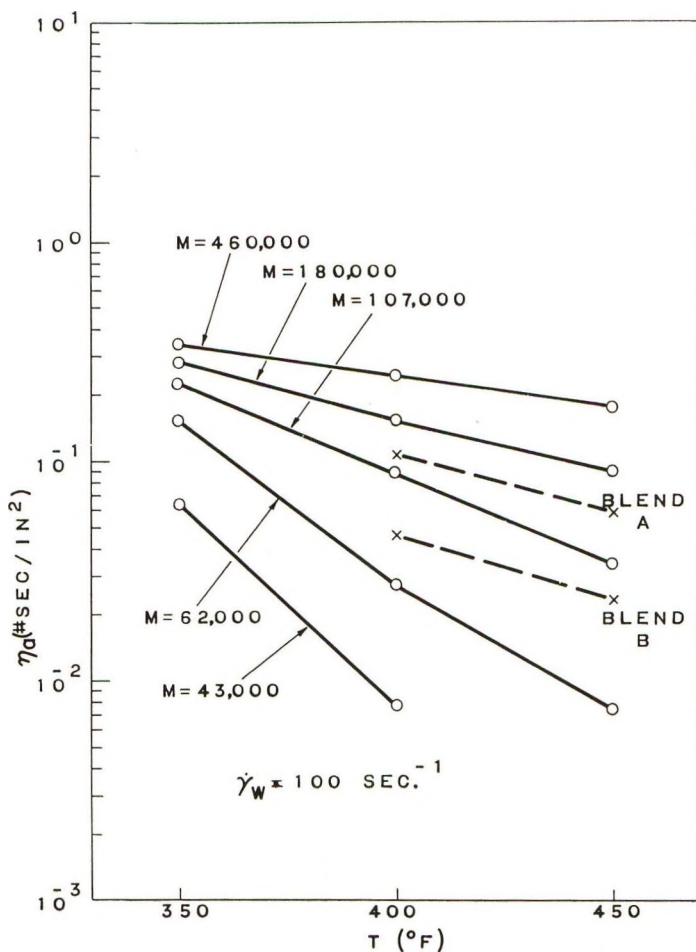


Fig. 7. Temperature dependence of apparent melt viscosity of narrow molecular-weight distribution polystyrene at constant shear rate of 100 sec.<sup>-1</sup>.

### Effect of Temperature

Traditionally the effect of temperature on viscosity is expressed by an Arrhenius equation

$$\eta_a = Ke^{\Delta E/RT}$$

where  $R$  is the gas constant,  $T$  is the absolute temperature, and  $\Delta E$ , the activation energy of viscous flow, is the same at zero shear whether calculated at constant shear rate or at constant stress. However Philippoff and Gaskins<sup>16</sup> have shown that widely different values are obtained for  $\Delta E_{\dot{\gamma}=k}$  and  $\Delta E_{\tau=k}$  for polymers in the non-Newtonian region. McKelvey<sup>17</sup> shows that the two  $\Delta E$ 's are related through the power law exponent  $n$ , so that  $\Delta E_{\dot{\gamma}} = n\Delta E_{\tau}$ .

Rudd<sup>2</sup> shows that  $\Delta E_\gamma$  has a value of ca. 23 kcal./mole and that this is invariant with molecular weight and molecular weight distribution. Our work confirms this, as shown in Figure 5.

For those processes which do not operate at constant shear stress, however, it is important to know the relationship between viscosity and molecular weight under other conditions of shear. For example, at a constant shear rate of 100 sec.<sup>-1</sup>, Figure 7 shows considerable dependence of  $\Delta E_\gamma$  on  $M$  with higher molecular weights having lower values of  $\Delta E_\gamma$ . The same is true at the lower shear rate of 10 sec.<sup>-1</sup>, as shown in Figure 6. In the latter figure, the curves for the blends show that they have a smaller  $\Delta E_\gamma$  than do the monodisperse polymers. Other data not shown here confirm this conclusion, i.e., that broad molecular-weight distribution polymers measured under these conditions give less temperature-sensitive melt viscosities than do narrow distribution materials, particularly at low rates of shear.

### Shear Rate-Temperature-Molecular Weight Superposition

The molecular theory of F. Bueche<sup>5</sup> relates viscosity and shear rate for polymer melts by

$$\frac{\eta}{\eta_c} = 1 - \frac{6}{\pi^2} \sum_{m=1}^N \frac{\dot{\gamma}^2 \lambda_1^2}{m^2(m^4 + \dot{\gamma}^2 \lambda_1^2)} \left( 2 - \frac{\dot{\gamma}^2 \lambda_1^2}{m^4 + \dot{\gamma}^2 \lambda_1^2} \right)$$

where  $\lambda_1$ , the characteristic relaxation time, is equal to  $12 \eta_0 M / \pi^2 \rho R T$ ,  $\rho$  being the density. As the only quantities affected by changing materials and temperature are  $\eta_0$  and  $\lambda_1$ , a plot of  $\eta/\eta_0$  versus  $\dot{\gamma} \lambda_1$  should therefore provide a master curve covering all polymers of all molecular weights and distributions and at all temperatures for which the assumptions made in Bueche's theory are valid. Such a "universal" curve was subsequently published by Bueche and Harding<sup>6</sup> based on data from concentrated solutions of polystyrene and polymethyl methacrylate. Figure 8 shows that the same procedure can be used to prepare a master curve for polystyrene melts. In this case, all the data for the monodisperse polymers shown in Figure 1 plus similar data at 350 and 450°F. were combined to give a single curve by plotting  $\eta/\eta_0$  versus  $\dot{\gamma} \eta_0 M / T$ . The superposition was excellent, with no systematic deviation for any materials at any of the three temperatures. Also impressive was the nearly nine decades of shear covered by the data superposition.

The generality of the master curve was found to be limited, however, by changes in molecular weight distribution as shown in Figure 9. Here are given master curves, based on  $\bar{M}_w$  (covering various temperatures), for two polystyrene blends and for another sample with a "normal" molecular-weight distribution. It is to be noted that the published Bueche-Harding curve fits this last curve of Figure 9 almost exactly. It is curious that the 70:30 blend (blend B) should show considerably greater deviation from the monodisperse master curve than does the 50:50 blend (blend A) even though its polydispersity ratio ( $\bar{M}_w/\bar{M}_n$ ) is somewhat less.

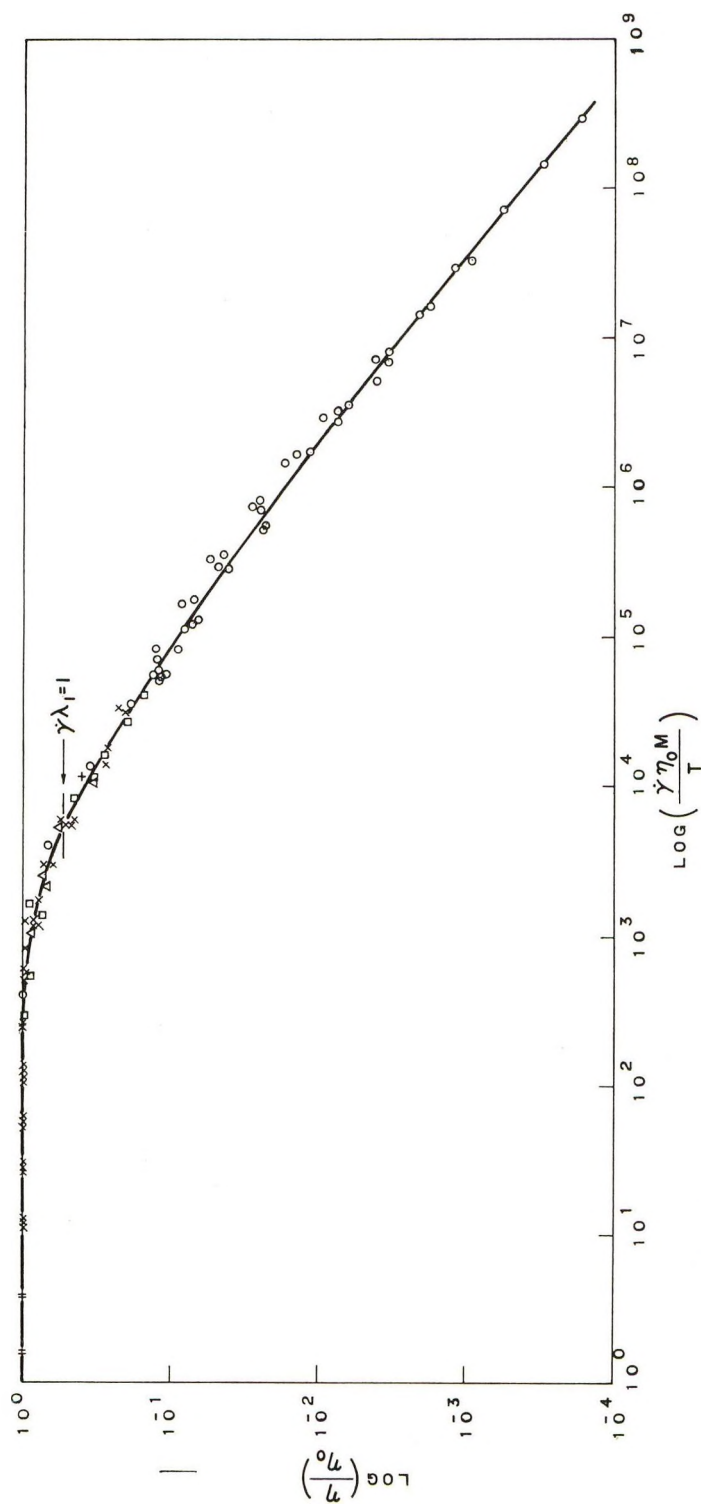


Fig. 8. Master curve of steady-state viscosity vs. reduced shear rate for monodisperse polystyrene.

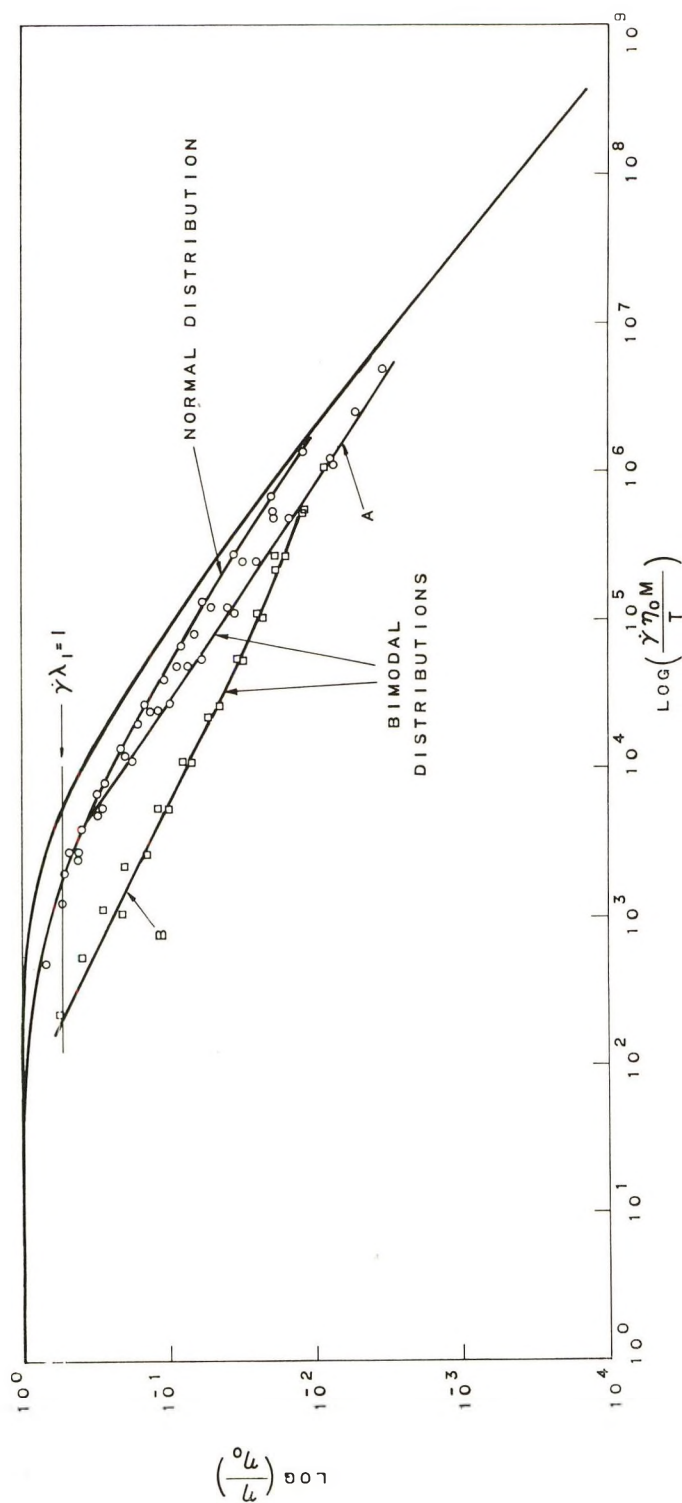


Fig. 9. Viscosity master curves showing the effect of polystyrene molecular-weight distribution.

Therefore it appears that the Bueche-Harding curve, while not general for various molecular weight distributions, is still a very useful technique for combining and generalizing data for a family of materials of similar molecular-weight distributions.

### Steady-State versus Dynamic Viscosity

Various workers have tried to relate steady-state and dynamic viscosities. DeWitt and his co-workers<sup>18-20</sup> have correlated apparent viscosity,  $\eta_a$ ,

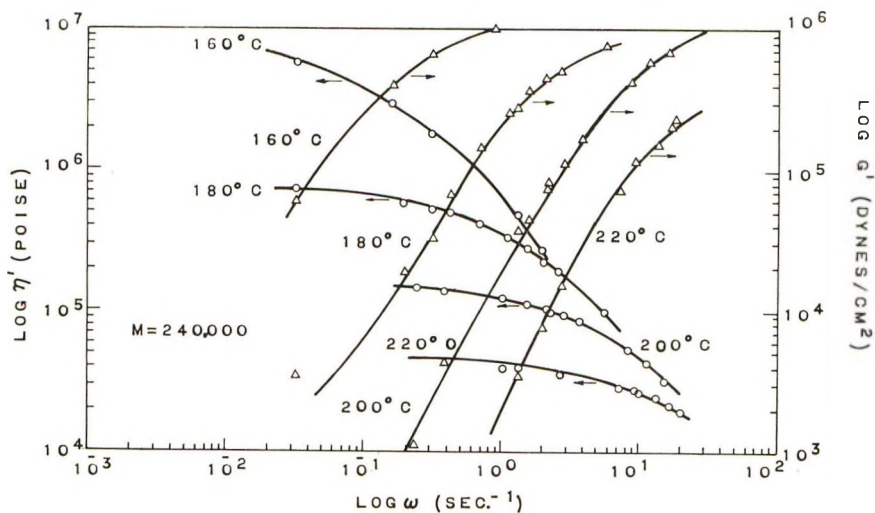


Fig. 10. Dynamic viscosity and modulus of monodisperse polystyrene.

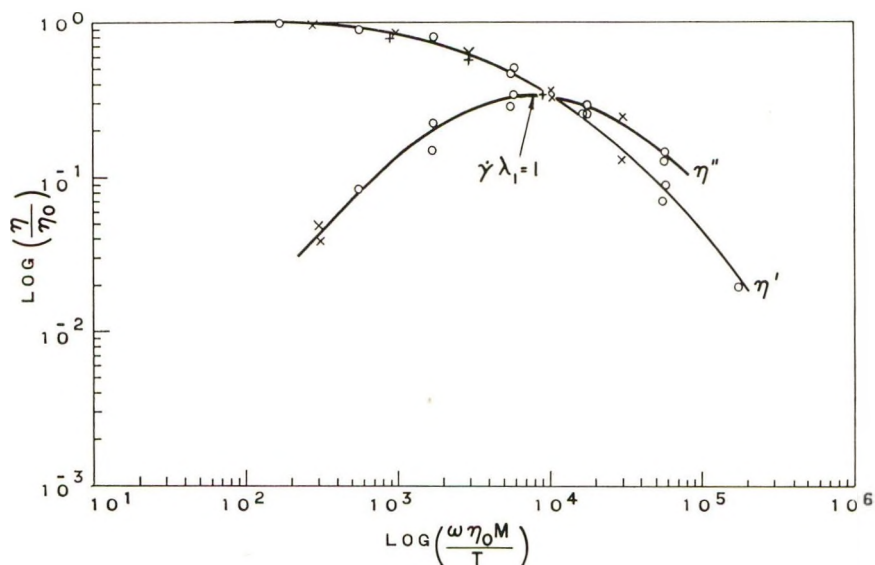


Fig. 11. Master curves of the components of the dynamic viscosity of monodisperse polystyrene.

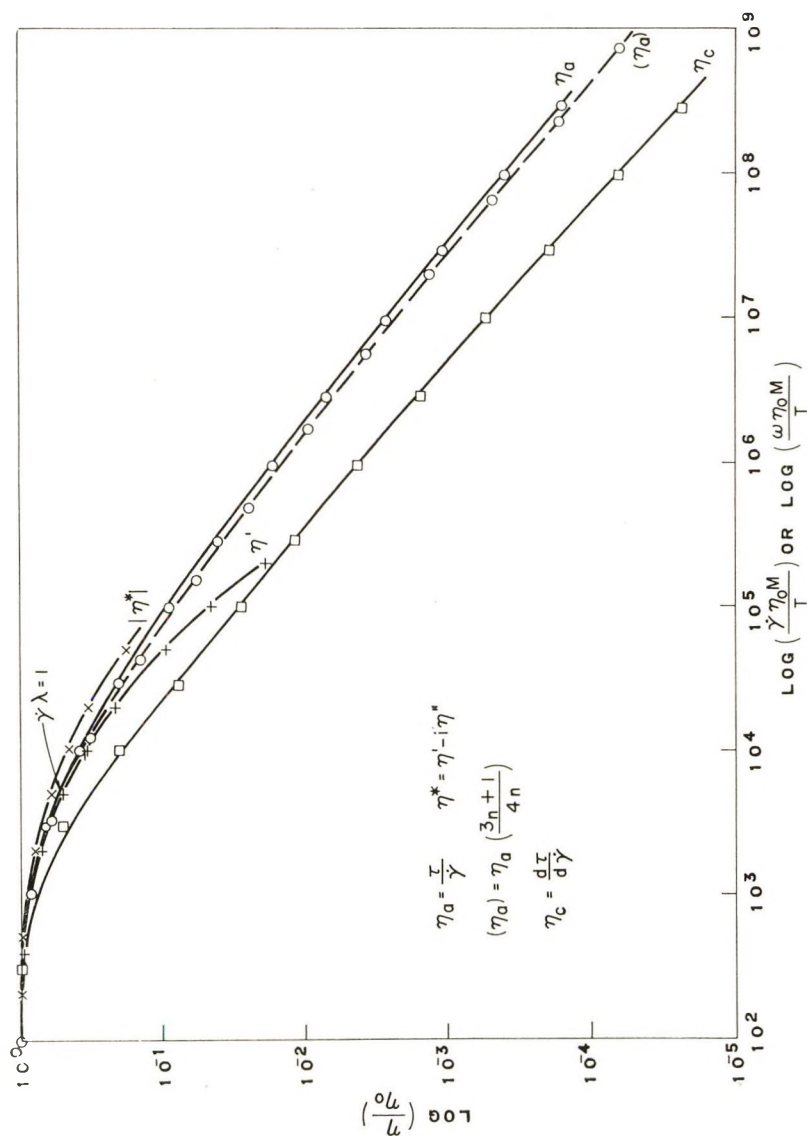


Fig. 12. Master curves comparing steady-state and dynamic viscosities of monodisperse polystyrene.

with the real part,  $\eta'$ , of the complex dynamic viscosity  $\eta^*$ . On the other hand, Merz and Cox,<sup>21,22</sup> and later Strella<sup>24</sup> have shown  $\eta_a$  to correspond to the absolute magnitude of the complex viscosity  $|\eta^*|$  and  $\eta'$  to correspond to the melt consistency,  $\eta_c = d\tau/d\dot{\gamma}$ .

The success of the construction of the master curve for polystyrene afforded a good opportunity to make a new comparison of steady-state and dynamic viscosities over a very broad range of shear.

Figure 10 shows dynamic viscosity and shear modulus data of Cox<sup>7</sup> as a function of frequency obtained on the elastoviscometer using fractionated polystyrene.<sup>23</sup> From these data the imaginary component  $\eta''$  was calculated and this along with  $\eta'$  plotted against  $\omega\eta_0 M/T$  (where  $\omega$  is frequency), giving the master curves shown in Figure 11. All the data fell without systematic deviation on the generalized curves.

The dynamic viscosity master curves of  $\eta'$  and  $|\eta^*|$  were then compared with the steady-state viscosity master curves of  $\eta_a$  and  $\eta_c$  as shown on Figure 12. The Rabinowitsch correction was applied to the  $\eta_a$  curve to give the parallel dotted line. The lack of correlation of dynamic and

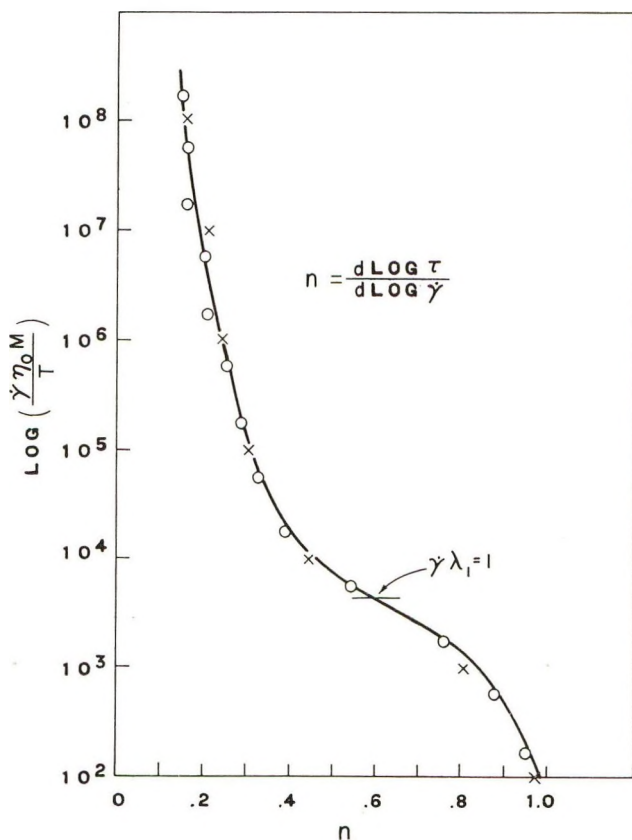


Fig. 13. Power law exponent vs. reduced shear rate for monodisperse polystyrene.

steady-state viscosities is evident, although there does seem to be good agreement between  $\eta'$  and the corrected  $\eta_a$  up to a reduced shear rate of  $10^4 \text{ sec.}^{-1}$ .

### Effect of Terminal Relaxation Time

According to Bueche's theory, when the molecular relaxation time  $\tau$  is comparable to the time required for one molecular revolution ( $1/\dot{\gamma}$ ), then the elastic response of the molecule to the shear field is maximized. If  $\dot{\gamma}\lambda_1 = 1$ , then  $\eta/\eta_0$  of Bueche's equation becomes 0.53. This point is marked on the monodisperse master curve in Figure 12. It occurs at a reduced shear rate of 5300 on this curve and at 7600 on the  $|\eta^*|$  curve. On Figure 11 it is apparent that the  $\eta''$  master curve goes through its maximum at 7600 and on Figure 13 it is also noted that the power law exponent for steady-state viscosity goes through an inflection point at 5300. This is a striking confirmation of the Bueche equation and points out an interesting relationship between the elastic contribution to the complex dynamic viscosity and the exponential index of non-Newtonian flow.

### CONCLUSIONS

Examination of a number of polystyrene melts of various molecular weights and distributions have shown that low shear viscosity is a function of  $\bar{M}_w$  and high shear viscosity of  $\bar{M}_n$ . The exponential dependence of zero shear viscosity on molecular weight is not appreciably changed by changing temperature in the range of 350–500°F. nor is the general form of the relationship changed with increasing shear stress although the value of the exponent decreases linearly with increasing stress.

The effect of temperature on melt viscosity measured at constant shear stress is independent of the molecular weight and distribution. This is not true at constant shear rate, where the activation energy decreases with increasing molecular weight and increasing breadth of distribution.

The Bueche-Harding procedure provides a means of expressing the flow behavior of different molecular weights at various temperatures by means of a single plot of  $\eta/\eta_0$  versus  $\dot{\gamma}\eta_0\bar{M}/T$ . The general curve is limited to specific molecular weight distributions, however.

The correlation of steady-state and dynamic viscosities was not successful except for the correspondence of  $\eta_a$  and  $\eta'$  up to  $10^4$  units of reduced shear. However the point at which  $\omega = \dot{\gamma} = 1/\lambda_1$  in the master curves did correspond with the maximum of  $\eta''$  versus  $\omega$ , and the inflection point of  $n$  versus  $\dot{\gamma}\eta_0\bar{M}/T$ , thereby giving a good check of the Bueche equation and a key to the correlation of steady-state and dynamic viscosities.

Helpful discussions with Dr. T. Boyd on polymerization technique are acknowledged with pleasure.

The authors wish to thank Messrs. G. W. Ingle and L. A. Cohen for their helpful suggestions in the preparation of the manuscript.

## References

1. McCormick, H. W., F. M. Brower, and L. Kin, *J. Polymer Sci.*, **39**, 87 (1959).
2. Rudd, J. F., *J. Polymer Sci.*, **44**, 459 (1960).
3. Rudd, J. F., *J. Polymer Sci.*, **60**, 57 (1962).
4. Cox, W. P., and R. L. Ballman, *J. Appl. Polymer Sci.*, **4**, 121 (1960).
5. Bueche, F., *J. Chem. Phys.*, **22**, 1570 (1954).
6. Bueche, F., and S. W. Harding, *J. Polymer Sci.*, **32**, 177 (1958).
7. Cox, W. P., unpublished data.
8. Merz, E. H., and R. E. Colwell, *ASTM Bull. No.* **232**, 63 (1958).
9. Ballman, R. L., and J. J. Brown, Instron Application Series SA-2 (1961).
10. Cox, W. P., L. E. Nielsen, and R. Keeney, *J. Polymer Sci.*, **26**, 365 (1957).
11. Rabinowitsch, B., *Z. Physik. Chem.*, **A145**, 1 (1929).
12. Bagley, E. B., *J. Appl. Phys.*, **28**, 624 (1957).
13. Bagley, E. B., and D. C. West, *J. Appl. Phys.*, **29**, 1511 (1958).
14. Porter, R. S., and J. F. Johnson, *J. Appl. Phys.*, **32**, 2326 (1961).
15. Fox, T. G, Jr., and P. J. Flory, *J. Polymer Sci.*, **14**, 315 (1954).
16. Philippoff, W., and F. H. Gaskins, *J. Polymer Sci.*, **21**, 205 (1956).
17. McKelvey, J. M., *Polymer Processing*, Wiley, New York, 1962.
18. Padden, F. J., and T. W. DeWitt, *J. Appl. Phys.*, **25**, 1086 (1954).
19. DeWitt, T. W., *J. Appl. Phys.*, **26**, 889 (1955).
20. DeWitt, T. W., H. Markovitz, F. J. Padden, and L. J. Zapas, *J. Colloid Sci.*, **10**, 174 (1955).
21. Cox, W. P., and E. H. Merz, *ASTM Special Technical Publication No. 247*, Am. Soc. Testing Materials, Philadelphia, 1958.
22. Cox, W. P., and E. H. Merz, *J. Polymer Sci.*, **28**, 619 (1958).
23. Merz, E. H., and R. W. Raetz, *J. Polymer Sci.*, **5**, 587 (1950).
24. Strella, S., *J. Polymer Sci.*, **60**, 59 (1962).

## Résumé

La viscosité de plusieurs espèces de polystyrène monodispersé à l'état fondu a été mesurée au moyen d'un rhéomètre à capillaire. Les échantillons couvraient une gamme de poids moléculaire s'étendant de 43000 à 460000. On a étudié des vitesses de cisaillement comprises entre 1.54 et 1540  $\text{sec}^{-1}$  et des températures de 350 à 450°F. On a également mesuré l'effet de la distribution des poids moléculaires du polystyrène polydispersé. On a montré qu'alors que la viscosité à faible cisaillement dépendait de  $\bar{M}_w$ , les viscosités à plus haut cisaillement à l'état fondu, dépendaient des moyennes entre  $\bar{M}_w$  et  $\bar{M}_n$  et ce jusqu'à 1000–2000  $\text{sec}^{-1}$  où  $\bar{M}_n$  déterminait la viscosité. L'accord entre la dépendance de la viscosité à cisaillement nul à la puissance 3.4 était bon. On a trouvé des relations exponentielles similaires pour des vitesses plus élevées de cisaillement correspondant à des valeurs plus petites de l'exposant. Des valeurs constantes de l'exposant ont été obtenues à tension de cisaillement constante mais non à vitesse de cisaillement constante. L'accord entre la constance de l'énergie d'activation du flux visqueux pour différents poids moléculaires et des distributions à tension de cisaillement constantes était bon. Cependant à des vitesses de cisaillement constantes,  $\Delta E$  diminuait lorsque le poids moléculaire croissait ou la distribution s'étalait. Les courbes principales viscosité/vitesse de cisaillement ont été construites grâce au procédé de Bueche-Harding. Tous les polystyrènes monodispersés étaient en accord avec ces courbes principales; d'autres distributions de poids moléculaires ne l'étaient pas. Les courbes-maitresses ont également été construites pour la mesure des viscosités dynamiques en fonction de la fréquence de monodispersion du polystyrène. Ces courbes lorsque comparées aux viscosités à l'état stationnaire, ne confirmaient pas la correspondance de  $\eta_a$  soit avec  $|\eta^*|$  ou avec  $\eta'$ .

### Zusammenfassung

Die Viskosität einer Reihe von monodispersen Polystyrolschmelzen wurde mit einem Kapillarrheometer gemessen. Die Molekulargewichte der untersuchten Stoffe lagen im Bereich von 43000 bis 460000. Untersucht wurden Schergeschwindigkeiten von 1,54 bis 1540  $\text{sek}^{-1}$  und Temperaturen von 350 bis 450°F. Auch der Einfluss der Molekulargewichtsverteilung von polydispersem Polystyrol wurde untersucht. Während sich die Viskosität bei niedrigem Schub als Funktion von  $\bar{M}_w$  erwies, hing sie bei höherem Schub von Mittelwerten zwischen  $\bar{M}_w$  und  $\bar{M}_n$  ab, bis schliesslich bei 1000–2000  $\text{sek}^{-1}$   $\bar{M}_n$  die bestimmende Grösse wurde. Es bestand gute Übereinstimmung mit einer 3,4-Potenzabhängigkeit der Viskosität beim Schub Null. Ähnliche Exponentialbeziehungen wurden bei höheren Schubgeschwindigkeiten mit kleineren Werten des Exponenten gefunden. Bei konstanter Schubspannung, nicht aber bei konstanter Schubgeschwindigkeit, ergaben sich konstante Werte für den Exponenten. Mit der Annahme einer konstanten Aktivierungsenergie für das viskose Fliessen bei verschiedenem Molekulargewicht und verschiedener Verteilung bestand bei konstanter Schubspannung gute Übereinstimmung. Bei konstanter Schubgeschwindigkeit nahm jedoch  $\Delta E$  mit steigendem Molekulargewichtsmittel und mit breiter werdender Verteilung ab. Nach dem Verfahren von Bueche und Harding wurden die Hauptkurven für die Viskosität-Schubgeschwindigkeitsabhängigkeit konstruiert. Alle monodispersen Polystyrole zeigten ausgezeichnete Übereinstimmung mit der Hauptkurve, andere Molekulargewichtsverteilungen aber nicht. Hauptkurven wurden auch für die Messung der dynamischen Viskosität in Abhängigkeit von der Frequenz an monodispersen Polystyrol konstruiert. Diese Kurven liessen beim Vergleich mit der Viskosität im stationären Zustand weder eine Übereinstimmung von  $\eta_a$  mit  $|\eta^*|$  noch mit  $\eta'$  erkennen.

Received July 23, 1963

## Stress Relaxation in Fibers: Effect of Water and Temperature

CYNTHIA KOLB WHITNEY\* and R. L. HAMILTON,† *Celanese Corporation of America, Summit, New Jersey*

### Synopsis

The effect of water on stress relaxation was studied for several fibers as a function of water temperature and other parameters. A quantitative measure of the effect was developed. A statistical model was developed, and it was found that the observed behavior could be interpreted in terms of a redistribution of forces among the various bonds within the fiber. The measure of the water effect, as defined here, could be used to study the connection between stress relaxation and other fiber properties.

### Introduction

Stress relaxation is usually used to connect measured mechanical properties of fibers with various "spring and dashpot" models of mechanical behavior. Several studies have shown, however, that relaxation measurements provide a relatively simple and sensitive means of studying the interaction of various chemical agents with the polymer. It appears that the utility of stress relaxation measurements lies in understanding the interaction of a polymer with its environment rather than in investigating purely mechanical behavior. Lemiszka<sup>1</sup> gives examples of such studies on environmental effects.

This work was part of a program to examine the connection between mechanical and diffusional properties of polymers. Most of these properties are affected by water, for example, and consequently, it was of interest to investigate this effect. At least part of the action of water is in solvating some of the intermolecular bonds in a fiber. These bonds are usually assumed to be involved in stress relaxation. The effect of water, therefore, on these bonds would be expected to be reflected in the effect of water on stress relaxation. This effect is examined in detail here. A quantitative measure of the effect is developed, and the effect is examined theoretically.

### Experimental Apparatus and Procedure

The stress relaxometer was similar to that used by Lemiszka,<sup>1</sup> except that a Satham wire strain gage was used to measure force, and strain rates of  $6.6 \times 10^3$  %/min. could be obtained. A temperature-controlled container

\* Present address: Department of Physics, Massachusetts Institute of Technology, Cambridge, Massachusetts.

† Present address: Bell Telephone Laboratories, Inc., Murray Hill, New Jersey.

was arranged so the fiber could be submerged in water at any time during the test. Submersion of the fiber could be completed within 0.5 sec.

Experiments were made with secondary cellulose acetate, Arnel triacetate, experimental nitril, experimental polyester, and Dacron 55 fibers at temperatures from 23 to 95°C. in air and in water. The fibers were strained 2% in air and relaxed for a time,  $\theta_a$ , and then water at specified temperatures was added around the fiber. The force  $F$  (used as a measure of stress) was recorded continuously on a Sanborn recorder.

### Experimental Results

Typical relaxation curves in air are shown in Figure 1. The equation of these lines is

$$F = F_1\theta^{-A} \quad (1)$$

which is a simplified form of the Nutting equation<sup>2</sup> for constant strain, where  $F_1$  is force at unit time and  $A$  is a dimensionless empirical constant. The slope,  $A$ , of the lines in Figure 1 was extremely reproducible. This behavior has been observed previously<sup>2,3</sup> and is not unexpected at the low strains used here.

After the fiber had relaxed in 23°C. air for a time  $\theta_a$ , water at a specified temperature was added. The resulting plot of  $\ln$  force, versus  $\ln$  time (with time measured from  $\theta_a$ ) showed two straight portions (Fig. 2). The first was steeper and lasted up to several seconds. The second portion was similar in slope to the curve in air at the temperature of the experiment.

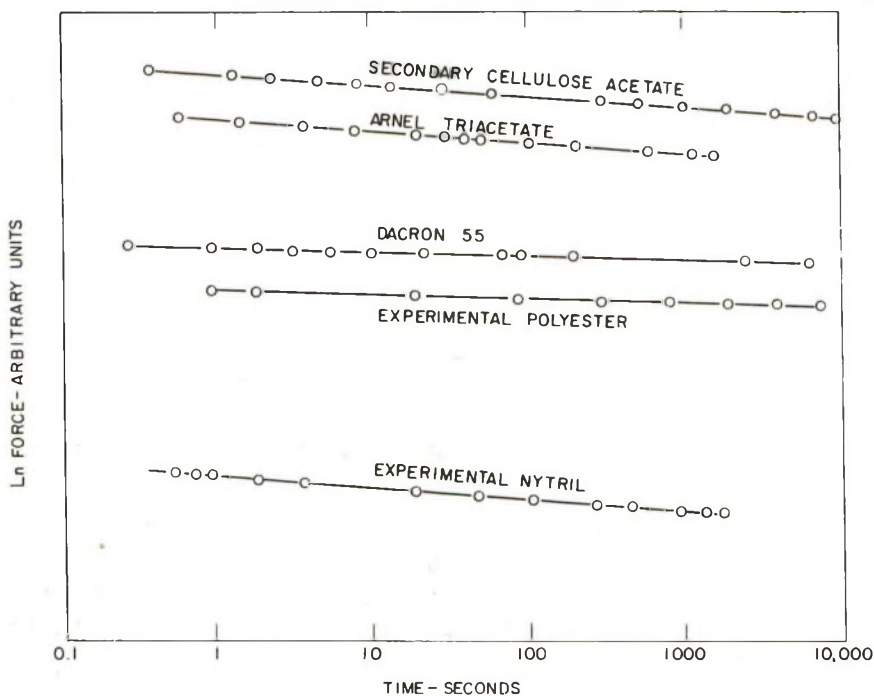


Fig. 1. Typical stress relaxations in air at 23°C.

It was first surmised that the first portion, called the "water effect," was merely the reflection of the advancing water front as the water diffused into the fiber. If such were so, two fibers of the same morphological structure but different diameters would show a different behavior in this first portion. This hypothesis was tested with two such Arnel fibers and discarded. Calculation of the rate of water uptake also showed that essentially equilibrium sorption is reached in much less time than the time (up to 10 sec.) for completion of the water effect. The literature on stress relaxation gave no information on such an effect; although stress relaxation in water has been studied, no one seems to have commented on the two separate portions of the curve. Note that the lower curve in Figure 2 is plotted with time measured from  $\theta_a$ . If the water portion of the relaxation curve is plotted simply as a continuation of the air portion, the water effect is obscured because at large times on a logarithmic scale the relatively short duration of the water effect appears as a nearly vertical line. Previous workers presented their curves in this manner and therefore could not readily discern these features of the water portion of the curve.

An extensive investigation of the first portion was made to determine the factors which influenced it. It was found that the magnitude of the water effect was best described in terms of the function  $(F_a - F_w)/F_a$ , as shown in Figures 3 and 4. ( $F_a$  is the force in air at the time  $\theta_a$  at which water is added, and  $F_w$  is the force at the end of the water effect. In Figure 2, the break in the lower curve corresponds to  $F_w$ .) This function was greatest for hydrophilic fibers such as cellulose acetate and much less for hydrophobic fibers; the polyester fibers, for example, showed no water effect except at water temperatures above 80°C. This agrees with the small effect of water on other properties of polyester fibers.

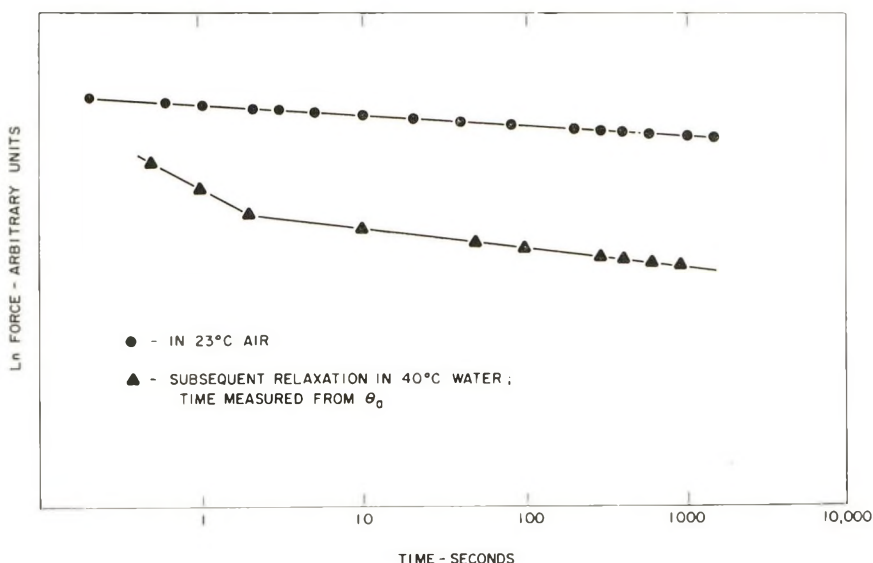


Fig. 2. Effect of hot water on strained secondary cellulose acetate: (●) in air at 23°C.; (▲) subsequent relaxation in water at 40°C., time measured from  $\theta_a$ .

The observed dependence of the water effect on water temperature,  $T_w$ , is:

$$\ln [(F_a - F_w)/F_a] = K_1 - (K_2/T_w) \quad (2)$$

where  $K_1, K_2$  are constants. This is the equation of the lines in Figure 3. The water effect also depended slightly on the relaxation time in air (Fig. 4); the effect was decreased by letting the fiber relax in air for longer times. Empirically,

$$\ln [(F_a - F_w)/F_a] = K_3 - K_4 \ln \theta_a \quad (3)$$

where  $K_3, K_4$  are constants. This relation was followed also by Arnel and nitril fibers. The last two equations summarize the significant empirical features of the water effect as measured by  $(F_a - F_w)/F_a$ .

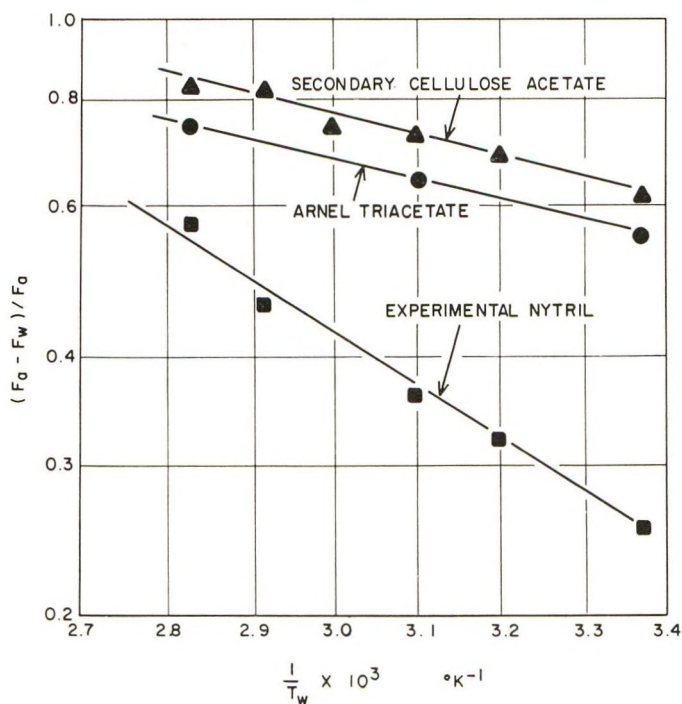


Fig. 3. Magnitude of water effect as a function of water temperature.

### Development of Model

A statistical model was developed to describe and investigate the features of this water effect. This model is described as follows: a cross-sectional plane of the fiber contains a total number  $N$  of force-supporting bonds. The total force is distributed among the bonds such that, in air,  $n_{ia}$  bonds have force from  $f_i$  to  $f_i + \Delta f$  each, where  $f_i$  is the force supported by a single bond. Just before the water is added, the total force is

$$F_a = \sum f_i n_{ia} \quad (4a)$$

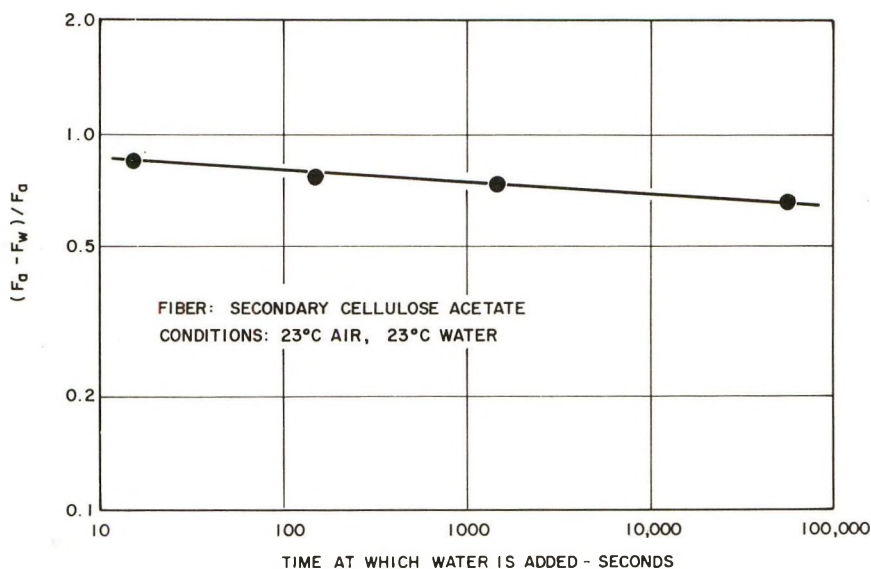


Fig. 4. Dependence of water effect on relaxation time  $\theta_a$  in air.

Also,

$$N = \sum_i n_{ia} \quad (4b)$$

If these equations are to be used, the  $f_i$  must be determined as a function of the  $n_{ia}$ . There is no experimental way to determine this functional relationship, but a rational method of making the least biased and best estimate has been shown to be similar to the method of statistical mechanics.<sup>4,5</sup> An "uncertainty"  $U$  is defined in terms of the  $n_{ia}$ :

$$U = - \sum_i [(n_{ia}/N) \ln (n_{ia}/N)] \quad (5)$$

The ratio  $n_{ia}/N$  can be considered a probability, and eq. (5) is analogous to the definition of entropy used in statistical mechanics. Jaynes<sup>4</sup> and Tribus<sup>5</sup> develop this equation and discuss its connection with statistics. To maximize  $U$  its total derivative with respect to all the  $n_{ia}$  is set equal to zero. Subsidiary conditions are:  $N$  is constant and  $F_a$  is constant. By the method of Lagrange multipliers:

$$\sum_i [\ln (n_{ia}/N) + 1 + \beta + \mu f_i] dn_{ia}/N = 0 \quad (6)$$

where  $\beta$  and  $\mu$  are constants. For this equation to be identically true,

$$n_{ia} = N \exp\{-1 - \beta - \mu f_i\} \quad (7)$$

This gives the number of bonds,  $n_{ia}$ , with force between  $f_i$  and  $f_i + \Delta f$ . By proportion, the differential number of bonds,  $dn_a$ , in a differential force element,  $df$ , is

$$dn_a = (N \exp\{-1 - \beta\} \exp\{-\mu f\})/\Delta f \quad (8)$$

Because  $N$ ,  $\exp\{-1 - \beta\}$ , and  $\Delta f$  are all constants,

$$dn_a = B \exp\{-\mu f\} df \quad (9)$$

where  $B$  is a constant. The conditions

$$N = \sum_i n_{ia} = \int_{f=0}^{\infty} dn_a \quad (10)$$

and

$$F_a = \sum_i f_i n_{ia} = \int_{f=0}^{\infty} f dn_a \quad (11)$$

determine the constants  $B$  and  $\mu$ :

$$B = N^2/F_a \quad (12)$$

$$\mu = N/F_a$$

Combining eqs. (9) and (12) gives:

$$dn_a = (N^2/F_a) \exp\{-Nf/F_a\} df \quad (13)$$

This is the distribution function sought. The effect of water will be described as a rearrangement of this distribution.

The fiber is now plunged in water. There will be some probability,  $p_i$ , that a given bond in the  $i$ th force cell will be attacked by the water. The problem is in constructing  $p_i$  as a function of the variables in eq. (13) and the experimental parameters. This can be done by using the experimental results as a guide. For example, the water effect was larger for fibers with greater water uptake. In terms of this model, this means that  $p_i$  will be greater for greater water uptake. The same argument applies to water temperature. It was also found that the water effect was larger for larger  $F_a$ . Because  $F_a$  is a reflection of the  $f_i$ ,  $p_i$  will be larger for larger  $f_i$ . In this way the following function was derived for the  $p_i$ :

$$p_i = \exp\{-1/\alpha f_i T_w\} \quad (14)$$

The quantity,  $\alpha$ , contains the water uptake and a proportionality constant. Equation (14) gives the fractional number of bonds in cell  $i$  which are affected by water.

After water is added, a certain redistribution of force among the bonds will occur, and a new total force,  $F_w$ , will result. The number of bonds,  $n_{iw}$ , left intact in the  $i$ th cell is:

$$n_{iw} = (1 - \exp\{-1/\alpha f_i T_w\}) n_{ia} \quad (15)$$

The force in water is

$$F_w = \sum_i f_i n_{iw} = \int_{f=0}^{\infty} f dn_w \quad (16)$$

Substituting eq. (13) and (15) into the right-hand side of eq. (16) gives:

$$F_w = \int_{f=0}^{\infty} (fN^2/F_a) \exp\{-Nf/F_a\} (1 - \exp\{-1/\alpha f T_w\}) df \quad (17)$$

An approximate value of the integral can be found if  $\exp\{-1/\alpha f T_w\}$  is expanded as a series and the integration carried out term by term. This will give:

$$F_w \cong F_a(1 - \exp\{-N/\alpha F_a T_w\}) \quad (18)$$

Introducing a correction factor  $X$ , eq. (18) can be written as an equality,

$$F_w = F_a (1 - X \exp\{-N/\alpha F_a T_w\}) \quad (19)$$

$X$  will involve to a small extent  $\alpha$ ,  $F_a$ , and  $T_w$ . For calculation purposes, it will be treated as an empirical constant characteristic of the experiment.

### Comparison with Data

Equation (19) is the relation between  $F_w$  (force at the end of the water effect) and  $F_a$  (the force in air just before water is added). It can be used to compare the predictions based on the model with the data shown in Figures 3 and 4. Equation (19) can be rearranged to give

$$\ln [(F_a - F_w)/F_a] = \ln (X \exp\{-N/\alpha F_a T_w\}) \quad (20)$$

The right-hand side of eq. (20) is a linear function of  $1/T_w$ , so that it clearly agrees with Figure 3. The predictions of the model can be compared with the data in Figure 4 by substituting eq. (1) into the right-hand side of eq. (20):

$$\ln [(F_a - F_w)/F_a] = \ln (X \exp\{-N\theta^4/\alpha F_a T_w\}) \quad (21)$$

From the temperature data in Figure 3 the empirical parameter  $X$  can be calculated. For secondary cellulose acetate it is approximately 2. This value can be used to plot a theoretical curve of  $\ln [(F_a - F_w)/F_a]$  as a function of  $\ln \theta_a$ . The function on the right-hand side of eq. (21) is found to be essentially linear in  $\ln \theta$  over the range of the data, which agrees with Figure 4.

### Discussion

To summarize briefly, the model proposed here consists of a distribution of force-supporting elements. This distribution was found by the principal of maximum uncertainty. The effect of water on this distribution was examined by constructing a function representing the probability that a certain bond is broken by water. A new distribution was then calculated and from this the force at the end of the water effect was found in terms of the experimental parameters. The model was found to agree substantially with the empirical observations.

To get this agreement it was necessary to assume that bonds affected by water are completely relaxed and therefore support no force. Lemiszka<sup>1</sup> used such an idea to measure the "accessibility" of fibers by means of stress relaxation. It is suggested that the water effect as defined here would afford a more consistent measure of this accessibility. The accessibility measured in this way would give information on the fraction of bonds that are completely broken by water.

The magnitude of the water effect is related to mass diffusional properties in water. For example, the dye diffusion coefficients of the fibers studied increase in the order: polyester, nitril, cellulose acetate. This is also the order in which the water effect increases, which indicates a correspondence between the bonds which support force and those which retard diffusion.

### References

1. Lemiszka, T., Doctorate dissertation, Princeton University, Princeton, N. J., 1954.
2. Meredith, R., *The Mechanical Properties of Textile Fibres*, Interscience, New York, 1956, p. 42.
3. Tobolsky, A. V., *Properties and Structure of Polymers*, Wiley, New York, 1960, p. 186.
4. Jaynes, E. T., *Probability Theory in Science and Engineering*, Colloquium Lectures in Pure and Applied Science, No. 4; Field Research Laboratory, Socony Mobil Oil Company, Incorporated; Dallas, Texas, 1959.
5. Tribus, M., *Thermostatics and Thermodynamics*, Van Nostrand, New York, 1961, pp. 29-88.

### Résumé

L'effet de l'eau sur la tension de relaxation a été étudié dans le cas de diverses fibres en fonction de la température de l'eau et d'autres paramètres. On a développé un mode de mesure quantitative de cet effet. Un modèle statistique ayant été mis au point, il s'est avéré que le comportement observé pouvait s'interpréter sur la base d'une redistribution de forces entre les différents liens existant dans la fibre. La mesure de l'effet de l'eau, comme définie ici, peut être utilisée pour l'étude des rapports existant entre la relaxation et les autres propriétés des fibres.

### Zusammenfassung

Der Einfluss von Wasser auf die Spannungsrelaxation wurde an einigen Fasern in Abhängigkeit von der Temperatur des Wassers und anderen Parametern untersucht. Ein quantitatives Mass für den Effekt wurde gewonnen. Ein statistisches Modell wurde entwickelt und das beobachtete Verhalten als eine Neuverteilung von Kräften unter den verschiedenen Bindungen in der Faser gedeutet. Das hier definierte Mass für den Wassereffekt konnte zu einer Untersuchung des Zusammenhanges zwischen Spannungsrelaxation und anderen Fasereigenschaften benutzt werden.

Received July 24, 1963

## Viscosity of Amorphous Polymers

A. T. DIBENEDETTO, *Department of Chemical Engineering, University of Wisconsin, Madison, Wisconsin*

### Synopsis

An amorphous polymer is characterized as a homogeneous array of  $N$  identical,  $n$ -center polymer segments which can be described in terms of four molecular constants. A mechanism for viscous flow (or self diffusion) is visualized as a positional exchange of two adjacent polymer segments in a hole the size of a segment-pair. The activation energy for the viscous flow is the energy required to overcome the cohesive bonding to neighboring segments plus the work of compression required to form a hole of molecular dimensions. The effect of chain entanglement is estimated by using the theories of Bueche. An equation is derived for the viscosity in terms of a characteristic temperature,  $T_0$ , a free volume expansion coefficient,  $\beta'$ , a fractional free volume for the glassy state  $f_{g0}$ , an average segmental length,  $2\lambda n$ , and the four measurable molecular constants. This equation describes the lower limiting viscosity of polyisobutylene, polystyrene, and poly(vinyl acetate) over a viscosity range of up to a factor of  $10^8$  and for the whole temperature range of available data. It is shown that the characteristic temperature,  $T_0$ , is close to the measured glass transition temperature, the free volume expansion coefficient,  $\beta'$ , is about 0.4 of the thermal expansion coefficient of the rubber and the fractional free volume,  $f_{g0}$ , is 0.1 for all the polymers. The size of the jumping unit in viscous flow is calculated to be about 0.1-0.3 of the size of an equivalent freely orienting segment.

### Introduction

In prior work<sup>1-3</sup> an amorphous polymer was characterized as a homogeneous one-component phase containing  $N$  identical  $n$ -center polymer segments. The behavior of this model was then defined in terms of four molecular parameters;  $\epsilon^*$  was a force constant which was a measure of the strength of interaction between two polymer segments,  $\rho^*$  was a range parameter which was a measure of the average separation between segments,  $c_m$  was a parameter which was related to the average number of external degrees of freedom for a segment, and  $n$  was a parameter which was a measure of the length of an average segment in the model.

These quantities were evaluated, for eight amorphous polymers,<sup>1</sup> by curve fitting of thermal expansion and compressibility data. Their absolute values may not have any special significance, since they are strongly dependent on the model that is used to represent the polymer structure. Rather, it is felt that their major value is for predicting hard-to-measure properties from experimental data on easy-to-measure properties, and also, simply for correlating data. Thus, an oversimplified, perhaps not too realistic model, with four molecular constants, replaces a complex polymeric structure. Three of the constants are fixed by the thermodynamic behav-

ior of the polymer while the fourth remains as an adjustable parameter. One may then utilize this model to predict and/or correlate data for other physical properties. Cohesion energy densities,<sup>1</sup> glass transition temperatures,<sup>1</sup> and gaseous diffusion through films<sup>2,3</sup> have been interpreted in this manner. The concept of "segmental motion" arises naturally from this approach and the value of the parameter  $n$  is a measure of an "ideal" segment length involved in a given phenomenon.

This paper extends these concepts in order to evaluate the effect of temperature on the viscosity of amorphous polymers in the limit of zero shear rate. Along with the idea of replacing the real polymeric structure with an "ideal" model, the development utilizes Eyring's idea of the activated state for segmental flow,<sup>4</sup> Bueche's ideas on the effects of chain entanglement,<sup>5</sup> and the effect of free volume on the viscosity as embodied in Bueche's work<sup>6</sup> and the WLF equation.<sup>7</sup> Equations are presented for three amorphous polymers which accurately predict their viscosities over the whole temperature range of available data and over a viscosity range of up to a factor of  $10^8$ .

### Theory

There is strong evidence that the viscous flow and self-diffusion of amorphous polymers are functions of two separable factors: a temperature-dependent factor which indicates that the basic flow process involves the flow of polymer segments and a molecular weight-dependent factor which indicates that the motion of a whole molecule involves a coordinated sequence of segmental jumps. Fox et al.<sup>8</sup> have summarized the basic assumptions which are used in most molecular theories. The viscous flow may be regarded as an activated rate process wherein a small segment of a polymer chain, the flow unit, jumps from one equilibrium position to another. Since the chain segments are connected by primary valence bonds and by entanglements, their motions are not independent of one another. The viscosity of a polymer is therefore expressible as the product of the reciprocal of a segmental jump frequency and some function of the chain length. The segmental jump frequency will be a function of temperature and the local configurational arrangement of the nearest neighbor segments, while the molecular weight factor will be independent of temperature and the same for all long flexible chains.

In this paper, the normal state of the polymer is a homogeneous array of  $N$   $n$ -center segments each with a coordination of four nearest neighbors (Figs. 1a and 1b). In the absence of external force fields, segmental self-diffusion will occur when two adjacent cells expand to twice their average volume (Fig. 2), i.e., a hole the size of the segment is created. Assume an activated complex is formed by the coupling of two adjacent segments to form a "segment-pair" capable of an exchange of positions and that the complex may be regarded as being situated at the top of an energy barrier between two equivalent states (Fig. 3). The frequency of exchange is approximated by assuming that the activated complex has a translational

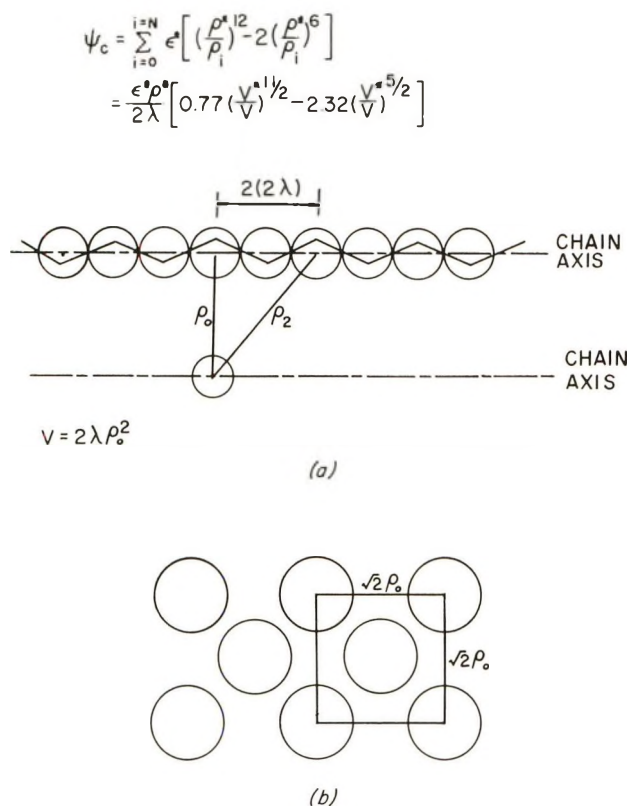


Fig. 1. Models for (a) chain interaction; (b) an amorphous polymer.

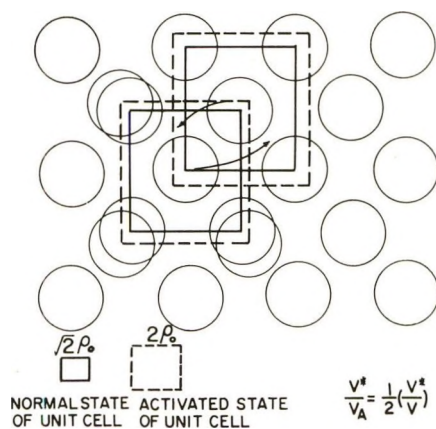


Fig. 2. Self-diffusion of a pair of polymer segments by a rotational exchange.

degree of freedom along the decomposition coordinate. The average rate of passage of the activated segment-pair over the barrier is then:

$$r_D = [kT/(2\pi) (2mn)]^{1/2} \quad (1)$$

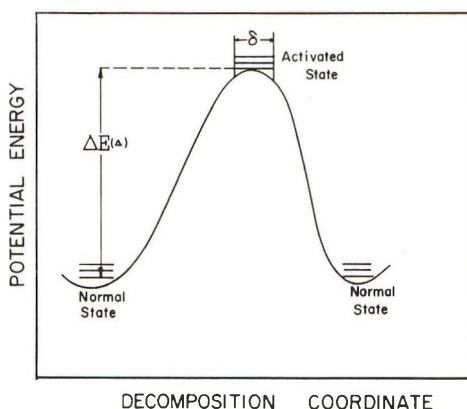


Fig. 3. Formation of an activated complex.

where  $k$  is the Boltzmann constant,  $T$  is absolute temperature,  $m$  is the mass of a center on a polymer chain (e.g.,  $-\text{CH}_2-$  in polyethylene), and  $n$  is the number of centers per segment. The mean life of an activated segment-pair is then:

$$\tau = \delta / r_D = \delta (4\pi mn / kT)^{1/2} \quad (2)$$

where  $\delta$  is the length of the top of the barrier. The number of decompositions per unit volume of polymer per unit time,  $k_D^*$ , is:

$$k_D^* = (c^* / \delta) (kT / 4\pi mn)^{1/2} \quad (3)$$

where  $c^*$  is the concentration of the activated segment pairs. The average jumping frequency of a polymer with a concentration of  $c$  pairs of segments per unit volume is thus:

$$k_D = (c^* / c) (1 / \delta) (kT / 4\pi mn)^{1/2} \quad (4a)$$

$$= (Z^* / Z_S^2) (1 / \delta) (kT / 4\pi mn)^{1/2} \exp \{ - \Delta E(0) / RT \} \quad (4b)$$

where  $k_D$  is the jumping frequency,  $Z^*$  is the total partition function of the activated segment-pair,  $Z_S$  is the total partition function for a single center segment,  $R$  is the universal gas constant, and  $\Delta E(0)$  is the activation energy per mole of activated segment-pairs at  $0^\circ\text{K}$ . The partition functions must be evaluated for a unit volume and relative to zero energy in each case.

The first problem is to estimate the ratio of the partition functions. As was the case in the prior work,<sup>1</sup> the normal state of the system is approximated as a homogeneous array of  $N$   $n$ -center segments, each in a "cell" formed by four nearest neighbors, and acted upon by a cylindrically symmetric potential. If each segment has  $3c_m n$  degrees of external<sup>1</sup> translational freedom, the partition function may be written as:<sup>1</sup>

$$Z_S = (Z_{\text{int}}) (2\pi mKT / h^2)^{3c_m n / 2} Q \quad (5)$$

where  $(Z_{\text{int}})$  is the contribution of internal degrees of freedom,  $h$  is Planck's

constant, and  $Q$  is the configurational partition function for the system. In prior work,<sup>1</sup> a square-well approximation to a 6-12, point center interaction was used to evaluate the configurational partition function. The true, angle-dependent potential of a segment was made cylindrically symmetric by evaluating an integrated average for a polymer segment as its center moved on a cylinder of radius  $r$  (Fig. 4). It was then shown that this symmetric potential could be approximated by a square well. From that paper:<sup>1</sup>

$$Q = \pi^{3c_m n/2} (\rho_0 - 0.83\rho^*)^{3c_m n} \exp(-E_0/RT) \quad (6)$$

$$E_0 = (2N\epsilon^*\rho^*/2\lambda)/[0.77 (v^*/v)^{11/2} - 2.32 (v^*/v)^{5/2}] \quad (7)$$

where  $\rho_0$  is the average nearest neighbor distance between chain axes,  $\rho^*$  is the distance parameter in the 6-12 potential energy function,  $2\lambda$  is the chain length per center,  $v$  is the volume per center,  $v^*$  is a volume parameter ( $v^* = 2\lambda\rho^{*2}$ ),  $\epsilon^*$  is the energy parameter in the 6-12 potential,  $N$  is Avogadro's number, and  $E_0$  is the total lattice energy (in calories per mole).

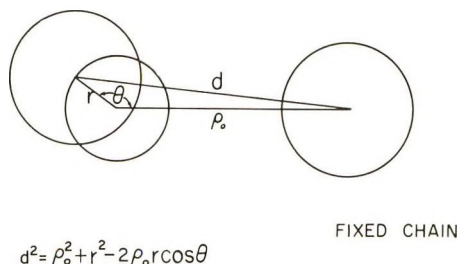


Fig. 4. Polymer segment with its center moving on a cylinder of radius  $r$ .

Assume that an activated state is attained when two adjacent cells expand to twice their average volume (i.e., a hole the size of the segment is formed) and two adjacent segments couple to form a "segment-pair" consisting of  $2n$  units. If a square-well approximation is still adequate, the motion of the segment-pair may still be represented by  $6c_m n$  degrees of translational freedom, since all  $(2n)$  particles are moving in a cage with a constant potential. An exchange of positions can occur when there is a cooperative, coordinated translation of two segments in opposite directions. The activated segment-pair must have one additional degree of translational freedom along the decomposition coordinate. Thus, the activated state differs from the normal state in that it has one extra translational degree in the decomposition coordinate and one less internal vibrational degree of freedom. The flow of a polymer molecule occurs when a coordinated sequence of these segmental exchanges is realized. For a lattice model with the square-well approximation, the partition function for the activated segment-pair is:

$$Z^* = (Z_{\text{int}}^*) [(2\pi) (2mn) (kT)/h^2]^{1/2} \delta (2\pi^2 m k T / h^2)^{3c_m n} \times (\rho_0 - 0.83\rho)^{6c_m n} \exp\{-2E_0/RT\} \quad (8)$$

Combining eqs. (4)–(8), one obtains a jump frequency for a polymer segment:

$$k_D = (kT/h) (Z_{\text{int}}^*/Z_{\text{Sint}}^2) \exp\{-\Delta E(0)/RT\} \quad (9)$$

The ratio of the internal partition functions is probably still close to one, in spite of a difference of one degree of freedom, so eq. (9) may be rewritten as:

$$k_D = (kT/h) \exp\{-\Delta E(0)/RT\} \quad (10)$$

The next problem is to evaluate the activation energy,  $\Delta E(0)$ , for the segmental exchange. This quantity represents the amount of energy that must be added to the two normal, adjacent cells, at  $0^\circ\text{K}$ ., before the polymer segments can become an activated pair. The proposed mechanism is shown in Figure 2. When two adjacent cells expand sufficiently to "loosen" the Van der Waals bonding of the two adjacent segments, a segmental exchange is possible. The total energy change,  $\Delta E(0)$ , is the energy required to overcome the cohesion of the surroundings plus the work of compression necessary to create the free volume.<sup>2,3</sup> The potential energy of interaction of one center to an adjacent polymer segment is:<sup>1</sup>

$$\varphi_T = N\epsilon^*\rho^*/2\lambda [2.32 (v^*/v)^{5/2} - 0.77 (v^*/v)^{11/2}] \quad (11)$$

For a unit cell of parallel,  $n$ -center, polymer segments with a coordination number of four (Figs. 1 and 2),  $6n$  bonds must be broken. At absolute zero,  $(d\varphi/dv)_{0^\circ\text{K}} = 0$ ,  $v^*/v = 1.11$  in the normal state, and  $v^*/v_A = 0.555$  in the activated state. Thus, the total energy required to overcome the cohesion energy of the polymer is:

$$6n (\Delta\varphi_T) = 3.42n N\epsilon^*\rho^*/\lambda \quad (12)$$

If the polymer is in a molten state, the only compression work is against the external pressure, since neighboring polymer segments are able to readjust to local volume fluctuations (i.e., relaxation is very rapid). Since the internal pressure (cohesion energy density) of polymers is on the order of  $10^3$ – $10^4$  atm., one can always neglect this relatively small contribution. Thus, for a molten polymer:

$$\Delta E(0)_m = 3.42nN\epsilon^*\rho^*/\lambda \quad (13)$$

When a polymer is in the glassy state (i.e., below the glass transition temperature), the polymer segments have a very low mobility and cannot readjust to volume fluctuations (i.e., relaxation is very slow). For relatively small volume changes and a constant cohesion energy density, the work of compression,  $W_{c\theta}$ , is simply the product of the internal pressure and the volume change. At absolute zero:

$$\begin{aligned} W_{c\theta} &\simeq (\beta T/\kappa) (2nv) \\ &\simeq (2nv) N\epsilon^*\rho^*/\lambda v [2.32 (v^*/v) - 0.77^{5/2} (v^*/v)]^{11/2} \\ &= 3.28n N\epsilon^*\rho^*/\lambda \end{aligned} \quad (14)$$

The quantity  $\beta$  is the thermal expansion coefficient,  $\kappa$  is the compressibility, and the product  $(\beta T/\kappa)$  is approximately the cohesion energy density. Thus, for a glassy polymer:

$$\begin{aligned}\Delta E(0)_g &\simeq (3.42 + 3.28)n N\epsilon^*\rho^*/\lambda \\ &= 1.96(\Delta E_0)_m\end{aligned}\quad (15)$$

A polymer will not be truly "glassy" until it is below its glass transition temperature, nor will it be truly molten until it is 200–400°K. above its glass transition temperature. In the region between the molten mass and the perfect glass, the true activation energy should be somewhere between the limits of eqs. (13) and (15). Thus, for a rubbery polymer, the activation energy for self diffusion,  $\Delta E(0)_R$ , is

$$\Delta E(0)_R = 3.42 n(N\epsilon^*\rho^*/\lambda) (1 + 0.96x) \quad (16)$$

where  $x$  is the fraction of the maximum work of compression that is required. This will be a function of the jump frequency of the polymer segments, varying from zero in the molten state (very high jump frequency) to one in the glassy state (very low jump frequency).

The Williams-Landel-Ferry equation<sup>7</sup> and the work of Doolittle<sup>9</sup> have shown that the apparent activation energy for the viscous flow of polymers is a relatively simple function of the free volume. On this basis, it appears reasonable to suppose that the quantity  $x$  is also a simple function of free volume. By analogy with the work of Bueche,<sup>6</sup> it is assumed that the relative fraction of compressive work at two temperature levels is inversely proportional to the relative probability that the segments can move into new positions.

$$\frac{x}{1} = \frac{\exp\{V_{fc}/V_{fT}\}}{\exp\{V_{fc}/V_{fT_0}\}} \quad (17)$$

The quantity  $V_{fc}$  is the critical amount of free volume required for segmental motion, and  $V_{fT}$  is the free volume effective in promoting molecular motion. The temperature  $T_0$  is the highest temperature at which a maximum of compressive work is required. It is fairly well established that the free volume at temperature  $T$  is equal to the free volume at  $T_0$  plus the thermal expansion in excess of the Van der Waals expansion of the glass:

$$\begin{aligned}V_{fT} &= V_{fT_0} + V_{T_0}(\beta_m - \beta_g)(T - T_0) \\ &= V_{fT_0} + V_{T_0}\beta'(T - T_0)\end{aligned}\quad (18)$$

where  $\beta_m$  and  $\beta_g$  are the thermal expansion coefficients of the molten polymer and glassy polymer, respectively, and  $V_{T_0}$  is the specific volume at temperature  $T_0$ . Since the critical free volume for segmental motion is equal to the size of the segment itself,  $V_{fc}$  is equal to  $V_T$  and is fairly constant over a wide temperature range. Thus eq. (19) may be rewritten as:

$$\ln x = - \frac{(1/f_{g0})(T - T_0)}{(f_{g0}/\beta) + T - T_0} \quad (19)$$

where  $f_{g0}$  is the fraction of the total volume at temperature  $T_0$  that is free volume and  $\beta'$  is the difference in expansion coefficients in the molten and glassy states. The temperature,  $T_0$ , is the temperature at which the polymer becomes a true glass in the sense that a maximum amount of work of compression must be done to create a "hole" in the structure. It should be close to, but not necessarily equal to, the measured glass transition temperature. The quantity  $f_{g0}$  should be a constant and have the same value for all glass-forming polymers. In theory, the quantity  $\beta'$  can be obtained from thermal expansion data, but in practice it might be better to leave it as an adjustable parameter to improve the curve fitting of data.

The self-diffusion coefficient for a polymer molecule with no entanglements may be evaluated from the jumping frequency. Consider a polymer of molecular weight  $M$  consisting of  $L$  freely orienting segments. (It is not known *a priori* how large a freely orienting segment is, but there are indications that it is larger than the jumping unit of  $n$  centers.<sup>10a</sup>) If each segment is displaced by a distance  $\rho_0$  at the rate of  $k_D$  times per second, the center of mass of the molecule will move a distance  $\rho_0/L$  at the rate of  $k_D L$  times per second. The self-diffusion coefficient, if there are no entanglements, is by definition:

$$D = k_D \rho_0^2 / 6L \quad (20)$$

The effect of entanglements is to reduce the self-diffusion coefficient. The exact computation of this effect presents a very difficult problem, but an approximate solution has been obtained by Bueche.<sup>5</sup> Utilizing his results, one obtains the true self-diffusion coefficient for a high molecular weight polymer ( $M > M_B$ ):

$$D_E = (k_D \rho_0^2 / 6L) (M_B / M)^{2.5} \quad (21)$$

where  $M_B$  is the molecular weight above which the viscosity varies with the 3.4-power of the molecular weight. Bueche has tabulated values of  $M_B$  for several polymers. The viscosity is related to the self-diffusion coefficient by eq. (22).<sup>10b</sup>

$$\eta = (6L / k_D \rho_0^2) (M / M_B)^{2.5} (RT / 36V) (\bar{R}_s^2 / M) \quad (22)$$

where  $\eta$  is the viscosity,  $V$  is the specific volume, and  $(\bar{R}_s^2)$  is the mean square end-to-end distance for the polymer chain. Since the model we are using is a homogeneous array of independent polymer segments, each segment may also be considered as a freely orienting unit. Thus, if a polymer chain of molecular weight  $M$  consists of  $L$  freely orienting segments, each containing  $n_f$  centers, the square of the end-to-end distance divided by the molecular weight is:

$$\begin{aligned} \bar{R}_s^2 / M &= (1/M) (2\lambda n_f)^2 L \\ &= (1/M) (2\lambda n_f)^2 (M / n_f M_0) \end{aligned} \quad (23)$$

$$(\bar{R}_s^2 / M) L = (2\lambda)^2 M / M_0^2 \quad (24)$$

where  $2\lambda$  is the distance between centers along the polymer chain and  $M_0$  is the molecular weight of a single center. Combining eqs. (10), (22), and (24), and taking the liberty of changing the exponent on the molecular weight from 3.5 to 3.4 to conform to experimental fact, one obtains:

$$\eta_R = (\bar{X}_w)^{3.4} (V^*/V)^2 \exp \{ \Delta E(0)/RT \} \quad (25)$$

$$\eta_R = (3/4N^2h) (V^{*2} M_B^{2.5}/\lambda^3 M_0^{0.5}) \eta \quad (26)$$

where the weight-average degree of polymerization is given as

$$\bar{X}_w = M/M_0 \quad (27)$$

and where

$$V^*/V = \left( \frac{\rho^*}{\rho} \right)^2 \quad (28)$$

$$2\lambda\rho_0^2 N/M_0 = V \quad (29)$$

$$\Delta E(0) = 3.42 nN\epsilon^*\rho^*/\lambda (1 + 0.96 x) \quad (30)$$

$$-\ln x = \frac{(1/f_{g0}) (T - T_0)}{(f_{g0}/\beta') + T - T_0} \quad (31)$$

The foregoing equations define unambiguously the viscosity of homogeneous polymer fractions. It has been found experimentally that if a molecular weight distribution exists, the weight-average degree of polymerization gives a good correlation.

Equations (25)–(31) describe the Newtonian viscosity of amorphous polymers, in the limit of zero shear rate, in terms of a number of molecular and thermodynamic properties which are easy to measure, plus three constants. The constant  $f_{g0}$  should be the same for all polymers,  $T_0$  should be very close to the glass transition temperature, and  $n$  is an adjustable constant which is a measure of the size of the jumping unit.

## Results

Table I lists experimental data and molecular parameters for four amorphous polymers. The data were obtained from a variety of literature sources and the molecular parameters were evaluated by curve fitting of thermal expansion and compressibility data to a square-well potential cell model.<sup>1</sup>

The viscosity data were obtained from the empirical equations for long chain polymers presented by Fox et al., which they based on a wide variety of literature sources. Table II presents these equations and gives the apparent temperature range of the data on which they are based.

Table III lists the constants that were obtained for polyisobutylene polystyrene and poly(vinyl acetate) by curve fitting of the viscosity data to eq. (25). The theoretical curves are shown in Figures 5–7 and, for clarity, theoretical and experimental values are compared in Table IV.

TABLE I  
 Thermodynamic and Molecular Properties of Some Amorphous Polymers

Polymer	$M_B$ , g./mole <sup>a</sup>	$M_0$ , g./mole <sup>b</sup>	$\lambda$ , Å. <sup>b</sup>	$\rho^*$ , A. <sup>b</sup>	$N\epsilon^*\rho^*/\lambda$ , cal./g.- mole <sup>b</sup>	Volume expansion for rubbery state ( $v/v^*$ )
Polyisobutylene	17,000	28	0.580	6.52	934	0.905 + 5.71 $\times 10^{-4}T^c$
Polystyrene	40,000	52	0.625	8.22	3000	0.782 + 5.60 $\times 10^{-4}T^c$
Poly(vinyl acetate)	22,000	43	0.625	7.10	2130	0.765 + 6.79 $\times 10^{-4}T^d$
Poly(methyl methacrylate)	10,000	50	0.625	7.60 <sup>e</sup>	2720 <sup>e</sup>	0.781 + 5.75 $\times 10^{-4}T^d$

<sup>a</sup> Data of Bueche.<sup>10c</sup><sup>b</sup> Reference 1.<sup>c</sup> Data of Eirich.<sup>8</sup><sup>d</sup> Estimated from density and expansion data of DiBenedetto<sup>1</sup> and Wood.<sup>11</sup><sup>e</sup> Data of Di Benedetto.<sup>12</sup>
 TABLE II  
 Empirical Viscosity Relationships For Long Chain Polymers

Polymer	Empirical equation <sup>a,b</sup>	For $\bar{X}_w \geq$	Apparent temp. range of data, °C.
Polyisobutylene	$\log \eta = 3.4 \log \bar{X}_w + 5.5 \times 10^5/T^2 - 10.93$	610	-10-217
Polystyrene	$\log \eta = 3.4 \log \bar{X}_w + 2.7 \times 10^{16}/T^6 - 9.51$	730	125-217
Poly(vinyl acetate)	$\log \eta = 3.4 \log \bar{X}_w + 9.77 \times 10^{10}/T^4 - 10.05$	—	60-200
Poly(methyl methacrylate) <sup>c</sup>	$\log \eta = 3.4 \log \bar{X}_w + 4.5 \times 10^{34}/T^{13} - 7.40$	208	110-140

<sup>a</sup> Viscosity in poises.<sup>b</sup> These equations will not predict viscosity below the glass transition temperature.<sup>c</sup> Most experimental data for PMMA is in the glass transition region so that this equation must be based on relatively few usable points.

When the constants in Table II are used in eqs. (25)–(31), good fits of experimental data are obtained over the whole temperature range for the three polymers listed. The last column of Table IV indicates that the differences are well within the experimental accuracy of the data. The quantity  $f_{g_0}$  is the fraction of the total volume that is free volume at temperature  $T_0$ . A value of 0.10 is higher than the 0.025 predicted by the WLF equation,<sup>7</sup> but is perhaps more reasonable, since it is on the order of magni-

tude of  $\beta_g T_g$ , where  $\beta_g$  is the expansion coefficient of the glass and  $T_g$  is the glass transition temperature. The values of  $\beta'$  are on the order of 0.3–0.5 of the expansion coefficients for the molten polymers. Since  $\beta'$  is theoretically the expansion coefficient of the molten mass minus the expansion coefficient for a perfect glass, these are reasonable. The values of  $T_0$  are seen to be close to the measured glass transition temperatures. The values listed in Table III are only average values and may easily vary by 5 or 10 degrees, depending on the measuring technique and the sample used. The temperature  $T_0$  is, by definition, the highest temperature at which a maxi-

TABLE III  
Constants for Viscosity Equation

	From viscosity data				Measured value <sup>a</sup>	
	$n$	$f_{g0}$	$T^0, ^\circ\text{K.}$	$\beta', ^\circ\text{K.}^{-1}$	Glass transition temp.	$\beta_m$ from thermal data
					$T_g, ^\circ\text{K.}$	
Polyisobutylene	3.210	0.10	190	$2.69 \times 10^{-4}$	203	$5.9 \times 10^{-4}$
Polystyrene	1.205	0.10	374	$2.01 \times 10^{-4}$	373	$5.5 \times 10^{-4}$
Poly(vinyl acetate)	1.35	0.10	313	$1.65 \times 10^{-4}$	303	$6.0 \times 10^{-4}$

<sup>a</sup> These are average values from the literature and should only be considered approximate.

TABLE IV  
Comparison of Experimental and Theoretical Values of Viscosity For Three Amorphous Polymers

Polymer	Temp., $^\circ\text{K.}$	$-\log \eta / \bar{X}_w^{3.4}$		$\eta$ (theoretical)
		Experimental <sup>a</sup>	Theoretical	$\eta$ (experimental)
Polyisobutylene	230	0.53 <sup>b</sup>	0.17	(2.29)
	250	2.13	2.03	1.26
	275	3.68	3.61	1.18
	300	4.83	4.96	0.74
	350	6.43	6.48	0.89
	400	7.49	7.46	1.07
	450	8.23	8.17	1.15
	500	8.73	8.73	1.00
Polystyrene	383	1.01 <sup>b</sup>	1.01	1.00
	400	2.92	3.04	0.76
	450	6.24	6.25	0.98
	500	7.78	7.70	1.20
	550	8.54	8.55	0.98
Poly(vinyl acetate)	333	2.14	2.12	1.05
	353	3.80	3.84	0.91
	373	5.02	5.10	0.83
	423	7.02	7.00	1.05
	473	8.12	8.06	1.15

<sup>a</sup> Data from Table II; probably no better than  $\pm 25\%$ .

<sup>b</sup> Extrapolation of equations in Table II.

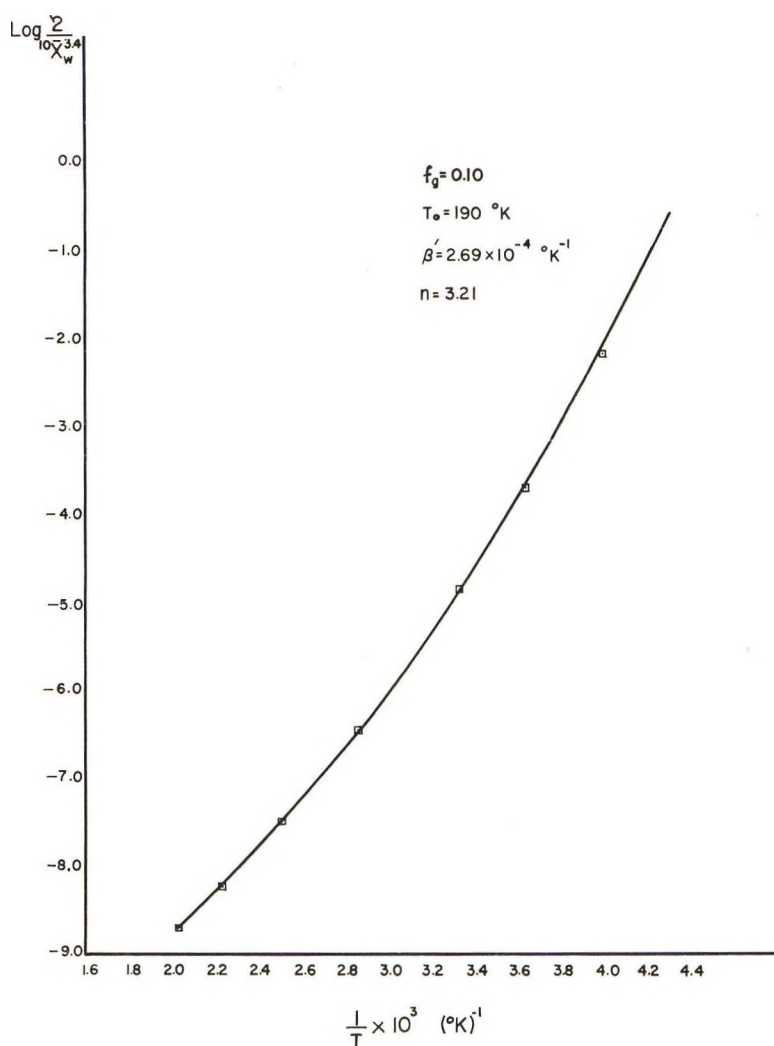


Fig. 5. Viscosity of polyisobutylene.  $f_g = 0.10$ ;  $T_0 = 190^\circ \text{K}$ ;  $\beta' = 2.69 \times 10^{-4} \text{ } ^\circ \text{K}^{-1}$ ;  $n = 3.21$ .

imum amount of compression work is required to form a hole of molecular dimensions. Although one would expect this to be very close to the glass transition temperature, it may not be exactly the same.

An interesting result of this development is that a sudden, sharp drop in apparent activation energy (the slope of a  $\log \eta$  versus  $1/T$  curve) is predicted below  $T_0$  (see Fig. 6 for an example) and that as the temperature increases to more than  $200^\circ \text{C}$ . above  $T_0$ , the log of viscosity is about linear with respect to  $(1/T)$ . This is in qualitative agreement with most viscosity data on amorphous polymers.

The values of  $n$  that were obtained imply that a jumping unit consists of 1-3 centers or, in other words, 1-3 carbon atoms in the backbone chain.

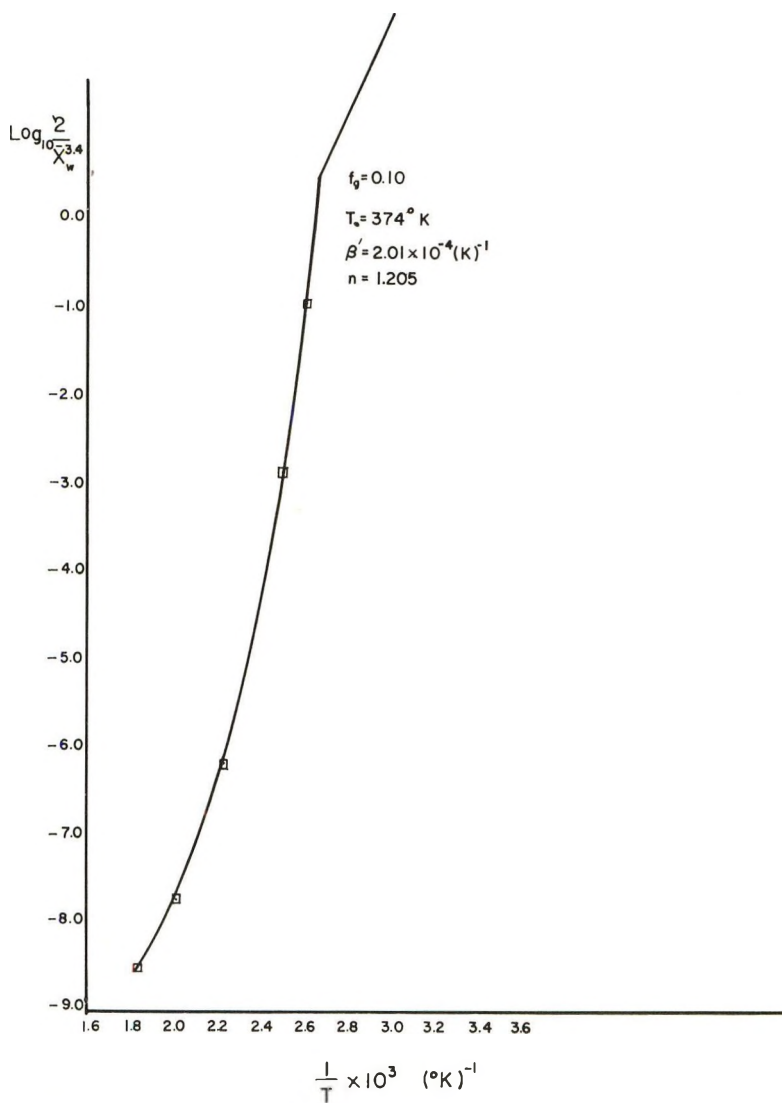


Fig. 6. Viscosity of polystyrene.  $f_g = 0.10$ ;  $T_0 = 374^\circ \text{K}$ .;  $\beta' = 2.01 \times 10^{-4} \text{K}^{-1}$ ;  $n = 1.205$ .

It is doubtful whether the magnitude of this number is meaningful, in an absolute sense, since the experimentally observed value of  $n$  is highly dependent upon the assumed model and flow mechanism. Bueche has stated, however, that the flow unit is probably much smaller than a freely orienting segment.<sup>10a</sup> The size of a freely orienting segment,  $n_f$ , for this model, is related to the square of the end-to-end distance for the polymer chain, as shown by eq. (23). Flory<sup>13</sup> has given some experimental values of this constant for various polymers in theta solvents. (A polymer molecule will have the same random configuration in a pure polymer as it does

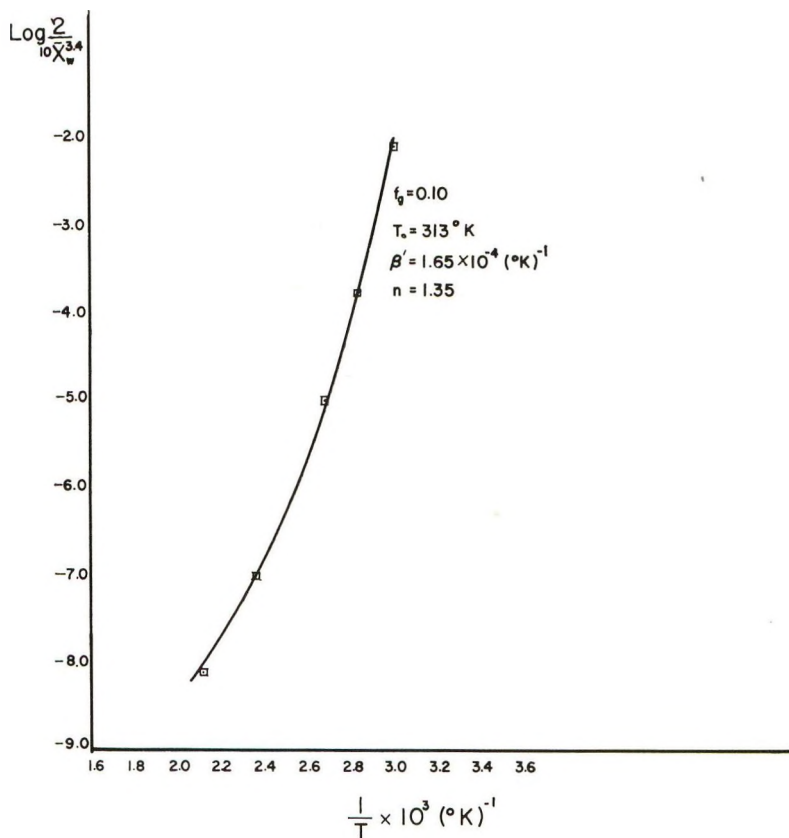


Fig. 7. Viscosity of poly(vinyl acetate).  $f_g = 0.10$ ;  $T_g = 313^\circ \text{K}$ ;  $\beta' = 1.65 \times 10^{-4} \text{°K}^{-1}$ ;  $n = 1.35$ .

in a theta solvent.) Table V shows the values for  $n_f$  for polystyrene, polyisobutylene, and natural rubber. Also tabulated are values of  $n_{fD}$  which were obtained by this author from gaseous diffusion through polymers.<sup>2</sup>

TABLE V  
Size of Freely Orienting Segments For Amorphous Polymers

Polymer	Temp., °K.	$\bar{R}_s^2/M$ , Å. <sup>a</sup>	$2\lambda n_f$ , Å.	$2\lambda n_{fD}$ , Å. <sup>b</sup>	$2\lambda n$ , Å. <sup>c</sup>
Polyisobutylene	297	0.632	15.2	14.2 <sup>d</sup>	3.72
	368	0.573	13.8		3.72
Polystyrene	298	0.540	22.4	—	1.51
	343	0.505	21.0	—	1.51
Natural rubber	300	0.689	9.9	10.7	—

<sup>a</sup> Data of Flory.<sup>13</sup>

<sup>b</sup> Data of DiBenedetto.<sup>2</sup>

<sup>c</sup> From Table III of this paper.

<sup>d</sup> Average for temperature range.

In that paper it was assumed that a diffusional jump for a gas molecule was a translation motion, parallel to a chain axis, from one end of a freely orienting segment to the other. Thus,  $n_{fD}$  should be approximately equal to  $n_f$ .

It appears that the jumping unit in viscous flow is on the order of 0.1–0.3 of the size of an equivalent freely orienting segment. This is, at least, in qualitative agreement with Bueche's statement.

Throughout the discussion it has been assumed that the adjustable parameter,  $n$ , was independent of temperature. This may be approximately true for flexible chains without too much steric hindrance. The polymers that we have been studying, on the other hand, do show a slight temperature dependence for the mean square end-to-end distance and thus would probably also show a slight temperature dependence of  $n$ . As long as this change is small, however, it can be masked in the curve fitting by slight adjustments in  $T_0$  or  $\beta'$  (which probably account for the slight variations from expected values). Intuitively, one would expect, however, that in moving through the transition temperature, relatively large changes in  $n$  might occur. Since polymer mobility is rapidly decreasing, steric hindrance becomes much more important and  $n$  would probably increase to a different constant value. There are viscosity data available for poly(methyl methacrylate) which cover the range  $T_g - 45 < T_g < T_g + 35$ .<sup>14</sup> An initial curve fitting was attempted by extrapolating the WLF equation<sup>15</sup> (based on stress relaxation data at 40–125°C.) into the higher temperature region but a good fit was not attainable. Thus, it was tentatively assumed that  $T_0 = 393^\circ\text{K}$ .,  $\beta' = 2.1 \times 10^{-4}$ , and  $f_{g0} = 0.10$ . The results for different values of  $n$  are shown in Figure 8 along with the experimental data.

The high temperature region (obtained by extrapolation of the equation in Table II) appears to be fitted with  $n$  equal to 1.00. The low temperature region can probably be fitted with  $n$  equal to about 2.13. The transition region of  $420 > T > 340^\circ\text{K}$ . cannot be fitted unless  $n$  is allowed to increase from 1.00 to 2.13 as the temperature decreases. The insert on Figure 8 shows that  $T_0$  marks the point where  $n$  starts to change rapidly and the measured glass transition temperature lies in about the middle of the zone. It could very well be that the curve fitting of the data for polystyrene and poly(vinyl acetate) masked the start of this variation which could account for the slightly high values of  $T_0$ .

Tentatively, it appears that the viscosity of a rubbery or molten polymer in the limit of zero shear rate can be determined by eqs. (25) – (31). Over a temperature range of at least  $(T_0 + 200) > T > (T_0 + 25)$ , the polymer may be characterized by a single value of the adjustable constant  $n$ , a "characteristic" temperature,  $T_0$ , which is close to the glass transition temperature, and a free-volume expansion coefficient,  $\beta'$ . It is necessary to have one viscosity measurement at least 200 degrees above  $T_g$  ( $x \approx 0$ ) to fix the value of  $n$  and it is desirable to have at least two other measurements, closer to  $T_g$ , to adjust  $T_0$  and  $\beta'$  to the best possible values. It

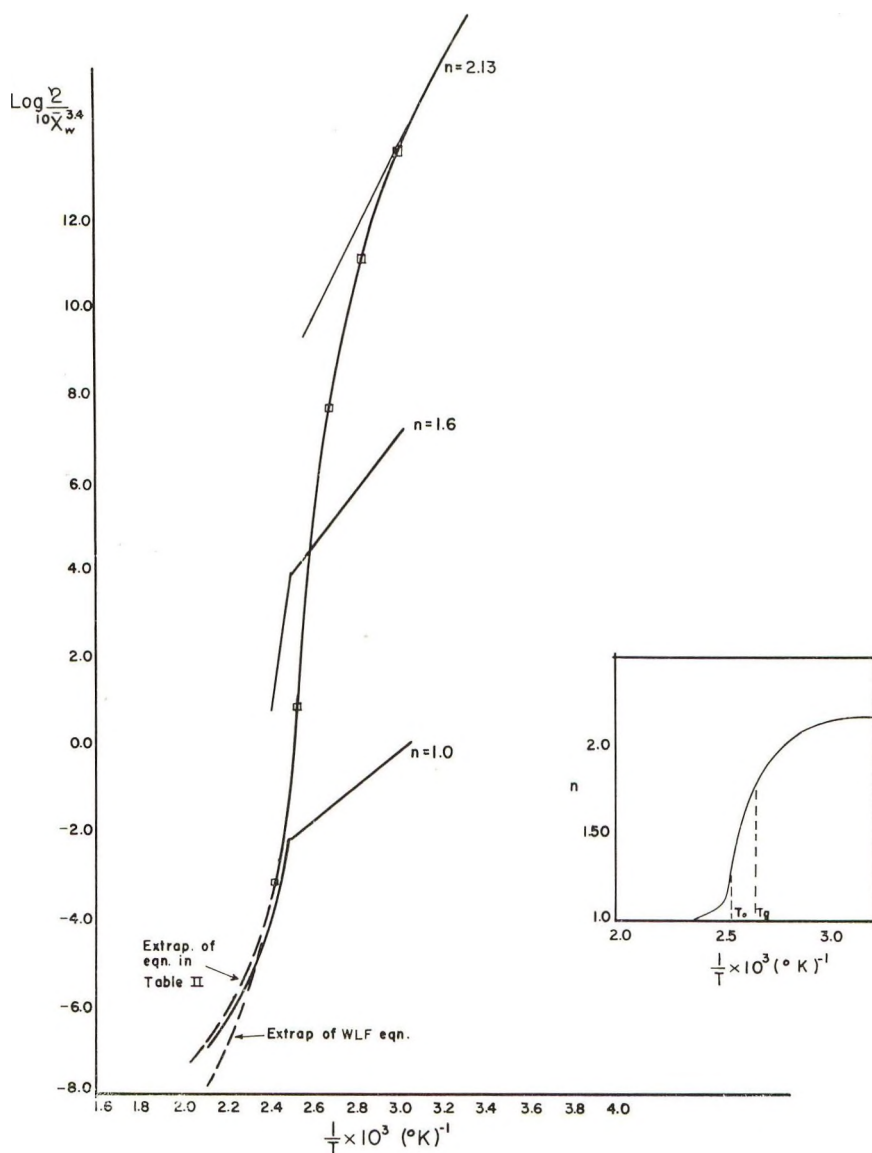


Fig. 8. Viscosity of poly(methyl methacrylate) in the glass transition region.

may also be possible to predict self-diffusion coefficients (or viscosities) in the glassy state from a single measurement below  $T_g$ , since the glassy state may be described by one constant,  $n$  [see eq. (15)].

This project has been supported in part by the Research Committee of the Graduate School from funds supplied by the Wisconsin Alumni Research Foundation.

### References

1. DiBenedetto, A. T., *J. Polymer Sci.*, **A1**, 3459 (1963).
2. DiBenedetto, A. T., *J. Polymer Sci.*, **A1**, 3477 (1963).

3. DiBenedetto, A. T., and D. R. Paul, *J. Polymer Sci.*, in press.
4. Glasstone, S., K. J. Laidler, and H. Eyring, *The Theory of Rate Processes*, McGraw-Hill, New York, 1941, Chap. 9.
5. Bueche, F., *J. Chem. Phys.*, **20**, 1959 (1952); *ibid.*, **25**, 599 (1956).
6. Bueche, F., *J. Chem. Phys.*, **21**, 1850 (1953); *ibid.*, **24**, 418 (1956); *ibid.*, **30**, 748 (1959).
7. Williams, M. L., R. F. Landel, and J. D. Ferry, *J. Am. Chem. Soc.*, **77**, 3701 (1955).
8. Fox, T. G., S. Gratch, and F. Loshaek in *Rheology*, F. R. Eirich, Ed., Vol. 1, Academic Press, New York, 1956, Chap. 12.
9. Doolittle, A. K., *J. Appl. Phys.*, **22**, 1471 (1951).
10. Bueche, F., *Physical Properties of Polymers*, Interscience, New York, 1962, Chap. 3 (a) p. 64; (b) p. 72; (c) p. 76.
11. Wood, L. A., *J. Polymer Sci.*, **28**, 319 (1958).
12. DiBenedetto, A. T., unpublished results.
13. Flory, P. J., *Principles of Polymer Chemistry*, Cornell Univ. Press, Ithaca, N. Y., 1953, p. 618.
14. Bueche, F., *J. Appl. Phys.*, **26**, 738 (1955).
15. Bischoff, J., E. Catsiff, and A. V. Tobolsky, *J. Am. Chem. Soc.*, **74**, 3378 (1952).

### Résumé

Un polymère amorphe est caractérisé par un ensemble de  $N$  segments polymériques identiques à  $n$  centres qui peut être décrit par quatre constantes moléculaires. Le mécanisme d'écoulement visqueux (ou d'autodiffusion) est visualisé par l'échange de position de deux segments polymériques adjacents dans une cavité de dimension égale à une paire de segments. L'énergie d'activation d'écoulement visqueux est l'énergie nécessaire pour vaincre les liaisons de cohésion entre segments voisins, plus le travail de compression nécessaire pour former la cavité de dimensions moléculaires. On estime l'effet dû à l'enchevêtrement des chaînes en utilisant la théorie de Bueche. On déduit une équation de la viscosité en fonction d'une température caractéristique  $T_0$  d'un coefficient d'expansion de volume libre  $\beta'$ , d'un volume fractionnaire libre pour l'état vitreux  $f_{g0}$ , d'une longueur segmentaire moyenne  $2\lambda n$  et des quatre constantes moléculaires mesurables. Cette équation décrit la viscosité limite inférieure du polyisobutylène, du polystyrène et de l'acétate de polyvinyle sur une gamme de viscosité s'étendant jusqu'à un facteur de  $10^8$  et pour tout le domaine de température couvert par les résultats expérimentaux accessibles. On montre que la température caractéristique  $T_0$  est proche de la température de transition vitreuse, que le coefficient d'expansion de volume libre  $\beta'$  est égal aux  $4/10$  du coefficient d'expansion thermique du caoutchouc et que le volume fractionnaire libre  $f_{g0}$  est de 0.1 pour tous les polymères. On calcule que la dimension de l'unité se mouvant au cours de l'écoulement visqueux égale 0.1 à 0.3 fois la dimension d'un segment équivalent, s'orientant librement.

### Zusammenfassung

Ein amorphes Polymeres wird als homogener Bereich von  $N$  identischen  $n$ -zentrigen Polymersegmenten charakterisiert, der mit vier Molekülkonstanten beschrieben werden kann. Ein Mechanismus für viskoses Fließen (oder Selbstdiffusion) wird als Stellungen- austausch zweier benachbarter Polymersegmente in einem Loch von der Grösse eines Segmentpaares anschaulich gemacht. Die Aktivierungsenergie für das viskose Fließen ist der Energiebedarf für die Überwindung der kohäsiven Bindung an die Nachbarsegmente vermehrt um die Kompressionsarbeit zur Bildung eines Loches in Molekülgrösse. Der Einfluss der Kettenverschlingung wird mittels der Theorien von Bueche bestimmt. Eine Viskositätsgleichung wird auf Grundlage einer charakteristischen Temperatur,  $T_0$ , eines Expansionskoeffizienten für das freie Volumen,  $\beta'$ , eines freien Volumenbruchteils für den Glaszustand  $f_{g0}$ , einer mittleren Segmentlänge,  $2\lambda n$ , und der vier messbaren

Molekülkonstanten abgeleitet. Diese Gleichung gibt die untere Grenzviskosität von Polyisobutylen, Polystyrol und Polyvinylacetat in einem Viskositätsbereich bis zu einem Faktor von  $10^8$  und im ganzen Temperaturbereich der erhaltenen Daten wieder. Die charakteristische Temperatur,  $T_0$ , liegt nahe bei der gemessenen Glasumwandlungstemperatur, der Expansionskoeffizient für das freie Volumen,  $\beta'$ , beträgt etwa 0,4 des thermischen Ausdehnungskoeffizienten von Kautschuk und der freie Volumbruchteil ist bei allen Polymeren 0,1. Die Grösse des Sprungelements beim viskosen Fließen wird zu etwa 0,1 bis 0,3 der Grösse eines äquivalenten, sich frei orientierenden Segments berechnet.

Received August 8, 1963

Revised October 7, 1963

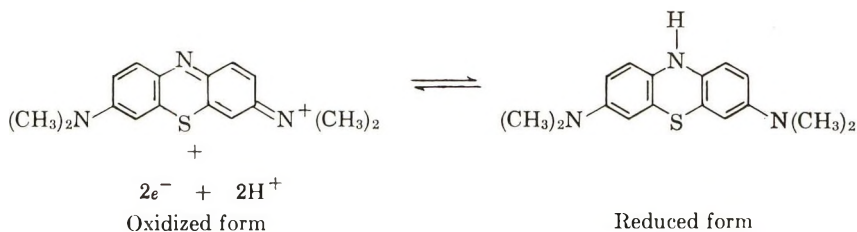
## Electron Exchange Polymers. XXII. Preparation and Properties of Poly-2-vinylphenothiazine

HIROYOSHI KAMOGAWA, JOEL MARIE LARKIN, KYOJI TÔEI,  
and HAROLD G. CASSIDY, *Department of Chemistry, Yale University,  
New Haven, Connecticut*

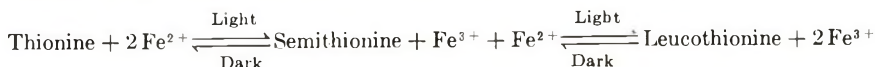
### Synopsis

A new electron exchange polymer, poly-2-vinylphenothiazine, was prepared from 2-vinylphenothiazine by thermal polymerization in an acetylating solvent (acetic anhydride) to form poly-2-vinyl-*N*-acetylphenothiazine. This was hydrolyzed with alcoholic alkali to yield greyish white poly-2-vinylphenothiazine, which is soluble in pyridine, dimethylformamide, chloroform, dioxane, and tetrahydrofuran, but not in aqueous solvents. The polymer could be oxidized with air in the presence of light, and oxidation with ferric chloride or bromine in tetrahydrofuran could be followed spectrophotometrically. On treatment with bromine followed with aqueous dimethylamine, the polymer became soluble in 90% acetic acid, in which solvent it could be reduced with titanium trichloride and reoxidized with bromine.

The phenothiazine functional group is of interest because of its derivatives which show reversible redox behavior. For example, methylene blue shows the following behavior:<sup>1</sup>



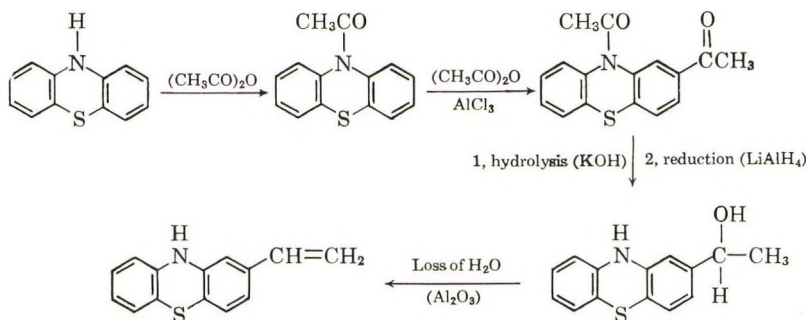
This behavior is particularly interesting because the redox reactions take place through semiquinone intermediates, the stabilities of which are dependent on the hydrogen ion activity of the medium.<sup>2,3</sup> Further, thionine, the corresponding unmethylated diaminophenothiazine, undergoes an interesting reaction with ferrous iron in the presence of light:<sup>4</sup>



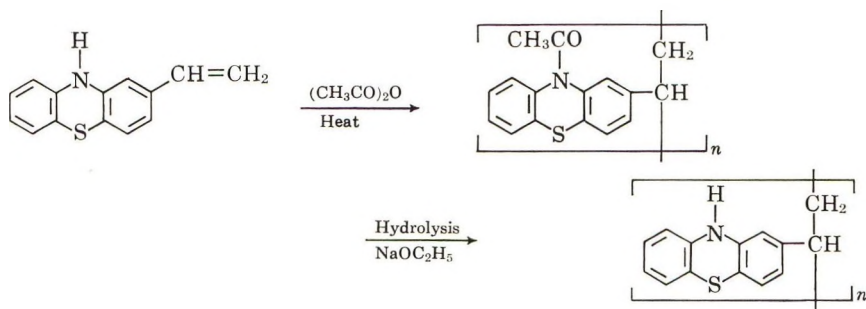
It seemed desirable, therefore, to enter the series of phenothiazine-based polymers as a new series of redox, or electron exchange polymers,<sup>5</sup> through the synthesis of poly-2-vinylphenothiazine. The objective, as in all our previous work, has been to prepare well-characterized, stable polymers, and

we have centered attention upon vinyl polymers. Sansoni has prepared crosslinked redox polymers by mixed condensation of methylene blue, formaldehyde, and resorcinol,<sup>6</sup> and he has also devised and studied redox resins made by loading cation exchangers with organic redox systems (including methylene blue).<sup>7</sup>

In this paper we report the preparation and some oxidative properties of poly-2-vinylphenothiazine. To prepare 2-vinylphenothiazine, the following reaction sequence was employed, starting with phenothiazine. The first two steps were previously known.<sup>8-10</sup>



This substance was simultaneously acetylated and polymerized by acetic anhydride and heat. Hydrolysis then yielded poly-2-vinylphenothiazine.



This polymer was found to be quite insoluble in water. It was made soluble by treating it with bromine in dimethylformamide, followed by aqueous dimethylamine in excess, a sequence of reactions of a type by means of which Kehrman<sup>11</sup> produced methylene blue from phenazine. The polymer so modified could be reduced and reoxidized.

## EXPERIMENTAL

### 2-Vinylphenothiazine

**10-Acetylphenothiazine.** This compound was prepared by the method of Bernthsen<sup>8</sup> by refluxing 250 g. of acetic anhydride with 125 g. of technical grade phenothiazine for 5 hr. On cooling, greyish-green crystals formed. These were filtered off and washed with a small amount of acetic acid.

The yield was 145 g. (97%), m.p. 198–200°C., of material pure enough for the next step.

**2,10-Diacetylphenothiazine.** The method of Cauquil and Casadevall,<sup>9</sup> a typical Friedel-Crafts reaction, served in the preparation of this compound. To 24.1 g. (0.1 mole) of 10-acetylphenothiazine and 54 g. (0.4 mole) of powdered anhydrous aluminum chloride in 380 ml. carbon disulfide was added 10.4 ml. (11.3 g., 0.11 mole) of acetic anhydride with stirring at room temperature. The mixture was refluxed, with stirring, for 7 hr. After cooling, carbon disulfide was decanted, and the tarry complex was decomposed by ice and concentrated hydrochloric acid, added slowly. The mixture was extracted with ether and the yellow ether layer washed successively with 10% hydrochloric acid, water, sodium carbonate solution, and then thoroughly with water until the aqueous layer was neutral to litmus. After drying over anhydrous sodium sulfate, the ether solution was evaporated to yield a yellow powder which was recrystallized from ethanol to give a product having m.p. 105–107°C. (lit.<sup>9,10</sup> 105–106°C.) in 20% yield.

**2-Acetylphenothiazine.**<sup>9</sup> To 23.6 g. (0.08 mole) of 2,10-diacetylphenothiazine dissolved in hot ethanol was added 6.6 g. (0.12 mole) of potassium hydroxide dissolved in 75 ml. 95% ethanol. Crystals began to form immediately, and the mixture was refluxed for 1 hr. Upon cooling, golden-orange crystals formed which were filtered off and washed with water until the washings were neutral to litmus. The product was recrystallized from ethyl acetate; yield 85%, m.p. 190–192°C. (lit.<sup>9</sup> 193°C.). In this step, crude 2,10-diacetylphenothiazine may be used, thereby considerably increasing the overall yield.

**2-(1-Hydroxyethyl)phenothiazine.** The acetylphenothiazine (24 g., 0.1 mole) in a Soxhlet thimble was extracted into 1.5 l. of dry ether containing 6 g. (0.15 mole) of finely powdered lithium aluminum hydride until the yellow extract ceased (about 12 hr.). The solution gradually became green. At the end of the reaction, 100 ml. ethyl acetate was added dropwise to destroy excess hydride, then 300 ml. water was added. The solution became pink, and a suspension of aluminum hydroxide appeared in the aqueous layer. The organic layer, upon evaporation, yielded a greyish white powder. This was taken up in refluxing 95% alcohol, the solution was treated with decolorizing charcoal, filtered, diluted with an equal volume of water, and cooled. White, fibrous crystals, m.p. 144–146°C., separated with a yield of 71%. The infrared spectrum showed no carbonyl absorption but showed a broad absorption at 3300–3400  $\text{cm}^{-1}$  assignable to —OH and —NH groups. Repeated recrystallization from ethanol–water afforded an analytical sample.

ANAL. Calcd. for  $\text{C}_{14}\text{H}_{13}\text{ONS}$ : C, 69.10%; H, 5.38%; N, 5.76%; S, 13.18%. Found: C, 68.88%; H, 5.39%; N, 5.75%; S, 12.93%.

**2-Vinylphenothiazine.** Activated alumina, 7 g., and 3 g. of 2-(1-hydroxyethyl)phenothiazine were ground in a mortar, then heated at 220–

240°C./1 mm. Hg for 2 hr. in a sublimation apparatus. The yellow sublimate was dissolved in 100 ml. hot ethanol and brought out by adding 25 ml. water to give yellow crystals, m.p. 178–180°C. yield 25%. The infrared spectrum of this compound (in KBr) shows a much reduced absorption at 3330  $\text{cm}^{-1}$  as compared with that of the starting material, and vinyl bands at 990 and 900  $\text{cm}^{-1}$ . A —CN stretching band was observed at 1310  $\text{cm}^{-1}$ . The evidence, taken with the analytical data, strongly supports the identification of this material as 2-vinylphenothiazine.

ANAL. Calcd. for  $\text{C}_{14}\text{H}_{11}\text{NS}$ : C, 74.63%; H, 4.92%; N, 6.22%; S, 14.23%. Found: C, 74.88%; H, 5.05%; N, 6.22%; S, 14.19%.

### Poly-2-vinyl-*N*-acetyl phenothiazine

**Attempted Polymerization of 2-Vinylphenothiazine.** It was not found possible to polymerize 2-vinylphenothiazine by conventional methods. For example, 0.5 g. 2-vinylphenothiazine, dissolved in 2 ml. toluene, with 0.005 g.  $\alpha, \alpha'$ -azobisisobutyronitrile, and sealed in a small tube under 1 mm. Hg gave no evidence of polymer formation after heating at 80°C. for 72 hr. Boron trifluoride etherate gave a red color with the vinylphenothiazine but no polymer, nor did the anionic initiator lithium metal yield polymer.

**Polymerization Procedure.** Polymerization was achieved by sealing 0.1 g. of 2-vinylphenothiazine with 0.2 ml. acetic anhydride in a small tube under 1 mm. mercury and heating at 130°C. for 5 hr. The monomer dissolved completely to a clear yellow solution, which became viscous. The tube was opened, a small amount of tetrahydrofuran was added, and the mixture poured into a large amount of ethanol. A white precipitate was obtained with a yield of 42%. The product softened at about 215°C. It was soluble in tetrahydrofuran, pyridine, chlorinated hydrocarbons, and acetic anhydride. Its intrinsic viscosity in tetrahydrofuran was 0.23 at 29.7°C. In a similar experiment, 0.40 g. monomer and 0.80 ml. acetic anhydride were heated at 130°C. for 24 hr. In this case some sticky white polymer separated during the polymerization. The whole, dissolved in tetrahydrofuran and poured into ethanol gave a 52% yield of polymer with an intrinsic viscosity in tetrahydrofuran of 0.33 at 29.7°C. The polymerization can be carried out under nitrogen and with larger amounts of monomer.

The infrared spectrum of this polymer, in KBr, showed a strong —CO absorption band of the tertiary amide at 1660  $\text{cm}^{-1}$ , a —CN stretching band at 1300  $\text{cm}^{-1}$ , and a C—CH<sub>3</sub> band at 1360  $\text{cm}^{-1}$ . Other characteristic bands of phenothiazine were present, but no vinyl bands could be recognized. The ultraviolet spectrum of the polymer in chloroform is very similar to that of *N*-acetylphenothiazine (Fig. 1). It is therefore concluded that at least the major structure of the polymer corresponds to poly-2-vinyl-*N*-acetylphenothiazine.

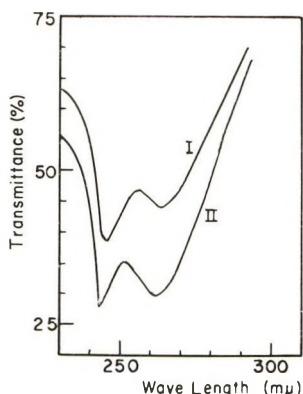


Fig. 1. Ultraviolet spectra in chloroform of (I) poly-2-vinyl-*N*-acetylphenothiazine and (II) *N*-acetylphenothiazine.

ANAL. Calcd. for  $(C_{16}H_{13}ONS)_n$ : C, 71.91%; H, 4.88%; N, 5.26%; S, 11.98%. Found: C, 69.16%; H, 5.09%; N, 4.85%; S, 11.88%.

As a check on the polymerization method, glacial acetic acid was substituted for acetic anhydride, and the experiment carried out in an otherwise identical manner, i.e., at 130°C. for 5 hr. No viscosity rise was observed after 5 hr., but there was some precipitate present. On pouring the mixture into methanol, a red-violet precipitate appeared. This did not melt at 220°C. but turned into a black powder. The red-violet precipitate dissolved in tetrahydrofuran to a yellow solution. The infrared spectrum of the precipitate was very similar to that of poly-2-vinylphenothiazine (see below). No double bond was recognized, and it appears most probable that although no high polymer was obtained there was formed some oligomer.

The addition of a radical initiator ( $\alpha, \alpha'$ -azobisisobutyronitrile) in the polymerization led to the formation of insoluble material with the progress of time.

### Poly-2-vinylphenothiazine

The polymer, 0.05 g., obtained as described above, was dissolved in 2 ml. tetrahydrofuran and warmed to give a clear solution. To this was added 0.2 ml. ethanol in which had been produced, by the addition of sodium, enough alcoholate to keep the mixture alkaline during the reaction. The mixture was refluxed under nitrogen for 2 hr. A yellow solution containing some precipitate was obtained. Upon pouring the mixture into aqueous sodium sulfate, a greenish grey precipitate separated. This was washed thoroughly with water and dissolved in tetrahydrofuran. The filtered tetrahydrofuran solution, poured into a large amount of methanol, with vigorous stirring, threw down a fine greyish white polymer. The yield was about 80%. The hydrolyzed polymer is soluble in pyridine, dimethylformamide, chloroform, dioxane, and tetrahydrofuran. On standing in

air it slowly becomes greenish grey, and insoluble. The infrared spectrum of hydrolyzed polymer is much like that of vinylphenothiazine, except that no vinyl absorptions at 990 and 900  $\text{cm}^{-1}$  can be seen, and alkane  $\text{---CH}_2\text{---}$  bands at 2920 and 2850  $\text{cm}^{-1}$  are clearly present. The  $\text{---CO}$  absorption at 1660  $\text{cm}^{-1}$  and the  $\text{C---CH}_3$  band at 1360  $\text{cm}^{-1}$  which characterized the starting polymer are no longer present. The ultraviolet spectrum of the polymer is quite similar to that of phenothiazine (Fig. 2 and Table I).

ANAL. Calcd. for  $(\text{C}_{14}\text{H}_{11}\text{NS})_n$ : C, 74.63%; H, 4.92%; N, 6.22%; S, 14.23%. Found: C, 73.85%; H, 5.31%; N, 6.40%; S, 13.94%.

These data support the conclusion that the polymer structure is mainly that of poly-2-vinylphenothiazine.

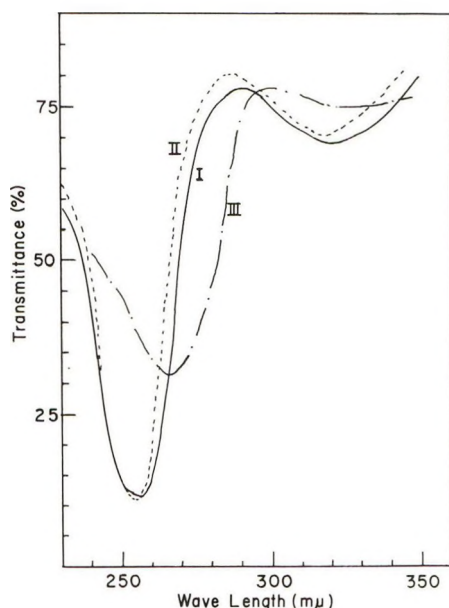


Fig. 2. Ultraviolet spectra in chloroform of (I) poly-2-vinylphenothiazine, (II) phenothiazine, and (III) 2-vinylphenothiazine.

### Redox Behaviors

**Potentiometric Titration.** Poly-2-vinylphenothiazine, as prepared by the above described procedure, is insoluble in water. Redox titrations in organic media are not very successful.<sup>12</sup> Michaelis, Granick, and Shubert<sup>3</sup> titrated phenothiazine in aqueous acetic acid, but the polymer did not give good stoichiometry when titrated with bromine in tetrahydrofuran or pyridine, with or without addition of a small amount of water. Ferric chloride titration in tetrahydrofuran was also unsuccessful. It seemed, therefore, that some means had to be taken to make the polymer soluble in an aqueous liquid—preferably 90% acetic acid, as used by Michaelis et al.<sup>3</sup>

TABLE I  
Ultraviolet Spectra of Poly-2-vinylphenothiazine and Related Compounds  
(Solvent: Chloroform)

Compound	Maximum absorption, $m\mu$	Molar extinction coefficient, l./mole cm.
Poly-2-vinylphenothiazine	256	26,100
	320	3,370
Phenothiazine	255	44,400
	316	5,180
2-Vinylphenothiazine	268	39,800
	332	4,520
Poly-2-vinyl- <i>N</i> -acetylphenothiazine	245	17,500
	263	15,600
<i>N</i> -Acetylphenothiazine	243	19,200
	262	14,600

The procedure typically used was as follows. Poly-2-vinylphenothiazine (26.6 mg.) was dissolved in 10 ml. of dimethylformamide to give a pale yellow solution. To this was added bromine in dimethylformamide until the color, passing through green, changed to red-brown. The solution was then treated with 5% aqueous dimethylamine to give a red-violet solution which contained an excess of the amine (by odor). This was poured into aqueous sodium sulfate solution to precipitate violet polymer. From this point the polymer must always be kept wet, otherwise it becomes insoluble. The precipitated polymer was centrifuged, suspended in distilled water, and centrifuged again. After several repetitions of this washing process, the wet polymer was dissolved in 100 ml. 90% acetic acid to give a red-violet solution. To this solution was added excess aqueous 0.08*N* titanium trichloride solution (about 5 ml.) until the violet color disappeared completely. The leuco polymer thus obtained was titrated under nitrogen with 0.1*N* bromine solution in 90% acetic acid, using platinum and saturated calomel electrodes.<sup>3</sup> A titration curve is shown in Figure 3. Calculation of an equivalent weight would not be possible because yields in the procedural steps are not known.

**Oxidation by Air.** Phenothiazine is readily oxidized in the presence of sunlight.<sup>13</sup> A solution of polymer in chloroform was bubbled with air under a 275 w. sunlight lamp. (The possible effect of oxidation of chloroform was found to be negligible under these conditions.) With the progress of oxidation, the color of the solution first changed to red, then to orange, with precipitation of the oxidized polymer. During this time the absorption in the visible was broad, with no apparent peak, but in the ultraviolet the sharp absorption of unoxidized polymer at 250  $m\mu$  was replaced by a peak at 242  $m\mu$ . Phenothiazine and 2-vinylphenothiazine treated in the same way showed the same responses (Fig. 4).

**Spectrophotometric Titration.** The colors developed on oxidation of poly-2-vinylphenothiazine are susceptible to conditions of the medium,

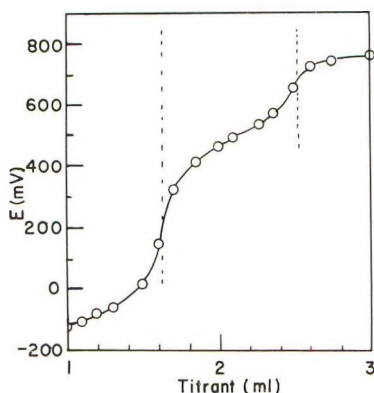


Fig. 3. Oxidative titration of the  $\text{TiCl}_3$ -reduced modified polymer. The first part of the curve shows titration of excess titanous chloride; the portion enclosed in dashed lines represents the oxidation of the polymer.

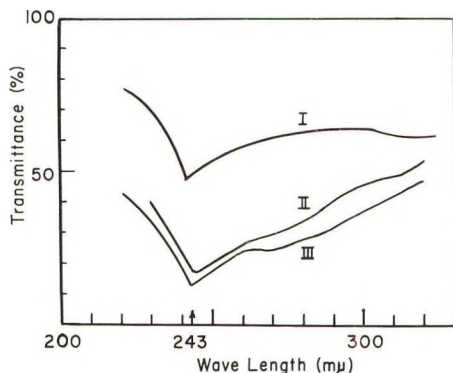


Fig. 4. Ultraviolet spectra of the air-oxidized (*I*) poly-2-vinylphenothiazine, (*II*) 2-vinylphenothiazine, and (*III*) phenothiazine. Solvent was chloroform.

such as pH change, kind of solvent, and ratio of mixtures of solvents; however, it was thought possible to determine equivalence points by spectrophotometric means (Spectronic 505, Bausch & Lomb Co.) with the use of an oxidant such as aqueous bromine or ferric chloride, and with tetrahydrofuran, dimethylformamide, or pyridine as solvents for the polymer. The procedure was to introduce into the spectrometer cell, equipped with a platinum wire stirrer, 3 ml. of solution containing 0.05–0.5 mg. of sample. Titration was carried out with standardized oxidant by use of a micrometer buret. In tetrahydrofuran the polymer gives a strong red-violet color on addition of bromine or ferric chloride solutions. The absorption maximum is at  $530\text{ m}\mu$ , at which wavelength the titrants scarcely absorb. The titration does not give an exact endpoint because a cloudy violet precipitate forms. The dimethylformamide solution remains transparent to the end, but the endpoint is not exact. It is dependent upon the sample concentration, and probably reflects some reaction with the solvent. At the end,

the "molecular" absorption coefficients for the polymer and phenothiazine were  $6 \times 10^5$  (at  $526 \text{ m}\mu$ ) and  $4 \times 10^6$  (at  $542 \text{ m}\mu$ ), respectively. With pyridine as a solvent, the spectra in the visible for the polymer and for phenothiazine are somewhat different. The former has no maximum around  $450 \text{ m}\mu$ , whereas the latter does. In both cases the color changes to orange, then green, with the addition of aqueous bromine titrant. When optical density at  $450 \text{ m}\mu$  was plotted against the amount of bromine added, endpoints corresponding to a four-electron system were obtained (Figs. 5 and 6).

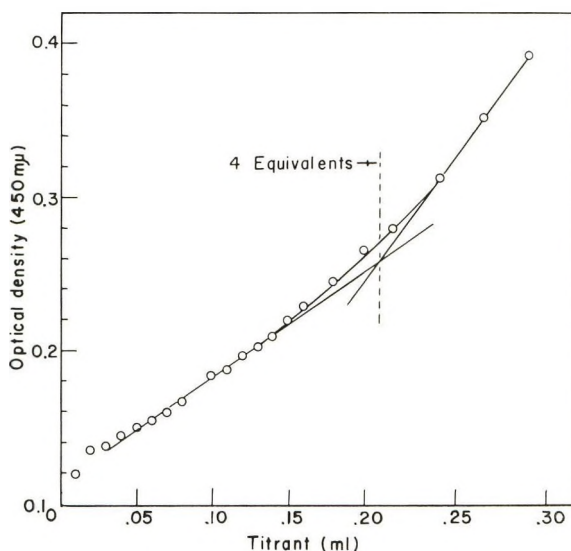


Fig. 5. Spectrophotometric titration of poly-2-vinylphenothiazine: 0.396 mg. in 3 ml. pyridine, with 0.0338*N* aqueous bromine solution.

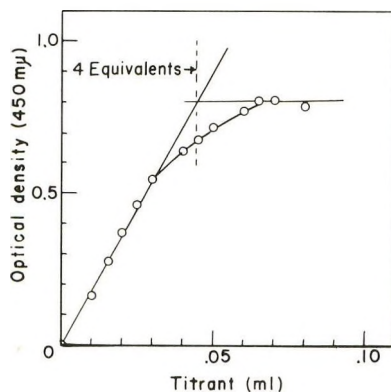
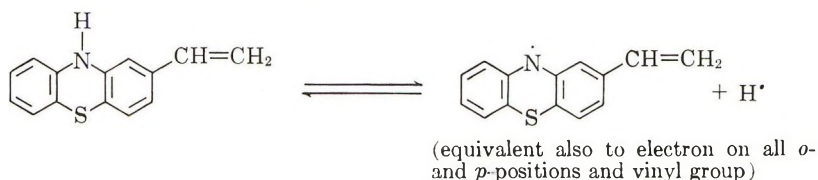


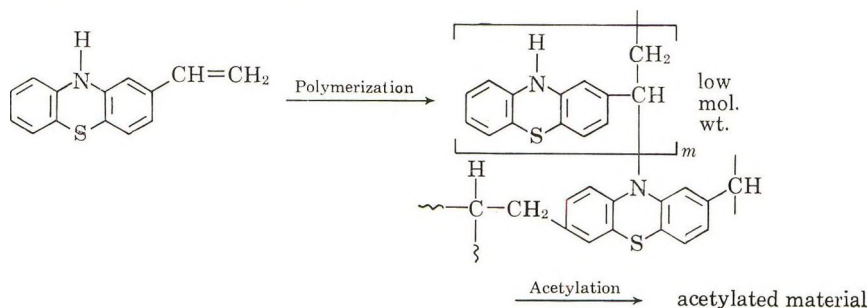
Fig. 6. Spectrophotometric titration of phenothiazine: 0.0848 mg. in 3 ml. pyridine with 0.0388*N* aqueous bromine solution.

## DISCUSSION

Difficulty in polymerizing 2-vinylphenothiazine is thought to be due to the hydrogen on the basic nitrogen. This should readily decompose to free radicals, capable of terminating growing radical chains.



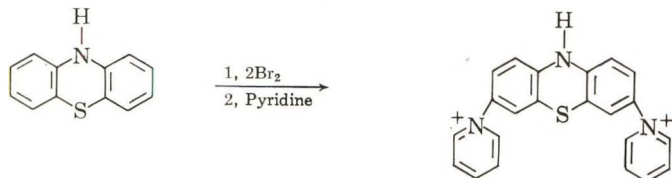
Phenothiazine is, indeed a polymerization inhibitor.<sup>14</sup> The monomer reacts with anionic initiators and forms complexes with Lewis base cationic initiators. It was therefore decided to replace this hydrogen with an acetyl group since this makes the nitrogen less basic and also deactivates the *ortho* and *para* positions. It might be thought that the same procedures employing acetic anhydride might be applied to the monomer as served with phenothiazine,<sup>8,13</sup> but the conditions are severe enough that thermal polymerization of the vinyl groups occurred even in the presence of additional inhibitors such as hydroquinone or picric acid. In these latter runs some oligomers were produced. No better results were obtained when acetyl chloride in pyridine and a lower temperature, were employed. It seemed, therefore, that a virtue might be made of necessity, and polymerization carried out in the acetylating medium, acetic anhydride. Free radical initiators were found to be undesirable; presumably they initiated free radical formation at too early a stage, and insoluble polymers of low molecular weight were produced. The process could be described as in the introduction. Presumable side reactions could be formulated to show a source of crosslinking, thus:



It is thought that a radical initiator may accelerate the polymerization of this type in which case active sites of the phenothiazine nucleus, including *ortho* and *para* positions, would serve as mechanisms of chain termination and crosslinking.

Poly-2-vinylphenothiazine is not soluble in conventional solvents suitable for oxidation, such as water and acetic acid. It is difficult to determine

the final oxidation product in such oxidation-sensitive solvents as tetrahydrofuran, dimethylformamide, and pyridine. It is known that pyridine will react with phenothiazine in the presence of bromine in an inert solvent.<sup>3,15</sup> The reaction is formulated (with a perbromide intermediate):



The endpoints of Figures 5 and 6 may correspond to this reaction. The product is still in a reduced state, and this may explain why the color continues to change beyond this point during bromine titration. In the case of phenothiazine, the absorption peak shifts to shorter wavelengths after the endpoint, and the intensity of 450 m $\mu$  apparently remains constant.

This same type of reaction served to obtain the acid-soluble polymer. Thus, according to Kehrmann,<sup>11</sup> methylene blue is readily formed from the perbromide intermediate from phenothiazine on reaction with dimethylamine at room temperature. Thus we suppose that the polymer titrated in Figure 3 contained an appreciable amount of dimethylamino groups which served to hold it in solution in the acetic solvent. The infrared spectra of bromine-oxidized polymer showed a new absorption band at 1610 cm.<sup>-1</sup> which might be ascribed to  $\text{>C=N-}$ .

As can be seen in Table I, these polymers show the usual hypochromic effect compared with the monomer or monomeric functional group. The small effect shown by the *N*-acetyl polymer suggests that this effect is related to interactions within or between polymer chains, for the acetyl group should block such interaction, or suppress it. We are following up this matter.

We are glad to acknowledge that this investigation was supported by a PHS research grant GM 10864, National Institute of Arthritis and Metabolic Diseases, Public Health Service.

## References

1. See, for example, W. M. Clark, *Oxidation Reduction Potentials of Organic Systems*, Williams & Wilkins, Baltimore, 1960.
2. Michaelis, L., M. P. Schubert, and S. Granick, *J. Am. Chem. Soc.*, **62**, 204 (1940); S. Granick, L. Michaelis, and M. P. Schubert, *ibid.*, **62**, 1802 (1940).
3. Michaelis, L., S. Granick, and M. P. Schubert, *J. Am. Chem. Soc.*, **63**, 351 (1941).
4. Rabinowitch, E., *J. Chem. Phys.*, **8**, 551 (1940). We are indebted to Dr. Donald E. Sargent for calling this reaction to our attention.
5. Kamogawa, H., and H. G. Cassidy, *J. Polymer Sci.*, **A2**, 2409 (1964).
6. Sansoni, B., *Naturwiss.*, **41**, 212 (1954).
7. Sansoni, B., *Naturwiss.*, **39**, 281 (1952).
8. Bernthsen, A., *Ann.*, **230**, 73 (1885).

9. Cauquil, G., and A. Casadevall, *Bull. Soc. Chim. France*, **1955**, 768.
10. Baltzly, R. M., M. Harfenist, and F. J. Webb, *J. Am. Chem. Soc.*, **68**, 2673 (1946).
11. Kehrman, F., *Ber.*, **49**, 53 (1916).
12. Kolthoff, I. M., R. Belcher, V. A. Stenger, and G. Matsuyama, *Volumetric Analysis*, Interscience, New York, 1957, Vol. III, p. 663 ff.
13. Massie, S. P., *Chem. Revs.*, **54**, 797 (1954).
14. See, for example, L. F. Fieser and M. Fieser, *Advanced Organic Chemistry*, Reinhold, New York, 1961.
15. Kehrman, F., and L. Diserens, *Ber.*, **48**, 318 (1915); R. Pummerer, F. Eckert, and S. Gassner, *Ber.*, **47**, 1494 (1914); R. Pummerer and S. Gassner, *Ber.*, **46**, 2310 (1913).

### Résumé

Un nouveau polymère, donnant lieu à des réactions d'échanges électroniques, la poly-(2-vinylphénothiazine), a été préparé à partir de 2 vinylphénothiazine par polymérisation thermique dans un solvant acétylant (l'anhydride acétique) qui fournit le poly(2-vinyl-*N*-acétylphénothiazine). Ce dernier a été hydrolysé au moyen d'alcoolate alcalin pour donner le poly(2-vinylphénothiazine) blanc grisâtre, soluble dans la pyridine, le diméthylformamide, le chloroforme, le dioxanne et le tétrahydrofurane, mais non dans les solvants aqueux. Le polymère peut être oxydé à l'air en présence de lumière et le processus d'oxydation par le chlorure ferrique ou le brome dans le tétrahydrofurane peut être suivi spectrophotométriquement. Si on le traite par le brome puis par la diméthylamine en solution aqueuse, le polymère devient soluble dans l'acide acétique à 90% solvant dans lequel il peut être réduit par le trichlorure de titane et réoxydé par le brome.

### Zusammenfassung

Ein neuer polymerer Elektronenaustauscher, Poly-(2-vinylphenothiazin) wurde aus 2-Vinylphenothiazin durch thermische Polymerisation in einem acetylierenden Lösungsmittel (Essigsäureanhydrid) unter Bildung von Poly(2-vinyl-*N*-acetylphenothiazin) dargestellt. Dieses wurde mit alkoholischem Alkali zu grauweissem Poly(2-vinylphenothiazin) hydrolysiert, das in Pyridin, Dimethylformamid, Chloroform, Dioxan und Tetrahydrofuran, nicht aber in wässrigen Lösungsmitteln löslich war. Das Polymere liess sich mit Luft in Gegenwart von Licht oxydieren und die Oxydation mit Ferri-chlorid oder Brom konnte spektralphotometrisch verfolgt werden. Bei Behandlung mit Brom und darauffolgend mit wässrigem Dimethylamin wurde das Polymere in 90% Essigsäure löslich und konnte in diesem Lösungsmittel mit Titantrichlorid reduziert und mit Brom rückoxydiert werden.

Received August 23, 1963

## Determination of a Mark-Houwink Type Relationship for Poly-*N-tert*-butylacrylamide in Methanol

E. A. S. CAVELL, I. T. GILSON, B. R. JENNINGS, and H. G. JERRARD, *Departments of Chemistry and Physics, The University, Southampton, England*

### Synopsis

Viscosity and light-scattering measurements have been made on five samples of poly-*N-tert*-butylacrylamide in methanol, for which brief preparative details are given. Specific viscosities  $\eta_{sp}$  have been determined at 25°C. with two U-tube viscometers, No. 0 and No. 1, over a range of concentrations  $c$ . The mean flow gradients lie in the range 360–750 sec.<sup>-1</sup> for No. 0 and 535–940 sec.<sup>-1</sup> for No. 1. Graphs of  $\eta_{sp}/c$  against  $c$  are linear for concentrations between 0.18 and 1.0 g./dl. at all gradients less than about 640 sec.<sup>-1</sup> with samples having weight-average molecular weights of 24.5, 5.46, 4.04, 3.79, and  $1.65 \times 10^5$ . At lower concentrations, which give correspondingly higher gradients, the linear relation ceases. Possible reasons for this are suggested. By extrapolation of the linear portions of the appropriate curves to zero concentration, apparent limiting viscosity numbers  $[\eta]_{\substack{c=0 \\ G=760}}$  have been obtained, where the value  $G = 760$  sec.<sup>-1</sup> is the

gradient for pure methanol. Light-scattering data have been employed to obtain the molecular weights of the samples using the Zimm technique. Depolarization ratios, determined for different concentrations at wavelengths 4358 and 5461 Å. and extrapolated to zero concentration, were negligible. The constants  $\kappa_1$  and  $\alpha$  in the expression  $[\eta]_{\substack{c=0 \\ G=760}}$

$= \kappa_1 \bar{M}_w^\alpha$  have the values  $8.87 \pm 0.44 \times 10^{-4}$  and  $0.525 \pm 0.026$ , respectively.

### I. INTRODUCTION

During a study of the kinetics of polymerization of *N-tert*-butylacrylamide (NTBA) in methanol, the need arose to determine the molecular weight of the polymers produced under kinetic conditions, in order to supplement the information obtainable from the measurements of rate alone. Molecular weights are often found by determining the apparent limiting viscosity  $[\eta]$  for zero concentration and a known flow gradient by employing a suitable solvent<sup>1</sup> and deriving the molecular weight  $M$  from an empirical relation of the form

$$[\eta] = \kappa_1 M^\alpha$$

where  $\kappa_1$  and  $\alpha$  are constants for the particular polymer-solvent system studied. For solutions of poly-NTBA in methanol, the values of  $\kappa_1$  and  $\alpha$  do not appear to be known, so that in this paper details are given of experiments from which the constants have been found over a given molecular weight range. Viscosity measurements were made with U-tube viscometers and weight-average molecular weights determined from light-scattering measurements.

## II. EXPERIMENTAL

### Preparation of Polymers

Solutions of monomer in methanol were deaerated in the usual way and then transferred to a thermostat bath for a suitable period of time. Polymerization was initiated by means of either azo bis- $\gamma$ -cyanovaleric acid (ACV), for which preparative details have been given elsewhere<sup>2</sup> or by azobisisobutyronitrile (AIBN). Details of the concentrations and temperatures employed are summarized in Table I. The polymer was precipitated by the gradual addition of the methanolic solution to cold water, removed by filtration and allowed to dry overnight in a vacuum desiccator. The samples were not fractionated. An appropriate quantity of the dried polymer was redissolved in a known volume of methanol. In light-scattering experiments it is of the utmost importance to remove any dust or insoluble impurities large compared with the polymer molecules. The solutions were therefore cleaned by centrifuging in an M.S.E. nonrefrigerated centrifuge at 15,000*g* for 1 hr. and then by filtering through a 1.2  $\mu$  ultrafine sintered glass filter to produce stock solutions. Methanol used to dilute stock solutions to give the required polymer concentration was similarly cleaned.

TABLE I  
Apparent Limiting Viscosity Numbers  $[\eta]_{c=0}$  and Weight-Average Molecular Weights  $\bar{M}_w$  of Poly-NTBA in Methanol

Polymer	Monomer concn., mole/l.	Initiator concn., mole/l.	Temp. of polymerization, °C.	$[\eta]_{c=0}$ <sup>a</sup> $G=760$	$\bar{M}_w \times 10^{-5}$
A	0.25	$10^{-4}$ ACV	25	1.95	24.5
B	0.20	$10^{-2}$ AIBN	15	0.94	5.46
C	0.20	$10^{-3}$ AIBN	5	0.76	4.04
D	0.20	$10^{-3}$ AIBN	18	0.80	3.79
E	0.20	$10^{-2}$ AIBN	25	0.465	1.65

<sup>a</sup> Viscosities determined at 25°C.

Absolute polymer concentrations of the stock solutions of each sample were measured by two methods, (1) by precipitating the polymer with water and drying to constant weight, and (2) by using a Rayleigh interferometer to determine the refractive index of the solution relative to that of the pure solvent. The variation of refractive index with polymer concentration ( $\partial n / \partial c$ ) was determined in a series of auxiliary experiments. The results of the two methods were in agreement.

### Measurement of Viscosity

Viscosities of the solutions prepared as above were measured by means of U-tube viscometers. As is well known, the velocity profile for flow of a non-Newtonian liquid in the capillary of such viscometers has the shape

of a flattened paraboloid, so that the velocity gradient  $G$  is variable. In this study a mean value for  $G$  was calculated<sup>3</sup> from the relationship

$$G = adg\Delta h/2l\eta \quad (1)$$

in which  $a$  and  $l$  are the capillary radius and length, respectively,  $g$  is the acceleration due to gravity,  $\eta$  is the viscosity of the solution of density  $d$ , and  $\Delta h = (h_1 - h_2)/\ln h_1/h_2$ , where  $h_1$  and  $h_2$  are the hydrostatic heads at the beginning and end of the measurement. Equation (1), although strictly valid only for a Newtonian liquid, is assumed to be a sufficiently good approximation for present purposes.

The majority of readings were obtained with a No. 0 viscometer (British Standard Specification No. 188, 1937) having a capacity of 10 ml. and with a capillary 12 cm. long and 0.04 cm. in diameter for which  $\Delta h$  was 6.445 cm. Times of flow varied from 1057 sec. for pure methanol to 2220 sec. for the most viscous polymer solution (sample D, concentration 1.03 g./dl.) and were consistent to within  $\pm 0.2$  sec. The corresponding gradients were 760 and 360 sec.<sup>-1</sup>. Some measurements were also taken with a No. 1 viscometer having a capillary diameter of 0.06 cm. and length 10 cm. for which  $\Delta h = 4.766$  cm. The gradient with this instrument was 1009 sec.<sup>-1</sup> for methanol and for the most viscous solution used (sample A, concentration 0.36 g./dl.) was 535 sec.<sup>-1</sup>. The temperature of measurement was in all cases  $25.00 \pm 0.01^\circ\text{C}$ .

### Light-Scattering Measurements

The apparatus used compares the intensity of light scattered at an angle  $\theta$  to the primary beam to that of the primary beam itself by means of a null modulation method and has been described elsewhere.<sup>4</sup> Observations were made at nine different values of  $\theta$  from  $35^\circ$  to  $135^\circ$  at a wavelength of 4358 Å., and for three or four concentrations of each sample. For one sample readings were also taken at 5461 Å. All readings were corrected for the volume, Fresnel, and refraction effects.<sup>5</sup>

From the theory of light scattering,<sup>5</sup> the Rayleigh scattering ratio  $R_\theta$  corrected by the factor  $(1 + \cos^2\theta)$  of a solution of concentration  $c'$  (in grams per liter) at wavelength  $\lambda_0$  is related to the weight-average molecular weight  $\bar{M}_w$  by an expression of the form

$$Kc' = R_\theta f(\bar{M}_w, c')$$

in which  $f(\bar{M}_w, c')$  is a function of  $\bar{M}_w$  and  $c$ , and

$$K = 2\pi^2 n_0^2 (\partial n / \partial c')^2 / \lambda_0 N \quad (2)$$

In eq. (2),  $n_0$  and  $n$  are the refractive indices of the solvent and solution, respectively, and  $N$  is the Avogadro number. Zimm<sup>6</sup> has shown that if  $Kc'/R_\theta$  is plotted against  $\sin^2\theta/2 + g'c'$ , in which  $g'$  is a constant so chosen to make  $g'c'$  of the same order of magnitude as  $\sin^2\theta/2$ , a gridlike graph is obtained. From this, lines corresponding to  $\theta = 0$  and  $c' = 0$  can be obtained, each of which has as its intercept on the ordinate axis the recipro-

cal of the apparent molecular weight. If the depolarization factor ( $\rho_u$ ) of the solution is negligibly small at zero concentration, then the apparent molecular weight equals the weight-average molecular weight.

### III. RESULTS AND DISCUSSION

Values of  $\partial n/\partial c$  were found by using a Rayleigh interferometer with 1 cm. cells. At 4358 and 5461 Å. they were 0.249 and 0.234 cm.<sup>3</sup>/g., respectively. At these wavelengths the values of  $\rho_u$  at zero concentration were found to be 0.0046 and zero, respectively. These values were obtained from measurements on sample A, for which the values of  $\rho_u$  at different concentrations are shown in Figure 1. This justifies identifying the molecular weight found from a Zimm plot with the weight-average value. A typical Zimm plot is shown in Figure 2. The molecular weights obtained for all the samples studied are summarized in Table I.

The results of the viscosity measurements are shown in Figures 3 and 4, in which  $\eta_{sp}/c$  has been plotted against polymer concentration, for Nos. 0 and 1 viscometers, respectively. No. 0 viscometer gives the lower gradients. With No. 0 viscometer, the variation of  $\eta_{sp}/c$  with  $c$  was linear for sample A, increasing from 2.12 to 4.20 for a change in concentration of 0.015 to 0.09 g./dl. and for gradients within the range 550–750 sec.<sup>-1</sup>. (This is not shown in Figure 3 because of the large ordinate values involved.) For samples B to E over an approximately fourfold variation in polymer concentration within the range 0.18–1.0 g./dl., the reduced

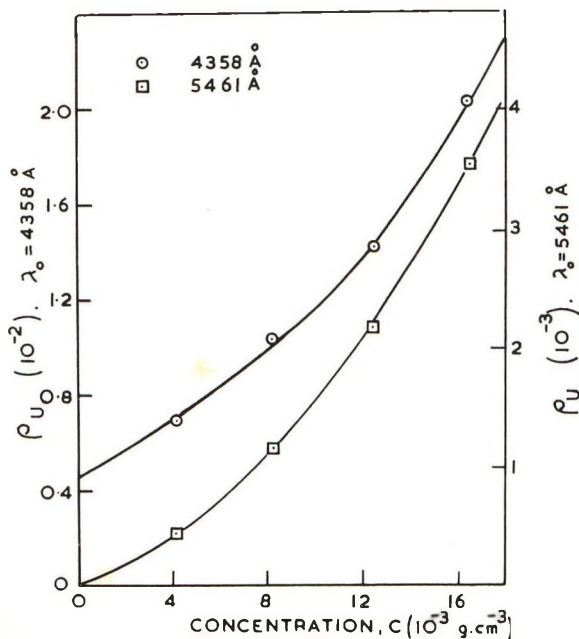


Fig. 1. Variation of depolarization ratio ( $\rho_u$ ) for poly-NTBA (sample A) in methanol, with concentration for wavelengths 4358 and 5461 Å.

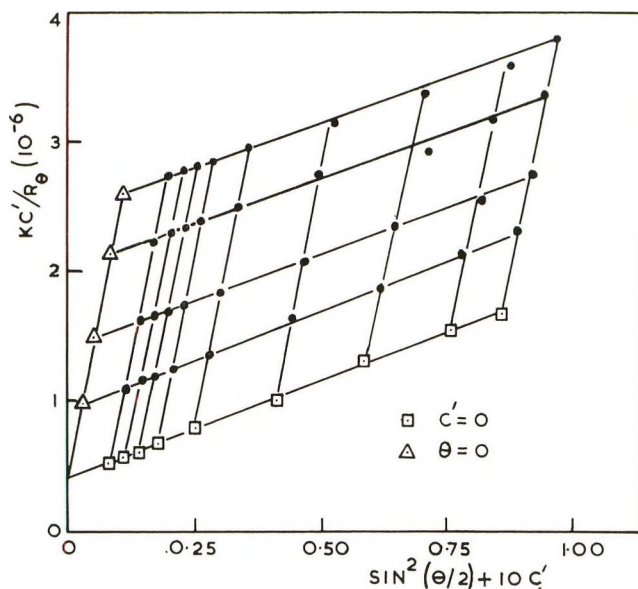


Fig. 2. A typical Zimm plot for poly-NTBA in methanol. Sample A, wavelength 4358 Å.

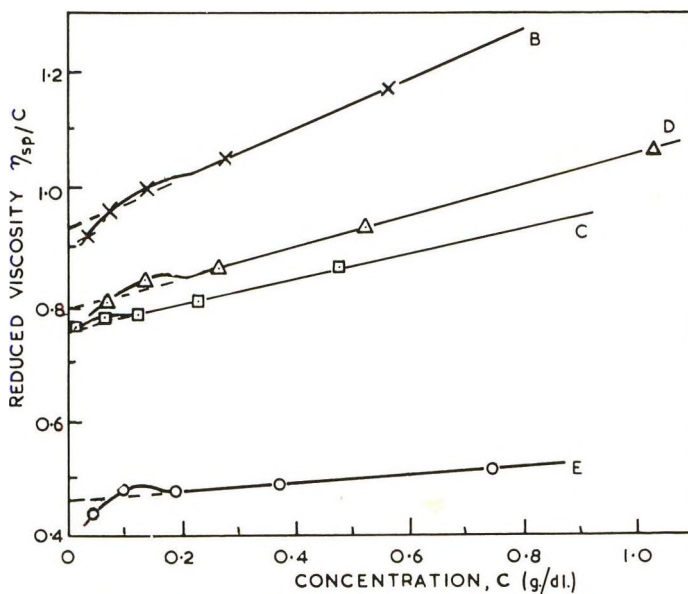


Fig. 3. Variation of reduced viscosity with concentration for samples B, C, D, and E of molecular weights 5.46, 4.04, 3.79, and  $1.65 \times 10^5$ , respectively, at various gradient ranges: (B) 460–736  $\text{sec.}^{-1}$ , (C) 453–750  $\text{sec.}^{-1}$ ; (D) 362–723  $\text{sec.}^{-1}$ ; (E) 551–745  $\text{sec.}^{-1}$ .

viscosity  $\eta_{sp}/c$  varies linearly with concentration. For concentrations less than 0.18 g./dl., there is a tendency for the graphs to curve downward. However, with the higher gradients obtained with No. 1 viscometer an upward trend occurred at concentrations below about 0.18 g./dl. as shown in

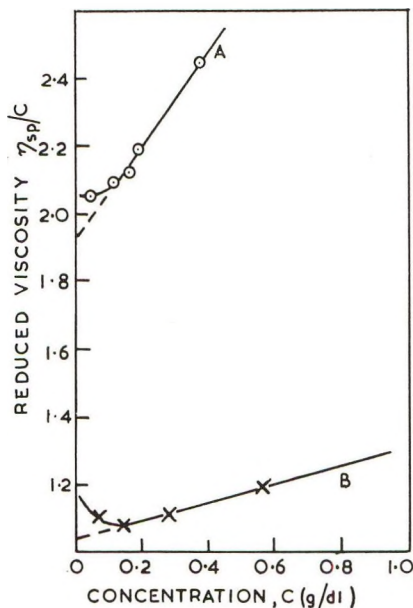


Fig. 4. Variation of reduced viscosity with concentration for samples A and B of molecular weights 24.5 and  $5.46 \times 10^5$ , respectively, at various gradient ranges: (A) 535–940  $\text{sec.}^{-1}$  and (B) 605–936  $\text{sec.}^{-1}$ .

Figure 4 for samples A and B. A change of  $\eta_{sp}/c$  with change of gradient has been confirmed in these laboratories by experiments made with a concentric cylinder viscometer.

Nonlinear behavior similar to this has been reported often.<sup>7</sup> In this particular case, the cause of the upward curvature in the graphs does not seem to be adsorption of polymer on the capillary walls as proposed by Ohrn,<sup>8</sup> because the effect becomes increasingly apparent with larger rather than smaller diameter capillaries, i.e., with smaller rather than larger gradients. However, the polymer concentration at which the minimum value of  $\eta_{sp}/c$  occurs does seem to increase as the molecular weight of the polymer is decreased. Since methanol is a "good" solvent for poly-NTBA, a dependence of viscosity on shear gradient might be expected. Consequently, both intermolecular hydrogen bonding between solvent and polymer and between polymer molecules themselves and intramolecular hydrogen bonding between contiguous *N-tert*-butylamido groups are possible reasons for nonlinear behavior.

The existence of a nonlinear dependence of  $\eta_{sp}/c$  upon  $c$  at low polymer concentrations does not prevent the formulation of a useful empirical relation between molecular weight and an apparent limiting viscosity number obtained by extrapolating the linear portion of the graphs given in Figures 3 and 4 to zero concentration, provided that the range of validity of the relationship is recognized, which here is for concentrations between 0.18 and 1.0 g./dl. and for gradients of less than about 640  $\text{sec.}^{-1}$ . Apparent limiting viscosity numbers obtained in this way are summarized in Table

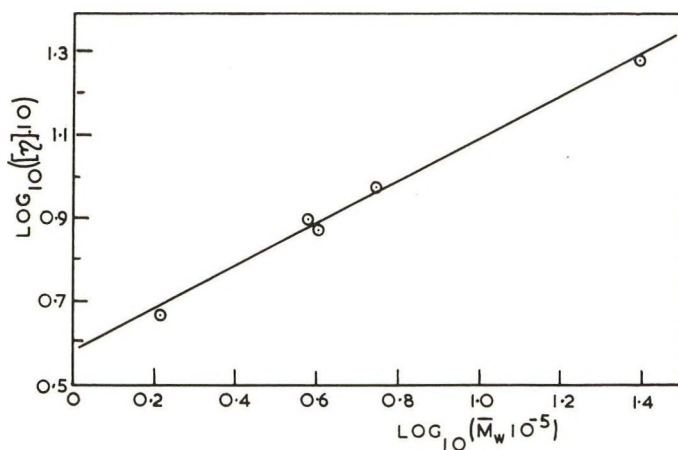


Fig. 5. Variation of the apparent intrinsic viscosity  $[\eta]_{c=0}$  with the weight-average molecular weight of poly-NTBA samples in methanol.  
 $G = 760$

I. It is evident from the logarithmic plot shown in Figure 5 that over the range of molecular weights studied the experimental data are adequately represented by an equation of the form

$$[\eta]_{c=0}^{G=s} = \kappa_1 \bar{M}_w^\alpha$$

in which  $\kappa_1 = 8.87 \pm 0.44 \times 10^{-4}$ ,  $\alpha = 0.525 \pm 0.026$ , and  $s$  is the numerical value of the gradient  $G$ . It should be emphasized that the limiting viscosity number  $[\eta]_{c=0}^{G=0}$  will most probably have a different value from the apparent values  $[\eta]_{c=0}^{G=s}$ , where  $s \leq 760 \text{ sec.}^{-1}$ , found in this investigation.

The light-scattering data have also been used to determine the radius of gyration  $\bar{R}_n$  and the number-average molecular weight  $\bar{M}_N$ . These are related by the equation

$$\bar{R}_n = \kappa_2 \bar{M}_N^\beta$$

in which  $\kappa_2$  and  $\beta$  are constants. The value of  $\beta$  was found to be greater than 0.5, which indicates polymer-solvent interaction. This is consistent with the above value of  $\alpha$ , which suggests that the polymer chains are not freely draining. Intermolecular hydrogen bonding may well account for the major part of the polymer-solvent interaction.

One of us (I. T. G.) wishes to thank the U. S. Air Force (Aeronautical Systems Division) and another (B. R. J.) the Department of Scientific and Industrial Research for research awards during the tenure of which this work was done. Thanks are also due the American Cyanamid Co. for a gift of *N*-*tert*-butylacrylamide.

## References

1. Cantow, H. J., and G. V. Schulz, *Z. Physik. Chem. (Frankfurt)*, **1**, 365 (1954).
2. Cavell, E. A. S., *Makromol. Chem.*, **54**, 70 (1962).

3. Yang, Jen Tsi, *Advan. Protein Chem.*, **16**, 375 (1961).
4. Jerrard, H. G., and D. B. Sellen, *Appl. Optics*, **1**, 243 (1962).
5. Stacey, K. A., *Light Scattering in Physical Chemistry*, Butterworth, London, 1956.
6. Zimm, B. H., *J. Chem. Phys.*, **16**, 1099 (1948).
7. Takeda, M., and E. Tsuruta, *Bull. Chem. Soc. Japan*, **25**, 80 (1952); D. J. Streeter and R. F. Boyer, *J. Polymer Sci.*, **14**, 5 (1954); S. Claesson, *Makromol. Chem.*, **35**, 75 (1960).
8. Ohrn, O. E., *J. Polymer Sci.*, **17**, 137 (1955); *ibid.*, **19**, 199 (1956).

## Résumé

On a effectué des mesures de viscosité et de diffusion lumineuse sur cinq échantillons de poly-*N-tert* butylacrylamide dans le méthanol et on donne quelques précisions sur la préparation de ce polymère. Les viscosités spécifiques ( $\eta_{sp}$ ) ont été déterminées à 25°C au moyen de viscosimètres N° 0 et N° 1, en forme de U dans un domaine de concentrations  $[c]$ . Les gradients d'écoulement moyen se situent entre 360 et 750  $\text{sec}^{-1}$  pour N° 0 et entre 535 et 940  $\text{sec}^{-1}$  pour N° 1. Pour les échantillons de poids moléculaire moyen en poids de 24.5, 5.46, 4.04, 3.79 et  $1.65 \times 10^5$ , si on porte  $\eta_{sp}/c$  en fonction de  $c$ , on obtient une droite dans le domaine de concentration intermédiaire entre 0.18 et 1 g./dl. pour tous les gradients inférieurs à 640  $\text{sec}^{-1}$  environ. Aux plus faibles concentrations, qui fournissent des gradients comparativement plus élevés, il n'y a plus de relation linéaire. On suggère quelques explications de ce phénomène. Par extrapolation à concentration nulle de la partie linéaire des courbes, on obtient des valeurs de la viscosité limite apparente  $[\eta]_{G=760}^{c \rightarrow 0}$  où  $G = 760 \text{ sec}^{-1}$  et le gradient du méthanol pur. Les résultats de la diffusion lumineuse ont servi à obtenir les poids moléculaires des échantillons par la technique de Zimm. Les rapports de dépolarisation déterminés pour différentes concentrations aux longueurs d'onde 4358 et 5461 Å. et extrapolés à concentration nulle sont négligeables. Les constantes  $\kappa_1$  et  $\alpha$  figurant dans l'expression  $[\eta]_{G=760}^{c \rightarrow 0} = \kappa_1 \bar{M}_w^\alpha$  possèdent les valeurs  $8.87 \pm 0.44 \times 10^{-4}$  et  $0.525 \pm 0.026$  respectivement.

## Zusammenfassung

An fünf Poly-*N-tert*-butylacrylamidproben, deren Darstellung kurz beschrieben wird, werden Viskositäts- und Lichtstreuungsmessungen in Methanol durchgeführt. Die spezifische Viskosität ( $\eta_{sp}$ ) wurde bei 25°C in zwei U-Röhrenviskosimetern, No. 0 und No. 1, bei verschiedenen Konzentrationen  $[c]$  bestimmt. Der mittlere Strömungsgradient liegt für No. 0 in Bereich von 360 bis 750  $\text{sek}^{-1}$  und für No. 1 im Bereich von 575 bis 940  $\text{sek}^{-1}$ . Bei allen Gradienten kleiner als etwa 640  $\text{sek}^{-1}$  liefert die Auftragung von  $\eta_{sp}/c$  gegen  $c$  bei Konzentrationen zwischen 0,18 und 1,0 g./dl. für Proben mit Gewichtsmittelwerten des Molekulargewichts von 24,5, 5,46, 4,04, 3,79 und  $1,65 \times 10^5$  eine lineare Abhängigkeit. Bei kleineren Konzentrationen, die entsprechend höhere Gradienten ergeben gilt die lineare Beziehung nicht mehr. Mögliche Gründe dafür werden angegeben. Durch Extrapolation des linearen Teils der geeigneten Kurven auf die Konzentration Null wurden scheinbare Grenzviskositätszahlen  $[\eta]_{G=760}^{c \rightarrow 0}$  erhalten, wo der Wert von  $G = 760 \text{ cm}^{-1}$  der Gradient für reines Methanol ist. Aus den Lichtstreuungsdaten wurden die Molekulargewichte der Proben nach dem Verfahren von Zimm erhalten. Das bei verschiedenen Konzentrationen bei den Wellenlängen 4358 und 5461 Å. bestimmte und auf die Konzentration Null extrapolierte Depolarisationsverhältnis war vernachlässigbar klein. Die Konstanten  $\kappa_1$ , und  $\alpha$  in der Beziehung  $[\eta]_{G=760}^{c \rightarrow 0} = \kappa_1 \bar{M}_w^\alpha$  besitzen den Wert  $(8,87 \pm 0,44) \times 10^{-4}$  bzw.  $0,525 \pm 0,026$ .

Received September 11, 1963

## General Conclusions about the Copolymerization of Ethylene with Other Monomers by Free Radical Catalysis

FRANCIS E. BROWN and GEORGE E. HAM, *Spencer Chemical Company, Research Center, Merriam, Kansas*

### Synopsis

The behavior of ethylene in copolymerization with methyl acrylate, methyl methacrylate, vinyl acetate, diethyl fumarate, and diethyl maleate was investigated, and reactivity ratios for these systems reported. Significant deviations of all systems investigated, except ethylene-vinyl acetate, from the conventional copolymerization equation are noted and interpreted on the basis of substantial penultimate and penpenultimate effects. The consistency of the reactivity ratios developed in the systems ethylene-methyl acrylate and ethylene-methyl methacrylate with reported values for methyl acrylate-methyl methacrylate is shown by application of the relationship  $P_{ab}P_{bc}P_{ca} = P_{ac}P_{cb}P_{ba}$ .

The copolymerization of ethylene with various monomers, polar and non-polar, by free radical catalysis has been previously reported.<sup>1,2</sup> Mortimer and co-workers investigated the copolymerization of ethylene ( $M_1$ ) and propylene ( $M_2$ ), analyzed the products by a  $C^{14}$  tracer technique, and reported reactivity ratios  $r_1 = 3.30 \pm 0.15$  and  $r_2 = 3.1 \pm 1.7$ . An  $r_1r_2$  product of 10.2 was obtained.

These results create new questions about the physical nature of ethylene copolymerization as compared with most other free radical copolymerizations. The prospect of block-type copolymerizations (preferred addition of either radical to its own monomer arising from  $r_1r_2 > 1$ ) is difficult to explain in the light of present knowledge of the nature of free radical copolymerization in homogeneous phase. In addition, ethylene monomer possesses a "duality" in copolymerization not shared by any other monomer. Either end may add equally well to growing radicals, which could lead to higher effective concentrations in copolymerization.

Zutty and Burkhart<sup>2</sup> reported copolymerizations of ethylene with *n*-butyl acrylate, vinyl chloride, vinyl acetate, and vinyl fluoride at 1000 atm. Their studies showed, on the contrary, reactivity ratio products ( $r_1r_2$ ) equal to unity within experimental error for the last three systems and equal to  $0.36 \pm 0.12$  for ethylene-*n*-butyl acrylate. The last result would indicate an appreciable alternating tendency in this system, but for the fact that  $r_1$  (ethylene =  $M_1$ ) = 0.03. Such a low value cannot be determined with great precision, so the most that can be concluded is that some tendency

TABLE I

Run no.	Monomer	Feed				Product					
		$M_2$ , moles	$M_1$ , moles	$M_1/M_2$	$\frac{M_1}{M_1+M_2}$	$\frac{M_2}{M_1+M_2}$	$m_2$ , moles	$m_1$ , moles	$m_1/m_2$	$m_2/m_1$	$\frac{m_1}{m_1+m_2}$ $\frac{m_2}{m_1+m_2}$
1308	Vinyl acetate	0.031	3.64	117.4	0.992	0.008	1.82	0.0211	166.3	0.006	0.994
1307	Vinyl acetate	0.153	3.47	22.7	0.961	0.039	11.18	0.130	24.4	0.041	0.961
1309	Vinyl acetate	1.68	1.37	0.815	0.688	0.312	60.75	0.706	1.40	0.504	0.665
1256	Methyl acrylate	0.031	3.64	117.4	0.992	0.008	12.51	0.145	22.5	0.041	0.957
1255	Methyl acrylate	0.153	3.49	22.8	0.961	0.039	48.30	0.562	3.29	0.304	0.767
1333	Methyl acrylate	2.00	1.29	0.645	0.393	0.607	97.4	1.145	0.0929	12.3	0.0750
1334	Methyl acrylate	2.00	1.22	0.610	0.379	0.621	99.1	1.150	0.0321	35.82	0.027
1276	Diethyl fumarate	0.306	2.94	9.6	0.925	0.075	65.4	0.380	1.24	0.306	0.765
1277	Diethyl fumarate	0.153	3.31	21.6	0.969	0.031	23.11	0.134	2.75	0.049	0.954
1279	Diethyl fumarate	0.84	1.66	1.97	0.815	0.185	80.9	0.470	0.68	1.42	0.691
1429	Diethyl fumarate	1.0	1.28	1.28	0.562	0.438	96.0	0.557	0.143	3.895	0.204
1429	Diethyl fumarate	1.0	1.28	1.28	0.562	0.438	95.5	0.554	0.160	3.463	0.224
1430	Diethyl fumarate	1.0	1.21	1.21	0.547	0.453	91.4	0.530	0.307	1.726	0.367
1432	Diethyl fumarate	1.0	1.00	1.00	0.500	0.500	99.0	0.574	0.0356	16.123	0.058
1282	Methyl methacrylate	0.031	3.63	117.0	0.992	0.008	13.4	0.134	23.0	0.043	0.958
1281	Methyl methacrylate	0.153	3.44	22.8	0.961	0.039	15.2	0.152	3.03	0.050	0.952
1283	Methyl methacrylate	0.84	2.39	2.84	0.815	0.185	86.8	0.867	0.471	1.84	0.352
	Methyl methacrylate	1.53	1.295	0.846	0.458	0.541	98.4	0.984	0.057	17.2	0.0547
1274	Diethyl maleate	0.031	3.61	116.4	0.992	0.008	16.11	0.093	2.99	0.031	0.971
1275	Diethyl maleate	0.84	1.69	2.01	0.815	0.185	86.21	0.501	0.49	1.02	0.494

toward alternation exists. Unfortunately, no compositions were reported containing more than 55 wt.-% ethylene, so no firm conclusions about  $r_1 = K^{aaa}/K^{aab}$  can be drawn. A similar difficulty in assessing  $r_1 = K^{aaa}/K^{aab}$  for the system ethylene ( $M_1$ )-vinyl chloride ( $M_2$ ) exists, since no compositions containing more than 40 wt.-% ethylene were reported. Their conclusions about ethylene-vinyl acetate do not suffer from this limitation. However, data at low vinyl fluoride contents in the system ethylene ( $M_1$ )-vinyl fluoride ( $M_2$ ) raise substantial doubts about the reported  $r_1$  value ( $4.39 \pm 0.77$ ) and suggest possibly large differences among  $K^{aaa}/K^{aab}$ ,  $K^{baaa}/K^{baab}$ , and  $K^{baa}/K^{bab}$ .

In our study, ethylene has been copolymerized with vinyl acetate, methyl acrylate, methyl methacrylate, diethyl maleate, and diethyl fumarate at 150°C. and pressures of 12,000 psi (Table I).

The calculated reactivity ratios for the best fit of the conventional copolymer composition equation are given in Table II.\*

TABLE II  
Reactivity Ratios

$M_1$	$M_2$	$r_1$	$r_2$	$r_1 r_2$
Ethylene	Vinyl acetate	1.01	1	1
Ethylene	Methyl acrylate	0.2	11	2.2
Ethylene	Methyl methacrylate	0.2	17	3.4
Ethylene	Diethyl maleate	0.25	10 <sup>a</sup>	2.5 <sup>a</sup>
Ethylene	Diethyl fumarate	0.25	10	2.5

\* The value for  $r_2$  in this system raises questions because of the experimental difficulties of producing copolymer at high levels of diethyl maleate. Other systems such as VAc-diethyl maleate would suggest that this  $r_2$  value may be lower. Our higher operating temperatures, however, would tend to increase  $r_2$ .

The fitting of data to the conventional equation unfortunately leads to a theoretical curve in the case of ethylene-methyl acrylate which is substantially divergent from experimental points (Fig. 1) particularly at high ethylene proportions in the charge. By employing Barb's equation,<sup>3</sup> where penultimate effects can be assessed:

$$n - 1 = r_1' x (r_1 x + 1) / (r_1' x + 1) \quad (1)$$

where  $x = A/B$  the ratio of monomers in the charge,  $n = a/b$  the ratio of monomers in the copolymer, and

$$r_1 = K^{aaa}/K^{aab}$$

$$r_1' = K^{baa}/K^{bab}$$

would be possible if addition of methyl acrylate to methyl acrylate free radical were unimportant at higher ethylene concentrations. However, since  $r_2 = 11$ , the more precise equation<sup>4</sup> is required.

\* The copolymer compositions were determined by calibrated infrared techniques devised by Dr. R. H. Hughes.

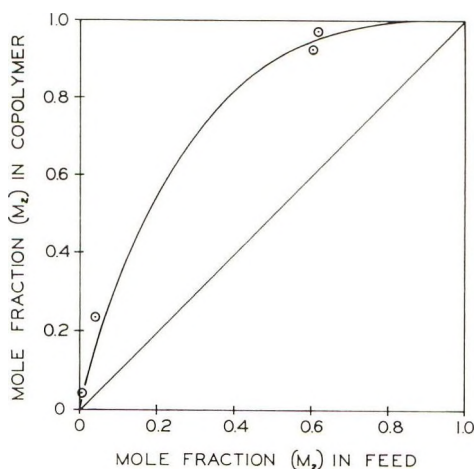


Fig. 1. Ethylene-methyl acrylate copolymerization.

$$\frac{a}{b} = \frac{[r_1' x (r_1 x + 1)/(r_1' x + 1)] + 1}{(r_2/x) + 1} \quad (2)$$

It was found that the latter equation fitted the data well with  $r_1 = 0.30$ ,  $r_1' = 0.15$ , and  $r_2 = 11$ .

The importance of the contribution to composition of additions of methyl acrylate monomer to methyl acrylate radical at various ethylene-methyl acrylate ratios is shown in the comparison given in Table III.

TABLE III

Monomer ratio $x(M_1/M_2)$	Copolymer ratio $n(m_1/m_2)$		
	Barb's equation	Eq. (2)	Experimental curve
49	14.8	12.1	11.5
24	7.4	5.08	6.15
15.7	5.0	2.94	3.76
5.0	2.075	0.65	0.85

A comparison of predictions of the conventional copolymer equation ( $r_1 = 0.20$ ,  $r_2 = 11$ ), eq. (2) ( $r_1 = 0.30$ ,  $r_1' = 0.10$ ,  $r_2 = 11$ ), and the preferred eq. (2) ( $r_1 = 0.30$ ,  $r_1' = 0.15$ ,  $r_2 = 11$ ) with experimental values is shown in Table IV.

It is of interest that, whereas (for  $r_1 = 0.30$ ,  $r_1' = 0.15$ ,  $r_2 = 11$ )  $r_1 r_2 = 3.3$ ,  $r_1' r_2 = 1.65$ . The latter result indicates a tendency toward random addition in copolymerization at other than high ethylene proportions. Our conclusions about  $r_1'(K^{\text{baa}}/K^{\text{bab}})$  suffer from lack of data in the intermediate range.

TABLE IV

Monomer Ratio $x(M_1/M_2)$	Copolymer ratio $n(m_1/m_2)$			Experimental curve
	Conventional copolymer eq. ( $r_1 = 0.2$ , $r_2 = 11$ )	Eq. (2) ( $r_1 = 0.30$ , $r_1 = 0.10$ , $r_2 = 11$ )	Eq. (2) ( $r_1 = 0.30$ , $r_1 = 0.15$ , $r_2 = 11$ )	
49	8.8	11.4	12.1	11.5
24	3.97	4.67	5.08	6.15
15.7	2.85	2.65	2.94	3.76
5	0.625	0.592	0.65	0.85
1	0.10	0.093	0.098	0.124

A related, but rather different situation exists in the system ethylene-methyl methacrylate (Fig. 2). The best fit of the data with the conventional copolymer equation leads to  $r_1 = 0.2$  and  $r_2 = 17$ . A remarkable  $r_1 r_2 = 3.4$  results. Such values do not give proper weight to low methyl methacrylate contents in copolymers in the intermediate regions.

Thus, a mole fraction of 0.721 methyl methacrylate in the copolymer is predicted at 0.185 mole fraction in the monomer whereas only 0.648 is actually obtained.

A better fit of the available data (Table I) is obtained with eq. (2) where

$$r_1 = K^{aaa}/K^{aab} = 0.2$$

$$r_1' = K^{baa}/K^{bab} = 1.0$$

$$r_2 = K^{bb}/K^{ba} = 17$$

It is apparent from Table V that the reactivity of methyl methacrylate for an ethylene free radical is considerably reduced if the penultimate unit

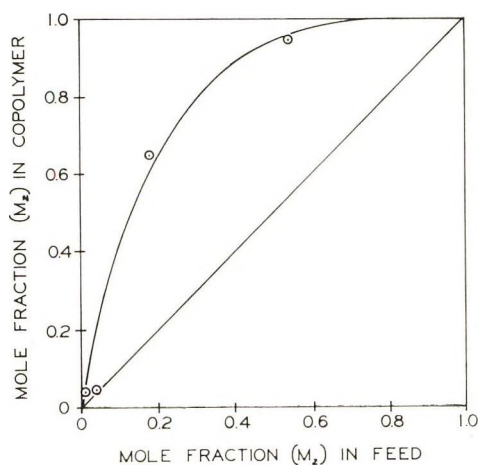


Fig. 2. Ethylene-methyl methacrylate copolymerization.

TABLE V  
 Ethylene-Methyl Methacrylate Copolymerization

Ratio of monomers <i>A/B</i>	Mole fraction of MMA in copolymer [ <i>b/(a + b)</i> ]		
	Points from expt. curve	$r_1 = K^{aa}/K^{ab} = 0.2,$ $r_2 = K^{bb}/K^{ba} = 17$	$K^{aaa}/K^{aab} = 0.2,$ $K^{baa}/K^{bab} = 1.0,$ $K^{bb}/K^{ba} = 17$
50	0.14	0.109	0.102
30	0.19	0.182	0.168
10	0.42	0.475	0.42
5	0.60	0.688	0.625
1	0.93	0.938	0.92

in the growing chain is methyl methacrylate. In the region where this effect is apparent, it is difficult to attribute the phenomenon to phase change effects. Much more feasible is the likelihood that polar and steric effects arising from penultimate methyl methacrylate units in the chain are much more readily transmitted across the terminal ethylene radical resulting in repulsion of adding methyl methacrylate monomer. Ethylene, as the smallest vinyl monomer and "chain unit component," exerts little shielding between penultimate methyl methacrylate unit and adding methacrylate monomer. On the other hand, it is doubtful that the addition of ethylene monomer to ethylene radical is influenced appreciably by whether the penultimate unit is ethylene or methyl methacrylate (except as this relates to "duality effects" involving ethylene monomer concentration). The consequence is that there is approximately 80% reduction in the reactivity of methyl methacrylate for an ethylene radical if the penultimate unit is methyl methacrylate rather than ethylene. This finding is of particular interest since methyl methacrylate does not contribute penultimate effects in most copolymerizations because of shielding effects of the other monomers involved, which, of course, have substituents not shared by ethylene.

Whether similar effects exist in the copolymerization of ethylene and methyl acrylate cannot be now ascertained because of the paucity of data in the intermediate region. It is probable that such effects are smaller (because of the greater configurational flexibility of methyl acrylate as a chain component).

It is interesting to examine the ternary system methyl methacrylate-methyl acrylate-ethylene and the three binary copolymer combinations which comprise it in the light of a new theory advanced by Ham.<sup>5</sup> This theory states that for systems of three monomers the following relationship holds:

$$P_{ab}P_{bc}P_{ca} = P_{ac}P_{cb}P_{ba} = \phi$$

where  $\phi$  is a constant. It follows that

$$r_{13}r_{21}r_{32} = r_{12}r_{31}r_{23} \quad (4)$$

Where the system is comprised of two conjugated monomers and one unconjugated monomer, experience has shown that  $\phi = 0.006$ . Thus, to examine the system methyl methacrylate ( $M_1$ )–methyl acrylate ( $M_2$ )–ethylene ( $M_3$ ) six reactivity ratios:  $r_{12}$ ,  $r_{21}$ ,  $r_{13}$ ,  $r_{31}$ ,  $r_{23}$ , and  $r_{32}$  are required to check the theory, or four ratios to predict the reactivity ratios for an untried combination. Thus, if  $r_{12}$ ,  $r_{21}$ ,  $r_{23}$ , and  $r_{32}$  are known,  $r_{13}$  and  $r_{31}$  can be predicted. For trial are chosen the values

$$r_{12} = 2.3 \text{ (Ref. 6)}$$

$$r_{23} = 11$$

$$r_{21} = 0.47 \text{ (Ref. 6)}$$

$$r_{32} = 0.2$$

From  $P_{ab}P_{bc}P_{ca} = 0.006$  and  $r_{12}r_{23}r_{31} = r_{13}r_{32}r_{21}$  it is determined that  $r_{13}$  (calcd.) = 16.4,  $r_{31}$  (calcd.) = 0.061;  $r_{13}$  (exptl.) = 17,  $r_{31}$  (exptl.) = 0.2.

The agreement with prediction for the copolymer system methyl methacrylate–ethylene is quite good, particularly when considered in the light of the “duality” of ethylene monomer. The high  $r_1r_2$  product (3.4) creates difficulties in generalization. If one accepts  $r_1$  and 0.1 and  $r_2 = 17$  ( $r_1r_2$  product = 1.7)

$$\begin{array}{cc} P_{ab}P_{bc}P_{ca} & = & P_{ac}P_{cb}P_{ba} \\ 0.0511 & & 0.00815 \end{array}$$

a result in good agreement with the prediction of equality and  $\phi = 0.006$ .

The copolymerization of ethylene and diethyl fumarate also exhibited anomalous behavior. The best fit of the experimental data (Fig. 3)<sup>7</sup> was afforded by eq. (3).

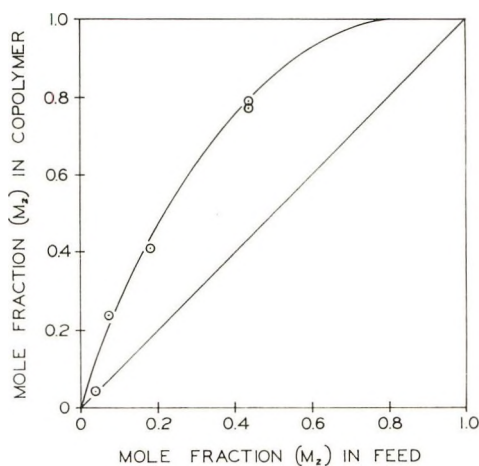


Fig. 3. Ethylene–diethyl fumarate copolymerization.

$$\frac{a}{b} = \frac{r_1''x\{[r_1x'(r_1x+1)/(r_1'x+1)]+1\}/(r_1''x+1)+1}{(r_2/x)+1} \quad (3)$$

where

$$r_1 = K^{aaaa}/K^{aaab} = 0.25$$

$$r_1' = K^{baaa}/K^{baab} = 2.0$$

$$r_1'' = K^{baa}/K^{bab} = 2.0$$

$$r_2 = K^{bb}/K^{ba} = 10.0$$

The necessity for invoking the effects of remote chain units of diethyl fumarate is shown by a comparison with theoretical points for  $r_1 = K^{aa}/K^{ab} = 0.25$  and  $r_2 = 10$  (Table VI).

TABLE VI  
Mole fraction in copolymer

Monomer ratio $x(A/B)$	Theoretical: $K^{aa}/K^{ab}$ $= 0.25$ , $K^{bb}/K^{ba}$ $= 10$	Theoretical: $K^{aaa}/K^{aab}$ $= 0.25$ , $K^{baa}/K^{bab}$ $= 1.0$ , $K^{bb}/K^{ba}$ $= 10$	Theoretical: $K^{aaa}/K^{aab}$ $= 0.25$ , $K^{baa}/K^{bab}$ $= 2.0$ , $K^{bb}/K^{ba}$ $= 10$	Theoretical: $K^{aaaa}/K^{aaab}$ $= 0.25$ , $K^{baaa}/K^{baab}$ $= 2.0$ , $K^{baa}/K^{bab}$ $= 2.0$ , $K^{bb}/K^{ba}$ $= 10.0$	Experi- mental curve
10	0.364	0.323	0.32	0.28	0.26
5	0.57	0.51	0.498	0.444	0.43
1	0.90	0.87	0.86	0.833	0.86

Here again there is evidence that a penultimate (or penpenultimate) diethyl fumarate in a growing chain ending in an ethylene radical actively repels adding diethyl fumarate monomer.

Our conclusions about the copolymerization of ethylene and vinyl acetate are in agreement with those of Zutty and Burkhart<sup>2</sup> ( $r_1 = 1.01$ ,  $r_2 = 1$ ). Copolymerization of ethylene and diethyl maleate yielded  $r_1 = 0.25$ ,  $r_2 = 10$ . Although our experiments were conducted at a relatively high temperature (150°C.)  $r_2$  is unusually high for a diethyl maleate copolymerization.

It is believed that the above conclusions are valid and proceed directly from the available data. However, an adequate means of assessing the "duality" of ethylene monomer in copolymerization will be required before a full understanding of ethylene copolymerization is possible.

## EXPERIMENTAL

### Equipment

The equipment used in carrying out the copolymerizations is illustrated in Figure 4. It consisted primarily of a 250-ml. Magna Dash autoclave, an injection pot, pump, strain gage, pressure recorder, temperature recorder, vent assembly, earphones, and cold trap assembly. The term Magna Dash refers to the type of agitation obtained from a small dasher moving verti-

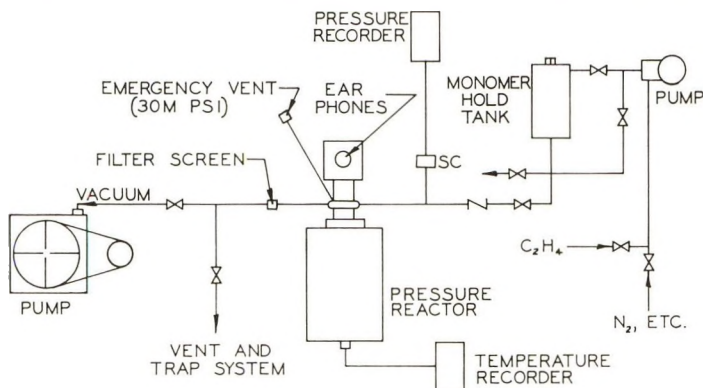


Figure 4.

cally up and down in the autoclave by a magnet cycling on and off exit the top section of the autoclave head. The autoclave internal temperature was recorded on a strip chart and regulated by steam pressure. A Baldwin-Lima 30,000 psi (max) strain cell was used. The pressure was recorded on an 8-hr. circular chart. The earphones were used to monitor the dasher action.

### Procedure

The stainless steel autoclave was solvent-cleaned, air-dried, and placed within the heating element. It was then sealed, purged twice with 2,000 psig ethylene, and pressured to 4,000 psig. The desired internal temperature of 150°C. was obtained. The autoclave was then pressured to 8,000 psig. The valve on the autoclave side of the injection pot was closed and the comonomer and catalyst placed in the injection pot. The additives were then swept into the reaction vessel while raising pressure to the desired value, which in all instances was 12,000 psig. The external heating was kept constant and the reaction allowed to proceed for 30 min. During the 30 min. period the reaction vessel was isolated from the ethylene source and the pressure drop recorded.

The reaction was terminated by venting into a large cylinder. The gas from the cylinder was passed through a cold trap for isolation of entrained liquids. Following each reaction elaborate procedures were followed in cleaning the reactor and dasher mechanism.

The copolymerizations were carried out at a temperature (150°C.), pressure (12,000 psig), and catalyst concentration ( $2.7 \times 10^{-4}$  moles of di-*tert*-butyl peroxide) which, for the homopolymerization of ethylene, resulted in a conversion of 6%. In the case of the copolymers the comonomers reached a higher conversion. The average total conversion, for example, of the methyl methacrylate runs, was about 7%. For methyl acrylate the average total conversion was about 13%.

### References

1. Boghetich, L., G. A. Mortimer, and G. W. Daues, paper presented before Polymer Division, 141st National American Chemical Society Meeting, Washington, D. C., March 1962; *Polymer Preprints*, **3**, No. 1 (1962).
2. Zutty, N. L., and R. D. Burkhart, in *Copolymerization*, G. E. Ham, Ed., Interscience, New York, 1964.
3. Barb, W. G., *J. Polymer Sci.*, **11**, 117 (1953).
4. Merz, E., T. Alfrey, and G. Goldfinger, *J. Polymer Sci.*, **1**, 75 (1946).
5. Ham, G. E., *J. Polymer Sci.*, **A2**, 2735 (1964).
6. Shima, M., and A. Kotera, *J. Polymer Sci.*, **A1**, 1115 (1963).
7. Ham, G. E., *J. Polymer Sci.*, **45**, 169 (1960).

### Résumé

On a étudié le comportement de l'éthylène lors de sa copolymérisation avec l'acrylate de méthyle, le méthacrylate de méthyle, l'acétate de vinyle, le fumarate de diéthyle, et le maléate de diéthyle et on donne les rapports de réactivité de ces différents systèmes. Pour tous ces systèmes étudiés sauf pour le système éthylène-acétate de vinyle, on constate d'importants écarts à l'équation classique de la copolymérisation et on les interprète sur la base d'effets pénultièmes et pen-pénultièmes non négligeables. L'accord entre les rapports de réactivité obtenus pour les systèmes éthylène-acrylate de méthyle et éthylène-méthacrylate de méthyle et les valeurs rapportées pour le système acrylate de méthyle-méthacrylate de méthyle est mis en évidence par l'application de la relation  $P_{ab}P_{bc}P_{ca} = P_{ac}P_{cb}P_{ba}$ .

### Zusammenfassung

Das Verhalten von Äthylen bei der Copolymerisation mit Methylacrylat, Methylmethacrylat, Vinylacetat, Diäthylfumarat, und Diäthylmaleat wurde untersucht und Reaktivitätsverhältnisse für diese Systeme mitgeteilt. Es treten bei allen untersuchten Systemen mit Ausnahme von Äthylen-Vinylacetat charakteristische Abweichungen von der konventionellen Copolymerisationsgleichung auf, die auf wesentliche Einflüsse der vorletzten und vorvorletzten Kettenglieder zurückgeführt werden. Die Konsistenz der im System Äthylen-Methylacrylat und Äthylen-Methylmethacrylat auftretenden Reaktivitätsverhältnisse mit Literaturwerten für Methylacrylat-Methylmethacrylat wird anhand der Beziehung  $P_{ab}P_{bc}P_{ca} = P_{ac}P_{cb}P_{ba}$  nachgewiesen.

Received October 8, 1963

## Proof of Validity of Expanded Copolymerization Equations

GEORGE E. HAM, *Research Center, Spencer Chemical Company, Merriam, Kansas*

### Synopsis

Generalized copolymerization equations which accounted for wide deviations from conventional copolymerization behavior of numerous systems involving highly polar or sterically hindered monomers had been previously proposed. This paper offers, for the first time, rigorous proof of the expanded equations for systems where one monomer is incapable of addition to its own radical. Employing these equations, effects as far removed as four units from the end of the growing chain can be accounted for.

In a series of papers<sup>1-4</sup> generalized copolymerization equations were proposed to account for the wide deviations from conventional copolymerization behavior observed for numerous systems involving highly polar or sterically hindered monomers. Excellent agreement between these new expanded equations and a substantial number of experimental systems was demonstrated. In addition to the experimental evidence the logical progressions implicit in these equations, proceeding as they did from the time-tested conventional copolymerization equation and the penultimate equation,<sup>5</sup> were presented as a reasonable basis for their validity.

The purpose of this paper is to offer for the first time rigorous proof of the expanded equations with special emphasis on systems where one monomer is incapable of addition to its own radical because of polar and steric considerations. For highly polar monomers which exhibit enhanced repulsion arising from more distant units, the equations allow for extra "spacer" units as required. This phenomenon has been shown to be related to the shielding power (mainly size) of the other monomer involved in the copolymerization.

For systems including very bulky monomers, such as  $\alpha$ -methylstyrene, free radical copolymerization allows addition of  $\alpha$ -methylstyrene to a radical ending in  $\alpha$ -methylstyrene only when highly polar monomers such as acrylonitrile and fumaronitrile are present. Here it was shown that  $\alpha$ -methylstyrene could not add to a sequence of three  $\alpha$ -methylstyrene units in free radical copolymerization,<sup>3</sup> and expanded equations for this circumstance were offered. Proofs of these equations are now given.

Maleic anhydride copolymerizations had been particularly difficult to treat theoretically before the offering of the expanded equations. Proofs

are now offered for equations matching these systems (such as styrene-maleic anhydride) where units as far back from the growing radical end as four (including the terminal unit) are effective in regulating competition of monomers for the radical.

For the proof of the expanded equations it is necessary to employ the theory of regular Markov chains. In a sequential process such as the addition of monomers to a growing chain in which a certain probability is associated with each addition of monomer, the probabilities of being in each of the possible states after  $n$  additions is  $\pi \mathbf{P}^n$  where  $\pi$  is the probability of the first addition and  $\mathbf{P}$  is a regular transition matrix. Furthermore, for any probability vector  $\pi$ ,  $\pi \mathbf{P}^n$  approaches the limiting vector  $\alpha$  as  $n$  approaches infinity. Since the number of monomer additions in a high polymer is large, we may safely say that the probabilities of being in a certain state after  $n$  additions is  $\alpha$ , the limiting vector for a Markov chain determined by  $\mathbf{P}$ , the regular transition matrix.

For copolymer systems where significant influences on the additivity of monomers can be effected by units as far back from the growing end as four (including influences of less distant units) a regular transition matrix is proposed. The only limitation is the assumption that B cannot add to a radical ending in B. For simplicity we have employed a binary number system for designation of all possible initial and final states. Thus, the initial state —aaaa· is designated as 0 and if monomer B is added, the resulting state, —aaab·, is designated as 1. Similarly, the initial state —baba· is 10 and, if monomer A is added, the resulting state —abaa·, is designated as 4. Thus  $P_{01}$  or  $1 - P_{00}$  is the probability associated with the former transition and  $P_{10-4}$  is that associated with the latter. It is readily apparent that all possible states of chain segments of four units, initial and final, may be designated by the numbers 0, 1, 2, . . . , 15. However, since two B's in sequence are ruled out, the states are limited to 0, 1, 2, . . . , 10. The transition matrix is

		Initial									
		0	1 2	3 4	5 6 7 8	9	10				
Final	0	$P_{00}$	0 0	0 0	0 0 0 $P_{80}$	0	0				
	1	$1 - P_{00}$	0 0	0 0	0 0 0 $1 - P_{80}$	0	0				
	2	0	1 0	0 0	0 0 0 0	1	0				
	3	0	0 0	0 0	0 0 0 0	0	0				
	4	0	0 $P_{24}$	0 0	0 0 0 0	0	$P_{10-4}$				
	5	0	0 1 $- P_{24}$	0 0	0 0 0 0	0	1 $- P_{10-4}$				
	6	0	0 0	0 0	0 0 0 0	0	0				
	7	0	0 0	0 0	0 0 0 0	0	0				
	8	0	0 0	0 $P_{48}$	0 0 0 0	0	0				
	9	0	0 0	0 1 $- P_{48}$	0 0 0 0	0	0				
	10	0	0 0	0	1 0 0 0	0	0				

For convenience all states expressed above are shown: 0, —aaaa—; 1, —aaab—; 2, —aaba—; 3, —aabb—; 4, —abaa—; 5, —abab—; 6, —abba—; 7, —abbb—; 8, —baaa—; 9, —baab—; 10, —baba—.

Since we need to find the limiting vector  $\alpha(a_0, a_1, a_2, a_4, a_5, a_8, a_9, a_{10})$  we must determine a probability vector such that  $\alpha P = \alpha$ . This statement is equivalent to saying that eqs. (1)–(9) must be satisfied for the system described by our matrix.

$$1 = a_0 + a_1 + a_2 + a_4 + a_5 + a_8 + a_9 + a_{10} \quad (1)$$

$$a_0 = P_{00}a_0 + P_{80}a_8 \quad (2)$$

$$a_1 = (1 - P_{00})a_0 + (1 - P_{80})a_8 \quad (3)$$

$$a_2 = a_1 + a_9 \quad (4)$$

$$a_4 = P_{24}a_2 + P_{10-4}a_{10} \quad (5)$$

$$a_5 = (1 - P_{24})a_2 + (1 - P_{10-4})a_{10} \quad (6)$$

$$a_8 = P_{48}a_4 \quad (7)$$

$$a_9 = (1 - P_{48})a_4 \quad (8)$$

$$a_{10} = a_5 \quad (9)$$

Solved in terms of  $a_1$  the following values result:

$$a_0 = \frac{P_{80}a_1}{1 - P_{00}} \quad (10)$$

$$a_1 = a_1 \quad (11)$$

$$a_2 = a_1 + [(1 - P_{48})a_1/P_{48}] \quad (12)$$

$$a_4 = a_1/P_{48} \quad (13)$$

$$a_5 = \frac{(1 - P_{24})}{P_{10-4}} \left[ a_1 + \frac{(1 - P_{48})a_1}{P_{48}} \right] \quad (14)$$

$$a_8 = a_1 \quad (15)$$

$$a_9 = (1 - P_{48})a_1/P_{48} \quad (16)$$

$$a_{10} = \frac{(1 - P_{24})}{P_{10-4}} \left[ a_1 + \frac{(1 - P_{48})a_1}{P_{48}} \right] \quad (17)$$

Since we are at the moment only interested in the copolymer composition  $a/b$ , this partial solution suffices.

$$a/b = (a_0 + a_2 + a_4 + a_8 + a_{10})/(a_1 + a_5 + a_9) \quad (18)$$

It is apparent that the numerator contains states which end in  $a$ 's, i.e., "generate"  $a$ 's and the denominator, states which generate  $b$ 's. Substitution of values for  $a_0 - a_{10}$  expressed in terms of  $a_1$  leads to the absolute copolymer composition (the  $a_1$ 's cancel).

$$\frac{a}{b} = 1 + \frac{[(1 - P_{00})P_{48} + P_{80}P_{48} + 1 - P_{00}]P_{10-4}}{(P_{10-4} - P_{24} + 1)(1 - P_{00})} \quad (19)$$

Expressed in simpler nomenclature where the final unit in the subscript represents adding monomer

$$\frac{a}{b} = 1 + \frac{P_{babaa}(P_{aaaab}P_{abaaa} + P_{baaaa}P_{abaaa} + P_{aaaab})}{P_{aaaab}(P_{babaa} - P_{aabaa} + 1)} \quad (20)$$

This equation may be used for any systems (B not adding to B) where effects exist in any region within the last four units in a growing chain. In the case of styrene-fumaronitrile substantial effects arise from fumaronitrile as the fourth unit as well as the penultimate unit from the chain end, but no effects arise beyond two terminal adjacent a units, hence eq. (20) becomes

$$\frac{a}{b} = 1 + \frac{P_{babaa}(P_{aab}P_{aaa} + P_{aan}P_{aaa} + P_{aab})}{P_{aab}(P_{babaa} - P_{aabaa} + 1)} \quad (21)$$

which reduces to

$$a/b = 1 + [P_{babaa}/P_{aab}(P_{aabab} + P_{babaa})] \quad (22)$$

This equation is readily shown to be equivalent to eq. (2) of the previous paper<sup>2</sup>

$$n - 1 = \frac{[r_1''x(r_1'x + 1)/(r_1''x + 1)](r_1x + 1)}{[r_1''x(r_1'x + 1)/(r_1''x + 1)] + 1} \quad (23)$$

It has been shown for the system styrene-fumaronitrile<sup>2</sup> with excellent agreement with eq. (23)

$$\begin{aligned} r_1 &= K^{aaa}/K^{aab} = 0.08 \\ r_1' &= K^{aabaa}/K^{aabab} = 0.3 \\ r_1'' &= K^{baabaa}/K^{babab} = 4.0 \end{aligned}$$

For the case of copolymer systems showing long range effects with respect to bunched a's, i.e., where additions to —BAA· are substantially different from additions to —AAA· eq. (20) may be partially reduced to

$$a/b = 1 + [P_{babaa}(P_{baaa} + P_{aaa})/P_{aaab}(P_{aabab} + P_{babaa})] \quad (24)$$

by equation  $P_{aaaab} = P_{aaab}$ ,  $P_{abaaa} = P_{baaa}$ ,  $P_{baaaa} = P_{aaaa}$ ,  $P_{aaaab} = P_{aaab}$ , and  $P_{abaab} = P_{baab}$ . This equation is readily shown to be the equivalent of eq. (4) of the previous paper<sup>3</sup>

$$n - 1 = \frac{[r_1'''x(r_1''x + 1)/(r_1'''x + 1)]\{[r_1'x(r_1x + 1)/(r_1'x + 1)] + 1\}}{[r_1'''x(r_1''x + 1)/(r_1'''x + 1)] + 1} \quad (25)$$

which exhibited close correlation with data for the system  $\alpha$ -methylstyrene-fumaronitrile. Reactivity ratios were found<sup>3</sup> to be

$$\begin{aligned}
 r_1 &= K^{aaaa}/K^{aaab} = 0 \\
 r_1' &= K^{baaa}/K^{baab} = 0.05 \\
 r_1'' &= K^{aaba}/K^{aabb} = 0.12 \\
 r_1''' &= K^{babaa}/K^{babab} = 0.17
 \end{aligned}$$

The broad utility of eq. (20) is further demonstrated by application to the system styrene-maleic anhydride. Here effects on reactivity arise only from single maleic anhydride units in segments ending growing chains but at considerable distance from the growing end (up to four units). In this case eq. (20) is reduced by equating  $P_{abaaa} = P_{baaa}$ ,  $P_{abab} = P_{baab}$ ,  $P_{babaa} = P_{baa}$ , and  $P_{aaba} = P_{baa}$  to yield

$$\frac{a}{b} = 1 + \frac{P_{baa}(P_{aaab}P_{baaa} + P_{baaaa}P_{baaa} + P_{aaaab})}{P_{aaab}(P_{baa} - P_{baa} + 1)} \quad (26)$$

$$a/b = 1 + [P_{baa}(P_{aaab}P_{baaa} + P_{baaaa}P_{baaa} + P_{aaaab})/P_{aaab}] \quad (27)$$

This expression is the same as eq. (6) of the previous paper<sup>4</sup>

$$n - 1 = r_1'''x \left\{ \frac{r_1''x \left[ \frac{r_1'x(r_1x + 1)}{r_1'x + 1} + 1 \right]}{r_1''x + 1} + 1 \right\} / (r_1'''x + 1) \quad (28)$$

which allowed a good fit of Barb's data<sup>6</sup> and made possible the calculation of reactivity ratios<sup>4</sup>

$$\begin{aligned}
 r_1 &= K^{aaaa}/K^{aaab} = 0.0084 \\
 r_1' &= K^{baaa}/K^{baab} = 0.01 \\
 r_1'' &= K^{aaba}/K^{aabb} = 0.0275 \\
 r_1''' &= K^{babaa}/K^{babab} = 0.063
 \end{aligned}$$

Finally, it is appropriate to point out that all of the expressions simplified from eq. (20), including eq. (20) may be reduced to the simple penultimate equation:

$$n - 1 = \frac{r_1'x(r_1x + 1)}{r_1'x + 1} \quad (29)$$

where  $r_1 = K^{aaa}/K^{aab}$ ,  $r_1' = K^{baa}/K^{bab}$ .

This is shown most simply from eq. (22) by equating  $P_{babaa} = P_{baa}$  and  $P_{aaba} = P_{bab}$  to yield eq. (29).

### References

1. Ham, G. E., *J. Polymer Sci.*, **45**, 169 (1960).
2. Ham, G. E., *J. Polymer Sci.*, **45**, 177 (1960).
3. Ham, G. E., *J. Polymer Sci.*, **45**, 183 (1960).
4. Ham, G. E., *J. Polymer Sci.*, **54**, 1 (1961).
5. Merz, E., T. Alfrey, and G. Goldfinger, *J. Polymer Sci.*, **1**, 75 (1946).
6. Barb, W. G., *J. Polymer Sci.*, **11**, 117 (1953).

### Résumé

On avait proposé précédemment des équations généralisées de copolymérisation qui s'accordaient avec les grands écarts à la copolymérisation classique, dus au comportement de nombreux systèmes composés des monomères hautement polaires ou encombrés stériquement. Cet article apporte pour la première fois, une preuve rigoureuse des équations généralisées pour les systèmes constitués par un monomère incapable de s'additionner à son propre radical. Sur la base de ces équations on peut justifier les effets à longue distance qui s'étendent jusqu'à la 4ème unité à partir de l'extrémité de la chaîne en croissance.

### Zusammenfassung

Verallgemeinerte Copolymerisationsgleichungen, die grosse Abweichungen vom normalen Copolymerisationsverhalten zahlreicher Systeme mit hochpolaren oder sterisch gehinderten Monomeren erklären können, wurden schon früher angegeben. Diese Arbeit ermöglicht zum ersten Mal eine strenge Überprüfung der entwickelten Gleichungen für Systeme, bei denen ein Monomeres zur Addition an sein eigenes Radikal unfähig ist. Bei Anwendung dieser Gleichungen kann Einflüssen von Gruppen, die bis zu vier Einheiten vom Ende der wachsenden Kette entfernt sind, Rechnung getragen werden.

Received July 15, 1963

## Radiation-Induced Polymerization of 2-Methyl-5-vinyl-pyridine

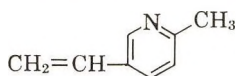
YONEHO TABATA and HIROKIMI KITANO, *Department of Nuclear Engineering and Department of Industrial Chemistry, University of Tokyo, Tokyo*, and HIROSHI SOBUE, *Nishin Spinning Co., Tokushima, Japan*

### Synopsis

Radiation-induced polymerization of 2-methyl-5-vinylpyridine was investigated in bulk in the temperature region of 50 to  $-196^{\circ}\text{C}$ . The activation energy was found to be 5.7 kcal./mole for the liquid-phase polymerization and 0.3 kcal./mole for the solid-phase polymerization. It was observed that the rate of polymerization is proportional to the square root of the dose rate in the liquid-phase polymerization and is proportional to the dose rate in the solid-phase polymerization. DPPH and benzoquinone inhibited strongly the liquid-phase polymerization, while the same inhibitors did not inhibit appreciably the solid-phase polymerization. On the other hand, the solid-phase polymerization was completely inhibited by acetone, pyridine, and methanol, while the liquid-phase polymerization was not inhibited by the same additives. It was concluded that the polymerization in the liquid phase proceeds by a radical mechanism and the polymerization in the solid phase proceeds by a nonradical mechanism, probably an ionic or electronic mechanism.

### Introduction

Though the catalytic polymerization of 2-methyl-5-vinylpyridine



has been carried out by several workers,<sup>1</sup> the polymerization initiated by high energy irradiation of the monomer does not appear to have been investigated.

We have investigated the radiation-induced bulk polymerization of the monomer in the liquid and solid state in the temperature range of 50 to  $-196^{\circ}\text{C}$ .

### Experimental

The 2-methyl-5-vinylpyridine was a sample obtained from Showa Denko Co. Ltd. The monomer was purified by distillation under reduced pressure in a nitrogen atmosphere just prior to use. The ampule containing solid monomer at  $-78^{\circ}\text{C}$ . was evacuated to  $10^{-2}$ – $10^{-3}$  mm. Hg. The polymerization was initiated by irradiation with  $\gamma$ -rays from a  $\text{Co}^{60}$  source.

Irradiation was carried out over the dose rate range of  $2.5 \times 10^4$  to  $3.1 \times 10^5$  r/hr. To determine yields of the polymer, the irradiated samples were opened at low temperature and petroleum ether was poured into the opened ampule. The polymer was separated by ultracentrifugation, the residue washed with petroleum ether, and weighed after drying at  $40^\circ\text{C}$ . The viscosity of the polymer was measured in methanol at  $25^\circ\text{C}$ . The molecular weight  $M$  of the polymer was determined from the relation:<sup>2</sup>

$$[\eta] = 1.8 \times 10^{-4} M^{0.83}$$

where  $[\eta]$  is the intrinsic viscosity (in units of milliliters/gram). X-ray diffraction of the polymer also was measured.

### Results

The conversion at  $25^\circ\text{C}$ . is shown in Figure 1 over the dose rate range of  $4.9 \times 10^4$ – $3.1 \times 10^5$  r/hr. An induction period was not observed in the polymerization. The conversion increases linearly with irradiation time up to about 10% yield; the rate of polymerization is then slowed down, but

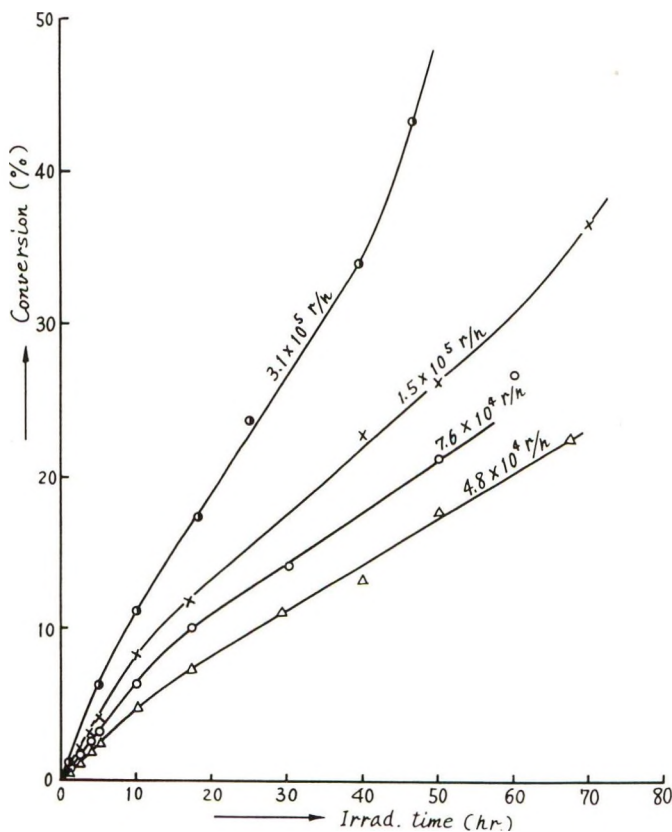


Fig. 1. Relation between per cent conversion and irradiation time in the liquid-state polymerization at  $25^\circ\text{C}$ .

in the final step of the polymerization, the rate is remarkably accelerated.

The dose rate dependency of the polymerization rate was investigated in the liquid-state polymerization at 25°C. The relation between the initial rate of polymerization  $R_p$  and the dose rate  $I$  is shown in Figure 2 on a logarithmic scale. From the result, the following relation was obtained.

$$R_p = 4.3 \times 10^{-8} I^{0.5}$$

The proportionality of  $R_p$  to  $I^{0.5}$  indicates that the polymerization in the liquid state proceeds by a typical radical mechanism.

The temperature dependence of the polymerization rate in liquid- and solid-state polymerizations was determined. The relation between the polymer yield and the irradiation time in both liquid- and solid-state polymerizations are shown in Figures 3 and 4, respectively.

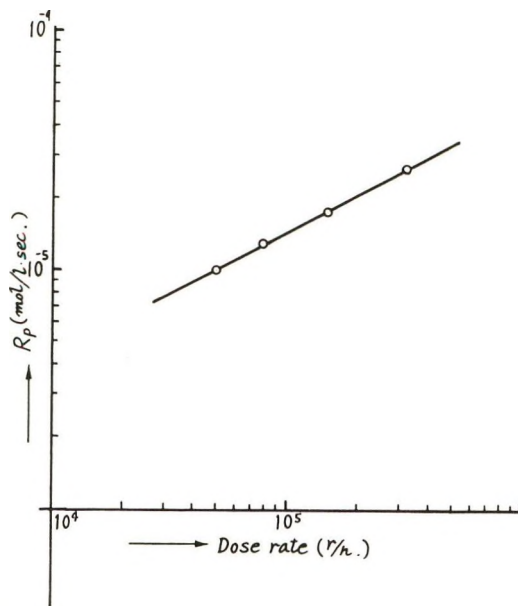


Fig. 2. Dose rate dependency of the initial polymerization rate at 25°C.

It is obvious that the temperature at which the irradiations were carried out had a marked effect on the polymerization in the region near room temperature but a minor effect at lower temperatures. The relation between the logarithmic rate of polymerization and the reciprocal absolute polymerization temperature is shown in Figure 5.

From this relation, an overall energy of activation of 5.7 kcal./mole was obtained for the liquid-phase polymerization, and about 0.3 kcal./mole for the solid-state polymerization.

The effects of several additives on the polymerization are summarized in Table I.

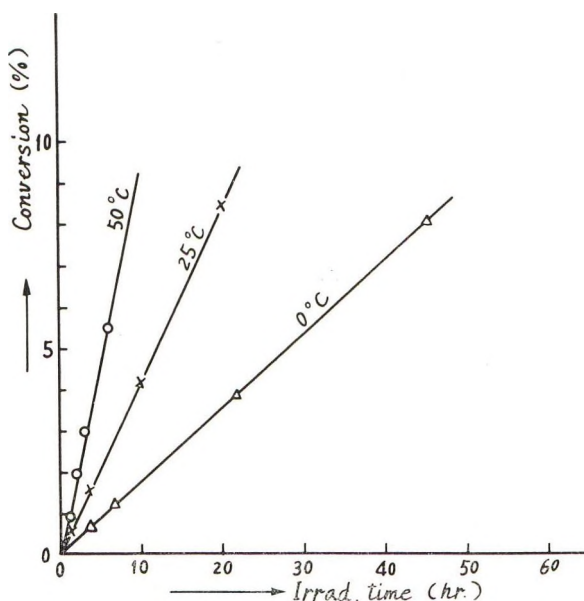


Fig. 3. Relation between per cent conversion and the irradiation time in the liquid-phase polymerization at various temperatures. Dose rate was  $1 \times 10^5$  r/hr.

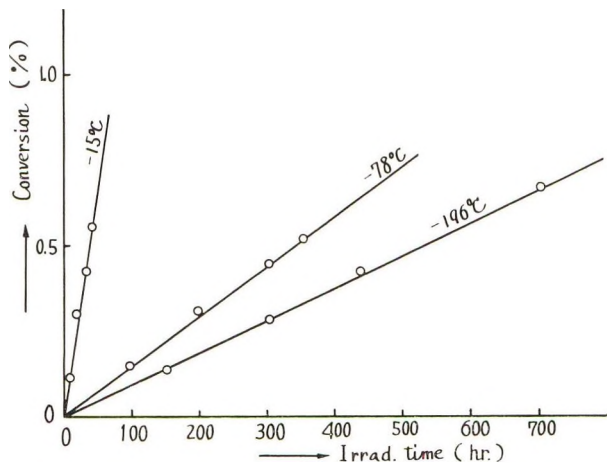


Fig. 4. Relation between per cent conversion and irradiation time in solid-phase polymerization at  $-15$ ,  $-78$ , and  $-196^\circ\text{C}$ . Dose rate was  $7.3 \times 10^4$  r/hr.

The radical inhibitors, DPPH and benzoquinone, are easily soluble in the monomer. The solid monomer containing the radical inhibitors was obtained by cooling the homogeneous solution. The weight fraction of the additives was 1%.

It is obvious from these results that the radical inhibitors strongly retard or inhibit the polymerization in the liquid-phase polymerization, while DPPH retards only about 40% and benzoquinone does not retard at all in

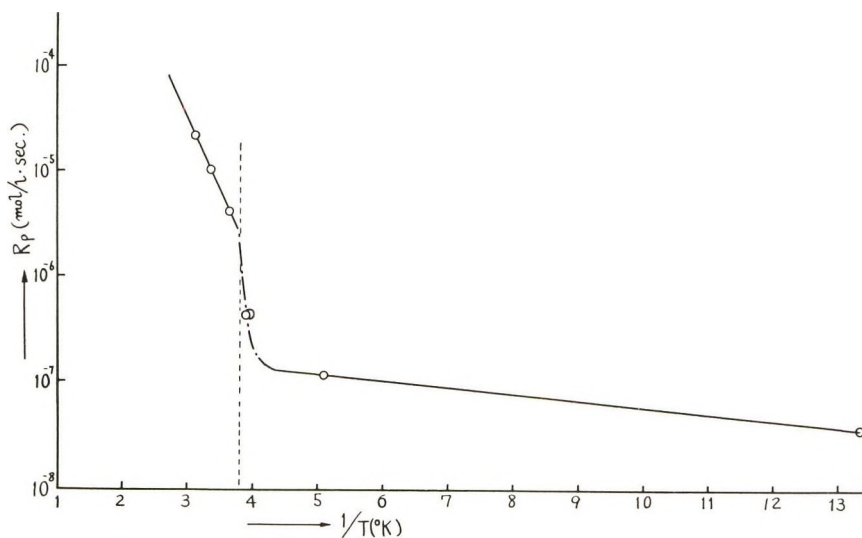


Fig. 5. Relation between the logarithmic rate of polymerization and the reciprocal, absolute, polymerization temperature.

TABLE I  
Effects of Several Additives on the Polymerization of 2-Methyl-5-vinylpyridine

Irradiation conditions	Additive	Relative yield
Dose rate $7.3 \times 10^4$ r/hr.; total dose $1.5 \times 10^6$ r; liquid phase at $20^{\circ}\text{C}$ .	None	1.00
	Methanol	1.11
	Pyridine	0.93
	Acetone	0.98
	DPPH	0.016
	Benzoquinone	0.022
Dose rate $7.3 \times 10^4$ r/hr.; total dose $1.1 \times 10^7$ r; solid phase at $-78^{\circ}\text{C}$ .	None	1.00
	Methanol	0
	Pyridine	0
	Acetone	0
	DPPH	0.63
	Benzoquinone	1.00

the solid-phase polymerization. On the other hand, methanol, pyridine, and acetone do not affect polymerization in the liquid state, while the same additives completely inhibit the polymerization in the solid state.

It is well known that a post-effect is usually observed in solid-state polymerizations. In this experiment, a post-polymerization was observed, more or less, if the monomer irradiated in solid phase was left at room temperature; the effect was negligible, however, if the irradiated monomer was dissolved in petroleum ether at about  $-40$  to  $-50^{\circ}\text{C}$ . This is confirmed also by the fact that the polymerization yield from the monomer containing benzoquinone (1%) is just the same as that from the pure monomer.

The dose rate dependence of the degree of polymerization was investigated in the liquid-phase polymerization. A log-log plot of the degree of polymerization,  $P$ , against the dose rate,  $I$ , is shown in Figure 6. The relation between  $1/P$  and the initial rate of polymerization is also shown in Figure 7.

It is obvious from these results that the degree of polymerization decreases exponentially with the dose rate, and the reciprocal degree of poly-

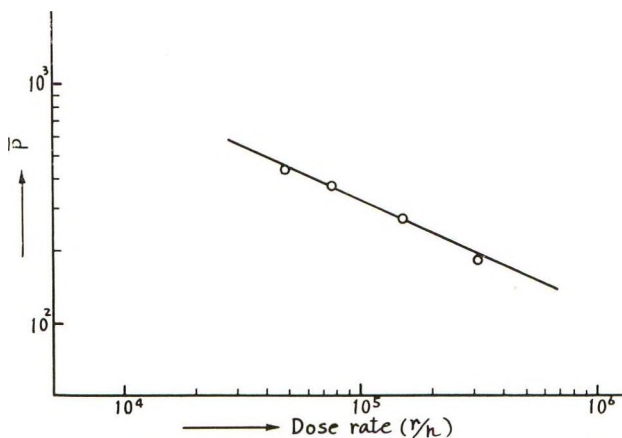


Fig. 6. Log-log plot of the degree of polymerization,  $P$ , against the dose rate,  $I$ .

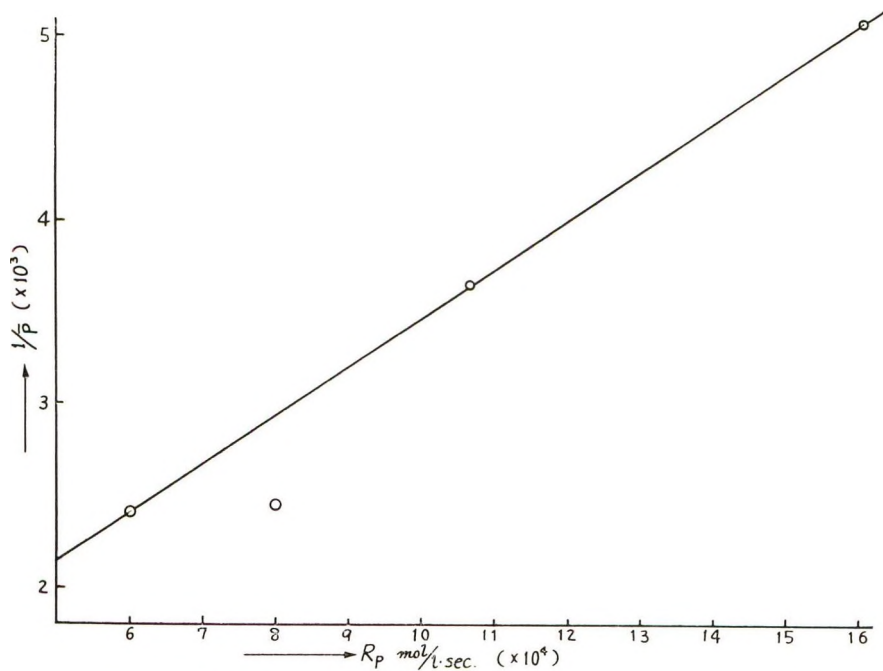


Fig. 7. Relation between  $1/P$  and the initial rate of polymerization.

merization  $1/P$  increases linearly with the initial rate of polymerization.

The x-ray diffraction patterns of the polymers indicated that the polymer obtained is amorphous.

### Discussion

In the polymerization of 2-methyl-5-vinylpyridine induced by  $\gamma$ -irradiation, the relation between the logarithmic polymerization rate and reciprocal absolute polymerization temperature in the liquid and solid states is very different from that in the cases of polymerization of acrylonitrile,<sup>3</sup> methacrylonitrile,<sup>4</sup> butadiene,<sup>5</sup> styrene,<sup>6</sup> hexamethylcyclotetrasiloxane,<sup>7</sup> and trioxane.<sup>8</sup>

At  $-17^{\circ}\text{C}$ . 2-methyl-5-vinylpyridine is in the glassy state, and the rate of polymerization at that temperature deviates from the Arrhenius plots in the liquid- and solid state polymerizations. The rate of polymerization in the transition region at  $-17^{\circ}\text{C}$ . has a value intermediate between that in the liquid and solid phases, indicating that the glassy state has an intermediate characteristic. The melting point of the monomer is  $-13.8 \pm 0.3^{\circ}\text{C}$ . In the polymerization at  $-17^{\circ}\text{C}$ ., although the monomer is in solid state before irradiation, the solid monomer gradually becomes a viscous fluid on irradiation. Apparently, the solid monomer is liquidized by irradiation for about 40 hr. at a dose rate of  $7 \times 10^4$  r/hr. This phenomenon appears to be due to the depression of the melting point of the monomer by the formation of polymer. We observed the same phenomenon in the radiation-induced polymerization of chloral at  $-78^{\circ}\text{C}$ ., that is, initially the monomer is in the solid state at  $-78^{\circ}\text{C}$ ., but the solid monomer is liquidized by irradiation for 20–30 hr. at a dose rate of about  $5 \times 10^4$  r/hr.<sup>9</sup>

Although the activation energy for the polymerization of 2-methyl-5-vinylpyridine is very small in the solid state as in the cases of acrylonitrile, methacrylonitrile, and butadiene, the rate of polymerization is much lower than in liquid-phase polymerization, in contrast with the behavior of the other monomers described above.

The lower rate of polymerization in the solid state is probably due to a peculiar state of aggregation of the monomer at low temperature. The solid monomer at low temperature may contain a major proportion of sterically nonpolymerizable region and a small quantity of polymerizable region in other words, the solid-state polymerization of 2-methyl-5-vinylpyridine may be characterized by a more negative entropy change than that of acrylonitrile, methacrylonitrile, or butadiene.

DPPH and benzoquinone are known to cause inhibition or retardation of free radical polymerizations but not to have any effect on ordinary ionic polymerizations. Although DPPH and benzoquinone inhibit or retard strongly the liquid-phase polymerization, the same inhibitors do not inhibit appreciably the solid-state polymerization. These results indicate that the polymerization in the liquid phase proceeds by a radical mechanism.

The activation energy, the dose rate dependencies of the polymerization rate, the degree of polymerization, and the inhibition of the polymerization by DPPH and benzoquinone all confirm that the ionizing radiation-induced polymerization in the liquid state proceeds by a radical mechanism.

The dose rate dependency of the polymerization rate in the solid state at  $-196^{\circ}\text{C}$ . is shown in Figure 8. This indicates that the rate of polymerization is approximately proportional to the dose rate and suggests that the termination may be a unimolecular reaction.

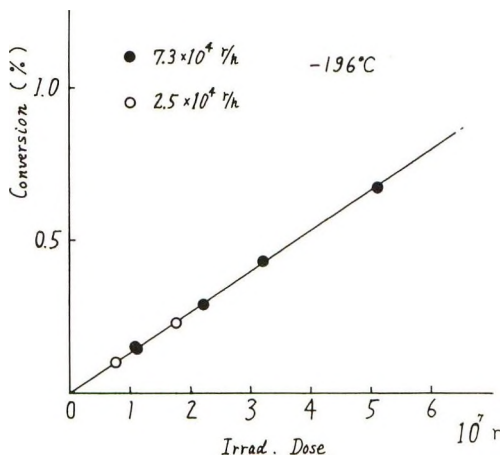


Fig. 8. Relation between per cent conversion and irradiation dose in the solid-state polymerization at  $-196^{\circ}\text{C}$ .

It is quite interesting that in the solid-state polymerization of the monomer at  $-78^{\circ}\text{C}$ ., the polymerization can be completely inhibited by addition of acetone, pyridine, and methanol, even in very small amounts (1 wt.-% based on monomer). This suggests that even in the solid state of the monomer, the molecules can diffuse into each other in the solid phase at  $-78^{\circ}\text{C}$ . or that a long-range energy transfer can take place in the solid system. We have observed in other experiments<sup>10</sup> that a radical postpolymerization of acrylonitrile in the temperature region of the melting point ( $-83^{\circ}\text{C}$ .) to the transition temperature of the monomer ( $-132^{\circ}\text{C}$ .) could be completely inhibited by radical scavengers. Recently, Kuri<sup>11</sup> has also observed that the radiation-induced copolymerization of styrene with sulfur dioxide is markedly inhibited by DPPH in the solid state of the monomers at  $-78^{\circ}\text{C}$ .

These experimental results indicate that the diffusion of molecules or an intermolecular energy transfer in the solid phase would play an important role for these polymerizations.

In the polymerization of 2-methyl-5-vinylpyridine, it seems to be possible also that a radical post-polymerization in the solid phase, if it occurs, could be inhibited by radical scavengers, as in the case of acrylonitrile. It is quite evident that the post-polymerization which would occur during

melting of the irradiated monomer can be excluded by the presence of the scavengers.

As described above, the polymerization of 2-methyl-5-vinylpyridine in the solid state was not inhibited by radical scavengers. On the other hand, the polymerization was completely inhibited by acetone, pyridine, and methanol.

It is obvious from these results that the polymerization in the solid state does not proceed by a radical mechanism in an ordinary sense.

The authors believe that in such solid-state polymerization at low temperature, there are two possibilities for the polymerization mechanism: one is an ionic type polymerization in which a propagating cation or anion plays an important role for the polymerization; the other is an electronic type polymerization (electronic polymerization) proposed by us<sup>12</sup> in which both the geometrical structure and the electronic state of the crystal as a whole are very important for the polymerization. The latter is a kind of cooperative phenomenon.

### References

1. Onyon, P. F., *Trans. Faraday Soc.*, **51**, 3400 (1959); Dannley, *J. Polymer Sci.*, **19**, 285 (1956).
2. Sato and Yamamoto, paper presented at Annual Meeting of Society of High Polymer Chemistry, Tokyo, 1958.
3. Sobue, H., and Y. Tabata, *J. Polymer Sci.*, **43**, 459 (1960).
4. Tabata, Y., and H. Sobue, *J. Polymer Sci.*, **45**, 469 (1960).
5. Tabata, Y., H. Sobue, and E. Oda, *J. Phys. Chem.*, **65**, 1645 (1961).
6. Chapiro, A., and V. Stannett, *J. Chim. Phys.*, **57**, 35 (1960).
7. Lawton, E. J., W. T. Grubb, and J. S. Balwit, *J. Polymer Sci.*, **19**, 355 (1956).
8. Okamura, S., K. Hayashi, and Y. Nakamura, *Doitai to Hoshasen*, **3**, 416 (1960).
9. Tabata, Y., and H. Shibano, unpublished data.
10. Tabata, Y., et al., papers presented at 4th Symposium on Radiation Chemistry in Japan, Kyoto, June 1961; papers presented at 5th Symposium of Radiation Chemistry in Japan, Tokyo, October 1962.
11. Kuri, Z. et al., paper presented at 6th Symposium of Radiation Chemistry in Japan, Kyoto, September 1963.
12. Sobu, H., Y. Tabata, M. Hiraoka, and K. Oshima, *J. Polymer Sci.*, **C4**, 943 (1964).

### Résumé

On a étudié la polymérisation en bloc de la 2-méthyl-5-vinylpyridine induite par radiation dans le domaine de température de 50°C à -196°C. On obtient une énergie d'activation de 5.7 Kcal/mole pour la polymérisation en phase liquide et 0.3 Kcal/mole pour la polymérisation en phase solide. On observe que la vitesse de polymérisation est proportionnelle à la racine carrée de la dose dans la polymérisation en phase liquide et est proportionnelle à la dose dans la polymérisation en phase solide. Le DPPH et la benzo-quinone inhibent fortement la polymérisation en phase liquide. Les mêmes inhibiteurs n'inhibent pas de façon appréciable la polymérisation en phase solide. D'autre part, la polymérisation en phase solide est complètement inhibée par l'acétone, la pyridine, et le méthanol, alors que la polymérisation liquide n'est pas inhibée par ces mêmes additifs. On en conclut que la polymérisation en phase liquide se fait par un mécanisme

radicalaire, tandis que la polymérisation en phase solide se fait par un mécanisme non-radicalaire, soit un mécanisme ionique ou électronique.

### Zusammenfassung

Die strahlungsinduzierte Polymerisation von 1-Methyl-5-vinylpyridin in Substanz wurde im Temperaturbereich von 50° bis -196°C untersucht. Die Aktivierungsenergie für die Polymerisation in flüssiger Phase ergab sich zu 5,7 kcal/Mol, diejenige für die Polymerisation in fester Phase zu 0,3 kcal/Mol. Bei der Polymerisation in flüssiger Phase ist die Polymerisationsgeschwindigkeit der Wurzel aus der Dosisleistung und in fester Phase der Dosisleistung selbst proportional. DPPH und Benzochinon waren wirksame Inhibitoren für die Polymerisation in flüssiger Phase, während die gleichen Stoffe die Polymerisation in fester Phase nicht wesentlich inhibierten. Andererseits wurde Polymerisation in fester Phase durch Aceton, Pyridin, und Methanol vollständig inhibiert, welche Stoffe wieder keine inhibierende Wirkung auf die Polymerisation in flüssiger Phase hatten. Es wird angenommen, dass die Polymerisation in flüssiger Phase über einen Radikalmechanismus, diejenige in fester Phase über einen ionischen oder elektronischen Mechanismus verläuft.

Received December 9, 1960

Revised October 24, 1963

## Radiation-Induced Copolymerization of Acrylonitrile with Styrene\*

YONEHO TABATA, *Department of Nuclear Engineering, University of Tokyo*, YOSHIO HASHIZUME, *Dainippon Celluloid Co., Central Research Laboratory, Ohii, Irymagun, Saitama*, and HIROSHI SOBUE, *Department of Industrial Chemistry, University of Tokyo, Tokyo, Japan*

### Synopsis

Radiation-induced copolymerization of acrylonitrile with styrene was carried out over a wide range of temperatures. It was found that the rate of copolymerization is proportional to the square root of the dose rate. An apparent activation energy of 6.90 kcal./mole was obtained for the copolymerization in an equimolar mixture of monomers. The rate of copolymerization increased with the molar concentration of acrylonitrile in the monomer mixture. Monomer reactivity ratios were determined as  $r_{AN} = 0.03$ ,  $r_{St} = 0.33$  for the copolymerization at 15 and 0°C.,  $r_{AN} = 0.28$ ,  $r_{St} = 0$  at -20°C. in the liquid state of monomers. On the other hand, the monomer reactivity ratios were obtained as  $r_{AN} \cong 0$  and  $r_{St} \cong 0$  for the copolymerization in the solid state at -78°C. It was concluded from these experimental results that there is a great difference between the liquid-state and solid-state copolymerizations, both in the polymerization mechanism and the structure of copolymers.

### INTRODUCTION

Radiation-induced copolymerization of acrylonitrile with styrene at low temperature has been reported by several workers.<sup>1-3</sup> However, most of the studies were brief ones, carried out to determine the mechanism of the polymerization of acrylonitrile or styrene at low temperature.

In our studies, the radiation-induced copolymerization in the same system was carried out precisely over a wide range of temperature.

### EXPERIMENTAL

Styrene and acrylonitrile monomers were carefully purified prior to use. The ampule containing solid monomers was evacuated to  $10^{-3}$ – $10^{-4}$  mm. Hg. Irradiation was carried out by  $\gamma$ -rays over a temperature range of 20 to -78°C. The overall reaction rates were determined by isolating and weighing the polymer. Polymer composition was determined by infrared analysis.

\* Published in part in *Kogyo Kagaku Zasshi*, **65**, 1883 (1962).

## RESULTS AND DISCUSSION

### 1. Solubility of Copolymers for Various Solvents and Separation of Homopolymer

Solubilities of the copolymers obtained were examined in various solvents, such as acetone, toluene, chloroform, carbon tetrachloride, and dimethylformamide at 20°C. No acrylonitrile or styrene homopolymer could be extracted by any solvent extraction technique, except in the case of the product of copolymerization of the monomers in the solid state at -78°C. A small amount of styrene homopolymer was extracted from monomers which were irradiated at -78°C. in the solid state.

### 2. Infrared Analysis of Composition of Copolymers

Infrared spectra of a mixture of homopolymers (60 mole-% acrylonitrile) and of the copolymers obtained are given in Figure 1. There are only small differences between the spectrum of the mixture of homopolymers and those of copolymers, unlike the case of the tetrafluoroethylene- $\alpha$ -olefin and acrylonitrile-methyl methacrylate systems.<sup>4-7</sup> Main differences were observed in the region of 1100-1300  $\text{cm}^{-1}$ .

The 2230  $\text{cm}^{-1}$  band is due to the CN stretching vibration in the unit of acrylonitrile; on the other hand, the 3020 and 1495  $\text{cm}^{-1}$  bands are due to

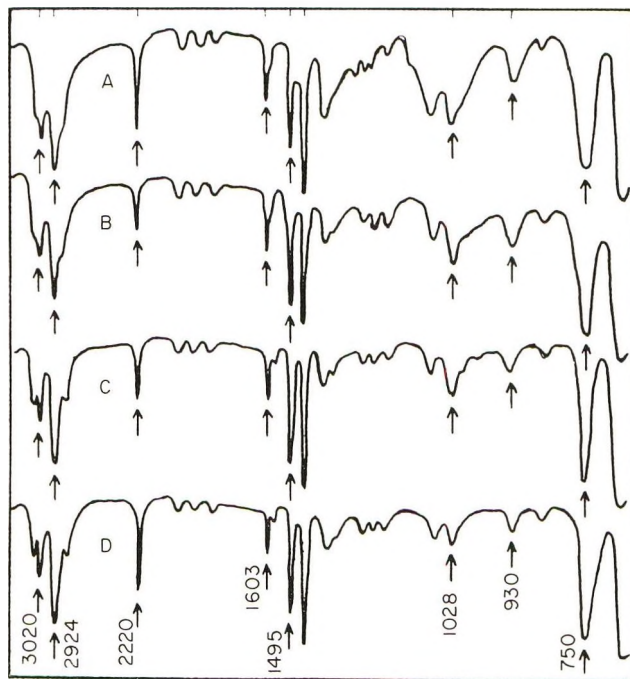


Fig. 1. Infrared spectra of (A) a mixture of acrylonitrile (mole fraction 0.6) and polystyrene (mole fraction 0.4) and of various acrylonitrile-styrene copolymers having mole fractions of acrylonitrile of (B) 0.30, (C) 0.43, and (D) 0.57.

the stretching and deformation vibrations of phenyl group in the styrene unit.

The relative intensities,  $D_{3020}/D_{2230}$  and  $D_{1496}/D_{2230}$  were plotted for the molar ratios of styrene to acrylonitrile in the copolymers, as shown in Figure 2. A tangential base line procedure was used for determining absorbances, and the molar concentration of acrylonitrile in the copolymer was determined by an elementary analysis.

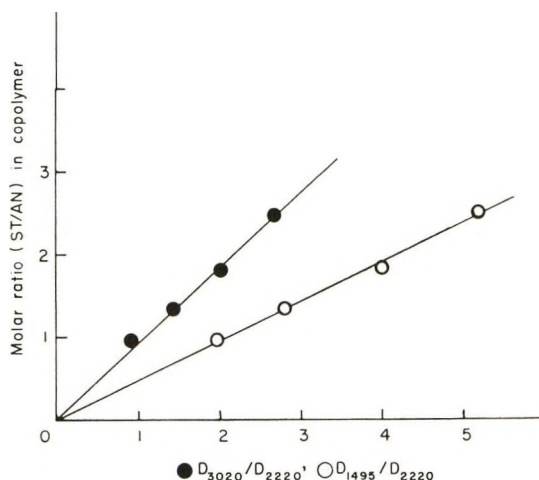


Fig. 2. Infrared calibration: (●)  $D_{3020}/D_{2220}$ ; (○)  $D_{1495}/D_{2220}$ .

It is obvious from these results that there is a linear correlation between the relative absorption intensity and the molar concentration of one component in the copolymer. Therefore, one can easily determine the acrylonitrile-styrene composition by means of these calibration curves.

### 3. Rate of Copolymerization

The copolymerization is not preceded by an induction period. The yield increases linearly with irradiation time up to 6–7% conversion; above this conversion, a retardation phenomenon was observed, probably due to the retardation of diffusion of monomers held inside of the polymer precipitated. The relation between the rate of polymerization and the dose rate is shown in Figure 3.

It is obvious from the results that the rate of copolymerization is proportional to the square root of the dose rate. It suggests that the termination would be a bimolecular reaction.

The relation between the rate of copolymerization and the molar concentration of acrylonitrile in the monomer mixture is shown in Figure 4. The rate of copolymerization increases linearly with the molar concentration of acrylonitrile in the monomer mixture.

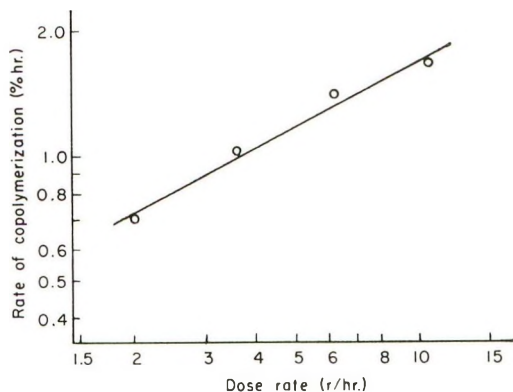


Fig. 3. Dose rate dependency of the rate of copolymerization at 15°C.

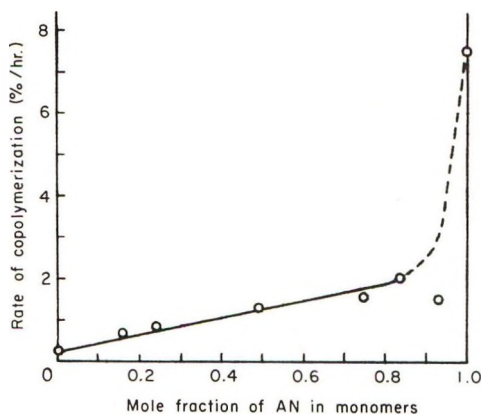


Fig. 4. Relation between the rate of copolymerization and the molar concentration of acrylonitrile at 15°C. Dose rate  $6.1 \times 10^4$  r/hr.

#### 4. Temperature Dependency of Rate of Copolymerization

An equimolar mixture of the monomers was irradiated at dose rates of  $6.1 \times 10^4$  r/hr. at various temperatures. An Arrhenius plot of the results is given in Figure 5. Apparent activation energy of 6.9 kcal./mole was obtained from the results for the copolymerization.

#### 5. Monomer Reactivity Ratio

Composition curves of acrylonitrile-styrene copolymers are shown in Figure 6. Experiments were carried out at 15, 0, -20, and -78°C. The compositions of the copolymers were determined below about 5% conversion. In the case of the solid-state copolymerization at -78°C., styrene homopolymer was excluded from the product by extraction.

It is well known that the monomer reactivity ratios are defined as,

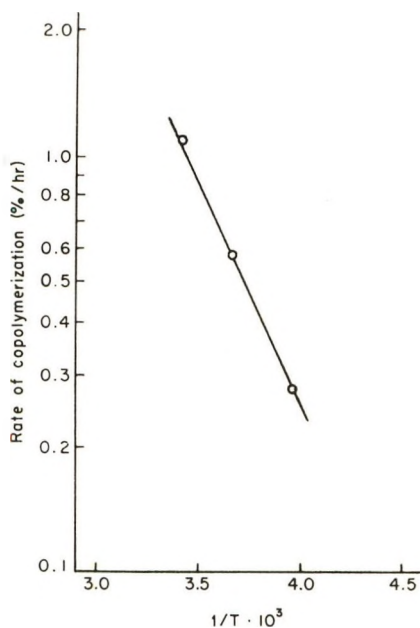


Fig. 5. Arrhenius plot of the rate of copolymerization.

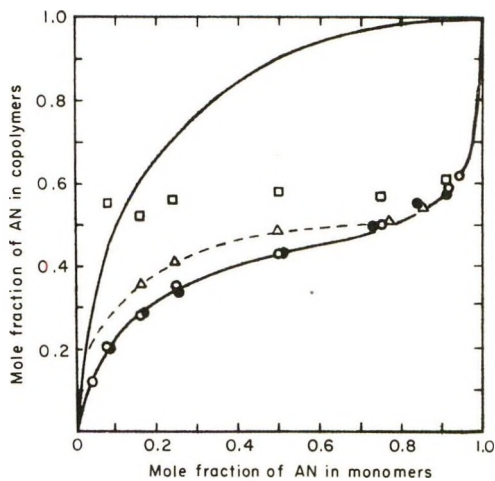


Fig. 6. Composition curve of acrylonitrile-styrene copolymers (liquid-phase polymerizations) at various temperatures: (O) 15°C.; (●) 0°C.; (Δ) 20°C.; (—) radical copolymerization.

$$r_1 = k_{11}/k_{12}$$

$$r_2 = k_{22}/k_{21}$$

where  $k$  is the propagation rate constant. From the acrylonitrile-styrene composition curve, the reactivity ratios can be determined. In the case of copolymerization in the solid state at  $-78^\circ\text{C}$ ., the composition curve was

determined both by an infrared method and by direct elementary analysis, as shown in Figure 7. The monomer reactivity ratios for the copolymerization are summarized in Table I.

TABLE I  
Monomer Reactivity Ratios for Acrylonitrile-Styrene Copolymerization

Polymerization temp., °C.	State	$r_1$ (AN)	$r_2$ (St)
15	Liquid	0.03	0.33
0	Liquid	0.03	0.33
-20	Liquid	0.28	0
-78	Solid	$\simeq 0$	$\simeq 0$

On the other hand, Zutty and Welch<sup>8</sup> carried out the copolymerization in the presence of various catalysts and they obtained  $r_1 = 0.03$ ,  $r_2 = 0.33$  for a radical copolymerization. Our results of the copolymerization at 0 and 15°C. coincide with their data. It is evident from Figure 7 that the composition in copolymer is always constant over the entire monomer composition range in the monomer mixtures, within experimental errors. The monomer reactivity ratio in the solid-state copolymerization at -78°C. could not be determined exactly from these data; however the values can be roughly determined to be  $r_1 \simeq 0$  and  $r_2 \simeq 0$ .

It appears to be an anomalous phenomenon that the concentration of acrylonitrile in the copolymer is so high in a region of high concentration of styrene in the monomer mixture, in spite of the fact that the copolymerization system is in the solid state. This peculiarity could be explained by postulating that there are two phases in the monomer mixture systems,

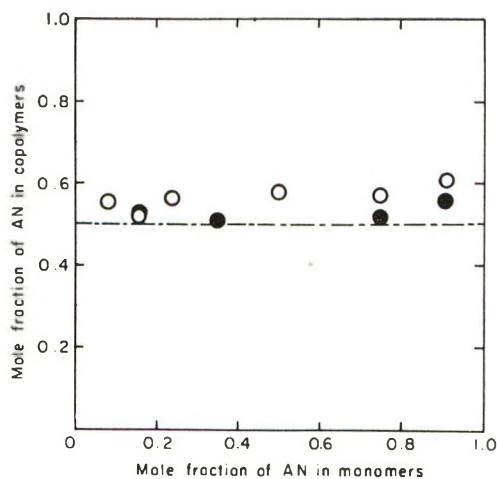


Fig. 7. Composition curve of acrylonitrile-styrene copolymers (solid-phase copolymerization at -78°C.): (O) infrared method; (●) elementary analysis.

i.e., one of the phases consists of pure styrene and the other is an acrylonitrile-styrene equimolar complex or something of this type. Though this is not a conclusive explanation, the authors wish to emphasize a possibility of alternating copolymerization in the solid state. In our system, as described above, the homopolymerization of styrene and the alternating copolymerization of acrylonitrile with styrene would proceed independently in the two solid phases.

### References

1. Abkin, A. D., et al., *J. Polymer Sci.*, **53**, 39 (1961).
2. Okamura, S., K. Hayashi, Nishii, and Nakamura, *Doitai To Hoshusen*, **3**, 344 (1960).
3. Tsuda, Y., *J. Polymer Sci.*, **54**, 193 (1961).
4. Tabata, Y., H. Shibano, and H. Sobue, *J. Polymer Sci.*, **A2**, 1977 (1964).
5. Tabata, Y., K. Ishigure, and H. Sobue, *J. Polymer Sci.*, in press.
6. Tabata, Y., K. Ishigure, K. Oshima, and H. Sobue, *J. Polymer Sci.*, in press.
7. Tabata, Y., Y. Hashizume, and H. Sobue, *J. Polymer Sci.*, in press.
8. Zutty, N. L., and F. J. Weleh, *J. Polymer Sci.*, **43**, 445 (1960).

### Résumé

La copolymérisation induite par radiation de l'acrylonitrile avec le styrène a été effectuée dans un large domaine de température. Les résultats suivants furent obtenus: (1) La vitesse de copolymérisation est proportionnelle à la racine carrée de la vitesse de dose. (2) L'énergie d'activation apparente de 6,90 Kcal/mole a été obtenue pour la copolymérisation d'un mélange équimoléculaire des monomères. (3) La vitesse de copolymérisation augmente avec la concentration molaire de l'acrylonitrile dans le mélange de monomères. (4) Le rapport des réactivités des monomères est  $r_{AN} = 0,03$ ,  $r_{St} = 0,33$  pour la copolymérisation à 15 et 0°C,  $r_{AN} = 0,28$ ,  $r_{St} = 0$  à -20°C pour les monomères à l'état liquide. D'autre part le rapport des réactivités des monomères est  $r_{AN} \cong 0$  et  $r_{St} \cong 0$  pour la copolymérisation à l'état solide à -78°C. Ces résultats expérimentaux montrent qu'il y a une grande différence entre les copolymérisations à l'état liquide et à l'état solide, du point de vue du mécanisme de la polymérisation et de la structure des polymères.

### Zusammenfassung

Strahlungsinduzierte Copolymerisation von Acrylnitril mit Styrol wurde in einem grossen Temperaturbereich ausgeführt. Folgende Resultate wurde erhalten: (1) Die Copolymerisationsgeschwindigkeit ist der Wurzel aus der Dosisleistung proportional. (2) Die scheinbare Aktivierungsenergie von 6,90 kcal/Mol wurde bei Copolymerisation einer äquimolaren Mischung der Monomeren erhalten. (3) Die Copolymerisationsgeschwindigkeit wächst mit der molaren Konzentration von Acrylnitril in der Monomermischung. (4) Die Monomerreaktivitätsverhältnisse wurden zu  $r_{AN} = 0,03$ ,  $r_{St} = 0,33$  für die Copolymerisation bei 15°C und 0°C bestimmt,  $r_{AN} = 0,28$ ,  $r_{St} = 0$  bei -20°C in flüssiger Monomerphase. Andererseits wurden die Monomerreaktivitätsverhältnisse für die Copolymerisation im festen Zustand bei -78°C zu  $r_{AN} \approx 0$  und  $r_{St} \approx 0$  erhalten. Aus diesen experimentellen Ergebnissen wurde geschlossen, dass zwischen der Copolymerisation im flüssigen und der im festen Zustand ein grosser Unterschied vom Standpunkt des Polymerisationsmechanismus und der Copolymerstruktur besteht.

Received September 17, 1963

Revised October 18, 1963

## CH<sub>2</sub> Rocking Vibrations of Polyethylene Oxybenzoate

MATAHUMI ISHIBASHI, *Research Institute, Nippon Rayon Company, Ltd., Uji, Kyoto, Japan*

### Synopsis

Infrared spectra of poly(*p*-ethylene oxybenzoate) and four of its diol oligomer series (from monomer to tetramer) have been obtained in the range of 400–4000 cm.<sup>-1</sup>. An assignment of the CH<sub>2</sub> rocking vibrations has been made on the basis of analysis of spectra of ethylene glycol and its derivatives, and with the help of data from related compounds containing —OCH<sub>2</sub>CH<sub>2</sub>OH endgroups linked to a phenyl and/or to a benzoyl residue and containing a —OCH<sub>2</sub>CH<sub>2</sub>O— group between a phenyl and a benzoyl residue. This assignment suggests that the —OCH<sub>2</sub>CH<sub>2</sub>O— groups of poly(*p*-ethylene oxybenzoate) are in the *trans* conformation. The similarity between the noncrystalline and the crystalline phase spectra of poly(*p*-ethylene oxybenzoate) suggests that the —OCH<sub>2</sub>CH<sub>2</sub>O— groups exist in essentially the same (*trans*) conformation in both phases.

### INTRODUCTION

The infrared spectrum of poly(ethylene terephthalate) (PETP) has been investigated by several authors.<sup>1–12</sup>

In almost all these cases,<sup>3,4,6–9</sup> it has been asserted that the bands whose intensity changes with the specimen crystallinity are associated with the —OCH<sub>2</sub>CH<sub>2</sub>O— group of the chain, and that the spectral changes originate from the *trans* conformation of this group in the crystalline region and the *gauche* conformation in the noncrystalline region. However, it has been suggested by Liang and Krimm<sup>10,11</sup> that the spectral changes which occur upon crystallization of PETP are not associated with different isomeric forms of the —OCH<sub>2</sub>CH<sub>2</sub>O— group of the chain, but associated rather with the changes in the symmetry and resonance characteristic of the framework of the O=CC<sub>6</sub>H<sub>4</sub>C=O group. It has been pointed out from the infrared

spectrum of poly(*p*-ethylene oxybenzoate) (PEOB)<sup>13</sup> that the spectral changes in PETP are associated with the relaxation of the symmetry of the O=CC<sub>6</sub>H<sub>4</sub>C=O group in the noncrystalline region. The molecular struc-

ture of PEOB,  $\left[ \text{C}_6\text{H}_4\text{COOCH}_2\text{CH}_2\text{O} \right]_n$ , is similar to that of PETP,  $\left[ \text{C}_6\text{H}_4\text{COOCH}_2\text{CH}_2\text{OCO} \right]_n$ .

During the course of a complete assignment of the spectrum of PEOB, some information on the vibrations of the —OCH<sub>2</sub>CH<sub>2</sub>O— group is necessary. In order to obtain these data, infrared spectra of related compounds containing a —OCH<sub>2</sub>CH<sub>2</sub>O— group are required.

This paper is concerned with an assignment of the  $\text{CH}_2$  rocking vibrations in PEOB, and in the series of linear, diol oligomers of *p*-ethylene oxybenzoate,  $\text{HOCH}_2\text{CH}(\text{OC}_6\text{H}_4\text{COOCH}_2\text{CH}_2)_n\text{OH}$ , because the  $\text{CH}_2$  rocking vibrations are particularly sensitive to the molecular configuration. Complete assignment of the infrared spectra of PEOB and oligomers was not attempted.

## EXPERIMENTAL

PEOB was prepared according to the method of Cook et al.<sup>14</sup> The series of linear diol oligomers was prepared from *p*- $\beta$ -oxyethoxy,  $\beta'$ -oxyethyl benzoate by a controlled condensation reaction. The melting points and the molecular weights of oligomers are shown in Table I. The method of preparation and the properties of oligomers will be reported in a subsequent paper.<sup>15</sup>

The infrared spectra were recorded on a Shimadzu double-beam spectrometer Model IR-600 with three gratings incorporating a KBr fore prism. The absorption measurements were made in the region of 400–4000  $\text{cm}^{-1}$ .

TABLE I  
Melting Points and Molecular Weights of Linear Diol Oligomers  
 $\text{HOCH}_2\text{CH}_2(\text{OC}_6\text{H}_4\text{COOCH}_2\text{CH}_2)_n\text{OH}$

<i>n</i>	Melting point, °C.	Mol. wt.	
		Obs. <sup>a</sup>	Calc.
1	77	228	226
2	114	377	390
3	136	597 <sup>b</sup>	554
4	156	825 <sup>b</sup>	718

<sup>a</sup> Molecular weight measured by cryoscopic method.

<sup>b</sup> These high molecular weight values are probably due to mixture with oligomers whose *n* are greater than 3 or 4.

## RESULTS

The infrared spectra of oligomers and polymer are shown in Figure 1, and the enlarged curves of the 850–950  $\text{cm}^{-1}$  range are shown in Figure 2.

It can be seen from Figure 1 that the infrared absorption curves of oligomers are dependent on the degree of polymerization, and that the absorption curves of oligomers of degree of polymerization greater than 3 are similar to that of the polymer exclusive of the 3  $\mu$  region associated with the  $-\text{OH}$  stretching vibrations of endgroups.

Two distinct bands appearing at about 2950 and 2880  $\text{cm}^{-1}$  can be assigned to the  $\text{CH}_2$  antisymmetric and symmetric stretching vibrations, respectively. A strong band appearing at about 1710  $\text{cm}^{-1}$  can be assigned to the  $\text{C}=\text{O}$  stretching vibration. The origin of the bands at about 1610, 1580, 1370, 1170, 1100, 690, 630, and 510  $\text{cm}^{-1}$  has been pointed out in a

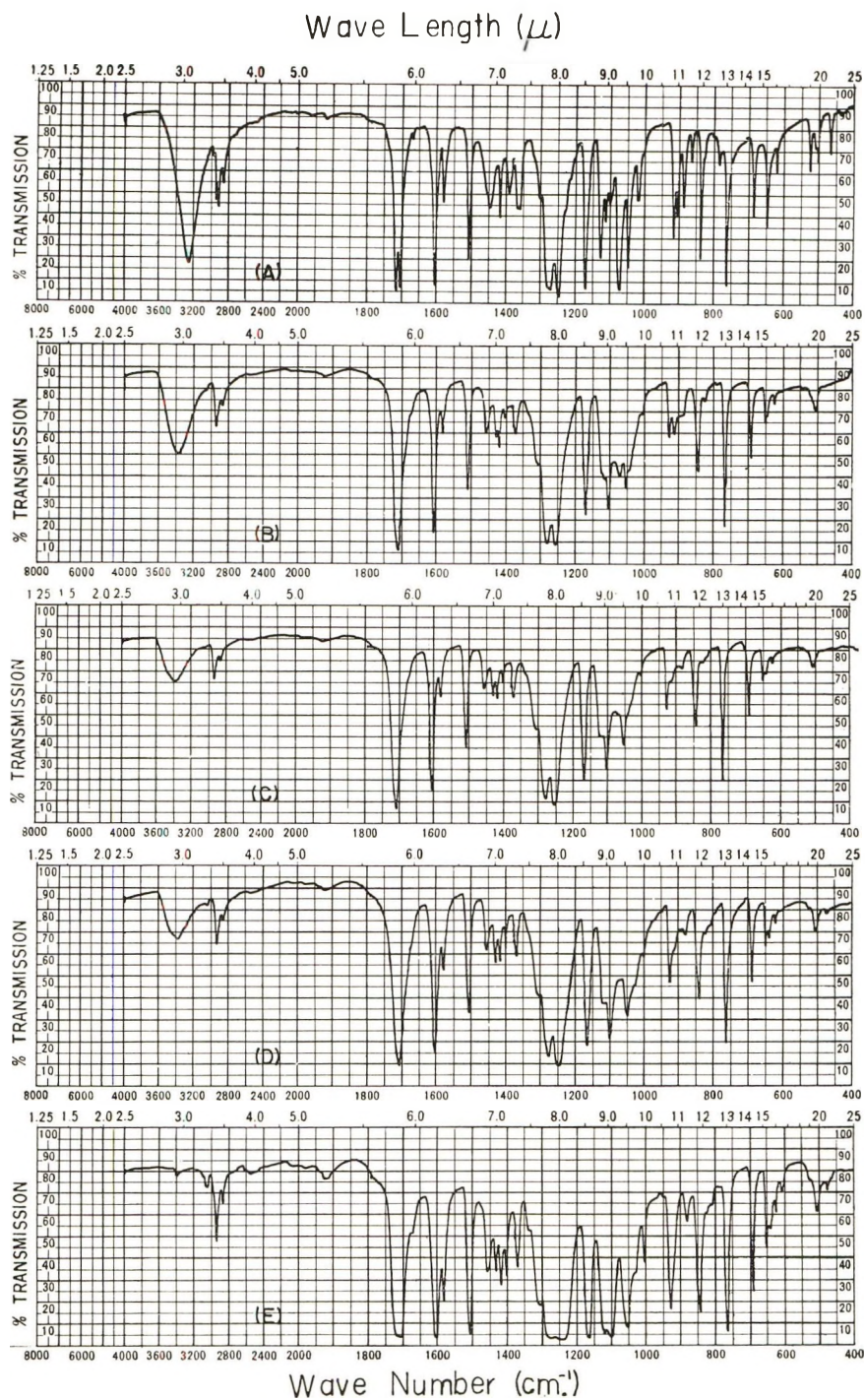


Fig. 1. Infrared spectra of linear diol oligomers of *p*-ethylene oxybenzoate and poly(*p*-ethylene oxybenzoate): (A) monomer; (B) dimer; (C) trimer; (D) tetramer; (E) polymer.

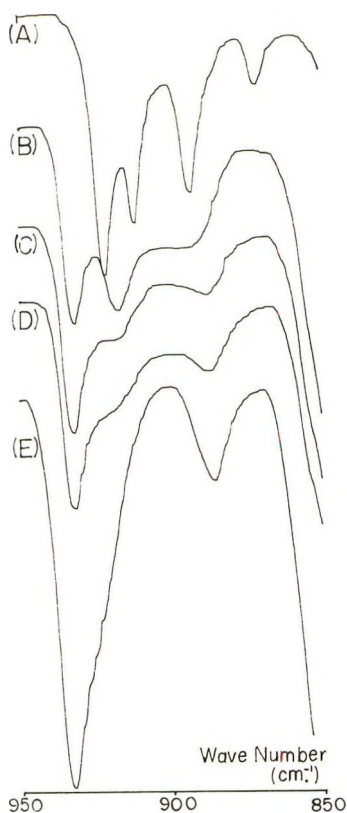


Fig. 2. Infrared spectra of the  $\text{CH}_2$ -rocking region: (A) monomer; (B) dimer; (C) trimer; (D) tetramer; (E) polymer.

preceding report.<sup>13</sup> The  $\text{CH}_2$  twisting, wagging, and bending vibrations have weak peaks at about 1310, 1340, and 1400, 1420, 1435, and 1460  $\text{cm}^{-1}$ , respectively.

In the  $11\ \mu$  region, shown in Figure 2, four distinct bands at 920, 911, 892, and 870  $\text{cm}^{-1}$  appear in the spectrum of the monomer. Two distinct bands at 930 and 918  $\text{cm}^{-1}$  and a shoulder band at 890  $\text{cm}^{-1}$  appear in the dimer. One distinct band, a shoulder, and one weak band at 931, 918, and 887  $\text{cm}^{-1}$ , respectively, appear in the trimer. One distinct band, one feeble shoulder, and one weak band appear at 932, 918, and 885  $\text{cm}^{-1}$ , respectively, in the tetramer. Two distinct bands at 932 and 885  $\text{cm}^{-1}$  appear in the polymer. These bands can be assigned to the  $\text{CH}_2$  rocking vibrations.

## DISCUSSION

In the monomer,  $\text{HOCH}_2\text{CH}_2\text{OC}_6\text{H}_4\text{COOCH}_2\text{CH}_2\text{OH}$ , one  $-\text{OCH}_2\text{CH}_2\text{OH}$  endgroup is linked to a phenyl residue and the other to a benzoyl residue. The infrared spectra of compounds containing the  $-\text{OCH}_2\text{CH}_2\text{OH}$  endgroup linked to a phenyl and/or to a benzoyl residue have been

investigated.<sup>9,16-18</sup> The wave numbers suggested by their infrared spectra in the solid and the molten states for the CH<sub>2</sub> rocking vibrations are given in Table II.

TABLE II  
CH<sub>2</sub> Rocking Vibrations of *p*-Ethylene Glycol Esters and Ethers

	State	Frequency, cm. <sup>-1</sup>			
HOCH <sub>2</sub> CH <sub>2</sub> OOCC <sub>6</sub> H <sub>4</sub> COOCH <sub>2</sub> CH <sub>2</sub> OH	Solid	909	898	875	860
	Molten		899	873	
HOC <sub>6</sub> H <sub>4</sub> COOCH <sub>2</sub> CH <sub>2</sub> OH	Solid	909			863
	Molten		900		
HOCH <sub>2</sub> CH <sub>2</sub> OC <sub>6</sub> H <sub>4</sub> COOH <sup>a</sup>	Solid	919		905	
	Molten		912		
HOCH <sub>2</sub> CH <sub>2</sub> OC <sub>6</sub> H <sub>4</sub> COOH <sup>a</sup>	Solid	920	912	901	890
	Molten		912		
HOCH <sub>2</sub> CH <sub>2</sub> OC <sub>6</sub> H <sub>4</sub> OCH <sub>2</sub> CH <sub>2</sub> OH	Solid	922			896
	Molten		912	899	
HOCH <sub>2</sub> CH <sub>2</sub> OC <sub>6</sub> H <sub>4</sub> COOCH <sub>3</sub>	Solid	923			883
	Molten		913		

<sup>a</sup> *p*-β-(Oxyethoxybenzoic acid has two modifications.

The spectrum of polyethylene glycol has been interpreted as arising from a predominantly *gauche* conformation in the molten state.<sup>19</sup> The bands at 909, 898, 870, and 861 cm.<sup>-1</sup> in HOCH<sub>2</sub>CH<sub>2</sub>OOCC<sub>6</sub>H<sub>4</sub>COOCH<sub>2</sub>OH have been assigned to the CH<sub>2</sub> rocking vibrations of the *trans* B<sub>g</sub>, *gauche* A, *gauche* B, and *trans* A<sub>u</sub> classes, respectively.<sup>16</sup>

According to the assignments mentioned above, in the related compounds containing the —OCH<sub>2</sub>CH<sub>2</sub>OH endgroup linked to a benzoyl residue, the bands at about 910 and 860 cm.<sup>-1</sup> should arise from the *trans* conformation, and the bands at about 900 cm.<sup>-1</sup> and at nearly 875 cm.<sup>-1</sup> should arise from the *gauche* conformation of the —OCH<sub>2</sub>CH<sub>2</sub>OH endgroups.

If it is assumed that the assignment to the CH<sub>2</sub> rocking vibrations in the related compounds containing the —OCH<sub>2</sub>CH<sub>2</sub>OH endgroup linked to a phenyl residue is analogous to that linked to a benzoyl residue, the bands at about 920 and 890 cm.<sup>-1</sup> could be assigned to the *trans* conformation, and the bands at about 912 and at nearly 900 cm.<sup>-1</sup> to the *gauche* conformation of —OCH<sub>2</sub>CH<sub>2</sub>OH endgroup linked to a phenyl residue.

From these suggestions, it should be concluded that the band at 920 cm.<sup>-1</sup> in the monomer originates from the *trans* conformation of the —OCH<sub>2</sub>CH<sub>2</sub>OH endgroup linked to a phenyl residue. Since the band at about 900 cm.<sup>-1</sup> does not appear in the monomer, it is reasonable to infer that there is no *gauche* conformation in the —OCH<sub>2</sub>CH<sub>2</sub>OH endgroup linked to a benzoyl residue.

The band at 911 cm.<sup>-1</sup> would be assigned to either the *gauche* conformation of the —OCH<sub>2</sub>CH<sub>2</sub>OH endgroup linked to a phenyl residue, or the *trans* conformation of the —OCH<sub>2</sub>CH<sub>2</sub>OH endgroup linked to a benzoyl residue. According to the preliminary x-ray analysis,<sup>20</sup> the monomer has a structure

whose cell dimensions are  $a = 11.27 \text{ \AA}$ ,  $b = 4.67 \text{ \AA}$ ,  $c = 22.45 \text{ \AA}$ ,  $\beta = 103^\circ$ , and has the space group  $C_{2h}^5 - P - 2_1/C$ . If the band at  $911 \text{ cm}^{-1}$  is assigned to the *gauche* conformation of the  $-\text{OCH}_2\text{CH}_2\text{OH}$  endgroup linked to a phenyl residue, the  $-\text{OCH}_2\text{CH}_2\text{OH}$  endgroup linked to a phenyl residue should have a different conformation in the monomer. This structure does not fit the space group. It is, therefore, reasonable to infer that the band at  $911 \text{ cm}^{-1}$  originates from the *trans* conformation of the  $-\text{OCH}_2\text{CH}_2\text{OH}$  endgroup linked to a benzoyl residue.

These estimations suggest that the band at  $892 \text{ cm}^{-1}$  in the monomer originates from the *trans* conformation of the  $-\text{OCH}_2\text{CH}_2\text{OH}$  endgroup linked to a phenyl residue, and the band at  $870 \text{ cm}^{-1}$  is associated with the *trans* conformation of the  $-\text{OCH}_2\text{CH}_2\text{OH}$  endgroup linked to a benzoyl residue.

It should be concluded from these suggestions that the two  $-\text{OCH}_2\text{CH}_2\text{OH}$  endgroups in the monomer are both in the *trans* conformation.

The dimer has two  $-\text{OCH}_2\text{CH}_2\text{OH}$  endgroups and one  $-\text{OCH}_2\text{CH}_2\text{O}-$  group between a phenyl and a benzoyl residue. As shown in Figure 2, the bands at  $930$  and  $890 \text{ cm}^{-1}$  which appear in the dimer should be associated with the  $-\text{OCH}_2\text{CH}_2\text{O}-$  group. The same bands appear in all the compounds containing the  $-\text{OCH}_2\text{CH}_2\text{O}-$  group between a phenyl and a benzoyl residue. Some of them are shown in Figure 3.

The number of  $-\text{OCH}_2\text{CH}_2\text{O}-$  groups increases with increasing degree of polymerization. The band at about  $920 \text{ cm}^{-1}$  decreases in intensity with increasing the degree of polymerization. This band arises from the  $-\text{OCH}_2\text{CH}_2\text{OH}$  endgroups. The bands appearing in the dimer at about

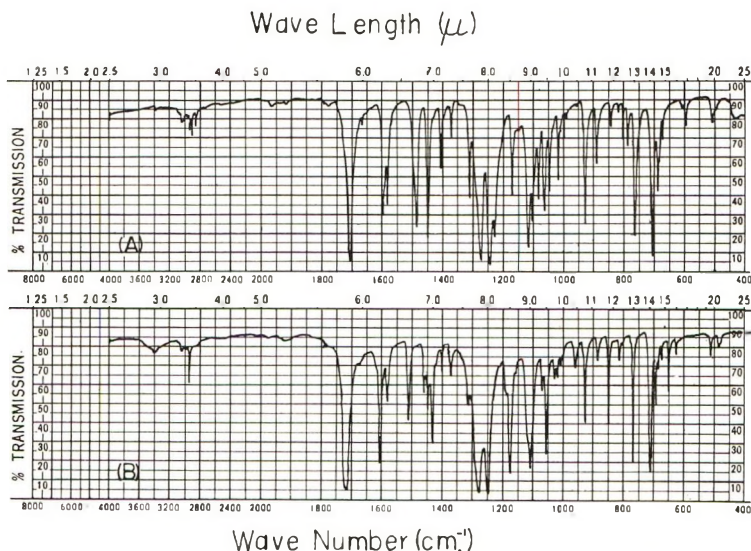


Fig. 3. Infrared spectra of related compounds containing the  $-\text{OCH}_2\text{CH}_2\text{O}-$  group between a benzoyl and a phenyl residue: (A)  $\text{C}_6\text{H}_5\text{COOCH}_2\text{CH}_2\text{OC}_6\text{H}_5$ ; (B)  $\text{C}_6\text{H}_5\text{COOCH}_2\text{CH}_2\text{OC}_6\text{H}_4\text{COOCH}_3$ .

930 and 890  $\text{cm}^{-1}$  increase in intensity with increasing degree of polymerization. It is proved from this result that these two bands are associated with the  $-\text{OCH}_2\text{CH}_2\text{O}-$  groups.

Clearly the assignment of the bands at about 930 and 890  $\text{cm}^{-1}$  must await further study on the diffraction patterns of oligomers and polymer. The above results suggest, however, that the  $-\text{OCH}_2\text{CH}_2\text{O}-$  groups of PEOB are in the *trans* conformation, because the difference in wave number of the two  $\text{CH}_2$  rocking vibrations at 932 and 885  $\text{cm}^{-1}$  is too large to permit the assumption that the bands originate from the *gauche* conformation. Both the  $\text{CH}_2$  antisymmetric and symmetric stretching vibrations show  $\sigma$  polarization in the spectrum of the oriented PEOB. The position of the 932 and 885  $\text{cm}^{-1}$  bands in PEOB does not change appreciably on crystallization. The similarity in spectra of both the noncrystalline and crystalline phases of PEOB suggests that the  $-\text{OCH}_2\text{CH}_2\text{O}-$  groups are essentially in the same (*trans*) conformation in both phases.

The author wishes to thank Drs. H. Kobayashi and H. Arimoto for fruitful discussion. He is particularly indebted to Messrs. M. Hirai and K. Yoshimura for much of the experimental work.

### References

1. Miller, R. G. J., and H. A. Willis, *Trans. Faraday Soc.*, **49**, 433 (1953).
2. Cobbs, W. H., Jr., and R. L. Burton, *J. Polymer Sci.*, **10**, 275 (1953).
3. Ward, I. M., *Chem. Ind. (London)*, **1956**, 905.
4. Ward, I. M., *Chem. Ind. (London)*, **1957**, 1102.
5. Tobin, M. C., *J. Phys. Chem.*, **61**, 1392 (1957).
6. Daniels, W. W., and R. E. Kitson, *J. Polymer Sci.*, **33**, 161 (1958).
7. Grimer, D., and I. W. Ward, *Trans. Faraday Soc.*, **54**, 959 (1958).
8. Seidel, B., *Z. Elektrochem.*, **62**, 214 (1958).
9. Miyake, A., *J. Polymer Sci.*, **38**, 479, 497 (1959).
10. Liang, C. Y., and S. Krimm, *J. Mol. Spectroscopy*, **3**, 554 (1959).
11. Krimm, S., *Fortschr. Hochpolymer.-Forsch.*, **2**, 51 (1960).
12. Tadokoro, H., K. Tatsuka, and S. Murahashi, *J. Polymer Sci.*, **59**, 413 (1962).
13. Ishibashi, M., *J. Polymer Sci.*, **B1**, 529 (1963).
14. Cook, J. G., J. T. Dickson, A. R. Lowe, and J. R. Whinfield, British Pat. 604,985 (Dec. 11, 1945).
15. Ishibashi, M., *Kobunshi Kazako*, in press.
16. Miyake, A., *Bull. Chem. Soc. Japan*, **30**, 361 (1957).
17. Miyake, A., *J. Am. Chem. Soc.*, **82**, 3040 (1960).
18. Ishibashi, M., unpublished data.
19. White, H. F., and C. M. Lovell, *J. Polymer Sci.*, **41**, 369 (1959).
20. Ishibashi, M., unpublished data.

### Résumé

On a obtenu les spectres infra-rouges de poly-*p*-oxybenzoate d'éthylène et de quatre oligomères du diol de cette série (depuis le monomère jusqu'au tétramère) dans le région de 400 à 4000  $\text{cm}^{-1}$ . On a déterminé les vibrations du  $\text{CH}_2$  sur la base de l'analyse du spectre de l'éthylène-glycol et de ses dérivés, et à l'aide des données de composés mentionnés et contenant des groupements terminaux  $\text{O}-\text{CH}_2-\text{CH}_2-\text{OH}$  liés à des restes phényles et/ou benzoyles et contenant des groupements  $-\text{O}-\text{CH}_2-\text{CH}_2-\text{O}-$  entre les résidus phényles et benzoyles. Cette détermination suggère que les groupements

$\text{—O—CH}_2\text{—CH}_2\text{—O—}$  du poly-oxybenzoate d'éthylène ont la configuration *trans*. La similitude entre la phase non-cristalline et la phase cristalline du spectre du poly-oxybenzoate d'éthylène suggère que les groupes  $\text{—O—CH}_2\text{—CH}_2\text{—O—}$  ont essentiellement la même conformation *trans* dans les deux systèmes.

### Zusammenfassung

Infrarotspektren von poly-*p*-äthylenoxybenzoat und vier Gliedern seiner Diololigomerreihe (von Monomeren bis zum Tetrameren) wurden im Bereich von  $400\text{--}4000\text{ cm}^{-1}$  aufgenommen. Eine Zuordnung der  $\text{CH}_2\text{—}$  rocking-Schwingungen wurde auf Grundlage einer Analyse den Spektren von Äthylenglykol und seinen Derivaten und mit Hilfe der Daten von verwandten Verbindungen mit einer  $\text{—OCH}_2\text{CH}_2\text{OH—}$  Endgruppe an einem Phenyl- oder Benzoylrest und mit der  $\text{—OCH}_2\text{CH}_2\text{O—}$  Gruppe zwischen einem Phenyl- und einem Benzoylrest vorgenommen. Diese Zuordnung lässt eine *trans*-Konformation der  $\text{—OCH}_2\text{CH}_2\text{O—}$  Gruppen von poly-*p*-äthylenoxybenzoat erkennen. Die Ähnlichkeit zwischen den Spektren von poly-*p*-äthylenoxybenzoat in nichtkristalliner und kristalliner Phase spricht dafür, dass die  $\text{—OCH}_2\text{CH}_2\text{O—}$  Gruppe in beiden Fällen im wesentlichen in der gleichen *trans*-Konformation vorliegt.

Received July 1, 1963

Revised October 11, 1963

## CH<sub>2</sub> Rocking Vibrations of Linear Oligomers of Poly(*p*-ethylene Oxybenzoate) Having Hydroxyl and Carboxylic Acid Endgroups

MATAHUMI ISHIBASHI, *Research Institute, Nippon Rayon Company, Ltd., Uji, Kyoto, Japan*

### Synopsis

Infrared spectra of poly(*p*-ethylene oxybenzoate) and four of its oligomers (from monomer to tetramer) having hydroxy and carboxylic acid endgroups have been obtained in the range of 400–4000 cm.<sup>-1</sup>. An assignment of the CH<sub>2</sub> rocking vibrations of the ethylene glycol linkage in the oligomers has been made on the basis of analysis of the spectra of the related compounds containing the —OCH<sub>2</sub>CH<sub>2</sub>OH endgroup linked to phenyl residue, and containing the —OCH<sub>2</sub>CH<sub>2</sub>O— group between phenyl and benzoyl residues. This assignment suggests that the ethylene glycol linkages of the oligomers exist in a *trans* conformation. The similarity of the CH<sub>2</sub> rocking vibrations in both the noncrystalline and crystalline phases of poly(*p*-ethylene oxybenzoate) suggests that the ethylene glycol linkages exist essentially in the same (*trans*) conformation in both phases.

### INTRODUCTION

It has previously been reported<sup>1</sup> in an investigation of the CH<sub>2</sub> rocking vibrations of the linear diol oligomers, HOCH<sub>2</sub>CH<sub>2</sub>[O—C<sub>6</sub>H<sub>4</sub>—COOCH<sub>2</sub>—CH<sub>2</sub>]<sub>n</sub>OH, that the ethylene glycol linkage of poly(*p*-ethylene oxybenzoate) (PEOB) may exist in the *trans* form.

In an effort to increase our knowledge of the structure of PEOB, the infrared spectra of a series of the linear oligomers having hydroxyl and carboxylic acid endgroups, HO[CH<sub>2</sub>CH<sub>2</sub>O—C<sub>6</sub>H<sub>4</sub>—COO]<sub>n</sub>H, were obtained.

An assignment of the CH<sub>2</sub> rocking vibrations of the oligomers is reported in the present paper on the basis of analysis of the spectra of the related compounds containing the —OCH<sub>2</sub>CH<sub>2</sub>OH endgroup linked to phenyl residue, and containing the —OCH<sub>2</sub>CH<sub>2</sub>O— group between phenyl and benzoyl residues.

### EXPERIMENTAL

#### Apparatus

Infrared spectra were recorded on a Shimadzu Model IR-600 high resolution spectrophotometer with three gratings incorporating a KBr foreprism. The absorption measurements were made in the region of

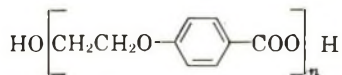
400–4000  $\text{cm}^{-1}$ . The instrument was carefully calibrated for wave number against hydrogen chloride, ammonia, methane, hydrogen bromide, carbon monoxide, and atmospheric carbon dioxide and water vapor.

### Materials

The polymer material was prepared according to the method of Cook et al.<sup>2</sup> The melting point and intrinsic viscosity of the polymer are 220°C. and 0.72, respectively.

The linear oligomers with hydroxyl and carboxylic acid endgroups were prepared from *p*- $\beta$ -oxyethoxy benzoic acid by a controlled condensation reaction. The melting points and molecular weights of the oligomers are shown in Table I.

TABLE I  
Melting Points and Molecular Weights of Linear Oligomers  
with Hydroxy and Carboxylic Acid Endgroups



<i>n</i>	Melting point, °C.	Mol. wt.	
		Obs. <sup>a</sup>	Calcd.
1	177	177	182
2	165	338	346
3	183	526	510
4	192	710 <sup>b</sup>	674

<sup>a</sup> Molecular weight was measured by cryoscopic method.

<sup>b</sup> This high molecular weight value is probably due to mixtures with oligomers higher than tetramer (for which *n* > 4).

The related compounds prepared were: 1,4-di-( $\beta$ -oxyethoxy)benzene, m.p. 103–105°C.; *p*-( $\beta$ -oxyethoxy)benzoic acid, m.p. 177°C. (This compound has two modifications; modification I, shown in Figure 3 and Table II, was used as the monomer for the condensation reaction); *p*-( $\beta$ -oxyethoxy)benzoic acid methyl ester, m.p. 69°C.; ethylene glycol monophenyl ether, b.p. 97–99°C./9 mm. Hg;  $\beta$ -(*p*-nitrophenoxy)ethyl alcohol, m.p. 81–83°C.;  $\beta$ -phenoxyethyl benzoate, m.p. 57–58°C.; methyl *p*-( $\beta$ -benzoyloxyethoxy)benzoate, m.p. 81°C.

All these compounds were prepared at this laboratory.

## RESULTS

### Polymer Spectra

The infrared spectra of polymer specimen were obtained in both non-crystalline and crystalline phases. The noncrystalline specimen was produced by quenching the polymer melt, and the crystalline specimen was

obtained by heating the noncrystalline one at 100°C. or higher temperatures for several hours. The crystallinity of the specimens was verified by x-ray diffraction measurement. Typical infrared spectra of noncrystalline and crystalline specimens of PEOB are shown in Figures 1 and 2. These spectra illustrate the effect of crystallization.

### Infrared Spectra of Oligomers

The infrared spectra of the oligomers were obtained in a crystalline phase from potassium bromide dies. Figures 3–6 show the spectra obtained for the oligomers.

These spectra are dependent on the degree of polymerization, and the principal absorption bands for that trimer and tetramer are much the same as those of PEOB, except for the  $3\ \mu$  region associated with the —OH stretching vibrations of endgroups. The enlarged curves of the 850–980  $\text{cm}^{-1}$  range are shown in Figure 7.

### Infrared Spectra of Related Compounds

Infrared spectra of the related compounds were obtained from potassium bromide dies or by the sandwich method by use of potassium bromide

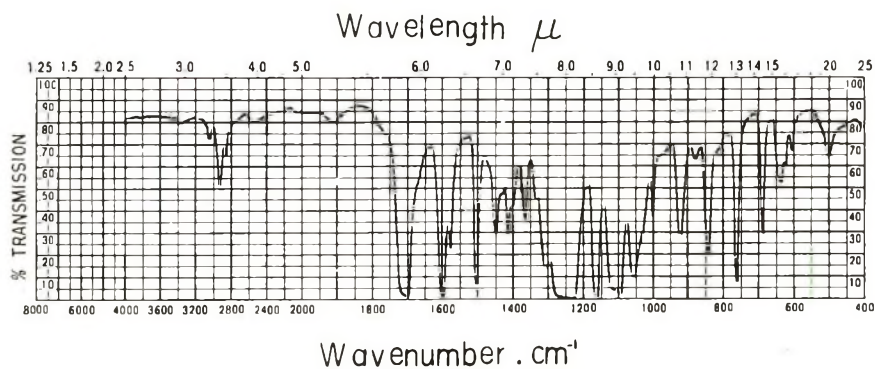


Fig. 1. Infrared spectrum of noncrystalline poly(*p*-ethylene oxybenzoate).

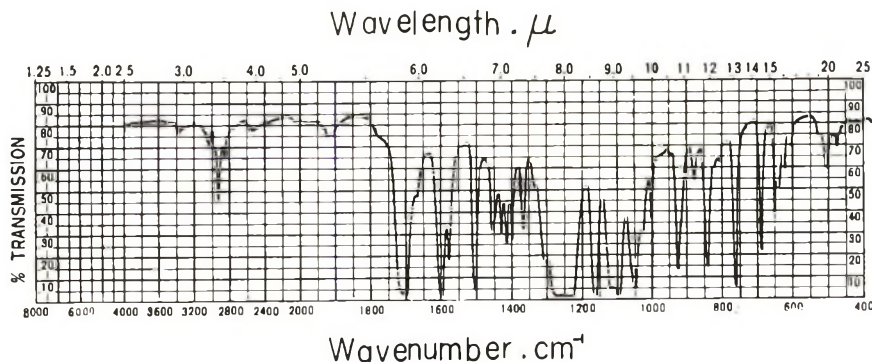


Fig. 2. Infrared spectrum of crystalline poly(*p*-ethylene oxybenzoate).

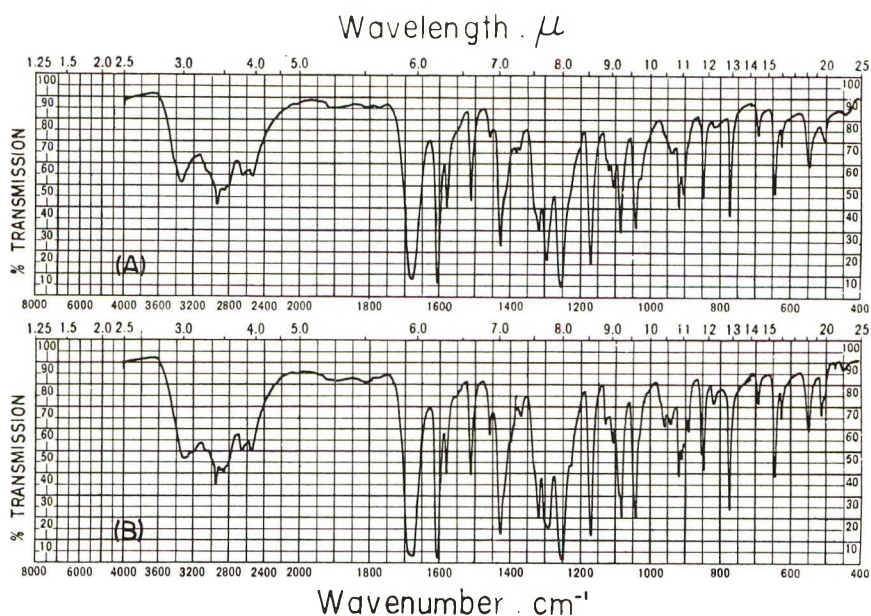


Fig. 3. Infrared spectra of *p*-( $\beta$ -oxyethoxy)benzoic acid: (A) modification I (this was used as monomer); (B) modification II.

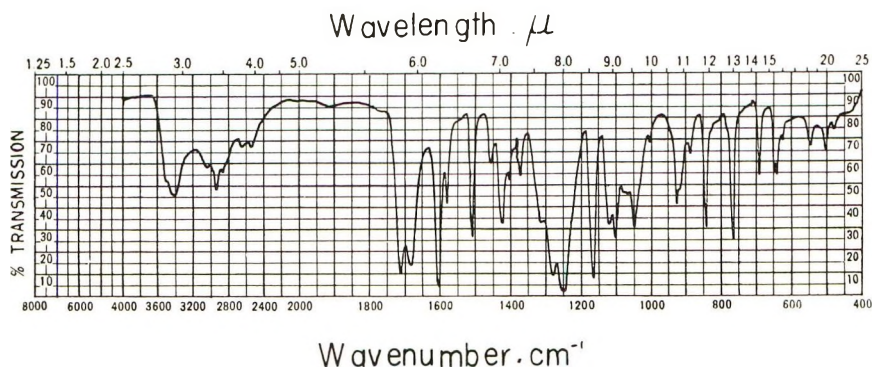


Fig. 4. Infrared spectrum of dimer,  $\text{HO} \left[ \text{CH}_2\text{CH}_2\text{O} - \text{C}_6\text{H}_4 - \text{COO} \right]_2 \text{H}$ .

plates. The spectra also were obtained on the related compounds in the molten state. The wave numbers suggested by their infrared spectra in the solid and molten states for the  $\text{CH}_2$  rocking vibrations are given in Table II.

### DISCUSSION AND CONCLUSION

In the monomer, *p*- $\beta$ -oxyethoxybenzoic acid, the  $-\text{OCH}_2\text{CH}_2\text{OH}$  end-group is linked to a phenyl residue. As shown in Figure 3 and Table II,

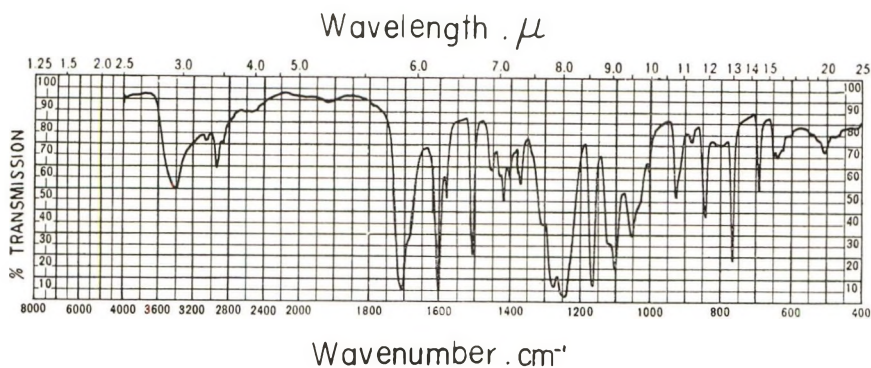


Fig. 5. Infrared spectrum of trimer,  $\text{HO} \left[ \text{CH}_2\text{CH}_2\text{O}-\text{C}_6\text{H}_4-\text{COO} \right]_3\text{H}$ .

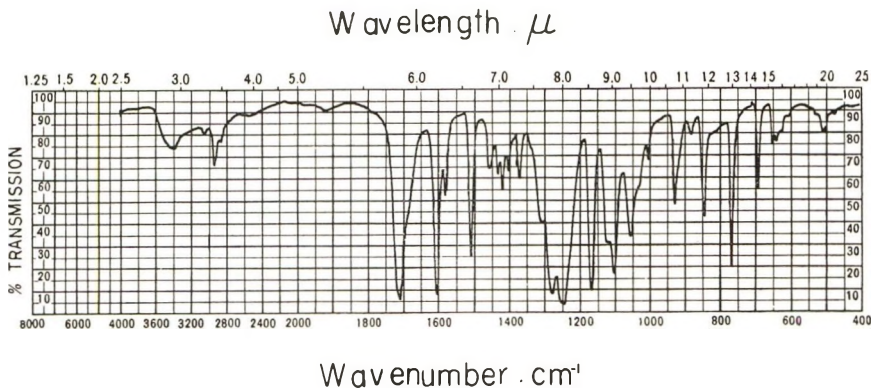


Fig. 6. Infrared spectrum of tetramer,  $\text{HO} \left[ \text{CH}_2\text{CH}_2\text{O}-\text{C}_6\text{H}_4-\text{COO} \right]_4\text{H}$ .

the monomer has two modifications. The principal absorption bands for these modifications are almost the same except for the  $11\ \mu$   $\text{CH}_2$  rocking vibration region. Modification I has two bands at  $919$  and  $905\ \text{cm}^{-1}$  in the  $\text{CH}_2$  rocking vibration region, and modification II has four bands at  $920$ ,  $912$ ,  $901$ , and  $890\ \text{cm}^{-1}$ . The former was used as the monomer for the condensation reaction. Both modifications have the same melting points and one distinct band at  $912\ \text{cm}^{-1}$  in the molten state.

The spectra of polyethylene glycol, ethylene glycol, and  $-\text{OCH}_2\text{CH}_2\text{OH}$  endgroups linked to benzoyl and/or phenyl residues have been investigated by several authors. White and Lovell<sup>3</sup> have suggested that the  $-\text{OCH}_2\text{CH}_2\text{OH}$  endgroup should have a certain amount of freedom in packing in the crystal and it probably would pack into the energetically stable *trans* conformation. Nakagawa<sup>4</sup> has shown that the  $\text{CH}_2$  rocking frequencies of disubstituted ethanes increase in the following order:  $A_u(\text{trans}) < B$

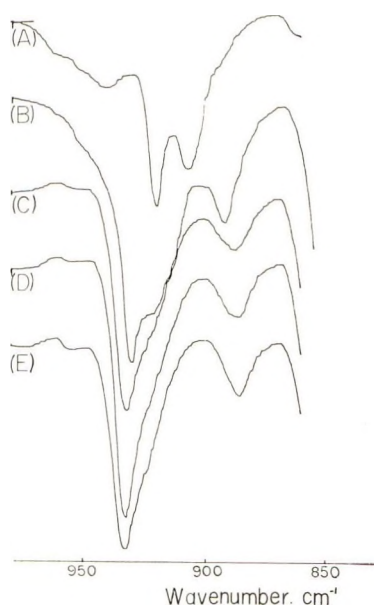



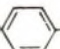


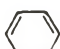


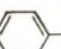


Fig. 7. Infrared spectra of CH<sub>2</sub> rocking vibration region: (A) monomer; (B) dimer; (C) trimer; (D) tetramer; (E) polymer.

TABLE II  
CH<sub>2</sub> Rocking Vibrations of Related Compounds

	State	Frequency, cm. <sup>-1</sup>			
 -OCH <sub>2</sub> CH <sub>2</sub> OH	Liquid	918			895
HOCH <sub>2</sub> CH <sub>2</sub> O-  -COOH <sup>a</sup>	Solid	919		905	
	Molten		912		
HOCH <sub>2</sub> CH <sub>2</sub> O-  -COOH <sup>b</sup>	Solid	920	912	901	890
	Molten		912		
HOCH <sub>2</sub> CH <sub>2</sub> O-  -COOCH <sub>3</sub>	Solid	923			883
	Molten		913		
HOCH <sub>2</sub> CH <sub>2</sub> O-  -OCH <sub>2</sub> CH <sub>2</sub> OH	Solid	922			896
	Molten		912	899	
HOCH <sub>2</sub> CH <sub>2</sub> O-  -NO <sub>2</sub>	Solid	918			896
	Molten		914	898	
 -COOCH <sub>2</sub> CH <sub>2</sub> O- 	Solid	931			892
	Molten	929			888
 -COOCH <sub>2</sub> CH <sub>2</sub> O-  -COOCH <sub>3</sub>	Solid	929			888
	Molten	928			887

<sup>a</sup> Modification I (this was used as a monomer).

<sup>b</sup> Modification II.

(*gauche*) < *A* (*gauche*) < *B<sub>g</sub>* (*trans*). Miyake<sup>5</sup> has assigned the bands at 909, 898, 870, and 861  $\text{cm}^{-1}$  in bis- $\beta$ -hydroxyethyl terephthalate to the  $\text{CH}_2$  rocking vibrations of the *trans* *B<sub>g</sub>*, *gauche* *A*, *gauche* *B*, and *trans* *A<sub>u</sub>* classes, respectively.

According to these suggestions, the bands at about 920 and 890  $\text{cm}^{-1}$  should arise from the *trans* form, and the bands at about 912 and 900  $\text{cm}^{-1}$  from the *gauche* form in the related compounds containing the  $-\text{OCH}_2\text{CH}_2\text{OH}$  endgroup linked to phenyl residue.

It is concluded from this suggestion that the conformation of the  $-\text{OCH}_2\text{CH}_2\text{OH}$  endgroup in modification I is *trans*, and in modification II both *trans* and *gauche*. The band at 912  $\text{cm}^{-1}$  of the monomer in the molten state is interpreted as arising from the *gauche* form.

The dimer shows a lower melting point than that of the monomer. This phenomenon is due to the ester linkage in the dimer. There is one  $-\text{OCH}_2\text{CH}_2\text{OH}$  endgroup and one  $-\text{OCH}_2\text{CH}_2\text{O}-$  group between phenyl and benzoyl residues in the dimer. The bands at 929 and 890  $\text{cm}^{-1}$  appearing in the dimer should be associated with the  $-\text{OCH}_2\text{CH}_2\text{O}-$  group. As shown in Table II, the same bands are noted in the related compounds containing the  $-\text{OCH}_2\text{CH}_2\text{O}-$  group between phenyl and benzoyl residues.

The number of  $-\text{OCH}_2\text{CH}_2\text{O}-$  groups increases with increasing degree of polymerization. The band at about 920  $\text{cm}^{-1}$  decreases in intensity as the degree of polymerization increases. It is concluded that this band arises from the  $-\text{OCH}_2\text{CH}_2\text{OH}$  endgroup. The bands appearing in the dimer at 929 and 890  $\text{cm}^{-1}$  increase in intensity as the degree of polymerization increases. It should be noted that these two bands are associated with the  $-\text{OCH}_2\text{CH}_2\text{O}-$  groups. The spacing between the two bands is about 40  $\text{cm}^{-1}$ . Miyake<sup>5</sup> has shown that the spacing between two *gauche* vibrations of the  $\text{CH}_2$  rocking mode of the ethylene glycol linkage between the phenyl residues and the benzoyl residues is only 20  $\text{cm}^{-1}$ . From his<sup>6</sup> and Nakagawa's<sup>4</sup> conclusions, the spacing between the bands at about 930 and 885  $\text{cm}^{-1}$  in the oligomers is too large to assign them to the *gauche* form of the  $-\text{OCH}_2\text{CH}_2\text{O}-$  groups; therefore, these bands should arise not from the *gauche* form, but from the *trans* form. As reported in the preceding paper<sup>1</sup> and as is shown in Figures 1 and 2 in the present paper, the position of the 932 and 885  $\text{cm}^{-1}$  bands in PEOB is not changed appreciably by crystallization.

The similarity between the  $\text{CH}_2$  rocking vibrations of the noncrystalline and crystalline phase spectra of PEOB suggests that the  $-\text{OCH}_2\text{CH}_2\text{O}-$  groups exist essentially in the same (*trans*) form in both phases.

## References

1. Ishibashi, M., *J. Polymer Sci.*, **A2**, 3657 (1964).
2. Cook, J. G., J. T. Dickson, A. R. Lowe, and J. R. Whinfield, British Pat. 604,985 (Dec. 11, 1945).
3. White, H. F., and C. M. Lovell, *J. Polymer Sci.*, **41**, 369 (1959).
4. Nakagawa, I., *Nippon Kagaku Zasshi*, **76**, 813 (1955).

5. Miyake, A., *Bull. Chem. Soc. Japan*, **30**, 361 (1957).
6. Miyake, A., *J. Am. Chem. Soc.*, **82**, 3040 (1960).

### Résumé

Des spectres infrarouges du poly-*p*-éthylène-oxybenzoate et de quatre de ses oligomères d'alcools et acides carboxyliques (du monomère au tétramère) ont été obtenus dans les régions de 400 à 4000  $\text{cm}^{-1}$ . On a pu attribuer les vibrations "rocking" du  $\text{CH}_2$  de la liaison éthylène-glycol dans les oligomères sur la base de l'analyse de spectres de composés analogues contenant le groupement terminal  $-\text{OCH}_2\text{CH}_2\text{OH}$  lié à un résidu phényle, et contenant le groupe  $-\text{OCH}_2\text{CH}_2\text{O}-$  entre le phényle et le benzyle. Cette attribution suggère que les liaisons éthylène-glycol des oligomères existent dans une conformation *trans*. La similitude des vibrations de "rocking" du  $\text{CH}_2$  dans les spectres de la phase non-cristalline et cristalline du poly-*p*-éthylène oxybenzoate fait penser que liaisons éthylène-glycol existent essentiellement dans la même conformation *trans* dans les deux phases.

### Zusammenfassung

Infrarotspektren von Poly-*p*-äthylenoxybenzoat und vier seiner Oligomeren mit Alkohol- und Carboxylendgruppen (vom Monomeren bis zum Tetrameren) wurden im Bereich von 400–4000  $\text{cm}^{-1}$  aufgenommen. Eine Zuordnung der  $\text{CH}_2$ -rocking-Schwingungen des Äthylenglykoltiels in den Oligomeren wurde auf Grundlage einer Analyse der Spektren verwandter Verbindungen mit der  $-\text{OCH}_2\text{CH}_2\text{OH}$ -Endgruppe am Phenylrest und mit der  $-\text{OCH}_2\text{CH}_2\text{O}-$  Gruppe zwischen Phenyl und Benzoylresten vorgenommen. Diese Zuordnung zeigt, dass die Äthylenglykolgruppe in den Oligomeren eine *trans*-Konformation aufweist. Die Ähnlichkeit der  $\text{CH}_2$ -rocking-Schwingungen in den Spektren der nichtkristallinen und kristallinen Phase von Poly-*p*-äthylenoxybenzoat weist auf eine im wesentlichen gleiche *trans*-Konformation der Äthylenglykoleinheit in beiden Phasen hin.

Received July 23, 1963

Revised October 11, 1963

## Determination of 1,2-Glycol Units in Polyvinyl Alcohol

HENRY E. HARRIS and J. G. PRITCHARD, *Chemstrand Research Center, Durham, North Carolina*

### Synopsis

A titrimetric method, involving the determination of the periodate consumption by means of iodine and arsenious oxide, was applied to the determination of 1,2-glycol units in polyvinyl alcohol by periodate cleavage. The method gave consistent results regardless of the molecular weight of the sample, and is believed to be accurate to  $\pm 0.05\%$  glycol units. In contrast, it was shown that the well-known Flory-Leutner viscometric method gave results which were about 20% lower than those obtained by the first method for samples of molecular weight greater than about 40,000, and gave grossly unrealistic results for samples of much lower molecular weight. Details of the methods and sources of error are discussed.

### INTRODUCTION

It is well known that the free radical-initiated polymerization of vinyl esters ( $\text{CH}_2=\text{CH}-\text{OAc}$ ) produces high polymers containing about 1% of the acyloxy groups in 1,2 sequence, instead of the preponderant 1,3 sequence along the hydrocarbon chain. This occurs mainly because a small fraction of the vinyl monomer units add to the growing polymer radicals in the orientation alternative to the preferred one, during the propagation step of the polymerization; also, mutual termination of straight-chain polymer radicals should contribute to the number of 1,2 sequences if the preferred addition takes place at the  $\beta$ -vinyl carbon atom, as is usually supposed.<sup>1,2</sup>

The proportion of 1,2 sequences in these polymers is commonly estimated through oxidative cleavage of the 1,2 glycol groups in the derived polyvinyl alcohols using periodate. The amount of reaction has usually been determined by the Flory-Leutner viscometric method<sup>2</sup> although, fairly recently, other methods have been mentioned.<sup>3,4</sup> The purpose of this paper is to present data for this determination by using the straightforward, standard technique for quantitative analysis of periodate, by titration with arsenious oxide,<sup>5</sup> which appears to have been neglected. This method is then compared with the viscometric method.

## EXPERIMENTAL

### Polyvinyl Alcohol Samples

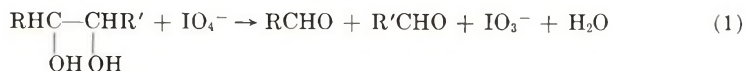
With the use of 2,2'-azoisobutyronitrile as initiator, vinyl acetate was polymerized to 10–20% conversion at various temperatures in the range 25–90°C., either in bulk or in the presence of selected chain-transfer agents, to yield polyvinyl acetate samples having widely different molecular weights and different contents of head-to-head placements. Conventional saponification of these with NaOH/MeOH yielded the polyvinyl alcohol samples labeled A through F in the tables. A sample of Vinol 125, obtained from the Air Reduction Chemical and Carbide Company, was also included.

### Periodate Cleavage and Titrations

The fact that 1,2-diols are cleaved by periodate ion according to eq. (1) is very well known. A typical experiment to determine the amount of cleavage in polymer was as follows. A weighed sample (0.2425 g., say  $w$ ) of polyvinyl alcohol was dissolved in ca. 35 ml. of distilled water at ca. 60°C. and about a twofold excess of aqueous sodium periodate\* was added to the cooled solution. After 30 min., about 1 g. of sodium bicarbonate, then 10.00 ml. of 0.1004*N* arsenious oxide solution (a measured excess), and finally ca. 0.1 g. of potassium iodide were dissolved in the solution in turn.<sup>6</sup> The effective overall reaction, which is catalyzed by the iodide ions present, is shown in eq. (2). The alkaline solution of unreacted arsenate was titrated with standard iodine and required 3.10 ml. ( $v$ ) of 0.1048*N* solution ( $n$  normal based on the equivalent of I). (The presence of sodium bicarbonate is important because, in acid solution, iodide reduces iodate as well as periodate. The back-titration procedure avoids the liberation of free iodine which would partly complex with the polyvinyl alcohol present.) Then, the above procedure was repeated in the absence of the polymer, 1.73 ml. ( $v_0$ ) of 0.1048*N* iodine solution being required for the titration. The appropriate expression for computing the number of 1,2-diol units present per 100 monomer units in the polymer is

$$100(v - v_0)nm/w$$

where  $m$  is the molecular weight of one polymer segment ( $-\text{CH}_2\text{CHOH}-$ ) or 44.1. The answer is 1.28% in the above case, and a summary of all the experiments is given in Table I.



\* We do not recommend the use of periodic acid hydrate because with this reagent we observed that, after completion of reaction (1) in an acid solution, about 10% more periodate was consumed on allowing the solution to stand for 5 hr. This occurred with both polyvinyl alcohol and the model system 2,3-butanediol and was presumably due to slow, acid-catalyzed oxidation of the aldehyde produced by reaction (1). This phenomenon was not observed when sodium periodate was used as the reagent.



The accuracy of the method was checked by use of aliquots of a solution of 2,3-butanediol in water, each containing about 0.003 g. of the diol. The value of  $m$  for the diol, which has two segments ( $\text{CH}_3\text{CHOH}-$ ), is 45.1; and the result expected for perfect purity and accuracy is 50% (cf. Table I). A practical grade of the diol was purified by distillation and collection of a center cut: b.p. 180–181°C./760 mm., m.p. 13°C., and  $n_D^{20}$  1.4385. (These characteristics indicate that the sample was probably derived via the fermentation of beet molasses and probably contained ca. 80% of the *meso* isomer and ca. 20% of optically active species.<sup>7,8</sup>)

Under the same conditions as above, no detectable reaction of isopropyl alcohol occurred on exposure to periodate for 2 hr., and methyl vinyl ketone consumed only 7% of an equivalent of periodate in 1 hr.

### Viscometry

The specific viscosity of each polyvinyl alcohol sample was determined at 25°C. over a range of concentrations in water by conventional viscometric technique in the Ubbelohde type of viscometer, in order to obtain intrinsic viscosities. Great care in the handling of solutions more concentrated than about 0.5 g./dl. was required to prevent bubbling and concentration of the polymer in the surface through evaporation. A mean of four flow times was taken for each determination. Solutions of ca. 1 g./dl. (known) concentration were then treated with a twofold excess of sodium periodate and, after standing for 30 min., the intrinsic viscosity was determined as above.

## RESULTS AND DISCUSSION

### Titrimetric Method

The mean of several estimations of the number of 1,2-diol segments per  $\text{CH}_3\text{CHOH}$  segment for samples of 2,3-butanediol gave a result very close to the theoretical one of 50% (cf. Table I) and constitutes satisfactory precision for the scale of operations employed.

The several polymers obtained by polymerization at 30°C., comprising types A and B in Table I, and having altogether about a 15-fold range of molecular weight, gave results for the 1,2-diol content in close agreement with the mean value of ca. 1.3%. Our one preparation of very low molecular weight, type C, gave the slightly lower value of ca. 1.2%, as is partly consistent with the lower polymerization temperature employed. It is thus established that this method is capable of yielding consistent results which are essentially independent of the molecular weights of the samples, and it may be employed successfully for polymers of such low molecular weights that the average number of 1,2-glycol units is only about one per

molecule. The accuracy of the method, for about six determinations per polymer, is well within 0.1% 1,2-glycol units.

An Arrhenius plot of the above results, combined with those for polymer types D, E, and F, made at higher temperatures, defines a difference of 1600 cal./mole between the activation energies for the head-to-head versus the head-to-tail monomer placement in the propagation step of the vinyl acetate polymerization, favoring the latter. The value found for the ratio of frequency factors is 0.19, also favoring the head-to-tail mode of propagation.<sup>9</sup>

TABLE I  
Data for the Titrimetric Determination of 1,2-Glycol Content of Polyvinyl Alcohol

No.	Type of sample <sup>a</sup>	Degree of polymerization	1,2-Glycol, %	R.M.S. deviation	Number of determinations
A	Bulk, 30°C.	1000-3000	1.30	±0.02	7
B	Methyl ethyl ketone, 30°C.	~200	1.27	0.04	8
C	<i>n</i> -Butyraldehyde, 25°C.	<80	1.16	0.02	5
D	Methyl ethyl ketone, 60°C.	~200	1.62	0.05	6
E	<i>tert</i> -Butyl alcohol, 77°C.	~2000	1.84	0.05	5
F	Amyl acetate, 90°C.	~2000	1.98	0.03	4
V	2,3-Butanediol vinol	~1000	1.66	0.07	5
			49.4	0.8	6

<sup>a</sup> Diluent and temperature used in the polymerization of the vinyl acetate.

### Viscometric Method

The type of precision which can be obtained in the determination of the intrinsic viscosity of polyvinyl alcohol samples, from the specific viscosity at various concentrations, is illustrated in Figure 1. (For values of  $[\eta]$  above about unity the slope of the plot increases markedly.<sup>10</sup>) The likely error for the extrapolation of such data to zero concentration is ca. 2% of  $[\eta]$ .

The equations for relating the intrinsic viscosities of initial and periodate-cleaved polymer to the content of 1,2-glycol units are, according to Flory and Leutner, as follows.<sup>2</sup>

$$[\eta] = 0.00020M^{0.76} \quad (3)$$

$$\% \text{ 1,2-glycol} = 1.89m[(1/M) - (1/M_0)]100 \quad (4)$$

The relationship between intrinsic viscosity and molecular weight was defined for 25°C. through osmotic pressure and viscosity measurements on several polymer fractions having presumably fairly narrow ranges of molecular weight [eq. (3)].<sup>2</sup> The appropriate conversion factor for application of this equation to nonfractionated polymers having the usual

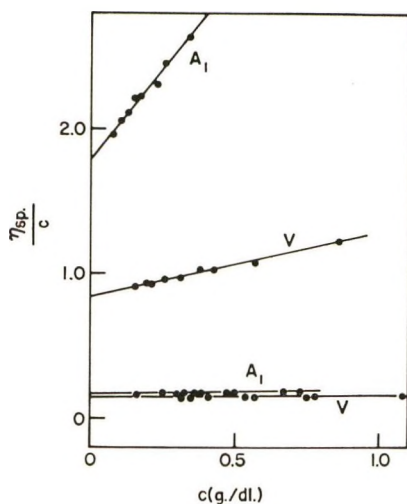


Fig. 1. Viscosity-concentration plot for two polyvinyl alcohol samples, before cleavage (upper lines) and after cleavage (lower lines).

TABLE II  
Data for the Viscometric Determination of 1,2-Glycol Content in Polyvinyl Alcohol

Polymer	Initial $[\eta]$	Final $[\eta]$	1,2-Glycol, %	Likely error <sup>a</sup>
A <sub>1</sub>	1.786	0.166	1.18	0.04
A <sub>2</sub>	0.975	0.168	1.04	0.04
A <sub>3</sub>	1.540	0.164	1.17	0.04
B	0.223	0.140	0.70	0.07
C	0.1008	0.0986	0.05	0.14
V	0.838	0.142	1.35	0.04

<sup>a</sup> This assumes  $\pm 2\%$  variation in  $[\eta]$ .

broad distribution ( $\bar{M}_w/\bar{M}_n = 1.89$ ) is included in eq. (4), where  $M_0$  represents the initial molecular weight and  $M$  the same after cleavage.<sup>2</sup>

The results for a representative set of six polymers for which the 1,2-glycol content was also determined by the titrimetric method are listed in Table II. Allowing for a 2% variation in the values of  $[\eta]$ , the likely error to be expected in the 1,2-glycol content for polymers containing 1-2% of same, on the basis of eqs. (3) and (4), is  $\pm 0.04\%$  for  $M_0 > 50,000$ , about  $\pm 0.07\%$  for  $M_0 \approx 10,000$ , and  $\pm 0.14\%$  for  $M_0 \approx 4000$  (or a degree of polymerization of ca. 80), as listed in the last column of Table II. It is evident that the values for the 1,2-glycol contents obtained by this viscometric method are all lower (far beyond the experimental errors) than the equivalent values obtained by the foregoing titrimetric method,\* progres-

\* Our "low" results obtained by the viscometric method are in fair agreement with previous results over the whole temperature range studied.<sup>2,11</sup> Our "high" results obtained by the titrimetric method are more consistent with results obtained by Japanese workers who used a polarographic method for estimating the periodate consumed.<sup>4</sup>

sively as the initial molecular weight of the polymer samples decreases until completely false results are obtained for  $M_0 < 10,000$ .<sup>11</sup>

The higher values for 1,2-glycol content obtained by the titrimetric method could be explained if structural features other than the 1,2-glycol units in polyvinyl alcohol consumed periodate but did not bring about cleavage.\* The most likely possibility would be  $\alpha,\beta$ -unsaturated ketonic structures, known to be present in polyvinyl alcohol.<sup>12</sup> However, their effect can be dismissed because we have shown that methyl vinyl ketone consumes less than one-tenth of an equivalent of periodate under the conditions of the titration, and because sample V has essentially no  $\alpha,\beta$ -unsaturated ketonic structures according to its ultraviolet spectrum,<sup>†</sup> but nevertheless gives a high and consistent value for the 1,2-glycol content by the titrimetric method.

The reasons for finding such discrepancies almost certainly lie in shortcomings of the viscometric method. For the samples of higher molecular weight, A and V, the discrepancy of ca. 20% in the 1,2-glycol content can not be accounted for by an error in the factor 1.89, which has the upper limiting value of 2.00, as the exponent of  $M$  in eq. (3) approaches the (unlikely) value of unity.<sup>13</sup> Rather, the explanation lies in that the  $\log [\eta]$ - $\log M$  relationship is not linear over the range of molecular weights considered and, indeed, that  $[\eta]$  becomes almost invariant with  $M$  for the lower molecular weight range. This last feature is demonstrated by our viscometric observation for polymer C (Table II), which we know to contain ca. 1.2% of 1,2-glycol units by the titrimetric method: the viscosity is practically unchanged on cleavage of the polymer. The osmotic pressure measurements on the polymers used to establish eq. (3) were probably in error as a result of leakage of low molecular weight polymer across the membrane,<sup>2</sup> most particularly for the lower range.<sup>14</sup> Also, we can find neither in the literature<sup>8,15</sup> nor empirically any linear  $\log [\eta]$ - $\log M$  equation which gives satisfactory results.

It should be emphasized that, in their original work, Flory and Leutner did not claim that their  $[\eta]$ - $M$  relationship was necessarily very reliable, but they rightly felt that it was useful for estimating the 1,2-glycol contents of their polyvinyl alcohol samples. However, it is our conclusion that the titrimetric method described here is more generally applicable and reliable, and is altogether to be preferred.

The authors wish to thank Mr. R. O. Cardwell for technical assistance.

\* We are indebted to a referee for pointing out this possibility.

† Measured by Mr. A. Ashbaugh of this laboratory.

## References

1. McLaren, A. D., and R. J. Davis, *J. Am. Chem. Soc.*, **68**, 1134 (1946); and refs. therein cited.
2. Flory, P. J., and F. S. Leutner, *J. Polymer Sci.*, **3**, 880 (1948); *ibid.*, **5**, 267 (1950).
3. Sakurada, I., and J. Takahashi, *Kyoto Daigaku Nippon Kagakuseni Kenkyusho Koenshu*, **14**, 37 (1957).
4. Imoto, S., J. Ukida, and T. Kominami, *Kobunshi Kagaku*, **14**, 214 (1957).
5. Jackson, E. L., in *Organic Reactions*, Vol. II, Wiley, New York, 1944, Chap. 8.
6. Kolthoff, I. M., and R. Belcher, *Volumetric Analysis*, Vol. III, Interscience, New York, 1957, p. 484.
7. Wilson, C. E., and H. J. Lucas, *J. Am. Chem. Soc.*, **58**, 2396 (1936).
8. Watson, R. W., J. A. R. Coope, and J. L. Barnwell, *Can. J. Chem.*, **29**, 885 (1951).
9. Rosen, I., G. H. McCain, A. L. Endrey, and C. L. Sturm, *J. Polymer Sci.*, **A1**, 951 (1963).
10. Matsumoto, M., and K. Imai, *J. Polymer Sci.*, **26**, 125 (1957).
11. Imai, K., and U. Maeda, *Kobunshi Kagaku*, **16**, 168 (1959).
12. Haas, H. C., H. Husek, and L. D. Taylor, *J. Polymer Sci.*, **A1**, 1215 (1963).
13. Flory, P. J., *Principles of Polymer Chemistry*, Cornell Univ. Press, Ithaca, N. Y., 1953, p. 313.
14. Schulz, G. V., *Z. Elektrochem.*, **60**, 199 (1956).
15. Beresniewicz, A., *J. Polymer Sci.*, **35**, 321 (1959).

## Résumé

On a appliqué une méthode titrimétrique pour la détermination des unités 1,2-glycol dans l'alcool polyvinylique par scission au périodate, impliquant la détermination de la consommation du périodate au moyen d'iode et d'oxyde arsénieux. La méthode donne des résultats concordants indépendamment du poids moléculaire de l'échantillon, et présente une précision de  $\pm 0.05\%$  d'unités glycols. Par contre, on a montré que la méthode viscosimétrique bien connue de Flory-Leutner donne des résultats qui sont environ 20% plus bas que ceux obtenus par la première méthode pour des échantillons de poids moléculaire plus élevé que 40.000 et donne grossièrement des résultats aberrants pour des échantillons de poids moléculaire beaucoup plus faible. On discute les détails des méthodes et les sources d'erreurs.

## Zusammenfassung

Zur Bestimmung der 1,2-Glykoleinheiten in Polyvinylalkohol wurde eine massanalytische Methode herangezogen, die auf einer Bestimmung des bei der Perjodatspaltung verbrauchten Perjodats mit Jod und Arsen(III)-oxyd beruht. Die Methode ergab unabhängig vom Molekulargewicht der Probe übereinstimmende Werte mit einer Genauigkeit von  $\pm 0,05\%$  Glykoleinheiten. Dagegen ergab die bekannte viskosimetrische Methode von Flory und Leutner für Proben mit höherem Molekulargewicht als etwa 40000 um etwa 20% niedrigere Werte als die erstgenannte Methode und für Proben mit viel niedrigerem Molekulargewicht ganz falsche Resultate. Einzelheiten der beiden Methoden und Fehlerquellen werden diskutiert.

Received August 30, 1963

Revised October 18, 1963

## Probability Theory of Asymmetric Chain Growth in Polymerization

TAKAYUKI FUENO and JUNJI FURUKAWA, *Department of Synthetic  
Chemistry, Kyoto University, Yoshida, Kyoto, Japan*

### Synopsis

Probability theory of Markov chains has been applied to the chain propagation step of binary and multicomponent copolymerizations. General equations are presented for the calculation of the fractional distribution of monomer units in linear copolymers of any arbitrary degree of polymerization. It is shown that in ordinary Markov processes, the effect of initiation progressively becomes unimportant as the chain length increases and that the polymer composition approaches its stationary limit determined by the transition probabilities alone. The possibility of preparing optically active polymers is discussed in the light of the theoretical results obtained.

### 1. INTRODUCTION

Ordinary kinetic theories of copolymerization utilize the fundamental assumptions that the statistical distribution of the active polymer end units, which select the reacting monomers according to the probabilities characterized by the monomer reactivity ratios, remains invariant in the region where the chain length of the growing polymer molecule is sufficiently large. This concept of statistical stationarity originates from an intuitive idea that the initiation of chains would hardly affect the monomer selection of the reactive end units of growing high polymers, and it is in fact justifiable on a mathematical background. Given the monomer feed ratios, one can then calculate the composition of high polymers with reasonable accuracy from known data of the monomer reactivity ratios or vice versa. The practical significance of the stationarity assumption admittedly has overshadowed a fair understanding of how the copolymer composition will vary with the progress of chain growth in the low molecular weight region. However, this last phase of the problem is currently receiving an increasing interest, both theoretically and experimentally, in connection with the configurational asymmetry induced in the resulting polymers.<sup>1-4</sup>

Insofar as the selection probability remains constant throughout the chain propagation step, the statistics of nonstationary chain growth of linear polymer is the one depicted by the theory of the one-dimensional finite Markov chain, and its rigorous expression is obtainable by means of a simple algebraic method.<sup>5</sup> In discussing the possibility of obtaining optically active polymers, Frisch, Schuerch, and Szwarc<sup>1</sup> have considered a special Markov chain in which two outcomes, *D* and *L*, follow their re-

spective predecessor units  $D$  and  $L$  with equal probabilities ( $DD = LL$ ). Their calculation indicates that in such a "symmetric" Markov process the mean specific rotation per monomer unit rapidly approaches zero as the molecular weight increases. They have also considered the polymerization mechanism governed by Bernoulli trials ( $DD = LD, DL = LL$ ) as a possible alternative to the "symmetric" Markov process and concluded that a Bernoulli trial scheme can yield a polymer with appreciable optical activity. However, a more general case, i.e., the "asymmetric" Markov process ( $DD \neq LL$ ), which is not necessarily Bernoullian, has never been treated explicitly with full attention to the asymmetric induction.

In recent years a number of investigators<sup>2,6-8</sup> have attempted to characterize stereoregular polymers on the basis of the theory of Markov chains in the ultimate stationarity. Among others, Price<sup>8</sup> presented a mathematical procedure which makes it straightforward to derive statistical expressions for discussing the influence of any number of preceding monomer units upon the reactivity of the end unit of the growing high polymer chain. Essentially, it was the mathematization of the stationary-state kinetics of multicomponent copolymerizations.

In the present paper, we will first deal with the nonstationary chain growth in the binary copolymerization. This is a generalization of the aforementioned work of Frisch et al. and covers even more important cases of "asymmetric" Markov processes. Second, we will extend the nonstationarity consideration to the multicomponent copolymerization. The approach is a formal extension of Price's procedure to cover the nonstationary region of the propagation. Finally, in the light of our results obtained, critical discussions will be made on the polymer composition, with particular reference to the asymmetric induction in polymerization.

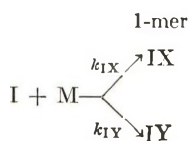
## II. BINARY COPOLYMERIZATIONS

### A. Finite Markov Process

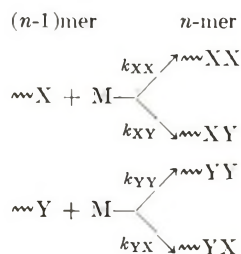
In discussing the probability process of chain growth in binary copolymerization we will consider homopolymerization of a monomer  $M$  which can take either of the two stereoisomeric forms  $X$  and  $Y$  in the resulting polymer chains. It is safe and convenient to classify such a homopolymerization into the category of binary copolymerization, inasmuch as every step of chain growth is subjected to the selection of one of the two possible monomeric configurations.

The mechanism of homopolymerizations of our present interest is represented by the appropriate sequence of the following elementary steps.

Initiation:



Propagation:



where I is an initiator,  $k$ 's are the bimolecular rate constants of the respective elementary steps specified by the subscripts, and  $n$  is, of course, any integer greater than unity. In this mechanism no termination or chain transfer is assumed to be operative.

Let  $x$  and  $y$  be the probabilities that the initiator selects the configurations X and Y, respectively. Obviously, we have the relations:

$$x = k_{IX}/(k_{IX} + k_{IY}) \quad (1a)$$

$$y = k_{IY}/(k_{IX} + k_{IY}) \quad (1b)$$

and

$$x + y = 1 \quad (2)$$

Next, let us denote by  $p_X$  and  $q_X$  the conditional probabilities that in the propagation step a growing polymer carrying an end unit X selects the X and Y configurations, respectively. Similar conditional probabilities of persistence and alternation of the end unit Y of a growing polymer chain on propagation will be respectively denoted by  $p_Y$  and  $q_Y$ . These four conditional probabilities should be related to the propagation rate constants in such a way that

$$p_X = k_{XX}/(k_{XX} + k_{XY}) \quad (3a)$$

$$q_X = k_{XY}/(k_{XX} + k_{XY}) \quad (3b)$$

$$p_Y = k_{YY}/(k_{YY} + k_{YX}) \quad (3c)$$

$$q_Y = k_{YX}/(k_{YY} + k_{YX}) \quad (3d)$$

which impose the following apparent restrictions on the persistence and alternation probabilities:

$$p_X + q_X = 1 \quad (4a)$$

and

$$p_Y + q_Y = 1 \quad (4b)$$

We are now ready to calculate the unconditional probability that the monomer unit occupying a given unit site of a polymer chain be in the X- (or Y-) configuration. Clearly, this calculation is mathematically identical

with calculating the probability that the end unit of a growing  $n$ -mer, sampled at random, be an X (or Y). We will denote such unconditional probabilities by the symbols  $\phi_X^{(n)}$  and  $\phi_Y^{(n)}$ . Now, let it be assumed that the conditional probabilities  $p$  and  $q$  remain constant throughout the course of polymerization, i.e., we assume that they are independent of both the conversion and the degree of polymerization. Then, our problem reduces to solving the simultaneous difference equations:

$$\phi_X^{(n)} = p_X \phi_X^{(n-1)} + q_Y \phi_Y^{(n-1)} \quad (5a)$$

$$\phi_Y^{(n)} = q_X \phi_X^{(n-1)} + p_Y \phi_Y^{(n-1)} \quad (5b)$$

under the initial conditions:

$$\phi_X^{(1)} = x \quad (6a)$$

$$\phi_Y^{(1)} = y \quad (6b)$$

It seems worthwhile to make some remarks on the probability process outlined above. In the first place, the present scheme of chain growth is essentially the statistical process governed by a simple finite chain of the Markov type and it has already been treated by Frisch, Schuerch, and Szwarc<sup>1</sup> for the special case where  $p_X = p_Y$ . In our treatment, however,  $p_X$  and  $p_Y$  may or may not be equal to each other, so that our scheme is more general than theirs. Secondly, the one-dimensional Markov process formulated above can readily be applied to real binary copolymerizations, insofar as we can invoke the usual hypothesis of low conversion. In such cases M is a mixture of two different monomeric species and it is only required to modify the conditional probabilities into

$$p_X = k_{XX}M_X/(k_{XX}M_X + k_{XY}M_Y) \text{ etc.} \quad (7)$$

where  $M_X$  and  $M_Y$  are the concentrations of the feed monomers.

Let us return to the problem of our finite Markov process. From eqs. (4) and (5) we have

$$\phi_X^{(n)} + \phi_Y^{(n)} = \phi_X^{(n-1)} + \phi_Y^{(n-1)}$$

which implies in conjunction with the restriction (2) and the initial conditions (6) the identity:

$$\phi_X^{(n)} + \phi_Y^{(n)} = 1 \quad (8)$$

Introduction of eqs. (4b) and (8) into eq. (5a) yields a difference equation for the component X alone:

$$\phi_X^{(n)} - (p_X + p_Y - 1)\phi_X^{(n-1)} - (1 - p_Y) = 0 \quad (9)$$

The general solution of eq. (9) is

$$\phi_X^{(n)} = \begin{cases} \alpha(p_X + p_Y - 1)^{n-1} + \frac{1 - p_Y}{2 - p_X - p_Y} & p_X + p_Y \neq 2 \\ C & p_X + p_Y = 2 \end{cases} \quad (10a)$$

$$(10b)$$

where  $\alpha$  and  $C$  are arbitrary constants to be determined from the initial condition (6a). Using eqs. (6a), (10a), and (10b) we find the final forms of  $\phi_X^{(n)}$ .

For case I,  $p_X + p_Y \neq 2$ :

$$\phi_X^{(n)} = \left( x - \frac{1 - p_Y}{2 - p_X - p_Y} \right) (p_X + p_Y - 1)^{n-1} + \frac{1 - p_Y}{2 - p_X - p_Y} \quad (11a)$$

For case II,  $p_X + p_Y = 2$ :

$$\phi_X^{(n)} = x \quad (11b)$$

The solution  $\phi_Y^{(n)}$  can be obtained either from the identity (8) or by mutually replacing subscripts X and Y as well as the quantities  $x$  and  $y$  appearing in eqs. (11a) and (11b).

It can be seen that if  $p_X + p_Y \neq 1$  in case I, the probability of finding an X unit in the  $n$ th site of a polymer varies with the increase in  $n$  and approaches, since  $|p_X + p_Y - 1| < 1$ , its limiting value determined by the conditional probabilities alone. Case II is trivial because the condition  $p_X + p_Y = 2$  requires that both  $p_X$  and  $p_Y$  must be unity. Since in such a case there should be no alternating chain propagation, it is obvious that the  $\phi_X^{(n)}$  averaged over many polymer molecules is all the time identical to the initial distribution  $x$  of 1-mers.

## B. Asymmetric Induction

In this section we will be concerned with the problem how and to what extent the asymmetry in population of the constituent configurational units is brought about to polymer chains.

The fraction,  $F_X^{(N)}$  or  $F_Y^{(N)}$ , of the units of one configuration involved in an  $N$ -mer is given, on the average, by

$$F_X^{(N)} = (1/N) \sum_{n=1}^N \phi_X^{(n)} \quad (12)$$

$$F_Y^{(N)} = (1/N) \sum_{n=1}^N \phi_Y^{(n)}$$

The fraction,  $\omega_X^{(N)}$  or  $\omega_Y^{(N)}$ , of one configuration in excess over that of the other in an  $N$ -mer is then given by

$$\omega_X^{(N)} = F_X^{(N)} - F_Y^{(N)} = (2/N) \sum_{n=1}^N \phi_X^{(n)} - 1 \quad (13a)$$

$$\omega_Y^{(N)} = -\omega_X^{(N)} \quad (13b)$$

Substitution of eqs. (11a) and (11b) into eq. (13a) results in the following expressions.

For case I,  $p_X + p_Y \neq 2$ :

$$\omega_X^{(N)} = 2 \left( x - \frac{1 - p_Y}{2 - p_X - p_Y} \right) \left[ \frac{1 - (p_X + p_Y - 1)^N}{(2 - p_X - p_Y)N} \right] + \frac{p_X - p_Y}{2 - p_X - p_Y} \quad (14a)$$

For case II,  $p_X = p_Y = 1$ :

$$\omega_X^{(N)} = 2x - 1 \quad (14b)$$

At this point let us consider two special, yet familiar, cases which can readily be reduced from case I. One is the case (case III) where  $p_X$  is equal to  $p_Y$ , while the other is a case (case IV) for which  $p_X + p_Y = 1$ . From eq. (14a) we have the following expressions of  $\omega_X^{(N)}$  for these special cases.

For case III,  $p_X = p_Y \neq 1$  (symmetric Markov chains):

$$\omega_X^{(N)} = [(2x - 1)/(2 - 2p_X)][1 - (2p_X - 1)^N]/N \quad (14c)$$

For case IV,  $p_X + p_Y = 1$  (Bernoulli trials):

$$\omega_X^{(N)} = [2(x - p_X)/N] + (2p_X - 1) \quad (14d)$$

Equation (14c) of case III is exactly identical with the familiar expression derived by Frisch et al.<sup>1</sup> In this special case the asymmetry of configurational composition induced by initiation rapidly decreases and does approach zero as the chain length  $N$  increases. This convergence is a direct consequence of the trend that when  $p_X = p_Y$  the unconditional probability,  $\phi_X^{(n)}$  or  $\phi_Y^{(n)}$ , of finding one configuration in the  $n$ th site approaches  $1/2$  as  $n$  increases. Both the fractions,  $F_X^{(N)}$  and  $F_Y^{(N)}$ , thus take on the same value of  $1/2$  in an infinitely long polymer chain. In this sense we may refer to case III as the case of "symmetric" Markov chains. In a subsequent section the conditions for such symmetric processes will be further discussed in a more general fashion.

In case IV the condition  $p_X + p_Y = 1$  greatly simplifies the unconditional probability. That is,  $\phi_X^{(1)} = x$  because  $(p_X + p_Y - 1)^{n-1} = 0^0 = 1$ , while  $\phi_X^{(n)} = p_X$  when  $n \geq 2$ . Furthermore, the above condition demands the equalities  $p_X = q_Y$  and  $q_X = p_Y$ . These characteristics are tantamount to the statement that in the propagation step ( $n \geq 2$ ) the configuration of adding monomers is selected in a manner independent of the nature of the growing polymer end. Thus, statistics of chain propagation in this case is one governed by Bernoulli trials. In particular, if the Bernoulli trial scheme extends over the initiation step so that  $x = p_X$ , then eq. (14d) is simplified to

$$\omega_X^{(N)} = 2p_X - 1 \quad (14e)$$

an expression which also was derived by Frisch et al.<sup>1</sup> from the random walk considerations.

It will be apparent from the foregoing that the asymmetry to be induced in an infinitely long linear polymer is not confined to Bernoullian cases.

It is possible to conclude that asymmetric induction does occur whenever the two persistence probabilities  $p_X$  and  $p_Y$ , and consequently the two alternation probabilities  $q_X$  and  $q_Y$ , are different. This conclusion is valid irrespective of which probability process the chain growth may follow, the Markov process or the Bernoulli trial scheme.

Generally, the fraction of X configurations in excess over that of Y configurations in an infinitely long chain,  $\omega_X$ , is given from eq. (14a) as

$$\omega_X = \lim_{N \rightarrow \infty} \omega_X^{(N)} = (p_X - p_Y)/(2 - p_X - p_Y) \quad (15)$$

except for the trivial case II, where  $\omega_X = 2x - 1$ . Cases III and IV need no separate consideration. Equation (15) transforms into

$$p_Y - 1 = [(1 + \omega_X)/(1 - \omega_X)] (p_X - 1) \quad (16)$$

which on plotting  $p_Y$  against  $p_X$  gives a group of straight lines radiating from a common point ( $p_X = p_Y = 1$ ) with various slopes  $(1 + \omega_X)/(1 - \omega_X)$ , as is illustrated in Figure 1.

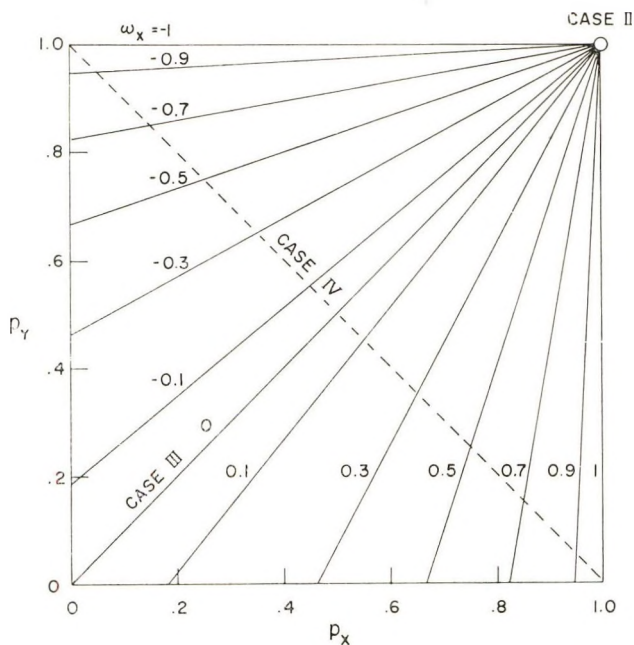


Fig. 1. Contour diagram of  $\omega_X$  as a function of  $p_X$  and  $p_Y$ .

### III. EXTENSION TO MULTICOMPONENT COPOLYMERIZATIONS

It is not difficult to extend the above nonstationarity considerations of copolymer compositions to cases in which there are more than two monomeric species entering into copolymerization. Here we intend to derive expressions for the fractional distribution of each constituent monomer unit which is present in a linear copolymer of a given degree of polymerization.

Although such multicomponent copolymerizations may be of little practical importance, the formulation extended to cover these cases does seem to be useful for understanding the feature characteristic of the process of asymmetric induction.

We shall consider a copolymerization system of  $m$  monomers ( $m \geq 2$ ). Let us denote by  $\phi_i^{(n)}$  the probability of finding a monomer unit  $i$  in the  $n$ th site of a polymer chain, the sites having been numbered in the order in which monomer units have been added to the growing chain. Clearly, we should have a constraint relation such that

$$\sum_{i=1}^m \phi_i^{(n)} = 1 \quad (17)$$

Let  $p_{ij}$  be the conditional probability that in polymer chains a monomer unit  $i$  follows its predecessor unit  $j$ , i.e., the probability that a growing polymer with the terminal unit  $j$  selects an adding monomer  $i$  in the chain propagation step. In the terminology of probability theory,  $p_{ij}$  is the conditional probability of transition from the initial state  $j$  to the final state  $i$ . Persisting to the hypothesis of low conversion, we write for  $p_{ij}$

$$p_{ij} = k_{ji}M_i / \sum_{h=1}^m k_{jh}M_h \quad (18)$$

where  $M$ 's are the feed concentrations of the monomers designated by the subscripts and  $k_{jh}$ , for instance, is the specific rate constant at which the monomer  $h$  adds to the polymer end unit  $j$ . Obviously, the transition probabilities are subject to the stochastic restriction:

$$\sum_{i=1}^m p_{ij} = 1 \quad j = 1, 2, \dots, m \quad (19)$$

Simultaneous difference equations corresponding to eq. (5) of the binary case can be written in a compact form:

$$\phi^{(n)} = \mathbf{P}\phi^{(n-1)} \quad (20)$$

with the initial conditions:

$$\phi^{(1)} = \mathbf{x} \quad (21)$$

where  $\phi^{(n)}$  is a column vector whose components are  $\phi_1^{(n)}, \phi_2^{(n)}, \dots, \phi_m^{(n)}$ ;  $\mathbf{x}$  is a column vector with the initial monomer unit distributions  $x_1, x_2, \dots, x_m$  as components; and  $\mathbf{P}$  is an  $m \times m$  stochastic matrix having  $p_{ij}$  as the elements, where  $i$  refers to the row and  $j$  the column.

Now, let us seek a particular solution  $\phi^{(n)}$  of the form:

$$\phi^{(n)} = \psi \lambda^{n-1} \quad (22)$$

where  $\lambda$  is a scalar parameter to be determined and  $\psi$  is a column vector  $\psi = \{\psi_1, \psi_2, \dots, \psi_m\}$  independent of the variable  $n$ . Substituting eq. (22) into eq. (20), we have upon cancellation

$$\mathbf{P}\psi = \lambda\psi \quad (23)$$

The value of  $\lambda$  can be obtained as one of the roots of the characteristic equation of  $\mathbf{P}$

$$K(\lambda) = \text{Det. } |p_{ij} - \lambda \delta_{ij}| = 0 \quad (24)$$

where  $\delta_{ij}$  is the Kronecker delta which equals unity when  $i = j$  and vanishes otherwise. The characteristic equation gives  $m$  eigenvalues including possible multiple roots. For the sake of simplicity we consider only the cases of no multiplicity for a moment and let these distinct eigenvalues be  $\lambda_1, \lambda_2, \dots, \lambda_m$  in decreasing order of magnitude. Corresponding to each  $\lambda_s$  there is an eigenvector  $\psi^{(s)}$ , which we normalize to unity here, i.e.,

$$\sum_{i=1}^m [\psi_i^{(s)}]^2 = 1$$

The general solution satisfying the difference equation is given by a linear combination of the particular solutions obtained as above. Thus we write

$$\phi_i^{(n)} = \sum_{s=1}^m \psi_i^{(s)} \alpha_s \lambda_s^{n-1} \quad i = 1, 2, \dots, m \quad (25)$$

Here the  $\alpha_s$ 's are the linear combination coefficients to be determined from the initial distributions. They can be obtained by solving

$$x_i = \sum_{s=1}^m \psi_i^{(s)} \alpha_s \quad i = 1, 2, \dots, m \quad (26)$$

which is a simultaneous set of nonhomogeneous linear equations in  $\alpha_s$ . Note that eqs. (25) and (26) are valid even when a  $\lambda_s$  takes on the value zero.

Our set of eigenvalues bears some important characteristics as a result of the stochastic restriction (19). It is possible to demonstrate<sup>5</sup> (a) that there always exists one eigenvalue equal to unity, (b) that it is the only unit eigenvalue if  $\mathbf{P}$  is not such a matrix that can be reduced to two or more isolated stochastic blocks, and (c) that all other eigenvalues are less than unity in the absolute magnitude. Thus, aside from the trivial case of blocked stochastic processes, our largest eigenvalue alone must be identically equal to unity, i.e.,  $\lambda_1 = 1$ , and other eigenvalues are such that  $|\lambda_s| < 1, s = 2, 3, \dots, m$ .

One can now formulate the average fractional distribution,  $F_i^{(N)}$ , of the monomer unit  $i$  existing in a linear polymer of the degree of polymerization  $N$ .

$$F_i^{(N)} = \frac{1}{N} \sum_{n=1}^N \phi_i^{(n)} = \psi_i^{(1)} \alpha_1 + \sum_{s=2}^m \frac{\psi_i^{(s)} \alpha_s (1 - \lambda_s^N)}{N(1 - \lambda_s)} \quad i = 1, 2, \dots, m \quad (27)$$

Clearly, the second term of eq. (27) tends to zero with the increase of  $N$ , and  $F_i^{(N)}$  approaches its limiting value  $\psi_i^{(1)} \alpha_1$  correspondingly. The  $\phi_i^{(n)}$  function (25) also converges to  $\psi_i^{(1)} \alpha_1$  as  $n$  increases infinitely.

Here, it is worthwhile to demonstrate one characteristic property attached to the eigenvectors of our stochastic matrix. Equation (23) can be represented by its algebraic version:

$$\lambda_s \psi_i^{(s)} = \sum_{j=1}^m p_{ij} \psi_j^{(s)} \quad s, i = 1, 2, \dots, m \quad (28)$$

Summing up both sides of eq. (28) over all  $i$ , we have

$$(\lambda_s - 1) \sum_{i=1}^m \psi_i^{(s)} = 0 \quad s = 1, 2, \dots, m \quad (29)$$

where the stochastic restriction (19) has been utilized. Equation (29) indicates that the total sum of the components of an eigenvector  $\psi^{(s)}$  vanishes if its eigenvalue  $\lambda_s$  is different from unity whereas it is not necessarily zero when and only when  $\lambda_s$  is equal to unity, the largest permissible value. To ensure the constraint relation (17), the summation for the case of  $\lambda_s = 1$  must take on a nonzero value. Thus,

$$\sum_{i=1}^m \psi_i^{(s)} \begin{cases} \neq 0 & \text{for } s = 1 \\ = 0 & \text{for } s \geq 2 \end{cases} \quad (30)$$

Use of eq. (30) leads to two important realizations in the following manner.

Firstly, by summing up eq. (26) over all  $i$  and utilizing eq. (30), one sees that

$$\alpha_1 = \left[ \sum_{i=1}^m \psi_i^{(1)} \right]^{-1} \quad (31)$$

where the constraint condition for the initial distribution,  $\sum x_i = 1$ , has been invoked. It follows that in an infinitely long copolymer the fractional distribution of each component monomer unit,  $F_i$ , is given by

$$F_i = \lim_{N \rightarrow \infty} F_i^{(N)} = \psi_i^{(1)} / \sum_{j=1}^m \psi_j^{(1)} = K_{ii}(1) / \sum_{j=1}^m K_{jj}(1) \quad (32)$$

Here,  $K_{jj}(1)$  is the diagonal minor determinant obtained by striking out the  $j$ th row and column of the characteristic determinant (24) corresponding to the unit eigenvalue  $\lambda_1 = 1$ . The last equality<sup>9</sup> in eq. (32) arises from the following identity holding between the diagonal and off-diagonal minors belonging to the same column of our singular determinant  $K(1)$ :

$$(-1)^{h+j} K_{hj}(1) = K_{jj}(1) \quad (33)$$

Thus we can conclude that the fraction of each monomer unit involved in a growing copolymer is relaxed with the progress of chain growth from its initial value  $F_i^{(1)} = x_i$  to its stationary value  $F_i$ , the latter of which is independent of the initial distributions and is a function of the transition probabilities alone.

Second, upon summing up eq. (27) over all  $i$  under cognizance of eq. (30), one can immediately verify the equality

$$\sum_{i=1}^m P_i^{(N)} = 1 \quad (34)$$

which is an obvious constraint relation to be satisfied by the fractional distributions of monomer units constituting a linear  $N$ -mer. The constraint relation (17) can be proved from eq. (25) by means of an analogous summation procedure.

So far, considerations have been limited to the cases in which the eigenvalues are distinct. The cases of multiple eigenvalues may be treated by similar methods, although certain modifications need to be introduced depending on the form of the matrix of transition probabilities. So far as the stationary copolymer composition is concerned, however, eq. (32) is valid even when some of the eigenvalues  $\lambda_s$  other than unity are multiple.

We now turn to the problem of the compositional "isometry" of infinitely long copolymers formed in the multicomponent copolymerizations.

In order that all the fractions of various monomers are identical in the stationary limit of copolymerization, it is required that the  $\psi^{(1)}$  be a column vector such that all the components are  $1/m$ , i.e.,

$$\psi_i^{(1)} = 1/m \quad i = 1, 2, \dots, m \quad (35)$$

Equation (28) for  $\lambda_s = 1$  is then reduced to

$$\sum_{j=1}^m p_{ij} = 1 \quad i = 1, 2, \dots, m \quad (36)$$

in formal contrast to the restriction (19). What eq. (36) implies is that the conditional probabilities of a unit  $i$  being preceded by various units in a chain must add up to unity. Thus we may conclude without elaborate calculations that the polymer composition tends to be isometric with the progress of our Markov chain growth if the process of the Markov chains is stochastic with respect to the predecessors also. Conversely, the stationary composition will be uneven if the Markov process is not doubly stochastic.

As an example of such Markov chains satisfying the stochastic reversibility one may conceive those stochastic chains in which the transition matrix  $\mathbf{P}$  is a symmetric matrix, i.e.,  $\mathbf{P}$  is identical with its transpose matrix  $\mathbf{P}^T$ . There, each conditional probability  $p_{ji}$  corresponding to the transition from  $i$  to  $j$  is equal to  $p_{ij}$  for the transition from  $j$  to  $i$ , so that the reversibility (36) is fulfilled whenever the stochastic restriction (19) holds. In such symmetric Markov processes the fractional distributions of various units accumulated in the chain must be uniform in the stationary limit. This statement does not appear to be intuitively obvious. Note that the relative magnitudes of various persistence probabilities  $p_{ii}$  are of no primary concern with the possibility of occurrence of the isometric copolymer composition.

Finally, it should be pointed out that in the case of binary copolymerization the requirement for the stochastic reversibility,  $p_X + q_Y = 1$ , is satisfied only when  $q_X = q_Y$  and consequently  $p_X = p_Y$ . Therefore, the

composition of infinitely long binary copolymers must be asymmetric in favor of one component monomer over the other, if the two alternation probabilities (and consequently the two persistence probabilities) are different from each other. This was the conclusion reached in Section IIB.

#### IV. SAMPLE CALCULATIONS

In binary copolymerizations the fraction of one component monomer existing in the polymer chain in excess over the other is calculated from either eq. (14a) or (14b) if the values of the four independent parameters  $N$ ,  $x$ ,  $p_X$ , and  $p_Y$  are given. In Figure 2, variations of the excess fraction  $\omega_X^{(N)}$  with increasing  $N$  are compared among various combinations of  $p_X$  and  $p_Y$  for a fixed initial distribution of  $x = 0.9$ . Figure 3 illustrates the variations of  $\omega_X^{(N)}$  for different initial distributions, where  $p_X$  has been kept constant at 0.9 while  $p_Y$  has been assigned various values.

From Figures 2 and 3 it can be seen that as the chain length  $N$  increases the effect of the initial distribution progressively wears off and the  $\omega_X^{(N)}$  approaches its stationary value depending on  $p_X$  and  $p_Y$  alone. The sway of  $\omega_X^{(N)}$  noticed in the low molecular weight region is due to the large alternation tendency in the chain propagation step. It occurs whenever  $p_X + p_Y < 1$  but is more marked, the smaller the sum  $p_X + p_Y$ .

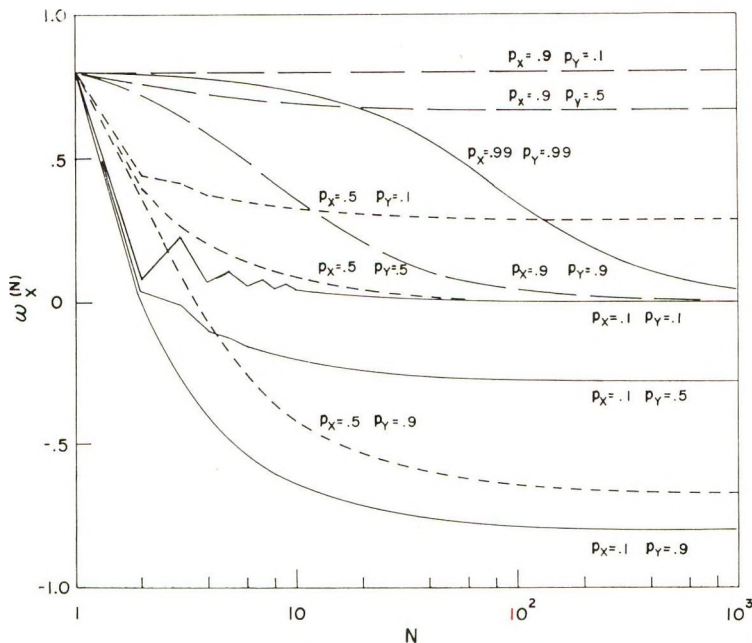


Fig. 2. Comparison of the variations of the excess fraction  $\omega_X^{(N)}$  among various combinations of  $p_X$  and  $p_Y$  in binary copolymerization. The 1-mer distribution  $x$  is fixed at 0.9.

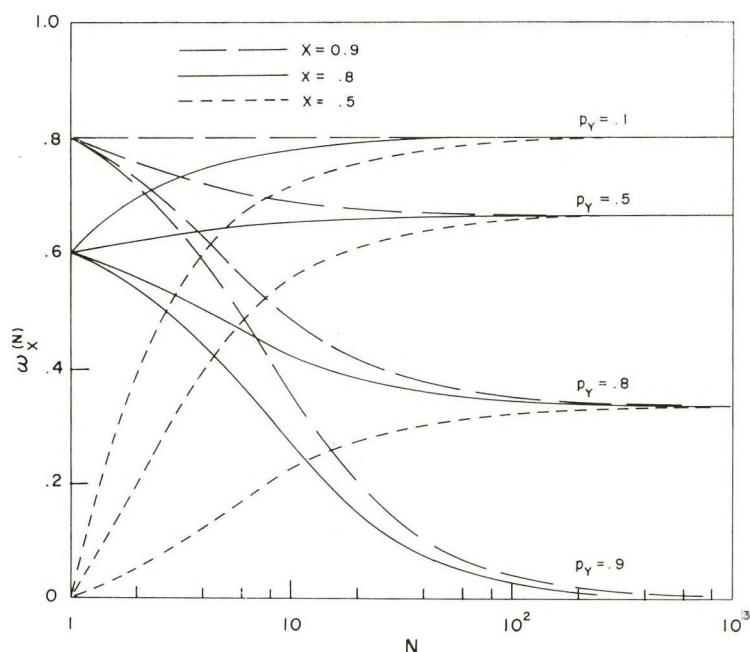


Fig. 3. Variations of the excess fraction  $\omega_X^{(N)}$  for different 1-mer distributions  $x$  in binary copolymerization. For each  $x$  the value of  $p_Y$  is varied while that of  $p_X$  is fixed at 0.9.

Figure 4 exemplifies the variations of the polymer composition with increasing  $N$  in ternary copolymerization. For the sake of comparison, two contrasting stochastic matrices have been selected for a fixed initial condition:  $x_1 = 1, x_2 = x_3 = 0$ .

$$\mathbf{P}_1 = \begin{pmatrix} 0.1 & 0.1 & 0.1 \\ 0.1 & 0.7 & 0.1 \\ 0.8 & 0.2 & 0.8 \end{pmatrix}$$

$$\mathbf{P}_2 = \begin{pmatrix} 0.6 & 0.2 & 0.2 \\ 0.1 & 0.2 & 0.7 \\ 0.3 & 0.6 & 0.1 \end{pmatrix}$$

$$\mathbf{x} = \begin{pmatrix} 1 \\ 0 \\ 0 \end{pmatrix}$$

In the case of  $\mathbf{P}_1$ , the monomer labeled 3 is favored for copolymerization, as is evident from the form of the matrix.  $\mathbf{P}_2$  provides an example of the equal stationary populations of the three monomers. Notice that the elements in  $\mathbf{P}_2$  add up to unity along every row as well as column. The eigenvalues of the former matrix are 1, 0.6, and 0 while for the latter they are 1, 0.4, and  $-0.5$ . The feature of wearing-off of the initial memory with the increase of  $N$  remains much the same as in binary copolymerizations.

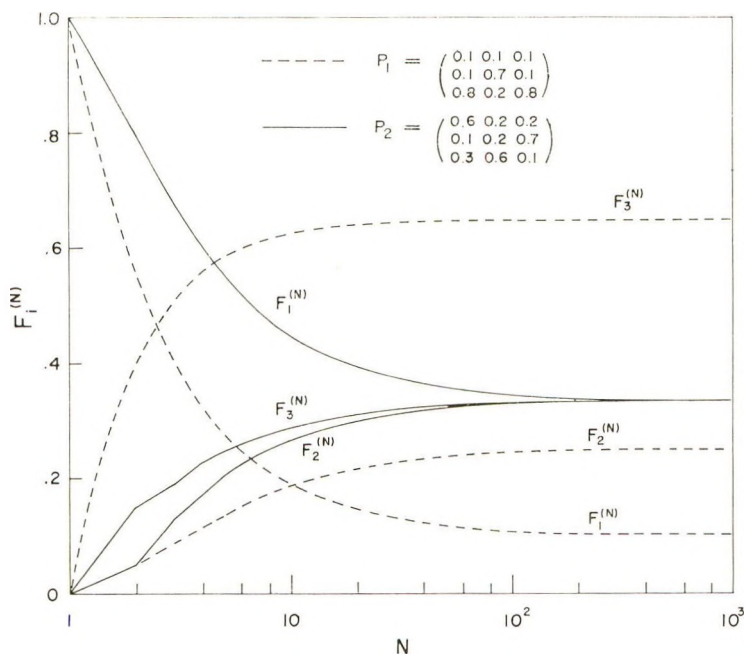


Fig. 4. Examples of the variation of the fractional distribution  $F_i^{(N)}$  in ternary copolymerization. The 1-mer distribution is:  $x_1 = 1$  and  $x_2 = x_3 = 0$ .

## V. DISCUSSION

Optical activity of the polymers prepared by asymmetric induction is attributed primarily to the prevalence of monomer units of one steric configuration  $D$  (or  $L$ ) over those of the other  $L$  (or  $D$ ) and to the conformational factors controlling the spacial arrangement of the monomer configurations. As has already been mentioned, Frisch, Schuerch, and Szwarc<sup>1</sup> revealed the theoretical aspect of the configurational contribution, by considering two extreme mechanisms governed by the statistics of the "symmetric" Markov chains ( $DD = LL$ ,  $DL = LD$ ) and the Bernoulli trials (or "biased" random walks such that  $DD = LD \neq DL = LL$ ). In the former mechanism the memory of asymmetric initiation, if any, rapidly wears off with the increase of the chain length, so that the optical activity of the resulting polymers tends to zero for very high molecular weights. In the latter case, on the other hand, the asymmetry of the polymer composition is maintained throughout the process of chain growth, yielding thus the polymer molecules of appreciable optical activity.

On the basis of the above criterion, Farina and Bressan<sup>3</sup> have discussed their experimental data on asymmetric polymerization of benzofuran in the presence of optically active  $\beta$ -phenylalanine and claimed that the effect of asymmetric growth is of exclusive importance relative to that of asymmetric initiation. However, it should be remarked here with some emphasis that the Bernoulli trial scheme is not the only probability process

leading to the asymmetric composition of the resulting high polymers. More specifically, the condition  $DD \neq LL$  does not necessarily guarantee the equalities  $DD = LD$  and  $DL = LL$ , which should be imposed on the propagation step if it is a process of Bernoulli trials. Instead, probability processes such that  $LD \neq DD \neq LL \neq DL$  may well be conceivable.

In such a more general Markov case, which is neither the case of symmetric Markov chains nor the Bernoulli trial scheme, the polymer composition can indeed be asymmetric in its stationary limit, as is clearly visualized in Figures 1-3. Thus, our treatment provides a sound theoretical basis to the otherwise not quite general reasoning of Farina and Bressan,<sup>3</sup> who correctly stress the importance of the asymmetric chain propagation ( $DD \neq LL$ ) in asymmetric polymerization.

Although in certain asymmetric polymerizations the mechanism of the asymmetric Markov chains could be even more important than that of the Bernoulli trial scheme, discrimination between the two mechanisms is not quite an easy practice. Even if the contribution of the conformational factor of polymer chains to the optical activity is negligibly small compared to that of the configurational factor, it is impossible to evaluate the probability parameters uniquely from the data for optical rotatory power of high polymers alone (see Fig. 1). Resolution of this point would have to await either establishment of the empirical relation between tacticity and asymmetry of high polymers or accumulation of experimental data on asymmetric polymerizations, especially in the low molecular weight region.

## VI. CONCLUSIONS

1. When the chain propagation step of copolymerization is governed by the mechanism leading to the statistics of Markov chains, each fraction of component monomers linked in the copolymer chain more or less rapidly converges, with the progress of chain growth, to its stationary value determined from the transition probabilities alone.

2. Asymmetric polymerization occurs whenever the two conditional probabilities of persistence ( $p_X$  and  $p_Y$ ), and consequently those of alternation ( $q_X$  and  $q_Y$ ), of the polymer end configuration are unequal to each other. In short, asymmetric polymerization is possible if the stochastic matrix

$$\begin{pmatrix} p_X & q_Y \\ q_X & p_Y \end{pmatrix}$$

is asymmetric.

3. The above conclusions can be generalized to cover the copolymerizations of more than two reacting monomers. Generally, if the Markov process does not contain two or more stochastic blocks, the copolymer composition in its stationary limit is calculated as the ratio among the diagonal minors derived from the characteristic determinant of the stochastic matrix corresponding to the unit eigenvalue. The stationary composition is iso-

metric over the component monomers in the polymer chain only when the Markov process is doubly stochastic.

### References

1. Frisch, H. L., C. Schuerch, and M. Szwarc, *J. Polymer Sci.*, **11**, 559 (1953).
2. Coleman, B. D., *J. Polymer Sci.*, **31**, 155 (1958).
3. Farina, M., and G. Bressan, *Makromol. Chem.*, **61**, 79 (1963).
4. Chu, N. S., and C. C. Price, *J. Polymer Sci.*, **A1**, 1105 (1963).
5. Feller, W., *An Introduction to Probability Theory and Its Application*, Wiley, New York, 1950, Chap. 16.
6. Miller, R. L., and L. E. Nielsen, *J. Polymer Sci.*, **46**, 303 (1960).
7. Johnsen, U., *Kolloid-Z.*, **178**, 161 (1961).
8. Price, F. P., *J. Chem. Phys.*, **36**, 209 (1962).
9. Fueno, T., and J. Furukawa, unpublished work.

### Résumé

On a appliqué la théorie des probabilités des chaînes de Markov à l'étape de propagation de chaînes en copolymérisation à composant linéaires et multiples. On présente des équations générales pour le calcul de la distribution fractionnée des unités de monomère dans le copolymère linéaire à n'importe quel degré arbitraire de polymérisation. On montre que, dans les processus de Markov habituels, l'effet de l'initiation devient progressivement négligeable quand la longueur de chaîne augmente et que la composition du polymère approche de sa limite stationnaire déterminée par les probabilités de transition seules. On discute la possibilité de préparer des polymères optiquement actifs à la lumière des résultats théoriques obtenus.

### Zusammenfassung

Die Wahrscheinlichkeitstheorie der Markov-Ketten wurde auf den Wachstumsschritt von Zwei- und Mehrkomponenten-Copolymerisationen angewandt. Es werden allgemeine Gleichungen zur Berechnung der Verteilung der Monomereinheiten in linearen Copolymeren von beliebigem Polymerisationsgrad angegeben. Bei gewöhnlichen Markov-Prozessen wird der Einfluss der Startreaktion mit steigender Kettenlänge in zunehmendem Masse vernachlässigbar und die Polymerzusammensetzung nähert sich dem nur durch die Übergangswahrscheinlichkeiten bestimmten stationären Grenzwert. Die Möglichkeit der Herstellung optisch aktiver Polymerer wird auf der Grundlage der gewonnenen theoretischen Ergebnisse diskutiert.

Received September 3, 1963

Revised October 21, 1963

## Polyethylene Crystallized from the Melt under Elevated Pressure\*

BERNHARD WUNDERLICH, *Department of Chemistry, Rensselaer Polytechnic Institute, Troy, New York*, and TAMIO ARAKAWA, *Department of Chemistry, Cornell University, Ithaca, New York*

### Synopsis

Polyethylene of the linear, low-pressure type has been crystallized under pressure (up to 5400 atm.) from the melt. Crystallization conditions of constant supercooling and constant cooling rates were employed. The resulting solid was analyzed at atmospheric pressure. In contrast to solution crystallization under pressure above 2000 atm., extended chain lamellae of increasing thickness become dominant. These show a maximum melting point of 140°C. and in this research, densities of up to 0.994 g./cm.<sup>3</sup>. Combining these data on large crystals with the experimental maximum melting temperatures and thickness data on low and atmospheric pressure crystallized lamellae yields a surface free energy of 91 ergs/cm.<sup>2</sup> for folded chain lamellae crystallized at low pressure.

### INTRODUCTION

In this paper an account will be given of experiments on crystallization of linear polyethylene from the melt under varied conditions of temperature and pressure. The experiments led to a highly crystalline state never before attained. The morphology of these high pressure crystals has been found to be of the extended-chain type and is described in a separate publication.<sup>1</sup> Here the melting behavior, crystallinity, and surface free energy of the crystals when removed from the high pressure autoclave will be discussed.

### EXPERIMENTAL

#### Crystallization

Linear unfractionated polyethylene (Marlex 50) ( $\bar{M}_w = 1.25 \times 10^5$ ;  $\bar{M}_n = 1.1 \times 10^4$ ) was used throughout this research. About 10 g. was melted under vacuum into brass bellows at 170°C. After being sealed, the bellows were placed into the pressure vessel. The pressure vessel was heated to the crystallization temperature under atmospheric pressure. After constant temperature was obtained, hydraulic oil was pumped into

\* Presented in part at the 142nd American Chemical Society Meeting, Atlantic City, September 1962.

the system and the crystallization pressure was applied within 1–3 min. The pressure was kept constant afterward by an automatic regulating device.<sup>2</sup>

The high-pressure apparatus used in this study is described elsewhere.<sup>2</sup> Heating up to 170°C. was carried out by immersion in a thermostatted oil bath, which was constant within  $\pm 0.1^\circ\text{C}$ . For temperatures higher than 170°C., the pressure vessel was heated with heating tapes. The temperature inside the bomb could in this case be controlled to within  $\pm 1^\circ\text{C}$ . The pressure was maintained constant during the course of the experiment with an accuracy of  $\pm 1.5\%$ .

The crystallizations were carried out in two ways. (a) For crystallization at constant degree of supercooling (samples 1–15 in Table I) the system was kept under constant temperature ( $t_c$ ) and pressure ( $P_c$ ) for a certain period of time (usually 8 hr.). Then cooling was carried out at the rate of  $4^\circ\text{C./hr.}$  at the same pressure.  $t_c$  and  $P_c$  were chosen to give approximately  $10^\circ\text{C.}$  of supercooling. (b) The second mode of crystallization (samples 16–24 in Table I) allowed different degrees of supercooling. The sample was first heated to 170°C. Cooling under constant pressure started at the rate of  $4^\circ\text{C./hr.}$  as soon as the crystallization pressure was reached. In both cases the pressure was released when the temperature dropped below  $50^\circ\text{C}$ . The samples were analyzed subsequently under atmospheric pressure.

### Analysis of the Samples

A density-gradient column consisting of toluene–chlorobenzene mixture was used. This column covered a density range of 0.96–1.00 g./cm.<sup>3</sup> with an accuracy of  $\pm 0.0002$  g./cm.<sup>3</sup>. The density variations within any one sample were  $\pm 0.001$ .

A General Electric XRD-5 diffractometer with a copper target tube was used. NaCl powder was the reference sample for the determination of (100) and (200) spacings. The method described by Hendus and Schnell<sup>3</sup> was followed to calculate crystallinity from the x-ray intensities.

The melting phenomena of the samples were studied by means of DTA. The description of the apparatus and the determination of melting points from a DTA chart are found elsewhere.<sup>4</sup> The weight of the sample was controlled to  $0.50 \pm 0.01$  g. The heating rate employed was  $1.46$ – $1.66^\circ\text{C./min.}$  The temperatures read from the DTA traces were the beginning of melting, peak temperatures, and the experimental maximum melting point. The beginning of melting was taken at the temperature where the temperature difference recording had increased to 5% of the total melting peak height. The experimental maximum melting point is that point where the last detectable amount of heat of fusion is absorbed. Its detection in DTA experiments is discussed elsewhere.<sup>4</sup> All thermal measurements described up to this point were carried out rapidly enough so that no appreciable reorganization could take place before the melting.<sup>5</sup>

Several of the samples (1-26) were cooled in the DTA setup rapidly after completion of the initial melting. After reaching room temperature these were rerun and showed independent of pressure crystallization history identical melting patterns, indicating that no permanent change was imparted to the polymer.

Samples crystallized at the highest pressures showed several small side peaks instead of the one low-temperature peak. To investigate these, samples 9, 11, and 24 with one small side peak and samples 15 and 26 with two small side peaks were rerun in the following way. The normal DTA heating was carried out up past the first peak; then the sample was quenched to room temperature and rerun. For samples 9, 11, and 24 this time the temperature was raised to the final melting point, while for samples 15 and 26 after going over the second peak the quenching was repeated, and in the third heating the samples were heated all the way to melting. For samples 9, 11, and 24 the side peak shifted in this series of experiments from the first heating to the second. In samples 15 and 26 in the second heating, two peaks appeared. In the last heating only one low temperature peak was found. The main melting peak was unaffected by all these experiments. From this it is concluded that these small peaks are no artifacts, but are the result of the actual defect distribution in the polymer sample, which can be altered by annealing.

Low-angle x-ray, and electron microscopy on fractured surfaces, were carried out by P. H. Geil at the Camille Dreyfus Laboratory and F. R. Anderson at the Chemstrand Research Center. The samples investigated by these techniques are labeled A-F in Table I. The techniques and results are presented in a separate paper.<sup>1</sup>

## RESULTS

Crystallization conditions as well as density, x-ray, and DTA results are summarized in Table I. The  $\Delta T$  column was calculated by using the equation

$$\Delta T = t_m + 0.02P_c - t_c$$

where  $t_m$  is the equilibrium melting point of the polymer investigated ( $t_m$  is 140°C., as will be discussed below). The crystallinity from density was calculated on the basis of values of using 1.001 cm.<sup>3</sup>/g. as the specific volume of the perfect crystal<sup>6</sup> at 25°C. and 1.173 cm.<sup>3</sup>/g. for the amorphous polyethylene<sup>7</sup> extrapolated to 25°C. The samples marked with an asterisk in the low-temperature peak column showed several small peaks instead of one low-temperature peak (see above and Fig. 1).

Figure 1 shows five DTA traces illustrating the disappearance of the low-temperature peak and the appearance of the high-temperature peak on increasing the crystallization pressure at constant supercooling.

Figure 2 shows the experimental maximum melting points and the position of the low- and high-temperature peaks.

TABLE I. Data of Polyethylene Crystallized under Different Pressures

Sample <sup>a</sup>	Crystallization conditions				Density			X-Ray measurement			DTA results		
	Temp., °C.	Press., atm.	Time, hr.	$\Delta T$ , °C.	$d$ (25°C.), g./cm. <sup>3</sup>	Cryst., %	[110] spacing, Å.	[200] spacing, Å.	Cryst., %	Beginning of melting, °C.	Low temp. peak, °C.	High temp. peak, °C.	Extrap. m.p., °C.
1 A	130	1	8	10.0	0.980	89	4.12	3.72	89	—	—	—	—
2 B	130	1	8	10.0	0.978	88	—	—	—	117.3	133.7	—	134.8
3 —	140	480	9	9.6	0.979	88	4.12	3.72	86	119.4	134.1	—	135.7
4 —	150	985	8	9.7	0.980	89	4.12	3.72	90	118.7	135.0	—	136.1
5 —	160	1530	18	10.6	0.981	89	4.12	3.72	90	119.8	133.9	—	135.6
6 C	170	2000	8.5	10.0	0.983	90	4.13	3.72	91	118.6	135.2	—	136.6
7 —	176	2300	8	10.0	0.980	89	—	—	—	126.1	133.4	—	134.8
8 —	181	2580	8	10.6	0.979	88	—	—	88	124.6	133.2	—	134.5
9 D	186	2760	8	9.0	0.986	92	—	—	91	124.5	133.2	138.5	—
10 —	186	2860	8	11.2	0.980	89	4.13	3.72	88	124.9	133.6	138.1	139.0
11 —	191	3060	8	10.2	0.984	91	—	—	91	120.7	132.5	137.4	138.5
12 —	201	3540	8	9.8	0.991	95	—	—	95	122.6	130.5	137.6	139.5
13 —	206	3810	8	10.2	0.991	96	4.12	3.72	95	113.4	130.5	137.6	139.6
14 E	226	4800	8	10.0	0.994	97	4.12	3.72	97	114.7	— <sup>b</sup>	138.8	140.1
15 F	236	5300	49	10.0	0.992	96	—	—	96	121.1	—	138.8	139.9
16 —	170	1	0	-30.0	0.977	87	—	—	—	—	—	—	—
17 —	170	740	0	-15.3	0.980	88	—	—	—	120.0	134.6	—	135.9
18 —	170	1290	0	-4.2	0.981	89	4.12	3.71	—	119.0	134.6	—	135.7
19 —	170	1290	0	-4.2	0.982	90	—	—	—	117.4	134.8	—	135.7
20 —	170	1940	0	+8.8	0.980	88	4.11	3.71	—	—	135.5	—	136.4
21 —	170	2580	0	21.6	0.976	86	4.12	3.72	—	121.8	133.6	—	135.2
22 —	170	2580	0	21.6	0.973	85	—	—	—	115.0	134.4	—	137.4
23 —	170	3880	0	47.6	0.983	91	4.12	3.72	—	111.2	129.3	137.9	139.4
24 —	170	3880	0	47.6	0.985	92	—	—	—	115.7	129.4	136.6	138.5
25 —	170	5170	0	73.4	0.983	90	4.13	3.72	—	115.1	— <sup>b</sup>	135.7	137.2
26 —	170	5170	0	73.4	0.983	90	—	—	—	118.3	— <sup>b</sup>	138.5	140.5

<sup>a</sup> Letters A-E refer to samples used in ref. 1. <sup>b</sup> Several small low-pressure peaks instead of one (see text).

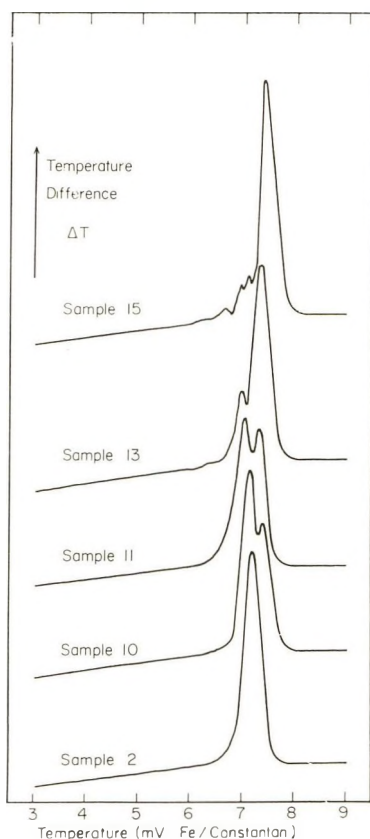


Fig. 1. DTA traces of the melting of polyethylene crystallized at constant degree of supercooling for various crystallization temperatures and pressures: sample 2, 130°C. and 1 atm.; sample 10, 186°C. and 2860 atm.; sample 11, 191°C. and 3060 atm.; sample 13, 206°C. and 3810 atm.; sample 15, 236°C. and 5300 atm.

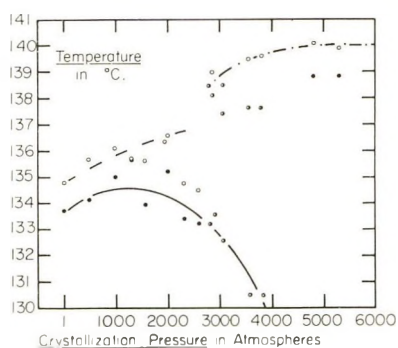


Fig. 2. Experimental maximum melting points of pressure-crystallized polyethylene: (--) folded chain lamellae; (—) extended chain lamellae; (O) experimental points, samples 2-8, 10-15, 18-20; (●) position of the melting peak, samples 2-8, 14-15; (◐) position of the two melting peaks, samples 9-13. The solid line summarizes the approximate trend of folded chain lamellae melting peaks.

## DISCUSSION

## Polyethylene under Pressure

The result of investigations of the high-pressure behavior of polyethylene<sup>8-11</sup> can be summarized as follows.

A pressure increase decreases the volume of amorphous polyethylene more than the volume of crystalline polyethylene.

X-ray measurements on crystalline paraffins<sup>12,13</sup> under pressure have shown that the crystallographic *a* and *b* axes are compressed most easily, while the *c* axis changes at least one order of magnitude less.<sup>13</sup>

The melting point of the crystalline phase increases approximately 0.02°C./atm.<sup>9-11,14</sup> For crystallization at constant supercooling the effects of increased pressure are diminished by the increase in temperature, necessary to keep the degree of supercooling constant. The overall effect, however, remains a reduction in specific volume of the crystalline polymer, an even larger reduction in specific volume of the amorphous polymer, and a substantial rise in temperature.

Figures 1 and 2 show clearly that two different types of crystals are grown, depending upon temperature and pressure. The following discussion is divided into three parts, covering the crystals grown below 2000 atm., above 3500 atm., and in the region between 2000 and 35000 atm.

## Polyethylene Melt-Crystallized below 2000 Atm. (Thin Lamellar Crystals)

A small increase was found for the density at atmospheric pressure of the polymer samples crystallized between 1 and 2000 atm. at constant degree of supercooling as well as for those crystallized at constant cooling rates (samples 1-6 and 16-19). The density increase is rather slight, ~0.003 g./cm.<sup>3</sup> per 2000 atm. for the constant supercooling samples. Parallel to the density increase goes an increase in melting point. Figure 2 shows an increase of about 1.5°C. in the experimental maximum melting point.

Comparing these results with the results from crystallizations of the same polymer from solution under elevated pressure<sup>14</sup> suggests that a slight increase in the thickness of the crystal lamellae can account for the density as well as melting point increase.

Electron microscope investigations<sup>1</sup> indicate that the main portion of samples A, B, and C consist of folded chain lamellae with some polymer (possibly low molecular weight polymer) crystallizing in thin extended chainlike lamellae. Thickness determinations by low angle x-ray methods<sup>1</sup> gave 400 Å. for sample A and 600 Å. for sample C.

Assuming that no recrystallization occurred on fast melting, a thickness increase from 400 to 600 Å. would correspond to a decrease in surface area of  $1.7 \times 10^5$  cm.<sup>2</sup>/g. of polymer, which could account for the increase in melting point.

The differences between the samples grown at constant degree of supercooling and the 4°C./hr. cooled probes are slight, which must mean that in

both cases crystallization occurred at about the same temperature to about the same extent. Figure 2 contains results of both sets of experiments. The dashed line indicates the trend of melting points using only values for samples crystallized below 2000 atm.

### Polyethylene Melt-Crystallized above 3500 Atm. (Extended Chain Crystals)

The character of the material resulted from crystallization above 3500 atm. is radically different from that of the low pressure samples. The amount of defects (expressed in terms of amorphous density or x-ray scattering) has decreased to one-third of the low-pressure samples crystallized at identical supercooling. The experimental maximum melting point is much higher and reaches a plateau of  $140.0 \pm 0.5^\circ\text{C.}$  at about 4000 atm. (Fig. 2, dash-dotted line). Figure 1 indicates that only a small amount of material melting at lower temperature is left, keeping the beginning of the melting at about the same temperature for all samples crystallized regardless of pressure.

Comparison of the experimental maximum melting point with the extrapolated melting point of infinite chain length paraffins, which was recently reevaluated by Broadhurst<sup>15</sup> to be  $141 \pm 2.4^\circ\text{C.}$ , shows that almost perfect extended chain crystals must be present—an assumption which was borne out by the electron microscopic observation. Up to several micron thick lamellae formed of extended chains were found to make up the bulk of this material. Low-angle x-ray measurements showed no discrete or diffuse scatter below 600 Å., the limit of the instrument. This seems to indicate that the residual low-temperature melting peaks of Figure 1 are not necessarily folded lamellae, but could be early melting of small or defect-laden crystallites, perhaps of lower molecular weight.

The above evidence gives strong support to the assumption that  $140.0 \pm 0.5^\circ\text{C.}$  is the equilibrium maximum melting point in the Flory<sup>16</sup> sense. Since the polymer used here still has approximately 0.5 chain ends and branch points per 100 carbons<sup>4,17</sup> the equilibrium melting point,  $T_m^0$ , of pure  $(\text{CH}_2)_\infty$  can be calculated from eq. (1):<sup>16</sup>

$$\ln X_A = (-\Delta H_u/RT_m) + (\Delta H_u/RT_m^0) \quad (1)$$

$X_A$  is the activity of  $\text{CH}_2$  in the melt, here estimated to be 0.995.  $\Delta H_u$  is the heat of fusion.<sup>18</sup>  $T_m$  represents the equilibrium melting point of the largest extended chain lamella in the bulk sample ( $413^\circ\text{K.}$ ).  $T_m^0$  is thus  $415^\circ\text{K.}$  or  $142^\circ\text{C.}$  Turning to the constant-rate, high-pressure crystallized samples (23–26), one can see that a large degree of supercooling was created during the 2–3 min. of application of pressure. This resulted in a reduced density, or crystallinity, if compared with the samples grown at constant supercooling. The maximum melting point, however, is at the same high level, although it is more difficult now to get a reliable extrapolated melting point. This same phenomenon was observed in comparing quenched and slowly cooled polyethylene calorimetrically.<sup>18</sup> In Figure 2

the experimental maximum melting points of samples 23–26 are not plotted because it is felt that they are less reproducible.

All the high-pressure samples of this group were extremely brittle. The highest crystallinity ones could easily be powdered in a mortar.

### **The Intermediate Region (2000–3500 Atm.)**

Into this region fall the experiments of Matsuoka,<sup>19</sup> who found a small density (and crystallinity) increase on crystallization at 160°C. up to 2600 atm., but (within  $\pm 0.5^\circ\text{C}.$ ) no increase in melting point on slow heating. The densities, in addition, fell with increasing crystallization pressure. Matsuoka's experiments are comparable to our samples 18–22. Typical for this region is a drop in the experimental maximum melting point and the development of initially a high temperature shoulder (sample 9) in the DTA trace and finally development of the high-temperature peak (see Figure 1, sample 11). Both the low-temperature peak and the high-temperature peak are at lower temperatures than expected by extrapolation from below 2000 atm. and from above 4000 atm., respectively. Density and crystallinity show a dip to values close to those found on atmospheric pressure crystallization.

From the previous paragraphs it must be concluded that a mixed crystallization has taken place in these samples. The puzzling feature remains the lower melting point of the low-pressure lamellae.

Electron microscopy indicated that for sample D the extended-chain lamellae averaged about 800 Å. against 380 Å. in samples A and B, 480 Å. in sample C, and 2500 Å. in samples E and F. The low-angle spacings, however, dropped to 400 Å. Since the extended-chain lamellae showed wide fluctuations in thickness in the samples investigated<sup>1</sup> and did not have corresponding low-angle x-ray scattering patterns, one might conclude that the folded chain lamellae alone are responsible for the low-angle pattern and thus get thinner at pressures above 2000 atm. when grown from the melt. The melting point data would be in accord with such an explanation, although any increase in defects caused by the simultaneous growth of extended and folded lamellae could also account for the drop in melting temperature.

The low experimental maximum melting point of  $133.9^\circ\text{C}.$  given previously<sup>1</sup> for sample D is a direct result of this picture of two types of melting crystals. The DTA trace has a small shoulder at  $138.5^\circ\text{C}.$  at the high-temperature side of the melting peak ( $133.2^\circ\text{C}.$ ). Using the normal procedure of determining the experimental maximum melting point<sup>4</sup> yields  $133.9^\circ\text{C}.$ , because it disregards the small  $138.5^\circ\text{C}.$  shoulder. In Table I the shoulder is listed as the position of the high-temperature peak, while no experimental maximum melting point is given.

### **Surface Free Energy**

Surface free energy estimates can be made as soon as lamella thickness and melting point are known. Three determinations of melting points

under conditions of no recrystallization on samples of known average lamella thickness are given in Table I (samples A-B, C, and D). Since the x-ray lamellar thickness corresponds to an average thickness, as average melting point the peak temperature was chosen.

The equation used for the estimation of the surface free energy of the lamellar surface,  $\sigma$ , follows from the description of the polymer melting process previously given.<sup>1</sup> One has to assume that each lamella is one subsystem and internal defects do not contribute appreciably to the melting point observed.<sup>20</sup>

$$T_m = T_m^0 [1 - (2\sigma/\Delta h_f l)] \quad (2)$$

where  $l$  is the lamellar thickness and  $\Delta h_f$  the heat of fusion per cubic centimeter of crystals. Equations of this type were first used for the melting of lamellar crystals constrained between glass plates by Tammann<sup>21</sup> and Meissner.<sup>22</sup>

Table II lists the calculated surface face energies which are in accord with previous estimates from our laboratory.<sup>14,20</sup>

TABLE II  
Surface Free Energy of Polyethylene

Sample	Mode of crystallization	Melting temp., °C.	Thickness, Å.	$\sigma$ , erg/cm. <sup>2</sup>
A-B	130°C. from melt	133.7	400	84
C	170°C. from melt	135.2	600	97
D	186°C. from melt	133.2	400	91

Some preliminary crystallizations and DTA-traces of constant cooling rate samples were done by Douglas Poland in 1960.

Financial support from the Office of Naval Research is gratefully acknowledged.

## References

1. Geil, P. H., F. R. Anderson, B. Wunderlich, and T. Arakawa, *J. Polymer Sci.*, **A2**, 3707 (1964).
2. Wunderlich, B., *Rev. Sci. Instr.*, **32**, 1424 (1961).
3. Hendus, H., and G. Schnell, *Kunststoffe*, **51**, 69 (1961).
4. Wunderlich, B., and D. Poland, *J. Polymer Sci.*, **A1**, 357 (1963).
5. Wunderlich, B., *Polymer*, in press.
6. Swan, P. R., *J. Polymer Sci.*, **56**, 403 (1960).
7. Average of values given by M. G. Gubler and A. J. Kovacs, *J. Polymer Sci.*, **34**, 551 (1959), and L. E. Nielson, *J. Appl. Phys.*, **25**, 1209 (1954).
8. Bridgman, P. W., *Proc. Am. Acad. Arts Sci.*, **76**, 55 (1948).
9. Parks, W., and R. B. Richards, *Trans. Faraday Soc.*, **45**, 203 (1949).
10. Weir, C. E., *J. Res. Natl. Bur. Std.*, **53**, 245 (1954).
11. Matsuoka, S., *J. Polymer Sci.*, **42**, 511 (1960).
12. Kabalkina, S. S., and Z. V. Troitskaya, *Zh. Strukt. Khim.*, **2**, 27 (1961).
13. Müller, A., *Proc. Roy. Soc. (London)*, **A178**, 227 (1941).
14. Wunderlich, B., *J. Polymer Sci.*, **A1**, 1245 (1963).
15. Broadhurst, M. G., *J. Chem. Phys.*, **36**, 2578 (1962).
16. Flory, P. J., *Trans. Faraday Soc.*, **51**, 858 (1955).

17. Bryant, W. M. D., *J. Polymer Sci.*, **34**, 569 (1959) (discussion).
18. Wunderlich, B., and M. Dole, *J. Polymer Sci.*, **24**, 201 (1957).
19. Matsuoka, S., *J. Appl. Polymer Sci.*, **4**, 115 (1960).
20. Wunderlich, B., P. Sullivan, T. Arakawa, A. B. DiCyan, and J. F. Flood, *J. Polymer Sci.*, **A1**, 3581 (1963).
21. Tammann, G., *Z. Anorg. Allgem. Chem.*, **110**, 166 (1920).
22. Meissner, F., *Z. Anorg. Allgem. Chem.*, **110**, 169 (1920).

### Résumé

On a fait cristalliser du polyéthylène linéaire du type basse pression, sous l'action de la pression (jusqu'à 5400 atm) sur le polymère fondu. On a utilisé des conditions de super-refroidissement constant et de vitesse de refroidissement constantes. On a analysé le solide résultant à pression atmosphérique. Par contraste avec la cristallisation de solution sous pression supérieure à 2000 atm, la lamelle de chaîne étendue, d'épaisseur croissante devient prédominante (voir article précédent). Le point de fusion maximum observé est de 140°C et dans ce cas les densités vont jusqu'à 0.994. Si l'on combine ces données sur les grands cristaux avec les températures expérimentales maxima de fusion et les épaisseurs observées pour les lamelles cristallisées à basse pression et à pression atmosphérique, on obtient une énergie libre de surface de 91 ergs/cm<sup>2</sup> pour les lamelles de chaîne plissée cristallisée à basse pression.

### Zusammenfassung

Lineares Niederdruckpolyäthylen wurde aus der Schmelze unter Druck (bis zu 5400 atm.) kristallisiert. Kristallisationsbedingungen von konstanter Unterkühlung und konstanter Abkühlrate wurden angewandt. Der sich ergebende Festkörper wurde unter Atmosphärendruck analysiert. Im Gegensatz zur Kristallisation aus Lösung unter Druck, wurden über 2000 atm. Lamellen aus gestreckten Ketten von zunehmender Dicke überwiegend. Diese zeigen einen maximalen Schmelzpunkt von 140°C und in dieser Arbeit, Dichten von bis zu 0.994. Kombiniert man diese Daten von grossen Kristallen mit den experimentellen maximalen Schmelztemperaturen und Dicke Bestimmungen von Nieder- und Atmosphärendruck kristallisierten Lamellen, so erhält man eine Freie Oberflächen-energie von 91 erg/cm<sup>2</sup> für bei niedrigem Druck kristallisierte Lamellen mit gefalteten Ketten.

Received August 21, 1963

Revised October 22, 1963

## Morphology of Polyethylene Crystallized from the Melt Under Pressure

PHILLIP H. GEIL,\* *Camille Dreyfus Laboratory, Durham, North Carolina*,  
FRANKLIN R. ANDERSON, *Chemstrand Research Center, Durham,*  
*North Carolina*, and BERNHARD WUNDERLICH,† and TAMIO  
ARAKAWA, *Department of Chemistry, Cornell University, Ithaca, New York*

### Synopsis

The morphology of linear polyethylene crystallized under pressures up to 5300 atm. has been investigated. Electron micrographs of fracture surfaces obtained from these samples show that the majority of the polymer, at the highest pressures, crystallizes in the form of extended chain lamellae which can be as thick as 3  $\mu$ . Electron diffraction patterns show that the molecules are normal to the lamellae. At lower pressures part of the polymer crystallizes in the form of folded chain lamellae, the proportion increasing with decreasing pressure. Well defined kink bands can be observed in the thicker extended chain lamellae. It is suggested that either molecular weight fractionation or an end-to-end alignment of the molecules and subsequent folding takes place during the growth of the extended chain lamellae.

### INTRODUCTION

Linear polyethylene crystallized under pressure may have a density approaching the theoretical perfect crystal density and a melting point close to the limiting value for large, perfect crystals.<sup>1,2</sup> The morphology of such a sample is thus of considerable interest. In this paper we present a report of the investigation of the internal morphology of linear polyethylene crystallized under pressures up to 5300 atm. and with densities as high as 0.994 g./cc. Further details concerning the properties of these and other similar samples are described in a paper in preparation.<sup>2</sup>

Wunderlich<sup>1,3</sup> has previously discussed the growth of polyethylene single crystals from dilute solution under elevated pressure. The crystals in general resemble those obtained at atmospheric pressure at similar supercoolings (the melting point and therefore the crystallization temperature increases with pressure). At constant supercooling the thickness or fold period increases only slightly with pressure.

Anderson has pointed out<sup>4,5</sup> that at least three morphologically distinct lamellar structures can be observed in linear polyethylene crystallized from the melt at atmospheric pressure. These he has labeled types I, II, and

\* Present address: Case Institute of Technology, Cleveland, Ohio.

† Present address: Rensselaer Polytechnic Institute, Troy, New York.

III lamellae. Type I consists of broad, folded chain lamellae resembling those found in single crystals grown from solution. The smaller of the two small-angle x-ray diffraction long periods from melt crystallized polyethylene is essentially equal to their thickness.<sup>5-7</sup> Type I lamellae are found in both whole polymers and in fractionated samples. Whereas in fractionated polymer they can be observed on both exterior and fracture surfaces, in whole polymer they are usually visible only on exterior surfaces. When whole polymer is fractured, microdrawing apparently takes place in regions occupied by type I lamellae. The resulting "fracture" surfaces are covered with broken fibrils. This microdrawing is believed to be due to the presence of tie molecules connecting neighboring lamellae.<sup>5,7</sup> Type II lamellae consist of narrow or ribbon-like layers whose thickness is essentially equal to that of type I. They have been found only in higher molecular weight, fractionated samples and were not found in the samples discussed in this paper. Therefore, type II lamellae will be of no further concern to us here.

As observed on fracture surfaces, type III lamellae have an appearance similar to the bands observed to essentially occupy the entire volume of highly crystalline polytetrafluoroethylene.<sup>7,8</sup> Anderson has suggested<sup>5</sup> that they are probably similar to paraffin crystals, consisting of fully extended chains. Type III lamellae are found in whole polymer and in the lower molecular weight fractions. Each individual crystal is of about the same thickness over its lateral extent, but the crystals in a given sample may vary considerably in thickness. By varying the temperature of crystallization the relative proportion and thickness of types I and III lamellae can be varied for a given sample. With increasing temperature the fold period of type I, the maximum thickness of type III and the relative proportion of material crystallizing in type III increases. Although, with fractionated polymer, type III lamellae were found only in fractions with molecular weights below 12,000, Anderson suggested<sup>5</sup> that by waiting for longer periods of time at still higher temperatures it should be possible to obtain type III lamellae from polymer of much higher molecular weight.

## EXPERIMENTAL

Table I lists many of the properties of the samples used for this investigation. Samples of a linear polyethylene (Marlex 50) were enclosed in brass bellows and heated to the crystallization temperature at atmospheric pressure. The chosen pressure was then applied in 1-2 min. by using a pressurestat previously described.<sup>9</sup> The pressure and temperature were kept constant for the time listed, after which the temperature was reduced at a rate of 4°C./hr. to about 50°C., at which time the pressure was released and the sample removed. (For a full description of the sample preparation techniques, see Wunderlich.<sup>2,3</sup>) The atmospheric pressure samples (A and B, Table I) were prepared by quenching the sample quickly from the molten state to the crystallization temperature.

TABLE I

Sample	Crystallization conditions			Density measurements		X-ray measurements		Extr. melting point (DTA) °C.
	Temp., °C.	Pressure, atm.	Time, hr.	Density (25°C.), g./cm. <sup>3</sup>	Crystallinity, %	Crystallinity, %	Long period, Å.	
A	130	1	8	0.9799	89	89	400	—
B	130	1	8	0.9785	88	—	—	134.8
C	170.1	2000	8.5	0.9826	90	91	600	136.6
D	186	2760	8	0.9860	92	91	400	133.9
E	226	4800	8	0.9938	97	97	No discrete	140.1
F	236	5300	49	0.9921	96	93	or diffuse scatter	139.9

The density was measured by using 1 mm.<sup>3</sup> pieces, microscopically checked for voids, in a density gradient column at 25°C. The density crystallinity was determined by use of the average of Nielson's<sup>10</sup> and Gubler and Kovacs'<sup>11</sup> value for  $\bar{V}_n$  (1.173 cm.<sup>3</sup>/g.) and Swan's<sup>12</sup> value for  $\bar{V}_c$  (1.001 cm.<sup>3</sup>/g.). The x-ray crystallinity was measured on a General Electric XRD-5 diffractometer, the calculation being made by the method described by Hendus and Schnell.<sup>13</sup> The small-angle patterns were obtained by using a Jarrell-Ash-Frank optically focussing small-angle x-ray camera with a resolution of about 500 Å.

The melting points are extrapolated maximum melting points obtained by a DTA method previously described.<sup>2,14,15</sup> In some of the samples more than one DTA peak was found. As suggested by Anderson,<sup>5</sup> this is probably related to the presence of more than one morphological structure as observed in the electron microscope. In Table I the upper tail of the highest temperature peak is listed. (Further details are given elsewhere.<sup>2</sup>)

The samples were prepared for electron microscopy by immersing them in liquid nitrogen for a sufficient period of time to cool them, then fracturing them while still immersed. The two most highly crystalline samples (E and F) fractured readily at room temperature during handling. In these samples no difference was observed between the surfaces obtained at room temperature and those obtained following cooling. The micrographs of these samples in this paper are from surfaces obtained at room temperature. Following fracture the surfaces were shadowed with platinum, stripped with poly(acrylic acid), and backed with carbon (as described in detail in Chapter 1, of reference 7).

## RESULTS

### Electron Microscopy Observations

The fracture surfaces of the sample crystallized at atmospheric pressure resemble those described previously.<sup>5,7</sup> Over much of the surface, presumably in the areas corresponding to the occurrence of type I or folded chain lamellae, only an irregular, fibrillar structure was present. In a few

regions areas were observed of the order of  $100\ \mu$  in size in which there were primarily the type III or extended chain lamellae. Within these areas fracture had occurred both between and within the lamellae. Those which were measurable varied between 300 and 600 Å. in thickness, the 87 measured averaging 380 Å. thick.

Considerably larger proportions of the samples crystallized at the intermediate pressures (C and D) are found to consist of the extended chain lamellae. In both samples, however, there is evidence of the presence of folded chain lamellae, i.e., there are regions which have a drawn, fibrillar appearance. The extended chain lamellae in sample C (Fig. 1) varied in thickness between 200 and 1000 Å., averaging about 480 Å. In sample D they varied between 300 and almost 3000 Å., averaging about 800 Å. in thickness (Fig. 2). The thicknesses of 68 and 115 lamellae were measured for the two samples, respectively.

No correction was made for the possible tilt of the lamellae with respect to the surface. In addition, a meaningful distribution of step heights would require a more random selection of areas (in general only areas displaying groups of larger lamellae were photographed) and some correction should be made for the presence of thin lamellae beneath the resolving power of the replicas.

The thicker lamellae, in sample D, as indicated by Anderson,<sup>5</sup> are similar in appearance to the bands observed in highly crystalline polytetrafluoroethylene.<sup>7,8</sup> Although generally the type III lamellae of various thicknesses

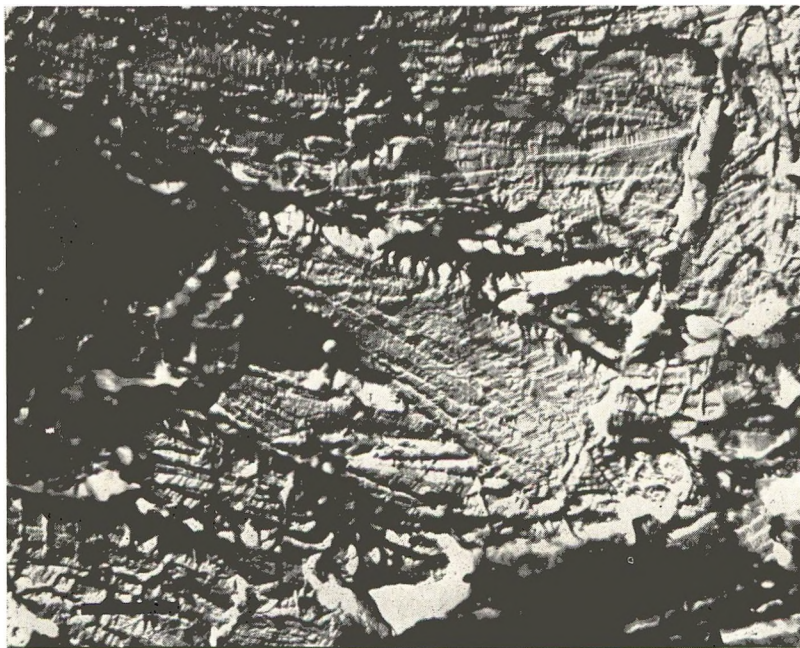


Fig. 1. Fracture surface of sample C (Table I). The scale bar on this and subsequent micrographs represents  $0.5\ \mu$ .



Fig. 2. Fracture surface of sample D. The dark areas in this and the other micrographs are a result of polyethylene adhering to the replica.

were intermixed, as in Figure 2 a significant number of regions were observed in which all the lamellae were of the same thickness, this being on the order of 300–400 Å. The relative length of the striations, with respect to their separation, in the type III lamellae causes the thicker lamellae to have a different appearance than the thinner ones. However, there appears to be no basic difference in their structure. Structures similar in appearance to the thinner lamellae have been observed in moderately crystalline polytetrafluoroethylene ( $\sim 50$ – $70\%$ ).<sup>7,16,17</sup> In that case, however, all of the bands present were of about the same thickness and considerably smaller in lateral extent than in the case of the more highly crystalline polymer. In sample D the thick and thin lamellae appear to have equivalent lateral dimensions.

The general appearance of the fractured type III lamellae in sample C (Fig. 1) differs from that of the lamellae of corresponding thickness in sample D (Fig. 2); the fracture surface of each lamella and the whole surface appears smoother. Whether this is characteristic of the thermal treatment of the two samples during crystallization or a result of possible differences in the fracturing and replicating process is not known. One notes that the striations in Figure 1 (sample C) in many cases make an angle of other than  $90^\circ$  with the lamellae (this occurred only infrequently in sample D) and also appear more closely spaced than those in Figure 2.

The entire fracture surface of samples E and F and thus probably the whole sample is occupied by extended chain lamellae of various thicknesses

(Fig. 3). Samples E and F appear nearly identical, E perhaps having a few lamellae somewhat thicker than F. In both samples optical microscope observations of the replicas and also of the fracture surfaces themselves, indicates that the lamellae are organized in incipient spherulites, i.e., sheaf-like clusters are found. The center of such a sheaf is located at the lower left of Figure 3.

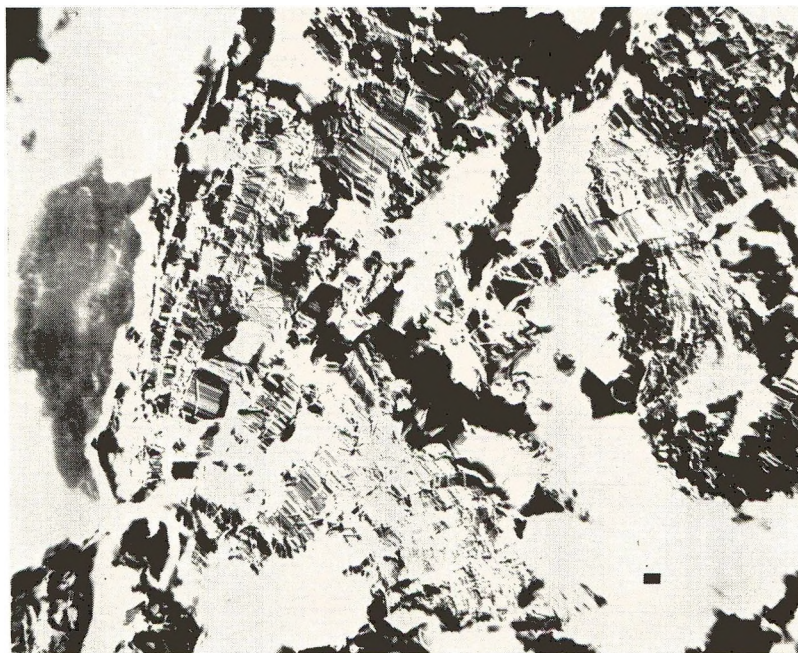


Fig. 3. Fracture surface of sample F. An entire lamella is attached to the replica on the left of the micrograph. This figure is printed as a negative.

The fracture process occurred both through the type III lamellae (right side of Figure 3) and between them (left side). In the latter case, entire lamellae often remained attached to the replica permitting the obtaining of single crystal electron diffraction patterns described in the next section. Although the striations could be observed on the fractured edges of the attached lamellae, the interlamellar surface was obscure. Apparently the large amount of attached polymer caused the replica to break up under the action of the beam. By limiting the beam current, as for the electron diffraction studies, somewhat better micrographs were obtained (Fig. 8), although at low magnification. These suggest that the thickness of a given lamella may vary somewhat, regions on the order of  $1 \mu^2$  being of nearly uniform thickness. Although no obvious structure was present within these regions, further investigation at higher magnification would be useful.

Lamellae have been observed with thicknesses of up to  $3 \mu$  in samples E and F. The average thickness, from low magnification micrographs covering areas representative of the whole sample, is about 2500 Å. The

most prominent feature of the lamellae are the striations (Fig. 3 and subsequent figures). It appears that in nondeformed lamellae the striations are perpendicular to the broad faces of the lamellae. In the case of polytetrafluoroethylene, drawing<sup>17</sup> or rolling<sup>7</sup> causes the striations to tilt within the lamellae. Deformation is probably also related to the presence of a few lamellae in these samples in which the striations are uniformly tilted and most certainly is the cause of the kinks to be described later.

The striations in samples E and F have a spacing of about 200 to 300 Å and are continuous across an entire lamella. The contrast between the striations is due in part to individual ribbons of material, one or more striations wide, adhering to the replica and in part due to the surface roughness of the fractured lamella. Each striation appears to correspond to a distinct structural entity. In a few regions it was possible to observe type III lamellae which had a smooth fracture surface (Fig. 4). Where the fracture plane changes levels, near the center of the micrograph, the appearance suggests that the striations correspond to the fracture edges of sheet-like structures. The structure of the lamellae would thus resemble that suggested by Speerschneider and Li<sup>17</sup> for polytetrafluoroethylene, except that the high crystallinity of these samples precludes an "amorphous" layer between the sheets.

It appears that the sheets can readily be broken up into nearly cylindrical structures, several hundred Angstroms in diameter and with a length corresponding to the lamella thickness (Fig. 5) or even larger (Fig. 6). In

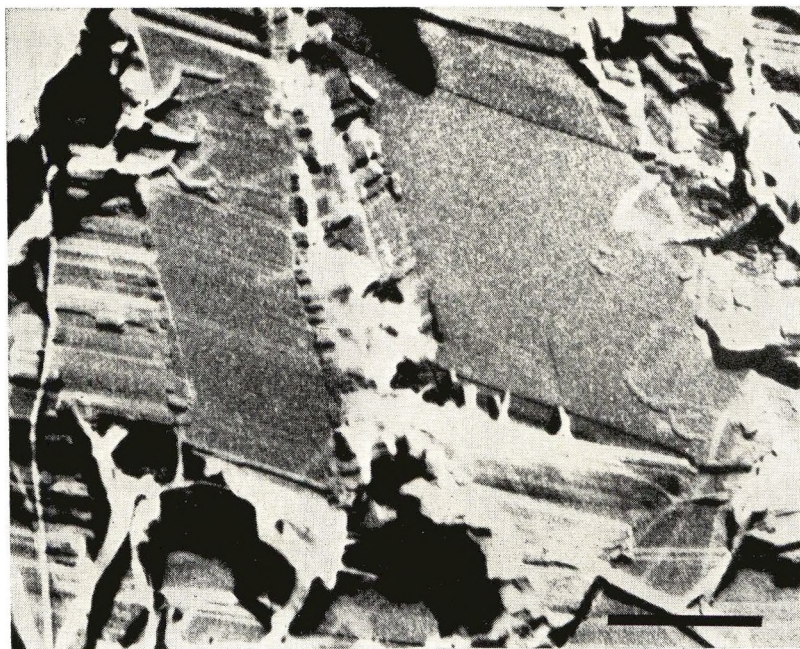


Fig. 4. Fracture surface of sample E, showing smooth fracture surface.



Fig. 5. Portion of the fracture surface of a large lamella in sample E. Several small kinks are present near the top center of the micrograph. This micrograph is printed as a negative.

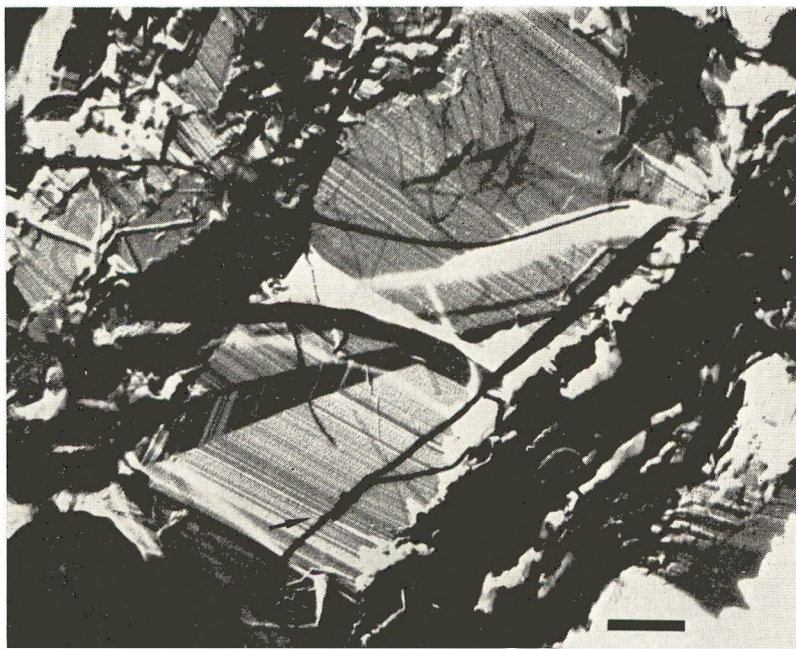


Fig. 6. Long "fiber" (arrow) and large kink on the fracture surface of a lamella in sample E. The surface structure of the lamella is also visible to an extent.

Figure 5 a piece of the lamella two striations wide has been partially removed from the surface and folded back on itself. The overall length is just equal to the lamella thickness. In Figure 6, however, the "fiber" lying parallel to the lamella is more than twice as long as the corresponding lamella thickness. It remained attached to the lamella on the right side, the thicker portion corresponding to the width of the lamella at that point. At the end of the thick region it has split into "fibers." It is believed that these fibers are portions of the sheets, as is the piece in Figure 5. The fact that it is wider than the striations is probably due to its being cylindrically coated with platinum and carbon. The implications of the fact that it is longer than the lamella thickness is discussed in the last section of this paper. Similar fibers have also been observed on other micrographs of these samples to be several times as long as the thickness of the lamella to which they are attached; the most prevalent type of fiber or ribbon, however, is that whose length is equal to the corresponding lamella thickness. The fibers of low contrast on these two, and other figures, were formed when the Pt replica was stripped from the sample.

Many of the thicker type III lamellae have one or more kinks visible on their fracture surface. Usually, as in Figure 6, they extend from one side of the lamella to the other, the striations clearly changing direction at the kink. There is often a related change in the fracture plane. The change in level and slope of the fracture plane at the kinks makes it difficult to determine the angle through which the striations kink. It can be as large as  $90^\circ$  and often appears to be about that angle. Occasionally, instead of extending directly from one surface of the lamella to the other, the kink results in the formation of an isolated patch of displaced material, as to the right and above the partially removed piece of material in Figure 5, or it may reverse directions several times within the lamella. The latter structure may also be due to the presence of several intersecting kinks.

### Electron Diffraction Observations

Geil has shown<sup>7</sup> that it is often possible to remove portions of the polymer from the surface along with the replica by using the technique utilized for these preparations. Electron diffraction patterns from this material have been related to the single-crystal nature of the lamellae in polyethylene<sup>7</sup> and annealed polyoxymethylene.<sup>18</sup> It was also found, as mentioned previously, that considerable quantities of the polymer in samples E and F remained attached to the replicas. Some of the contrast of the striations and the fibers observed on the fracture surfaces are due to this polymer.

An electron diffraction pattern and corresponding bright field micrograph of the material adhering to a fracture surface of the lamella is shown in Figure 7. The diffraction patterns here and from other similar samples are fiber-like (on the original of Figure 7 both  $\{110\}$  and  $\{200\}$  reflections are visible) and of relatively low intensity. The length of the crystals is such that one would expect the  $\{002\}$  reflection to be visible. Even with longer

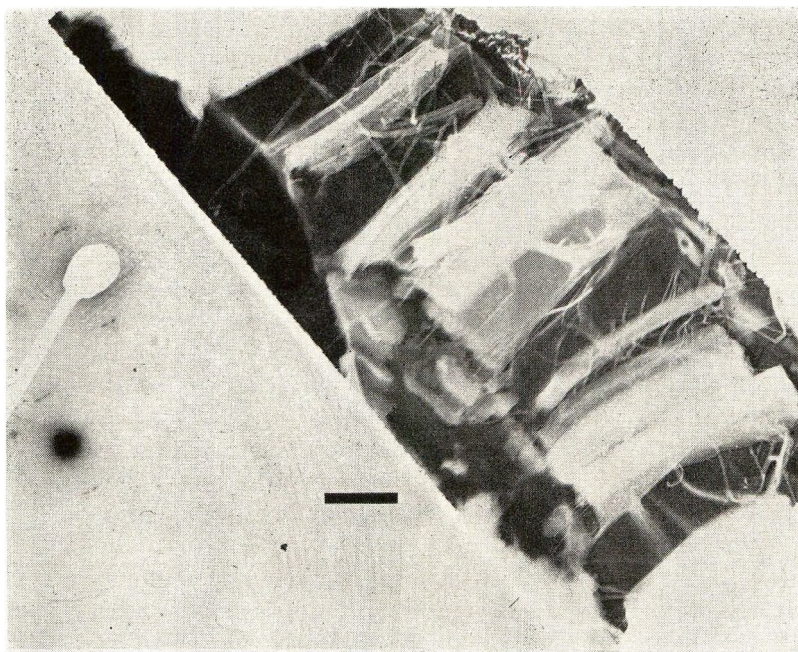


Fig. 7. Selected area electron diffraction patterns from the material adhering to the fracture surface of a type III lamella in sample E. The area giving rise to the patterns was recorded on the same plate as the pattern; the patterns should be rotated counter-clockwise about  $10^\circ$  to compensate for the rotation of the image in the microscope. This figure is printed as a negative.

exposure times and larger areas it was not possible to observe it. This may be due to a tilting of the lamella surface, however, and not to its absence. Likewise, the low intensity of the  $\{110\}$  and  $\{200\}$  reflections is probably due to the fact that only a few of the crystal's planes may be properly oriented to reflect. The alignment of the molecules parallel to the striations has been confirmed by observation of the optical birefringence of lamellae attached to the replica.\*

Good single-crystal diffraction patterns, sometimes with several orders of reflections and resembling those obtained from solution grown polyethylene single crystals, were obtained from regions in which an entire lamella remained attached to the replica (Fig. 8). Tilting of these lamellae with respect to the beam resulted in the type of pattern shown, the center of intensity of the pattern being displaced from the center of the pattern. Comparison of the selected area image that was taken at low intensity in conjunction with Figure 8 and which was unfortunately out of focus, and the subsequent micrograph shown in Figure 8, which was focused using an intensity sufficient to give a visible image on the microscope screen, indicates that some beam damage had occurred. However, the appearance of various regions of nearly uniform thickness is believed to be real.

\* The optical birefringence measurements were made by E. W. Fischer.



Fig. 8. Selected area diffraction pattern and corresponding bright field image of a Type III lamella in sample E. The area giving rise to the pattern is indicated on the micrograph, which is printed as a negative.

## DISCUSSION

Anderson suggested<sup>5</sup> that the molecules in the type III lamellae lie parallel to the striations. The electron diffraction patterns demonstrate this conclusively. The cause of the striations and the arrangement of the chains within the lamellae is somewhat more difficult to interpret. As indicated previously, it appears as if the type III lamellae are made up of sheet-like structures on the order of 300 Å. thick, of indeterminate, but large, length and of a width equal to the thickness of the lamella. In an undeformed lamella these sheets are oriented normal to the lamellae. However, they can easily be broken up into rod-like units of nearly square or circular cross section. It has not yet been possible to determine the orientation of the unit cell within the sheets or the rods, except for the parallel alignment of the molecules with the rod's axis. The rods may be nearly perfect crystals, the boundaries between the rods being similar to subgrain boundaries in metals. The individual lamellae would correspond to the grains.

One can visualize at least two possible ways of incorporating the molecules in the rods and thus the lamella: (1) the length of the rods (and thus the thickness of the lamella) corresponds to the length of the molecules incorporated in that rod; (2) the molecules within a given rod may be of any length, being arranged end to end; folding may take place at the end of the rod similar to that which occurs in solution-grown single crystals, or may be such as to connect adjacent rods.

The first possibility, as suggested by Bunn et al.<sup>8</sup> and Anderson,<sup>5</sup> requires that a fractionation in terms of molecular weight takes place during crystallization. In the case of the samples crystallized at the lower pressures (C and D) and that crystallized at atmospheric pressure it also suggests that the low molecular weight material is segregated into regions which may be microns in dimension, and that it crystallizes independently of the high molecular weight material which is crystallizing in the form of type I lamellae. Anderson's work with the fractionated polymer<sup>5</sup> would be in agreement with this suggestion. The observed thicknesses of the type III lamellae in the E and F samples is also reasonable in terms of this suggestion; the average thickness corresponds to a sort of number-average molecular weight of 28,000. Corrections need to be made for the lack of counting many of the thinner type III lamellae (because of low replica resolution and sample distortion during replica stripping), tilt of the lamellae with respect to the surface, and the volume occupied by the lamellae of various thicknesses.

If this possibility of fractionation during crystallization is correct, it indicates that molecules can move over large distances during crystallization. In addition, it indicates that even in the case of the largest molecules the effect of size on the thermodynamic properties remains significant. At first glance this possibility appears unlikely. However, evidence for molecular motion over distances of up to 1 mm. during crystallization at atmospheric pressure has been published.<sup>7,19</sup> Keith and Padden<sup>20</sup> also postulate (and have some evidence for) a not too different type of motion to occur during spherulite growth. Proposed experiments using fractionated polyethylene should prove or disprove this possibility. The implications of this fractionation, segregation process for the mechanical properties of polymers, as for instance mechanical relaxations, stress-strain relations and stress crack, are rather obvious and will not be discussed here.

The second possibility above also raises a considerable number of problems which cannot be answered until more is known of the crystallization process. For instance, what determines the thickness of the lamellae; it is not believed likely that they form at different temperatures as the sample is cooled. In addition, one is still faced with the problem of unentangling the supposedly randomly coiled molecules in the melt, aligning them and then placing them end to end. The high density precludes the existence of large quantities of defects in the crystals. If this possibility is correct, it is believed most likely that the molecules are folded at the ends of the rods and re-enter the same rod. However, the presence of a few fibers considerably longer than the rods, as in Figure 6, suggests also the possibility that the molecules are grouped into fibers corresponding to the rods and that these fibers are folded to form the sheets. Further investigation of the structure and formation of these long fibers is needed.

With either possibility the cause of the formation of rod-like crystals and their association in the form of sheets within the lamellae is not clear. We suggest that the lateral size of the rods may be limited by the accumulated

strain at the ends of the crystal, whether this consists of reentrant folds or of endgroups. If the entire crystal is folded at the end the size might be limited because of this. If the molecules are folded at the ends and re-enter the same rod, one wonders why the lamellae have a different characteristic fracture than the type I lamellae in which they are presumably also folded.

It is not known just when during the sample preparation process the kinks formed in the lamellae. One suspects that they are due to some increase in pressure following growth; possibly they may have formed during the fracture process. Deliberate attempts to induce their formation may help explain the deformation process in polymers. As in the case of polytetrafluoroethylene,<sup>7,17</sup> the presence of these large morphological structures should simplify study of polymer deformation.

At the present time we cannot interpret the small-angle x-ray diffraction measurements listed in Table I. The values for samples C and D are in satisfactory agreement with the relative melting points but not with the lamella thicknesses observed in the electron microscope. Also, one wonders that the diameter of the rod-like crystals does not contribute to the diffraction pattern. The measured spacings were near the maximum resolution of the presently available camera; it is hoped to remeasure the samples in the near future. The relative melting points of C and D are also difficult to explain in view of the fact that the thicker type III lamellae, as observed in the microscope, are in the sample with the lower melting point.

It should be evident from this discussion that there remains a considerable area of research in this field of the structure of polymers crystallized under high pressure. It is believed likely that polymers other than polyethylene can also be crystallized in the form of these extended chain lamellae. The structure of the bands in polytetrafluoroethylene, which was first explained in terms of a structure like that discussed in possibility (1) above<sup>8</sup> and then in terms of folded chains,<sup>7,21</sup> is probably related to these type III lamellae.

Appreciation is expressed for financial support of several of the authors by the Camille and Henry Dreyfus Foundation, the Office of Naval Research and the Advanced Research Projects Agency. The authors also wish to express their appreciation to R. L. Miller and E. W. Fischer for helpful discussions.

## References

1. Wunderlich, B., T. Arakawa, and D. Poland, paper presented at 142nd American Chemical Society Meeting, Atlantic City, Sept. 1962.
2. Wunderlich, B., and T. Arakawa, *J. Polymer Sci.*, **A2**, 3697 (1964).
3. Wunderlich, B., *J. Polymer Sci.*, **A1**, 1245 (1963).
4. Anderson, F. R., paper BB4 in *Electron Microscopy*, S. S. Breese, Jr., Ed., Academic Press, New York, 1962.
5. Anderson, F. R., *J. Appl. Phys.*, **35**, 64 (1964).
6. Geil, P. H., *Bull. Am. Phys. Soc.*, **7**, 206 (1962).
7. Geil, P. H., *Polymer Single Crystals*, Interscience (Wiley), New York, 1963.
8. Bunn, C. W., A. J. Cobbold, and R. P. Palmer, *J. Polymer Sci.*, **28**, 365 (1958).

9. Wunderlich, B., *Rev. Sci. Instr.*, **32**, 1424 (1961).
10. Nielson, L. E., *J. Appl. Phys.*, **25**, 1209 (1954).
11. Gubler, M. G., and A. J. Kovacs, *J. Polymer Sci.*, **35**, 551 (1959).
12. Swan, P. R., *J. Polymer Sci.*, **56**, 403 (1962).
13. Hendus, H., and G. Schnell, *Kunststoffe*, **51**, 69 (1961).
14. Wunderlich, B., and D. Poland, *J. Polymer Sci.*, **A1**, 357 (1963).
15. Wunderlich, B., *Polymer*, in press.
16. Geil, P. H. unpublished data.
17. Speersneider, C. J., and C. H. Li, *J. Appl. Phys.*, **33**, 1871 (1962).
18. Geil, P. H., in preparation.
19. Geil, P. H., *J. Polymer Sci.*, **47**, 65 (1960).
20. Keith, H. D., and F. J. Padden, Jr., *J. Appl. Phys.*, **34**, 2409 (1963); see H. D. Keith, in *The Physics and Chemistry of the Organic Solid State*, A. Weissberger, D. Fox, and M. M. Labes, Ed., Interscience (Wiley), New York, 1963.
21. Keller, A., *Makromol. Chem.*, **34**, 1 (1959).

### Résumé

La morphologie du polyéthylène linéaire cristallisé sous des pressions allant jusqu'à 5300 atmosphères a été examinée. Des micrographies électroniques des surfaces de rupture obtenues à partir de ces échantillons montrent que la majorité du polymère, aux pressions les plus élevées, cristallise sous forme de lamelles de chaînes étirées, qui peuvent atteindre une épaisseur de 3 microns. Des spectres de diffraction électronique montrent que les molécules sont normales par rapport aux lamelles. A des pressions plus basses une partie du polymère cristallise sous forme de lamelles à chaînes repliées, dont la proportion augmente avec une diminution de la pression. Des bandes de superposition bien définies peuvent être observées dans des lamelles à chaînes étendues plus épaisses. On suppose que le fractionnement du poids moléculaire ou bien un alignement des molécules bout-à-bout, suivi par un repliement des chaînes, a lieu pendant la croissance des lamelles à chaîne étirée.

### Zusammenfassung

Die Morphologie von unter Drucken bis zu 5300 Atmosphären kristallisiertem linearen Polyäthylen wurde untersucht. Aus elektronenmikroskopischen Aufnahmen von an diesen Proben hergestellten Bruchflächen geht hervor, dass im Falle der höchsten Drucke der Grossteil des Polymeren in Form von bis zu 3 Mikron dicken, aus entfalteten Ketten bestehenden Lamellen kristallisiert. Elektronenbeugungsdiagramme zeigen, dass die Moleküle senkrecht zu den Lamellen stehen. Bei niedrigeren Drucken kristallisiert ein mit sinkendem Druck zunehmender Anteil des Polymeren in Form von aus gefalteten Ketten bestehenden Lamellen. In den dickeren, aus entfalteten Ketten bestehenden Lamellen konnten deutliche Knickbanden festgestellt werden. Es wird angenommen, dass während des Wachstums der aus entfalteten Ketten bestehenden Lamellen entweder eine Molekulargewichtsfractionierung oder eine End-zu-End-Ausrichtung der Moleküle und anschliessende Faltung auftritt.

Received August 21, 1963

Revised October 20, 1963

## Efficiency and Frequency of Grafting of Methyl Methacrylate to Granular Corn Starch

C. E. BROCKWAY, *Research Center, A. E. Staley Manufacturing Company, Decatur, Illinois*

### Synopsis

PMMA content of graft copolymers with granular starch can be determined by acid hydrolysis with sufficient precision to allow reasonable estimates of efficiency and frequency of grafting. Preparation of the graft copolymer by initiation of methyl methacrylate with hydrogen peroxide and activators results in products containing long PMMA side chains attached to the starch at very infrequent intervals, but the length and frequency of attachment can be varied considerably by changes in the ratios of reactants. The highest frequency achieved was with PMMA of number-average molecular weight of about 30,000, attached at a frequency of one chain per 230-250 glucose units in the starch. Under the more favorable conditions, oxidized starch yielded product of significantly more frequent grafting than did unmodified starch. Gradual addition of monomer, initiator, and activator to the starch slurry gave slightly higher frequency of grafting than did complete addition of all reactants at the start of the polymerization.

A previous publication<sup>1</sup> has presented evidence for the formation of graft copolymer when methyl methacrylate is polymerized in an aqueous slurry of granular corn starch by initiation with peroxide. More recently, procedures for removal of ungrafted homopolymer of methyl methacrylate have been studied.<sup>2</sup> This paper presents quantitative data concerning the efficiency of grafting of poly(methyl methacrylate) to the starch, and the length and frequency of attachment of the grafted chains.

### EXPERIMENTAL

#### Materials

**Starches.** Unmodified and alkaline hypochlorite-oxidized (Stayco C) starches were A. E. Staley production materials. Prior to use they were defatted by the procedure of Schoch;<sup>3</sup> samples were given five successive extractions with refluxing 85/15 methanol-water, and then four successive washings at room temperature with distilled water in order to remove methanol.

**Monomer.** Methyl methacrylate (Rohm & Haas) containing 0.01% of *p*-methoxyphenol was redistilled at a reflux ratio of at least 4:1. Forerun

and residue were discarded; the main fraction was stored at  $-18^{\circ}\text{C}.$  until used.

**Other Reagents.** Hydrogen peroxide, 50% (du Pont), was diluted with distilled water to about 10%, and the exact concentration determined. Reagent grade ferrous ammonium sulfate hexahydrate and USP ascorbic acid were used as received.

### Polymerization

This was carried out as previously described<sup>1</sup> except as noted in the tables. Air was removed from the starch slurry by repeated evacuation and breaking the vacuum with nitrogen. Thereafter a blanket of nitrogen was maintained throughout the run.

### Characterization of Products

**PMMA Content by Acid Hydrolysis.** A sample of about 10 g. of granular product was accurately weighed and then treated for 6 hr. with 250 ml. of refluxing 1*N* HCl. The recovered solid was filtered, thoroughly washed with water, and dried to constant weight at  $60^{\circ}\text{C}.$  and 1 mm. of Hg.

**Extraction of Homopolymer.** Granular products at about 25% moisture were extracted with 1,2-dichloroethane by the procedure described in detail elsewhere.<sup>2</sup> Moisture was established at the desired level either by drying the entire product to about 25% water, or by adding the necessary water to the suspension of sample in solvent. Two successive extractions were carried out on each sample, and the sum of the PMMA solids recovered from the two was used to calculate grafting efficiency. When intrinsic viscosity of the extracted PMMA was to be determined, a portion of the clarified solution from the first extract was evaporated to dryness and the solid residue dried to constant weight at  $60^{\circ}\text{C}.$  under vacuum. Intrinsic viscosity was determined in the usual manner in 1,2-dichloroethane at  $30^{\circ}\text{C}.$

**Recovery of Grafted Polymer.** After extraction as described above, the insoluble residue was freed of residual solvent in a vacuum oven at  $60^{\circ}\text{C}.$ , then subjected to hydrolysis by refluxing in 1*N* HCl for 6 hr. After drying the washed product to constant weight at  $60^{\circ}\text{C}.$  (vacuum oven), the sample was dissolved in 100–200 ml. of 1,2-dichloroethane. The treated solution was clarified by filtration through a pressure filter fitted with a Millipore pad of 1  $\mu$  pore size. This left on the pad a sediment of fine brown solid which amounted to not more than 1% of the solids in solution. The concentration of PMMA in the filtrate was determined, and the solution then used for determination of intrinsic viscosity.

**Determination of Molecular Weight.** Values of  $\bar{M}_n$  were calculated from the equation of Fox and co-workers:<sup>4</sup>

$$[\eta] = 8.69 \times 10^{-5}(\bar{M}_n)^{0.76}$$

where  $[\eta]$  is determined in benzene at  $30^{\circ}\text{C}.$  Since intrinsic viscosities on the present samples had been run in 1,2-dichloroethane, intrinsic viscosities

in benzene were estimated by means of the following equation, derived by eliminating the factor for molecular weight between the two equations relating intrinsic viscosity and molecular weight in benzene and in 1,2-dichloroethane:<sup>5</sup>

$$[\eta]_{\text{benzene}} = [\eta]_{\text{dichloroethane}} \times 0.872$$

**Frequency of Grafting.** The weight of grafted PMMA per 162 g. of starch (i.e., per mole of contained glucose unit), divided by the number-average molecular weight of the grafted PMMA, gives moles of grafted side chain per mole of glucose unit. This corresponds to the degree of substitution (D.S.) commonly used to describe derivatized starches. The reciprocal of D.S. is the number of glucose units per grafted side chain; this value is referred to in the present paper as "frequency of grafting." The larger the number, the less frequent the attachment of grafted chains.

## COMPOSITION OF POLYMERIZATION PRODUCTS

### Granular Products

Calculations of efficiency and of frequency of grafting require a reasonably accurate knowledge of the amount of PMMA contained in the products. Four techniques have been examined for determining PMMA content: Gravimetric determination of PMMA after acid hydrolysis to remove starch, carbon-hydrogen analyses, infrared estimation of carbonyl content, and material balance. The assay by acid hydrolysis was found to be most consistent and relatively convenient. Typical spread in per cent PMMA found is shown in the following examples: sample 13D-51, 51.3, 50.2, 50.6% PMMA; sample 13D-52, 51.1, 52.2, 50.7% PMMA. Acid hydrolysis was reported previously<sup>1</sup> to leave a small amount of carbohydrate material in the PMMA, detectable by infrared spectra. We have now found that a 6-hr. hydrolysis in excess 1*N* hydrochloric acid reduces the carbohydrate content to a level below that detectable by infrared. Possible loss of weight of PMMA by acid hydrolysis of ester groups was checked in a few instances by titration with alkali of acetone solutions of the recovered PMMA. In no instance was there more than 2% hydrolysis, usually much less. This agrees with the known resistance of PMMA to acid hydrolysis.<sup>6</sup> Gravimetric error due to hydrolysis of the PMMA ought therefore to be very slight.

Insufficient data have been accumulated to allow estimate of the standard deviation of the determination of PMMA. That there is an error, however, is indicated by the fact that some of the yields of PMMA reported in Table I are higher than theoretical. The magnitude of the effect of errors in PMMA analysis on parameters of interest in this paper are shown in Table II, which illustrates the effects for sample 13D-57 if it actually contained 50.0%, but were reported by analysis to contain 52.0% of PMMA.

TABLE I  
Distribution of Products Between Granular and Aqueous Phases

Run	Parts MMA <sup>a</sup>	H <sub>2</sub> O <sub>2</sub> /FAS/- ascorbic acid <sup>b</sup>	Pro- cedure <sup>c</sup>	Granular product		Solids in filtrate		
				Dry wt., g.	Wt. PMMA, g. <sup>d</sup>	Total wt., g.	Wt. PMMA, g. <sup>d</sup>	Wt. starch, g. <sup>e</sup>
Unmodified Starch								
13D-51	100	100/1/10	A	196.4	100.8	2.66	0.20	1.20
13D-60	50	100/1/10	A	148.5	51.2	2.00	0.07	0.67
13D-52	100	10/1/0	A	198.9	103.8	0.80	0.00	0.63
13D-61	50	10/1/0	A	148.9	52.7	0.55	0.00	0.38
13D-63	100	10/10/0	A	195.0	95.0	1.63	0.00	0.00
13D-64	50	10/10/0	A	148.7	50.4	1.56	0.00	0.00
13D-65	100	100/10/0	A	202.5	97.6	1.82	0.00	0.08
13D-66	50	100/10/0	A	147.7	48.2	1.73	0.00	0.00
94E-31	None	100/1/10	A			2.56	—	1.30

			Oxidized Starch					
13D-57	100	100/1/10	A	189.5	102.2	11.48	1.27	8.95
13D-59	50	100/1/10	A	140.7	51.2	9.53	0.50	7.77
35D-44	20	100/1/10	A	112.7	20.7	6.98	0.01	5.71
35D-45	10	100/1/10	A	101.3	9.5	8.74	0.05	7.43
94E-32	None	100/1/10	A			12.62	—	11.36
13D-58	100	10/1/0	A	193.4	102.2	7.64	0.14	7.33
13D-62	50	10/1/0	A	145.9	51.9	5.53	0.00	5.36
13D-100	100	100/10/20	B	184.5	96.7	12.24	0.28	8.04
13D-97 <sup>f</sup>	100	100/10/100	B	129.3	65.0	47.8	9.06	26.1
35D-54	100	100/10/20	C	188.5	97.8	11.02	0.26	6.84
35D-57*	100	100/10/20	C	189.6	97.7	11.24	0.40	6.92

<sup>a</sup> Parts (by weight) of MMA monomer per 100 parts of starch solids.

<sup>b</sup> Millimoles of hydrogen peroxide, ferrous ammonium sulfate, and ascorbic acid per mole of contained glucose unit in the starch.

<sup>c</sup> Procedures: (A) all reagents added at start of polymerization; (B) monomer, initiator, and activator all added in 10 equal increments at 10-min. intervals during polymerization; (C) monomer, initiator, and activator added continuously during polymerization.

<sup>d</sup> Calculated from per cent contained PMMA as determined by acid hydrolysis.

<sup>e</sup> Estimated by subtracting the weights of PMMA in the filtrate, of ferrous ammonium sulfate (anhydrous basis) charged, and ascorbic acid charged from the total weight of solids in the filtrate.

<sup>f</sup> Polymerization run at 57–60°C.; all others run at about 20–40°C.

\* Repeat of run 35D-54.

TABLE II

Parameter	Calculated from		Difference, %
	50.0% PMMA	52.0% PMMA	
Grafting efficiency of PMMA	68.9	70.1	+1.7
Grafted PMMA, g./100 g. starch	68.9	76.0	+10.3
Glucose units per grafted chain	400	370	-7.5

### Products in Aqueous Filtrate

It was previously reported<sup>1</sup> that in polymerization with oxidized, but not with unmodified starch, there is a little carbohydrate material in the filtrate separated from the granular product. Since some runs in the present series involved more drastic oxidizing conditions than those previously reported, it was of interest to determine the amount and kind of solid contained in the aqueous phase. Results of such determinations are shown in Table I. It is again seen that the oxidized starch produces significant amounts of carbohydrate in the mother liquor, and that the unmodified starch does not, except in some instances at higher peroxide levels. Runs which produce significant amounts of water-soluble starch material also tend to yield a certain amount of PMMA in the filtrate. It was not determined whether this PMMA was present as discrete polymer particles or actually represented a solution of graft copolymer.

### EFFICIENCY AND FREQUENCY OF GRAFTING

Table III summarizes pertinent data for the series of graft preparations.

It will be noted that the viscosity-average molecular weight of the extracted homopolymer is sometimes the same as, never less than half that of the grafted PMMA concurrently formed. Products recovered from other runs not included in the table show a similar trend in molecular weights.

Grafting frequency, expressed as the number of anhydroglucose units per grafted PMMA chain, ranges from 230 to 6100. While this represents considerable variation, the grafted products in general contain long side chains grafted at rare intervals. Calculation of the average number of graft chains per starch molecule is pointless because of the extreme range in molecular weight present in native starch, and because of the unknown extent of degradation of starch chains by the action of the initiating system. But, since the grafting frequency is only one side chain per hundreds to thousands of glucose units, there must be a large fraction of the starch chains containing no grafted PMMA at all. This qualitative result is similar to that reported by Stannett and co-workers<sup>7</sup> for cellulosic graft copolymers.

Table III shows that the hydrogen peroxide is quite inefficient in formation of graft side chains. At best, less than 5% of the added hydroxide undergoes reaction resulting in grafting.

TABLE III  
Efficiency and Frequency of Grafting PMMA

Run	PMMA in product, g./100 g. starch		Graft efficiency, %	$\bar{M}_n$ of homo- PMMA $\times 10^{-5}$	Grafted PMMA		Graft frequency <sup>b</sup>	$H_2O_2$ efficiency, moles <sup>c</sup>
	Total	Grafted			$\bar{M}_n \times 10^{-5}$	$\bar{M}_n \times 10^{-5}$		
Unmodified Starch								
13D-51	105	73	69	2.0	4.1	1.8	1500	150
13D-60	53	38	72	—	2.7	1.2	2000	200
13D-52	109	92	84	7.7	9.8	4.4	3000	30
13D-61	55	48	88	—	6.3	2.9	3700	37
13D-63	95	44	46	—	9.6	4.3	6100	61
13D-64	51	37	72	—	4.2	1.9	3200	32
13D-65	93	36	39	—	6.5	2.9	5000	500
13D-66	48	29	59	—	4.3	1.9	4100	410
Oxidized Starch								
13D-57	117	83	71	0.98	0.98	0.45	330	33
13D-59	57	43	75	0.56	0.53	0.24	350	35
35D-44	23	21	93	—	0.40	0.18	530	53
35D-45	10.3	10.2	98	—	1.2	0.58	3500	350
13D-58	112	92	83	6.3	9.3	4.1	2700	27
13D-62	55	50	90	—	6.3	2.8	3500	35
13D-100	110	87	79	—	0.78	0.33	230	23
13D-97	101	54	54	—	1.2	0.53	600	60
35D-54	108	77	72	—	0.65	0.30	240	24
35D-57	106	82	76	—	0.74	0.33	250	25

<sup>a</sup> Per cent of PMMA which is unextractable from the granular product.

<sup>b</sup> Frequency expressed as number of glucose units per grafted chain of PMMA.

<sup>c</sup> Moles of  $H_2O_2$  added per mole of grafted PMMA.

### Comparison of Unmodified and Oxidized Starch

To simplify the comparison of the two starches, selected data from Table III are presented in Table IV. When the initiating system is the same, grafting efficiencies of PMMA to the two starches are quite similar. With millimole levels of peroxide/iron at 10/1, the molecular weight of the grafted side chains and the grafting frequency are also quite similar. With peroxide/iron/ascorbic acid at millimole levels of 100/1/10, however, the oxidized starch undergoes significantly more frequent grafting with side chains of appreciably lower molecular weight than does the unmodified starch. The reason that the oxidized starch behaves like the unmodified starch at the lower but not at the higher initiator level is not clear; perhaps there is a complex interplay of factors, including relative diffusion rates of initiator, activator, and monomer into the granule.

TABLE IV  
Comparison of Unmodified with Oxidized Starch

Run	Parts MMA	Grafting efficiency, %		$\bar{M}_n$ of grafted PMMA $\times 10^{-5}$		Grafting frequency	
		Unmod- ified	Oxi- dized	Unmod- ified	Oxi- dized	Unmod- ified	Oxi- dized
13D-51, 57 <sup>a</sup>	100	69	71	1.8	0.45	1500	300
13D-60, 59 <sup>a</sup>	50	72	75	1.2	0.24	2000	350
13D-52, 58 <sup>b</sup>	100	84	83	4.4	4.1	3000	2700
13D-61, 62 <sup>b</sup>	50	88	90	2.9	2.8	3700	3500

<sup>a</sup> Peroxide/Fe<sup>II</sup>/ascorbic acid at millimole levels of 100/1/10.

<sup>b</sup> Peroxide/Fe<sup>II</sup>/ascorbic acid at millimole levels of 10/1/0.

### Effect of Level of MMA Monomer

In general, as the monomer is decreased from 100 to 50 parts, but with other conditions unvaried (Table III), the grafting efficiency increases, the molecular weight of the side chains decreases, but there is no significant change in the frequency of grafting. Lower grafting efficiency at the higher

TABLE V  
Effect of Monomer Level

Run	Parts MMA <sup>a</sup>	Graft efficiency, %	$\bar{M}$ of grafted PMMA $\times 10^{-5}$	Graft frequency	H <sub>2</sub> O <sub>2</sub> efficiency, moles
13D-57	100	71	0.45	330	33
13D-59	50	75	0.24	350	35
35D-44	20	93	0.18	530	53
35D-45	10	98	0.58	3500	350

<sup>a</sup> Parts per 100 parts of oxidized starch, all run at 100/1/10 mmole levels of peroxide Fe<sup>II</sup>/Ascorbic acid.

TABLE VI. Effect of Level of Initiator

Run	Initiator					$\bar{M}_n$ of grafted PMMA $\times 10^{-3}$	Graft frequency	$H_2O_2$ efficiency, moles
	Parts MMA	$H_2O_2$ , mmoles	FAS, mmoles	Ascorbic acid, mmoles	Graft efficiency, %			
Unmodified Starch								
13D-52	100	10	1	0	84	4.4	3000	30
13D-63	100	10	10	0	46	4.3	6100	61
13D-51	100	100	1	10	69	1.8	1500	150
13D-65	100	100	10	0	39	2.9	5000	500
Oxidized Starch								
13D-58	100	10	1	0	83	4.1	2700	27
13D-57	100	100	1	10	71	0.45	330	33
13D-62	50	10	1	0	90	2.8	3500	35
13D-59	50	100	1	10	75	0.24	350	35
76A-142	50	100	1	0	No polymerization			

TABLE VII. Effect of Gradual Addition of Monomer and Initiator<sup>a</sup>

Run	$H_2O_2$ /FAS/ascorbic acid	Procedure	Temp., °C.	Time, hr.	Graft efficiency, %	$\bar{M}_n$ of grafted PMMA $\times 10^{-5}$	Graft frequency	$H_2O_2$ efficiency, moles
13D-57	100/1/10	A	30-46	3.0	71	0.45	330	33
13D-100	100/10/20	B	33-37	1.9	79	0.33	230	23
13D-97 <sup>b</sup>	100/10/100	B	57-60	2.0	54	0.53	600	60
35D-54	100/10/20	C	30-36	2.0	72	0.30	240	24
35D-57 <sup>c</sup>	100/10/20	C	30-37	2.5	76	0.33	250	25

<sup>a</sup> All runs with 100 parts of MMA per 100 parts of oxidized starch.<sup>b</sup> Conversion of monomer, 74%; in all other runs, conversion was 98-100%.<sup>c</sup> Repeat of 35D-54.

monomer levels means that the relative rates of formation of homo- and graft copolymer shift in such a way that a higher proportion of homopolymer is formed in the later than in the earlier stages of the polymerization.

Moreover, constancy of the grafting frequency suggests that no new grafting sites are being formed in the later stages of the polymerization.

Table V summarizes the results from a series in which a wider range of monomer level is examined. The same trends apply as already noted, except for less frequent grafting and higher molecular weight at 10 parts of monomer.

### Effect of Initiator/Activator Level

Table VI illustrates the effects. In broad terms, increasing the amount of peroxide tends to give lower grafting efficiencies. With unmodified starch, increasing the level of peroxide causes slight trend toward lower molecular weight of grafted side chains and perhaps a slight tendency toward more frequent grafting. With the oxidized starch, high level of peroxide results in very significant lowering of molecular weight and improvement of grafting frequency. At a fixed peroxide level, increasing the amount of iron lowers grafting efficiency and frequency. An effect repeatedly observed is that with peroxide at the 10 mmole level, raising the iron from 1 to 10 mmoles resulted in significantly slower polymerization.

Raising the iron concentration at a fixed level of peroxide lowered the yield of grafted chain based on the peroxide present.

### Effect of Gradual Addition of Monomer and Initiator

The more frequent the grafting, and the shorter the grafted chains, the higher the grafting efficiency with respect to the starch. It was therefore of interest to search for those conditions which would favor frequent grafting of short chains. Evidence discussed above indicated that when monomer and initiator/activator were added in single portions prior to or at the start of the polymerization cycle, no new grafting sites were formed in the later stages of the process. This suggested that perhaps more frequent grafting might be obtained if both monomer and initiator/activator were added gradually throughout the course of the polymerization. Because of its greater susceptibility to grafting, oxidized starch was used for a series of such runs. Data are shown in Table VII.

Except for run 13D-97, the gradual addition of monomer and initiator does indeed show slightly higher grafting efficiency than the batch addition, while at the same time molecular weight of the grafted chains appear slightly lower and grafting frequency appreciably higher. Thus, the changes are in the expected direction, but the magnitudes are relatively slight. The products still contain long side chains grafted at relatively rare intervals.

### References

1. Brockway, C. E., and K. B. Moser, *J. Polymer Sci.*, **A1**, 1025 (1963).
2. Brockway, C. E., *J. Polymer Sci.*, **A2**, 3731 (1964).
3. Schoch, T. J., *J. Am. Chem. Soc.*, **64**, 2954 (1942).
4. Fox, T. G., et al., *Polymer*, **3**, 82 (1962).
5. Riddle, E. H., *Monomeric Acrylic Esters*, Reinhold, New York, 1954, p. 64.
6. Glavis, F. J., *J. Polymer Sci.*, **36**, 547 (1959).
7. Yasuda, H., J. A. Wray, and V. Stannett, *J. Polymer Sci.*, **C2**, 387 (1963).

### Résumé

La teneur en P.M.M.A. des copolymères greffés avec l'amidon granulé, peut être déterminée par hydrolyse acide avec suffisamment de précision pour permettre de juger d'une façon raisonnée de l'efficacité et de la fréquence du greffage. La préparation du copolymère greffé par initiation du méthacrylate de méthyle avec le peroxyde d'hydrogène et des activateurs fournit des produits contenant de longues chaînes de PMMA latérales attachées à l'amidon, à très peu d'intervalles, mais la longueur et la fréquence d'attachement peuvent être considérablement modifiées en changeant le rapport des réactifs. La plus haute fréquence a été atteinte avec le PMMA, d'un poids moléculaire moyen en nombre de 30.000, attaché avec une fréquence d'une chaîne par 230-250 unités de glucose dans l'amidon. Dans des conditions plus favorables, l'amidon oxydé fournit un produit à fréquence de greffage plus importante qu'avec l'amidon non modifié. L'addition graduelle du monomère, de l'initiateur et de l'activant à la suspension d'amidon donne un léger accroissement de la fréquence de greffage, si on le compare à l'addition complète de tous les réactifs au début de la polymérisation.

### Zusammenfassung

Der PMMA-Gehalt von Pfropfcopolymeren auf gekörnter Stärke kann durch saure Hydrolyse mit einer für die Berechnung von Pfropfungswirksamkeit und -häufigkeit genügenden Genauigkeit bestimmt werden. Bei der Herstellung der Pfropfcopolymeren durch Anregung der Methylmethacrylatpolymerisation mit Wasserstoffperoxyd und Aktivatoren entstehen Produkte, in denen lange PMMA-Seitenketten in sehr grossen Abständen an die Stärke gebunden sind. Die Kettenlänge und die Häufigkeit der Haftstellen können durch Änderung des Verhältnisses der Reaktionspartner variiert werden. Die grösste Häufigkeit wurde mit PMMA mit einem Molekulargewichtszahlenmittel von etwa 30000 erreicht, wobei eine Kette auf 230-250 Glucoseeinheiten der Stärke entfiel. Unter günstigeren Bedingungen ergab oxydierte Stärke Produkte mit bedeutend höherer Pfropfungshäufigkeit als unmodifizierte Stärke. Bei schrittweiser Zugabe von Monomerem, Starter und Aktivator zum Stärkebrei wurde eine etwas höhere Pfropfungshäufigkeit als bei gemeinsamer Zugabe aller Reaktionsteilnehmer zu Beginn der Polymerisation erreicht.

Received August 16, 1963

Revised October 26, 1963

## Extractability of Homopolymer of Methyl Methacrylate from Its Graft Copolymers with Starch

C. E. BROCKWAY, *Research Center, A. E. Staley Manufacturing Company  
Decatur, Illinois*

### Synopsis

A study has been made of factors which influence the efficiency of extraction of homopolymer of methyl methacrylate from its graft copolymers with granular corn starch. The moisture content plays a significant role in the extractability of homopolymer; about 25% moisture seems optimum for many samples, with extractability of homopolymer falling sharply at lower moisture levels. In a series of solvents, the efficiency of removal of ungrafted homopolymer varies in a manner roughly paralleling the relative solvating efficiencies of the various solvents for the homopolymer, as indicated by the reported values of appropriate parameters for polymer solutions. For the starch/PMMA system, chloroform and dichloroethane are about equally efficient, and either is superior to benzene, which in turn is better than toluene, methyl ethyl ketone, or acetone. Soxhlet extraction, though commonly used for graft copolymers, is not as effective for the granular starch/PMMA system as is tumbling the heated mixture of solvent and polymer in a closed container. This is probably due to inefficient percolation of the solvent through the swollen syrupy mass of graft copolymer in the Soxhlet thimble.

### INTRODUCTION

A previous paper<sup>1</sup> reported evidence for grafting when polymerization of methyl methacrylate is initiated by hydrogen peroxide and iron ( $\text{Fe}^{+2}$ ) in an aqueous slurry of granular corn starch. This paper discusses factors influencing the extractability of ungrafted homopolymer. A subsequent paper will report the influence of polymerization conditions on efficiency and frequency of grafting.

### EXPERIMENTAL

Polymerizations were conducted in aqueous slurries of granular corn starch as previously described,<sup>1</sup> with initiation by hydrogen peroxide and ferrous ammonium sulfate in every instance. Amounts of monomer and initiator were selected to give a range of both poly(methyl methacrylate) (PMMA) content and of grafting efficiency.

#### Control of Moisture Content

After completion of the polymerization cycle, the solid product was recovered by filtering, reslurrying in distilled water, and again filtering.

The product was dried either at room temperature or in a 50°C. oven with frequent blending, until weight loss indicated the desired moisture content was realized. The product was bottled and blended by rolling the bottle for several hours, after which moisture content was accurately determined.

In some instances, products were air-dried at room temperature to equilibrium moisture content (10% or less), and at the time of extraction treated with added water to bring the total moisture content to the desired level.

### Extraction

The solvents used for the extraction were reagent grade materials used as received, and were all found to contain less than 0.1 mg. of nonvolatile residue per 20 ml. of solvent.

Samples of 9–13 g. (dry basis) of starch-PMMA were extracted with 200 ml. of solvent. The mixtures, in 12-oz. crown-cap bottles, were tumbled end over end at about 45 rpm for 16 hr. or longer in a water bath held at  $50 \pm 1^\circ\text{C}$ . After each bottle was cooled to room temperature, the mixture was suction filtered through a medium porosity sintered glass filter. To avoid evaporating solvent from the filter cake, the vacuum was broken when the level of mother liquor in the funnel dropped just to the top of the filter cake. The extraction bottle was rinsed with 100 ml. of fresh solvent, which was then poured into the filter, where solvent and filter cake were gently slurried for 3–5 min. before drawing off the solvent through the filter. The extraction bottle, filter, and filter cake were rinsed in the same manner twice more with fresh 100 ml. portions of solvent. Then the combined filtrate and washings in the filter flask were concentrated by warming under a gentle stream of filtered air, and finally dried to constant weight at 110°C. Infrared curves of selected specimens so obtained indicated that these were indeed PMMA free of any detectable carbohydrate material.

### Solvent Content of Extraction Residue

After separation and washing, the insoluble residue was transferred in fresh solvent to a tared and stoppered centrifuge bottle. The slurry was clarified by centrifuging. It was then possible to decant the supernate cleanly from the syrupy to semisolid cake. After weighing (nearest 0.1 g.), bottle and residue were dried at 110°C. to constant weight. The amount of retained solvent was calculated as milliliters per gram of (a) dry basis graft mixture charged; (b) PMMA retained in the insoluble residue (see Table III).

### EFFECT OF MOISTURE LEVEL

Table I shows the results of extracting two different mixtures containing graft copolymer. These were selected because of similar levels of contained PMMA at different grafting efficiencies. Samples were dried at room temperature to varying moisture contents and finally oven-dried. As the final step in the sequence, water was added to the mixture of solvent and oven-dried sample.

Results in Table I indicate a pronounced relationship of extractability of homopolymer to moisture content. Particularly interesting is the higher extractability, seen with both products, resulting from heating followed by addition of solvent and water. It is not established whether this treatment simply promotes opening of the granule structure, thus allowing more efficient removal of ungrafted polymer, or whether degradation of starch results in release of some of the grafted polymer. In any event, reducing the moisture content to a very low value does not cause irreversible changes which prevent the homopolymer from being extracted on addition of solvent plus water.

TABLE I  
Extractions at Various Moisture Levels

Sample no.	Sample treatment	Moisture content of sample, %	PMMA extracted, % <sup>a</sup>
Product 76A-147, 98.4 parts PMMA/100 parts starch			
1	Dried in air at room temp.	54.7	13.0, 14.3
2	"	30.3	12.7, 13.4
3	"	6.4	7.2, 7.1
4	Sample 3, dried 4 hr. at 110°C.	0.0	4.7, 4.8
5	Sample 3, dried 17 hr. at 50°C. and 0.1 mm. Hg.	0.0	4.3, 4.1
6	Water added to suspension of sample 4 in solvent	25.0	16.3, 17.4
7	Water added to suspension of sample 5 in solvent	25.0	17.2, 14.1
Product 76A-151, 87.6 parts PMMA/100 parts starch			
8	Dried in air at room temp.	55.8	35.2, 34.7
9	"	35.0	36.8, 34.6
10	"	8.0	24.5, 24.1
11	Sample 10, dried 4 hr. at 110°C.	0.0	18.6, 18.6
12	Sample 10, dried 17 hr. at 50°C. and 0.1 mm. Hg.	0.0	18.3, 18.6
13	Water added to suspension of sample 11 in solvent	25.0	48.4, 46.7
14	Water added to suspension of sample 12 in solvent	25.0	40.1, 40.6

<sup>a</sup> Duplicate samples extracted with 1,2-dichloroethane.

Certain runs were carried out to define more closely the moisture content at which extractability of homopolymer falls off significantly. Results from samples dried to various water levels are shown in Figure 1. Figure 2 shows similar curves for products air-dried to about 10% moisture, and then with moisture added back at varying levels either to the solid product or to the mixture of solid and solvent. While it is not possible to draw the curves with precision, it is again evident that as moisture content falls below 20-30%, extractability of homopolymer usually drops significantly.

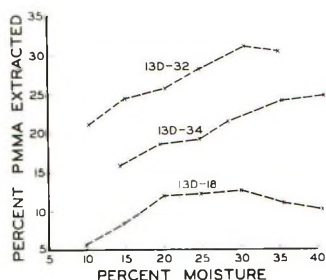


Fig. 1. Effect of moisture content on extractability of PMMA in dichloroethane: (13D-32) 96.8 parts PMMA/100 parts starch; (13D-34) 44.9 parts PMMA/100 parts starch; (13D-18) 95.0 parts PMMA/100 parts starch. Samples dried to varying moisture levels prior to extraction.

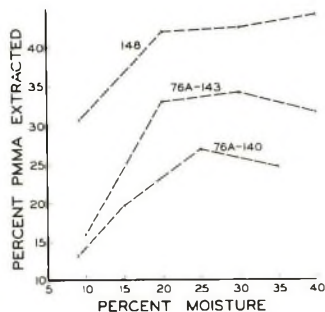


Fig. 2. Effect of moisture content on extractability of PMMA in dichloroethane: (76A-140) 49.9 parts PMMA/100 parts starch; (76A-143) 45.2 parts PMMA/100 parts starch; (76A-148) 86.9 parts PMMA/100 parts starch. All samples initially dried to ca. 10% moisture; for samples 76A-140 and 76A-143, additional water blended with sample prior to addition of solvent; for sample 76A-147, additional water added to suspensions of sample in solvent.

These results are consistent with the general experience that extraction of noncarbohydrate materials from granular starch with nonaqueous solvents is more efficient when the extracting solvent contains a small amount of water. As an example, both dioxane and methanol function more effectively for the removal of naturally occurring fatty material in granular corn starch when the solvent is diluted with a small amount of water.<sup>2</sup> This is undoubtedly related to the swelling of the starch granule on exposure to water.

### COMPARISON OF SOLVENTS

As reported earlier,<sup>1</sup> 1,2-dichloroethane was found to be more efficient than acetone for extraction of methyl methacrylate homopolymer. Benzene has been used for extracting PMMA from its block<sup>3</sup> or graft<sup>4</sup> copolymers with starch. It was therefore of interest to compare these two solvents in the tumbled bottle extraction. Figure 3 shows the results of

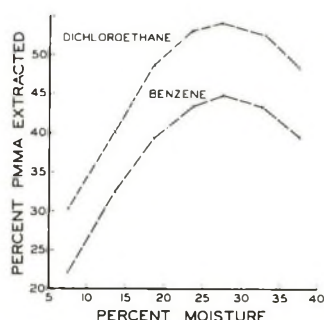


Fig. 3. Comparison of benzene and dichloroethane. Sample 76A-149, 71.2 parts PMMA/100 parts starch; dried to various moisture levels prior to extraction.

single extractions at various water levels. In addition to the usual trend of decreased extractability at low water levels, it is quite apparent that at any one water level 1,2-dichloroethane extracts more homopolymer than does benzene.

Fox and co-workers have recently published data indicating the relative solvating efficiency of various solvents for PMMA. For a given fraction of PMMA, the intrinsic viscosity is reported<sup>5</sup> to decrease from one solvent to another in the sequence shown in Table II. This is reflected by the change in the value of the exponent  $a$  in the empirical equation

$$[\eta] = K_1 M^a$$

Theta temperatures indicate the same sequence of relative solvating efficiency.<sup>6</sup> It was, therefore, of interest to check this series of solvents for relative efficiency in removing ungrafted homopolymer from starch-PMMA graft copolymers.

TABLE II  
Parameters for Solutions of PMMA in Various Solvents

Solvent	Value of exponent $a^a$	Theta temperature, °K. <sup>b</sup>
Chloroform	0.80	0
1,2-Dichloroethane	0.77	40
Benzene	0.76 <sup>c</sup>	50
Methyl ethyl ketone	0.72	175
Toluene	0.71	208
Acetone	0.70	218

<sup>a</sup> Data of Fox et al.<sup>5</sup> for the equation  $[\eta] = K_1 M^a$ .

<sup>b</sup> Data of Fox;<sup>6</sup> for limits of uncertainty see the original reference.

<sup>c</sup> For  $\bar{M}_w$  values greater than 35,000.

For this study, products were given a single extraction at 25% moisture content in tumbled bottles at 50°C. Table III shows that the amount of PMMA extracted runs consistently a little higher with 1,2-dichloroethane

TABLE III  
Comparison of Various Solvents<sup>a</sup>

Sample	PMMA content, parts/100 starch	$\bar{M}_n$ of PMMA $\times 10^{-4b}$	Solvent	PMMA extracted, %	Swollen residue	
					Solvent retained, ml./g. solid product charged	Solvent retained, ml./g. unextracted PMMA
13D-52A	104.5	44.0	Chloroform	17.1	3.2	6.9
			1,2-Dichloroethane	18.7	2.3	4.9
			Benzene	13.3	2.2	4.6
			MEK	10.1	1.4	2.8
			Toluene	8.9	1.8	3.7
			Acetone	9.5	1.3	2.7
13D-97A	101.3	5.3	Chloroform	47.4	4.6	13.3
			1,2-Dichloroethane	48.2	4.4	12.8
			Benzene	41.6	3.2	8.5
			MEK	40.3	1.8	4.8
			Toluene	37.3	2.4	6.2
			Acetone	41.5	2.1	5.5

13D-44A	22.5	1.8	Chloroform	9.4	1.2	6.5
			1,2-Dichloroethane	12.4	1.0	6.1
			Benzene	3.5	1.1	5.8
			MEK	2.2	0.8	4.5
			Toluene	1.7	1.2	6.7
			Acetone	1.3	0.8	4.1
13D-54A	107.9	3.0	Chloroform	26.5	4.6	10.4
			1,2-Dichloroethane	28.6	3.9	9.0
			Benzene	25.2	3.2	7.1
			MEK	13.8	1.5	3.0
			Toluene	21.9	2.4	5.2
			Acetone	15.0	1.4	2.9

<sup>a</sup> Each value is the mean from duplicate determinations.

<sup>b</sup> Values are for the unextractable portion of the PMMA calculated from intrinsic viscosities by means of the equation of Fox.<sup>7</sup>

than with chloroform, contrary to prediction. Benzene is consistently less efficient than either of the first two solvents. With the remaining three solvents, the results are less consistent. However, none of the three is in any instance as efficient as benzene, with the one exception of acetone for sample 13D-97A.

With respect to the amount of solvent imbibed by the insoluble solid, the sequence follows more nearly that which is predicted. Chloroform consistently causes greater swelling than 1,2-dichloroethane, which in turn is consistently better than benzene. Toluene does not cause as much swelling as benzene, but is better than either methyl ethyl ketone or acetone.

With a given solvent it might be expected that when the volume of swelling is calculated on the basis of milliliters of imbibed solvent per gram of PMMA retained in the residue, relatively constant values would be obtained. Actually, the low and high values differ by a factor of two or more, and do not seem to be related in any simple way to the content of PMMA or its molecular weight. However, with graft copolymers of similar initial PMMA content, the higher the proportion of PMMA that is extracted, the greater the volume of imbibed solvent per gram of unextracted PMMA. Perhaps removal of higher proportions of homopolymer from the granular products simply leaves more space available to be occupied by solvent.

In summary, while the relative efficiencies for extracting of homopolymer do not follow strictly the predicted solvating powers for the six solvents used, there is no question but that the most effective removal of homopolymer can be achieved by those solvents which are the "best" solvents for the homopolymer in question. With granular starch-PMMA, chloroform and 1,2-dichloroethane are about equally effective, and either is preferable to benzene.

### EFFECT OF EXTRACTION TECHNIQUE

The Soxhlet extractor has the advantage over the tumbled bottles that the sample is repeatedly exposed to distilled solvent. Moreover, Soxhlet extraction is evidently widely used for removal of homopolymer in grafted systems, and has recently been specifically reported as having been used for the separation of methyl methacrylate homopolymer from its block<sup>3</sup> or graft<sup>4</sup> copolymer with starch. It was therefore of interest to see if better

TABLE IV  
Comparison of Soxhlet with Tumbled Bottle Extractions<sup>a</sup>

Extraction	PMMA extracted, %	
	Bottle	Soxhlet
1st	30.0, 30.6	23.5, 22.6
2nd	— —	0.7, 0.9

<sup>a</sup> Product 13D-32, containing 96.8 parts PMMA/100 parts of contained starch, extracted at an initial moisture content of 35.1%.

extraction efficiencies could be realized in the Soxhlet extractor. Table IV shows the results of such a direct comparison. Duplicate samples were extracted by each technique.

In the Soxhlet extraction, samples were extracted for 24 hr. by the conventional technique, then the amount of solid extracted determined by drying an aliquot portion of the liquor in the boiling flask. The apparatus was then thoroughly rinsed with fresh solvent and the extraction continued with a charge of fresh solvent for about 24 hr. longer.

The Soxhlet extractor may be less efficient than the bottle because of accumulation of water droplets in the upper part of the barrel of the extractor, thus giving a lower effective moisture content. Another possible reason for the difference lies in the physical form of the insoluble solid during extraction. Upon exposure to solvent, the moist solid swells and becomes a compact syrupy mass. This undoubtedly interferes with efficient percolation of solvent through the sample. Although similar swelling occurs in the bottle, the end-over-end tumbling action prevents agglomeration of the solid to a single mass. In any event, in instances where the graft undergoing extraction tends to swell to a semi-impervious mass, the appropriateness of the Soxhlet extractor is questionable.

### References

1. Brockway, C. E., and K. B. Moser, *J. Polymer Sci.*, **A1**, 1025 (1963).
2. Schoch, T. J., *J. Am. Chem. Soc.*, **64**, 2954 (1942).
3. Ceresa, R. J., *Polymer*, **2**, 216 (1961).
4. Kimura, S., T. Takitani, and M. Imoto, *Bull. Chem. Soc. Japan*, **35**, 2014 (1962).
5. Cohn-Ginsberg, E., T. G. Fox, and H. F. Mason, *Polymer*, **3**, 97 (1962).
6. Fox, T. G., *Polymer*, **3**, 111 (1962).
7. Fox, T. G., J. B. Kinsinger, H. F. Mason, and E. M. Schuele, *Polymer*, **3**, 85 (1962).

### Résumé

On a effectué une étude des facteurs qui influencent l'efficacité de l'extraction de l'homopolymère du méthacrylate de méthyle de ses copolymères greffés au moyen de grains d'amidon de blé. La teneur en eau joue un rôle significatif dans l'extractibilité de l'homopolymère; environ 25% d'humidité semble être une valeur optimale pour beaucoup d'échantillons; pour des teneurs en eau plus faibles l'extractibilité de l'homopolymère décroît nettement. Dans une série de solvants, l'efficacité de l'extraction de l'homopolymère non-greffé varie d'une manière approximativement parallèle à l'efficacité relative de solvation des différents solvants pour l'homopolymère, comme l'indiquent les valeurs des paramètres, appropriés pour des solutions de polymères. Pour le système amidon/méthacrylate de méthyle, le chloroforme et le dichloroéthane sont d'une efficacité presque égale, et tous les deux sont supérieurs au benzène, qui à son tour est meilleur que le toluène, la méthyléthylcétone ou l'acétone. L'extraction au Soxhlet, bien que généralement employée pour des copolymères greffés, n'est pas aussi efficace pour le système amidon en grain/PMMA que l'agitation du mélange chauffé de solvant et de polymère dans un récipient fermé. Ceci est probablement dû à l'infiltration insuffisante du solvant à travers la masse gonflée et sirupeuse du copolymère greffé dans la carotte du Soxhlet.

### Zusammenfassung

Der Einfluss verschiedener Faktoren auf die Wirksamkeit der Extraktion des Methylmethacrylat-Homopolymeren aus Pffropfcopolymeren mit gekörnter Maisstärke wurde untersucht. Der Feuchtigkeitsgehalt spielt für die Extrahierbarkeit des Homopolymeren eine wichtige Rolle. Bei vielen Proben liegt das Optimum bei 25% Feuchtigkeitsgehalt; mit sinkendem Feuchtigkeitsgehalt nimmt die Extrahierbarkeit des Homopolymeren stark ab. Die Wirksamkeit der verschiedenen Lösungsmittel bei der Extraktion des ungepfropften Homopolymeren verläuft zum relativen Lösungsvermögen der einzelnen Lösungsmittel für das Homopolymere annähernd parallel, wie die Literaturwerte geeigneter Parameter von Polymerlösungen erkennen lassen. Im Falle des Stärke/PMMA-Systems sind Chloroform und Dichloräthan etwa gleich wirksam und besser als Benzol und dieses wiederum ist wirksamer als Toluol, Methyläthylketon oder Aceton. Die üblicherweise für Pffropfcopolymere verwendete Soxhlet-Extraktion ist im Falle des Systems gekörnte Stärke/PMMA nicht so wirksam wie das Schütteln des Gemisches von Lösungsmittel und Polymerem in einem geschlossenen Behälter, wahrscheinlich deshalb, weil das Lösungsmittel wirkungslos durch die gequollene sirupöse Masse des Pffropfcopolymeren in der Soxhlethülse durchläuft.

Received August 16, 1963

Revised October 26, 1963

## Statistical Theory of the Polymerization of Polyepoxide Monomers

KENICHI FUKUI and TOKIO YAMABE, *Faculty of Engineering, Kyoto University, Kyoto, Japan*

### Synopsis

A statistical study of the ring-opening polymerization of polyepoxides is made under the assumption of equal rates of initiation and propagation. The Poisson-type distribution and the gel point formula are characterized by the following equations:

$$M_{p,\nu} = [f(fp - p)]\nu^{p-1}/\{p!(fp - p + 1 - \nu)!\}\alpha^{p-1}\rho^{\nu+p-1}(1 - \rho)^{fp-p+1-\nu} \exp\{-\nu\alpha\rho\}$$

$$\rho_c = [I]^{1/2}/\{f(f-1)[M]_0\}^{1/2}$$

where  $p$  is the number of monomeric units,  $\nu$  is the number of propagating ends in a polymer,  $\alpha$  is  $f[M]_0/[I]_0$ ,  $\rho$  and  $\rho_c$  are the fraction of reacted functional groups and its critical value,  $f$  is the number of functional groups on the monomer, and  $[I]_0$  and  $[M]_0$  are the initial concentrations of initiator and monomer, respectively.

### INTRODUCTION

It is well known that there is a class of polymerization where the number of propagating chain ends in one polymer molecule remains invariant through the course of reaction, and in this case, the reaction of a polymer molecule with another polymer molecule is essentially not expected. Such is the case in ethylene oxide type polymerization, in which the effective initiation determines the number of propagating species.

The circumstances are entirely different in the polymerization of multifunctional monomers, such as polyepoxides, where the reaction between polymers can occur so that branched polymers are produced with a broad molecular weight distribution and gelation results<sup>1,2</sup> as is observed in the condensation or the addition polymerization of multifunctional monomers.<sup>3</sup>

A kinetical derivation of the molecular size distribution in linear polymers formed from a monofunctional monomer, such as ethylene oxide, was first given by Flory,<sup>4</sup> who obtained a Poisson distribution under the assumption that the rates of initiation and propagation were equal.

No theoretical attack has attempted, however, in regard to the polymerization of multifunctional monomers. In the present paper, the most general case is treated under the same assumption as Flory's, and a distribution similar to the Poisson type was obtained.

### Kinetic Formulation and Molecular Distribution

It should be remarked at the outset that the treatment presented below is applicable to all polymerization processes which fulfill the following conditions, first two of which characterized also the work of Flory,<sup>4</sup> except for the functionality of the monomer.

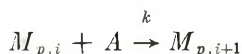
(1) Each monomer possesses  $f$  identical functional groups, and any unreacted functional group on the monomer or polymers can react with the initiator to be changed into propagating species. Therefore, the number of propagating species is equal to the number of initiator molecules consumed.

(2) At any stage during the course of reaction, throughout the initiation and propagation, all unreacted functional groups are considered to be equally reactive, and the rate of the initiation step is equal to that of the propagation step. Moreover, reactions proceed without termination. Such a situation may be realized, for example, in the polymerization of polyepoxides initiated by alcohols. In the case where the rate of initiation is markedly different from that of propagation, further research will be needed.

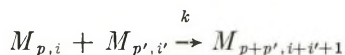
(3) Intramolecular reactions do not occur. This assumption was also introduced in the theory of branched polycondensation by Flory<sup>5</sup> and Stockmayer,<sup>6,7</sup> who pointed out that this assumption was available so far as the reaction did not proceed beyond the gel point, so that, for the first approximation, we also neglect the intramolecular reaction.

Then, the elementary reactions are as follows.

Initiation:



Propagation:



where  $M_{p,i}$  represents polymeric molecules which are composed of  $p$  monomeric units and have lost  $i$  functional groups ( $i - p + 1$ ) of which are due to the reaction with the initiator represented by  $A$ .

Hence,  $M_{p,i}$  bears  $(fp - i)$  unreacted functional groups and  $(i - p + 1)$  propagating species, with the condition

$$fp \geq i \geq p \quad (p \geq 1)$$

and, in addition,  $i = 0$ ,  $p = 1$  for the monomer.

If we suppose for the initial concentrations of the initiator and the monomer,  $[I]_0$  and  $[M]_0$ , then the instantaneous value of the initiator concentration,  $[I]$ , and that of the whole polymers including the monomer,  $[M]$ , are described in terms of one and the same rate constant,  $k$ , for both initiation and propagation.

For the reactions written above, the concentration of each polymer,  $[M_{p,i}]$ , satisfies the constraint and the conservation conditions

$$\begin{aligned}
\sum_{p,i} [M_{p,i}] &= [M] \\
\sum_{p,i} i[M_{p,i}] &= [M]_0 - [M] + [I]_0 - [I] \\
\sum_{p,i} p[M_{p,i}] &= [M]_0
\end{aligned} \tag{1}$$

and the time dependence of  $[I]$  and  $[M]$  is given by the following kinetic equations:

$$-d[I]/dt = k[I] \left\{ \sum_{p,i} (fp - i) [M_{p,i}] \right\} \tag{2}$$

$$-d[M]/dt = k([I]_0 - [I]) \left\{ \sum_{p,i} (fp - i) [M_{p,i}] \right\} \tag{3}$$

where the summation should cover all integers of  $p$  and  $i$  which satisfy the conditions of eq. (1).

It is convenient to introduce here several variables such a way as

$$\begin{aligned}
\alpha &= f[M]_0/[I]_0 \\
\beta &= [I]/[I]_0 \\
C &= [M]/[M]_0 \\
m_{p,i} &= [M_{p,i}]/[M]_0 \\
t' &= k[M]_0 t
\end{aligned} \tag{4}$$

whence eq. (1) is transformed into

$$\sum_{p,i} m_{p,i} = C \tag{1'a}$$

$$\sum_{p,i} i m_{p,i} = 1 - C + (f/\alpha)(1 - \beta) \tag{1'b}$$

$$\sum_{p,i} p m_{p,i} = 1 \tag{1'c}$$

Furthermore, we introduce a new variable,  $\rho$ , given by

$$\sum_{p,i} i m_{p,i} = f\rho \tag{5}$$

which represents the fraction of reacted functional groups.

On rewriting eqs. (2), (3), and (1'b) by the use of variables of eqs. (4) and (5), and differentiating eq. (1'b) with respect to  $t'$ , one obtains

$$\begin{aligned}
-d\beta/dt' &= f\beta(1 - \rho) \\
-dC/dt' &= (f^2/\alpha)(1 - \beta)(1 - \rho) \\
d\rho/dt' &= (d/\alpha)(1 - \rho)
\end{aligned} \tag{6}$$

which can be solved with the results

$$\rho = 1 - e^{-(f/\alpha)t'} \tag{7a}$$

$$\beta = e^{-\alpha\rho} \quad (7b)$$

$$C = 1 - f\rho + (f/\alpha)(1 - e^{-\alpha\rho}) \quad (7c)$$

These equations afford the time functions of the fraction of reacted functional groups, the initiator concentration, and the total concentration of monomers and polymers.

### Kinetic Derivation of Distribution Formula

The size distribution is derived from the following set of differential equations describing the polymerization process.

$$\begin{aligned} dm_{p,i}/dt' = & \sum_{s=1}^{p-1} \sum_{j=s}^{i-1} (\alpha/f)(j-s+1)[f(p-s) - (i-j-i)]m_{s,j} \cdot m_{p-s,i-j-1} + \\ & (f/\alpha)\beta[f p - (i-1)]m_{p,i-1} - f(1-\rho)(i-p+1)m_{p,i} - \\ & (f/\alpha)(1-\beta)(fp-i)m_{p,i} - (f/\alpha)\beta(fp-i)m_{p,i} \quad (8) \\ dm_{1,0}/dt' = & -(f^2/\alpha)(1-\beta)m_{1,0} - (f^2/\alpha)\beta m_{1,0} \end{aligned}$$

In this equation, the first sum represents the formation of molecules by the reaction between a pair of smaller molecules, the second term by the reaction of a  $M_{p,i-1}$  molecule with the initiator, and the remaining three terms correspond to the disappearance of  $M_{p,i}$  through the reaction of the propagating ends on a  $M_{p,i}$  molecule with unreacted functional groups on other molecules, the reaction of an unreacted functional group on  $M_{p,i}$  with propagating ends on other molecules, and the reaction of  $M_{p,i}$  with the initiator, respectively.

Using eqs. (6) and (7), we obtain

$$\begin{aligned} \frac{dm_{p,i}}{d\rho} + \left[ \alpha(i-p+1) + \frac{fp-i}{1-\rho} \right] m_{p,i} = & \sum_{s=1}^{p-1} \sum_{j=s}^{i-1} \alpha \frac{(i-s+1)[f(p-s) - (i-j-1)]}{f(1-\rho)} m_{s,j} \cdot m_{p-s,i-j-1} + \\ & \frac{fp-(i-1)}{1-\rho} \beta \cdot m_{p,i-1} \quad (8') \\ (dm_{1,0}/d\rho) + [f/(1-\rho)]m_{1,0} = & 0 \end{aligned}$$

For the monomer ( $m_{1,0}$ ), this latter equation can be solved directly with the result

$$m_{1,0} = (1-\rho)^f$$

In order to find the general solution, we put

$$m_{p,i} = C'(p,i)\alpha^{p-i} \cdot \rho^i (1-\rho)^{fp-i} e^{-(i-p+1)\alpha\rho}$$

where  $C'(p, i)$  is independent of  $\rho$ ; it is then easily seen that this expression  $m_{p,i}$  satisfies eq. (8) provided that

$$iC'(p, i) = \sum_{s=1}^{p-1} \sum_{j=s}^{i-1} \{ (j-s+1)[f(p-s) - (i-j-1)]/f \} C'(s, j) \cdot C'(p-s, i-j-1) + (fp - (i-1)) \cdot C'(p, i-1) \quad (9)$$

In Appendix A, it is shown that  $C'(p, i)$  can be expressed explicitly in terms of a function  $C(p, \nu)$  by the relation

$$C'(p, i) = C(p, \nu)$$

where

$$C(p, \nu) = \frac{f(fp - p)! \nu^{p-1}}{p!(fp - p + 1 - \nu)! \nu!} \quad (10)$$

The parameter  $\nu$  is equal to  $(i - p + 1)$ , which means the number of propagating ends of an  $M_{p,i}$  molecule.

Then, the molecular size distribution may be written

$$m_{p,\nu} = \frac{f(fp - p)! \nu^{p-1}}{p!(fp - p + 1 - \nu)! \nu!} \alpha^{p-1} \cdot \rho^{\nu+p-1} (1 - \rho)^{fp-p+1-\nu} e^{-\nu\alpha\rho} \quad (11)$$

which is a Poisson-type distribution, and a special case ( $f = 1$ , and therefore  $\nu = 1$ ) of this had been first deduced by Flory,<sup>4</sup> who showed the Poisson distribution

$$(M_{p,p}) = [I]_0(\alpha\rho)^{p-1}/p! \cdot e^{-\alpha\rho} \quad (12)$$

The concentration of  $p$ -mer is given as follows:

$$m_p = \sum_{\nu=0}^{fp-p+1} m_{p,\nu} \quad (13)$$

It is interesting to compare with the size distribution for the branched polycondensation which is given<sup>2</sup> by

$$m_p = \frac{f(fp - p)!}{p!(fp - 2p + 2)!} \rho'^{p-1} (1 - \rho')^{fp-2p+2} \quad (14)$$

where  $\rho'$  is the reacted fraction of the functional groups.

It is in the exponential factor that these two are entirely different from each other. Therefore, this type of distribution may be called a Poisson-type distribution.

### Average Molecular Size

If the weight of the initiator lost during the course of reaction is negligible, the average molecular sizes can readily be obtained, as seen in Appendix B. We may properly exclude the monomer ( $M_{1,0}$ ) from calculation.

The number-average is

$$\langle P_n \rangle = \frac{\sum_{p,i} p m_{p,i} - m_{1,0}}{\sum_{p,i} m_{p,i} - m_{1,0}} = \frac{1 - (1 - \rho)^f}{1 - f\rho - (1 - \rho)^f + (f/\alpha)(1 - e^{-\alpha\rho})} \quad (15)$$

while the weight-average is

$$\langle P_w \rangle = \frac{\sum_{p,i} p^2 m_{p,i} - m_{1,0}}{\sum_{p,i} p m_{p,i} - m_{1,0}} = \frac{1 + \alpha\rho^2 - (1 - \rho)^f - [1 - (f - 1)\alpha\rho^2]}{[1 - (1 - \rho)^f][1 - (f - 1)\alpha\rho^2]} \quad (16)$$

Considering the gel point defined by a critical value  $\rho_c$ , where the latter average approaches infinity, we can characterize  $\rho_c$  by the initial concentrations of the monomer and the initiator  $[M]_0$  and  $[I]_0$ , as follows:

$$\rho_c^2 = \frac{1}{\alpha(f - 1)} = \frac{[I]_0}{f(f - 1)[M]_0} \quad (17)$$

From this equation we know that  $\rho_c$  varies in proportion to  $([I]_0/[M]_0)^{1/2}$ .

From eq. (7) the time required from the start of reaction up to the gel point,  $t_{gel}$ , and the unreacted initiator concentration at this point  $[I_{gel}]$ , can be calculated as

$$t_{gel} = \frac{-1}{k[I]_0} \ln \left( 1 - \left\{ \frac{[I]_0}{f(f - 1)[M]_0} \right\}^{1/2} \right) \quad (18)$$

$$[I_{gel}] = [I]_0 \exp - \left\{ \frac{f[M]_0}{(f - 1)[I]_0} \right\}^{1/2} \quad (19)$$

When it is necessary to include initiators as 1-mer into the calculation of average sizes, the number-average is

$$\langle P_n \rangle' = 1 + \frac{f\rho}{1 - f\rho - (1 - \rho)^f + f/\alpha}$$

while the weight-average is

$$\langle P_w \rangle' = 1 + \frac{(f/\alpha)[(\alpha\rho)^2 + 2\alpha\rho + (f - 1)\alpha\rho^2]}{[1 - (1 - \rho)^f + (f/\alpha)][1 - (f - 1)\alpha\rho^2]}$$

For the special case  $f = 1$  (linear polymer)

$$\langle P_n \rangle'_{f=1} = 1 + \alpha\rho$$

$$\langle P_w \rangle'_{f=1} = (1 + \alpha\rho + \alpha\rho)/(1 + \alpha\rho)$$

which agree with Flory's result.<sup>4</sup>

## APPENDIX A

Equation (9) can be easily reduced to

$$C'(p, i) = \sum_{k=p}^i (k-1)! (fp-k)! \sum_{s=1}^{p-1} \sum_{j=s}^{k-(p-s)} (j-s+1) \\ [f(p-s) - (k-j-1)] C'(s, j) \cdot C'(p-s, k-j-1) / f \cdot i! (fp-i)!$$

After changing notations in this equation by setting

$$\begin{aligned} p-s &= q \\ k-j-1 &= l \\ k-p+1 &= \mu \\ j-s+1 &= m \\ l-q+1 &= n \\ i-p+1 &= \nu \end{aligned}$$

it may be rewritten as follows:

$$C(p, \nu) = \frac{\sum_{\mu=1}^{\nu} (\mu+p-2)! (fp-p+1-\mu)! S(p, \mu)}{f(fp-p+1-\nu)! (\nu+p-1)!} \quad (\text{A-1})$$

where

$$S(p, \mu) = \sum_{q+s=p} \sum_{m+n=\mu} m(fq-q+1-n) C'(s, m) \cdot C'(q, n) \quad (\text{A-2})$$

in which summation is carried out over all sets of  $(s, q)$  and  $(m, n)$  satisfying the conditions

$$\begin{aligned} s+q &= p \\ (s &\geq 1) \\ m+n &= \mu \\ (m &\geq 0) \end{aligned}$$

Now we define the following two functions:

$$\begin{aligned} F_1(\xi, \zeta) &= \sum_{p=1}^{\infty} \sum_{\nu=0}^{fp-p+1} \nu \cdot C(p, \nu) \xi^p \zeta^{\nu} \\ F_2(\xi, \zeta) &= \sum_{p=1}^{\infty} \sum_{\nu=0}^{fp-p+1} (fp-p+1-\nu) C(p, \nu) \xi^p \zeta^{\nu} \end{aligned} \quad (\text{A-3})$$

and recognize that

$$\begin{aligned}
F(\xi, \zeta) &= F_1(\xi, \zeta) \cdot F_2(\xi, \zeta) \\
&= \left[ \sum_{s=1}^{\infty} \sum_{m=0}^{fs-s+1} m C(s, m) \xi^s \zeta^m \right] \\
&\quad \left[ \sum_{q=1}^{\infty} \sum_{n=0}^{fq-q+1} (fq - q + 1 - n) C(q, n) \xi^q \zeta^n \right] \\
&= \sum_{p=2}^{\infty} \sum_{\mu=1}^{fp-p+1} \sum_{\substack{s+q=p \\ m+n=\mu}} m(fq - q + 1 - n) C(q, n) \cdot C(s, m) \xi^p \zeta^\mu
\end{aligned} \tag{A-4}$$

Equation (A-4) shows that  $S(p, \mu)$  is the coefficient of  $\xi^p \zeta^\mu$  in the power series defining  $F(\xi, \zeta)$ . Hence by Cauchy's theorem,

$$S(p, \mu) = \frac{1}{(2\pi i)^2} \oint \oint \frac{F(\xi, \zeta)}{\xi^{p+1} \zeta^{\mu+1}} d\xi d\zeta \tag{A-5}$$

But the right sides of eqs. (A-3) can be summed by the use of the relations obtained from eqs. (1') and (9'). The results are

$$F_1(\xi, \zeta) = f\rho(1 - e^{-\alpha\rho})/(1 - \rho) \tag{A-6}$$

$$F_2(\xi, \zeta) = f\alpha\rho \tag{A-7}$$

with

$$\xi = \alpha\rho(1 - \rho)^{f-1} \tag{A-8}$$

$$\zeta = \rho e^{-\alpha\rho}/(1 + \rho) \tag{A-9}$$

Introducing eqs. (A-6) and (A-9) into the integrand and evaluating those, we have

$$S(p, \mu) = \frac{f^2(fp - p)!}{p!\mu!(fp - p + 1 - \mu)!} [(p + \mu - 1)\mu^{p-1} - \mu(\mu - 1)^{p-1}] \tag{A-10}$$

Substituting eq. (A-10) into eq. (A-1) yields

$$\begin{aligned}
C(p, \nu) &= \frac{f(fp - p)!}{p!(fp - p + 1 - \nu)!(\nu + p - 1)!} \\
&\quad \left\{ \sum_{\mu=1}^p \left( \frac{(\mu + p - 1)! \mu^{p-1}}{\mu!} - \frac{(\mu + p + 2)! (\mu - 1)^{p-1}}{(\mu - 1)!} \right) \right\}
\end{aligned}$$

The only term  $\mu = \nu$  contributes to the sum, and therefore we obtain the expression  $C(p, \nu)$  stated in eq. (10) of the text.

In this calculation  $C(p, \nu)$  is not defined at  $p = 1$ , but by solving eq. (8') directly one can easily see that eq. (12) holds also at  $p = 1$ .

## APPENDIX B

From eq. (11)

$$\sum_{p,i} m_{p,i} = \sum_{p=1}^{\infty} \sum_{\nu=0}^{fp-p+1} \frac{f(fp-p)! \nu^{p-1}}{p! \nu! (fp-p+1-\nu)!} \alpha^{p-1} \cdot \rho^{p+\nu-1} \cdot (1-\rho)^{fp-p+1-\nu} \cdot e^{-\nu\alpha\rho} \quad (\text{B-1})$$

Expanding  $(1-\rho)^{fp-p+1-\nu}$  in such a way as

$$(1-\rho)^{fp-p+1-\nu} = \sum_{\lambda} \binom{fp-p+1-\nu}{\lambda} (-\rho)^{\lambda}$$

and putting  $\lambda + \nu = q$ , we can rewrite eq. (B-1) as follows:

$$\sum_{p,i} m_{p,i} = \sum_{q=0}^{\infty} \frac{(-\rho)^q}{q!} \sum_{\nu=0}^q \binom{q}{\nu} (-1)^{\nu} e^{-\nu\alpha\rho} \sum_{p=1}^{\infty} \frac{f(f-1)(fp-p-1)! (\nu\alpha\rho)^{p-1}}{(p-1)! (fp-p-1-q)!} \quad (\text{B-2})$$

Now consider a generating function (for  $q \geq 2$ )

$$\kappa_0(x; q) = [1 - \exp\{-\alpha\rho(1-x^{f-1})\}]^q \cdot x^{f-2} \quad (\text{B-3})$$

Repeated differentiations give

$$\left[ \left( \frac{d}{dx} \right)^{q-2} \kappa_0(x; q) \right]_{x=1} = \sum_{\nu=0}^q \binom{q}{\nu} (-1)^{\nu} e^{-\nu\alpha\rho} \sum_{p=1}^{\infty} \frac{(fp-p-1)! (\nu\alpha\rho)^{p-1}}{(p-1)! (fp-p+1-q)!} \quad (\text{B-4})$$

which is just the same as one of the summations to be evaluated in eq. (B-2). Since this  $(q-2)$ th derivative contains the factor  $(1 - \exp\{-\alpha\rho(1-x^{f-1})\})$ , the left side of eq. (B-4) is zero, and the sum of eq. (B-2) reduces to the terms of  $q=0$  and  $q=1$ . Evaluating these, we obtain

$$\sum_{p,i} m_{p,i} = 1 - f\rho + (f/\alpha)(1 - e^{-\alpha\rho})$$

which is wholly consistent with the constraint requirement, eq. (7c). Then

$$\sum_{p,i} pm_{p,i} = \sum_{p=1}^{\infty} \sum_{\nu=0}^{fp-p+1} \frac{f(fp-p)! (\nu\alpha\rho)^{p-1}}{(p-1)! (fp-p+1-\nu)!} \rho^{\nu} (1-\rho)^{fp-p+1-\nu} \cdot e^{-\nu\alpha\rho} \quad (\text{B-5})$$

Changing the function, eq. (B-3), slightly into the form

$$\kappa_1(x; q) = [1 - \exp\{-\alpha\rho(1 - x^{f-1})\}]^q \cdot x^{f-1} \quad (\text{B-6})$$

and similarly using the result of repeated differentiations we obtain finally

$$\sum_{p,i} pm_{p,i} = 1$$

which agrees precisely with the conservation condition, eq. (1'). For the calculation of weight-average molecular size, one has to obtain the sum

$$\begin{aligned} \sum_{p,i} p^2 m_{p,i} &= \\ \sum_{p=1}^{\infty} \sum_{\nu=0}^{fp-p+1} \frac{fp(fp-p)! (\nu\alpha\rho)^{p-1}}{(p-1)!(fp-p+1-\nu)!} \rho^{\nu} (1-\rho)^{fp-p+1-\nu} \cdot e^{-\nu\alpha\rho} \end{aligned} \quad (\text{B-7})$$

By using an identical equation

$$p(fp-p)! = \frac{(fp-p+1)! - (fp-p)!}{f-1}$$

and expanding the power of  $(1-\rho)$ , this equation is rewritten as follows:

$$\begin{aligned} \sum_{p,i} p^2 m_{p,i} &= \\ \frac{f}{f-1} \sum_{q=0}^{\infty} \frac{(-\rho)^q}{q!} \sum_{\nu=0}^q \binom{q}{\nu} (-1)^{\nu} e^{-\nu\alpha\rho} \sum_{p=1}^{\infty} \frac{(fp-p+1)! (\nu\alpha\rho)^{p-1}}{(p-1)!(fp-p+1-q)!} - \\ &\quad \frac{1}{f-1} \end{aligned} \quad (\text{B-8})$$

Now we define

$$\kappa_2(x; q) = [1 - \exp\{-\alpha\rho(1 - x^{f-1})\}]^q \cdot x^f \quad (\text{B-9})$$

Expanding multinominally and differentiating eq. (B-9)  $q$  times with respect to  $x$ , we obtain

$$\begin{aligned} \left[ \left( \frac{d}{dx} \right)^q \kappa_2(x; q) \right]_{x=1} &= \\ \sum_{\nu=0}^q \binom{q}{\nu} (-1)^{\nu} e^{-\nu\alpha\rho} \sum_{p=1}^{\infty} \frac{(fp-p+1)! (\nu\alpha\rho)^{p-1}}{(p-1)!(fp-p+1-q)!} \end{aligned}$$

which is evidently equal to the furthest right sum in eq. (B-8). A direct evaluation of this quantity from eq. (B-9) gives

$$= q! (-1)^q [\alpha\rho(f-1)]^q$$

Substituting this into eq. (B-8) we obtain

$$\sum_{p,i} p^2 m_{p,i} = \frac{1 + \alpha\rho^2}{1 - (f-1)\alpha\rho^2}$$

## References

1. Kakurai, T., and T. Noguchi, *Kogyo Kagaku Zasshi*, **64**, 398 (1961); *ibid.*, **65**, 827 (1962); *Kobunshi Kagaku*, **20**, 17 (1963); *ibid.*, **20**, 22 (1963); *ibid.*, **19**, 547 (1962); T. Kakurai, H. Asanuma, and T. Noguchi, *ibid.*, **20**, 27 (1963).
2. Tanaka, Y., and H. Kakiuchi, *J. Appl. Polymer Sci.*, **7**, 1063 (1963); G. Maerker, H. A. Monroe, and W. S. Port, *ibid.*, **7**, 301 (1963).
3. Flory, P. J., *Principles of Polymer Chemistry*, Cornell Univ. Press, Ithaca, N. Y., 1953, Chap. 9.
4. Flory, P. J., *J. Am. Chem. Soc.*, **62**, 1561 (1940).
5. Flory, P. J., *J. Am. Chem. Soc.*, **63**, 3083 (1941); *Chem. Revs.*, **39**, 137 (1946).
6. Stockmayer, W. H., *J. Chem. Phys.*, **11**, 45 (1943).
7. Stockmayer, W. H., and L. L. Weil, *Advancing Fronts in Chemistry*, Reinhold, New York, 1945, Chap. 6.

## Résumé

Une étude statistique a été effectuée sur la polymérisation par ouverture de cycle des polyépoxydes, en supposant que les vitesses d'initiation et de propagation sont égales. La distribution du type Poisson et la formule du point de gélification sont caractérisées par les équations suivantes:

$$M_{p,\nu} = [f(fp - p)! \nu^{p-1} / \{p!(fp - p + 1 - \nu)!\}] \alpha^{p-1} \cdot \rho^{\nu+p-1} (1 - \rho)^{p-p+1-\nu} \exp \{-\nu \alpha \rho\}$$

$$\rho_c = [I]_0^{1/2} / \{f(f-1)[M]_0\}^{1/2}$$

dans lesquelles  $p$  est le nombre des unités monomériques,  $\nu$  le nombre des fins des chaînes qui peuvent propager dans un polymère,  $\alpha$  est  $f[M]_0/[I]_0$ ,  $\rho$  et  $\rho_c$  sont la fraction des groupes fonctionnels qui ont réagi et sa valeur critique,  $f$  est le nombre des groupes fonctionnels d'un monomère, et  $[I]_0$  et  $[M]_0$  sont les concentrations initiales de l'initiateur et du monomère respectivement.

## Zusammenfassung

Die unter Ringöffnung verlaufende Polymerisation von Polyepoxyden wurde unter der Annahme gleicher Start- und Wachstumsgeschwindigkeit statistisch untersucht. Die Poisson-Verteilung und die Gelpunktsformel werden durch folgende Gleichungen wiedergegeben:

$$M_{p,\nu} = [f(fp - p)! \nu^{p-1} / \{p!(fp - p + 1 - \nu)!\}] \alpha^{p-1} \cdot \rho^{\nu+p-1} (1 - \rho)^{p-p+1-\nu} \exp \{-\nu \alpha \rho\}$$

$$\rho_c = [I]_0^{1/2} / \{f(f-1)[M]_0\}^{1/2}$$

Dabei ist  $p$  die Anzahl der Monomerseinheiten und  $\nu$  die Anzahl der wachsenden Enden im Polymeren.  $\alpha$  ist  $f[M]_0/[I]_0$ ,  $\rho$  und  $\rho_c$  sind der Bruchteil der umgesetzten funktionellen Gruppen und dessen kritischer Wert,  $f$  ist die Anzahl der funktionellen Gruppen an einem Monomeren und  $[I]_0$  und  $[M]_0$  sind die Anfangskonzentrationen von Starter bzw. Monomeren.

Received October 18, 1963

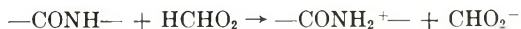
## Dilute Solution Properties of Polyamides in Formic Acid. Part I. Repression of Polyelectrolyte Effects by Means of Excess Counterions

P. R. SAUNDERS, *Chemstrand Research Center, Inc., Durham, North Carolina*

### Synopsis

The polyelectrolyte effects of nylon 66 have been studied as a function of the composition of the solvent system formic acid–water–sodium formate by means of viscometry and light scattering. The intrinsic viscosity and light-scattering second virial coefficient of nylon 66 in 90% formic acid decrease rapidly with addition of sodium formate. The apparent weight-average molecular weight increases initially and then becomes constant at salt concentrations greater than 0.025 mole/l. The changes in intrinsic viscosity and second virial coefficient are relatively small for changes in salt concentration above 0.2 mole/l. In the presence of 0.5 mole/l. of sodium formate, the polyelectrolyte effects are completely repressed and the polymer solvent interaction can be varied independently by adjustment of the quantity of water in the solvent. In these circumstances, there is a linear relation between intrinsic viscosity and second virial coefficient. Extrapolation yields a value of the intrinsic viscosity in an ideal solvent and an estimate of the unperturbed dimensions of nylon 66,  $(\bar{r}_0^2/M)^{1/2} = 9 \times 10^{-9}$  cm. mole<sup>1/2</sup> · g.<sup>-1/2</sup>. These results lead to a value for Flory's universal constant for randomly coiled chain molecules,  $\Phi = 2.5 \times 10^{21}$ .

It has been known for some time that polyamides dissolved in formic acid are ionized.<sup>1,2</sup> Evidence for this comes from viscosity measurements, where values of the reduced specific viscosity increase with decreasing polymer concentration in a manner typical of polyelectrolytes. The charge on the polyamides is believed to result from the protonation of the polymer amide groups.



The presence of electric charge on the polymer molecules complicates the interpretation of viscosity and light-scattering data owing to electrostatic interference and, in the absence of appropriate theory, the determination of molecular weights and dimensions in solution is impossible.

The electrostatic interaction can be diminished by decreasing the degree of ionization of the polymer or by increasing the ionic strength of the solvent.<sup>2</sup> Both of these requirements are satisfied when the solvent contains a simple electrolyte with a common counterion.<sup>3,4</sup>

In this paper, the viscosity and light scattering of polyamides have been

studied as a function of the composition of the solvent system formic acid-water-sodium formate.

## EXPERIMENTAL

Polymer 1 was a sample of nylon 66 prepared in the laboratory without acetic acid termination. Endgroup analyses gave  $58.2 \times 10^{-6}$  equiv.  $\text{NH}_2/\text{g.}$  and  $59.5 \times 10^{-6}$  equiv.  $\text{COOH}/\text{g.}$  These values correspond to a number-average molecular weight of 17,000.

Polymers 2 and 3 were commercial samples of nylon 66 and nylon 6, respectively.

Viscosities were measured at  $25.0^\circ\text{C.}$  in Cannon-Fenske viscometers. Flow times were approximately 200 sec., and kinetic energy corrections were not applied.

Light-scattering measurements were performed at  $25^\circ\text{C.}$  in a Brice-Phoenix photometer, incident unpolarized monochromatic light of wavelength 4358 Å. being used. The photometer was modified in order to permit use of the scattering cell assembly described by Dandliker and Kraut.<sup>5</sup> Solutions and solvent were freed from suspended matter by passage through a fine grade sintered glass filter, followed by ultracentrifugation at 50,000*g* for 90 min. The apparent dissymmetry  $I_{45}/I_{135}$  of the solvent was 1.07. Measurements made in a cylindrical scattering cell gave dissymmetries ranging from 1.01 to 1.03. However, the reduced intensities at  $90^\circ$  in both cell systems were identical. For the polymers studied here,  $M_w < 100,000$ , the dissymmetry would not be expected to be appreciably different from unity. All measurements reported here were made with the Dandliker and Kraut system. Only the  $90^\circ$  intensities have been used. The photometer was calibrated with the Cornell standard polystyrene as reference, the excess turbidity of a solution 0.5g./100 cc. toluene being taken to be  $3.51 \times 10^{-3} \text{ cm.}^{-1}$

Refractive index differences  $\Delta n$  between solutions and solvents were measured at  $25^\circ\text{C.}$  in a Brice-Phoenix differential refractometer which had been calibrated by means of sucrose solutions. Values of  $\Delta n$  were measured at four polymer concentrations; 0.5, 1.0, 1.5, and 2.0 g./100 ml.; the slope of the line through the origin was taken as the value of  $dn/dc$ .

## RESULTS AND DISCUSSION

### Intrinsic Viscosity

In Figure 1, the intrinsic viscosity of polymer 1 dissolved in 90% formic acid is shown as a function of the molarity of sodium formate present in solution. The increasing concentration of counterions, leading to a decreasing degree of ionization of the polymer and an increasing ionic strength of the solvent, results in a marked decrease in intrinsic viscosity. Beyond 0.2*M*  $\text{NaCHO}_2$ , the decrease in intrinsic viscosity is slight, and it seems probable that very little charge is left on the polymer molecules.

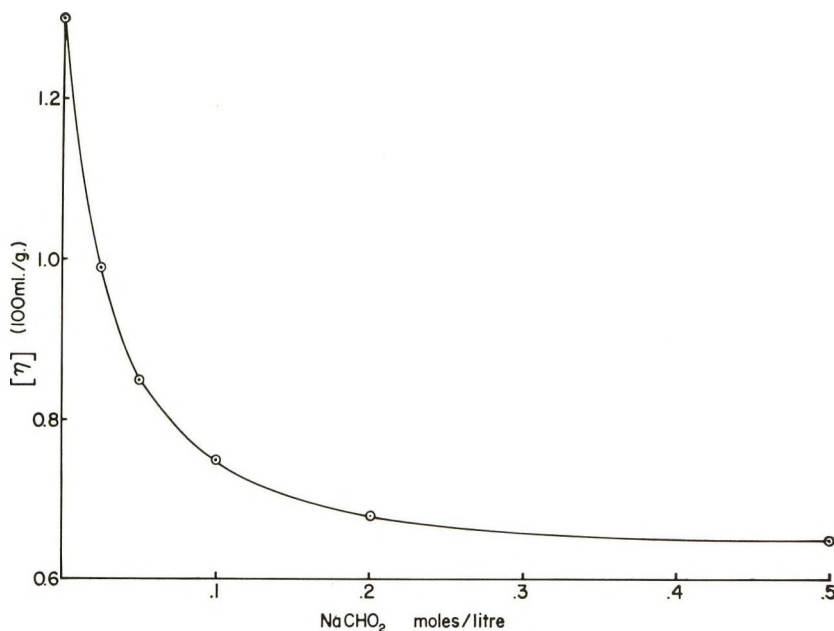


Fig. 1. Intrinsic viscosity of polymer 1 in 90% formic acid containing various additions of sodium formate.

This conclusion is confirmed by the light-scattering data. This small linear change in  $[\eta]$  with increasing salt illustrates the increasing poorness of the solvent, in complete analogy to the addition of nonsolvent to solutions of nonionic polymers.

From light-scattering evidence,<sup>4</sup> the polyelectrolyte effect can be reduced by increasing the concentration of water in the formic acid. This results from the increased ionization of the formic acid, with a consequent decrease in the degree of ionization of the polymer. In Figure 2, the intrinsic viscosity of polymer 1 is shown as a function of the amount of water present in the formic acid. The decrease in intrinsic viscosity with increasing concentration of water is due not only to the decrease in the degree of ionization of the polymer but also to changes in the polymer solvent interaction. This is illustrated by the fact that the polymer was insoluble in solvents containing more than 30% water. It is clear that water alone cannot be used to repress completely polyelectrolyte behavior, since the values of intrinsic viscosity obtained near the insoluble region are higher than those found in the presence of sodium formate.

### Differential Refractive Index

Values of the differential refractive index  $dn/dc$  for polymer 1 dissolved in 90% formic acid containing various quantities of sodium formate are shown in Table I. In Table II,  $dn/dc$  for polymer 1 is shown as a function of the concentration of water in the solvent, both without salt, and in the presence of 0.5M  $\text{NaCHO}_2$ .

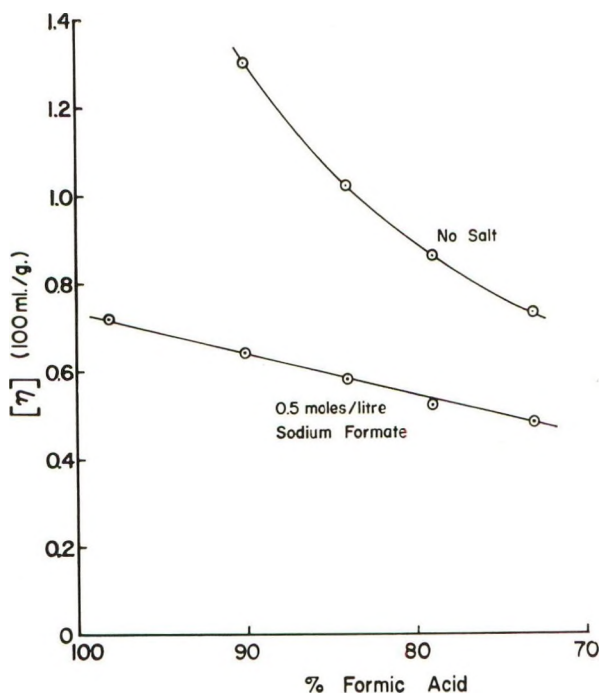


Fig. 2. Intrinsic viscosity of polymer 1 as a function of the formic acid strength.

TABLE I  
Differential Refractive Index of Polymer 1 in 90% Formic Acid  
Containing Varying Quantities of Sodium Formate

NaCHO <sub>2</sub> concn., mole/l.	$dn/dc$ , ml./g.
0	0.145
0.025	0.147
0.05	0.146
0.1	0.142
0.2	0.142
0.5	0.136
0.75	0.130
1.0	0.124

Analysis of these results shows that in circumstances where the degree of ionization of the polymer is changing, the variation of  $dn/dc$  is very different from what one would expect on the basis of variation of the refractive index of the solvent. This phenomenon is associated with the changing polarizabilities of the polymeric amide groups and their counterions.

### Light Scattering

The light scattering of polymer 1 in 90% formic acid with various additions of sodium formate is shown in Figure 3. The lines have a common

TABLE II  
Differential Refractive Index of Polymer 1 as a Function  
of the Concentration of Water Present

Water, %	$dn/dc$ , ml./g.	
	No salt present	0.5M NaCHO <sub>2</sub>
0	0.157	0.136
5	0.150	0.136
10	0.145	0.136
20	0.145	0.136
25	0.144	0.138

intercept, giving a weight-average molecular weight,  $M_w$ , of 32,000. The slope of the lines decreases with increasing concentration of sodium formate. This is in line with the decrease in intrinsic viscosity in similar solvent circumstances (Fig. 1). For sodium formate additions in excess of 0.5 mole/l., the scattering curves change very little with increasing salt concentration. This result backed up by the intrinsic viscosity results, means that the degree of ionization of the polymer in these conditions is close to zero.

The data of Figure 3 can be represented by the equation:

$$Hc/\tau = (1/M_w) (1 + M_w A_2' c)^2 \quad (1)$$

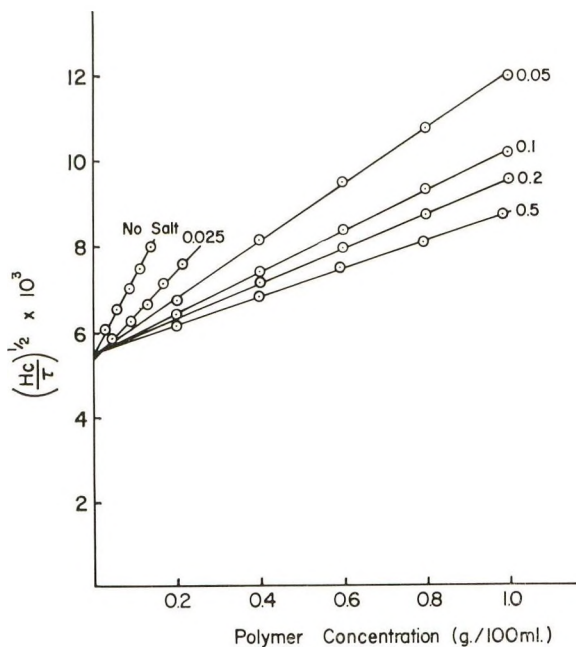


Fig. 3. Light scattering of polymer 1 in 90% formic acid containing various additions of sodium formate.

The apparent second virial coefficient  $A_2'$  is equal to the product of the slope and the intercept of the linear plots in Figure 3.

Values of  $A_2'$  calculated in this way are plotted against molarity of sodium formate in Figure 4. The resemblance to the viscosity data of Figure 1 is obvious. Figures 1 and 4 both show the change in molecular dimensions, at constant molecular weight, as a function of the electrolyte concentration. Interpretation of these results, on the basis of theories such as that of Hermans and Overbeek,<sup>6</sup> is complicated by the fact that the variation of the concentration of sodium formate varies the degree of ionization of the polymer as well as the ionic strength.

### Nonionic Polymer-Solvent Interaction

If we wish to study the nonionic polymer-solvent interaction, we must ensure that the electrostatic interaction is reduced to a minimum. Figures 1 and 4 both show that the ionic forces in solutions containing at least 0.5*M* NaCHO<sub>2</sub> are suppressed to the extent that their variation with further added NaCHO<sub>2</sub> is negligible. Consequently we may study the polymer solvent interaction as a function of the concentration of the precipitant component (water) in the solvent, keeping the concentration of sodium formate constant at 0.5 mole/l. The concentration of water is changed from zero up to the point where the polymer is insoluble, and the light-scattering and viscosity results are shown in Figures 2 and 5. As one might expect, the intrinsic viscosity decreases progressively as the concentration of precipi-

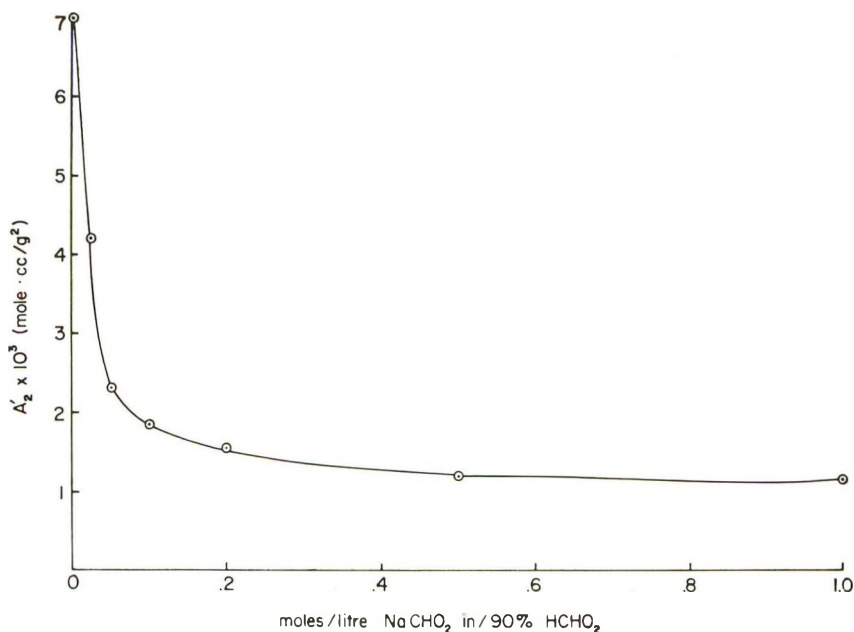


Fig. 4. Second virial coefficient of polymer 1 in 90% formic acid as a function of the addition of sodium formate.

tant increases. The light-scattering data extrapolate through a common point to give a value of  $M_w = 32,000$ , which is identical with the result obtained from the data of Figure 3. The constancy of  $M_w$ , independent of changes in the relative proportions of the individual components of the solvent system, indicates that the tendency of any one component of the solvent system to be preferentially absorbed on the polymer molecules is negligible. The square root plots fit the data very well, except at the very highest precipitant concentration. In the latter case, the unusually high scattering at the highest polymer concentrations, coupled with the very high dissymmetry of scattering,  $I_{45}/I_{135} > 2$ , suggests the formation of polymer aggregates in these solutions. Indeed, on standing for several days, the polymer precipitated from solution. The data of Figure 5 are interpreted by means of eq. (2):

$$(Hc/\tau)^{1/2} = (1/M_w)^{1/2} (1 + M_w A_2 c) \quad (2)$$

where the osmotic second virial coefficient  $A_2$  is identical with the quantity used for nonionic polymers and is independent of ionic interaction.

In the absence of electrostatic interaction  $[\eta]$  and  $A_2$  are both an index of the polymer-solvent interaction, since both of these quantities are sensitive to changes in the molecular dimensions in solution. As the polymer conformation is varied, e.g., by varying the solvent-nonsolvent ratio, we would expect a unique relationship between  $[\eta]$  and  $A_2$ . Several different models<sup>7,8</sup> have been used to deduce a relationship of this kind. Krigbaum<sup>7</sup> has suggested a relation, which can be used directly for unfractionated polymers:

$$[\eta] = [\eta]_0 + 3(136/105)(3/2 \pi)^{3/2} (\Phi/N) A_2 M_w + \dots \quad (3)$$

where  $[\eta]_0$  is the intrinsic viscosity in a theta solvent,  $\Phi$  is a universal constant with a mean experimental value of  $2.2 \times 10^{21}$  when the units of  $[\eta]$  are decilitres/g., and  $N$  is Avogadro's number.

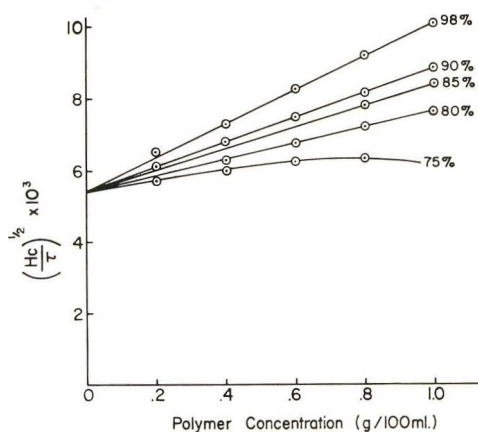


Fig. 5. Light scattering of polymer 1 in various concentrations of formic acid, all containing 0.5 mole/l. of sodium formate.

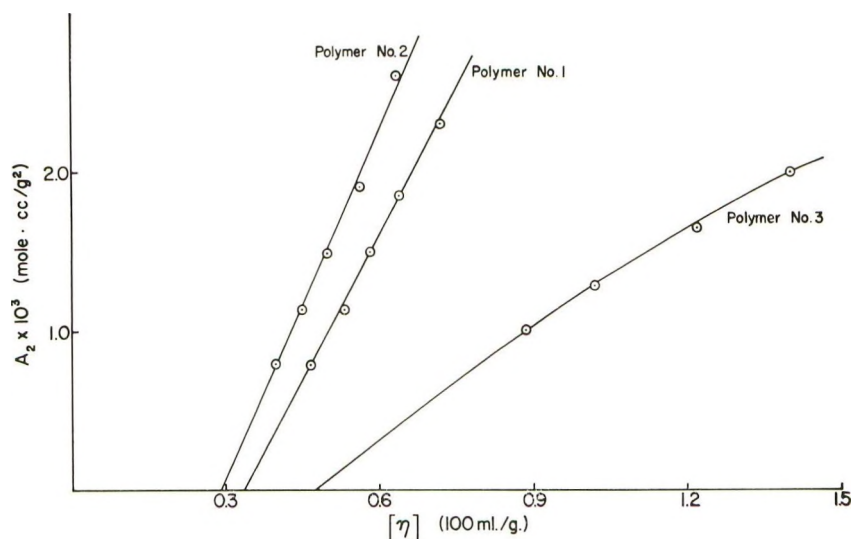


Fig. 6. Relations between second virial coefficient and intrinsic viscosity for polymers 1, 2, and 3 in the absence of polyelectrolyte effects.

Experimental values of  $A_2$  for polymers 1, 2, and 3, derived from data such as those in Figure 5, are plotted in Figure 6, against values of intrinsic viscosity measured in the corresponding solvents. A linear relation fits the data for polymers 1 and 2, while for the higher molecular weight polymer 3 the data fall on a curve. Equations (4)–(6) fit the data.

Polymer 1 ( $M_w = 32,000$ ):

$$[\eta] = 0.33 + 1.705 \times 10^2 A_2 \quad (4)$$

Polymer 2 ( $M_w = 26,000$ ):

$$[\eta] = 0.29 + 1.44 \times 10^2 A_2 \quad (5)$$

Polymer 3 ( $M_w = 68,000$ ):

$$[\eta] = 0.47 + 3.5 \times 10^2 A_2 + 6.5 \times 10^4 A_2^2 \quad (6)$$

From the intercept on the  $[\eta]$  axis, we obtain the intrinsic viscosity in a theta solvent,  $[\eta]_0$ , for each polymer. This quantity cannot be measured directly owing to the insolubility of the polymer in the hypothetical solvent.

From a direct comparison of these experimental relations and Krigbaum's equation, we can calculate values of  $\Phi$ . This is very useful, because the low molecular weights of these polymers precludes the possibility of estimating  $\Phi$  from light-scattering dissymmetry measurements. For all three polymers,  $\Phi = 2.5 \times 10^{21}$ , which is close to the accepted mean value of  $2.2 \times 10^{21}$ .

Approximate values for the constants  $K$  and  $(\overline{r_0^2}/M)^{1/2}$  which are characteristic of the polymer can be calculated from the eqs. (7) and (8):

$$[\eta]_0 = KM^{1/2} \quad (7)$$

$$K = \Phi(\bar{r}_0^2/M)^{3/2} \quad (8)$$

The values for the three polymer samples are given in Table III.

TABLE III

Sample	$K \times 10^4$	$(\bar{r}_0^2/M)^{1/2} \times 10^{11}$
Polymer 1	19	950
Polymer 2	18	940
Polymer 3	18	940

The molecular parameters for these unfractionated polymers are remarkably close to the values,  $K = 19.2 \times 10^{-4}$  and  $(\bar{r}_0^2/M)^{1/2} = 960 \times 10^{-11}$  calculated from viscosity and molecular weight measurements of nylon 66 fractions in a theta solvent.<sup>9</sup>

The values for nylon 6 are, within experimental error, identical with those for nylon 66. Therefore, the different molecular structures of these polymers has no effect on the conformation of the molecules in solution.

### References

1. Schaefgen, J. R., and C. F. Trivisonno, *J. Am. Chem. Soc.*, **74**, 2715 (1952).
2. Saunders, P. R., *J. Polymer Sci.*, **57**, 131 (1962).
3. Fendler, H. G., and H. A. Stuart, *Makromol. Chem.*, **25**, 159 (1957).
4. Saunders, P. R., *J. Polymer Sci.*, **43**, 273 (1960).
5. Dandliker, W. B., and J. Kraut, *J. Am. Chem. Soc.*, **78**, 2380 (1956).
6. Hermans, J. J., and J. T. G. Overbeek, *Rec. Trav. Chim.*, **67**, 761 (1948).
7. Krigbaum, W. R., *J. Polymer Sci.*, **18**, 315 (1955).
8. Orofino, T. A., and P. J. Flory, *J. Chem. Phys.*, **26**, 1067 (1957).
9. Saunders, P. R., *J. Polymer Sci.*, **A2**, 3765 (1964).

### Résumé

Les effets polyélectrolytiques du nylon 66 ont été étudiés en fonction de la composition du système de solvant acide formique-eau-formiate de sodium par viscosimétrie et diffusion de la lumière. La viscosité intrinsèque et le second coefficient viriel de la diffusion de la lumière du nylon 66 dans 90% d'acide formique, diminue rapidement avec l'addition de formiate de sodium. Le poids moléculaire moyen en poids apparent augmente au début et puis devient constant à des concentrations en sel plus grandes que 0,025 moles/litre. Les changements dans la viscosité intrinsèque et le second coefficient viriel sont relativement petits pour des changements dans la concentration en sel supérieurs à 0,2 moles/litre. En présence de 0,5 moles/litre de formiate de sodium les effets polyélectrolytiques sont complètement réprimés et l'interaction polymère-solvant peut être changée indépendamment en ajustant la quantité d'eau dans le solvant. Dans ces conditions, il existe une relation linéaire entre la viscosité intrinsèque et le second coefficient viriel. Par extrapolation on obtient la valeur de la viscosité intrinsèque dans un solvant idéal et une estimation des dimensions non-perturbées du nylon 66,  $(\bar{r}_0^2/M)^{1/2} = 9 \times 10^{-9}$  cm. mole<sup>1/2</sup>.g<sup>-1/2</sup>. Ces résultats conduisent à une valeur de la constante universelle de Flory pour les chaînes moléculaires enroulées statistiquement  $\Phi = 2,5 \times 10^{21}$ .

### Zusammenfassung

Die Polyelektrolyteffekte von Nylon 66 wurden als Funktion der Zusammensetzung des Lösungsmittelsystems Ameisensäure-Wasser-Natriumformiat mittels Viscosimetrie und Lichtstreuung untersucht. Die Viscositätszahl und der zweite Virialkoeffizient der Lichtstreuung von Nylon 66 in 90% Ameisensäure nimmt bei Zugabe von Natriumformiat schnell ab. Das scheinbare Gewichtsmittel des Molekulargewichts steigt am Anfang an und wird dann bei Salzkonzentrationen grösser als 0,025 Mol/Liter konstant. Die Änderung der Viscositätszahl und des zweiten Virialkoeffizienten sind für Änderungen der Salzkonzentration über 0,2 Mol/Liter relativ klein. Bei Anwesenheit von 0,5 Mol/Liter Natriumformiat sind die Polyelektrolyteffekte völlig zurückgedrängt, und die Wechselwirkung Polymer-Lösungsmittel kann unabhängig durch die Wassermenge im Lösungsmittel variiert werden. Unter diesen Umständen besteht eine lineare Beziehung zwischen Viscositätszahl und zweitem Virialkoeffizienten. Extrapolation ergibt einen Wert der Viscositätszahl in einem idealen Lösungsmittel und einen Wert für die ungestörten Dimensionen von Nylon 66 ( $\bar{r}_0^2/M$ ) =  $9 \times 10^{-9}$  cm. Mol<sup>1/2</sup>·g<sup>-1/2</sup>. Diese Ergebnisse führen zu einem Wert der universellen Konstanten von Flory für statistisch geknäuelte Kettenmoleküle  $\Phi = 2,5 \times 10^{21}$ .

Received September 13, 1963

Revised October 21, 1963

## The Unperturbed Dimensions of Nylon 66

P. R. SAUNDERS, *Chemstrand Research Center, Inc.,  
Durham, North Carolina*

### Synopsis

Light-scattering and viscosity measurements have been performed on nylon 66 fractions dissolved in an ideal solvent. The relation between intrinsic viscosity and weight-average molecular weight in this solvent is  $[\eta] = 19.2 \times 10^{-4} \bar{M}_w^{1/2}$ , which indicates that nylon 66 obeys random coil statistics in solution. The unperturbed coil dimensions are given by the parameter  $(r_0^2/M)^{1/2} = 96 \times 10^{-10}$  cm. mole<sup>1/2</sup> g.<sup>-1/2</sup>.

In order to calculate the unperturbed dimensions of a polymer molecule in solution, it is necessary to select a solvent having no net interaction with the polymer and in which polyelectrolyte effects are negligible. Polyamides dissolved in formic acid exhibit typical polyelectrolyte behavior.<sup>1,2</sup> These properties can be suppressed either by adding excess counterions to the solution, which decreases the degree of ionization of the polymer, or by adding simple electrolyte, which increases the ionic strength and screens the polymeric charges.<sup>3,4</sup> The removal of charge from the polymer by the addition of excess sodium formate would appear to be the safer method of eliminating polyelectrolytic affects. Unfortunately, it is not possible to find a composition of the solvent system formic acid-water-sodium formate in which the polymer-solvent interaction is zero. Decreasing the solvent power by addition of water and/or sodium formate always leads to precipitation before ideality can be attained. We are therefore obliged to use the solvent system formic acid-water-potassium chloride, which relies on high ionic strength to suppress polyelectrolyte effects. It was shown previously<sup>4</sup> that a whole range of ideal solvents is available for nylon 66, their composition being defined by the equation

$$S = 12.1m + 62.2 \quad (1)$$

where  $S$  is the formic acid strength (in weight per cent), and  $m$  is the molarity of potassium chloride. The solvent used throughout this paper was composed of 90% formic acid containing 2.3 moles/l. of potassium chloride.

The fact that the light-scattering function,  $Hc/\tau$  is independent of polymer concentration is not in itself enough to justify the assumption that the molecular dimensions are unperturbed by charge effects. However, this assumption is supported by the data in Figure 5 of a previous paper.<sup>4</sup> The intrinsic viscosity and second virial coefficient for a sample of nylon 66 in

various compositions of the solvent system formic acid–water–sodium formate are in linear relation. Extrapolation to  $A_2 = 0$  gives a value for the intrinsic viscosity in an ideal solvent where the degree of ionization of the polymer is zero. This value was identical to that measured in the solvent system formic acid–water–potassium chloride. This point could be checked more thoroughly by measuring intrinsic viscosities in different solvents defined by eq. (1) in which the degree of ionization of the polymer varies from solvent to solvent.

## EXPERIMENTAL

### Materials

The sample of nylon 66 used in this study was prepared in the laboratory without acetic acid termination. Endgroup analyses gave  $58.2 \times 10^{-6}$  equiv.  $\text{NH}_2/\text{g.}$  and  $59.5 \times 10^{-6}$  equiv.  $\text{COOH/g.}$  These values correspond to a number-average molecular weight of 17,000. The weight-average molecular weight of this sample, determined via light scattering, was 32,000.

The *m*-cresol as supplied contained colored impurities which were removed by distillation.

### Measurements

Viscosities were measured at 25°C. in Cannon-Uenske viscometers. Flow times were always greater than 100 sec., and kinetic energy corrections were not applied.

Light-scattering measurements were performed at 25°C. in a Brice-Phoenix photometer, incident unpolarized monochromatic light of wavelength 4358 Å. being used. The details of solution preparation and measurement have been described previously.<sup>3</sup>

### Fractionation Procedure

A 50-g. portion of polymer was dissolved in 2 l. of *m*-cresol, saturated with nitrogen, and placed in a 20 l. separatory funnel. The separatory funnel was enclosed in a water bath and thermostatted at 25°C. To produce a stable turbidity required 7.5 l. of cyclohexane saturated with nitrogen, and after being stirred for 10 min., the coacervate was allowed to separate overnight. An atmosphere of nitrogen was maintained over the solution at all times. This was necessary in order to avoid the formation of insoluble resins, which occurred when exposed to atmospheric oxygen. The coacervate was then drawn off and further cyclohexane was added. In this way five fractions were obtained, the last coming with a large excess of cyclohexane. The supernatant contained about 10% of the polymer which would have been tedious to reclaim and was consequently rejected. Each of the five coacervated fractions was placed in a 5 l. separatory funnel and refractionated into four to five fractions each.

The coacervates were dripped into beakers of acetone and the polymer precipitated. It should be noted that the form of the precipitate was excellent for further processing and recovery. Droplets precipitated individually and gave the appearance of a "snow storm." The acetone was decanted off and replaced with hot methanol in order to wash out the *m*-cresol. After a further washing with methanol, the fractions were dried in a vacuum desiccator over  $P_2O_5$ . The designation of the fractions is illustrated by the following example. Fraction 2-4 is the fourth fraction from the refractionation of the second fraction from the initial fractionation.

## RESULTS

Two separate fractionations were performed. The fractions produced in the first run had a slightly off white appearance, and it was feared that the polymer might contain some oxidation products. In the second fractionation, additional care was exercised to exclude atmosphere oxygen from all stages of the preparation. The second set of fractions was colorless.

Viscosity and light-scattering measurements were performed on the fractions dissolved in the solvent 90% formic acid containing 2.3 moles/l. of potassium chloride. A representative selection of the light-scattering results is shown in Figure 1. The ideality of the solvent is shown by the independence of the light-scattering function,  $Hc/\tau$ , on the polymer concentration. The measured values of the intrinsic viscosity,  $[\eta]$  and the weight-average molecular weight of the fractions are listed in Table I.

TABLE I  
Properties of Nylon Fractions in an Ideal Solvent

1st Fractionation			2nd Fractionation		
Fraction	$\bar{M}_w$	$[\eta]$	Fraction	$\bar{M}_w$	$[\eta]$
1-2	83,000	0.56	1-1	69,000	0.47
1-3	65,000	0.50	1-2	49,000	0.46
1-4	45,000	0.41	1-3	38,000	0.38
1-5	30,000	0.31	2-1	56,000	0.45
2-1	69,000	0.50	2-2	48,000	0.45
2-3	56,000	0.46	2-3	43,000	0.40
3-1	47,000	0.41	3-1	40,000	0.39
3-2	41,000	0.38	3-3	38,000	0.38
3-3	32,000	0.32	3-4	26,000	0.33
			4-1	28,000	0.34
			4-2	25,000	0.31
			4-3	20,000	0.26

For random coil molecules in an ideal solvent, the following relations hold:

$$[\eta] = KM_w^{1/2} \quad (2)$$

and

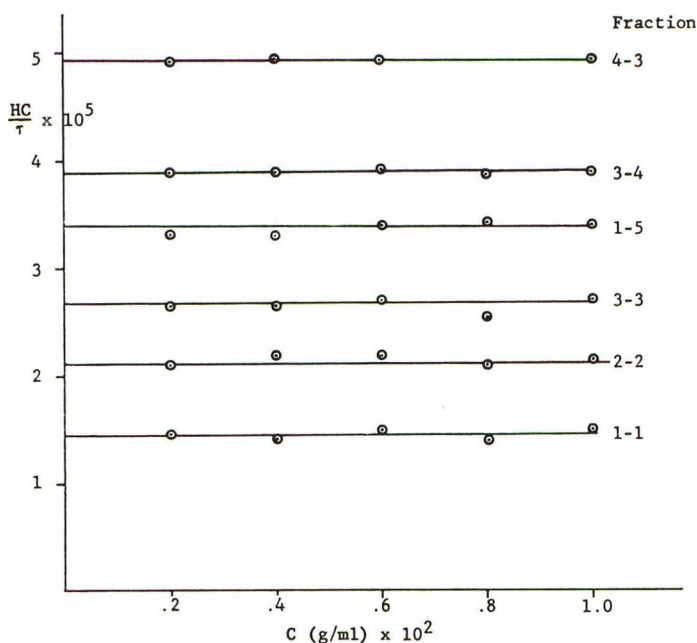


Fig. 1. Light scattering of nylon 66 fractions in an ideal solvent.

$$K = \Phi (\overline{r_0^2}/M)^{3/2} \quad (3)$$

where  $\Phi$  is a universal constant for random coil chains, having an accepted mean experimental value of  $2.2 \times 10^{21}$  and  $\overline{r_0^2}$  is the mean square value of the unperturbed end-to-end distance.

In Figure 2,  $\log [\eta]$  is plotted against  $\log \bar{M}_w$  for the fractions. The points are randomly scattered around a line of slope 0.5. This means that nylon 66 in this solvent obeys random coil statistics. The value of  $K$ , calculated from the data in Figure 2, is  $19.2 \times 10^{-4}$ . This leads to a value of  $(\overline{r_0^2}/M)^{1/2} = 96 \times 10^{-10}$  cm. mole<sup>1/2</sup> g.<sup>-1/2</sup>.

The molecular parameters for several other common polymers are shown in Table II.

TABLE II

Polymer	Temp., °C.	$(\overline{r_0^2}/M)^{1/2}$ $\times 10^{11}$	Reference
Polystyrene	25	735	Flory <sup>5</sup>
Poly(methyl methacrylate)	25	680	"
Poly(acrylic acid)	30	710	"
Polyethylene	140	1900	Tremontozzi <sup>6</sup>
		1070	Flory <sup>7</sup>
Nylon 66	25	960	This work

The nylon chain contains, on average, five methylene units for each amide group. In this respect we can think of nylon as consisting of polyethylene with each amide group replacing two methylene groups. The molecular

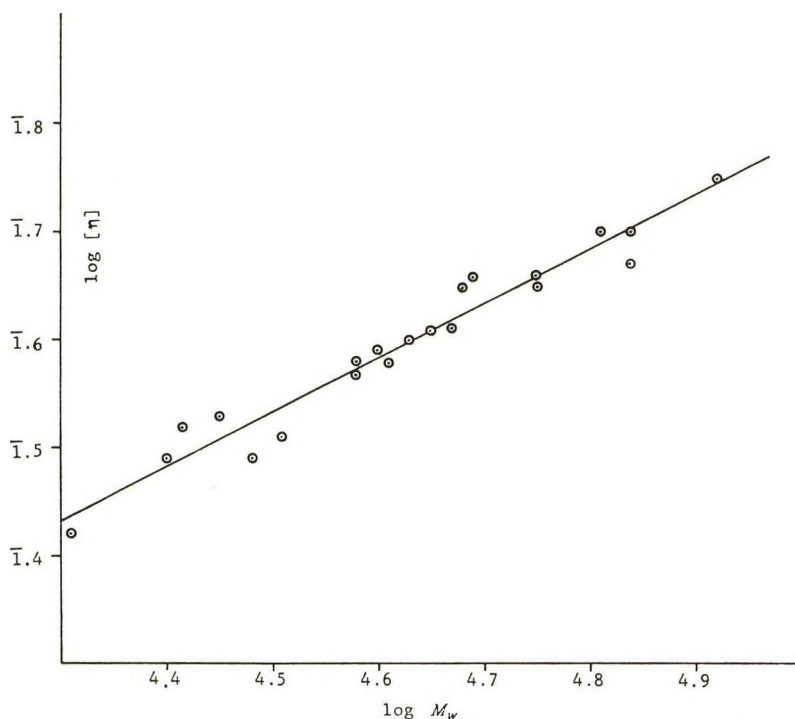


Fig. 2. Relation between intrinsic viscosity and molecular weight of nylon 66 fractions in an ideal solvent.

weight of the repeating unit of nylon 66 is greater than that of an equivalent length of the polyethylene chain in the ratio 113:98. This should be taken into consideration when comparing the values of  $(\overline{r_0^2}/M)^{1/2}$  for the two polymers. The relative extensibility of different polymer chains can be assessed from the values of  $(\overline{r_0^2})^{1/2}$  for equivalent chain lengths. The value of this parameter for nylon 66 is 4% less than that for polyethylene according to Flory et al.<sup>7</sup> The data for polyethylene were obtained at a higher temperature than those for nylon 66, and the temperature dependence of the unperturbed dimensions is not known in this region. If we assume that the temperature dependence is small, then polyethylene and nylon 66 have similar extensibilities.

### References

1. Schaeffgen, J. R., and C. F. Trivisonno, *J. Am. Chem. Soc.*, **74**, 2715 (1952).
2. Fendler, H. G., and H. A. Stuart, *Makromol. Chem.*, **25**, 159 (1957).
3. Saunders, P. R., *J. Polymer Sci.*, **43**, 273 (1960).
4. Saunders, P. R., *J. Polymer Sci.*, **57**, 131 (1962).
5. Flory, P. J., *Principles of Polymer Chemistry*, Cornell Univ. Press, Ithaca, N. Y., 1953, Chap. 14, Table XXXIX.
6. Tremontozzi, Q. A., *J. Polymer Sci.*, **36**, 113 (1959).
7. Flory, P. J., A. Ciferri, and R. Chiang, *J. Am. Chem. Soc.*, **83**, 1023 (1961).

### Résumé

Des mesures de diffusion de la lumière et de viscosité ont été effectuées sur des fractions de nylon 66 dissoutes dans un solvant idéal. La relation entre la viscosité intrinsèque et le poids moléculaire moyen en poids est dans ce solvant:  $[\eta] = 19.2 \times 10^{-4} \bar{M}_w^{1/2}$  ce qui indique que le nylon 66 obéit aux lois de la pelote statistique en solution. Les dimensions de la pelote non-perturbée sont données par le paramètre  $(\bar{r}_0^2/M)^{1/2} = 96 \times 10^{-10}$  cm. mole<sup>1/2</sup> g<sup>-1/2</sup>.

### Zusammenfassung

An Nylon-66-Fractionen in idealem Lösungsmittel wurden Lichtstreuungs- und Viskositätsmessungen durchgeführt. Die Beziehung zwischen der Viskositätszahl und dem Gewichtsmittel des Molekulargewichts in diesem Lösungsmittel lautet  $[\eta] = 19,2 \times 10^{-4} \bar{M}_w^{1/2}$ , was dafür spricht, dass Nylon 66 in Lösung den Gesetzmässigkeiten eines statistischen Knäuels folgt. Die ungestörten Knäueldimensionen werden durch den Parameter  $(\bar{r}_0^2/M)^{1/2} = 96 \times 10^{-10}$  cm. Mol<sup>1/2</sup>g<sup>-1/2</sup> gegeben.

Received September 13, 1963

Revised October 21, 1963

## Interaction of Polymethacrylic Acid and Bivalent Counterions. II

M. MANDEL and J. C. LEYTE, *Laboratorium voor Fysische Chemie der Rijksuniversiteit te Leiden, Netherlands*

### Synopsis

The Cu(II) chelate of polymethacrylic acid was investigated. Viscometric, electrophoretic, and spectrophotometric evidence is shown to confirm the potentiometric results reported previously which indicated the binding of two carboxylic groups by one Cu(II) ion.

### 1. INTRODUCTION

The investigation of the interaction between polymethacrylic acid (PMA) and Cu(II) with the help of potentiometric titrations<sup>1</sup> indicated the existence of a copper chelate involving two carboxylate groups over a large range of pH values of PMA-Cu(NO<sub>3</sub>)<sub>2</sub> solutions. To obtain these results from the experimental titration curves of PMA-Cu(NO<sub>3</sub>)<sub>2</sub> solutions with NaOH, some possibly serious approximations had to be made. As our results are in contradiction with those of previous investigations<sup>2,3</sup> it was thought useful to verify them by some independent experimental techniques.

The viscometric, electrophoretic, and spectrophotometric behavior of the system will be discussed here.

### 2. VISCOMETRIC TITRATIONS

The viscometric titrations were carried out by measuring the solution viscosity as a function of the degree of neutralization. In Figure 1 titrations of PMA solutions are compared for different concentrations of Cu(NO<sub>3</sub>)<sub>2</sub>. It is seen that the shape of the titration curves is not changed much by the Cu(NO<sub>3</sub>)<sub>2</sub> present, except for a displacement of the whole curve over a distance approximately equivalent to the amount of copper nitrate present. It may be seen that the viscosity of the solutions containing copper(II) ions begins to increase at approximately the point of equivalence of alkali and Cu(NO<sub>3</sub>)<sub>2</sub>. For each titration this point is indicated by an arrow in Figure 1. It may be recalled that the increase in the viscosity of solutions of weak polyacids in the course of a titration of such an acid is generally attributed to the repulsive forces between the fixed charges along the polymer chain, resulting from the ionization of the polymer. Thus the observed displacement of the titration curves may consequently be inter-

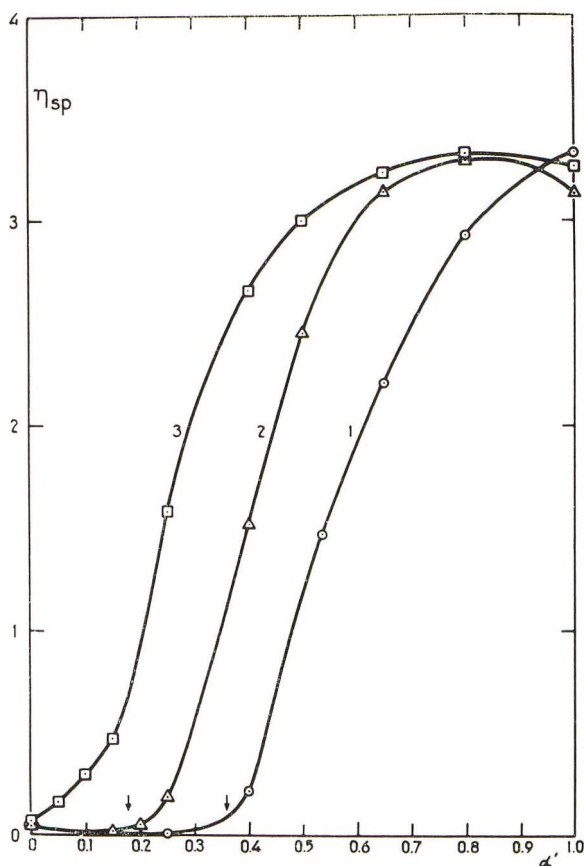


Fig. 1. Viscometric titrations of PMA ( $4.54 \times 10^{-3}$  eq./l.) in the presence of  $\text{NaNO}_3$  and  $\text{Cu}(\text{NO}_3)_2$ , respectively: ( $\square$ )  $1.67 \times 10^{-3}M$   $\text{NaNO}_3$ ; ( $\Delta$ )  $4.13 \times 10^{-4}M$   $\text{Cu}(\text{NO}_3)_2$ ; ( $\circ$ )  $8.26 \times 10^{-4}M$   $\text{Cu}(\text{NO}_3)_2$ .

puted as an absence of the usual charge increase during the first part of the titration. This means that the copper ions are bound to the polymer chain. Further information may be deduced from the fact that the general shape of the titration curve remains practically unchanged and that the highest viscosities reached are independent of the amount of copper ions present if an approximate correction is made for the ionic strength. For the highest copper concentration a comparable titration curve of a PMA solution containing  $\text{NaNO}_3$  is given. Thus, linking of polyions by copper ions does not seem to occur to an appreciable extent.

It is concluded, that the results of the viscometric titrations are consistent with the formation of a copper chelate involving two carboxylate groups.

### 3. ELECTROPHORESIS EXPERIMENTS

In the preceding section indications were found that, in the course of titrations of PMA containing  $\text{Cu}(\text{NO}_3)_2$ , little charge is formed on the poly-

mer before the point of equivalence with copper nitrate is reached. If this is true, it should be reflected in the electrophoretic behavior of the chelated polyacid as compared to the free polyacid. It must be observed, however, that changes in mobility related to charge variations will be somewhat obstructed by the tendency of the polyacid to expand with increase of charge. In Figure 2 the results of two electrophoretic titrations are plotted. The titration in the absence of copper nitrate shows a large increase of mobility between  $\alpha' = 0$  and  $\alpha' = 0.1$ . Here,  $\alpha'$  is the degree of neutralization. In the presence of copper nitrate a much slower increase of mobility is observed till the point of equivalence with  $\text{Cu}(\text{NO}_3)_2$  is reached. The

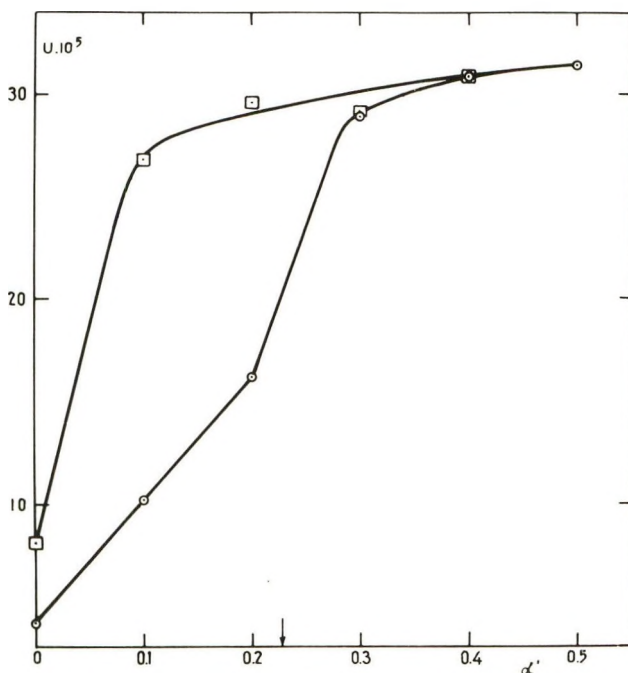


Fig. 2. Electrophoretic titrations of PMA ( $2.17 \times 10^{-2}$  eq./l.): (□)  $4.96 \times 10^{-3}M$   $\text{NaNO}_3$ ; (○)  $2.48 \times 10^{-3}M$   $\text{Cu}(\text{NO}_3)_2$ .  $U$  in units of  $\text{cm}^2$  v. sec.

electrophoretic mobility then rises quickly to the same level that was observed for PMA in the absence of copper ions. Thus, the electrophoresis experiments confirm the conclusions that were based on the results of viscometric titrations. The observed difference in mobility at  $\alpha' = 0$  is probably caused by a lowering of the charge of the polymer due to self-dissociation, by binding of copper ions, even at zero degree of neutralization.

It must be pointed out here, that the mobilities in Figure 2 must be considered only as approximate values of the PMA mobilities because boundary anomalies were observed (see the section on the experimental techniques).

#### 4. SPECTROPHOTOMETRY

In Figure 3 the ultraviolet absorption spectra for PMA in the absence and in the presence of copper nitrate are compared. It was impossible to follow the  $\text{PMA-Cu(NO}_3)_2$  spectrum to higher wave numbers, with the concentrations used, because strong absorption by the nitrate ions occurs. The copper containing PMA solutions were measured against a  $\text{Cu(NO}_3)_2$  reference solution.

It is seen that, in the presence of  $\text{Cu(NO}_3)_2$ , a new absorption region appears. Another absorption region was observed in the visible range, and some measurements were conducted in this region. The position of the absorption regions agrees with the results of previous investigations.<sup>2,3</sup>

In Figures 4-6 the results of some spectrophotometric titrations of  $\text{PMA-Cu(NO}_3)_2$  solutions with  $\text{NaOH}$  are presented (at a wave number where PMA does not absorb appreciably in the absence of  $\text{Cu}$ ). In all experiments the concentration of PMA exceeded that of  $\text{Cu(NO}_3)_2$ . It may be seen that, before the point of equivalence of  $\text{NaOH}$  with copper nitrate is reached, the absorbance  $A$  increases linearly with the amount of sodium hy-

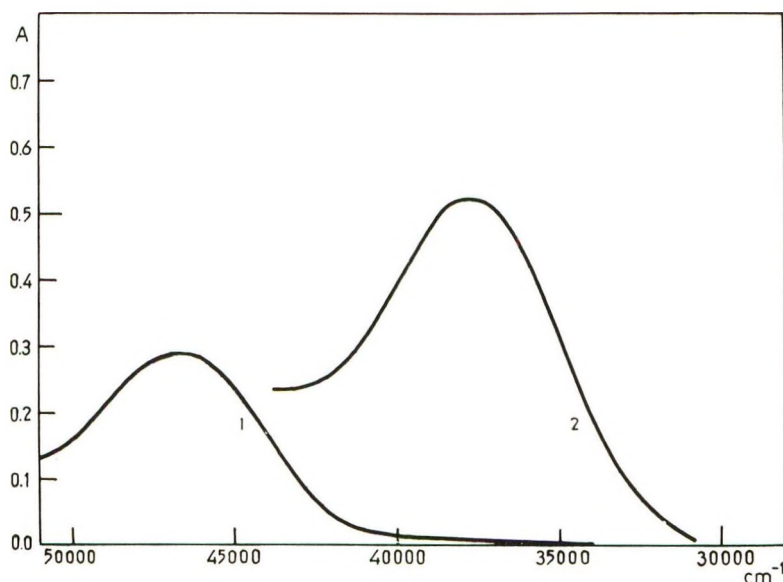


Fig. 3. Absorption spectra of PMA and  $\text{PMA-Cu(NO}_3)_2$  solutions: (1)  $2.26 \times 10^{-3}$  eq./l. PMA; (2)  $2.26 \times 10^{-3}$  eq./l. PMA,  $8.27 \times 10^{-4}M$   $\text{Cu(NO}_3)_2$ .

droxide added. This was established for different PMA concentrations and several  $\text{Cu(NO}_3)_2/\text{PMA}$  ratios. A smooth formation of the complex in the course of the titration is indicated. After the point of equivalence is reached the increase of absorbance levels off and, somewhat further, the absorbance starts to decrease. The measurements in the visible region (Fig. 6) are rather inaccurate, but the shape of the titration curve is essen-

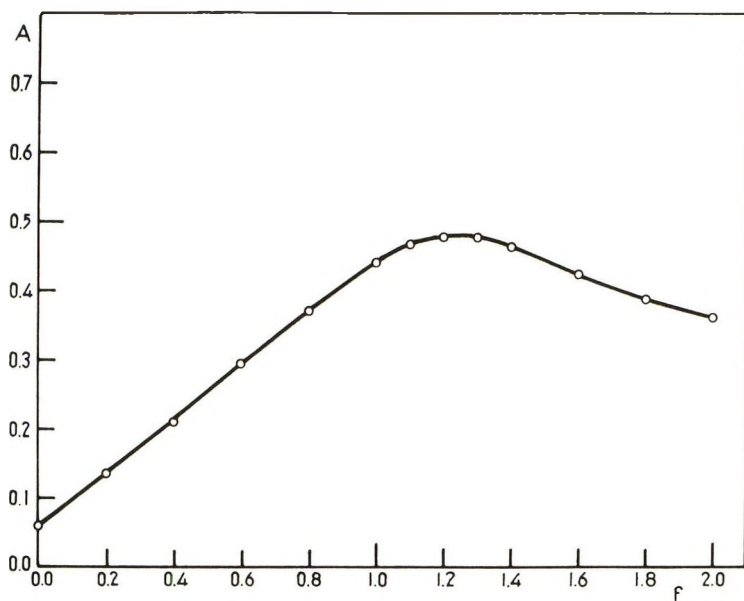


Fig. 4. Spectrophotometric titration of a PMA- $\text{Cu}(\text{NO}_3)_2$  solution.  $2.26 \times 10^{-3}$  eq./l. PMA;  $4.13 \times 10^{-4}M$   $\text{Cu}(\text{NO}_3)_2$ ; measured at  $32,800 \text{ cm}^{-1}$ ; cell length = 1 cm.;  $f$  = ratio of the amount of NaOH added and the amount of  $\text{Cu}(\text{NO}_3)_2$  present.

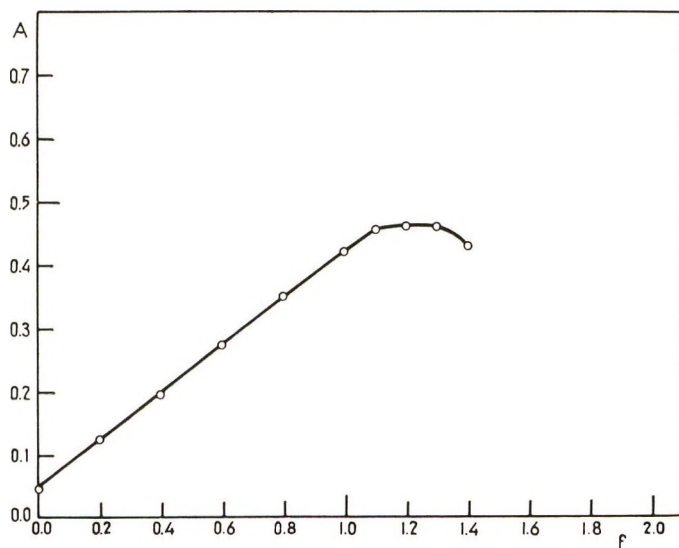


Fig. 5. Spectrophotometric titration of a PMA- $\text{Cu}(\text{NO}_3)_2$  solution.  $2.26 \times 10^{-3}$  eq./l. PMA;  $8.27 \times 10^{-4}M$   $\text{Cu}(\text{NO}_3)_2$ ; measured at  $31,800 \text{ cm}^{-1}$ ; cell length = 1 cm.;  $f$  = ratio of the amount of NaOH added and the amount of  $\text{Cu}(\text{NO}_3)_2$  present.

tially the same as in the ultraviolet region. It was observed that the ratio of the absorbance values of the maxima in the titration curves, if measured at the same wave number, is equal to the ratio of the copper nitrate concentra-

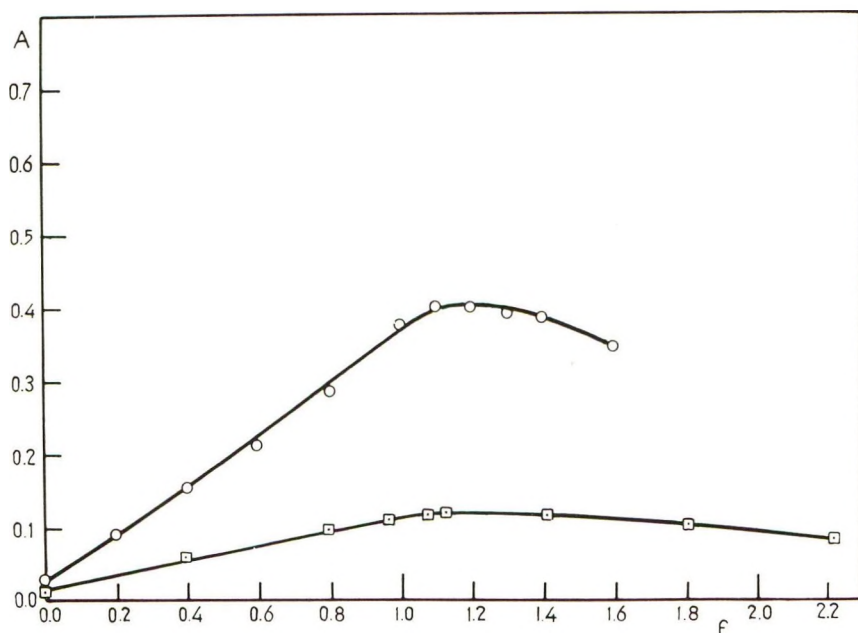


Fig. 6. Spectrophotometric titration of PMA- $\text{Cu}(\text{NO}_3)_2$  solutions: (O)  $4.54 \times 10^{-3}$  eq./l. PMA;  $1.24 \times 10^{-3}M$   $\text{Cu}(\text{NO}_3)_2$ ; measured at  $31,000 \text{ cm}^{-1}$ ; (□)  $4.54 \times 10^{-3}$  eq./l. PMA,  $8266 \times 10^{-4}M$   $\text{Cu}(\text{NO}_3)_2$ , measured at  $14,500 \text{ cm}^{-1}$ . Cell length = 1 cm.;  $f$  = ratio of the amount of NaOH added and the amount of  $\text{Cu}(\text{NO}_3)_2$  present.

tions (Table I). All this may be interpreted as follows. First, a copper-PMA complex is formed, involving two carboxylate groups. When all the copper ions are bound, this complex partially disintegrates in favor of some other form of binding. No new absorption region was observed, however. Therefore the exact nature of this new form of binding is not yet clear.

TABLE I

$\text{Cu}(\text{NO}_3)_2$ concn., $M$	$A_{\max}$ ( $31,000 \text{ cm}^{-1}$ )	$\frac{A_{\max}}{[\text{Cu}(\text{NO}_3)_2]}$
$1.24 \times 10^{-3}$	0.400	$3.23 \times 10^2$
$8.27 \times 10^{-4}$	0.285	$3.44 \times 10^2$
$4.13 \times 10^{-4}$	0.136	$3.30 \times 10^2$

In Figure 7 spectrophotometric data are compared with a formation curve that was calculated by the method discussed previously.<sup>1</sup> In a  $p([\text{HA}]/[\text{H}^+])$  region in which a given complex dominates, the average coordination number  $\bar{n}$  will be proportional to the concentration of this complex. If the complex absorbs at a certain frequency, there should be a linear relationship between  $\bar{n}$  and the absorbance of the solution. A potentiometric titration of a solution of copper nitrate and PMA was followed

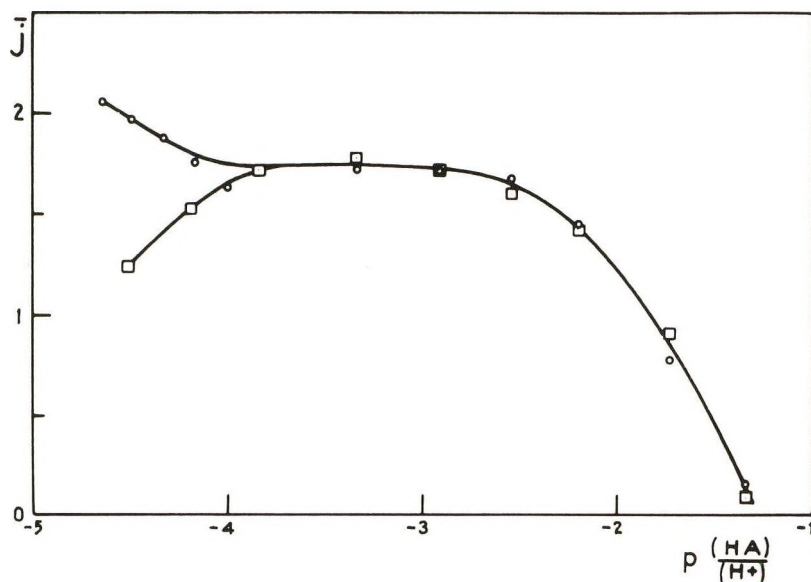


Fig. 7. Comparison of spectrophotometric titration and formation curve: ( $\square$ ) transformed absorbance at  $14,500\text{ cm}^{-1}$ ; ( $\circ$ ) mean coordination number  $\bar{j}$ .  $4.54 \times 10^{-3}$  eq./l. PMA;  $8.26 \times 10^{-4}M$   $\text{Cu}(\text{NO}_3)_2$ . See text.

spectrophotometrically. From the same titration, a formation curve was calculated. Then the factor was determined by which the absorbance at one point of the titration curve should be multiplied to obtain the value of  $\bar{j}$  at this point. Now the whole spectrophotometrical titration curve was transformed by use of the same factor. The result of this procedure is seen in Figure 7. Besides a confirmation of the general shape of the formation curve, Figure 7 reveals an interesting agreement of the results obtained by the two methods. Both, the spectrophotometrical and the potentiometric results show a breakdown of the chelate in the same  $p([HA]/[H^+])$  region.

## 5. SOLUBILITY OF THE CHELATE

In Figure 8 the results of some experiments on the solubility of the copper-PMA complex may be seen. For a given PMA concentration the pH region in which the polymer is insoluble was determined at different  $\text{Cu}(\text{NO}_3)_2$  concentrations. It is seen that, if a solution containing 90%  $\text{Cu}(\text{NO}_3)_2$  with respect to the PMA concentration, is titrated with alkali, the polymer starts to precipitate at a low pH value. After continued addition of alkali the solution becomes clear again at  $\text{pH} = 9$ . The dissolution always starts after the point of equivalence with  $\text{Cu}(\text{NO}_3)_2$  has been reached. Even at these high pH values no copper hydroxide precipitate is observed when the polymer becomes soluble again. The observed behavior is, again, consistent with the formation of an uncharged complex during the first part of the titration. At lower PMA concentrations the region of insolubility is shifted to the right.

## 6. DISCUSSION

In the preceding paragraphs it is shown that the principal result obtained by potentiometric investigations<sup>1</sup> (the existence of a copper complex involving two carboxylate groups) is confirmed by investigations with various independent experimental techniques. From the viscometric and electrophoretic titrations it may be seen that the formation of the complex does not appreciably influence the dependence of the spatial properties of the polymer chain on the charge. This suggests a binding of the copper(II) ions by neighboring carboxylate groups of the same chain.

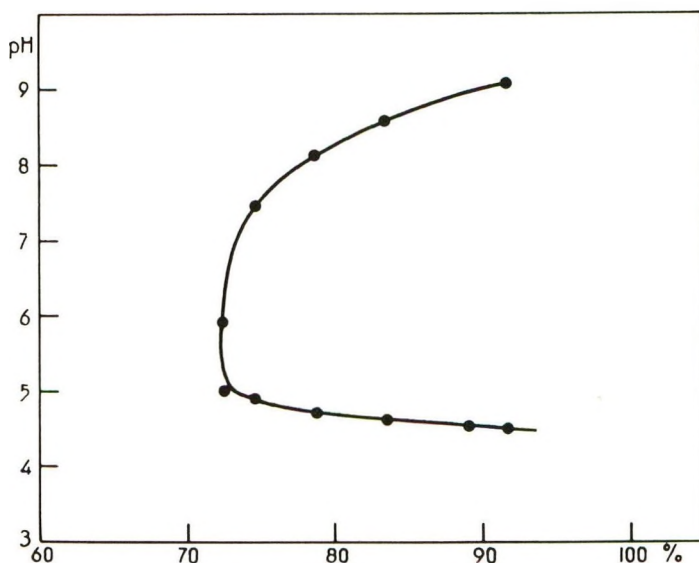


Fig. 8. Polymer solubility range. Precipitation occurs at the right-hand side of the drawn curve.  $4.7 \times 10^{-2}$  eq./l. PMA. pH against equivalent percentage of  $\text{Cu}(\text{NO}_3)_2$  with respect to PMA.

An interesting problem arises regarding the instability of this chelate at high charge densities of the polymer. The spectroscopic and potentiometric results agree about the region in which the concentration of the chelate involving two carboxylate groups starts to diminish. No precipitation of copper hydroxide was ever observed. On the other hand, the formation of a complex involving more carboxylate groups must be thought extremely improbable, first in view of the steric strains this would probably involve and second, with respect to the large electrostatic repulsion that would be the result of a densely coiled polyion at high charge densities. Also the viscometric results do not indicate a compact form of the charged polymer if copper(II) ions are present. Further experimental evidence will be necessary before definite conclusions may be reached.

## 7. EXPERIMENTAL

### Materials

The preparation of all materials used was described previously.<sup>1</sup>

### Viscometric Titrations

The viscometric titrations were performed with an Ubbelohde viscometer in which liquids could be mixed and viscosity measurements could be carried out in a nitrogen atmosphere. For water a flow time of 265.2 sec. was measured with this viscometer. All measurements were carried out at  $20 \pm 0.02^\circ\text{C}$ .

The actual titration was performed by adding to a  $\text{PMA-Cu(NO}_3)_2$  solution already in the viscometer, a 100% neutralized  $\text{PMA-Cu(NO}_3)_2$  solution of the same concentration by means of a microburet. After each addition and homogenization the viscosity of the mixture was measured. Thus, these titrations were conducted at constant polymer and  $\text{Cu(NO}_3)_2$  concentration.

Measured viscosities were presented in the form of specific viscosities.

### Electrophoresis Experiments

The experiments were performed at  $25^\circ\text{C}$ . with a L.K.B. 3023 Tiselius-Svenson electrophoresis apparatus and a Tiselius cell. The initial boundaries were  $\text{Cu(NO}_3)_2$ ,  $\text{PMA|NaNO}_3$  and, for the experiments in absence of copper ions  $\text{NaNO}_3$ ,  $\text{PMA|NaNO}_3$ . In both sets of experiments the degree of neutralization of PMA was varied. To avoid disturbing effects on the binding equilibrium of copper ions at the boundary the pH's of the  $\text{NaNO}_3$  solutions were adjusted to the pH's of the polymer phase ( $\text{HNO}_3$  and  $\text{NaOH}$  were used for this purpose). This, of course, does not guarantee an equality of pH at both sides of the moving boundary, because of the concentration boundary which may be formed at the place of the initial boundary.

In all experiments the velocity of the boundary moving into the polymer phase was measured. As in this phase the PMA concentration was always larger than the  $\text{Cu(NO}_3)_2$  concentration, the conditions for ideal free electrophoresis were clearly not fulfilled.<sup>4</sup> Rapid and asymmetric broadening of the descending boundary was observed. (The rising boundary tended to become sharper but could not be used because this boundary moves into a PMA-free solution.) However, for a qualitative comparison of the effects of equivalent amounts of sodium nitrate and copper nitrate the results may be used. The results given refer only to the maxima of the gradient curves.

All conductivity measurements were performed with a Leeds and Northrup bridge at  $25.00 \pm 0.01^\circ\text{C}$ . The measurements were carried out at 1200 cycles/sec. with a conductance cell (cell constant =  $10.04 \text{ cm.}^{-1}$ ).

### Spectrophotometric Experiments

An automatically recording SP 700 Unicam spectrophotometer was used with suprasil cuvetts of 10 mm. optical length. The measurements were conducted at room temperature (about 20°C. in this case).

### Solubility Experiments

These experiments consisted of slow titration of PMA-Cu(NO<sub>3</sub>)<sub>2</sub> solutions with NaOH in a thermostatted titration vessel at 20°C. In the course of the titrations the pH was measured with a pH meter (Radiometer 22) with the use of glass and calomel electrodes.

The points at which precipitate appeared and disappeared were observed visually.

### References

1. Mandel, M., and J. C. Leyte, *J. Polymer Sci.*, **A2**, 2883 (1964).
2. Kotliar, A. M., and H. Morawetz, *J. Am. Chem. Soc.*, **77**, 3692 (1955).
3. Morawetz, H., *J. Polymer Sci.*, **17**, 442 (1955).
4. Bier, M., *Electrophoresis. Theory, Methods and Applications*, Academic Press, New York, 1959.

### Résumé

On a étudié le chélate entre Cu(II) et l'acide polyméthacrylique. Les mesures viscosimétrique, électrophorétique et spectrophotométrique confirment les résultats potentiométriques rapportés précédemment, et qui montraient la liaison de deux groupements carboxyliques par ion Cu(II).

### Zusammenfassung

Das Cu(II)-Chelat von Polymethacrylsäure wurde untersucht. Viskosimetrische, elektrophoretische, und spektrophotometrische Ergebnisse bestätigen die früher aus potentiometrischen Resultaten gefolgerte Bindung von zwei Carboxylgruppen an ein Cu(II)-Ion.

Received September 17, 1963

Revised October 21, 1963

## Radiation Chemistry of Iodine-Octamethylcyclotetrasiloxane Solutions

CLARENCE J. WOLF\* and A. C. STEWART,† *Parma Research  
Laboratory, Union Carbide Corporation, Parma, Ohio*

### Synopsis

Post-irradiation polymerization of  $\gamma$ -ray-irradiated liquid octamethylcyclotetrasiloxane containing a small amount of iodine was observed. The effect occurs at room temperature without an additional stimulus, and we conclude that it results from catalysis by  $\text{HI}_3$ , i.e., a complex of  $\text{HI} + \text{I}_2$ . Hydrogen triiodide is produced when iodine-octamethylcyclotetrasiloxane solutions are irradiated with  $\gamma$ -rays from  $\text{Co}^{60}$ .  $\text{HI}_3$  is a good rearrangement catalyst for siloxane bonds. The dose is critical; short irradiations do not produce enough  $\text{HI}$ , while longer irradiations consume most of the  $\text{I}_2$ . The triiodide complex dissociates at temperatures equal to or greater than  $60^\circ\text{C}$ .; thus, the polymerization stops as the temperature is raised, but contrary to usual post-irradiation polymerization processes, resumes when the sample cools. Pure irradiated octamethylcyclotetrasiloxane polymerizes upon the addition of iodine. We assume that the irradiation produces silicon-hydrogen bonds which react with iodine yielding the catalyst  $\text{HI}_3$ . In all systems the  $\text{HI}_3$  was identified spectrophotometrically. However, its role in the polymerization was established directly when it was determined that an unirradiated iodine-octamethylcyclotetrasiloxane solution polymerized upon the addition of  $\text{HI}$ .

### Introduction

It is well known that ionizing radiation can polymerize many organic compounds. A few cases are reported<sup>1-4</sup> where the polymerization continues even after the sample is removed from the radiation field. The most acceptable explanation for post-irradiation polymerization of solids is as follows: radicals or reactive species produced when energy is absorbed are trapped in the crystal lattice. Under a different stimulus (e.g., temperature change) they are released and initiate chemical reactions. Such reactive species have been used to induce reactions in sensitive substances so that oriented copolymers, graft polymers, etc., resulted. In our reactions liquid octamethylcyclotetrasiloxane ( $[(\text{CH}_3)_2\text{SiO}]_4$ ), (hereafter referred to as octamethyl tetramer) containing a small amount of iodine undergoes post-irradiation polymerization following  $\gamma$ -ray irradiation.

\* Present address: McDonnell Aircraft Corporation, St. Louis, Missouri.

† Present address: Union Carbide Consumer Products Company, New York, New York.

## Experimental

Details of purification, product analysis, and a description of the  $\text{Co}^{60}$  irradiator are described elsewhere.<sup>5</sup> Results were readily reproducible, and the special sample preparation techniques described earlier<sup>5</sup> were unnecessary. Known amounts of iodine were added to the octamethyl tetramer and the solutions were deaerated by conventional freeze-pump-thaw techniques. The irradiations and spectrophotometric analysis were carried out in a fused silica cell (either 10 or 1 mm. path length). The disappearance of iodine and appearance of hydrogen iodide were determined by means of a Cary Model 14 recording spectrophotometer, as discussed elsewhere.<sup>5</sup> In several experiments methyl iodide was identified as a product, but its concentration was not determined.

The amount of polymer was determined by weighing the irradiation vessel with and without polymer. The vessel and polymer were pumped in a vacuum system until they attained a constant weight. The polymer was then removed with benzene, dried, and the vessel weighed.

The anhydrous iodide used for the chemical polymerization was prepared by boiling a solution of iodine in tetralin. The HI gas was stored in a 1 liter flask and added to the sample in a vacuum system by condensation at  $-196^\circ\text{C}$ .

## Results

Weber et al.<sup>6</sup> observed zero-order kinetics for the disappearance of iodine in the radiolysis of several iodine-hydrocarbon systems. In the iodine-octamethyl tetramer system, however, it was observed that the rate of iodine consumption is dependent on the dose. The different kinetic behavior may be due to chemical reactions induced by  $\text{HI}_3$  produced during irradiation; but more likely the difference is due to the reaction of HI (also produced during irradiation) with methyl radicals.

Figure 1 shows the iodine concentration as a function of dose for several different initial iodine concentrations. After a large initial rate of consumption of iodine, there is a gradual decrease until approximately two-thirds of the iodine is gone, then all curves exhibit another rapid rate of iodine consumption. This increase in the rate corresponds with the production of methyl iodide; little or no methyl iodide is formed before this point.

Post-irradiation polymerization which persists for several days occurs in these solutions. Its rate is dependent on both initial iodine concentration and dose. Figure 2 shows the per cent polymer produced in iodine solutions (initially,  $5.8 \times 10^{-3}M$ ) as a function of dose for four different aging times. A sample irradiated to 1 Mrad ( $6 \times 10^{19}$  e.v./g.) was converted to about 90% polymer after aging at room temperature for four days. However, a sample which received 2 Mrad contained only about 20% polymer after the same post-irradiation time interval.

For a given dose, the rate of post-irradiation polymerization at room temperature is strongly dependent on initial iodine concentration; this may be

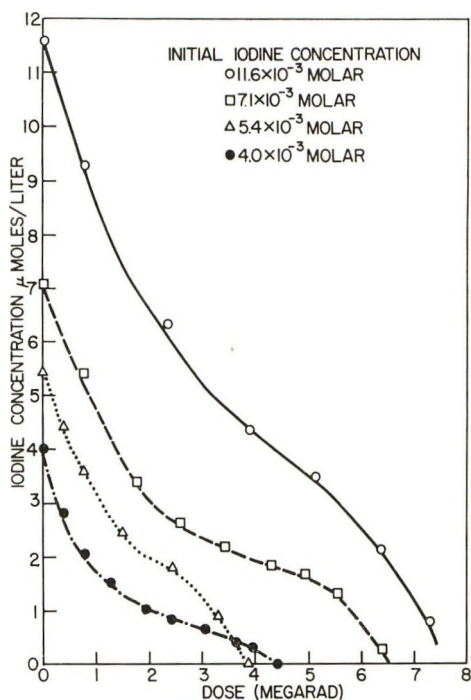


Fig. 1. Iodine consumption as a function of dose.

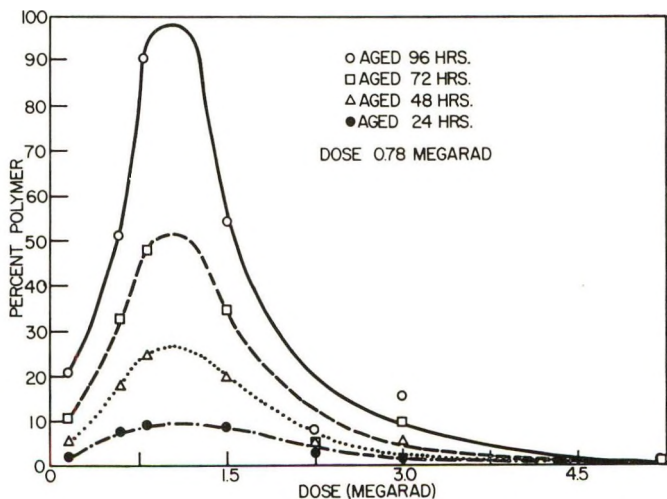


Fig. 2. Polymer formation as a function dose for different aging periods.

seen in Figure 3. Iodine concentrations ranged between  $17 \times 10^{-3}$  and  $4.5 \times 10^{-3} M$ . All samples received a dose of 0.78 Mrad at a dose rate of 1.4 Mrad/hr. A change in the radiation intensity by a factor of two (for the same total dose) did not alter the rate of post-irradiation polymerization.

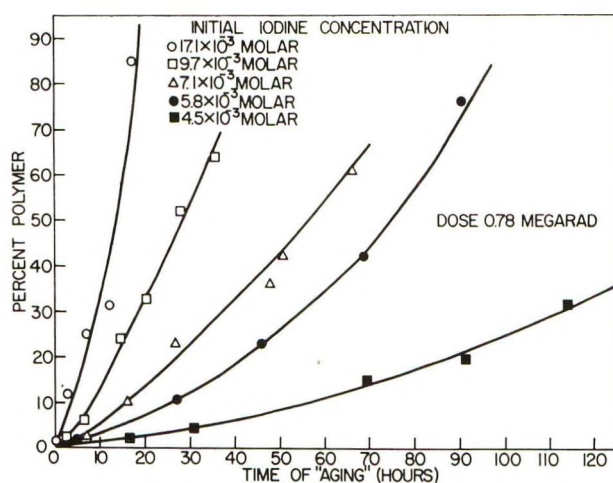


Fig. 3. Effect of iodine concentration on post-irradiation polymerization.

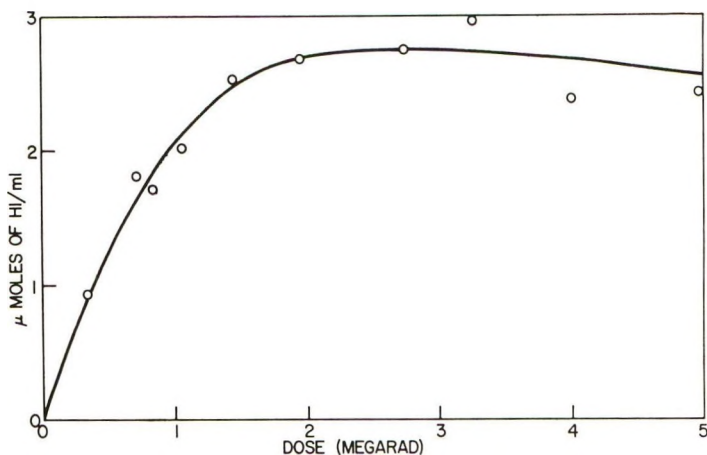


Fig. 4. Production of HI as a function of dose.

Hydrogen iodide is produced during the radiolysis (Fig. 4). However, our analytical technique did not enable us to distinguish between the iodide ion formed from HI and that formed by hydrolysis of silicon-iodine bonds. Since there is definitely more HI than  $\equiv\text{SiI}$  (according to spectrophotometric measurements), it is assumed that all the iodide ion observed results from the dissociation of hydrogen iodide. The iodide concentration rises rapidly with dose until the iodine and iodide concentrations are essentially equal. At this point the maximum amount of hydrogen iodide is present. Although further radiolysis converts iodine to hydrogen iodide, the hydrogen iodide is now in sufficient concentration to act as a radical scavenger. Pottie et al.<sup>7</sup> have shown that methyl radicals produced by photolysis are more susceptible to scavenging by HI than by  $\text{I}_2$ . This also explains the apparent induction period observed for the production of methane in these

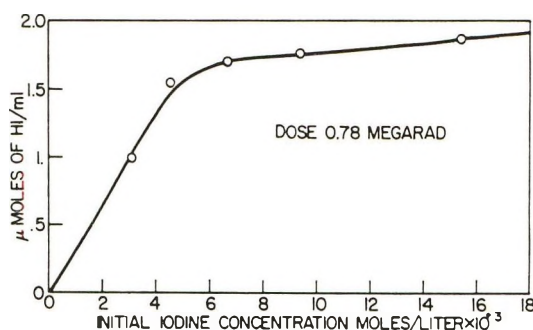


Fig. 5. Production of HI as a function of initial iodine concentration.

systems.<sup>5</sup> As shown in Figure 5, the amount of hydrogen iodide produced for a given dose is dependent on the initial iodine concentrations up to  $5 \times 10^{-3}$  M, but is essentially independent of initial iodine concentration for solutions between  $5 \times 10^{-3}$  and  $15 \times 10^{-3}$  M.

The post-irradiation polymerization of these systems is dependent upon aging temperature and not upon irradiation temperature. Solutions irradiated at various temperatures from room temperature up to 75°C. exhibited the same rate of polymerization when aged at room temperature. Figure 6 shows the per cent polymer formed during the 24-hr. aging period versus the aging temperature. All samples were initially  $5.8 \times 10^{-3}$  M with respect to iodine and received 0.78 Mrad. At 30°C. the rate of polymerization is at the maximum. Although post-irradiation polymerization virtually ceases in a sample stored above 60°C., it resumes when the sample cools. Thus, the polymerization process can be stopped and resumed repeatedly by raising and lowering the temperature.

In order to be certain that the decrease in reaction rate at elevated temperatures was not due to evaporation of iodine from the liquid phase, vessels which contained different liquid to vapor ratios were irradiated. These results are summarized in Table I. The agreement among the data indicates that loss of iodine to the gas phase is not responsible for the decreased rate of polymerization with a temperature increase.

TABLE I  
Effect of Vapor/Liquid Volume Ratios on the Polymerization of  
Irradiated Octamethyl Tetramer Solutions<sup>a</sup>

Portion of vessel volume occupied by the solution, %	Amt. polymerized, % <sup>b</sup>
~100	35.5
55	34.0
38	28.1
26	37.7
14	32.8

<sup>a</sup> Initial iodine concentration  $7.1 \times 10^{-3}$  M subjected to a total dose of 0.77 Mrad.

<sup>b</sup> All solutions aged at room temperature for 47 hours.

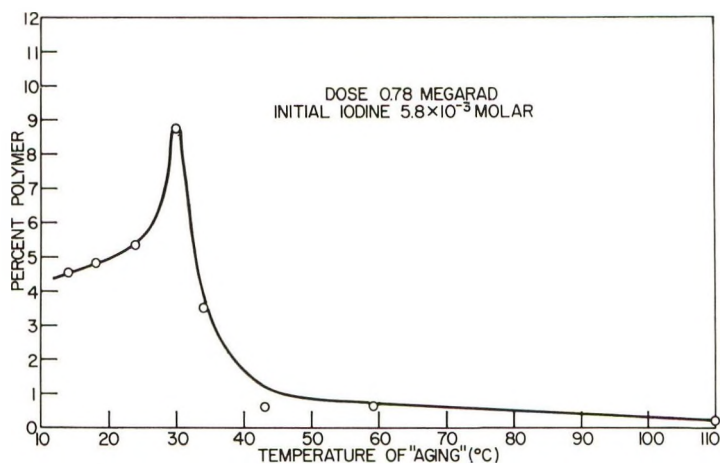


Fig. 6. Polymer production as a function of aging temperature.

Three principal new peaks appear in the absorption spectra of irradiated solutions of iodine in octamethyl tetramer. They are at  $226 \text{ m}\mu$ , corresponding to  $\text{HI}$  (or  $\text{I}^-$ ), at  $360 \text{ m}\mu$ , corresponding to  $\text{HI}_3$  (or  $\text{I}_3^-$ ), and at  $254 \text{ m}\mu$ , corresponding to  $\text{CH}_3\text{I}$ . The latter peak appears after most of the molecular iodine is consumed. The absorption spectra of both the irradiated and unirradiated solutions are shown in Figure 7. The single peak at  $515 \text{ m}\mu$  corresponds to uncomplexed iodine ( $6.6 \times 10^{-3} M$ ). After a dose of  $0.65 \text{ Mrad}$ , definite peaks appear at  $360$  and  $226 \text{ m}\mu$ . As a first approximation we can assume a molar extinction coefficient of 26,000 for triiodide, the value observed in water.<sup>8</sup> From this we can calculate the  $\text{HI}_3$  concentration and obtain an equilibrium constant in octamethyl tetramer at  $25^\circ\text{C}$ . of approximately  $10 \text{ l./mole}$  for the reaction:



$\text{HI}_3$  dissociates at elevated temperatures, and the peak at  $360 \text{ m}\mu$  disappears when the solution is heated and reappears when the solution cools.

Iodine induces polymerization when it is added to previously irradiated pure octamethylcyclotetrasiloxane. Although oxygen must be excluded from these samples during irradiation, post-irradiation polymerization will occur in the presence of air or oxygen.

Post-irradiation polymerization occurs when iodine is added to a sample of octamethyl tetramer which was warmed to room temperature after irradiation at  $-196^\circ\text{C}$ . Neither the gases which are volatile below  $-78^\circ\text{C}$ . (mainly  $\text{H}_2$ ,  $\text{CH}_4$ , and  $\text{C}_2\text{H}_6$ ) nor the nonvolatile portion (containing linear polymer and dimerized molecules) which remains when the sample is distilled *in vacuo* at room temperature can polymerize an iodine-tetramer solution. The fraction volatile at room temperature containing the unreacted monomer and lower molecular weight compounds produced by the irradiation polymerize upon addition of iodine.

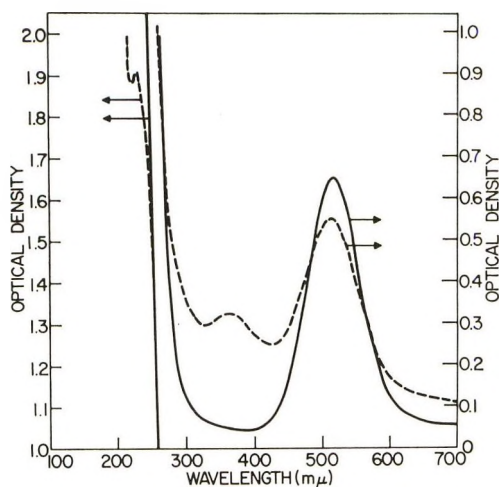
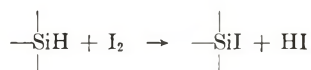


Fig. 7. Absorption spectra of  $I_2$ -octamethylcyclotetrasiloxane solutions: (—) before irradiation; (---) after irradiation.

Heptamethylcyclotetrasiloxane, a possible irradiation product with a vapor pressure similar to that of the octamethyl tetramer, was found to polymerize octamethyl tetramer solutions in the presence of iodine. When this compound (0.5 wt.-%) was added to an iodine-tetramer solution ( $9 \times 10^{-3}M I_2$ ), the sample polymerized without exposure to ionizing radiation. Solutions containing the heptamethyl tetramer exhibited a temperature-dependent absorption at 360  $m\mu$ . Presumably this is due to  $HI_3$  and its presence can be accounted for by the following sequence of reactions: (1) iodine reacts with the silicon-hydrogen bond in heptamethylcyclotetrasiloxane to form a silicon-iodine bond and  $HI$ :



(2)  $HI$  then complexes with the remaining iodine to form  $HI_3$ .



Several cyclic silicones were found to polymerize in the presence of iodine and anhydrous hydrogen iodide. A 2-g. octamethyl tetramer sample,  $20 \times 10^{-3}M$  with respect to iodine, polymerized to a gel in a few hours upon the addition of 1 cc. at STP of anhydrous hydrogen iodide. Several other cyclic silicones, such as decamethylcyclopentasiloxane and hexamethylcyclotrisiloxane, were readily polymerized by the addition of  $HI$  to an iodine solution. All of these solutions exhibited a strong room temperature absorption at 360  $m\mu$  which disappeared upon heating.

### Discussion

The acid- or base-catalyzed polymerization<sup>9,10</sup> of cyclic siloxanes to form linear siloxanes is usually considered to proceed via an ionic mechanism.

The crosslinking mechanism, on the other hand, appears to involve free radicals. Johannson<sup>11</sup> prepared the ethylene-bridged dimer by adding a free radical catalyst (*tert*-butyl perbenzoate) to the octamethyl tetramer. Attempts to polymerize the hexamethyl trimer  $(\text{Me}_2\text{SiO})_3$  into linear polydimethylsiloxanes with free radical catalysts were unsuccessful.<sup>12,13</sup> It is proposed, therefore, that the observed post-irradiation polymerizations are catalyzed by the polarizable triiodide complex.

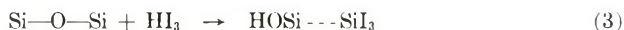
The kinetics of the post-irradiation polymerization of iodine-octamethyl tetramer solutions depend on the iodine and hydrogen iodide concentrations as well as on the temperature. The active species ( $\text{HI}_3$ ) is considered in its molecular form, although it is possible that the actual entities involved in the polymerization are ions. The following mechanism is proposed to explain the observations. In irradiated solutions hydrogen iodide is probably produced by iodine scavenging of radiogenic hydrogen atoms:



The HI then complexes with iodine



with a room temperature equilibrium constant of about 10 l./mole. The siloxane bonds are rearranged by  $\text{HI}_3$  via the same general mechanism proposed for the  $\text{H}_2\text{SO}_4$ -catalyzed polymerization:<sup>9</sup>

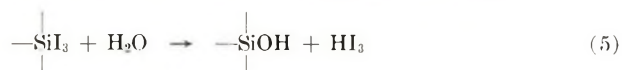


A reversal of this reaction by other opened cyclic siloxane molecules leads to chain propagation.

Hurd<sup>9</sup> showed that silanol groups alone do not catalyze polymerization of the tetramer, but he did observe that water was formed when tetramethyl-disiloxanediol was heated with the tetramer. Thus, the silanol groups *per se* probably cannot open rings, but once they are present they can lead to polymerization via coupling:



Water can hydrolyze the silicon triiodide bond, regenerating  $\text{HI}_3$ :



In several instances traces of water were produced during the polymerization reaction and, due to the iodine which dissolved in it, appeared as finely divided black specks near the bottom of the reaction vessel. The amount of water was not measured and the distribution of  $\text{HI}_3$  in the two phases is not known. Therefore, a kinetic analysis of the triiodide polymerization cannot be made.

### Conclusion

The postulated mechanism enables us to explain qualitatively the experimental observations. The maximum in the rate of polymerization with dose results from a maximum concentration of  $\text{HI}_3$ . This condition is reached when the  $\text{HI}$  concentration times the iodine concentration is a maximum. The higher the initial iodine concentration, the greater the amount of  $\text{HI}_3$  for a given dose. The complex dissociates at elevated temperatures, thereby stopping the polymerization. The complex reforms and polymerization resumes when the solution cools.

The radiolysis of the pure octamethyl tetramer produces a small concentration of silicon-hydrogen bonds which react with added iodine to yield  $\text{HI}$ . The  $\text{HI}$  complexes with the excess iodine producing  $\text{HI}_3$ . If oxygen is present during radiolysis, silicon-hydrogen bonds are not formed, but if the hydride is already present, oxygen does not affect the polymerization.

Pure octamethyl tetramer does not polymerize when iodine is present in its molecular form. In fact, Osthoff et al.<sup>14</sup> have used iodine to stop the base-catalyzed ( $\text{KOH}$ ) polymerization of the tetramer at room and elevated temperatures.

We are deeply indebted to Dr. J. A. Ghormley for his helpful advice and constructive criticism given to us during the course of this work.

### References

1. Bamford, C. H., A. D. Jenkins, M. C. R. Symons, and M. G. Townsend, *J. Polymer Sci.*, **34**, 181 (1959).
2. Bensasson, B., and A. Bernas, *J. Polymer Sci.*, **30**, 163 (1958).
3. Adler, G., and P. Colombo, *J. Polymer Sci.*, **37**, 390 (1959).
4. Fadner, T. A., I. Rubin, and H. Morawetz, *J. Polymer Sci.*, **37**, 549 (1959).
5. Wolf, C. J., and A. C. Stewart, *J. Phys. Chem.*, **66**, 1119 (1962).
6. Weber, E. N., P. F. Forsyth, and R. H. Schuler, *Radiation Res.*, **3**, 68 (1955).
7. Pottie, F. R., W. H. Hamill, and R. R. Williams, *J. Am. Chem. Soc.*, **80**, 4224 (1958).
8. Autrey, A. D., and R. E. Connick, *J. Am. Chem. Soc.*, **73**, 1812 (1951).
9. Hurd, D. T., *J. Am. Chem. Soc.*, **77**, 2998 (1955).
10. Kantor, S. W., W. T. Grubb, and R. C. Osthoff, *J. Am. Chem. Soc.*, **76**, 5190 (1954).
11. Johansson, O. K. (assigned to Dow Corning Corp.), U. S. Pat. 2,762,827 (1958).
12. Lawton, E. J., W. G. Grubb, and J. S. Balwit, *J. Polymer Sci.*, **19**, 455 (1956).
13. Kohima, K., N. Tarumi, and S. Wakatuki, *Nippon Kagaku Zasshi*, **76**, 1205 (1955); *Chem. Abstr.*, **51**, 17639 (1957).
14. Osthoff, R. C., A. M. Bueche, and W. T. Grubb, *J. Am. Chem. Soc.*, **76**, 4659 (1954).

### Résumé

On a observé une polymérisation lors de la post-irradiation aux rayons-gamma de l'octaméthylcyclotétrasiloxane liquide, contenant une petite quantité d'iode. Ce phénomène se fait à température ordinaire sans aucun stimulant supplémentaire et nous concluons que cela provient de la catalyse par  $\text{HI}$ , c'est à dire un complexe de  $\text{HI}$  et  $\text{I}_2$ . Le triiodure d'hydrogène se forme en irradiant avec des rayons gamma provenant du  $\text{Co-60}$  des solutions d'iode-octométhylcyclotétrasiloxane.  $\text{HI}_3$  est un bon catalyseur de

réarrangement pour les liaisons siloxane. La dose est critique, des courtes irradiations ne produisent pas assez de HI tandis que des irradiations plus longues consomment trop de  $I_2$ . Le complexe triiodé se dissocie à une température égale ou plus grande que  $60^\circ$ ; ainsi la polymérisation s'arrête lorsqu'on augmente la température mais, contrairement au processus habituel de polymérisation par post-irradiation, recommence après refroidissement. L'octaméthylcyclotétrasiloxane pur, lorsqu'il est irradié, polymérise par addition d'iode. Nous supposons que l'irradiation produit des liaisons silicone-hydrogène qui réagissent avec l'iode pour donner le catalyseur  $HI_3$ . Dans tous les systèmes,  $HI_3$  a été identifié par spectrophotométrie. Cependant son rôle dans la polymérisation a été établi directement lorsqu'on a déterminé qu'une solution d'iode-octaméthylcyclotétrasiloxane non-irradiée polymérise par addition de HI.

### Zusammenfassung

Polymerisation als Nacheffekt bei gammabestrahltem flüssigen Octamethylcyclotetrasiloxan mit geringer Menge von Jod wurde beobachtet. Der Effekt tritt bei Zimmertemperatur ohne zusätzliche Anregung auf, und wir folgern, dass dies durch Katalyse durch  $HI_3$ , d.h. einen Komplex von  $HI + I_2$  erfolgt. Wasserstofftriiodid entsteht bei Bestrahlung von Iod-Octamethylcyclotetrasiloxanlösungen mit Co-60 Gammastrahlen.  $HI_3$  ist ein guter Umlagerungskatalysator für Siloxanbindungen. Die Dosis ist kritisch; kurze Bestrahlungszeit erzeugt nicht genügend HI, während längere Bestrahlung einen Grossteil des  $I_2$  aufbraucht. Der Triiodidkomplex dissoziiert bei Temperaturen gleich oder grösser als  $60^\circ$ ; daher hört die Polymerisation bei steigender Temperatur auf, während sie im Gegensatz zu gewöhnlichen Nacheffektpolymerisationsprozessen bei Abkühlung wieder auftritt. Reines bestrahltes Octamethylcyclotetrasiloxan polymerisiert bei Zugabe von Iod. Wir nehmen an, dass die Bestrahlung Silizium-Wasserstoffbindungen erzeugt, die mit Iod unter Bildung des Katalysators  $HI_3$  reagieren. In allen Systemen wurde  $HI_3$  spektrophotometrisch identifiziert. Seine Rolle bei der Polymerisation wurde aber direkt festgestellt, da erwiesen wurde, dass eine unbestrahlte Iod-Octamethylcyclotetrasiloxanlösung bei Zugabe von HI polymerisiert.

Received September 18, 1963

Revised October 25, 1963

## Elastic Effects and Extrudate Distortions in Capillary Flow of Molten Polyethylene Resins

HANS SCHOTT, *Research Center, Lever Brothers Company, Edgewater,  
New Jersey*

### Synopsis

During the flow of polymer melts, distortions of the emerging stream begin at well defined critical shear conditions and increase in severity at higher shear. End-corrected critical shear stresses in the capillary extrusion of molten polyethylene are independent of the length/radius ratio of the capillary but increase somewhat with rising temperature. The recoverable shear strain reaches its maximum value at the critical conditions, where it was calculated as the elastic component of the end effects and by applying Hooke's law in shear. Critical recoverable shear strain as well as the derived quantities shear modulus and normal force increase with increasing temperature. Linear polyethylene has higher values for these three parameters than two branched resins. Relaxation times calculated as the ratio viscosity/shear modulus agree rather well with values determined by other means.

### INTRODUCTION

Capillary flow data of viscoelastic liquids can be used to obtain information on their elastic as well as viscous characteristics.<sup>1</sup> Of special interest are the conditions leading to incipient distortion of the extruded jet observed in the case of molten plastics, since such distortions result from elastic failure in shear.<sup>2</sup> There is considerable disagreement on the effect of temperature and capillary dimensions on these conditions.

Accurate data are presented for three commercial polyethylene resins to illustrate the influence of these two factors, and to calculate elastic parameters of the molten resins. Two are low density resins, DYNH-3 (Resin A) and DFD-0114 (Resin B) of Union Carbide Plastic Co. The third is a high density polyethylene, Marlex Series 6000 Type 50 of Phillips Chemical Co. (Resin C). Their characteristics and viscous flow properties have been described.<sup>3</sup>

### TREATMENT OF DATA

For flow in a capillary of radius  $R$  and length  $L$ , the nominal maximum shear stress  $\tau$  at the wall is calculated according to

$$\tau = PR/2L \quad (1)$$

and the nominal shear rate  $D$  at the wall is

$$D = 4Q/\pi R^3 \quad (2)$$

where  $P$  is the pressure drop and  $Q$  the volumetric flow rate. This nominal shear rate is corrected for non-Newtonian behavior according to eq. (3):

$$\dot{\gamma} = [(3 + n')/4]D \quad (3)$$

$n'$  being the slope of the  $\log D$ - $\log \tau$  plot. Since the pressure drop is measured not only across the length of the capillary but includes the inlet as well, the nominal maximum shear stress is corrected for entrance losses according to Bagley<sup>4</sup> to give the effective shear stress at the wall:

$$\tau_{\text{eff}} = \tau/[1 + m/(L/R)] \quad (4)$$

That eq. (4) can be applied to the flow of polymer melts is shown by the fact that plots of  $P$  versus  $L/R$  at constant shear rate are linear in the range of  $L/R$  from 0 to 30 or more, provided that only dies with similar inlet angles are compared.<sup>4-6</sup> Within experimental error, points obtained with tapers in the 42-60° range fall on the same lines.<sup>3</sup>

Equation (4) has also been confirmed by an energy balance across a capillary die with  $L/R = 65$  and a 60° included inlet angle.<sup>3</sup> End effects calculated as the difference between the overall energy input  $PQ$  and the energy dissipated by viscous friction and transformed into heat  $Qc_r\Delta T$ , were 9.2% of  $PQ$ . End effects calculated as  $\tau D - \tau_{\text{eff}} D$  amounted to 8.7% of  $\tau D$ . The two percentage values of the end effects differ by only 6%, which is well within experimental error.

### End Correction

The end correction defined by eq. 4 consists in adding a multiple  $m$  of the radius to the capillary length in order to obtain an effective length. Neglecting the kinetic energy correction,  $m$  can be broken down into two or three components:

$$m = m_1 + (\gamma_{\text{el}}/2) + m_2 \quad (5)$$

The Couette correction  $m_1$  is a geometric end effect. The second component is one-half of the recoverable shear strain at the wall. It corrects for the elastic energy stored by the melt under shear, which is imparted at the inlet and not dissipated inside the capillary.<sup>1</sup>

The third component depends on the taper of the inlet to the capillary. The melt flowing into die inlets with included angles of 110°<sup>7</sup> and 180°<sup>8-10</sup> adopts a funnel-shaped path on entering the capillary, the funnel having an included angle of 30-40° for low density polyethylene. The melt outside this conical influent zone above the shoulders of the die inlet remains trapped there, in circulatory motion. The energy spent in maintaining the circulatory flow of this stagnant melt is corrected for by  $m_2$ . With dies of small inlet angles equal to that of the natural approach funnel, the stagnant zone is filled up by metal and  $m_2$  is zero.

Since the volume of the stagnant zone depends on the entry angle, so does  $m_2$  and therefore  $m$  as well. Until the dependence of  $m_2$  on the entry angle has been evaluated, it is necessary to apply end corrections to flow data obtained with dies of the same angle. As all of the work described below was done with flat entry dies (included inlet angle  $180^\circ$ ), the  $m$  values Schott and Kaghan<sup>3</sup> obtained with dies of  $45^\circ$  inlets are inapplicable. Therefore, values of  $m$  were taken from Ryder<sup>5</sup> and calculated from the  $188^\circ\text{C.}$  data of Schott and Kaghan,<sup>9</sup> both of which refer to resin A and flat entry dies. The crossing over of the  $292$  and  $265^\circ\text{C.}$  lines in Figure 4 of reference 5 is probably due to thermal degradation at high temperature and low shear rates. The lower temperature data agree roughly with those calculated from reference 9 (see Fig. 1).

While  $\gamma_{e1}$  and  $m_2$  are functions of shear and temperature,  $m_1$  is assumed to be constant. The importance of  $m_2$  is illustrated in Figure 1, where  $m$  values for resin A obtained with flat entry dies are compared to values obtained with dies of  $42$ – $60^\circ$  inlet angles, for which  $m_2$  is zero. At comparable temperatures and shear rates, the values of the former are about twice those of the latter. Therefore,  $m_2$  is of the same order of magnitude as  $m_1 + \gamma_{e1}/2$  for this low density resin.

The only end correction values published for resin B refer to dies of  $42$ – $60^\circ$  included inlet angles.<sup>3</sup> End correction values corresponding to flat entry dies were estimated by assuming the same  $m_2$  value as for resin A at

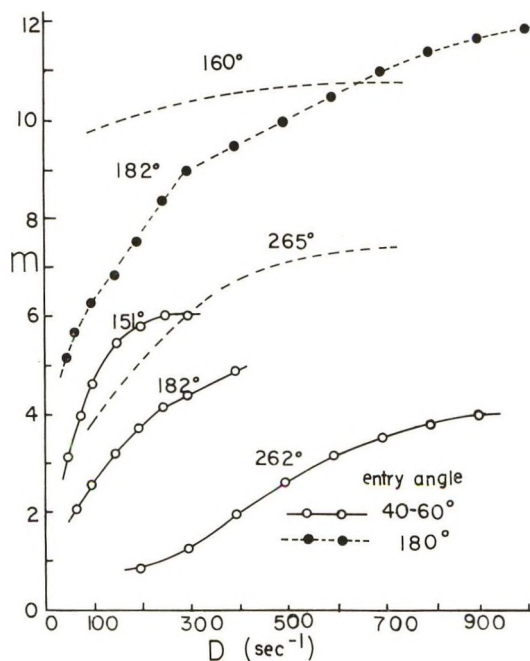


Fig. 1. Comparison of end effect parameter  $m$  of resin A determined with dies of flat and tapered entries at various shear rates. The  $160$  and  $265^\circ\text{C.}$  curves are taken from the data of Ryder.<sup>5</sup>

comparable temperature and rate of shear, and increasing the remainder of  $m$  in the proportion of the  $m$  values of resin A and B obtained with dies of small taper.<sup>3,5</sup> The risk inherent in this procedure is mitigated by the fact that the flow data of resin B were obtained with a die of a high  $L/R$  ratio. The end corrections used for resin C were estimated by extrapolating  $m$  values for linear resins of lower melt indices.<sup>5</sup>

## VARIABILITY OF CRITICAL SHEAR STRESS

When molten plastics are extruded through capillaries, melt fracture sets in at well defined shear stresses and shear rates, which are designated as critical;<sup>11</sup> they are marked by the subscript  $c$ . If the capillary inlets are flat or have a large angle, melt fracture manifests itself as distortions of the extrudate which begin at the critical shear conditions and increase in severity as the shear goes up.<sup>7,9-12</sup>

There is considerable disagreement in the literature on whether the critical shear stress depends on the length/radius ratio of the capillary and on the melt temperature. For polystyrene, the critical shear stress was reported independent of temperature between 175 and 225°C.<sup>12</sup> For polyethylene, it was found to increase with increasing temperature and decreasing length/radius ratio.<sup>9,11</sup> Other investigators claim that the critical shear stress decreases with increasing temperature,<sup>13,14</sup> or that it is independent of temperature.<sup>6,15</sup> These critical shear stresses are nominal values calculated from eq. (1). Moreover, the rather narrow temperature range covered by some investigators, combined with the possibility of thermal degradation, renders some of the conclusions doubtful. Bagley's extensive measurements were all made at 190°C.<sup>2,4,10,16</sup>

It is shown below that the effective critical shear stress, obtained by correcting the nominal critical shear stress corresponding to incipient waviness<sup>9</sup> for end effects according to eq. (4), is independent of length/radius ratio in the range of 7-80 and increases by about 0.75% for every degree of temperature rise.

Tables I-III summarize critical data of the three resins obtained with square-edged capillary dies. Most of the values for resins A and B were measured with a viscometer driven by a screw extruder<sup>3,9,17</sup> and a few with a piston-driven apparatus applying the instrumental correction of Marker, Early, and Aggarwal.<sup>18</sup> The data of resin C were measured with a gas-driven viscometer.<sup>19</sup> The critical shear values obtained with the screw extruder are by far the most reliable. Because the reservoir of resin is unlimited, flow rate or pressure and temperature can be increased or decreased very gradually or held constant for hours. Meanwhile, high flow rates and the continual churning of the melt prevent degradation due to prolonged contact of one portion with hot metal. Critical shear rates were found reproducible within  $\pm 5\%$ .

There is no systematic relation between  $L/R$  and  $\tau_{c,eff}$  or  $\dot{\gamma}_c$  for resin A. When plotting  $\log \tau_{c,eff}$  or  $\log \dot{\gamma}_c$  versus reciprocal absolute temperature, the

TABLE I  
Critical Flow Data of Resin A, Determined with Square-Edged Capillary Dies

Die	Die dimensions		Mean melt temperature, °C.	Critical shear stress, dyne/cm. <sup>2</sup> × 10 <sup>-5a</sup>		Critical shear rate, sec. <sup>-1b</sup>	
	Length, cm.	Length Radius		$\tau_c$	$\tau_{c,eff}$	$D_c$	$\dot{\gamma}_c$
F	0.80	7.42	170	15.2	6.61	180	246
			184	15.8	6.99	249	332
			200	17.9	7.76	475	628
			221	20.7	8.84	987	1404
			248	23.2	10.75	1967	—
D	1.86	7.65	158	13.0	5.70	100	139
			192	15.6	7.04	307	406
			210	18.1	7.98	632	841
S	2.56	10.7	183	11.5	6.11	250	334
			188	11.6	6.18	294	391
C	13.86	79.3	136	5.51	4.89	34	50
			147	5.90	5.23	56	81
			164	6.49	5.78	129	178
			194	9.29	8.36	239	314
			221	10.3	9.21	581	761
			277	13.2	12.4	5130	—

<sup>a</sup>  $\tau_c$  is defined by eq. (1),  $\tau_{c,eff}$  by eq. (4).

<sup>b</sup>  $D_c$  is defined by eq. (2),  $\dot{\gamma}_c$  by eq. (3).

TABLE II  
Critical Flow Data of Resin B<sup>a</sup>

Mean melt temperature, °C.	Critical shear stress, dyne/cm. <sup>2</sup> × 10 <sup>-5</sup>		Critical shear rate, sec. <sup>-1</sup>	
	$\tau_c$	$\tau_{c,eff}$	$D_c$	$\dot{\gamma}_c$
150	6.04	5.20	57	82
183	7.83	6.60	126	172
204	8.80	7.56	244	319
228	10.1	8.81	529	684

<sup>a</sup> Die dimensions:  $L = 13.86$  cm.,  $L/R = 79.3$ , entry angle = 180°.

TABLE III  
Critical Flow Data of Resin C<sup>a</sup>

Melt temperature, °C.	Critical shear stress, dyne/cm. <sup>2</sup> × 10 <sup>-5</sup>		Critical shear rate, sec. <sup>-1</sup>	
	$\tau_c$	$\tau_{c,eff}$	$D_c$	$\dot{\gamma}_c$
150	27.9	22.1	1250	1560
190	32.0	25.6	3100	4260

<sup>a</sup> Data of Mills, Moore, and Pugh.<sup>19</sup> Die dimensions:  $L = 0.447$  cm.,  $L/R = 18.24$ , entry angle = 180°.

points obtained with the different dies are scattered about the straight lines obtained by the method of least squares in random fashion. The equation for the critical shear stress is

$$\log \tau_{c,\text{eff}} = 7.2950 - 665.6/T \quad (6)$$

The apparent activation energy for the effective critical shear stress calculated according to the Arrhenius equation is  $-3,040$  cal./mole for resin A, approximately  $-2,840$  cal./mole for resin B, and  $-1,430$  cal./mole for resin C.

A similar value can be predicted for resin A by comparing the published values of the temperature dependence of the critical shear rate and of the viscosity. The Arrhenius equation was found to apply to the critical shear

$$D_c = A \exp \{ \Delta U_c / RT \} \quad (7)$$

rate. The constants for resin A are  $A = 8.00 \times 10^9$  and  $\Delta U_c = -15,600$  cal./mole.<sup>9</sup> When the critical shear rate is corrected for non-Newtonian behavior according to eq. (3), the constants become  $A = 1.576 \times 10^9$  and  $\Delta U_c = -14,000$  cal./mole. Zero shear viscosity and apparent viscosity at constant stress  $\eta^*$  obey the Arrhenius equation

$$\eta^* = \tau / \dot{\gamma} = A \exp \{ \Delta E / RT \} \quad (8)$$

from which results

$$R[d \ln \tau / d(1/T) - d \ln \dot{\gamma} / d(1/T)] = \Delta E \quad (9)$$

This relation holds at the critical conditions.

As mentioned above,  $R[d \ln \dot{\gamma}_c / d(1/T)] = \Delta U_c = -14,000$  cal./mole. For resin A,  $\Delta E$  is  $12,000$  cal./mole.<sup>3</sup> Therefore,  $R[d \ln \tau_c / d(1/T)] = \Delta E + \Delta U_c$  equals approximately  $-2,000$  cal./mole. In view of the experimental uncertainties, the discrepancy between  $-2,000$  and  $-3,040$  cal./mole is not serious.

The conclusion that the effective critical shear stress is independent of the length/radius ratio of the capillary would seem incompatible with the experimental observation that, at comparable shear rate and temperature, extrudate distortions become less severe for capillaries of higher  $L/R$ , i.e., for longer dwell times of the melt inside the capillary. A tenfold increase in  $L/R$  attenuates the distortions by more than two-thirds according to visual rating. No distortions at all were obtained with a tube of "infinite" length.<sup>6</sup> Since distortions are caused by surges of melt from the stagnant zone, of low strain or orientation, into the stream of highly oriented melt, the average melt viscosity and  $\tau_{c,\text{eff}}$  should vary with  $L/R$ .<sup>16</sup> The precision of the present data is too low and the  $L/R$  range too narrow to permit such comparatively small changes to be observed if they did occur.

### RECOVERABLE SHEAR

Philippoff has shown that viscoelastic liquids in steady flow store an elastic potential energy, which can be represented by the product of the

effective shear stress and the recoverable shear strain at the capillary wall. It equals the normal force at the capillary wall in the direction of flow, which causes an axial tension:<sup>1</sup>

$$P_{11} = \tau_{\text{eff}} \gamma_{\text{el}} \quad (10)$$

Since melt fracture results from exceeding the limit of elastic deformation in shear,<sup>2,20</sup> the recoverable shear strain reaches its maximum value at incipient melt fracture. This value should be a characteristic for a given resin at a given temperature, just like critical shear stress and critical rate of shear. Several methods for determining recoverable shear have been discussed by Philippoff.<sup>1</sup> Those used below were also employed by Bagley.<sup>2</sup>

The first method is based on eq. (5). It is important in the case of low density polyethylene to use values of  $m$  obtained with capillaries of small inlet angles similar to the angle of the natural approach funnel, so that  $m_2$  is zero. For high density polyethylene the use of small taper entries may have the opposite effect of increasing  $m_2$ . Since there is little or no stagnant melt even in flat inlets, streamlining of the inlet would disturb the natural flow pattern.<sup>21</sup>

Extrapolating the  $m$  values of resin A at 151°C.<sup>3</sup> as a function of shear stress to zero shear, at which point  $\gamma_{\text{el}}$  is zero, gives the value of 1.24 for  $m_1$ . The  $m$  values at 204°C. converge to a similar figure but are more scattered so that the extrapolation is less precise. The third column of Table IV gives the values of  $\gamma_{\text{el}}$  calculated by this method.

TABLE IV  
Recoverable Shear Strain, Shear Modulus, and Normal Force for Three Polyethylene Resins at Critical Conditions

Resin	Temperature, °C.	$\gamma_{\text{el},c}$		$\mu$ , dyne/cm. <sup>2</sup> $\times 10^{-5}$		$P_{11, c}$ dyne/cm. <sup>2</sup> $\times 10^{-6}$	
		From eq. (5)	From eq. (11)	From eqs. (5) and (11a)	From eqs. (11) and (11a)	From eqs. (5) and (10)	From eqs. (10) and (11)
A	151	5.04	3.45	1.06	1.54	2.68	1.84
A	204	6.66	4.76	1.20	1.67	5.29	3.78
A	262	7.24	6.26	1.56	1.80	8.15	7.05
B	151		3.58		1.46		1.87
B	204		4.81		1.58		3.65
B	262		6.17		1.70		6.49
C	150		7.42		2.98		16.4
C	190		8.08		3.17		20.7

The second method, using Hooke's law in shear,<sup>22</sup> is based on data less subject to experimental error than the previous method, but its theoretical basis is not as reliable. For low density polyethylenes, measurements of recoverable strain on rotational instruments as a function of shear stress indicate that the direct proportionality between the two holds only below  $10^5$

dyne/cm.<sup>2</sup>.<sup>23</sup> Hooke's law in shear, applied to the point of incipient melt fracture, is:

$$\tau_{c,\text{eff}} \bar{M}_w = RT\rho\gamma_{el,c} \quad (11)$$

Values of the density  $\rho$  are calculated<sup>18</sup> according to

$$1/\rho = 0.88875 + 0.000936 T \quad (12)$$

where  $T$  is absolute temperature. Weight-average molecular weights  $\bar{M}_w$  calculated from intrinsic viscosities are 178,000 for resin A, 188,000 for resin B, and 92,000 for resin C.<sup>3</sup> Introducing these values of  $\bar{M}_w$  of resins A and B into eq. 11 may result in error because of long chain branching. Effective critical shear stresses were calculated from the data of Tables I and II by applying the method of least squares to the linear relation between  $\log \tau_{c,\text{eff}}$  and reciprocal temperature. Using these values in eq. (11) results in the recoverable shear values given in the fourth column of Table IV.

The values of critical recoverable shear of resin A calculated by the two methods are in fair agreement. Both sets increase with increasing temperature. Apparent activation energies are approximately  $-1,500$  cal./mole for the data based on eq. (5) and  $-2,400$  cal./mole for those based on eq. (11). Recoverable shear strains at incipient melt fracture of the three polyethylene resins range from 4 to 8, i.e., the melts have limits of elastic deformation in shear of 400–800%, beyond which that relief mechanism sets in.

For comparison, Bagley<sup>2</sup> calculated the following values of  $\gamma_{el,c}$  from the polystyrene data of Spencer and Dillon<sup>12</sup> using Eq. (11): 7.67 (175°C.), 7.37 (200°C.), and 7.08 (225°C.). These strain values decrease with increasing temperature whereas those of polyethylene were found to increase. This discrepancy may be due to the fact that the polystyrene values are based on uncorrected values of critical shear stress. Additional values of  $\gamma_{el,c}$  are 7.2 (190°C.) for poly(methyl methacrylate), 6.6 (190°C.) for high density polyethylene but 14.8 (190°C.) for low density polyethylene.<sup>2</sup> Tordella, on the other hand, reported a value of approximately 5 for  $\gamma_{el,c}$  not only of poly(methyl methacrylate) (200°C.), formaldehyde polymer (200°C.), and high density polyethylene, but for three low density polyethylenes at 150°C. as well.<sup>24</sup> He measured instantaneous shear moduli on a rotational viscometer<sup>1</sup> and calculated recoverable shear strain at the critical point as the ratio of critical shear stress to modulus, assuming the modulus independent of shear stress. The actual values of  $\gamma_{el,c}$  taken from Figure 12 of Tordella's publication<sup>24</sup> are 3.0, 4.2, and 8.5 for low and 4.1 for high density polyethylene. This last value is lower than the 7.4 figure of resin C, but the melt index of resin C is ten times as high, and it has been observed for linear resins at 150°C. that  $\tau_c$  increases with increasing melt index (Fig. 11 of ref. 19), and therefore  $\gamma_{el,c}$  should increase as well. Tordella's  $\gamma_{el,c}$  values for low density polyethylene are of the same order as those of Table IV but considerably smaller than the 14.8 figure reported by Bagley.<sup>2</sup> This discrepancy is either due to differences in resin or to the

fact that Bagley used square-edged dies and did not subtract  $m_z$  from the total end effect. As shown earlier, this correction is important for low density polyethylene and tends to reduce  $\gamma_{el}$ .

Shear moduli calculated according to

$$\mu = \tau_{c,eff} / \gamma_{el,c} \quad (11a)$$

are also listed in Table IV. They increase with increasing temperature as predicted by theory.<sup>22</sup> The higher modulus of the linear resin compared to the branched resins is to be expected. Branched molecules are more compact than linear molecules and are therefore less entangled with each other. Considering each point of intermolecular entanglement as a temporary crosslink, the higher density of crosslinking in the melt of linear resin C should result in a proportionally higher modulus in shear than for resins A or B.<sup>3</sup>

### NORMAL STRESSES

Normal stress values at critical conditions, defined by eq. (10) and calculated from  $\gamma_{el,c}$  determined by the two methods described above, are recorded in Table IV. Since recoverable shear strain, the ratio of normal stress to shear stress, varied from 4 to 8 at critical conditions, normal stresses are between four and eight times larger than shear stresses, and are likely to play a dominant role in melt fracture. Published  $P_{11}$  values obtained by different methods<sup>1,23</sup> agree rather well with those of Table IV.

### RELAXATION TIMES

Hoff measured relaxation times of molten low density polyethylene resins with an oscillating coaxial viscometer at small strains.<sup>25</sup> The resins behaved nearly like Maxwell models, and a single relaxation time was sufficient to describe their mechanical behavior at a given temperature. Clegg found that stress relaxation, measured with a concentric cylinder viscometer at larger strains, was also nearly Maxwellian.<sup>7</sup> Since values of both apparent viscosity and shear modulus are available from capillary flow measurements, it is formally possible to calculate a relaxation time for each temperature as the ratio of the two. It is interesting to compare these values with the relaxation times previously published.

For resin A, the values at critical conditions are 50 msec. (151°C.), 10.5 msec. (204°C.), and 2.3 msec. (262°C.). These relaxation times, corresponding to conditions at the wall of the capillary, are from 5 to 95 times smaller than the average dwell times of the melt inside the capillary dies at critical conditions. The latter are 0.45 sec. (die D, 151°C.), 4.6 sec. (die C, 151°C.), 11 msec. (die D, 262°C.) and 111 msec. (die C, 262°C.).

Hoff reported relaxation times of 10–20 msec. between 135 and 203°C., but his values increased slightly with increasing temperature because his shear moduli as well as his viscosity values decreased with increasing tem-

perature. Clegg's relaxation times of 0.2–0.3 sec. (130°C.) are in better agreement with the present data than with those of Hoff.

## CONCLUSIONS

The lowest end-corrected shear stress producing melt fracture, measured with square-edged capillary dies, is independent of capillary dimensions within a tenfold range of length/radius ratio, but increases slightly with increasing temperature. In view of the small differences and of the experimental uncertainties, it is not possible to state whether the apparent activation energy of  $\tau_{c,eff}$  for linear polyethylene is actually lower than that of branched resins.

Critical shear rates increase rapidly with increasing temperature. The apparent activation energy of  $\dot{\gamma}_c$  is greater for the two branched than for the linear polyethylene resin. This is a consequence of the greater apparent activation energy for viscous flow of the former.

Since melt fracture is the result of elastic failure in shear, the maximum attainable value of the recoverable shear strain is a good parameter for characterizing the critical conditions corresponding to incipient melt fracture. From a mechanistic viewpoint,  $\gamma_{el,c}$  can be considered a dimensionless parameter expressing the ratio of viscous to elastic forces  $\dot{\gamma}\eta^*/\mu$ .<sup>20,26</sup> Melt fracture occurs when  $\tau_{eff}/\mu$  exceeds the critical value of  $\gamma_{el}$ .

Reported values of  $\gamma_{el,c}$  for different polymers are all in the range of  $6 \pm 2.5$ . However, these polymers have rather flexible chains. It should be interesting to study the effect of greater chain stiffness (less entanglement) as well as of crosslinking on  $\gamma_{el,c}$ .

## References

1. Philippoff, W., and F. H. Gaskins, *Trans. Soc. Rheol.*, **2**, 263 (1958).
2. Bagley, E. B., *Trans. Soc. Rheol.*, **5**, 355 (1961).
3. Schott, H., and W. S. Kaghan, *J. Appl. Polymer Sci.*, **5**, 175 (1961).
4. Bagley, E. B., *J. Appl. Phys.*, **28**, 624 (1957).
5. Ryder, L. B., *SPE J.*, **17**, 1305 (1961).
6. Metzner, A. B., E. L. Carley, and I. K. Park, *Mod. Plastics*, **37**, No. 11, 133 (1960).
7. Clegg, P. L., in *Rheology of Elastomers*, P. Mason and N. Wookey, Eds., Pergamon Press, New York-London, 1958, pp. 174–189.
8. Tordella, J. P., *Trans. Soc. Rheol.*, **1**, 203 (1957).
9. Schott, H., and W. S. Kaghan, *Ind. Eng. Chem.*, **51**, 844 (1959).
10. Bagley, E. B., and A. M. Birks, *J. Appl. Phys.*, **31**, 556 (1960).
11. Tordella, J. P., *J. Appl. Phys.*, **27**, 454 (1956).
12. Spencer, R. S., and R. E. Dillon, *J. Colloid Sci.*, **4**, 241 (1949).
13. Westover, R. F., and B. Maxwell, *SPE J.*, **13**, No. 8, 27 (1957).
14. Hogg, R. W., *Plastics (London)*, **24**, 69 (1959).
15. Beynon, D. L. T., and B. S. Glyde, *Brit. Plastics*, **33**, 414 (1960).
16. Bagley, E. B., and H. P. Schreiber, *Trans. Soc. Rheol.*, **5**, 341 (1961).
17. Schott, H., and W. S. Kaghan, *J. Appl. Polymer Sci.*, **4**, 368 (1961).
18. Marker, L., R. Early, and S. L. Aggarwal, *J. Polymer Sci.*, **38**, 381 (1959).
19. Mills, D. R., G. E. Moore, and D. W. Pugh, *SPE Trans.*, **1**, 40 (1961).
20. Tordella, J. P., *Rheol. Acta*, **1**, 216 (1958).

21. Schreiber, H. P., E. B. Bagley, and A. M. Birks, *J. Appl. Polymer Sci.*, **4**, 362 (1960).
22. Treloar, L. R. G., *Trans. Faraday Soc.*, **39**, 36 (1943).
23. Benbow, J. J., and E. R. Howells, *Polymer*, **2**, 429 (1961).
24. Tordella, J. P., *J. Appl. Polymer Sci.*, **7**, 215 (1963).
25. Hoff, E. A. W., *J. Polymer Sci.*, **9**, 41 (1952).
26. Vinogradov, G. V., A. Y. Malkin, and A. I. Lenov, *Kolloid-Z.*, **191**, 25 (1963).

### Résumé

Au cours du coulage de polymères fondus, des distortions du courant superficiel apparaissent pour des valeurs critiques bien définies des conditions de cisaillement et croissent en importance pour des valeurs plus élevées de cisaillement. Les tensions de cisaillement critique, corrigées pour les extrémités dans l'extrusion capillaire du polyéthylène fondu sont indépendantes du rapport longueur/rayon du capillaire mais augmentent quelque peu avec la température. La tension de cisaillement maximale est atteinte pour les conditions critiques où elle a été calculée comme étant la composante élastique des effets terminaux et en appliquant la loi de Hooke relative du cisaillement. La tension de cisaillement critique observable ainsi que les grandeurs dérivées du module de cisaillement et de la force normale augmentent avec la température. Le polyéthylène linéaire présente des valeurs de ces trois paramètres plus élevées que pour deux résines ramifiées. Les temps de relaxation calculés par le rapport viscosité/module de cisaillement s'accordent plutôt bien avec les valeurs calculées par d'autres voies.

### Zusammenfassung

Während des Fließens von Polymerschmelzen beginnen Störungen des austretenden Stromes bei gut definierten kritischen Scherungsbedingungen und nehmen bei höherer Scherung bedeutend zu. Endeffektkorrigierte kritische Scherspannungen bei der Kapillarextrusion von geschmolzenem Polyäthylen sind vom Länge-Radius-verhältnis der Kapillare unabhängig, nehmen aber etwas mit steigender Temperatur zu. Die rückbildbare Scherverformung erreicht bei kritischen Bedingungen ihr Maximum, wo sie als die elastische Komponente der Endeffekte unter Anwendung des Hookeschen Gesetzes auf die Scherung berechnet wurde. Sowohl die kritische rückbildbare Scherverformung als auch die abgeleiteten Größen, Schermodul und Normalkraft, nehmen mit steigender Temperatur zu. Lineares Polyäthylen weist für diese drei Parameter höhere Werte auf als zwei verzweigte Harze. Relaxationszeiten, berechnet als Verhältnis Viskosität:Schermodul stimmen recht gut mit anderweitig bestimmten Werten überein.

Received September 20, 1963

Revised November 4, 1963

## Synthesis and Polymerization of 1-(Perfluoroacyl)aziridines

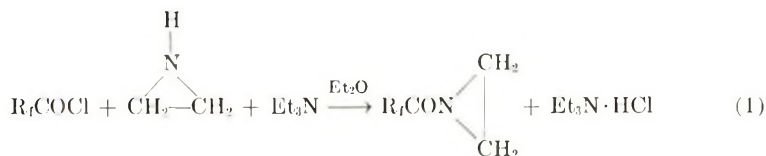
A. G. PITTMAN and R. E. LUNDIN, *Western Regional Research Laboratory, Agricultural Research Service, U. S. Department of Agriculture, Albany, California*

### Synopsis

The preparation and polymerization of representative 1-(perfluoroacyl)aziridines were examined. Polymerization of the aziridines was induced by heat, by certain inorganic nucleophiles such as cyanide, fluoride, and chloride, and by organic bases. Certain other inorganic nucleophilic reagents such as KI and KBr effected the rearrangement of the 1-(perfluoroacyl)aziridines to the isomeric 2-perfluoroalkyl-2-oxazolines. A possible reaction mechanism involving anionic polymerization in competition with oxazoline formation was discussed.

### INTRODUCTION

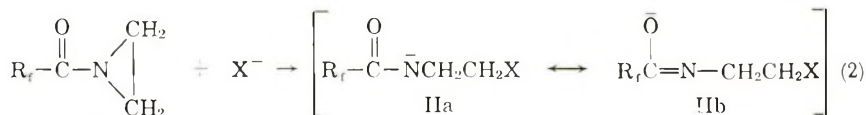
The 1-(perfluoroacyl)aziridines represent a versatile group of fluorine-containing compounds which has received little attention. Brace and McCormack<sup>1</sup> described a displacement reaction between ethylenimine and an  $\alpha,\alpha$ -dichloroperfluoroalkyl ester in which ring-opened products were obtained instead of the 1-(acyl)aziridines. We found that the 1-(perfluoroacyl)aziridines could be prepared in a straightforward manner by reaction of the corresponding perfluoro acid chlorides with ethylenimine, as shown in eq. (1).



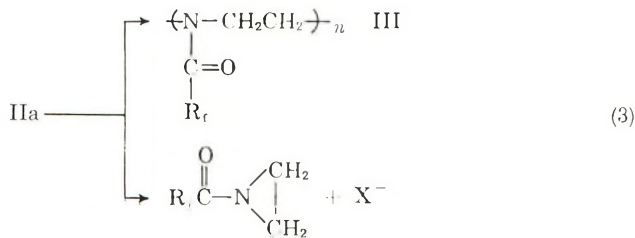
Removal of triethylamine hydrochloride and solvent from the crude reaction product left a heat-labile concentrate which could be stored at  $-78^\circ\text{C}$ . for an indefinite period. At room temperature the concentrate normally polymerized exothermically within 2 hr. Instability of the crude product is apparently due to the presence of traces of the free bases  $\text{Et}_3\text{N}$  or ethylenimine. Purification of the aziridines was carried out by removing them from the concentrate under vacuum without application of external heat to the distillation pot. After purification, the aziridinyl derivatives ex-

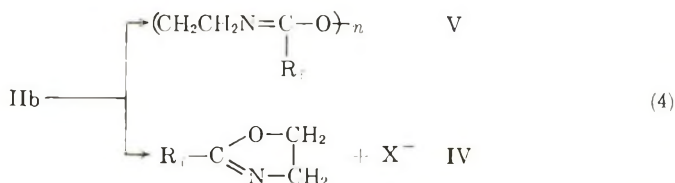
hibited increased stability, i.e., no sign of polymerization was noted with purified 1-(perfluorobutyryl)aziridine (I) until after 4 hr. at 24°C.

The polymerization of the 1-(perfluoroacyl)aziridines evidently follows a different course from ethylenimine, which is not polymerized by bases<sup>2,3</sup> but undergoes acid-catalyzed polymerization involving positively charged nitrogen. Addition of small quantities (ca. 1%) of 50% acetic, trifluoroacetic, or 6*N* hydrochloric acid to I at room temperature did not effect polymerization. Attempts to polymerize I with  $\text{BF}_3$  in ether or  $\text{AlCl}_3$  in *n*-heptane were also unsuccessful. In both cases, monomer was recovered after 2 hr. at room temperature. On the other hand, addition of catalytic amounts of triethyl amine, pyridine, or ethylenimine to I at room temperature caused an instantaneous exothermic conversion to polymer. Polymerization was also effected by using other nucleophiles such as chloride, cyanide, or fluoride ion in diglyme. The relative stability of the 1-fluoroacylaziridines toward acidic substances and their susceptibility to nucleophilic attack is best explained on the basis of an electron deficiency in the aziridinyll ring caused by the strong electron-withdrawal properties of the perfluoroalkyl group. Heine and co-workers<sup>4</sup> have shown that nucleophilic reagents such as sodium iodide or sodium thiocyanate are effective catalysts for the rearrangement of certain 1-(aroyl)aziridines to the isomeric oxazoline derivatives and have postulated mechanisms involving initial attack of the nucleophile on the carbonyl and on the aziridine ring. Similar mechanisms can be invoked for the 1-(perfluoroacyl)aziridines in which the intermediates serve either as a polymerization catalyst or are converted to a 2-perfluoroalkyl-2-oxazoline. It was observed that, in a series of experiments with a catalytic quantity (2 mole-%) of potassium halide in diglyme, iodide ion gave virtually complete conversion of I to 2-perfluoropropyl-2-oxazoline, bromide gave an 80% conversion to polymer and 20% conversion to oxazoline, whereas chloride and fluoride gave polymer and no oxazoline. Considering an initial attack of halide on one of the carbons of the aziridine ring,



where  $\text{X}^-$  = halide anion





it can be seen that reformation of the aziridine could occur by intramolecular displacement of halide by nitrogen in a reversible reaction or that intramolecular displacement of halide by the oxy anion would yield an oxazoline (IV). Polymer formation is presumably a competing intermolecular reaction which occurs when the C—X bond is not easily broken by displacement. Polymer structures III and V appear feasible depending on whether initiation occurs through negatively charged nitrogen (IIa) or the oxy anion (IIb). The fact that the ease of oxazoline formation follows the order of ease of displacement of halides,  $\text{I}^- > \text{Br}^- \gg \text{Cl}^-$ , lends credence to the mechanism proposed. The NMR and infrared spectra of poly-1-(perfluorobutyryl)aziridine were similar to the spectra obtained from a sample of polyethylenimine which received a treatment with perfluorobutyryl chloride. On the basis of this spectral evidence, we favor structure III as being representative of the poly-1-(perfluoroacyl)aziridines.

## EXPERIMENTAL

Boiling points and melting points are uncorrected. Melting points and polymer softening temperatures were obtained on a Fischer-Johns melting point block. Proton NMR spectra were taken on a Varian Associates 60 mcycle high resolution NMR spectrometer. Infrared spectra were obtained on a Perkin-Elmer Model 137 spectrophotometer. Infrared scans were run on the undiluted pure samples unless otherwise indicated.

### Preparation of Monomers

**Preparation of 1-(Perfluorobutyryl)aziridine (I).** A three-necked 500 ml. flask equipped with a stirrer, nitrogen inlet, and rubber septum was dried and flushed with nitrogen. Then 200 cc. of anhydrous diethyl ether, 13.3 g. (0.13 mole) triethylamine and 5.6 g. (0.13 mole) ethylenimine were added to the flask, and the contents were placed under a nitrogen blanket and cooled in a Dry Ice-acetone bath to ca.  $-30^\circ\text{C}$ . The mixture was stirred and 30 g. (0.13 mole) of perfluorobutyryl chloride was added slowly with stirring. The precipitated triethylamine hydrochloride was rapidly filtered from the cold ethereal solution; 17 g. of the hydrochloride was collected, indicating 94% conversion of the acid chloride. The ether was removed on a rotary evaporator, leaving 22 g. of a light brown liquid product. The crude material was distilled in a vacuum system (0.05–0.1 mm.) without applying external heat, and 20 g. (63%) of product was collected in a Dry Ice trap. The purified material was a clear liquid, b.p.

36°C./11 mm.,  $n_D^{23}$  1.3401. The infrared absorption spectra showed the C—H stretching at 3.25 and 3.35  $\mu$  and carbonyl absorption at 5.8  $\mu$ .

The 60 mcycle proton NMR spectrum of this material as a dilute solution in carbon tetrachloride showed a single sharp peak at 7.50  $\tau$ . To establish the shielding value of aziridine protons, 1-(3,5-dinitrobenzoyl)-aziridine was prepared by the method of Heine.<sup>4</sup> The four equivalent protons on the aziridine ring produced a sharp peak at 7.52  $\tau$ , confirming that I was an aziridine.

Because of the instability of the monomer, combustion analysis was carried out on the polymer as described subsequently.

A ring-opened derivative, *N*-(2-bromoethyl)perfluorobutyramide, was prepared as follows. A 0.5-g. (0.0021 mole) portion of I was added, with stirring, to 20 cc. of a cold (ca. 5°C.) 48% aqueous HBr solution. A white solid was formed immediately. It was filtered from the solution, washed several times with H<sub>2</sub>O and dried; 0.61 g. (91% yield) of *N*-(2-bromoethyl)-perfluorobutyramide was obtained, m.p. 57–59°C. Sublimation of the solid at 0.7 mm. gave the pure product, m.p. 63–64°C.

ANAL. Calcd. for C<sub>6</sub>BrF<sub>7</sub>H<sub>4</sub>NO: C, 22.50%; Br, 25.00%; F, 41.56%; H, 1.5%; MW, 320. Found: C, 22.30%; Br, 24.99%; F, 39.7%; H, 1.8%; MW, 343 (Rast).

Infrared spectra of the product in CCl<sub>4</sub> had the bands expected for a secondary amide: N—H at 2.95  $\mu$ , carbonyl at 5.78  $\mu$ , and N—H deformation at 6.5  $\mu$ .<sup>5a</sup>

The proton NMR spectrum of this compound in carbon tetrachloride showed a very broad band with its center at 3.10  $\tau$  arising from the amide proton, and a complex multiplet of the A<sub>2</sub>B<sub>2</sub>X type centered at 6.40  $\tau$ . Integration showed that the latter band represented 4.1 protons on the basis of the assignment of one proton to the broad peak. To confirm the assignment of the multiplet to the hydrogens of the methylene groups attached either to amide nitrogen or to bromine, the spectrum of *N*-(2-bromoethyl)octanoamide was obtained. The methylene protons of the bromoethyl moiety produced an incompletely resolved band centered at 6.46  $\tau$ .

**1-(Perfluorooctanoyl)aziridine (VI).** In a procedure analogous to that described for I, VI was prepared as a clear liquid, b.p. 44°C./0.1–0.2 mm.,  $n_D^{23}$  1.3330. Elemental analysis was carried out on the polymer obtained by allowing VI to stand overnight at 23°C.

ANAL. Calcd. for C<sub>10</sub>F<sub>15</sub>H<sub>4</sub>NO: C, 27.33%; F, 64.92%; H, 0.9%. Found: C, 26.82%; F, 64.2%; H, 1.12%.

**1,1'-(Perfluoroglutaryl)bisaziridine (VII).** A procedure was used similar to that described by Heine for the preparation of 1-(aroyl)aziridines.<sup>4</sup> Into a Waring Blendor were placed 50 g. ice, 50 g. benzene, 4.0 g. (0.1 mole) NaOH, and 4.3 g. (0.1 mole) ethylenimine. After the mixture had been stirred for a few minutes to dissolve NaOH, 14 g. (0.05 mole) of perfluoroglutaryl chloride was added over a period of 10–15 min. The temperature was maintained at ca. 5°C. by addition of ice when needed. The benzene

layer was separated and dried over  $\text{CaSO}_4$ . The water layer was extracted once with about 20 cc. of diethyl ether and the ether and benzene layers combined. The ether and benzene were removed on a rotary evaporator leaving 20 g. of a liquid product which contained residual benzene. The infrared spectrum of the residue confirmed the 1-(acyl)aziridine structure. Absorption was noted at  $3.25\ \mu$  and  $3.35\ \mu$  for the C—H stretching,  $5.8\ \mu$  for the carbonyl, and in the  $8\text{--}9\ \mu$  region for the C—F absorption. Several unsuccessful attempts at purification were made via high vacuum distillation. The higher boiling point of VII necessitated some heating during the distillation attempts which always resulted in a highly exothermic polymerization.

The polymer derived from the crude monomer had properties expected of a highly crosslinked structure in that it was extremely brittle, insoluble, and did not melt. Charring of the polymer commenced at  $270\text{--}280^\circ\text{C}$ .

### Polymerizations

**Uncatalyzed Polymerization of I.** Purified I was placed in a 2-oz. screw-cap vial and allowed to stand at  $23^\circ\text{C}$ . A viscosity increase was noted after 4 hr. and complete solidification after 12 hr. A white, opaque solid polymer was obtained which softened at  $190^\circ\text{C}$ . and yielded a clear, somewhat brittle film on pressing at  $175^\circ\text{C}/1000\ \text{psi}$ . The inherent viscosity of the polymer was 0.07 at  $23^\circ\text{C}$ . (1% solution in 1,3-bis(trifluoromethyl)benzene). The polymer was soluble in acetone, 1,3-bis(trifluoromethyl)benzene, and DMF and insoluble in  $\text{CCl}_4$  and heptane.

Infrared analysis of the polymer revealed the disappearance of the carbonyl band at  $5.8\ \mu$  and the presence of new bands at  $5.98\ \mu$  (strong) and  $3.02\ \mu$  (weak). The band at  $5.98\ \mu$  is presumably due either to amide carbonyl or  $\text{—N=C—O}^{5b}$  and the weak band at  $3.05\ \mu$  to N—H stretching of secondary amide chain ends. The proton NMR spectrum of the polymer dissolved in trifluoromethylbenzene and run at  $80^\circ\text{C}$ . showed a single broad peak (line width approximately 9 cycles/sec.) centered at  $6.15\ \tau$ . This peak is not present in the spectrum of the solvent when run under the same conditions. This peak was somewhat asymmetric with the extra intensity on the high-field side. The position of the observed band is not unreasonable for the methylene protons in III and IV. The sensitivity was not sufficient to observe any terminal group resonances.

ANAL. Calcd. for  $\text{C}_6\text{F}_7\text{H}_4\text{NO}$ : C, 30.12%; F, 55.64%; H, 1.7%; N, 5.85%. Found: C, 29.90%; F, 54.35%; H, 1.9%; N, 5.93%.  $\bar{M}_n = 3,728$  (Mechrolab osmometer).

**Modification of Polyethylenimine to a Structure III.** An aqueous sample of polyethylenimine (MW 30,000–40,000) was dried by repeated azeotropic distillations with benzene and reacted with an excess of perfluorobutryl chloride in acetone/chloroform with triethylamine as an acid acceptor.

The proton NMR spectrum of the modified polyethylenimine dissolved in trifluoromethylbenzene and run at  $80^\circ\text{C}$ . showed a single broad peak

(line width at one-half height approximately 30 cycles/sec.) centered at  $6.15 \tau$ .

An infrared scan (KBr) showed absorption bands similar to those observed for poly-1-(perfluorobutyl)aziridine.

**Polymerization of a Crude Reaction Product of VI.** Ether was stripped from a reaction mixture as described for the preparation of VI. After standing at room temperature for 45 min., the concentrate underwent a spontaneous exothermic polymerization, giving a clear, light-brown solid polymer with an inherent viscosity of 0.15 at  $22^\circ\text{C}$ . (1% solution in 1,3-bis(trifluoromethyl)benzene). The polymer melted at  $142\text{--}145^\circ\text{C}$ ., yielded a clear brittle film on pressing at  $135^\circ\text{C}/1000$  psi, and was soluble in benzo-trifluoride and 1,3-bis(trifluoromethyl) benzene and insoluble in  $\text{CCl}_3$ , DMF, and hydrocarbon solvents.

ANAL. Calcd. for  $\text{C}_{10}\text{F}_{15}\text{H}_1\text{NO}$ : C, 27.33%; F, 64.92%; H, 0.9%; N, 3.2%. Found: C, 27.32%; F, 64.2%; H, 1.34%; N, 3.4%.

The carbonyl band at  $5.8 \mu$  had disappeared and new bands occurred at  $5.98 \mu$  (strong) and  $3.05 \mu$  (weak).

**Polymerization vs. Oxazoline Formation.** A series of reactions with the use of 2 mole-% of the potassium halides KF, KCl, KBr, and KI in diglyme were carried out as follows. A 25-cc. round-bottomed flask was dried, flushed with nitrogen, and charged with the proper amount of halide and 5 cc. anhydrous diglyme. The solution was stirred and cooled to  $-30^\circ\text{C}$ ., and 1.6 g. I was added with a syringe. The cooling bath was removed and the solution was stirred overnight (12 hr.) at room temperature. After ca.  $1\frac{1}{2}$  hr., solid polymer was noted on the walls of the flask when KBr, KCl, and KF were used. A clear homogeneous solution resulted when KI was employed. The liquid was then distilled into a Dry Ice trap *in vacuo* without applying external heat to the distillation pot. The solid polymer which remained in the distillation pot was then washed with  $\text{H}_2\text{O}$ , dried, and weighed. The distillate was diluted with 6 cc.  $\text{H}_2\text{O}$  and the upper  $\text{H}_2\text{O}$ -diglyme phase removed. The fluorocarbon layer was washed once with 2 cc.  $\text{H}_2\text{O}$ , dried, and examined by infrared spectroscopy and gas chromatography. The results of the experiments are summarized in Table I.

TABLE I  
Effect of Halide

Halide	Polymer obtained, %	Liquid recovered, %	Composition of recovered liquid
KF	73	20	Monomer
KCl	80	20	Monomer
KBr	73	20	Oxazoline
KI	<1	>99	Oxazoline

Control experiments without added halide verified the catalytic action of the potassium halides. The polymers obtained were similar to the polymer obtained by the uncatalyzed polymerization of I. The oxazoline obtained from I is 2-perfluoropropyl-2-oxazoline, b.p. 135–136°C./760 mm.,  $n_D^{23}$  1.3345.

ANAL. Calcd. for  $C_6F_7H_4NO$ : C, 30.12%; F, 55.64%; H, 1.7%; N, 5.85%. Found: C, 30.98%; F, 55.8%; H, 2.1%; N, 5.82%.

The infrared spectrum of 2-perfluoropropyl-2-oxazoline revealed C—H stretching at 3.4–3.5  $\mu$  and —C=N— stretching (medium intensity) at 5.98  $\mu$ . This compound in carbon tetrachloride had a proton NMR spectrum that consisted of a single complex multiplet of the  $A_2B_2$  type centered at 5.75  $\tau$ . The high-field half of this band showed an additional incompletely resolved triplet splitting ( $J \approx 1.5$  cycle/sec.) presumably arising from spin-spin coupling between the two equivalent fluorines on the  $\alpha$  carbon and the protons of the methylene group attached to the unsaturated nitrogen. To confirm the assignment of this band to the four oxazoline protons, the spectrum of 2-(3,5-dinitrophenyl)-2-oxazoline, prepared by the method of Heine<sup>6</sup> was obtained. The oxazoline hydrogens gave rise to a multiplet of identical appearance (except for the absence of the fluorine splitting) centered at 5.70  $\tau$ .

The oxazoline was also obtained when diglyme was used as a solvent with either a 1/50 or 1/1 mole ratio of NaI to 1-(perfluorobutyl)aziridine. Polymer formation was not observed under any of the conditions in which NaI or KI were used.

Reference to a company or product name does not imply approval or recommendation of the product by the U. S. Department of Agriculture to the exclusion of others that may be suitable.

### References

1. Brace, N. O., and W. B. McCormack, *J. Org. Chem.*, **26**, 5091 (1961).
2. Barb, W. G., *J. Chem. Soc.*, **1955**, 2564.
3. Barb, W. G., *J. Chem. Soc.*, **1955**, 2577.
4. Heine, H. W., M. E. Fetter, and E. M. Nicholson, *J. Am. Chem. Soc.*, **81**, 2202 (1959).
5. Bellamy, L. J., *The Infra-red Spectra of Complex Molecules*, Methuen, London, 1958 (a) p. 204; (b) p. 267.
6. Heine, H. W., and J. Proctor, *J. Org. Chem.*, **23**, 1554 (1958).

### Résumé

La préparation et la polymérisation de représentants de la classe des 1-(perfluoro-acyl)aziridines ont été examinées. La polymérisation des aziridines était initiée par la chaleur, par certaines substances nucléophiles inorganiques tels des cyanures, fluorures, chlorures et par des bases organiques. Certains autres réactifs nucléophiles tels que KI et KBr ont produit le réarrangement des 1-(perfluoroacyl)aziridines en isomères 2-perfluoroalcoyl-2-oxazolines. La possibilité d'un mécanisme de réaction impliquant une polymérisation anionique en compétition avec la formation d'oxazoline a été discutée.

### Zusammenfassung

Die Herstellung und Polymerisation von repräsentativen 1-Perfluoracylaziridinen wurde untersucht. Die Polymerisation der Aziridine wurde durch Hitze, bestimmte anorganische Nucleophile wie Cyanid, Fluorid und Chlorid und organische Basen angeregt. Gewisse andere anorganische nucleophile Reagenzien wie KI und KBr bewirkten die Umlagerung der 1-Perfluoracylaziridine zu den isomeren 2-Perfluoralkyl-2-Oxazolinen. Ein möglicher Reaktionsmechanismus mit anionischer Polymerisation und gleichzeitiger Oxazolinbildung wird diskutiert.

Received December 6, 1963

Revised January 20, 1964

## BOOK REVIEW

N. G. GAYLORD, Editor

**Polymerization of Aldehydes and Oxides (Polymer Reviews, Vol. 3),**  
J. Furukawa and T. Saegusa, Interscience, New York, 1963, xii + 482 pp.,  
\$18.50.

This is a clear and well-written review of the field of polymerization of aldehydes and oxides through 1962. Initially, one would wonder why the publisher would publish two books on the same subject in one year (the other being *Polyethers*, edited by N. G. Gaylord). However, although there is some duplication of coverage, the two books complement each other. Their orientation is different in that they emphasize different areas. The present book emphasizes the reaction mechanisms involved in the polymerizations and does not deal with the applications of the polymers. Gaylord's book very nicely combines the chemistry of the polymerization reaction with a good amount of information on the industrial application of the polymers and their technology.

The reviewer feels that the patent information compiled in Chapter IX should not be segregated from the main chapters dealing with the subject. If the tables of patent examples were made part of the main chapters, they would be more useful for reference usage.

The utility of the patent index as such escapes the reviewer. It is not often that a specific patent number is known. More often, it is known that a specific company has obtained a patent in a field. Indexing by company would make the patent index much more useful from this point of view. Actually, the patent index should probably be indexed by subject and the company name appear along with the patent number for maximum utility.

*Arthur M. Schiller*

American Cyanamid Company  
Stamford Research Laboratories  
Stamford, Connecticut

## ERRATA

### Thermal Degradation of *N*-Substituted Polycarbamates

(article in *J. Polymer Sci.*, **A2**, 1-14, 1964)

BY ELIZABETH DYER and RICHARD J. HAMMOND

*Department of Chemistry, University of Delaware, Newark, Delaware*

On p. 9, para. 1, line 1, reference should have been made to cyclic urethans described by H. Zahn and M. Dominik, *Angew. Chem.*, **72**, 273 (1960); W. Kern, K. J. Rauterkus, and W. Weber, *Makromol. Chem.*, **43**, 98 (1961); W. Kern, K. J. Rauterkus, W. Weber, and W. Heitz, *Makromol. Chem.*, **57**, 241 (1962); and W. Kern and K. J. Rauterkus, *Chimia (Aarau)*, **16**, 114 (1962).

### Estimation of Copolymer Reactivity Ratios: An Example of Nonlinear Estimation

(article in *J. Polymer Sci.*, **A2**, 645-668, 1964)

By D. W. BEHNKEN

*American Cyanamid Company, Central Research Division, Stamford, Connecticut*

On page 651, line 3, eq. (16) should read:

$$(\hat{\theta} - \hat{\theta})' [\mathbf{P}'\mathbf{P}] (\hat{\theta} - \hat{\theta}) = p s^2 F_{\alpha}(p, \nu)$$

On page 666, sections 5.4.1, line 7 should read (denoted by  $\bar{z}_1$  and  $\bar{z}_2$ , respectively). . . .

On page 666, para. 3, eq. (44) should read:

$$s^2 = \frac{\sum_{u=1}^n (z_{1u} - \bar{z}_1)^2 + \sum_{u=1}^n (z_{2u} - \bar{z}_2)^2}{N - 2}$$

On page 667, line 7 should read to obtain  $\hat{r}_1, \hat{r}_2$  after the first cycle.

On page 667, line 20 should read Since  $x_i = [M_1]_0/[M_2]_0 = \text{constant}$  . . .